OFFICE OF NAVAL RESEARCH
STRUCTURAL MECHANICS SERIES

Already published in this series:

STRUCTURAL MECHANICS, Proceedings of the First symposium on Naval Structural Mechanics.

Edited by J. NORMAN GOODIER and NICHOLAS J. HOFF, 1960

PLASTICITY, Proceedings of the Second symposium on Naval Structural Mechanics.

Edited by E. H. LEE and P. S. SYMONDS, 1960

HIGH TEMPERATURE STRUCTURES AND MATERIALS, Proceedings of the Third symposium on Naval Structural Mechanics.

Edited by A.M.FREUDENTHAL, B. A. BOLEY and. H. LIEBOWITZ, 1964

MECHANICS AND CHEMISTRY

OF SOLID PROPELLANTS

PROCEEDINGS OF THE FOURTH SYMPOSIUM

ON NAVAL STRUCTURAL MECHANICS

Held at Purdue University, Lafayette, Indiana

April 19–21, 1965

Sponsored by the Office of Naval Research

and Purdue University

Edited by

A. C. ERINGEN

H. LIEBOWITZ

S. L. KOH

J. M. CROWLEY

PREFACE

THE Fourth Symposium on Naval Structural Mechanics, which was also the International Conference on the Mechanics and Chemistry of Solid Propellants, was held from April 19 to April 21, 1965, at Purdue University under the joint sponsorship of the Structural Mechanics Branch of the Office of Naval Research of the U.S. Department of the Navy and the School of Aeronautics, Astronautics and Engineering Sciences of Purdue University.

This conference was organized mainly to provide a forum for scientists and engineers active in the research, development and utilization of solid propellants to review and evaluate the present status of the field, attempt to consolidate the vast amount of significant information presently available in various widely-scattered depositories, and establish useful guidance for further work. The conference covered the many branches of studies that touch upon the science and technology of solid propellants. Integrated reviews and tutorial lectures were presented on the mathematical and physical theories underlying the behavior of solid propellant materials (e.g. nonlinear and linear theories of viscoelasticity), recent advances in solid propellant binder chemistry, combustion and its effects on the structural integrity of the solid propellant grain, and design and other engineering problems.

This volume contains the full text of the papers presented at the conference (with the exception of two papers for which abstracts are published here). The various addresses delivered at the opening session are also included in this volume.

Following is the complete program of the conference:

MONDAY, 19 April

OPENING SESSION

Chairman: Dr. JOHN CRAVEN, Chief Scientist, Department of the Navy.

    9.00   Welcoming Address:
            Dr. F. L. HOVDE, President, Purdue University.
            Opening Remarks: Dr. F. J. WEYL, Chief Scientist, Office of Naval Research.

SESSION I—ENGINEERING PROBLEMS

    9.30   Rear Admiral GEORGE H. MILLER, Director of Navy Long Range Objectives Group, United States Department of the Navy, Navy Projections of Long-Range Objectives.
   10.15   Dr. I. SILVER, Bureau of Naval Weapons, U.S. Navy, Navy Requirements for Solid Propellant Grain Integrity.
   11.00   Mr. J. E. FITZGERALD, Director of Research and Engineering, Lockheed Propulsion Company, Analysis and Design of Solid Propellant Grains.
   11.45   Discussion

* Indicates Speaker

WEDNESDAY, 21 April

SESSION V—EXPERIMENTAL RESEARCH

Chairman: Dr. H. M. SHUEY, Director of Technical Liaison and Service, Rohm and Haas.

8.30   Dr. F. J. LOCKETT, Mathematics Division, National Physical Laboratory, Teddington, Middlesex, England, Experimental Characterization of Non-linear Viscoelastic Materials.

9.00   Professor H. KOLSKY, Division of Applied Mathematics, Brown University, Experimental Studies of the Mechanical Behaviour of Linear Viscoelastic Solids.

10.15 Professor A. DURELLI, Mechanics Division, The Catholic University of America, Experimental Strain Analysis of Propellant Grains and Pro-pellant Grain Models.

11.40 Professor E. H. DILL, School of Aerospace Engineering, University of Washington, Photoviscoelasticity.

SESSION VI—STRENGTH AND FAILURE

Chairman: Dr. T. L. SMITH, Stanford Research Institute.

1.00   Professor A. M. FREUDENTHAL†, Department of Civil Engineering, Columbia University; Dr. E. L. ALEXANDER* and A. CAPUTO, Rocketdyne Division of North American Aviation, Reinforced Propellants and Related Structures

1.45   Dr. F. R. SCHWARZL, Central Laboratory T.N.O. Delft, Holland, On Mechanical Properties of Unfilled and Filled Elastomers

3.00   Dr. J. H. WIEGAND, Aerojet-General Corporation, The Failure Mechan-ism of Solid Propellant Grains

3.45   Dr. R. F. LANDEL, Jet Propulsion Laboratory, California Institute of Technology, The Effect of Fillers on Deformation and Fracture

* Indicates Speaker.

† Professor Freudenthal was not able to present his paper at the conference; however, the full text of his paper is included in these *Proceedings*.

The editors are grateful to the many individuals who contributed to the success of the conference, particularly to the authors, the chairmen of sessions and other participants in the meeting. The presence and active participation of many scientists and engineers from abroad contributed towards the broadening of the scope of the meeting. Special thanks go to them. Thanks also go to the members of the different committees that planned the conference and made possible the arrangements for the smooth conduct of the meeting, and especially to Mrs. Karen Schmidt and Mrs. Anna Hickman for their efficient discharge of the voluminous detailed secretarial work that developed with the organization of the conference.

WELCOMING ADDRESS

Frederick L. Hovde

President, Purdue University

WE at Purdue University are both pleased and complimented by the fact that the Office of Naval Research has convened on this campus this International Conference on the Mechanics of Chemistry and Solid Propellants, the fourth in a series of Symposia on Naval Structural Mechanics. To be selected from among the many places in the United States where such a conference might be held is a high honor for this University.

Twenty-five years ago when I was much younger and was personally and directly involved in the field of rocket ordnance research in the Office of Scientific Research and Development, I might possibly have understood and even been capable of contributing in a small way to the subject matter of this particular symposium. I believe I am correct in saying that the first important research efforts in this country to develop heterogeneous cast propellants were made at the Allegany Ballistics Laboratory, one of the principal research laboratories of the Rocket Ordnance Research Division of OSRD. When World War II ended and OSRD disbanded, it was apparent that this early work was so promising that special arrangements were made with the appropriate Naval agencies to continue to support these investigations.

During the war years, the relationships between the civilian scientists and the United States Navy personnel in the field of research and development involving all aspects of weapons and instrumentalities of war were friendly, cooperative, and mutually helpful. Our collaborators in the Naval organization were deeply interested and extremely competent in the advancement of the science of warfare. It might even be said that our Naval officers were technologically more sophisticated than their brother officers in the Department of the Army at that time. In any event, the men of the United States Navy know, understand, and appreciate the importance of using the nation's scientific resources continuously to strengthen the Naval arm of our military establishment.

Many of you present may not know much about Purdue University. Since you are here, perhaps a few words about it will be helpful. Purdue is the land-grant institution of the State of Indiana and therefore has had a scientific and technical orientation since its founding in 1869. During the last quarter-century Purdue has maintained on this campus the largest fulltime undergraduate enrollment in engineering and is the largest producer of Bachelor of Science degrees in the various engineering disciplines in the United States. Supporting the profession schools of engineering, agriculture, veterinary medicine, pharmacy, industrial management, and home economics are four basic science departments

—chemistry, physics, biological sciences, and mathematics. These four basic science departments daily, semester after semester, operate the largest instructional program in the United States under the jurisdiction of any single institution. The basic science instructional program, from beginning freshman courses to the most advanced courses in the graduate school, is truly an enormous operation involving the handling and scheduling of literally thousands and thousands of students at all levels of the scientific spectrum.

Purdue University is approximately fifteenth in size in the United States in enrollment of full-time resident students. Its major orientation in teaching, research, and public service is scientific, with equal interest in pure science and in applied science.

This conference which you as delegates have come to participate in and learn from is an example of the service and relationship of the modern university to the ongoing public and private organizations functioning in the American complex—in this case in cooperation with the Office of Naval Research of the United States Navy. Similar conferences and symposia are held on the campus in cooperation with industrial, technical, and scientific organizations of many different kinds.

At the time of its formation the Office of Naval Research was a pioneer governmental effort to encourage and strengthen collaboration between the scientific forces of the universities and the technical establishment of the Navy. Today the Departments of the Army and the Air Force have similar organizations. On a broader scale, the National Science Foundation, the Atomic Energy Commission, the National Aeronautics and Space Administration, and the National Institutes of Health support the structure of American science in the universities and in the industrial establishments.

The scientific work reported during the sessions of this conference is, of course, pertinent to the Navy weapon and missile development programs, but these scientific investigations will also have value for industry because the basic work in the field of structural mechanics has many applications important to our industrial technology.

I should like at this time to give an official, as well as personal, welcome to Admiral Miller, Chief of the Long Range Objectives Branch of the United States Navy, and to Doctor Weyl, Chief Scientist for the Office of Naval Research, who will also speak on this program.

I know you will be keenly interested in the papers presented because these and the discussions which will ensue are the reasons why you are here. Aside from this, I hope that you will enjoy your short stay in our Purdue environment, that you will meet members of the University's scientific staff, and that you will know the genuine hospitality and pride that we have in this institution, its work, and our Indiana environment. Therefore, on behalf of all of us at Purdue, I extend to you a welcome that is sincere and warm. When the program has been completed, I hope that all of you will return to your institutions better informed and stimulated by this experience. We are grateful for your presence here.

OPENING REMARKS

F. JOACHIM WEYL

Chief Scientist, Office of Naval Research

WITH his warm welcome, Dr. Hovde has joined the word to the action. We are grateful, indeed, to be Purdue University's guests—not only in the sense of physical fact, but no less by finding ourselves under her many-gabled intellectual roof.

For the amenities which, under the first of these viewpoints, contribute to the success of this Conference, our appreciation is owed to the local arrangements committee under the chairmanship of Dr. Lianis. Regarding the intellectual fare, on the other hand, we pay our respects to Dr. Eringen and Dr. Liebowitz, together with their colleagues on the Planning Committee for their deft design of the menu.

And finally, the Office of Naval Research is deeply appreciative of your interest in this venture as expressed by your presence and participation involving much hard work and long hours of travel, especially on the part of those of you who have come from abroad to make this a truly international conference.

We have come here to learn what is happening in the mechanics and chemistry of solid propellants. Before we do so, let me make two remarks about these happenings to assure you that the moral to be drawn from them has not been lost on ONR.

For many years now the Navy has had a firm and broad commitment to solid propellants and has invested much money and effort in developing, testing, and procuring them. Concerning the reasons for this, the speaker who follows me will have more to say. Under such conditions, there is a pervasive danger that engineering development proceeds on the basis of massive, rapidly accumulating experience rather than firm understanding. It is an unfortunate habit of such experience to leave you in the lurch when you least expect it or can least afford it. It has been the objective of the Polaris Long Range Program, under the aegis of which this Conference is held, to provide for the research that would in the end develop the required solid understanding of the physics and the phenomena involved. For insurance reasons alone, it seems that one should want to conduct such a program. Yet we have faced, at the same time, great and continuing administrative difficulties in maintaining and continuing such a program, even though its cost is but a small fraction of the total commitment. The moral we have drawn from this experience lies in the importance of the effort to continue work on the scientific foundations even in areas of engineering where massive means for empirical approaches are available.

As this first remark of mine addressed itself to the depth to which one must

lay the scientific foundations for disciplines on which major expectations of achievement are placed, so will my second remark address itself to the span of these foundations. To get as high a peak in engineering performance as the Navy requires in its reliance on solid propellants, the scientific base from which these endeavours spring must have a corresponding breadth and coverage in a multitude of the traditional disciplines. Once the task of laying it firmly is seen in proper perspective, it is found to touch upon many challenging problems of fundamental interest in these disciplines—problems that are worth of the preoccupation of the best minds in them. This has been achieved in the Navy's program, as your presence shows. However, let me assure you that it does not come automatically—this is the second lesson. Much work and thought must go into the architecture of a program which is built effectively to tap this source for its momentum. And, so let the Conference proceed to make its history!

Keynote Address

NAVY PROJECTIONS OF LONG-RANGE OBJECTIVES

Rear Admiral George H. Miller, U.S. Navy,
Director, Navy Long Range Objectives Group

IT is a distinct honor to be here today to talk to you about the future of the Navy.

I am particularly happy to return to my home state of Indiana and to take part in this important conference. As a naval officer I take pride in the close association between Purdue University and the Navy which has made this meeting possible.

The world, as you know, is experiencing unprecedented growth in the whole area of military technologies. Break-throughs are being experienced in many important fields. Some of them are occurring in the area of particular interest to you who are assembled here—that is, the area of solid fuel propulsion.

The Army, the Air Force and the Marine Corps, as well as the Navy, are participating in a broad technological advance. Each service is making important progress. Today, however, I shall confine my remarks to naval matters.

My discussion will be addressed to the indefinite future—that period of time which lies somewhat beyond the parameters of present policy and guidance, and in some cases, beyond present technology. Much of what I talk about will not, and cannot, advance beyond the talking stage unless groups like yours—using your time, your knowledge, your effort and your imagination—provide the scientific and technical base from which new capabilities, new systems and new hardware can grow.

To begin with, let us look at the ocean environment itself. Much is being said and written these days about oceanographic research. We are learning more about the ocean depths and the vast land areas which extend beneath them. Much of what we are learning is being made available to the public. We in the Navy are encouraged by the interest which people are taking in our oceanographic efforts.

The Navy is anxious to learn as much as possible about this oceanic domain in furtherance of our country's naval effectiveness. But our concern in this area transcends what is normally regarded as a strictly military interest. It is becoming increasingly clear that in these vast, relatively unexplored regions of the earth lie the future of our country, for better or for worse. Tremendous food resources are available in the sea waters themselves. Beneath the seas, in the lands which extend beneath international waters, lie incalculable deposits of mineral wealth. There can be little doubt that these resources, virtually unclaimed and unexploited, will greatly influence, and perhaps even dictate, the course of future world events.

More needs to be learned about this tremendous frontier area, which extends over two-thirds of the surface of our earth. More needs to be done to comprehend the world ocean, its boundaries, its properties, and its processes. We need to exploit this comprehension in the public interest, in enhancement of our security, our culture, our international posture and our economic growth. This suggests a need for an increased interest in maritime matters within our educational community and increased seamindedness among our people and government.

Turning now to specific considerations of security, it is generally recognized that the great oceans which wash our shores can no longer be regarded as the barriers of a generation ago. But they can provide added security for our country, provided we use them properly. We see the rising pressure of weapon technology compelling the United States to look well beyond its own continental borders to gain the space and maneuvering room needed for adequate security in the modern military environment. This space and maneuvering room are immediately available in the ocean areas, to which it is our nation's good fortune to have direct, unrestricted geographical access.

Of particular interest to those of you assembled here is the technology which can provide ballistic missiles with greatly increased efficiency during the next decade. This technology will of course be available to other peoples as well as to ourselves.

Missiles with greater payload and greater accuracy could diminish the relative effectiveness of hardness as a defense against ballistic missiles. Smaller ballistic missiles could permit greater flexibility in ballistic missile deployment, and an opportunity to employ greater mobility to reduce the relative vulnerability of our forces. Smaller missiles would be adaptable to a greater variety of mobile launch platforms, heretofore considered impractical because of the greater weight and bulk of today's generation of missiles. Sea-based launch platforms such as destroyers and even smaller ships can take their place alongside the ballistic missile submarines of today.

Smaller, more accurate ballistic missiles would have many uses in a sea-based version, in addition to the conventional strategic deterrent use as we know it today. Tactical ballistic missiles aboard ships of our carrier task forces could add significantly to the over-all offensive power of naval striking forces. The naval aircraft and the tactical ballistic missile could team up on offense, just as the ship-board guided missile and intercept aircraft team up so effectively on defense today.

Along with the all-important reduction of size which we can see coming along, is the continually increasing accuracy which technology can provide. This means that at some point in time it may be practical for ballistic missiles to have the additional option of delivering non-nuclear payloads.

Turning now to the limited and cold war areas, we see a future need for increased naval capabilities to provide continuous, effective support of U.S. foreign policies in distant areas,

One can read almost daily of some kind of new difficulty or crisis arising in

some part of the world. In the beginning, trouble is usually minor and local in character—the issue not clearly drawn. But trouble has a habit of growing when not attended to at once.

One of the fundamental principles underlying the employment of naval force is to make your moves early—before trouble grows into conflict. Naval forces can be moved into a crisis area by sea without making a big military production of it.

In a tense, pre-military environment, it is possible for ships to visit foreign ports without creating an international incident. They can remain close to a crisis area in the earliest stages, in close touch with Washington and in close touch with the senior U.S. representative on the scene. They can remain in sight of land—or remain out of sight, as the situation may require. They can remain at sea for long periods of time, relatively safe from sabotage and surprise attack.

We therefore foresee a need to place greater emphasis on thinking ahead and looking ahead. There will be increasing requirements for close, direct collaboration at all echelons with those who make and implement our foreign policy. The trend will be toward adapting more quickly and reacting more quickly to unusual, and perhaps unforeseen, situations, while they are still little situations.

New naval technologies will be utilized as they are developed, to provide our government with more freedom of action and the options needed in support of U.S. foreign policy. In addition, there will be a need for adapting present naval capabilities to unorthodox situations which may not have assumed a formal military character. For example, a small commando unit may be needed here, just to be near at hand. A U.S. mobile sea-based airfield may be needed there— not necessarily to fight a formal war—but perhaps just to be available to strengthen an Ambassador's hand, or to serve as a U.S. base of good will and assistance, where comparable facilities are not available on land.

Navies, over the centuries, have served with distinction as peace-keeping machines, as well as war machines. Peace-keeping, as we have seen, oftentimes involves more than spreading good will across the seas. The more successful nations of history sometimes found it necessary to take corrective naval actions in time of formal peace, as well as in formal war. Maritime nations were often able to achieve security through continuous naval vigilance and initiative—day after day, around the clock. Maintaining and exercising control of the seas was a never-ending process. While landsmen of rival powers dined and chatted in chancellories ashore, rival naval units oftentime were in conflict at sea—without benefit of formal recognition of a state of war.

The future, I think, will see circumstances moving the United States toward a concept of continuous control and peace-keeping, exercised on and from the world oceans. In extension of this concept we foresee a need for a greatly increased naval capability for world-wide surveillance of the ocean areas. The United States will need to know what is going on, beneath as well as on the surface of the seas. Maritime surveillance and control measures at the lower end of the spectrum will receive increasing attention as a practical alternative to the total peace of the Idealist and the total war of the Nucleist.

Turning now to ships themselves, what might be expected in the way of future developments? With the new technologies becoming available, we can anticipate increasingly more naval power per individual ship, increasingly more cargo capacity per merchant ship. Bigger, more powerful ships will be going to sea with fewer people on board to operate them.

In the Navy we will continue to seek new techniques which will permit combat ships to remain at sea for longer periods of time. This requirement may be imposed in support of cold or limited war situations. It certainly will be imposed by a growing need to keep major combat units on the move at sea because of the vulnerability of port areas to surprise nuclear attack.

Fortunately, new technologies are providing increasingly efficient techniques for replenishing and repairing ships at sea or on distant stations. Nuclear propulsion and other new developments are bringing endurance characteristics to shipboard equipment and machinery which will permit ships to remain at sea for much longer periods of time. To minimize the hardship effects of long periods at sea, techniques are already available for moving relief crews on board ships in the operating area. Complete replenishment of major ships at sea, including routine repairs and relief of personnel will eventually minimize the time which needs to be spent in vulnerable ports and will increase the percentage of time ships can be continuously in readiness at sea.

To carry this concept of greater utilization one step further, we look to the day when it may be feasible to package major components of a combat ship's equipment, to further reduce the time a major ship is required to remain in port. The day may come, for example, when a ship can enter a Navy yard and exchange ballistic missile suits, main propulsion units, and other packaged components and be back operating at sea in a matter of hours. Repair and overhaul of major components could then be accomplished effectively ashore without immobilizing a valuable unit of the fleet for several weeks or months.

Turning now to the matter of speed of ships, we have in the experimental stage today smaller ships of advanced hull design, capable of speeds in the 60 to 90 knot bracket. There are indications that still greater advances in this area can be anticipated in the next decade.

We are familiar with how quantum advances in air transport speeds have revolutionized world air transport patterns and how high speed has affected the strategy and tactics of air warfare. We can be certain that significant advances in ship speeds will also have revolutionary effects on the strategy and tactics of naval warfare, as well as on world shipping patterns.

The progress which has been made in air transportation is a direct outgrowth of the vigorous, large-scale air research and development effort which has been in progress since World War II. In comparison to what has been achieved in aircraft development, advances in marine hull and machinery design have not been very spectacular. A notable exception of course is development of the nuclear reactor which is slowly replacing the oil-fired boiler in marine propulsion.

Achieving the high ship speeds, which appear to be within the reach of technology, will of course take some effort in research and development. Since over

98 per cent of all material moving overseas still goes by ship, in war and in peace, the conclusion can be drawn that the nation which undertakes this developmental effort will get a significant jump on its competitors. For economic as well as military reasons, we can anticipate that an increasing share of our nation's research, development and production dollar will in time be channelled into ship research, design and construction.

I have ranged across a rather broad spectrum of possibilities for the future. I have discussed the new potentials which lie within the grasp of our nation through development of the oceanic environment and the underlying land areas. I have touched on new ballistic missile technology, new versatility in the employment of naval forces, and new capabilities which technology can achieve in the performance and utilization of ships.

In closing I want to repeat and emphasize that few of these advances will be possible without your interest, your vigorous support and your future accomplishment. The security of the Free World and the well-being of mankind depend on the way we employ our imagination and collective talents—military, academic and industrial—toward the achievement of better understanding and utilization of our tremendous maritime resources.

NAVAL ROCKET MOTORS AND
STRUCTURAL INTEGRITY CONSIDERATIONS

I. SILVER

Missile Propulsion Division, Bureau of Naval Weapons,
Washington, D.C.

Abstract—The handling, storage and operational environments which various types of Navy solid rocket motors are exposed to are discussed. The Navy motors are classified mainly according to their launch and service use environments. Each class has its own unique characteristics and limitations, but the extreme environments and man-safety requirements for air-launched rocket motors present the most difficult problem in safety and reliability.

Future Navy rocket motors are not expected to vary much in size or configuration from many of those currently in development or production; however, current deficiencies may be further accentuated by more extreme environments coupled with the use of more advanced and energetic propellants. Current programs in mechanical behavior of solid propellants, improved binder systems and grain design studies are now beginning to make possible the development of solid rocket motors with high reliability and the accurate prediction of the behavior of the solid rocket motors under service use conditions.

THE development of solid rocket motors in the Navy in the last decade and a half has generally followed a pattern of continuing change dictated by requirements for higher ballistic performance under more vigorous environmental and operational conditions. Rocket motor technology has grown dynamically from the small, simple JATO units of the early 1950's to the larger and more sophisticated motors in the Navy inventory today. The early axioms of low cost, high reliability, and simplicity are no longer necessarily true, particularly in the light of the high degree of sophistication now required in the manufacture of solid rocket motors. High reliability is achievable only at the cost of increasing the requirements for detailed and precise material and processing specifications, and increased level of inspection and quality control, including greater use of sophisticated nondestructive test methods.

However, considerable potential for performance improvement in both large and small rocket motors continues to exist and remains to be exploited in future motor development programs. Research in propellants, materials, designs and associated problem areas is being supported at close to the levels established several years ago, but certain signs are now beginning to emerge which indicate new possibilities and trends. For one, new concepts of managing development programs have resulted in more orderly and logical procedures of justifying and introducing these new programs into the budget structure, albeit at the cost of a certain though possibly temporary delay in the process. Secondly, the support of the high energy synthesis program has essentially shifted back to the Services from the Advanced Research Projects Agency. This is significant in that the trend to

higher performing solid propellants is entering a phase of evaluation and con-
solidation of the ideas and results achieved to-date. Finally, large motor strategic
requirements are no longer serving as the major impetus to advancing the rocket
propulsion technology in the development phase, as was typical of the earlier
versions of Polaris.

On the other hand, efforts to develop solid propellant motors since the Korean
War have generated several new, well-characterized families of solid propellants.
These efforts have also produced new engineering materials able to withstand
the severe environment of combustion products of the propellants. Growth
in new areas of missile technology, changes in the characteristics of the targets
available, development of carriers and delivery vehicles to place the rockets
in the selected launch environment, and the accompanying changes in military
tactics collectively have presented a continually varying set of ground rules for
the development of rocket armament.

Table 1 summarizes some pertinent characteristics of naval rocket motors
developed and produced in the last decade. Among some of the earliest motors

TABLE 1. TACTICAL ROCKET MOTOR CHARACTERISTICS

MOTOR CLASS	THRUST RANGE LBS - F	PRESSURE RANGE PSIA	MASS RATIO
AIRCRAFT LAUNCH (JATOS)	1000 - 5000	1000	0.55
PERSONNEL ESCAPE ROCKETS	2700 - 6500	400 - 700	0.25
SOUNDING ROCKETS	1400 - 8000	550 - 1150	0.67 - 0.75
UPPER STATE (PROBES)	470 - 21,000	340 - 580	0.86 - 0.94
AIR TO SURFACE	6000 - 8000	1400 - 1700	0.25 - 0.54
AIR TO AIR	2700 - 7700	750 - 1150	0.6 - 0.7
SURFACE TO AIR	800 - 490,000	760 - 2600	0.66 - 0.73
SURFACE TO SURFACE	60 - 185,000	540 - 1250	0.44 - 0.91

were the JATO's used for aircraft launch purposes. These motors are relatively
low performing systems but are still in constant demand and are being produced
not only as JATO's but for propelling track sleds for accelerations and other
environmental tests. The personnel escape rockets for pilot ejection systems do
not represent, at the present time, any significant advance in propulsion tech-
nology; however, they are required to be designed for maximum safety and
optimum performance if the escape functions are to be performed successfully.
High structural integrity is required if a catastrophic blow on ignition is to be
avoided. The pilot and his seat must be blown clear of the aircraft over a wide
range of altitudes and speeds without exceeding a maximum on-set rate of 250
g/sec^2 and sufficiently high to permit complete opening and functioning of the
parachute. To achieve this performance, close control over the internal ballistics
of the escape rockets over a wide temperature range is required.

Sounding rocket propulsion systems require moderate thrust and long durations and must be highly reproducible in ballistic performance. Long duration thrust is generally required for sounding rockets so that peak altitudes can be achieved with moderate acceleration loading, low drag and minimal aerodynamic heating. End burning grains are frequently used for maximum propellant loading density. Future requirements may include the use of frangible or consumable cases.

Space probes and upper stage rockets require very high mass fraction, generally above 0.90, and propellants and nozzle designs which generate the highest possible specific impulse at high altitudes are used. The Navy has been successful in developing a whole series of third- and fourth-stage Scout motors for upper altitude performance, growing out of its work on the Vanguard program using glass-reinforced cases, lightweight design and high specific impulse propellants.

Guided air-to-air and air-to-ground missiles are carried as external stores aboard the aircraft. These missiles must be capable of resisting high aerodynamic heating and temperature extremes, and the propulsion systems must resist moderate heating and temperature extremes and deliver a moderate thrust for a short time. Future air-to-air and air-to-surface missions will have longer stand-off ranges and will be based on requirements for longer burning times, higher speeds, and increased performance flexibility made possible by thrust controllable solid rocket motors. Also associated with this class of missiles is the requirement for performance reliability, and in particular, safety in view of the possible catastrophic damage to personnel and aircraft.

In guided surface-to-air and surface-to-surface missiles, with a relatively short time to target, high thrusts are required. This high thrust, coupled with maneuvering in flight, subject these missiles to high-g loadings during flight and high, although brief, aero-heating. Because these missiles are ship-launched, greater weight than for air-launched missiles can generally be tolerated, although the launcher loading requirements do place very specific limits on weight and dimensions. Future requirements will necessitate increased sophistication in motor design and propellant development to achieve higher boost accelerations. Increased propellant burning rate, higher strength/low weight cases and grain configurations capable of accommodating high-g loading under Navy service conditions will be required.

Finally, submarine-launched surface-to-surface missiles such as Polaris are severely limited in both volume and weight. In addition, they must have long stowage life in a vertical attitude where they are subjected to ships' vibration and launch tube pressure cycle. Extreme temperature capabilities are not required since the environments are controlled in the logistic cycle. Because of the volume limitation, maximum impulse density is required. Long burning times with moderate thrust levels and minimum acceleration forces are desired to meet near future requirements. The follow-on Polaris, or *Poseidon*, motor will be larger, but no significant or unique requirements in rocket motor technology are envisioned.

Research has provided solutions and insights to the numerous problems

associated with the development of current rocket motors. Nevertheless, basic problems affecting performance reliability still exist of which the mechanical integrity of the grain is possibly the single greatest area of concern. At every phase of its life, from early development through flight, the solid rocket propellant grain is subject to environmental and operational forces tending to degrade and destroy its integrity.

Table 2 represents a categorization of tactical Navy missile systems in terms of launch platform environments. A major objective of Table 2 is to emphasize the critical differences between the environments in the surface- and air-launched motors and to indicate the effects of the more extreme requirements on the structural integrity of these rocket motors.

TABLE 2. NAVY ENVIRONMENTAL CONDITIONS

LAUNCH PLATFORM ENVIRONMENT	SURFACE LAUNCHED		AIR LAUNCHED	
	CURRENT	FUTURE	CURRENT	FUTURE
TRANSPORTATION (TRUCK, RAIL)				
TEMPERATURE	0-120 P	SAME	(-65 F)-(+160 F)	SAME
VIBRATION	5-300 CPS	SAME	5-300 CPS	SAME
SHOCK	30g-0.030 SEC. BASE	SAME	30g-0.030 SEC. BASE	SAME
R.H.	40%	SAME	40%	SAME
DEPOT LAND STORAGE				
TEMPERATURE	0-120 F	SAME	(-65 F)-(+160 F)	SAME
SHOCK (HANDLING)	30g-0.030 SEC BASE	SAME	30g-0.030 SEC BASE	SAME
R.H.	40-90%	SAME	40-90%	SAME
SHIPBOARD STOWAGE				
TEMPERATURE	40-100 F	SAME	40-100 F	SAME
SHOCK	15g-0.015 SEC BASE	SAME	15g-0.015 SEC. BASE	SAME
VIBRATION	5-33 CPS	SAME	5-33 CPS	SAME
AIRCRAFT CAPTIVE FLIGHT				
VIBRATION			0-2000 CPS	SAME
TEMPERATURE			(-65 F)-(+325 F)	SAME
SHOCK (CATAPULT AND LANDING)			20g-0.010 SEC. BASE	SAME
POWERED FLIGHT				
TEMPERATURE				
FIRING	20-110 F	SAME		
IN-FLIGHT (MAX.)	400 F	>400 F	(-65 F)-(+325 F)	(-65 F)-(+325 F)
ACCELERATION				
LONGITUDINAL	40g	>100g		
SPIN RATES	60 RPS	>200 RPS	40g	>100g

The temperature limitations on surface-launched motors are less rigorous than those for air-launched motors. Although it may be obvious that temperature conditions on ships at sea are naturally limited, the actual determination and fixing of such limits are made with a consideration for the actual temperatures experienced at sea and elsewhere and the frequency with which serious deviations from such limits would result in the creation of a critical structural integrity defect in the motor. The environmental temperatures for surface-launched motors resulted from a four year study of temperature data from selected Weather Bureau stations along transcontinental shipping routes, considering the various probabilities of occurrence. From these data, a reasonable estimate of temperature exposure during transportation was obtained. Storage environment was obtained from a study of ambient diurnal ranges and magazine temperatures of both coastal and inland Navy ammunition depots. Use environments resulted from a survey of actual ambient and magazine temperatures experienced by a number of ships in extreme locations where naval vessels might reasonably be expected to operate.

In conjunction with the above, a corollary study was made of the temperature response characteristics of typical surface-launched motors. These studies

showed that for critical defects, i.e. those involving personal safety, it is desirable that a design criterion of 99.9 per cent of the units shall be successful with a 95 per cent confidence level. For major defects, i.e., those of performance and function, a 97.5 per cent compliance with 95 per cent confidence level is generally required.

From a practical viewpoint, it is logical that the same statistical reasoning be applied to extreme temperature occurrence as that which is applied to the design of the rocket. If the rockets are exposed for significant periods of time to ambient temperatures outside of the range for which they were qualified, and if the exposure is undetected and results in catastrophic failure at launch, then the exposure would be considered as critical in the same sense as a critical design criterion. The probability of occurrence of the specified extreme environment for a critical exposure should not exceed 0.1 per cent at a 95 per cent confidence level. Based on thermocouple measurements, a significant period of exposure for surface-to-air rockets would be 24 consecutive hours at − 15°F or lower.

In looking ahead to future uses of and requirements for surface-launched motors, there appears to be no need to extend any of the existing temperature requirements. It is conceivable that for special cases, where land launchings may be required, a broadening of these ranges to − 65°F to + 160°F may be required. In other cases where special precautions and equipment to control the ambient temperature are available and practicable, a significant reduction in the temperature range to + 30°F to + 80°F may be warranted.

In most instances, a requirement to withstand longitudinal accelerations in flight of about 40 g's is normal. As we look ahead to future requirements where high speed or shorter times to intercept become more predominant, motors will be required to accelerate to greater than 100 g's. The ability of grain structures to resist such forces appears to be possible within the present date of rocket motor design. No overwhelming structural problems are foreseen provided the temperature ranges for service use can be reasonably restricted.

Air-launched motors require a degree of safety and reliability which demands the most stringent development and qualification test programs prior to release to production service use. The extreme temperature requirements are determined as in the case of the surface-launched motors, after a careful consideration of the exposures which these motors will experience from the time of manufacture to and during operational use. Since the complete life history of a particular air-launched motor is almost impossible to predict, the development test program is based mainly on the theory of testing at temperature extremes under a series of test conditions sequentially arranged. The reasoning for this is very clear when one considers the real environment which an air-launched motor sees from the moment of launching to its free flight condition after firing, or if unfired, on return to the aircraft carrier or land base. As external stores on the aircraft, the motor is subject to catapult forces, aircraft vibration under captive flight, and to various temperature extremes for varying durations, depending upon the particular flight regime of the aircraft. In recent years, the capability of aircraft to cover a wide range of altitudes at supersonic speeds has increased

the stresses imposed on the grain structure by aero-heating and the severe thermal cycling which may occur within relatively short periods of time. The situation is further aggravated by the fact that in many missions in peacetime, the missiles are not fired but are returned to the flight deck and further subjected to arrested landing forces. This cycle of takeoff, flight, and landing may be repeated dozens of times over a period of years. The structural integrity of the grain must be adequate to resist these various stresses and give a reliability for safe performance as great as 0.9999.

In flight, the high Mach numbers generate stagnation heating conditions which are additive to those imposed by captive flight conditions. For relatively long burning times with case-bonded motors, the interface effects caused by high temperatures, between liner, case and propellant can become very serious and cause separations leading to catastrophic failures. Future requirements envision higher accelerations and flight speeds for volume limited motors, thus generating more stringent demands for structural integrity and higher reliability. Improvements in insulators, case materials, and the thermal stability and mechanical strength of propellants will be necessitated by these advanced operating requirements.

Spin accelerations represent another environment which has demonstrated some unusual effects on the performance of various rocket motors. Spin rates in the order of several revolutions per second have been observed to affect burning rates and internal gas dynamics, resulting in unusual erosion effects and serious aberrations in thrust. Once the associated mechanisms were understood, changes in propellant formulations and grain and motor design have reduced or eliminated these effects.

A more serious problem arises in those instances where spin rates in the order of over 200 r.p.s. are required for aerodynamic stability. A study of the stresses in propellant grains has been made at several spin rates. As a first approximation of the stresses developed in a spinning motor, an elastic stress analysis of a thin spinning disk was made. The maximum stresses occur at the center of the grain where the tangential and radial stresses are the same. In an unsupported grain, the radial stresses decrease to zero at the outer surface. The tangential stresses also decrease radially outward, but at a lower rate to a positive value at the outer surface. As a result, spin failures in isotropic materials originate at the center under primarily a biaxial tensile load and develop into radial cracks because of the higher tangential stress away from the center. If a grain is in a strong liner, it may be supported by the liner, depending on the grain liner separation. In Fig. 1 are curves of the maximum tangential stresses at the center of an isotropic disk versus spin rate for several values of grain liner separation. The highest stress are shown to occur in the unsupported disk.

Spin tests were made on several types of propellant systems. Photographs of the exposed surface of a number of typical grains are shown in Fig. 2. This illustration includes tests in which several different methods of grain preparation and motor loading were used. Pictures A, B, and C show the effect on single extruded grains. The failure cracks originated at the center and spread in radial

direction indicating tangential tensile failure. To relieve the center stresses, grains were sectioned as shown in G and H. Although neither grain cracked up when spun at 300 r.p.s., appreciable flow of the epoxy from the center in G and cracking of the epoxy in H were observed. Results also show that crack growth was very rapid in more rigid materials and markedly slower in the low modulus
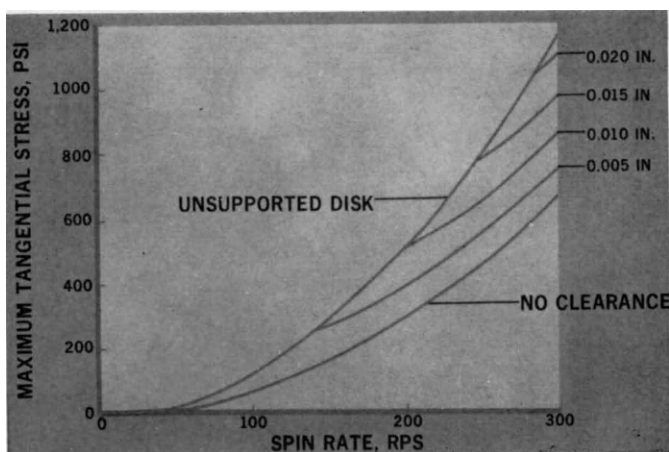

FIG. 1. Center tangential stresses vs. maximum tangential stress.

propellant. The advantage of low modulus propellants was their ability to undergo appreciable axial deformation to relieve the transverse stresses. For higher modulus propellants, the importance of adequate initial liner support was shown.

As part of this study, motors were accelerated to the desired spin rate and then fired. X-ray motion pictures were used as a data-gathering technique. Figure 3 shows a cutaway view of the test hardware. The area outlined by the dotted lines denotes the field of view of the X-ray coverage. X-ray movies showed that a cone was being formed in the center of the grain and that the magnitude of the covering was a function of the spin rate. Figure 4 shows this effect in a series of frames taken from the X-ray movies. Figure 5 shows an actual grain obtained from an interrupted motor firing.

The history of rocket motor development is replete with examples of grain integrity failure. A representative case is one described by Figs. 6 and 7. In early phases of development, on exposure to elevated temperature the sustainer or outer grain in a dual thrust motor exhibited serious propellant degradation with separation of booster from the sustainer grain, bond separation, and general disintegration of the mechanical structure of the propellant as shown in Fig. 6. This behavior was attributed to the use of an ingredient which caused the depolymerization of the sustainer binder at elevated temperatures. This problem was readily corrected through a change in the propellant formulation, and in due time, the motor was properly qualified for Service use. In early production it was soon discovered that cracks emanating from the star points in the booster

(A) SINGLE EXTRUSION
0.010 INCH CLEARANCE
FAILED AT 214 RPS

(B) SINGLE EXTRUSION
POTTED IN FLEXIBLE EPOXY
FAILED AT 270 RPS

(C) SINGLE EXTRUSION
POTTED IN RIGID EPOXY
NO FAILURE

(D) SINGLE EXTRUSION
ANNEALED IN LINER
NO FAILURE

(E) REEXTRUDED GRAIN
POTTED IN FLEXIBLE EPOXY
FAILED AT ~ 300 RPS

(F) REEXTRUDED STRANDS
0.080 INCH CLEARANCE
FAILED AT 242 RPS

(G) SINGLE EXTRUSION
SPLIT GRAIN
POTTED IN
FLEXIBLE EPOXY
NO GRAIN FAILURE

(H) SINGLE EXTRUSION
TRISECTED
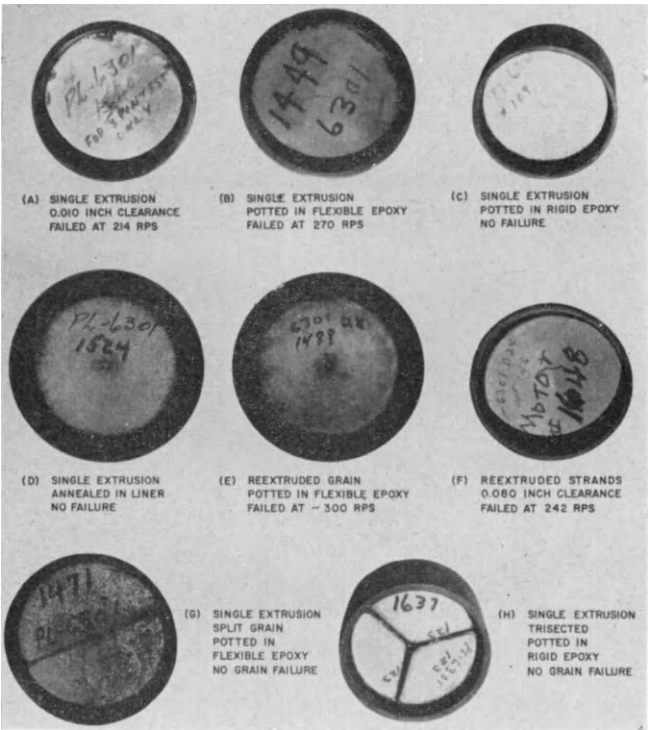POTTED IN
RIGID EPOXY
NO GRAIN FAILURE

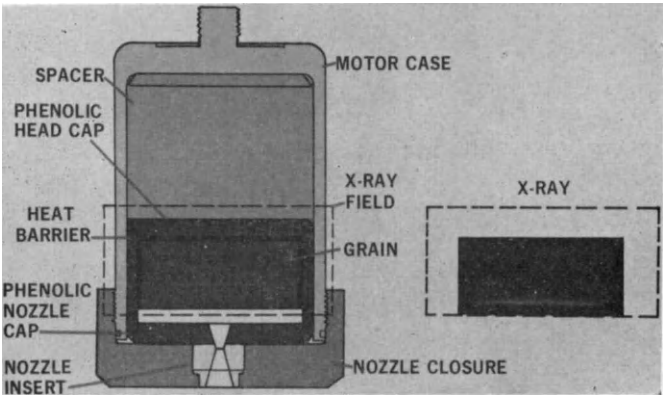FIG. 2. Spin-tested grains of fluorocarbon propellant PL6301.

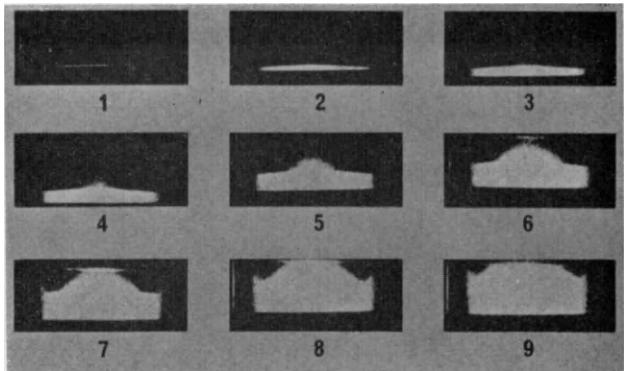FIG. 3. Motor orientation showing X-ray field of view.
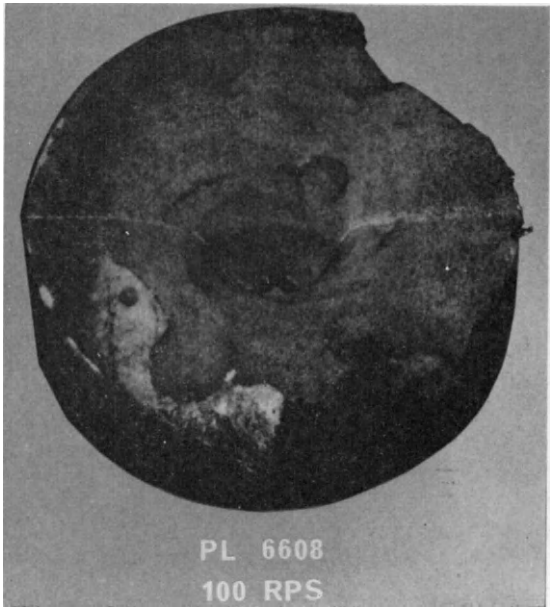
FIG. 4. X-ray single nozzle.

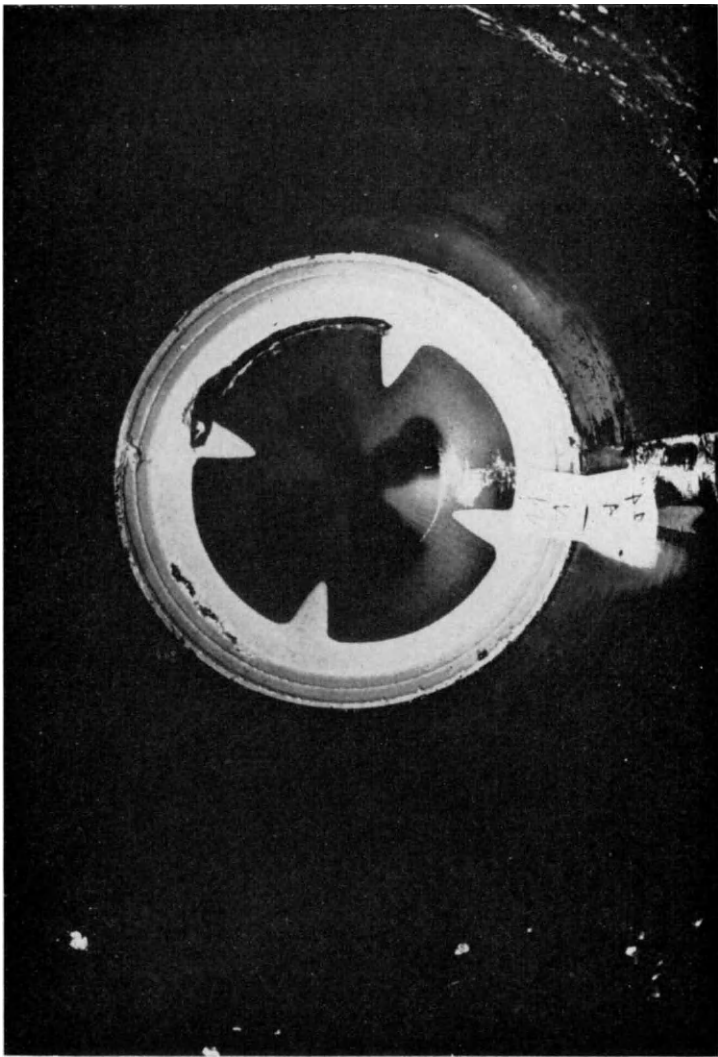

FIG. 5. Spin tested—interrupted firing.

Fig. 6. Chemical degradation.

FIG. 7. Grain cracking.

occurred when motors were subjected to temperature cycling as shown in Fig. 7. A careful stress analysis and a determination of the available strain in the grain showed that at 0°F, particularly in the presence of moisture, the presence of a negative margin of safety resulted contrary to early design studies and qualifica-
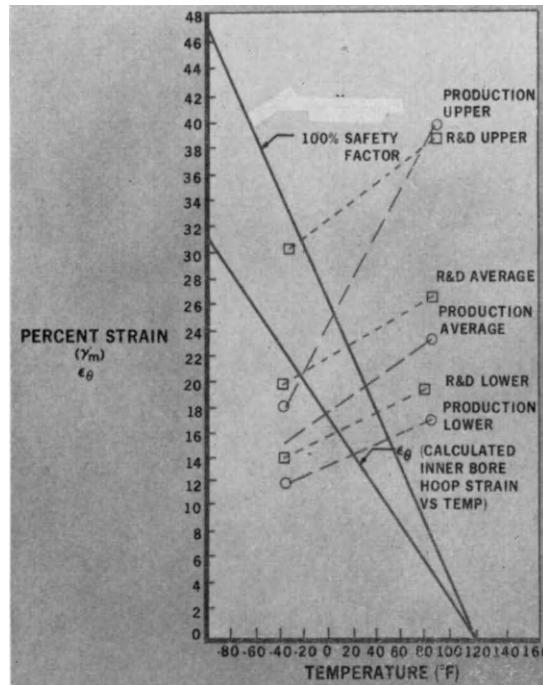

FIG. 8. Grain strain capability.

tion testing. Investigations revealed that inadequate control over the materials and processing gave a propellant which was borderline in available strain as shown in Fig. 8. The range of strain data for R&D and Production fell well below the inner bore hoop strain indicating no margin of safety at the lower temperatures. To correct this deficiency several parallel courses of action were adopted. The more immediate action was to mount a process and material variable investigation to improve the elongation to the propellant and decrease its sensitivity to moisture at low temperatures. The other approach, and in the long run, the more effective one, was to redesign the inner bore configuration so that the stresses imposed on the grain in the bore at the lowest Service temperatures would be significantly below the available strain in the propellant, even though the latter would be reduced considerably under constant strain conditions at the lower temperatures.

This case history illustrated the need for an early and complete characterization of the time- and temperature-dependent mechanical properties of a propellant,

as a basis for determining grain structural integrity. At the inception of this particular motor program, the techniques for stress analysis, methods of characterization of propellants, and the necessary information on the chemistry of the propellant were not generally available. Since then, considerable progress has been made and as a result propellant characterization and substantiation of motor grain integrity are now required prior to the fixing of the design and propellant in development.

TABLE 3.

MAJOR SOLID PROPELLANT GRAIN CHARACTERISTICS

	PRESENT	FUTURE
PROPELLANT	CAST DOUBLE-BASE POLYURETHANE POLYVINYL CHLORIDE	CAST DOUBLE-BASE POLYURETHANES HYDROCARBON BINDERS FLUOROCARBON BINDERS
GRAIN DESIGN	CARTRIDGE LOADED CASE-BONDED INTERNAL AND END BURNERS	CASE-BONDED INTERNAL BURNERS END BURNERS REINFORCED PROPELLANTS

**SPECIAL
CHARACTERISTICS**
		HIGH SOLIDS LOADING
		HIGHER ENERGY PROPELLANTS
		HIGHER PROPELLANT REPRODUCIBILITY
		DECREASED PROPELLANT MOISTURE
		    SENSITIVITY
		IMPROVED PROPELLANT AGING
		GRAIN DESIGNS CAPABLE OF RESISTING
		    HIGHER ACCELERATION AND SPIN
		    RATES
		HIGH BURNING RATES FOR SOME
		    APPLICATION (AIR AUGMENTATION)

Table 3 lists general trends and characteristics for propellants and grain designs for both surface- and air-launched motors. Since most Navy missiles, whether they are large as Polaris or as small as a Sidewinder, are generally volume- as well as weight-limited, due to limitations in ship and aircraft storage space and capacities of handling gear, there is an ever-present need to upgrade the performance of Navy rocket motors. Efforts in this area are mainly directed to the development of Service acceptable propellants with specific impulse increases in the order of 10–20 per cent higher than presently available propellants. The degree of success will depend very largely on our ability to make physically tractable propellants with acceptable thermal and explosive sensitivities.

At present, the Navy has essentially narrowed the propellant systems for its major rocket development programs down to cast modified double base, polyurethanes and polybutadienes. Each propellant system has its own unique set of characteristics which define its area of applicability. The double-base propellants (nitrocellulose/nitroglycerine) offer the highest specific impulses, but are limited for both high and low temperature applications, particularly in case-bonded motors. The polybutadienes, particularly the carboxy-terminated variety, offer the promise of good physical properties over a wide temperature range and high solids loading, thus providing for a slight impulse advantage over poly-

urethane propellants. The latter are competitive with polybutadienes for many rocket motor applications, but have been somewhat limited for low temperature use, particularly after exposure to moisture. Certain polyurethanes exhibit a tendency to crystallize under certain time-dependent conditions, but recent formulation work has largely overcome this problem by the addition of ingredients which provide for better wetting of the solid particles.

Fluorocarbon binders in extruded propellants offer the advantage of high density, thermal stability and high tensile strength. These characteristics are expected to prove attractive for a number of applications, particularly in certain boost and barrage rockets where high impulse density and resistance to acceleration forces are required.

An interesting approach to the fabrication of rocket motors is the use of metal wire-reinforced propellant systems. Rocket motors using reinforced propellants have been investigated fróm the viewpoint of achieving high mass fraction through a reduction in requirements for case support. A secondary characteristic which may be a major advantage over the long range is the resistance of wire-reinforced propellants to the effects of high shock, acceleration and thermal cycling as a result of the inherent toughness of the propellants.

Future applications envision the general upgrading of the structural integrity of solid propellants by the optimization of the mechanical properties of the binder. It is evident that the chemistry of the binder has major effects on the structural integrity of rocket grains and that a basic understanding of the effects of binder or polymer molecular weight, molecular weight distribution, unsaturation, chemical structure and cross-linking density is required to optimize the propellant for mechanical properties including reproducibility, stability and processability.

With respect to the carboxy-terminated polybutadiene, the structure of the curing agent itself, aside from the reactive functional groups, can affect the properties of the final products, particularly if large quantities are used relative to the amount of prepolymer. Large bulky groups can physically retard free rotation and cause chain crystallization. Short non-functional chains between the active functional groups can cause tightening of the networks and areas of tension in its vicinity. Certain curing agents react with the antioxidants, removing their ability to protect. In addition, the curing agents can react with the newly formed functional groups resulting from the curing agent carboxyl group condensation. This means an additional cross-link or branching in a random positioning. The use of less curing agent equivalents than carboxyl equivalents is a device for arriving at a looser network. It is not surprising to find that physical properties are still changing after long periods of cure in an inert environment. One area requiring more extensive study is that of the effects of various ingredients and small traces of impurities on the chemical reactions of the binder. These include for example, oxygen, ozone, ammonium perchlorate, water, etc., all of which can result in the deterioration of physical properties. A need continues to exist to develop binders with high thermal stability, good aging properties, resistance to the aforementioned environmental effects and adequate tensile

and elongation properties over the entire temperature range particularly for the air-launched environment.

Finally, to appreciate more fully the various factors involved in establishing the structural integrity of Navy rocket motors, a brief exposition of development and test philosophy followed by the Navy is described. It is generally required that the initiation of any new engineering development program be contingent upon the prior completion of feasibility, and that no new state-of-the-art research is required. The first major step in the development program is to establish the design, followed by the development of one or more prototypes and critical environmental testing thereof until the final prototype is obtained. Early in this phase, critical stress analyses and propellant characterization of all pertinent physical properties of the propellant are conducted.

The following types of test programs are considered necessary to provide the design engineer with the information he needs to evolve a grain design consistent with the mechanical stresses and ballistic requirements imposed on the system. Early work involves the testing of several charges of less than 2 lb in the laboratory, generally followed by testing of 40–100 lb charges. In large motor developments such as Polaris the use of full-scale heavy-weight hardware may be preceded by work on 1/3 scale models for a variety of developmental objectives, e.g. ballistic, physical and material evaluation, and propellant processing. Smaller motor developments of the tactical variety may proceed immediately to full-scale heavy-weight hardware with a minimum of effort on scale models.

In order to complete the design analysis in the early phases of development, mechanical properties must be defined. Various test methods are available which have general acceptance in the Interagency Rocket Propulsion Group (ICRPG) Solid Propellant Mechanical Behaviour Manual. These include:

(a) Uniaxial Test Methods as a basis for developing stress, strain modulus curves based on the time-temperature superposition of data.

(b) Constant Strain Test to determine the failure of a propellant when held at constant strain for an extended time.

(c) Stress Relaxation Modulus Test.

(d) Multiaxial Test Methods. Strength analysis of a grain depends not only on having an adequate stress or strain analysis under various modes of loading, but also on knowledge of the stress and/or strain at which either excessive deformation or a fracture threshold is reached. Uniaxial tests yield some information, but in general, prediction of a fraction threshold depends on propellant material behavior in a state of multiaxial stress. Multiaxial tests include the strip biaxial and poker chip or triaxial test methods.

(e) Thermal Strain Evaluation Cylinder Test. Failure on cool-down of case bonded, cylindrical grains are commonly the longitudinal type, initiating near the inner bore and propagating radially into the web arising principally from inner bore circumferential strain. In such instances, hoop strain is of major concern in: (1) comparison of propellants with regard to the low temperature storage limits as a function of grain geometry, or (2) the critical strain at failure of a certain propellant for a given grain design. The ICRPG Mechanical

Behavior Manual describes a test method which permits scale or model testing to generate information to characterize the resistance of the propellant to various thermal strain histories.
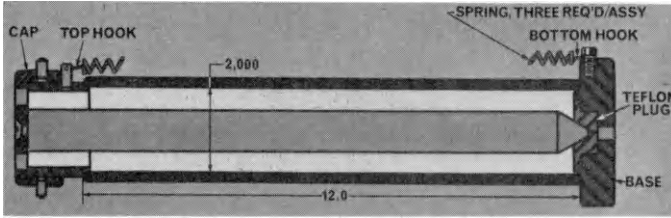

Fig. 9. Strain evaluation cylinder.

Figure 9 illustrates a typical 2 × 12 Strain Evaluation Cylinder (SEC) and Casting Fixture in which propellant samples with various web fractions and bonded to thick walled metal cylinders are cooled to failure. Bore measurements are made at each temperature from which hoop strain is calculated. The inner bore is inspected visually for evidence of propellant failure. Figure 10 shows
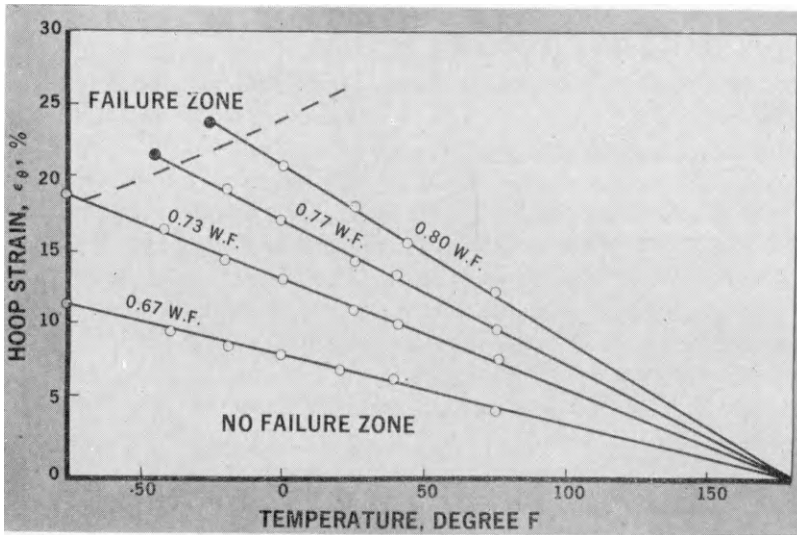

Fig. 10. SEC data for polybutadiene propellant.

typical SEC data for a polybutadiene propellant, indicating the temperatures and strains at which failure will not occur. At higher web fractions (W.F.) and at lower temperatures, greater hoop strains are developed and therefore the propellant must have higher strain capability to resist failure by cracking.

(f) Bond Tests. Finally, the prediction of structural integrity of a solid propellant grain requires a knowledge of the structural integrity of the interfaces between the grain and the liner. Peel and double lap shear tests are both used to evaluate the resistance of propellant-liner metal bonds to failure resulting from shear forces.

The culmination of the effort leading to a final prototype is followed by pre-liminary flight rating tests (PFRT). In this phase, certain extreme environmental tests are performed on rocket thrust units fabricated to the specifications of the final prototype design developed in the previous phase. It is in this phase that the major design deficiencies are most likely to be uncovered and necessary changes made in design, propellant, materials, or processing. The results of this program provide the basis for the release of the motor for experimental flight tests prior to the completion of the qualification testing. The PFRT tests may include, but are not limited to, the following:

(a) Static Firings at the high and low operating temperature extremes and simulated maximum specified pressure altitudes.

(b) Thermal Cycling Tests.

(c) Vibration Tests (as applicable).

(d) Drop Tests.

(e) Acceleration Tests (including simulated missile launch and flight loads).

The final or qualification phase of development is intended as a complete evaluation program to prove the capabilities of the developed rocket thrust unit to meet all design, performance, environmental and service use require-ments, prior to release of the motor design to production.

The reliability requirement for an air-launched motor may be as high as 99.99 per cent at a 95 per cent confidence level. The number of firings necessary to establish this degree of reliability are generally prohibitive in time and cost for a qualification program. The test program is generally arranged so that tests are carried out under extreme environmental conditions and are generally sequential in arrangement so that the transient and cumulative effects to which motors are exposed in their life history can be simulated.

A simplified but representative motor qualification program is given in Table 4. The sequential exposure to thermal cycling, vibration, aero-heat and acceleration forces represent an extreme combination of conditions design to prove the integrity of the motor design. For a case bonded motor, the critical loading and critical regions for the various test conditions listed in Table 4 are indicated in Table 5.

CONCLUSIONS

The history of recent years in development and production would indicate that major problems resulting in loss in time and increase in program costs are largely associated with the structural integrity of the solid propellant grains. The results of our research effort in this area of technology are now beginning to be used with considerable degree of effectiveness, but it is also evident that further work is required before we can establish stress analysis as a reliable engineering tool in the design of structurally sound propellant grains. A wider range of propellant mechanical properties is needed so that demands for performance under wider temperature extremes, improved ruggedness, higher acceleration loads, and larger motor sizes can be met.

2

TABLE 4.

SIMPLIFIED MOTOR QUALIFICATION PROGRAM

TEST CONDITIONS	FIRING -65°F	+165°F
1. TEMP. CONDITIONING (-65°F, +165°F)	X	X
2. THERMAL CYCLING (-65°F TO +165°F)	X	X
3. THERMAL CYCLING, CATAPULT & ARRESTED LANDING. ACCELERATION	X	X
4. THERMAL CYCLING, ACCELERATION	X	X
5. THERMAL CYCLING , VIBRATION	X	X
6. THERMAL CYCLING, VIBRATION, AERO HEAT	X	X
7. CATAPULT AND ARRESTED LANDING, AERO HEAT	X	X
8. AERO HEAT	X	X
9. DROP	X	X
10. ACCELERATION	X	X
11. ACC. AGING, ACCELERATION	X	X
12. RAIN, SALT SPRAY, ACCELERATION, HUMIDITY	X	X
13. VIBRATION, ACCELERATION	X	X

TABLE 5.

CRITICAL LOADING AND REGIONS FOR CASE BONDED MOTOR

TEST CONDITION	CRITICAL LOADING	CRITICAL REGION
1. AERODYNAMIC HEATING		
A. LOW INITIAL TEMPERATURE-SLOW	GRAIN COLD, CASE HOT, CASE BOND HOT	1. STARPOINT HOOP STRAIN 2. BOND TENSILE STRESS
B. HIGH INITIAL TEMPERATURE-SLOW	GRAIN COLD, CASE HOT, CASE BOND HOT	1. STARPOINT HOOP STRAIN 2. BOND TENSILE STRESS
C. LOW INITIAL TEMPERATURE-FAST	GRAIN COLD. CASE HOT. CASE BOND HOT	1. STARPOINT HOOP STRAIN 2. BOND TENSILE STRESS
D. HIGH INITIAL TEMPERATURE-FAST	GRAIN COLD. CASE HOT. CASE BOND HOT	1. STARPOINT HOOP STRAIN 2. BOND TENSILE STRESS
2. FIRING		
A. LOW TEMPERATURE FIRING (-50°F) B. HIGH　　　　FIRING (+160°F)	CURE SHRINKAGE. THERMAL SHRINKAGE. PRESS. LOADING (NOT CRITICAL)	STARPOINT HOOP STRAIN BOND TENSILE STRESS (NOT CRITICAL)
3. THERMAL CYCLING		
A. LOW INITIAL TEMPERATURE (-65 F)	GRAIN COLD , CASE HOT, CASE BOND HOT	1. STARPOINT HOOP STRAIN 2. BOND TENSILE STRESS
B. HIGH INITIAL TEMPERATURE (+160 F	GRAIN COLD. CASE HOT. CASE BOND HOT	1. STARPOINT HOOP STRAIN 2. BOND TENSILE STRESS
4. VIBRATION TEST		
A. LOW TEMPERATURE VIBRATION (-65°F)	GRAIN AXIAL G LOAD. GRAIN LATERAL G LOAD	AXIAL SHEAR ON CASE BOND BENDING AT BASE OF RAY
B. HIGH TEMPERATURE VIBRATION (+160°F)	GRAIN AXIAL G LOAD. GRAIN LATERAL G LOAD	AXIAL SHEAR ON CASE BOND BENDING AT BASE OF RAY .
5. DROP TEST (50°F)	GRAIN AXIAL G LOAD GRAIN AXIAL G LOAD GRAIN LATERAL G LOAD	AXIAL SHEAR ON CASE BOND AXIAL SHEAR ON CASE BOND BENDING AT BASE OF RAY
6. SIMULATED CATAPULT AND ARRESTED LANDING		
A. LOW TEMPERATURE SHOCK (-65°F)	GRAIN AXIAL G LOAD GRAIN LATERAL G LOAD GRAIN AXIAL G LOAD	AXIAL SHEAR ON CASE BOND BENDING AT BASE OF RAY AXIAL SHEAR ON CASE BOND
B. HIGH TEMPERATURE SHOCK (+160°F)	GRAIN AXIAL G LOAD GRAIN AXIAL G LOAD GRAIN LATERAL G LOAD	AXIAL SHEAR ON CASE BOND AXIAL SHEAR ON CASE BOND BENDING AT BASE OF RAY
7. ACCELERATION TEST		
A. LOW TEMP. ACCELERATION (-50°F)	GRAIN G LOAD GRAIN LATERAL G LOAD	AXIAL SHEAR ON CASE BOND BENDING AT BASE RAY
B. HIGH TEMP. ACCELERATION (+170°F)	GRAIN AXIAL G LOAD GRAIN LATERAL G LOAD	AXIAL SHEAR ON CASE BOND BENDING AT BASE OF RAY

ANALYSIS AND DESIGN OF
SOLID PROPELLANT GRAINS

J. Edmund Fitzgerald

Lockheed Propulsion Company
Redlands, California

Abstract—The present paper covers in some detail several pertinent aspects of engineering grain stress analysis:

(1) A brief review of linear viscoelastic theory with emphasis on time-temperature relations
(2) More details on thermal relations including a redefinition of Lee's reduced time parameter
(3) Presentation of a master relaxation curve for typical 84 percent solids loaded systems
(4) Discussion of relative thermal equilibrium and relaxation times for several motor sizes and design implications therefrom
(5) A generalization of the "freezing point" concept for uniformly cooled grains resulting in a new "material characteristic"
(6) Thermo-mechanically coupled experimental data
(7) Comments on creep-relaxation reciprocal relations and finally
(8) Recommendations relative to methods of analysis for physically non-linear materials which appear promising for future engineering utilization.

1. INTRODUCTION

Several years ago the author presented a paper [1] at the JANAF Solid Propellant Group Meeting at Pittsburgh, Pennsylvania. It was therein pointed out that the use of isothermal linear viscoelasticity theories employing the Laplace transforms of finite linear differential operators and the correspondence principle of Alfrey [2] were useful in obtaining solutions to the following problems:

(1) Propellant grain thermal stress (isothermal).
(2) Grain pressurization (isochoric).
(3) Gravitational slump (infinite cylinder).

The governing infinitesimal strain, incompressible, isothermal stress–strain relations used were either the finite differential operator form

$$P\sigma(t) = Qe(t) \tag{1.1}$$

where

$$P = \sum_{i=0}^{n} a_i \frac{\partial^i}{\partial t^i}, \qquad Q = \sum_{i=0}^{n} b_i \frac{\partial^i}{\partial t^i} \tag{1.2}$$

or the hereditary integral form

$$\sigma(t) = \int_0^t G(t - \tau)\,\dot{\epsilon}(\tau)\,\mathrm{d}\tau \tag{1.3}$$

$$\epsilon(t) = \int_0^t J(t - \tau)\,\dot{\sigma}(\tau)\,\mathrm{d}\tau$$

19

with the superposed dot being the time derivative of the quantity so indicated.

The general methods of this essentially one-dimensional linearized theory and its application had previously been extensively discussed by Lee [3] and Williams [4] as well as treated in detail in the monograph of Bland [5].

The fact that application of the above-mentioned methods required either closed form elastic solutions of rather restricted form with respect to the elastic moduli or, alternatively, rather simple isothermal and isochoric problems for finite difference numerical evaluation, confined their use essentially to the problems discussed in the author's 1962 paper [1].

Those associated with the solid propellant industry almost without exception began generating elastic solutions for the various propellant grain problems at a great rate. These solutions were generally numerical in nature and gave rise to much controversy relative to the merits of finite difference methods, stiffness methods, and redundant force methods for computer utilization. A rather comprehensive review of these methods is given by Parr [6]. Needless to say, these numerical solutions were applicable only to isothermal and isochoric or elastic bulk behavior where synchronous separation of variables was evident; that is, where the viscoelastic solution could be obtained by Alfrey's [2] correspondence principle and where the relaxation or creep function entered as a simple multiplier of the elastic solution.

The transient thermal problem was not successfully attacked until the publication of the paper by Muki and Sternberg [7] followed by the work of Lianis and Valanis [8, 9] utilizing real relaxation moduli found in rubber-base propellants by Jones $et\ al.$ (LPC) [10].

2. HEREDITARY STRESS–STRAIN RELATIONS

At this point it might be well to present the pertinent equations for the linear theory of viscoelasticity generally used throughout the solid propellant industry.

The displacement gradient-strain relations for small strains are

$$\epsilon_{ij} = \tfrac{1}{2} (u_{i,\,j} + u_{j,\,i}) \tag{2.1}$$

where $u_i(\mathbf{x}, t)$ and $\epsilon_{ij}(\mathbf{x}, t)$ are respectively the components of the displacement and the strain at the material point with the position vector $\mathbf{x}$ where,

$$\mathbf{x} = f(x_1, x_2, x_3)$$

and time t and $u_{i,\,j}$ is the displacement gradient. Subscripts take values 1, 2, 3 and the comma indicates partial differentiation with respect to the coordinate following it.

The deviatoric components of stress and strain are, respectively

$$s_{ij} = \sigma_{ij} - \tfrac{1}{3} \delta_{ij}\sigma_{\kappa\kappa} \qquad \left(\delta_{ij} = \begin{matrix} 0, & i \neq j \\ 1, & i = j \end{matrix} \right)$$

and

$$e_{ij} = \epsilon_{ij} - \tfrac{1}{3} \delta_{ij}\epsilon_{\kappa\kappa} \tag{2.2}$$

The local instantaneous temperature is $T(\mathbf{x}, t)$ and T_0 is an arbitrary reference temperature usually taken at the upper value of interest of T. The temperature field history is designated by θ, where

$$\theta = T - T_0 \tag{2.3}$$

Occasionally it is more desirable to use a dimensionless temperature, where

$$\bar{\theta} = \frac{T - T_0}{T_0} \tag{2.4}$$

or in some cases to normalize the temperature history over the range of interest between T_0 and, say, T_1, so that the reduced temperature, $\hat{\theta}$, is

$$\hat{\theta} = \frac{T - T_0}{T_1 - T_0} \quad (0 \leq \hat{\theta} \leq 1) \tag{2.5}$$

The linear coefficient of thermal expansion, $\alpha(T)$, usually varies with temperature so that we define an average coefficient, $\bar{\alpha}$, where

$$\bar{\alpha}(T) = \frac{1}{\theta} \int_T^{T_0} \alpha(T') \, dT' \tag{2.6}$$

and use this instead of $\alpha(T)$. Some authors have used the value of $\alpha(T)_0$ and a reduced temperature, $\hat{\theta}$, where

$$\hat{\theta} = \frac{1}{\alpha(T)_0} \int_{T_0}^{T(\mathbf{x},\, t)} \alpha(T') \, dT' \tag{2.7}$$

It is felt, however, that the use of an average coefficient of expansion and a temperature history whose units are in degrees F or C is to be preferred, particularly when comparing theory with experimental results. (As will be seen shortly, the term, α, always comes as a multiplier of θ so that $\alpha(T)_0\hat{\theta} = \alpha\theta = \hat{\alpha}\hat{\theta} = \bar{\alpha}\theta$; the choice therefore does not affect the mathematics.)

Now employing a general stress-strain law for linear viscoelastic materials relating the stress component σ_{ij} with the strain component $\epsilon_{\kappa l}$ through a convolution integral on the tensorial component, $G_{ij\kappa l}$, where $\mathbf{G}(t)$ is a fourth-order tensor, where $G_{ij\kappa l}(t) = G_{ji\kappa l}(t) = G_{ijl\kappa}(t)$ for every t in $[-\infty, \infty]$, we have

$$\sigma_{ij} = \epsilon_{\kappa l}{}^* \, dG_{ij\kappa l} \tag{2.8}$$

where $\mathbf{G}(t)$ is the tensorial relaxation function as is shown in Gurtin and Sternberg [11].

Although the above conditions for the existence of the Stieltjes convolution integral are sufficient according to Theorem 9–26 of Apostol's text [12], there is often added, for reasons shown in [11] that

$\mathbf{G} = 0$ on $[-\infty, 0]$
$\mathbf{G}$ is continuous on $[-\infty, \infty]$
$\mathbf{G}$ and ϵ are at least once differentiable on $[0, \infty]$
$\epsilon = 0$ on $[-\infty, 0]$

(It should be mentioned that both ϵ and $\mathbf{G}$ need not be continuous; rather they shall not have a common discontinuity at any time, t [12].)

With the above, admittedly over-restrictive conditions on ϵ and $\mathbf{G}$ including the exception noted, we can write

$$\sigma_{ij} = \epsilon_{\kappa l}{}^* \, dG_{ij\kappa l} = G_{ij\kappa l}{}^* \, d\epsilon_{\kappa l} \tag{2.9}$$

or

$$\sigma_{ij}(\mathbf{x},\ t) = \int_{-\infty}^{t} \epsilon_{\kappa l}(t\ -\ \tau)\ dG_{ij\kappa l}(\tau) \tag{2.10}$$

and

$$\sigma_{ij}(\mathbf{x},\ t) = \int_{-\infty}^{t} G_{ij\kappa l}(t\ -\ \tau)\ d\epsilon_{\kappa l}(\tau) \tag{2.11}$$

By assuming isotropy in our linear material description, the stress–strain relations for the deviatoric and dilatational components of stress are then

$$s_{ij} = e_{ij}{}^* \, dG_1$$

and

$$\sigma_{\kappa\kappa} = (\epsilon_{\kappa\kappa} - 3\bar{a}\theta)^* \, dG_2 \tag{2.12}$$

where, G_1 is the relaxation shear modulus and G_2 is the relaxation bulk modulus.

Using the commutative property of the convolution integral, eqn. (2.9), and either integrating by parts or referring to Apostol [12] in order to change the limits of integration from $[-\infty,\ t]$ to $[0,\ t]$, we obtain for eqn. (2.12) the following

$$s_{ij}(\mathbf{x},\ t) = G_1(t)\ e_{ij}(\mathbf{x},\ 0) + \int_{0}^{t} G_1(t\ -\ \tau)\ \frac{de_{ij}}{d\tau}\ (\mathbf{x},\ \tau)\ d\tau \tag{2.13}$$

and

$$\sigma_{\kappa\kappa}(\mathbf{x},\ t) = G_2(t)[\epsilon_{\kappa\kappa}(\mathbf{x},\ 0) - 3\bar{a}\theta(\mathbf{x},\ 0)]$$
$$+ \int_{0}^{t} G_2(t\ -\ \tau)\left[\frac{d\epsilon_{\kappa\kappa}}{d\tau}\ (\mathbf{x},\ t) - 3\bar{a}\ \frac{d\theta}{d\tau}\ (\mathbf{x},\ t)\right]\ d\tau \tag{2.14}$$

or

$$s_{ij}(\mathbf{x},\ t) = G_1(0)\ e_{ij}(\mathbf{x},\ t) + \int_{0}^{t} e_{ij}(\mathbf{x},\ t\ -\ \mathbf{x},\ \tau)\ \frac{dG_1(\tau)}{d\tau}\ d\tau \tag{2.15}$$

and

$$\sigma_{\kappa\kappa}(\mathbf{x},\ t) = G_2(0)[\epsilon_{\kappa\kappa}(\mathbf{x},\ t) - 3\bar{a}\theta(\mathbf{x},\ t)]$$
$$+ \int_{0}^{t} [\epsilon_{\kappa\kappa}(\mathbf{x},\ t\ -\ \mathbf{x},\ \tau) - 3\bar{a}\theta(\mathbf{x},\ t\ -\ \mathbf{x},\ \tau)]\ \frac{dG_2(\tau)}{d\tau}\ d\tau \tag{2.16}$$

Since G_1 and G_2 are generally monotonically decreasing, then dG_1 and dG_2 are negative.

In the case where G's are constants, the above relations reduce to the usual

elastic relations where G_1 equals twice the shear modulus and G_2 equals thrice the bulk modulus.

Where the assumption is made that $G_1(t)$, $G_2(t) \rightarrow 0$ as $t \rightarrow \infty$, then it is convenient to regard G as the increment of modulus in excess of the equilibrium modulus $G(\infty)$ or G_{eq}. This definition then requires the addition of a term $G_1(\infty) \, \epsilon_{ij}(\mathbf{x}, t)$ in eqn. (2.13) and similar terms in the other equations.

In real materials, $G_1(t)$, is a strong function of time varying by four or five orders of magnitude from $t = 0$ to $t = \infty$. The term, $G_2(t)$, on the other hand, is a weak function of time varying by a factor of less than two over the entire time span. As a result the value of $G_2(t)$ is often with sufficient accuracy taken as a constant for solid propellants with a value of approximately 500,000 psi. For problems dominated by shear response, the value of $G_2(t)$ is taken as infinite, i.e. incompressible material with a Poisson's ratio of 0.5 for infinitesimal strains.

3. THERMAL EFFECTS

For problems involving temperature change, a change in the time variable, t, to a reduced time variable, ξ, is usually employed. The physics of the real materials used in solid propellant charges produce the following types of changes.

1. For equilibrium conditions, the relaxation modulus is proportional to the absolute temperature as a consequence of the theory of rubber elasticity as expounded by Tobolsky [13].

2. The relaxation modulus is proportional to the density ratio over the temperature difference considered [14].

3. A change of temperature translates the relaxation modulus (throughout the transition region only) horizontally on a plot of log G versus log t, $t =$ time, by an amount

$$\log A_T = f(T_0) - f(T) \tag{3.1}$$

where $T =$ temperature and $T_0 =$ an arbitrary reference temperature. This form of shift was first proposed by Leaderman [15] for elastic and creep properties and was earlier used by Wagner [16] in 1914 for shifting dielectric data.

Derivation of the effect of temperature change consists in multiplying all reciprocal relaxation times, $a_i = 1/\tau_2$, by a common factor $a'(T)$, where $a'(T)$ is a function of temperature only [17, 18]. The combination of these factors then leads to a relationship between the relaxation modulus, $G(t, T_0)$, at the reference temperature to the modulus at a new temperature, T, such that

$$\frac{\rho_0 T_0}{\rho T} \, G\left(\frac{t}{a'_T}, T\right) = G(t, T_0) \tag{3.2}$$

or since

$$\rho = \frac{\rho_0}{1 + 3\bar{a}\theta}, \qquad \theta = T - T_0$$

$$\frac{(1 + 3\bar{a}\theta)}{(\theta + T_0)} \, T_0 G\left(\frac{t}{a'_T}, T\right) = G(t, T_0) \tag{3.3}$$

For most solid propellants, $\bar{a}$ is of the order of 5×10^{-5} °F^{-1} so that for any range of θ of interest the term $1 + 3\bar{a}\theta$ varies by less than 1 % and is generally impossible to reproducibly measure experimentally. Equation (3.3) then becomes

$$\frac{T_0}{T} \, G\left(\frac{t}{a'_T}, \, T\right) = G(t, T_0) \tag{3.4}$$

Although it is quite common in the literature reporting experimental work to use the above relation, introduction of the multiplier, T_0/T_1, results in undue complication of the constitutive equations (2.13) through (2.16). It is thus convenient and quantitatively not too incorrect to define a new shift factor a_T such that

$$G\left(\frac{t}{a_T}, \, T\right) = G(t, T_0) \tag{3.5}$$

In this formulation, the relaxation moduli curves of $G(t, T)$ superpose those of $G(t, T_0)$ when shifted along the log time axis by an amount log a_T. This last relationship has been used to define a material as "thermorheologically simple" by Schwarzl and Staverman [19].

A new variable, ξ, the reduced time, may be used where

$$\xi = \frac{t}{a_T} \tag{3.6}$$

and

$$G(\xi, T) = G(t, T_0) \tag{3.7}$$

For transient temperature conditions Moreland and Lee [20] have introduced the reduced time as

$$\xi(t) = \int_0^t \frac{dt'}{a_T[T(t')]} \tag{3.8}$$

(In the above paper, however, the reciprocal, ϕ, of a_T is used, whereby $\phi = 1/a_T$.)

A series of precision uniaxial stress relaxation tests was carried out on a polybutadiene acrylic acid (rubber) based copolymer with an 84 per cent by weight solids loading (approximately 70 per cent by volume) of aluminum powder and granular ammonium perchlorate oxidizer. The relaxation tests were performed over four decades of time at many isothermal temperature conditions ranging from −110°F to +174°F. The uncorrected data are shown as circles in Fig. 1 [21] with the logarithm of the uniaxial relaxation modulus, $E(t)$ plotted versus the logarithm of time in seconds. The dashed horizontal lines give the values of a_T used to shift the data. Figure 2 [21] is a plot of a_T versus temperature and of the relaxation modulus versus the logarithm of the reduced time, $\xi = t/a_T$, using a +70°F reference temperature. The reduced curve ranges over fifteen decades of reduced time.
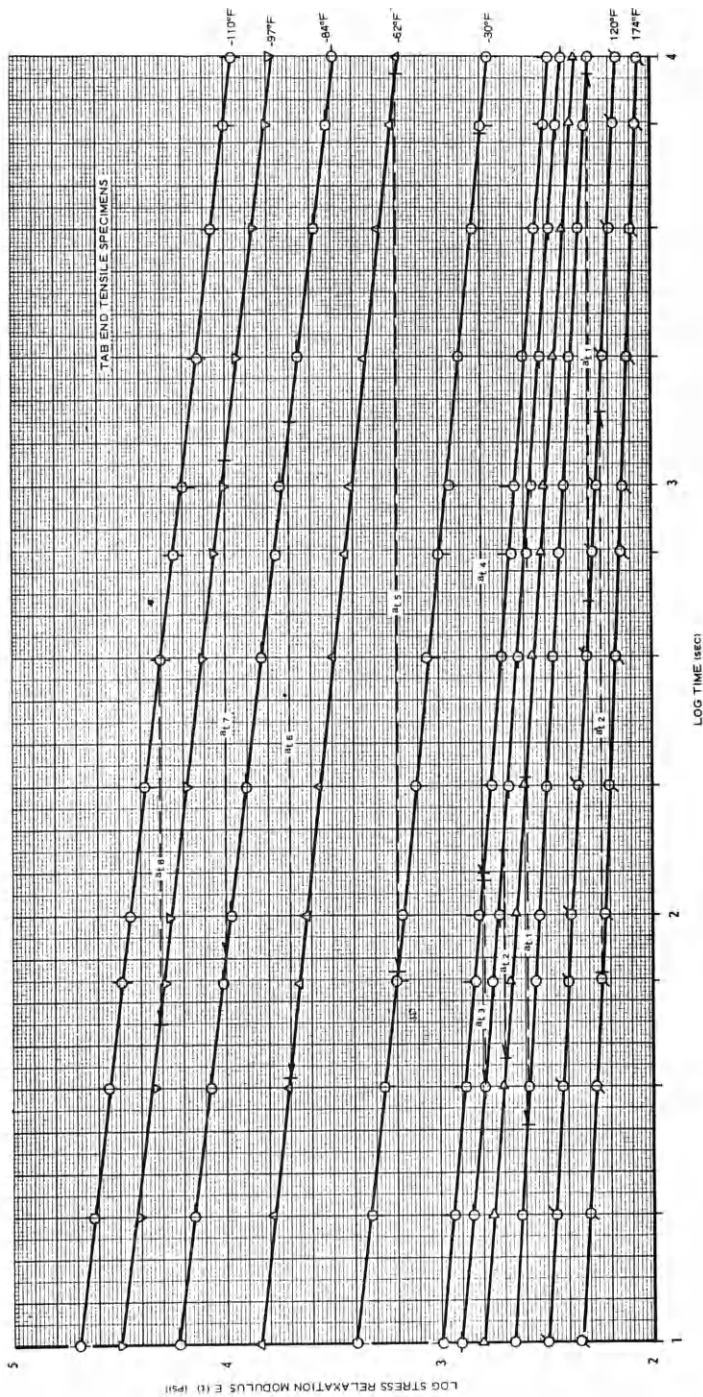
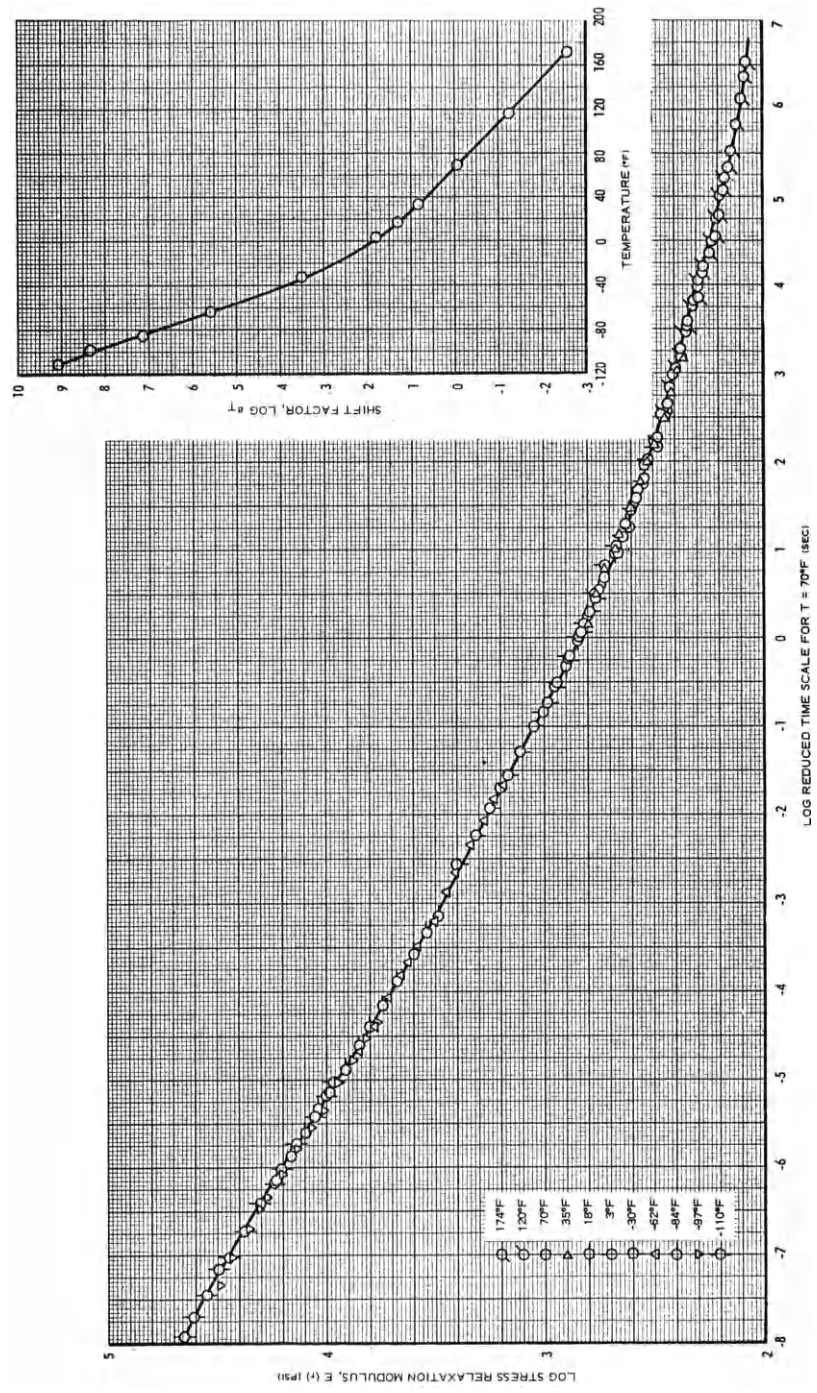FIG. 1. Stress relaxation data for temperatures between $-110°F$ and $+174°F$, PBAA propellant.

FIG. 2. Master stress relaxation modulus at $T = 70°F$ and shift factor, PBAA propellant.

Returning to consideration of eqns. (2.13) and (2.14), we introduce the reduced time into them. In addition, let us take

$$e_{ij}(\mathbf{x}, 0) = \epsilon_{\kappa\kappa}(\mathbf{x}, 0) = \theta(\mathbf{x}, 0) = 0$$

since step functions of strain or temperature are unattainable in practice. Assuming further that the bulk relaxation modulus, G_2, is a constant, Fig. 3
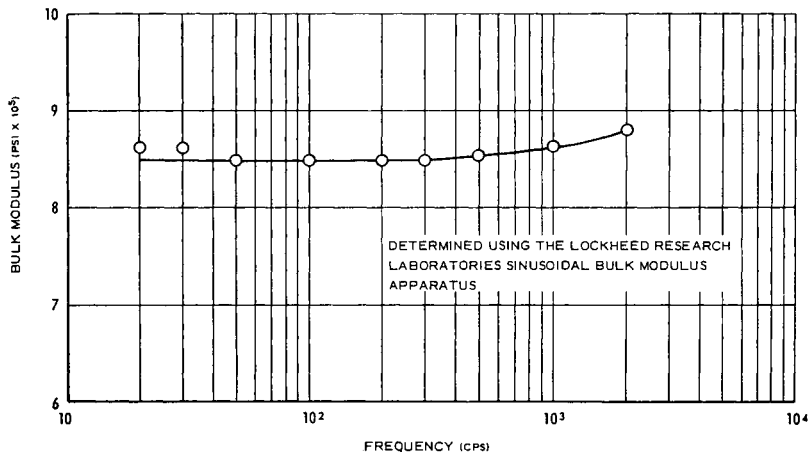
FIG. 3. Bulk modulus of PBAA propellant at 77°F.

shows the relative insensitivity of G_2 to rate processes [22] for a solid propellant; Fig. 4 shows the rather small variation of bulk modulus of polyisobutylene over ten decades of reduced time [23]. Then eqns. (2.13) and (2.14) become

$$s_{ij}(\mathbf{x}, \xi) = \int_0^{\xi} G_1(\xi - \xi') \frac{de_{ij}}{d\xi}(\mathbf{x}, \xi')\, d\xi' \tag{3.9}$$

and

$$\sigma_{\kappa\kappa}(\mathbf{x}, \xi) = G_2(0)[\epsilon_{\kappa\kappa}(\mathbf{x}, \xi) - 3\bar{a}\theta(\mathbf{x}, a_T\xi)] \tag{3.10}$$

where

$$\xi(\mathbf{x}, t, T) = \int_0^{t} \frac{dt'}{a_T[T(\mathbf{x}, t')]} \tag{3.11}$$

and

$$G_2(0) = 3K$$

Equations (3.9) and (3.10) are the forms of the constitutive equations most generally used in the formulation of solid propellant stress analysis problems. It will be noted from a comparison of log a_T versus temperature that the

relaxation modulus is much more strongly affected by changes in temperature than by changes in time. This attribute has enabled many solutions to be greatly simplified by assuming essentially constant time or piecewise constant time during thermal transients [8, 9, 23].
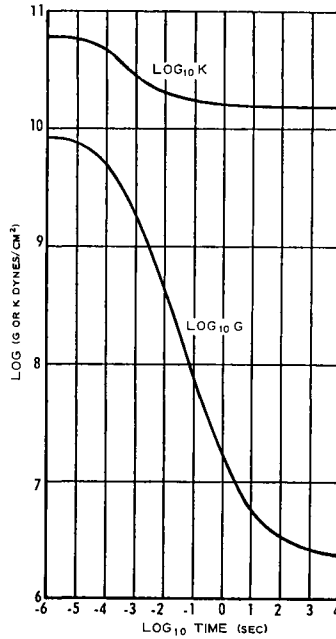

FIG. 4. Relaxation moduli of polyisobutylene in dilation (K) and shear (G).

A rather complete discussion of the formulation of equations, uniqueness of solutions, and bibliography is given in Sternberg's monograph on thermo-rheologically simple materials [24]. A second monograph by Taylor with some examples of thermo-mechanically uncoupled systems is also available [25].

4. THERMAL STRESS PROBLEMS

In spite of the several problems relating to transient thermal states in thermo-rheologically simple materials, little has been published using realistic tempera-ture variations imposed on real solid propellants [26] and essentially nothing has appeared in the open literature. The report of Jones, Fitzgerald, and Francis [26] makes use of Biot's approximation method for calculating the temperature field in a case-bonded, circular-port solid propellant grain. The method is described in detail in the referenced report and also in the textbook by Boley and Weiner [27].

We define a diffusion parameter, η^2

$$\eta^2 = \frac{\kappa t}{w^2} \tag{4.1}$$

where $\quad\quad\quad\quad\quad\quad$ κ = propellant diffusivity, in²/min

$\quad\quad\quad\quad\quad\quad\quad\quad$ t = real time, min

$\quad\quad\quad\quad\quad\quad\quad\quad$ w = web thickness, in.

The scaled diffusivity, $\bar{\kappa}$, is defined as

$$\bar{\kappa} = \frac{\kappa}{w^2}, \text{ min}^{-1} \tag{4.2}$$

so that eqn. (4.1) becomes $\eta^2 = \bar{\kappa}t$.

The time, t_a, for an external step temperature change, $\theta U(t)$, to be felt at the inner port surface is [26].

$$t_a \simeq \frac{w^2}{10\kappa} = \frac{0.1}{\bar{\kappa}} \tag{4.3}$$

The time, t_{90}, for the inner port surface to reach 90 per cent of the value of the input temperature change, θ, is given by [26]

$$t_{90} \simeq \frac{w^2}{\kappa} = 10\, t_a = \frac{1}{\bar{\kappa}} \tag{4.4}$$

The reduced times, η^2, are repectively given by

$$\eta_a^2 = \bar{\kappa}t_a = 0.1; \quad \eta_{90}^2 = 10\,\eta_a^2 = 1.0 \tag{4.5}$$

Thus the inverse of the scaled diffusivity, $\bar{\kappa}$, is a close measure of the real time needed to bring a grain to near equilibrium temperature.

Consider, for example, three sizes of solid rocket motors whose outer diameters and webs, for web fractions of 50 per cent or greater, are

	Diameter (in)	Web thickness (in)
Small motor, S.M.	4.0	1.0
Medium motor, M.M.	36.0	10.0
Large motor, L.M.	156.0	50.0

Using the measured diffusivity of the PBAA propellant previously used (Fig. 2),

$$\kappa = 193 \times 10^{-4}\, \frac{\text{in}^2}{\text{min}} = 1.16\, \frac{\text{in}^2}{\text{hr}} \simeq 1\, \frac{\text{in}^2}{\text{hr}} = 7.5\, \frac{\text{cm}^2}{\text{hr}}$$

Thus the reciprocal scaled diffusivities for the three motors, which are the times, t_{90}, for achieving near temperature equilibrium, are:

Motor	Diameter (in)	Web (in)	κ^{-1} (hr)	κ^{-1} (min)	
S.M.	4.0	1.0	1	60	
M.M.	36	10	100	6000	= 4 days
L.M.	156	50	2500	150,000	= 3+months

A more accurate value for the time for penetration is given in [26] as

$$t_a = \frac{b^2}{30\kappa} \left(\frac{2\lambda^3 - 3\lambda^2 + 1}{\lambda^3} \right) \tag{4.6}$$

where b = outer grain radius

　　a = inner grain port radius

　　$\lambda = b/a$

and

　　$t_{90} = 10\, t_a$

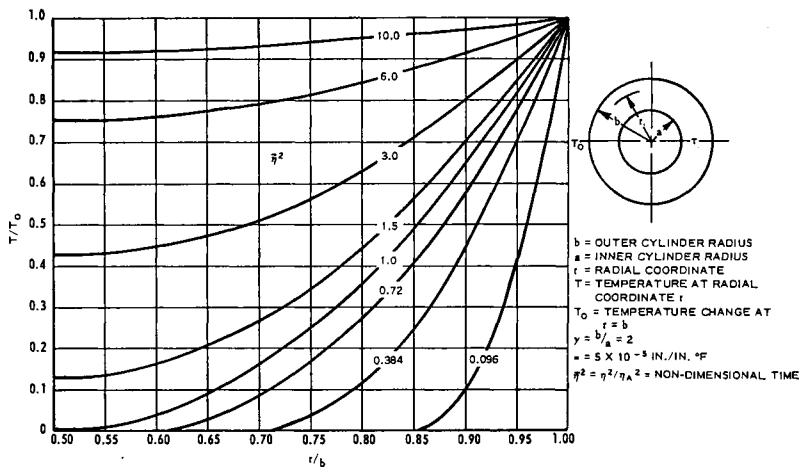A plot of $\bar{\eta}^2 = t/t_a$ is shown in Fig. 5.

FIG. 5. Time–temperature distribution of a hollow cylinder with zero initial temperature and a suddenly applied surface temperature, T_0 (inner port insulated).

Consider a grain unbonded from the case and instantaneously cooled from its equilibrium initial temperature by $\theta°F$. Now apply an outwardly directed normal tension to its outer surface until it comes in contact with the case wall again. Apply this tension gradually, taking a time, t_{90}, fully to achieve contact. This sequence of events is more severe than the gradually cooling down of a case-bonded grain. For the motors under discussion these times are 60 minutes, 4 days, and 3 months. The logarithms of the above times are 1.8, 3.8, and 5.2, respectively.

There exists a unique temperature, with $+70°F$ as a reference temperature, therefore, for each of these motors whereby the shift factor, a_T (Fig. 2), reduces the time by these same equilibrium times. The following table gives these relations (both a_T and ξ have been adjusted from seconds to minutes for the listed values).

Motor	$t_{90} = \kappa^{-1}$(min)	$\log t_{90}$(sec)	T (°F)	θ (°F)	$\dot{\theta}_{av}$ (°/m)	T_{ext}
S.M.	60	3.5	−25	−95	−95	−35
M.M.	6000	5.8	−65	−135	−1.35	−75
L.M.	150,000	7.8	−90	−160	−0.064	−105

Thus, if each of these motors were instantaneously reduced in temperature by $\theta°F$ as listed and then allowed to rest for times equal to t_{90}, the effective relaxation modulus would be identical to the value obtained at $+70°F$ and time equal to one second, i.e. $\log E = 2.82$ or $E = 660$ psi.

Although the average modulus of a real motor cannot, therefore, approach the glassy regime under conditions of thermal stresses, certain portions on the outer periphery may obtain higher moduli because of the greater cooling rates. In order to calculate the effective reduced time more accurately, use is made of an equivalent reduced time.

Returning to the definition of reduced time as given in eqn. (3.11)

$$\xi(\mathbf{x}, t, T) = \int_0^t \frac{dt'}{a_T[T(\mathbf{x}, t')]}$$

and noting that $d\theta = \dot{\theta} dt$, we have

$$\xi(\mathbf{x}, t, T) = \int_0^\theta \frac{d\theta'}{a_T[T(\mathbf{x}, t')] \dot{\theta}} \tag{4.7}$$

which is dependent on both temperature and the rate of temperature history change. Assuming that the temperature changes uniformly with respect to time, $\dot{\theta} = $ constant, we may write (4.7) as

$$\xi(\mathbf{x}, \theta, T) = \bar{\xi}(\mathbf{x}, T)\dot{\theta} = \int_0^\theta \frac{d\theta'}{a_T[T(\mathbf{x})]} \tag{4.8}$$

The integral expression above is a function of the material property only. For the PBAA propellant of Fig. 2, a graph of $\bar{\xi}$ versus θ with a reference temperature of $+70°F$ is shown in Fig. 6.

For a constant rate of change of temperature, $\dot{\theta}$, and from eqn. (4.8) we obtain

$$t = \frac{\theta}{\dot{\theta}} = \frac{\dot{t}}{\dot{\theta}} \text{ where } \theta = \dot{t}$$

and

$$\xi = \frac{\bar{\xi}}{\dot{\theta}} \tag{4.9}$$

Curves of this sort for specific temperature change histories have been previously obtained by Lee and Rogers [28] and Taylor [25] but neither author puts the relations into the reduced form shown herein.

For uniform continuous cooling, curve A of Fig. 6 applies. For the case where cooling is uniform to a certain temperature, θ, and that temperature is then held constant, curve A holds to θ_1 and the tangent to $\bar{\xi}$ versus θ at θ_1 holds henceforth. Curve C in Fig. 6 depicts this relationship for $\theta_1 = 30°F$

$(T = +40°F)$. The applicable part of curve C from $\theta = 30°$ onward is then

$$\bar{\xi} = \frac{\bar{\xi}_0}{\theta} + \frac{\bar{t}}{\theta a_T} \text{ for all } \bar{t} > \theta \tag{4.10}$$

or again from eqn. (4.9) the reduced time

$$\xi = \frac{\bar{\xi}_0}{\theta} + \frac{t}{a_T} \text{ for all } t > \frac{\theta}{\bar{\theta}} \tag{4.11}$$

where $\bar{\xi}_0$ is the vertical intercept of the tangent to $\bar{\xi}$ versus θ taken at $\theta = \theta_1$.

Equations (4.10) and (4.11) point out the reason for looking upon the temperature history θ as a type of equivalent time, $\bar{t}$. Equation (4.11) makes clear the point that the reduced time ξ in thermal cooling problems must be
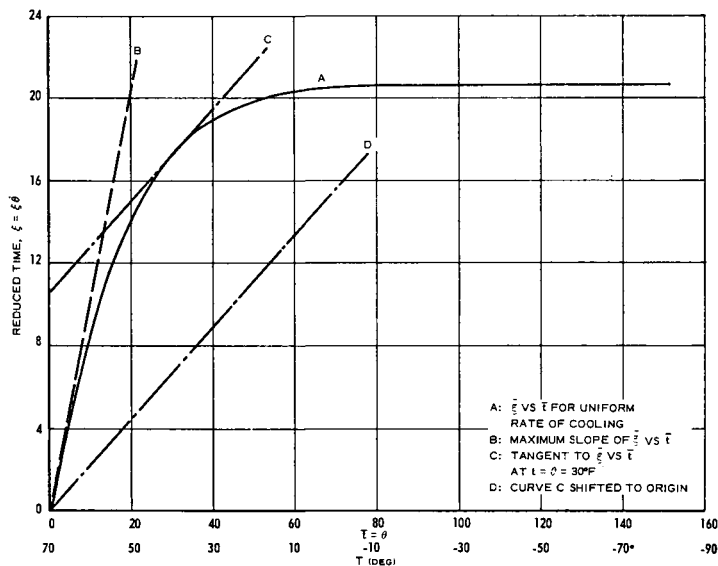
FIG. 6. Reduced time $\bar{\xi} = \xi\theta$ versus temperature history θ, °F.

equal to or greater than the instantaneous value of ξ given by $\xi = t/a_T$ by an amount equal to $\bar{\xi}_0/\theta$. For the physically unrealizable case where cooling is instantaneous, $\theta \to \infty$ and $\xi = t/a_T$.

For the case of our motor examples uniformly cooling from, say, $+70°F$ to $+40°F$ ($\theta = 30°F$) the relations are from eqn. (4.9) and the average cooling rates of the previous table:

Motor	$\dot{\theta}_{av}$ (°F/hr)	ξ vs.t for $t > \theta/\dot{\theta}$
S.M.	-95	$\xi = 0.11 + 0.25t$, hr
M.M.	-1.35	$\xi = 7.8 + 0.25t$, hr
L.M.	-0.064	$\xi = 165 + 0.25t$, hr

For a uniform cooling to $T = -5°F$ ($\theta = 75°F$) however, the relations become

Motor	ξ vs. t for $t > \theta/\dot{\theta}$
S.M.	$\xi = 0.21 + 0.01t$, hr
M.M.	$\xi = 14.7 + 0.01t$, hr
L.M.	$\xi = 310 \ \ + 0.01t$, hr

The above tables show that for the small motor (S.M.) cooled to $+40°F$, the value of ξ will double within less than one-half hour. For the large motor (L.M.) cooled to $-5°F$, the value of reduced time ξ will not double for a time less than three years. Of even more interest is the fact that if the motors were allowed to cool continuously below $-5°F$, the intercept values of ξ would not change from those listed in the second of the above two tables. This value of θ or T ($-5°F = T$ for PBAA) has been called the freezing temperature by Lee and Rogers [28]. The above examples clarify this definition. The "freezing point" of a propellant is that temperature where the reduced time, ξ, does not continue to increase within meaningful measure with real time, t, while the propellant is undergoing continuous cooling. Effectively, this means that the relaxation modulus achieved on a plot of E_{relax} versus ξ does not change with increasing time or decreasing temperature beyond the "freezing point". However, when the cooling rate stops and the propellant is held at the temperature then achieved, θ_1, the relaxation modulus decreases as the reduced time, ξ, increases at a rate

$$\xi = t/a_T$$

where a_T is taken at the value of T reference minus θ_1. Thus any residual stresses frozen in at the "freezing temperature", $-5°F$ for PBAA, then ultimately relax to zero.

It should be mentioned in passing that the $\bar{\xi}$ versus θ curve of Fig. 6 is readily constructed from the a_T curve of Fig. 2 with a half-hour effort on a slide rule. The observed circumferential strain at the inner bore of a solid propellant motor after thermal equilibrium is reached is given by [1]

$$\epsilon_\theta(a, t) = -\frac{(1 + \nu) \, a\theta(\lambda^2 - 1)}{(1 - 2\nu) \, \lambda^2 + 1} \, PK_2 \tag{4.12}$$

where ν = Poisson's ratio

λ = ratio of outer radius to equivalent inner bore radius

P = Parr factor for finite length effects [29]

K_2 = stress concentration factor [30]

Knowing that the value of Poisson's ratio, ν, is time dependent because of the relation between the nearly constant bulk modulus, K, and the highly time-

3

dependent uniaxial relaxation modulus, E, where

$$\nu = \frac{1}{2} \left(1 - \frac{E}{3K} \right) \tag{4.13}$$

several authors have included this variation in the thermal stress equation (4.12) [ref. 25, for example].

The ensuing computational difficulties are, however, not worth the trivially increased accuracy thus obtained. For example, letting

$$\phi = \frac{1 + \nu}{(1 - 2\nu) \lambda^2 + 1} \text{ and } \lambda = 2 \tag{4.14}$$

the values of ϕ, ν, and $1-2\nu$ are calculated in Fig. 7 versus log $E/6K$. For $K = 500,000$ psi for PBAA, the resulting values of E are also shown on the graph.
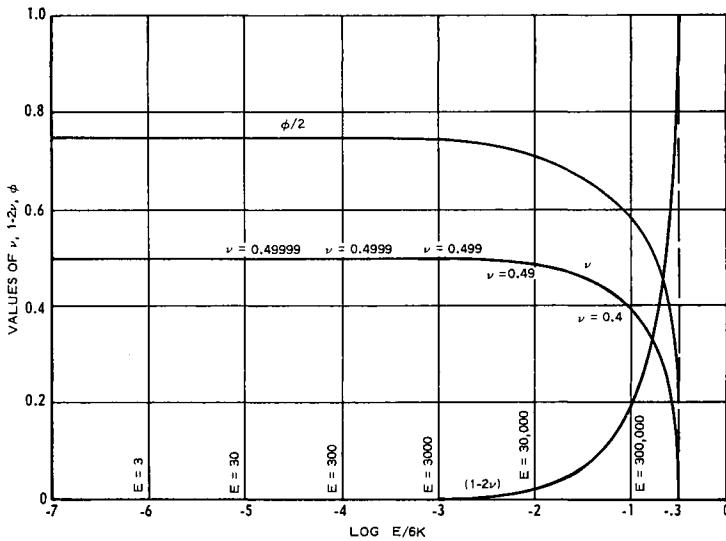
FIG. 7. ν, $1-2\nu$, and $\phi/2$ versus log $E/6K$.

It becomes rather apparent from Fig. 2, the relaxation modulus versus ξ, and the variations of ξ versus temperature previous discussed, that values of E in excess of 30,000 psi are essentially unobtainable in realistic solid rocket motors. The variations in the value of ϕ is thus restricted to less than 1 per cent of its asymptotic value of 1.5 over the entire time–temperature range achievable in thermal cycling problems. Thus even if a 50 per cent web fraction grain of PBAA propellant were instantaneously cooled from $+70°F$ down to $-40°F$, a physically impossible situation, the bore strains and radial displacements observed one second thereafter would be in agreement with incompressible theory to within less than 1 per cent.

For engineering analysis, the simplified form of eqn. (4.12) is used where

$$\epsilon_\theta(a) = \frac{3}{2} \, \bar{a}\theta(\lambda^2 - 1) \, PK_2 \qquad (4.15)$$

is used for the observed strains and radial port displacements based on the original mandrel diameter and

$$\epsilon_\theta(a) = \frac{3}{2} \, \bar{a}\theta\lambda^2 \, PK$$

is used to compare the stress producing strains with laboratory test data (see Fig. 17 for comparison) [47]. For application to star grains, stress concentration factors derived from photoelastic models are commonly used.

There are materials, however, and certain experimental propellants, where the above simplification does not hold even closely. An example of such materials with a largely varying value of ν is to be found in a very interesting and excellent article by Theocaris [31].

All of the foregoing discussion has been centered on the thermo-mechanically uncoupled problem. For propellant materials commonly used, the viscous dissipation is quite large over a wide range of temperatures. The vibration of rocket grains over this temperature range of interest gives rise to rather large temperature increments. Indeed, actual and dramatic failure of rocket grains under vibration testing has been observed and reported [32]. Work is presently being conducted experimentally at LPC based on guidance obtained from Schapery's theoretical efforts at Purdue [33]. Some rather interesting preliminary results obtained by Cantey [33] for the thermo-mechanically coupled problem are discussed below.

The test apparatus consists of two pieces of PBAA propellant (each 1 in. high by 4 in. long by 0.5 in. wide) mounted so as to be subjected to a sinusoidally varying simple shear strain. Two types of loading were used:

1. Constant shear-strain amplitude as shown in Fig. 8; and
2. Inertial shear-strain as shown in Fig. 9.

Two test conditions were maintained for each of the above test devices:

1. Isothermal boundary condition as shown in Figs. 8 and 9; and
2. Adiabatic boundary conditions where insulated wooden blocks replaced the cooled supports shown.

Thermocouples were installed on both the inner and outer propellant faces in contact with the supporting members as well as in the center of the propellant samples. The constant strain amplitude tests were run with a 45 c/s sinusoidal input of 2.5 per cent nominal peak strain value. The input strain and the output strain and force were recorded. The real, G', and imaginary, G'', parts of the dynamic modulus were calculated from the above measurements using the observed phase angle.

The results of the test, including the loss tangent, tan ϕ, are shown in Fig. 10 for the adiabatic case and in Fig. 11 for the isothermal condition. It will be noted that the temperature at all points in the adiabatic condition rise rather

rapidly from $+70°F$ to $+150°F$ in less than an hour. The outer boundary temperatures lag the other temperatures, indicating either a non-ideal test geometry for adiabatic conditions or a variation in the strain distribution through the sample.
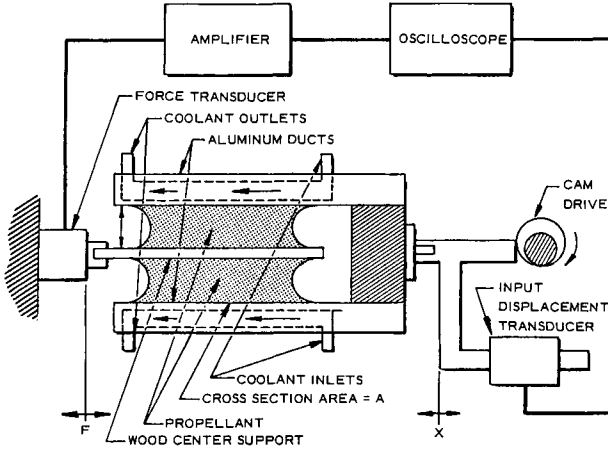

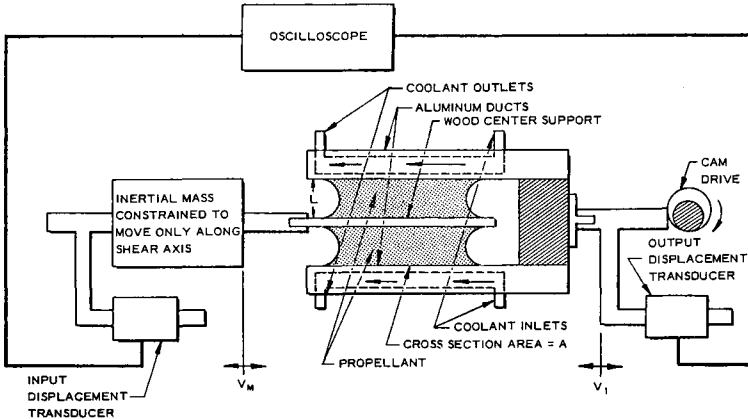FIG. 8. Schematic of constant shear–strain amplitude test device.

FIG. 9. Schematic of inertial test device.

The inertial loading test results show the ratio of output amplitude, V_M, and input amplitude, V_I, where the input amplitude was the same as in the previous tests (0.0246 in. peak). The inertial weight equalled 25.1 lb and the test was conducted at 18.6 c/s. (An amplitude ratio of 1.0 produces a 2.46 per cent strain in the sample.) The adiabatic condition is shown in Fig. 12 and the isothermal results are given in Fig. 13. Both sets of isothermal data show good control of the outer boundary temperature over the duration of the test.

Figure 14 [46] shows, perhaps more clearly, the results of another isothermal test of longer duration. Rather interestingly, the value of the reciprocal scaled

diffusivity, which is also approximately 60 min for this sample, coincides with the temperature equilibrium time, t_{90}, on the graph.

The point to be made here is that the rather rapid temperature changes that
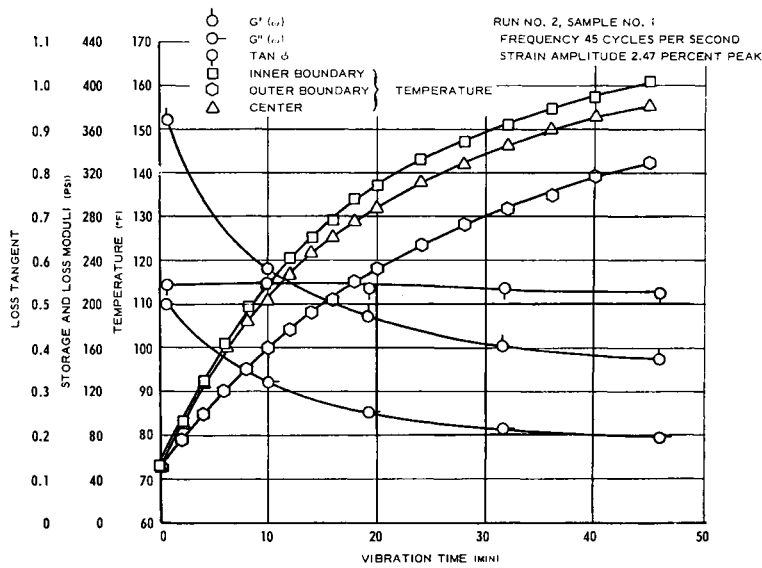
FIG. 10. Thermomechanical response, constant strain amplitude excitation, adiabatic boundary conditions, PBAA propellant.
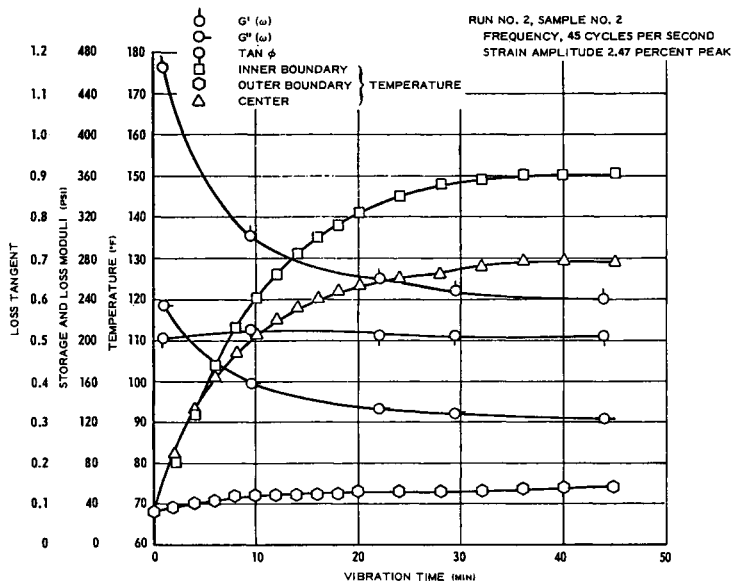
FIG. 11. Thermomechanical response, constant strain amplitude excitation, isothermal boundary conditions, PBAA propellant.

result with a 2.5 to 5 per cent oscillatory strain input on a real propellant sample
(40°F in 10 min and above 80°F in less than an hour) are equaled by a step-
temperature input of the same magnitude on a 1-in. web motor case ($\bar{\kappa}^{-1} = 60$
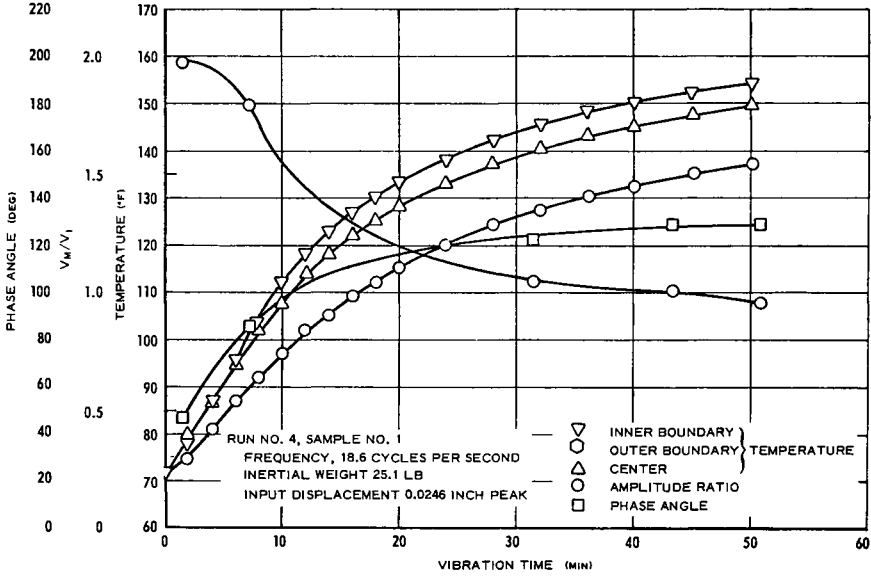
FIG. 12. Thermomechanical response, inertial loading, adiabatic boundary conditions,
PBAA propellant.
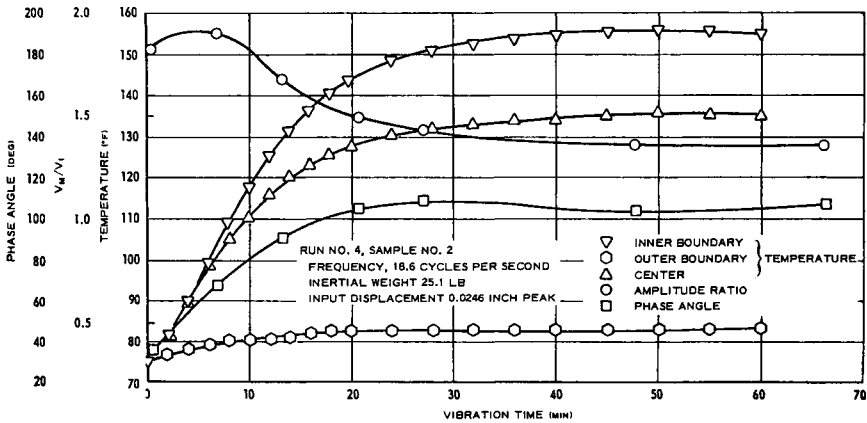
FIG. 13. Thermomechanical response, inertial loading, isothermal boundary conditions,
PBAA propellant.

min) but are far more rapid than can be achieved throughout larger web fraction
motor grains. Thus the thermo-mechanically coupled response associated with
solid propellant motor grain vibration is indeed a real problem requiring solu-
tion. At this time there is, to the author's knowledge, no published solution for
even simple grain geometries.
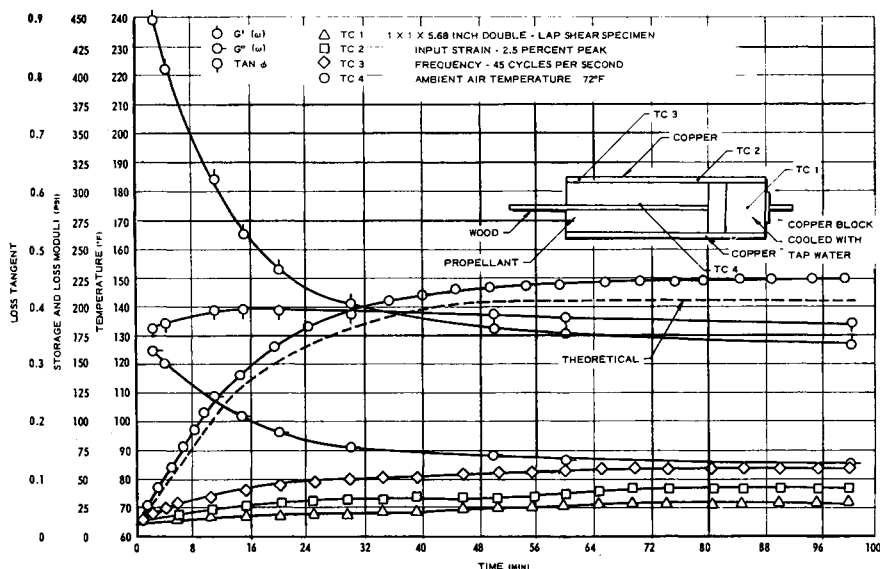
FIG. 14. Dynamic heating, isothermal boundary conditions, PBAA propellant.

5. NONLINEAR BEHAVIOR

Highly loaded solid propellant formulations generally exhibit two types of nonlinearities:

- ● Kinematic or geometric nonlinearity
- ● Material or physical nonlinearity

The subject of kinematic nonlinearity, occasioned by large deformation gradients, has been dealt with in theory by Green, Rivlin, and Spencer in various volumes of the *Archive for Rotational Mechanics and Analysis* as well as by Noll in the same publication. Eringen [34] and Bernstein [48] cover the various aspects of the subject quite well. Lianis [35], Pipkin and Rivlin [36], and Ko and Blatz [37] cover the problem of small deformations superposed on large deformations in materials with fading memory. In most of these formulations, a nonlinear constitutive equation with a single hereditary integral suffices even if certain simplifying assumptions must be made to obtain the single integral form.

From a solid rocket engineer's point of view, the necessity to apply the above results is somewhat limited. The reasons are rather straightforward:

- ● Modern high energy, hence high solids-loaded propellants, are limited to extension ratios much less than 1.5.
- ● Long-term strains are not permitted to exceed 10 or 20 per cent (the case of long-term thermal strains greater than 10 per cent is generally handled by a stepwise calculation equivalent to the historic Hencky or natural strain).

- Gravitational slump deformation gradients are generally kept much below the 10 per cent level because the ensuing grain surface distortion could and would effect ballistic performance.
- Lastly, it just does not appeal to the designer's esthetic sense to see large deformations in a rocket grain.

There are specific areas, unseen by the eye of the sometimes less than wary designer, where large deformation gradients can indeed occur. These regions are usually in the vicinity of grain discontinuities where mathematical singularities arise in the solution of the governing equations. Most of these singular regions are long term in nature and, hence, fall into the realm of finite elasticity rather than finite viscoelasticity as a problem area. In actual design practice, the singularities occurring at grain boundary discontinuities are removed from the propellant material. This is done by the insertion of local, highly compliant rubber relief flaps or boots. The problem is thus simply avoided with respect to the propellant. By using relief flaps, material with 800 per cent strain capability, the entire problem becomes one of large deformation gradient rubber elasticity.

The situation with respect to intrinsic material nonlinearity or physical nonlinearity is quite different. Studies of very highly loaded propellants (85 to 90 per cent solids by weight, 70 to 80 per cent by volume) over a $-24°F$ to $+174°F$ temperature range [33] have shown marked nonlinearities in the deformation gradient or strain range from 1 to 5 per cent in relaxation tests. Conversion of this relaxation data to complex compliance moduli and subsequent comparison with dynamic measurements in the 6×10^{-3} per cent strain range were rather discouraging. The discrepancy increases at lower frequencies and higher temperatures. In addition, the time–temperature superposition of the data was found to be poor.

Theoretical developments applicable to intrinsic material nonlinearities have been rather more sparse for hereditary materials than the developments for finite deformations. Some of the applicable theories may be found in Truesdell [38], Ward and Onat [39], and Dong [40]. The general approach appears to have been treated in depth initially by Green and Rivlin in their now classic 1957 paper [41]. In general, the above mentioned papers demonstrate for example, that the one dimensional nonlinear equivalent to eqn. (13) can be approximated by:

$$\sigma(t) = \sum_{n=1}^{n} \int_{-\infty}^{t} \int_{-\infty}^{t} \dots \int_{-\infty}^{t} G_n(t - \tau_1, \dots, t - \tau_n) \, \dot{\epsilon}(\tau_1) \dots \dot{\epsilon}(\tau_n) \, d\tau_1 \dots d\tau_n$$

$$(5.1)$$

or

$$\sigma(t) = \int_{-\infty}^{t} G_1(t - \tau_1) \, \dot{\epsilon}(\tau_1) \, d\tau_1 + \int_{-\infty}^{t} \int_{-\infty}^{t} G_2(t - \tau_1, t - \tau_2) \, \dot{\epsilon}(\tau_1) \, \dot{\epsilon}(\tau_2) \, d\tau_1 d\tau_2$$

$$+ \iiint_{-\infty}^{t} G_3(t - \tau_1, t - \tau_2, t - \tau_3) \, \dot{\epsilon}(\tau_1) \, \dot{\epsilon}(\tau_2) \, \dot{\epsilon}(\tau_3) \, d\tau_1 d\tau_2 d\tau_3 \dots$$

It readily becomes apparent that the experimental determination of the above relaxation functions requires the strain, ϵ, to be applied at n discrete times for example, or the use of n different generalized loadings.

In spite of the obvious experimental difficulties involved, Lifshitz [42] has conducted such tests on polyethylene. Lockett and Gurtin [43] have described methods for applying oscillatory loadings for the determination of the G_n, and Huang and Lee [44] have applied the methods to short time ranges using polypropylene data.

As Dong [40] has illustrated in his thesis, a linear material function, $G(\tau_1)$, may be described by a single curve with respect to one time coordinate. A nonlinear second order function, $G(\tau_1, \tau_2)$, is describable by a surface with respect to two time coordinates; and a third order function, $G(\tau_1, \tau_2)$, is describable by a four-dimensional hypersurface with respect to three time coordinates; and so on. If one were now to add the concept of nonlinear thermoviscoelasticity as discussed by Koh and Eringen [45] the situation would indeed become complex.

Previously published work by Cantey et al. [33] demonstrated that the shift factor, a_T, was identical to the experimentally determined dielectric shift factor, b_T, where b_T was based on shifting the dielectric dispersive loss parameters. Some preliminary observations indicate that the optical birefringence also has a shift factor, c_T, possibly identical to a_T. However, the actual curves of mechanical relaxation or retardation, dielectric relaxation or loss, and birefringence in relaxation or creep while quite grossly similar are definitely not identical, Even the symmetries of the curves are not similar as can be readily seen for birefringence and mechanical relaxation in the papers of Theocaris [31] and Williams and Arenz [50]. In Fig. 15, Theocaris most nicely shows this lack of symmetry between birefringence and mechanical properties for a cold setting epoxy polymer. Figure 15 quite nicely illustrates the hazard of using the approximate relation between creep and relaxation where

$$[E_{\text{relax}}(t)][D_{\text{creep}}(t)] = 1.0$$

Zener [51] has shown that

$$[E_{\text{relax}}(t)][D_{\text{relax}}(t)] \leq 1.0$$

and Fig. 15 demonstrates that the value of the product can be as low as 0.15.

It should, therefore, prove most interesting to compare the thermo-mechanical nonlinearities under varying load histories with, say, the dielectric response under the same load histories. The comments by Truesdell [52] relative to the need for a "theory of theories" to determine the proper nonlinear formulation invoking the principle of equipresence are certainly applicable here. (See also Eringen [34].)

Needless to say, the state of the art in solid propellants is such that no real attempts have been made to characterize propellants by the methods briefly outlined above. The problem of severe nonlinearity is present in the material, but no applications to solid rockets have yet been published. The real state of

Creep and relaxation contraction ratio of linear viscoelastic materials
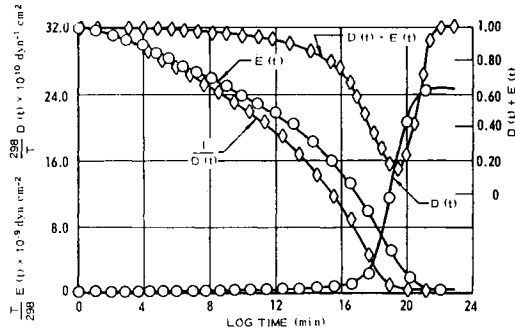
Master Curves of the Extension Creep Compliance and Relaxation
Modulus as Well as of the Product of These Functions for the Pure
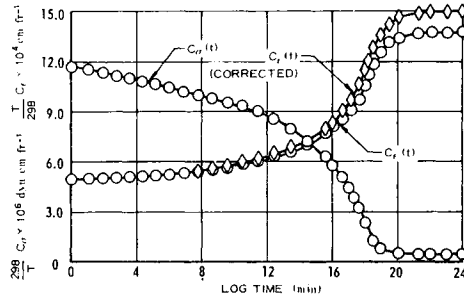Cold-Setting Epoxy Polymer C-100-0-8

FIG. 15. Curves of the stress- and strain-optical coefficients for C-100-0-8.

analytical capability of the solid propellant industry is most aptly summarized
in the survey paper by Williams [49].

6. SUMMARY

The applicable constitutive equations for materials with memory are com-
mented upon. Their applicability and limitations for solid propellants are noted.
The rather pronounced thermo-mechanical coupling effects in solid propellants
are demonstrated and the lack of suitable analytical methods for solid rockets
is pointed out. The uncoupled thermo-mechanical problem is discussed and it
is well in hand analytically. A method for characterizing a given propellant by
a general reduced time for uniform cooling is presented and its implications
for various size motors are discussed. The problem of intrinsic material or
physical nonlinearity for highly loaded solid propellants is discussed and the
lack of use of multiple integral characterization is brought out. Finally, the
principle of equipresence is mentioned as a possible approach to determining
the proper nonlinear formulation for strongly coupled thermo-mechanical non-
linear problems. The engineering aspects of failure criteria are manifold.
Several other papers in this conference will be covering the subject which of
necessity must remain semi-empirical so long as the previous difficulties remain
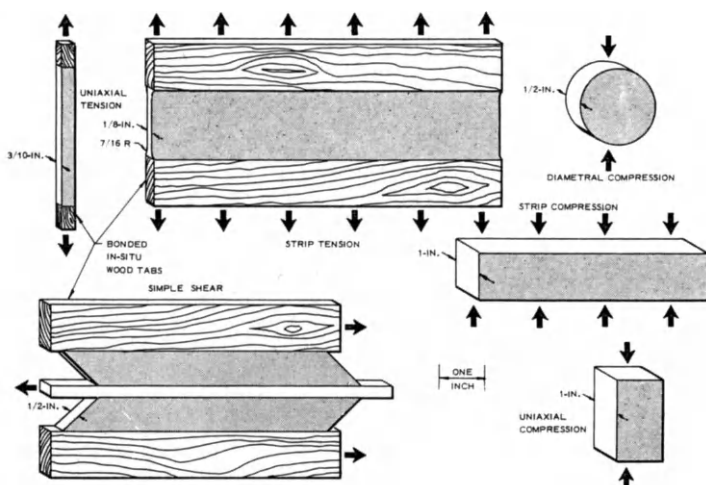
FIG. 16. Test specimens.
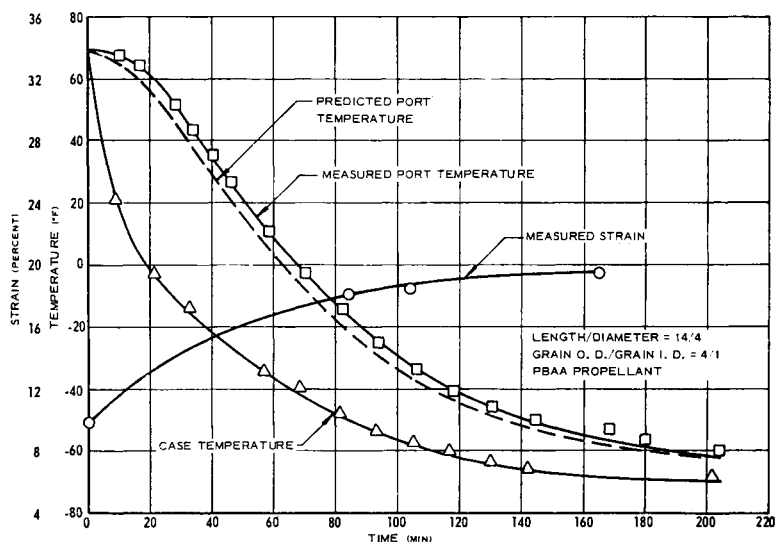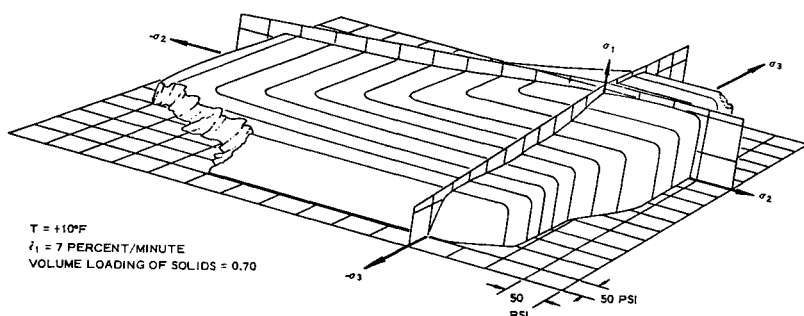

FIG. 17. Analog motor test data.

FIG. 18. Failure surface for PBAN propellant.

unresolved. At this point in time, the best engineering failure theory is one based on similitude in its experimental determination for solid propellant motors.

Multi-axial tests of propellants presently used are shown in Fig. 16. The results plotted in stress space are shown in Fig. 18. It is not implied here that a maximum stress failure criterion is valid. The data are, however, valid and any failure theory should be capable of utilizing them.

REFERENCES

[1] FITZGERALD, J. E., "Some comments on the present status of grain structural integrity analysis", *Proc. 19th JANAF-ARPA-NASA Solid Propellant Group Meeting*, Pittsburgh, Pennsylvania (1962).

[2] ALFREY, T., "Nonhomogeneous stresses in viscoelastic media", *Quart. Appl. Math.*, 2, 113–119 (1944).

[3] LEE, E. H., "Viscoelastic stress analysis", *Proc. First Symposium on Structural Mechanics*, Pergamon Press, Oxford, England, 456–482 (1960).

[4] WILLIAMS, M. L., Jr., *et al.*, *Fundamental Studies Relating to Systems Analysis of Solid Propellants*, GALCIT-101, SM 61-5, Guggenheim Aeronautical Laboratory, California Institute of Technology (1961).

[5] BLAND, D. R., *The Theory of Linear Viscoelasticity*, Pergamon Press, New York, New York (1960).

[6] PARR, C. H., "The application of numerical methods to the solution of structural integrity problems of solid propellant rockets", *Solid Rocket Structural Integrity Abstracts*, GALCIT, 1 (1964).

[7] MUKI, R. and STERNBERG, E., "On transient thermal stresses in viscoelastic materials with temperature-dependent properties", *J. Appl. Mech.*, 28, 2 (1961).

[8] LIANIS, G. and VALANIS, K. C., *The Linearization of the Problem of Transient Thermo-visco-elastic Stress*, Purdue University Report A & ES 62-2 (1962).

[9] VALANIS, K. C. and LIANIS, G., *Methods of Analysis of Transient Thermal Stresses in Thermorheologically Simple Viscoelastic Solids*, Purdue University Report A & ES 62-3 (1962).

[10] JONES, J., FRANCIS, E. and CANTEY, D., *Thermal Grain Structural Analysis*, Lockheed Propulsion Company Reports on Contract AF 04(611)-8013 (1962).

[11] GURTIN, M. E. and STERNBERG, ELI, "On the linear theory of viscoelasticity", *Archives for Rational Mechanics and Analysis*, 291–356 (1962).

[12] APOSTOL, TOM M., *Mathematical Analysis*, Addison-Wesley Publ. Co., Reading, Massachusetts (1957).

[13] TOBOLSKY, A. V. and ANDREWS, R. D., *J. Chem. Physics*, 13, (1945).

[14] FERRY, J. D., *J. Am. Chem. Soc.*, 72, 3746 (1950).

[15] LEADERMAN, H., "Elastic and creep properties of filamentous materials and other high polymers", The Textile Foundation (1943).

[16] WAGNER, K. W. in 1914, discussion remark by G. Gross, *Kolloid Z.*, 134, 197 (1953).

[17] STUART, H. A., *Die Physik der Hochpolymeren*, Springer-Verlag, Berlin (1956).

[18] FRANCIS, E. and CANTEY, D., *Structural Integrity of Propellant Grains*, Lockheed Propulsion Company Report No. 556, Contract DA-04-495-ORD-3260 (1962).

[19] SCHWARZL, F. and STAVERMAN, A. J., *J. Appl. Physics*, 23, 838 (1952).

[20] MORELAND, L. W. and LEE, E. H., "Stress analysis for linear viscoelastic materials with temperature variation", *Trans. Soc. Rheol.*, 4, 223–263 (1960).

[21] FITZGERALD, J. E., *Engineering Methods for Grain Structural Integrity Analysis*, Lockheed Propulsion Company Report 578/556-F-3, Contract No. AF 04(611)-9013 and DA-04-495-ord-3260 (1963).

[22] CANTEY, D., *Solid Propellant Structural Integrity Investigations*, Lockheed Propulsion Company Final Report No. 618-F, Contract AF 04(611)-8539 (1964).

[23] HUANG, N. G., LEE, E. H. and ROGERS, T. G., *On the Influence of Viscoelastic Compressibility in Stress Analysis*, Stanford University Technical Report No. 140 (1963).

[24] STERNBERG, ELI, *On the Analysis of Thermal Stresses in Viscoelastic Solids*, Tech. Report No. 19, Division of Applied Mathematics, Brown University, Cont. Nonr 562 (25) (1963).

[25] TAYLOR, R. L., *Problems in Thermoviscoelasticity*, University of California, Berkeley, California (1963).

[26] JONES, J., FITZGERALD, J. E. and FRANCIS, E., *Thermal Stress Investigation of Solid Propellant Grains*, Vol. 1, *Theory and Experiment*, Lockheed Propulsion Company Report 578–F–1, Contract No. AF 04(611)–8013 (1963).

[27] BOLEY, B. and WEINER, *The Theory of Thermal Stresses*, John Wiley & Sons, Inc., New York (1960).

[28] LEE, E. H. and ROGERS, T. G., *On the Generation of Residual Stresses in Thermo-Viscoelastic Bodies*, Tech. Report No. 139, Stanford University, Contract No. NOw 63–0175c (1963).

[29] PARR, C. H., *Deformations and Stresses in Case-Bonded Solid Propellant Grains of Finite Length by Numerical Methods*, Rohm and Haas Co. Report No. P–61–17 (1962).

[30] FOURNEY, M. E. and PARMERTER, R. R., *Stress Concentrations for Internally Perforated Star Grains*, BuWeps, NAV Weps Report 7758 (1961).

[31] THEOCARIS, P. S., "Creep and relaxation contraction ratio of linear viscoelastic materials", *J. Mech. and Phys. of Solids*, **12**, (1964).

[32] TORMEY, J. F. and BRITTON, S. C., "Effect of cyclic loading on solid propellant grain structures", *AIAA Journal*, **1**, 1763–1770 (1963).

[33] Lockheed Propulsion Company, *Solid Propellant Structural Integrity Investigations: Dynamic Response and Failure Mechanisms*, Contract No. AF 04(611)–9953 (1965) and earlier reports on same contract.

[34] ERINGEN, A. C., *Nonlinear Theory of Continuous Media*, McGraw Hill, Inc. (1962).

[35] LIANIS, G., *Small Deformations Superposed on an Initial Large Deformation in Finite Linear Viscoelastic Material*, University of Washington Report 03–4 (1963).

[36] PIPKIN, A. C. and RIVLIN, R. S., "Small deformations superposed on large deformations in materials with fading memory", *Archive for Rational Mechanics and Analysis*, **8** (1961).

[37] KO, W. L. and BLATZ, P. J., *Application of Finite Viscoelastic Theory to the Deformation of Rubberlike Materials*, GALCIT SM 64–4 (1964).

[38] TRUESDELL, C. and TOUPIN, R., "The classical field theories", *Handbuch der Physik*, Springer-Verlag, Berlin, **3** (1960).

[39] WARD, I. M. and ONAT, E. T., "Non-linear mechanical behavior of oriented polypropylene", *J. Mech. and Phys. of Solids*, **11** (1963).

[40] DONG, R., *Studies in Mechanics of Nonlinear Solids*, Ph.D. Thesis, University of California, UCRL–12039 (1964).

[41] GREEN, A. E. and RIVLIN, R. S., "The mechanics of non-linear materials with memory, I", *Archive for Rational Mechanics and Analysis*, **1** (1957).

[42] LIFSHITZ, J. M., *Multiple Integral Representation of Mechanical Behavior of Polyethylene*, Brown University Report No. 10, Cont. Nonr 562(30) (1964).

[43] LOCKETT, F. J. and GURTIN, M. E., *Frequency Response of Non-linear Viscoelastic Solids*, Brown University Report C11–90, Nonr 562(10) and (30) (1964).

[44] HUANG, N. C. and LEE, E. H., *Nonlinear Viscoelasticity for Short Time Ranges*, Stanford University Technical Report Nol 151, Cont. Nonr. 225(69), (1964).

[45] KOH, S. L. and ERINGEN, A. C., "On the foundations of non-linear thermo-viscoelasticity", *Int. J. Engng. Sci.*, **1** (1963).

[46] JONES, J. and CANTEY, D. C., *Investigations of Propellant Dynamic Response, Viscoelastic Linearity and Thermorheological Behavior*, Lockheed Propulsion Company Research Report T.N. 113 (1964).

[47] JONES, J. W. and FITZGERALD, J. E., *Thermal Grain Structural Analysis*, Lockheed Propulsion Company Report No. 578–P–13, Contract No. AF 04(611)–8013 (1963).

[48] BERNSTEIN, B., KEARSLEY, E. A. and ZAPAS, L. J., "A study of stress relaxation with finite strain", *Trans. Society of Rheology*, **7**, 391–410 (1963).

[49] WILLIAMS, M. L., "Structural analysis of viscoelastic materials", *AIAA Journal*, 785–808 (1964).

[50] WILLIAMS, M. L. and ARENZ, R. J., "The engineering analysis of linear photoviscoelastic materials", *Journal of Experimental Mechanics* (1964).

[51] ZENER, C., *Elasticity and Anelasticity of Metals*, University of Chicago Press, Chicago (1948).

[52] TRUESDELL, C., "Modern theories of materials", *Trans. Soc. Rheology*, **4**, (1960).

RECENT ADVANCES IN SOLID PROPELLANT BINDER CHEMISTRY*

K. KLAGER and J. M. WRIGHTSON

Aerojet-General Corporation
Sacramento, California

Abstract—Modern solid propellants have three basic components: an organic elastomeric binder, a solid oxidizer, and a metallic fuel additive. The binder is the continuous matrix of the system and has a primary effect on the ballistic and mechanical properties.

Because of the complexities of the thermodynamic calculations, high-speed computers are used for propellant performance calculations. The general method of calculation and the resulting performance curves illustrate the potential for various polymeric binder materials.

The mechanical behavior of the propellant depends on the number of crosslinks and the number of dangling chains in the polymeric binder and its interaction with the solid ingredients. Approaches have been made toward achieving an ideal polymer network by using bifunctional prepolymers and bifunctional or trifunctional curing agents with a minimum of monofunctional materials and absence of side reactions. Evidence indicates that failure in strained solid composite propellants starts in the binder phase by the formation of voids and propagates to the solid materials. "Bonding agents" designed to increase the modulus of the binder in the immediate vicinity of the solid ingredients has proved to be very useful in forestalling the propagation of voids, which ultimately leads to complete "dewetting" and the irrecoverable loss of mechanical properties.

1. INTRODUCTION

1.1. Solid Propellant Description

A solid propellant is a complex and stable mixture of oxidizing and reducing ingredients which, when ignited, burns in a controlled manner to form predominantly very hot, low-molecular-weight gases. The tremendous increase in volume resulting from formation of the hot, low-molecular-weight gases and the great increase in temperature provide the kinetic energy which is released through the exhaust nozzle of the solid-rocket motor. The solid propellant can be either homogeneous or heterogeneous depending on the ingredients. A propellant prepared from nitroglycerin and nitrocellulose is homogeneous and is commonly referred to as a *double base propellant*. The oxidizing and reducing functions are contained within the same molecule and the nitroglycerin plasticizes the high-molecular-weight nitrocellulose to yield a rubbery mass. Modern solid composite propellants are heterogeneous and consist of three basic components: an organic polymer which serves as both a binder and gas-forming, combustible fuel, a solid oxidizer (which may also contribute to gas formation), and a combustible metal additive, which provides the primary source of thermal energy. The binder can also contain, in its molecular structure, oxidizing

---

groups similar to those in double base propellants. Indeed double base propel-
lant, in some cases, actually becomes the binder. The most energetic solid
propellants result when the oxidizing and reducing agents exist in discrete
molecules. Thus, from the standpoint of energy potential, the best binders are
the hydrocarbons, such as polybutadiene, and the best fillers are inorganic
oxidizers, such as ammonium perchlorate, and fuels, such as aluminum metal.

1.2. *General Considerations*

Modern solid rockets are propelled by motors in which the heterogeneous or
homogeneous propellant is bonded to the chamber wall (case-bonded) and com-
bustion takes place in the internal bore of the grain. This discussion deals
mainly with binder polymer chemistry as applied to these motors and how it is
influenced by ballistic and mechanical property requirements. Figure 1 is a
diagram of a case-bonded solid rocket motor and indicates the three major
areas in which propellant chemists are contributing vital information.
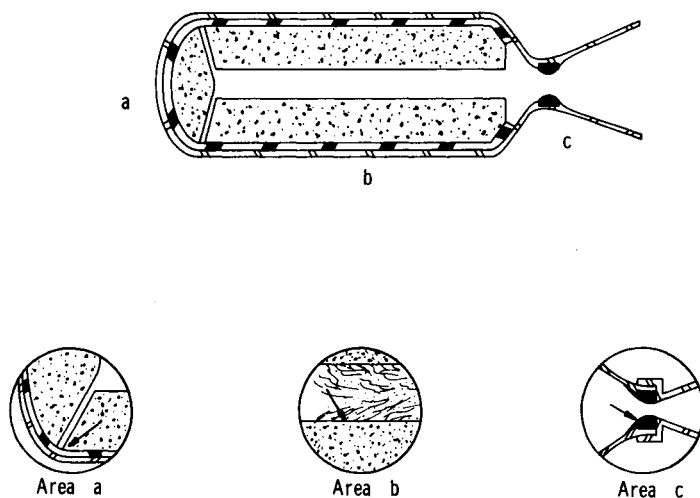
FIG. 1. Rocket motor areas of critical interest to the chemist.

Area "a" shows the fore end of the case-bonded motor, in which the case-
bonded system is most apt to fail because of the concentration of strain in the
propellant and insulating liner. Failure, usually in the propellant, can be either
adhesive or cohesive. The same considerations apply to the aft end of the motor
which is similarly constructed.

Strain in the propellant and liner has two principal independent causes. First,
a strain within the bonded propellant charge (grain) can be induced by pro-
pellant shrinkage during cure. In current practice, the cure reaction is carried
out under conditions which result in essentially no strain in the grain at ambient
temperature. The cure reaction will be discussed in detail later, but at this point

it should be remarked that the reaction must be efficient. The optimum mechanical properties of the elastomeric binder in the propellant must be obtained by forming the least number of chemical bonds so as to insure minimum shrinkage of the propellant during cure.

The second and most important cause of strain is the difference in thermal expansion between the chamber, the insulating material, and the propellant which are all bonded together in the motor. For example, when a steel chamber is used with conventional solid propellants, the coefficient of thermal expansion for the propellant can be 10 to 13 times greater than that of the chamber. The environmental temperature, except for very large motors, is usually not controlled. It is not unusual to test and to expect the motor to operate over a temperature range of -75 to $+180°F$. If the propellant loses its elastomeric properties at low temperature, it will become brittle and may fracture because of induced tensional strain resulting from differences in thermal contraction or because of the sudden compressive strains produced by rapid pressurization of the motor during ignition of the propellant surface.

Area "b" depicts the burning of the propellant. The chemistry of combustion is a fascinating and important field of investigation, and has been the subject of many publications.* This subject is beyond the scope of this discussion. However, a few general comments are in order. Propellants are formulated to burn at specified rates required for the particular designed operating pressure of a motor. This enables the rocket engineer to program the motor's thrust and duration. The factors which control the combustion parameters, such as burning rate, change of burning rate with pressure (pressure exponent), change in burning rate with propellant temperature (temperature coefficients), and extinguishment are generally understood and controlled empirically. However, the detailed burning mechanism in solid rocket motors is not completely understood and is a very active area of investigation. The type, particle size, and concentration of oxidizer all have a direct influence on burning rate. With ammonium perchlorate, the burning rate increases with decreasing particle size and increasing concentration. Many metals and their oxides or salts act as burning accelerators.

Area "c" is a sketch of the throat area of the motor nozzle. The material used for throat insert depends on the flame temperature and the erosive and/or corrosive effect of the exhaust gases. Erosion of carbon throat inserts can sometimes be directly attributed to the chemical reaction of certain species in the exhaust gas. These reactions are discussed in detail in reports by the Union Carbide Research Institute [2].

1.3. Selection of Oxidizer

Selection of the oxidizer for composite solid propellants must necessarily be limited to those that are produced or can be produced in large quantities by the chemical industry. The best oxidizer for producing chemical energy for

---

* For example. see M. Summerfield [1].

rocket propulsion is one with the optimum combination of low heat of formation, high density, and reaction with fuels to yield a high number of moles of gaseous products.

Table 1 gives some of the properties of available oxidizers. Selection of which oxidizer to use will depend on the specific solid-rocket motor requirements. Ammonium perchlorate is commonly used for high performance rockets; ammonium nitrate is usually preferable for gas generators and slow-burning propellants.

TABLE 1. PROPERTIES OF AVAILABLE OXIDIZERS

Oxidizer	Available oxygen *vt.* %	Density lb/in^3	Heat of formation kcal/100g	*Moles of gas per 100g
KClO$_4$	46.0	0.090	−32	0
KNO$_3$	39.5	0.076	−118	0.495
NH$_4$ClO$_4$	34.0	0.070	−59	2.55
NH$_4$NO$_3$	20.0	0.061	−110	3.75
LiClO$_4$	60.6	0.087	−86.5	0

* Gas produced by the oxidizer other than that formed by the reaction of oxygen with fuel components.

1.4. Selection of Fuel

The binder which is the continuous phase of the propellant is the major reducing agent and gas-producing fuel in the propellant composition. It must be chemically and physically stable in the presence of the ozidizer at normal storage and operating temperatures.

Most modern high-energy solid propellants contain metallic fuels such as aluminum. These metallic fuels increase the chemical energy of solid propellants not only through their highly exothermic reaction with the oxidizer but also because they exclude water vapor from the exhaust product and increase its hydrogen content. Thus, use of metallic fuels prevents energy losses due to the water–gas equilibrium and the dissociation of the water molecule into radicals at the combustion temperature. Although use of metallic fuels produces a large net increase in specific impulse, the metallic oxides formed detract from the efficient conversion of chemical energy to propulsive force by the rocket nozzle. Compared with gases these nongaseous oxides release their heat more slowly (thermal lag) and accelerate more slowly (velocity lag) during the expansion process in the nozzle.

2. SIGNIFICANCE OF THE BINDER

The binder is the elastomeric matrix which contains the oxidizer and metallic fuel particles in composite propellants. Since it is the continuous phase of a solid propellant, the binder must serve a multitude of functions. Besides being the main source of fuel for the propellant, it must bind together the discrete oxidizer and metallic fuel particles to form a tough rubbery mass capable of

withstanding severe strains produced by thermal and mechanical stresses. Therefore, it largely determines the propellant mechanical properties. The binder must be capable of bonding to plastic insulating materials and metal parts of the motor. To achieve optimum mechanical properties, it must also form a tough membrane around each individual oxidizer and metallic fuel particle.

The binder can be formed from linear, either amorphous or crystalline, and crosslinked polymers. The binders used in modern solid propellants are formed from crosslinked and from linear crystalline polymers. Table 2 summarizes the chemistry of propellant binders by dividing them into two categories—cured and uncured. The cured propellants are further separated into two categories depending on whether the cure mechanism is a chemical crosslinking or physical plasticization and swelling of crystalline linear polymers.

TABLE 2. TYPES OF PROPELLANT BINDERS AND THEIR CURE SYSTEM

Cured				Uncured
Chemical		Physical		
Prepolymer	Curing agent	Prepolymer	Swelling agent	
Vinyl polyester	Hydroperoxides	Nitrocellu-lose	Nitroglycerin or other fluid nitrato esters	Asphalt
Hydroxy terminated polyesters and poly-ethers	Isocyanates	Polyvinyl chloride	Ester plasticizers	Polyisobutylene
Carboxy terminated polybutadiene	Aziridines Epoxides			
Polysulfides	Metal oxide and epoxides			
GRS & GRI rubbers	Sulfur or other standard rubber cure systems			

Many of the binders and prepolymers listed are not sufficiently fluid at normal processing temperatures to use the preferred simple fluid propellant casting technique. Therefore, special processing techniques and equipment must be devised. Table 3 relates the processing technique to the structure of the binder.

After the propellant has been cast and cured in a motor, the dimensional stability of the propellant, or grain integrity, under motor operational conditions of temperature, vibration and acceleration etc., becomes extremely important. Propellants prepared with a linear amorphous polymer have very poor dimensional stability at temperatures of 160°F or higher. At higher temperatures, propellants with polycrystalline binders have poor dimensional stability because the polymer crystallites dissolve in the plasticizer. The chemically crosslinked

TABLE 3. PROPELLANT PROCESSING TECHNIQUES RELATED TO BINDER STRUCTURE

Structure	Process	Example
Linear Polymer		
Amorphous	Casting (hotmelt)	Asphalt
	Extrusion (hot)	Polyisobutylene
Polycrystalline	Casting and curing by fusion through swelling agents (plastistol)	Polyvinylchloride Nitrocellulose
	Extrusion (hot)	
Crosslinked	Casting and curing by polymerization	Polysulfide Polyurethane Carboxy-terminated polybutadiene GRS and GRI rubbers

polymers yield propellants with the best thermal stability and do not show any abnormal behavior until chemical degradation of the binder starts.

Most current high energy composite solid propellants are prepared with three castable binder systems. These are the chemically crosslinked polybutadiene and polyurethanes and the linear polycrystalline nitrocellulose plastisols.

3. ROLE OF THE BINDER IN SOLID PROPELLANTS

3.1. *Ballistic Considerations*

A typical propellant consisting of polybutadiene binder, ammonium per-chlorate oxidizer, and aluminum metal additive burns with an energy evolution of about 1500 cal/g (under conditions of constant pressure, or zero work). The maximum thermodynamic efficiency of such a propellant depends primarily on the pressure ratio (chamber pressure to exhaust pressure) at which the propellant is fired. This is illustrated in Fig. 2 which shows that, if chamber
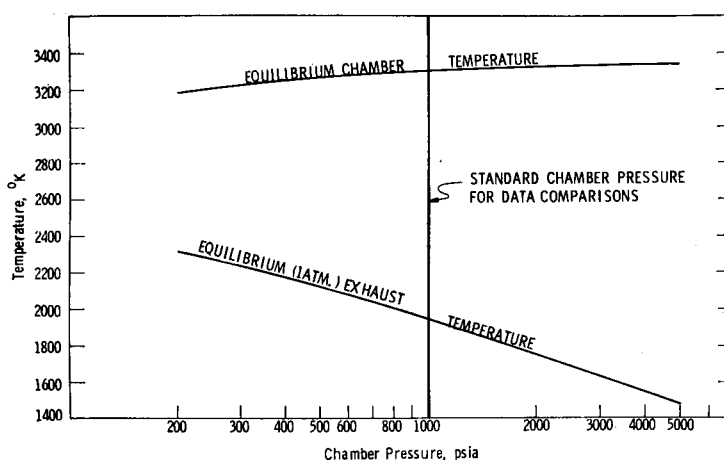
FIG. 2. Variation of equilibrium chamber and exhaust temperatures with chamber pressure (ideal expansion to one atmosphere).

pressure increases while exhaust pressure remains constant at 1 atm (14.7 psia), the equilibrium chamber temperature increases while the equilibrium exhaust temperature decreases. Thus, as P_c/P_e increases, T_c/T_e (and therefore thermo-dynamic efficiency) increases. For data comparison, a standard pressure ratio (1000 : 14.696 psia) is normally used. Under these conditions, roughly 50 per cent of the total evolved thermochemical energy, or about 750 cal/g is converted into kinetic energy.

The unit of comparison used is specific impulse or (pounds-force × seconds/pounds-mass). The theoretical specific impulse is computed from the enthalpy change under equilibrium expansion (both adiabatic and isentropic) from chamber to exhaust pressure [3]:

$$I_s = \sqrt{\frac{2J}{g}} (H_c - H_e)$$

I_s = specific impulse
J = mechanical equivalent of heat
g = acceleration due to gravity
H_c = enthalpy of combustion products in chamber
H_e = enthalpy of combustion products at the exhaust plane.

This is the equation used in computing an exact theoretical I_s. However, since evaluation of this equation involves simultaneous solution of many complex equilibrium constant equations, it is usually accomplished with the aid of high-speed computers.

For rough data comparison a "short method" of calculation has been derived [4]. The basic equations used for these calculations are as follows:

$$I_s = k \sqrt{T_c \cdot N} \quad \text{or} \quad k' \sqrt{\frac{T_c}{M}}$$

N = moles of gas per unit propellant weight
M = average molecular weight of combustion products
T_c = equilibrium flame temperature in the chamber
k, k' = constants

A triangular composition diagram (Fig. 3) for a propellant consisting of aluminum, polybutadiene, and ammonium perchlorate shows lines of constant N (moles of gas per 100 g of propellant) and contours of constant flame tempera-ture. The diagonal solid line across the triangle is the "OMOX" line. This is a line of constant chemical stoichiometry, representing all propellant compositions in which the amount of oxygen present is exactly that required to form CO and Al_2O_3 (no CO_2, H_2O or other oxygen compounds). As the binder content is decreased along either a line of constant oxidizer or constant aluminum content, flame temperature increases while the number of moles of gas decreases. The optimum combination of flame temperature and gas formation is shown in Fig. 4, which is a triangular diagram for the same system showing contours of constant I_s. In this example, the maximum specific impulse occurs near the
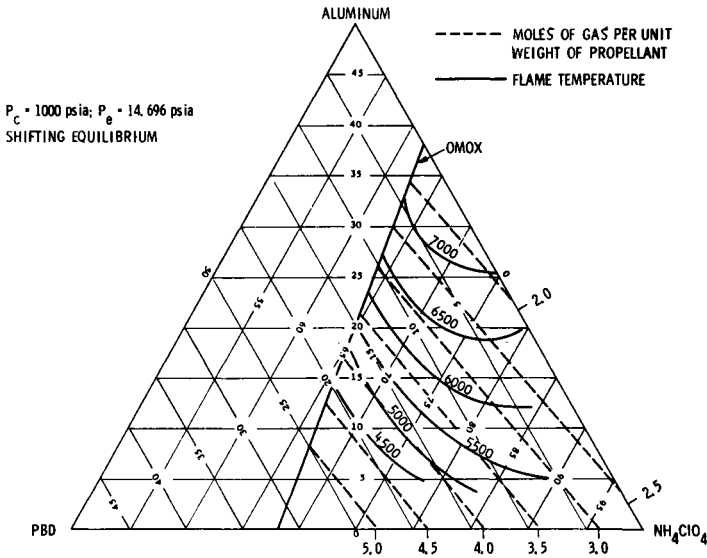
FIG. 3. Composition diagram of chamber flame temperature, °F, and moles of gas per unit weight of propellant, for ammonium perchlorate–aluminum–polybutadiene propellant.
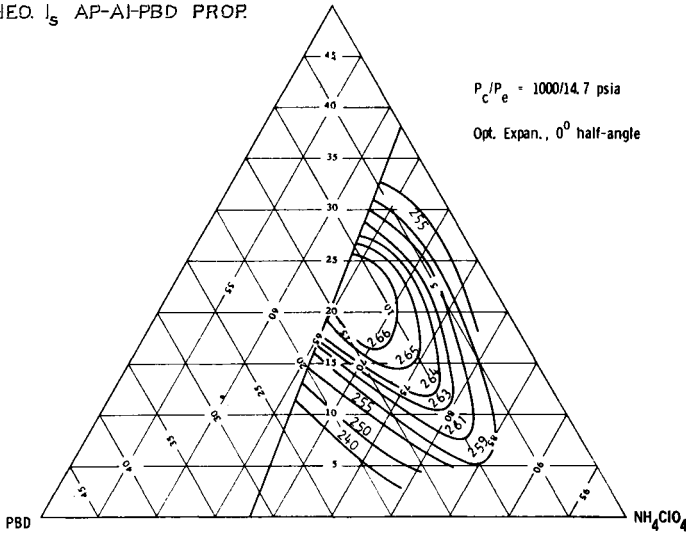

FIG. 4. Theo. I_s: AP–Al–PBD prop.

OMOX line at some point between 15 per cent and 10 per cent binder (85 to 90 per cent solids).

Figure 5 shows a comparison of typical binder types in propellant systems containing typical types of binder with aluminium and ammonium perchlorate. As we move from the pure fuel polybutadiene to binders containing increasing

amounts of oxygen, peak I_s is reached at progressively lower solids loadings. Polybutadiene is a better fuel than polyurethane, showing a peak I_s approximately three units higher; however, the solids loading required to reach the peak I_s imposes problems in propellant processing. When nitroplasticizers of high oxygen content are added to polyurethane, the magnitude of the peak I_s does not change but is achieved with a lower portion of solid oxidizer. The use of
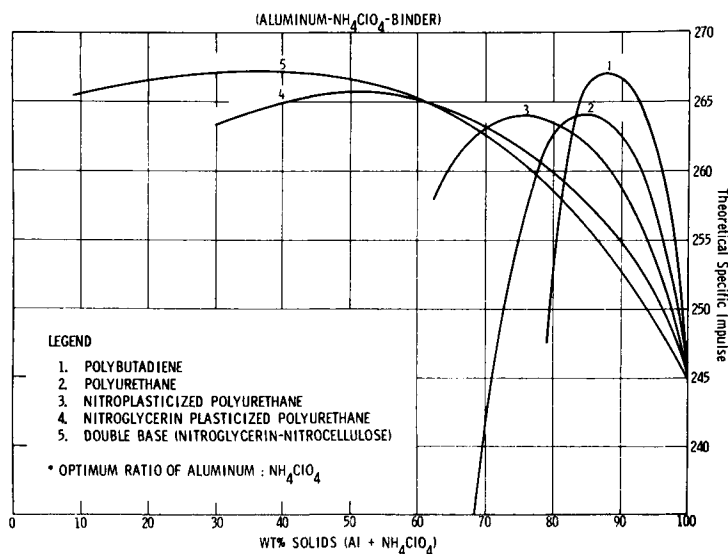
FIG. 5. Theoretical specific impulse vs. WT per cent solids.

nitrate plasticizers and polymers such as nitroglycerin and nitrocellulose not only shifts the peak I_s to a lower solids loading, but also increases the peak value (compared with polyurethane). The disadvantage of propellant systems with peak I_s at low solids loadings is lower density and consequently lower impulse per unit volume.

3.2. Mechanical Properties

As noted previously, the elastomeric binder that holds together the solid oxidizer and fuel phases is a high polymer. For the purposes of this discussion, a high polymer is a material composed of molecules with high-molecular-weight (> 1000) structural units chemically bound in a repeating pattern. Figure 6 illustrates schematically the arrangement of repeating units in large molecules. The pattern may be linear, as shown at the top of the figure, or crosslinked as at the bottom. The linear polymer contains long chains which are not interconnected, but can slip past each other. The crosslinked polymer containing random interchain connections achieves greater dimensional stability. When the interchain connections are few, the polymer is elastomeric. It may be deformed by an applied stress, but recovers its original dimensions when the stress is released.

LINEAR POLYMER

A—A + B—B· —►-A—A-B—B-A—A-B—B-A—A-B—B-A—A-B—B-

CROSS LINKED POLYMER

A—A + A—A + B—B —►
        |
        A
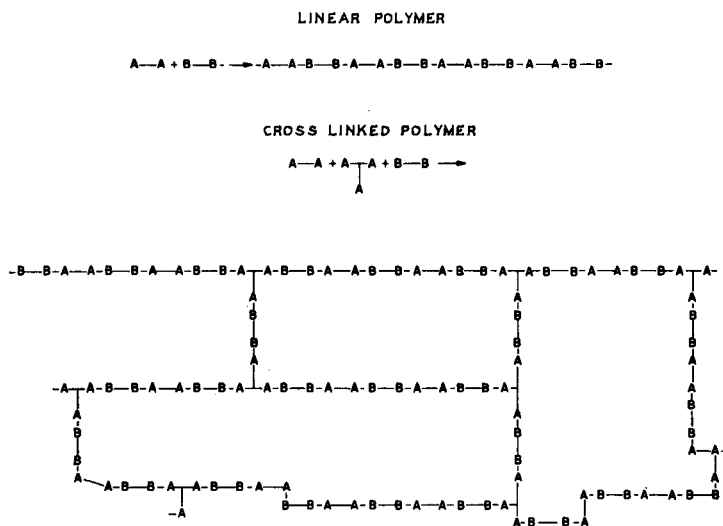
FIG. 6. Polymer formation.

For example, a polyurethane binder can be diagramed (Fig. 6) with A—A, A—A, and B—B representing, a diol, a triol, and a diisocyanate. Each "A"
  |
  A
represents the functional group OH and each "B" the functional group NCO. Reaction of these two groups produces a urethane line (A—B in Fig. 6). Some typical diols, triols, and diisocyanates used to prepare solid propellant binders are given in Table 4.

Some of these ingredients are themselves linear polymers. Since the crosslinked network structure is built up in random fashion, the chains between the branch points vary in length and the resulting network is disordered.

In following discussions we will continue using polyurethane polymers to illustrate the principles involved. The generalizations made are applicable, with proper modifications, to all the types of polymer binders previously mentioned.

The mechanical behavior of the crosslinked polymer depends upon the number of crosslinks in the polymer network and on the number of dangling chains; i.e. chains in which each is attached by only one end to the crosslinked network. The nature of this dependence is illustrated schematically in Fig. 7. At the top of the illustration is a randomly coiled portion of an idealized polymer network before extension. The effect of extending this section of network is shown next. If an additional crosslink is introduced into the network, the network is no longer capable of the original extension. Some crosslinking must be introduced to prevent the plastic flow which would readily occur under the influence of pressure and heat in a purely linear polymer. The result must be a compromise to obtain some reinforcement while allowing reasonable extension. To prevent excessive crosslinking, the branching of the polymer is accomplished by the use of trifunctional ingredients, since trifunctionality is the lowest func-

TABLE 4. TYPICAL INGREDIENTS USED FOR PREPARATION OF POLYURETHANE
BINDERS

$H(OCH_2CH_2CH_2CH_2)_nOH$	Poly-(1,4-oxybutylene) glycol
$H(OCH_2CH)_nOH$	Polypropylene glycol

$$CH_3$$
$$HOCH_2C(CH_3)CH_2[OCO(CH_2)_7COOCH_2C(CH_3)_2CH_2]_nOH \quad \text{Poly (neopentylglycol azelate)}$$

$HO(C_4H_6)_nOH$	Hydroxy-terminated polybutadiene

$$CH_2OH$$
$$|$$
$$CH_3CH_2CCH_2OH \qquad \text{Trimethylolpropane}$$
$$|$$
$$CH_2OH$$

$$CH_3$$
$$|$$
$$CH_2(OCH_2CH)_xOH$$
$$|$$
$$CH_3CH_2CCH_2(OCH_2CH)_mOH \qquad \text{Poly-(proplyene oxide) adduct}$$
$$| \qquad\qquad\qquad | \qquad\qquad\qquad\qquad \text{trimethylolpropane}$$
$$\qquad\qquad CH_3$$
$$|$$
$$CH_2(OCH_2CH)_nOH$$
$$|$$
$$CH_3$$

$$OCN(CH_2)_6NCO \qquad\qquad \text{Hexamethylene diisocyanate}$$

2,4 Tolylene diisocyanate

tionality which will allow crosslinking. The crosslink density, branch points per cc, is further controlled by varying the ratio of bifunctional to trifunctional units. In this manner, the mechanical behavior of the solid propellant may be varied over a wide range.

Extensibility is also diminished if a considerable amount of the material of the network section consists of dangling chains, as shown at the bottom of the figure. The dangling chains may come from many sources. Some of these are: (1) Presence of monofunctional impurities in the starting materials, (2) excess of any of the functional groups, and (3) loss of functional groups by side reactions which do not contribute to the elastomer formation.

The chemistry of building the network must be directed toward the reaction of bifunctional units in exactly a one-to-one relationship to achieve long chains while introducing a small number of multifunctional units to join the linear chains into a crosslinked network. The factors which interfere most with attaining this ideal structure are (1) impurities which consume functional units in non-network building reactions, (2) the variability in functionality of the structural

FIG. 7. Schematic representation of binder network behavior.

units being used to construct the network, and (3) incomplete reaction, which increases the number of dangling chains.

A typical effect of an impurity which consumes functional groups without contributing to the formation of the network is shown below. This illustrates the reaction of moisture with isocyanates. [5].

REACTION OF ISOCYANATE WITH WATER

$$RNCO + H_2O \longrightarrow RNHCOOH \xrightarrow[\text{$-CO_2$}]{} \begin{array}{c} \text{$\xrightarrow{RNCO}$ (RNHCO)$_2$O} \\ \text{$\xrightarrow{-CO_2}$ (RNH$_2$)$_2$CO $\xleftarrow{RNCO}$} \end{array} RNH_2$$

The water reacts with the isocyanate and eliminates it from possible reaction with the diols and triols. The extent to which these side reactions occur is a function of (1) the relative rates of side reaction and the network-building reaction and of (2) the relative concentration of the interfering impurity.

Table 5 indicates various reactions which may occur with isocyanates and their relative rates [6]. The reaction of isocyanate with hydroxyl groups is favored over reaction with water, but the water reaction rate is competitive enough to be troublesome. All ingredients must be carefully dried to prepare polyurethane propellants and control of the humidity is necessary during mixing and curing of the propellants.

When the bifunctional units A—A and B—B are condensed in the presence of some monofunctional units —A, the chain length of the resulting polymer is

TABLE 5. REACTION RATE CONSTANTS AT 100° C FOR
2,4-TOLYLENE AND HEXAMETHYLENE DIISOCYANATES
WITH VARIOUS FUNCTIONAL GROUPS

Functional group	Rate constant, 1/mole-sec $\times 10^4$	
	TDI	HDI
Amine	36.0	2.4
Hydroxyl	21.0	8.3
Water	5.8	0.5
Urea	2.2	1.1
Urethane	0.7*	0.2*

* 130° C.

shorter than when —A is not present. The effect of the functionality of the A units on the length of the polymer chain can be surmised on theoretical grounds [7].

The effect is shown by the following modified equations:

For condensation of bifunctional units A—A and B—B in the presence of monofunctional impurity —A

$$\bar{X}_n = \frac{r + \dfrac{f}{2}}{2r + f - 2rpf}$$

$\bar{X}_n$ = average number of repeating units in polymer
      (number average degree of polymerization)
r = ratio of A groups to B groups
f = average functionality of the units containing A groups
p = extent of reaction

If $r = 1$ and the reaction is complete ($p = 1$)

$$\bar{X}_n = \frac{1}{2}\left[\frac{2 + f}{2 - f}\right]$$

If $r = 1$ and no monofunctional units are present ($f = 2$)

$$\bar{X}_n = \frac{1}{2(1 - p)}$$

The average degree of polymerization depends upon the ratio of the reacting functional groups, the extent or completeness of reaction, and the functionality of the reacting units. In Fig. 8, the equation is plotted to illustrate the effect of the reactants ratio and of functionality on the average degree of polymerization when the reaction is complete. The curves are symmetrical about $r = 1$, and the peak of each curve is very sensitive to a change in functionality. Figure 9 is an additional plot of the equation, which illustrates the effect of functionality and of the completeness of reaction on the chain length when the number of reacting

groups is equal. The figure shows dramatically how sensitive the chain length is to the extent of reaction.

The divergence of the reactants ratio from a value of one, incompleteness of reaction, and amount of monofunctional impurities all lower the length of the polymer chain. At a reactants ratio of one with complete reaction the chain length (average number of repeating units) is given by the expression $\frac{1}{2}[(2 + f)/2 - f)]$. The chain length is infinite when no monofunctional material is present. When 5 mol. per cent of a monofunctional unit (1 mole in 20) is present, the average number of repeating units in the chain drops to 40.
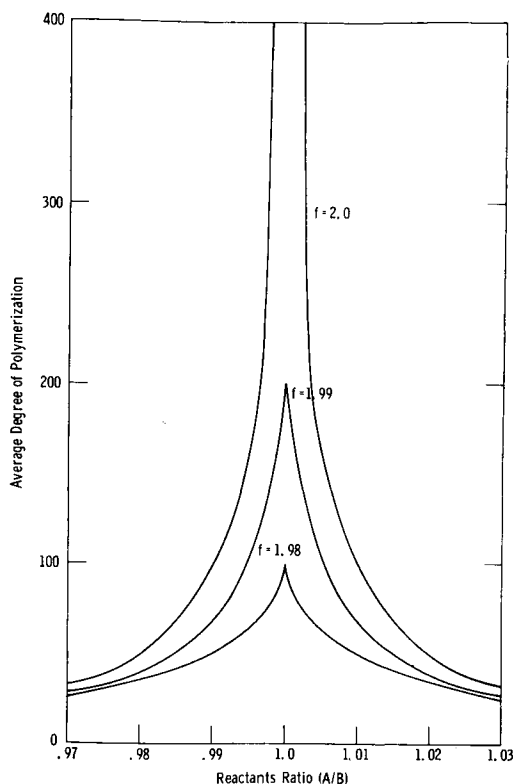
FIG. 8. Effect of reactants ratio on the average degree of polymerization of bifunctional A–A and B–B in the presence of monofunctional –A.

When the functionality of one of the reacting species is greater than two, a combination of A—A and A—⊤—A for example, there is a probability that the
                                        |
                                        A
polymer will be crosslinked into an infinite network. Formation of a network structure is accompanied by the occurrence of a sharp "gel point". At the gel point, which occurs at a well-defined stage during the polymerization, the polymer transforms suddenly from a viscous liquid to an elastic gel. Prior to the gel

point all of the polymer is soluble in suitable solvents and also fusible; beyond the gel point, it is no longer fusible and is not entirely soluble in solvents. These characteristics result from the restraining effects of three-dimensional network structures of infinite size within the polymer.
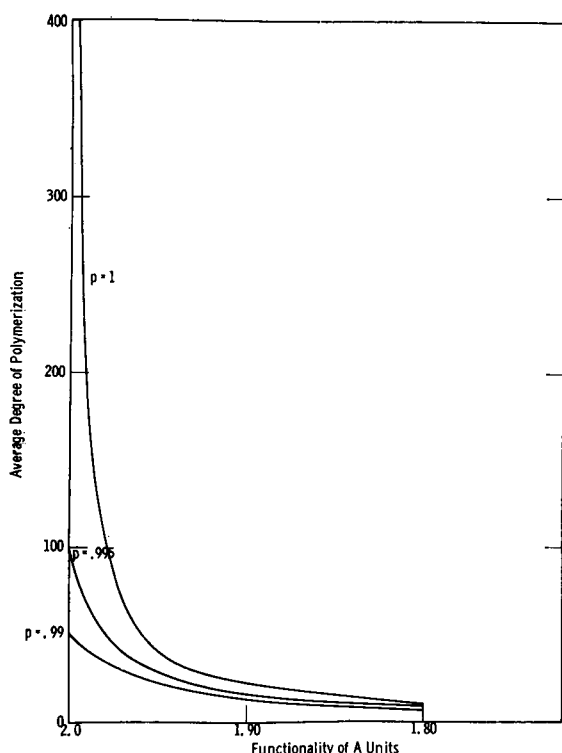
FIG. 9.   Effect of functionality on the average degree of polymerization of bifunctional A—A and B—B in the presence of monofunctional —A.

The probability of forming a crosslinked network and the chance that a given chain terminates in a branch has been treated theoretically [8], as shown in the next equation.

For condensation of A—A, A—$\overset{\overset{\textstyle A}{|}}{\text{A}}$, with B—B

$$\alpha = \frac{rp^2\rho}{1 - rp^2(1 - \rho)}$$

α = probability that chain ends in branch
r = ratio of A groups to B groups
p = extent of reaction
ρ = ratio of A groups in multifunctional unit to total A groups

Gelation occurs when α reaches a critical value α_c

$$\alpha_c = \frac{1}{f-1}$$

f = average functionality of the multifunctional groups

The probability α varies as the reaction proceeds until it reaches a critical value. At the critical value, the probability of branching exceeds that of chain extension, and the polymer rapidly crosslinks into an infinite network. At gelation, the viscosity of the polymer increases rapidly. The relation of the various parameters for polymerization of succinic acid (A—A), tricarballylic acid (A$\underset{\underset{A}{|}}{{}_{\top}}$A). and di-

ethylene glycol (B—B) are shown in Fig. 10 [9]. Here $r = 1.002$ and $\rho = 0.404$; the observed extent of reaction at gelation is 0.894 compared with the calculated 0.843.
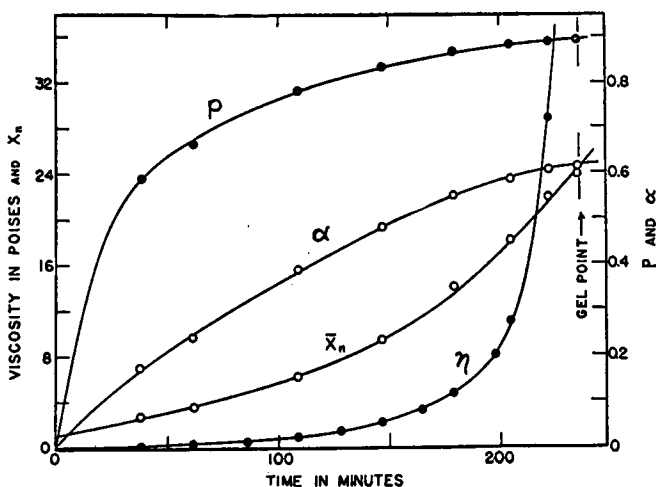
FIG. 10. The course of a three dimensional polyesterification (*Principles of Polymer Chemistry*, P. J. Flory).

The presence of a gel point is important not only because crosslinking is required to obtain a true elastomer but also because of its effects on the processing of a solid propellant. To be castable, a propellant must have a viscosity which will allow it to flow readily for a number of hours after mixing. A polymer which reaches its gel point before the casting is complete would lead to poor consolidation of the propellant in the motor resulting in unreliable ballistic performance.

Both theoretical and practical considerations indicate that the extent of reaction has an important effect on the chain length and degree of crosslinking of a polymer. In turn, the length of the chain and the degree of crosslinking normally determine the mechanical behavior of the polymer. The reaction that leads to the final network structure, complete polymer cure, continues beyond the gelation point.

The completeness of the cure of a solid propellant may be determined in several ways, but one of the better ways is to determine the mechanical properties of the propellant and to consider the reaction complete when these properties become constant. Figure 11 illustrates this point for a typical polyurethane propellant. The nominal maximum stresses for the two propellants illustrated are approaching constant values. The propellant represented by the upper curve may be considered fully cured. The other propellant is approaching a complete cure.
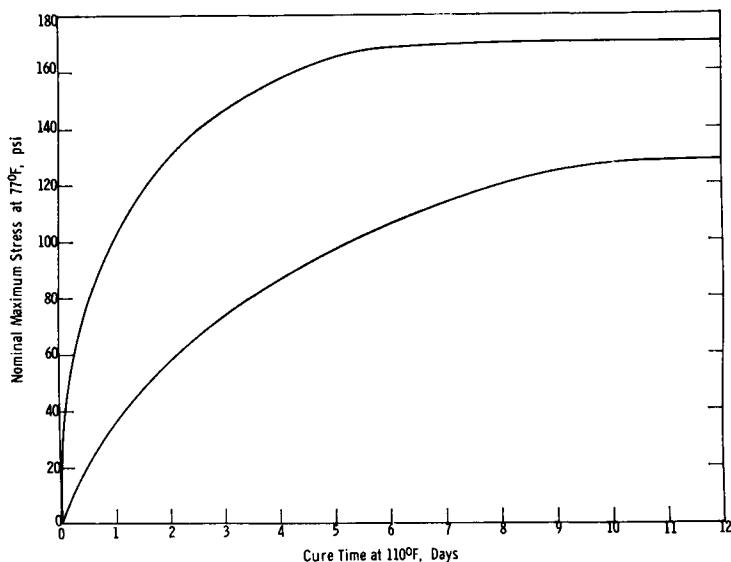
FIG. 11. Effect of cure time on the tensile strength of typical polyurethane propellants.
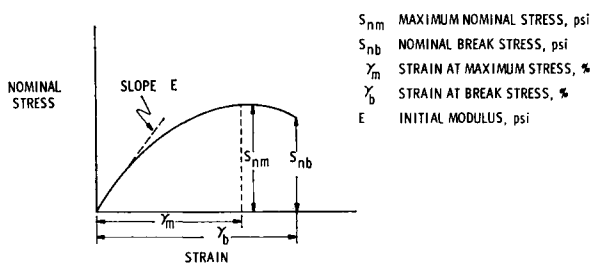
FIG. 12. Definitions of mechanical properties.

Before proceeding further in the discussion of the mechanical behavior of solid propellants, we will define the terms used.

Figure 12 shows a typical stress–strain curve for a solid propellant and designates some salient features important to the propellant chemist. The important variables are the initial modulus (E), the maximum and break stress (S_{nm} and S_{nb}) and the elongations at maximum and at break stress (γ_m and γ_b).

The shape of the stress–strain curve is a function of the viscoelastic behavior of the polymer phase and the interactions which occur between the polymer and the fillers. The effect of fillers on the modulus of an elastic material has been treated theoretically. The equation proposed by Eilers and Van Dyck [10] and an experimental verification are shown in Fig. 13 [11]. It is seen that the relative

$$\frac{E}{E_0} = \left[1 + \frac{k\phi}{1-S^{1}\phi} \right]^2$$

k and S^1 are Empirical Constants

▲ Polyisobutylene - Glass Beads
O Polyurethane, Type I - Glass Beads
✕ Polyurethane, Type II - Glass Beads
⊖ Polyurethane Propellant A
● Polyurethane Propellant B
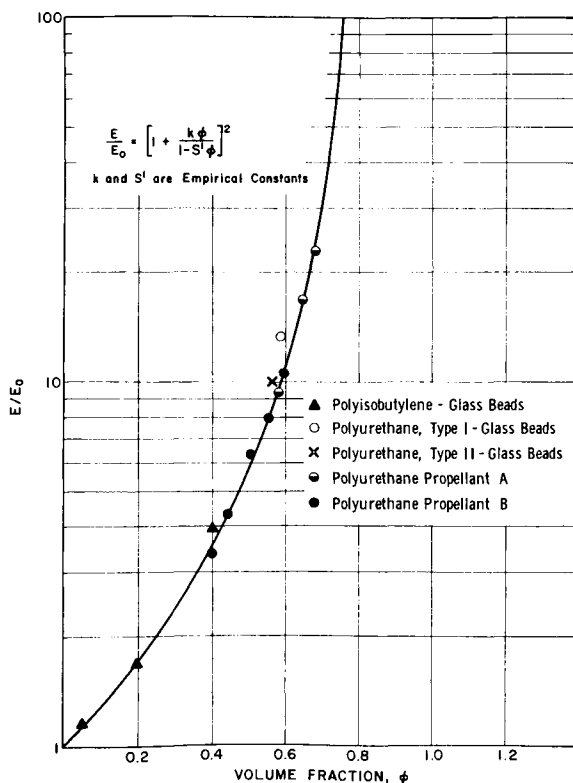
FIG. 13. Dependence of relative modulus on volume fraction of filler.

modulus is a function only of the volume fraction of filler. That this is true is further illustrated in Fig. 14, which indicates that a polyurethane filled with 19 vol. per cent of various fillers has the same initial modulus although the tensile strength and elongation vary with the nature of the filler.

The mechanical behavior of a propellant varies also with the temperature at which the measurement is made and with the rate of strain. These are illustrated in Table 6 and Fig. 15.

A decrease in temperature increases the modulus and the maximum stress and decreases the elongation at maximum stress. An increase in the strain rate has the same effect as a decrease in temperature. In fact, the effect of strain rate and of temperature can be correlated [12] by expressions similar to the Williams, Landel, Ferry equation [13] for elastomers.
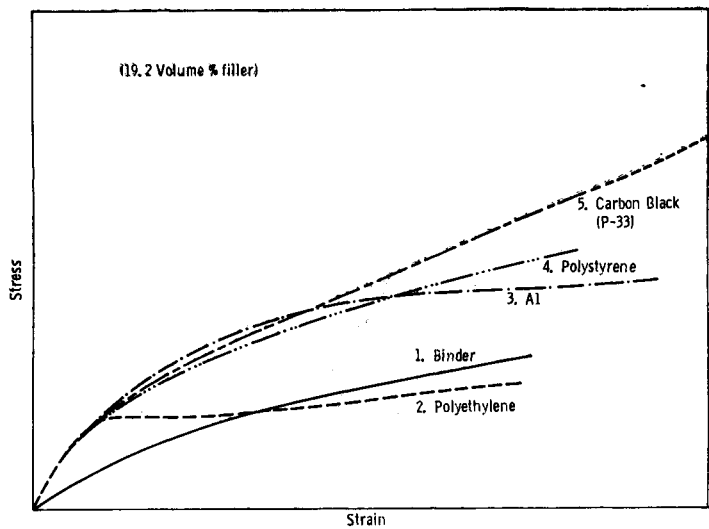
FIG. 14. Effect of different fillers on a polyurethane binder system.

TABLE 6. EFFECT OF TEMPERATURE ON THE MECHANICAL PROPERTIES OF A POLYURETHANE PROPELLANT

Temperature °F	S_{nm} psi	γ_m %	E psi
−40	767	5.2	23,090
0	400	21.6	4230
40	189	36	1185
77	121	42	594
110	94	45	398
150	76	46	314
180	70	43	284
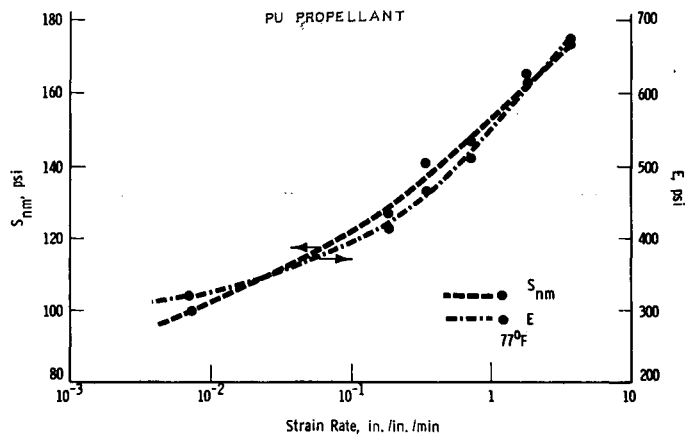
FIG. 15. Mechanical properties.

The dimensional changes which occurred when a solid propellant was strained were adequate to indicate that the propellant volume increased during straining [14], a phenomenon that was not observed in the unfilled binder at the same strain. To study further this behavior, a gas phase dilatometer was developed which measured both the stress–strain relation and the volume change induced
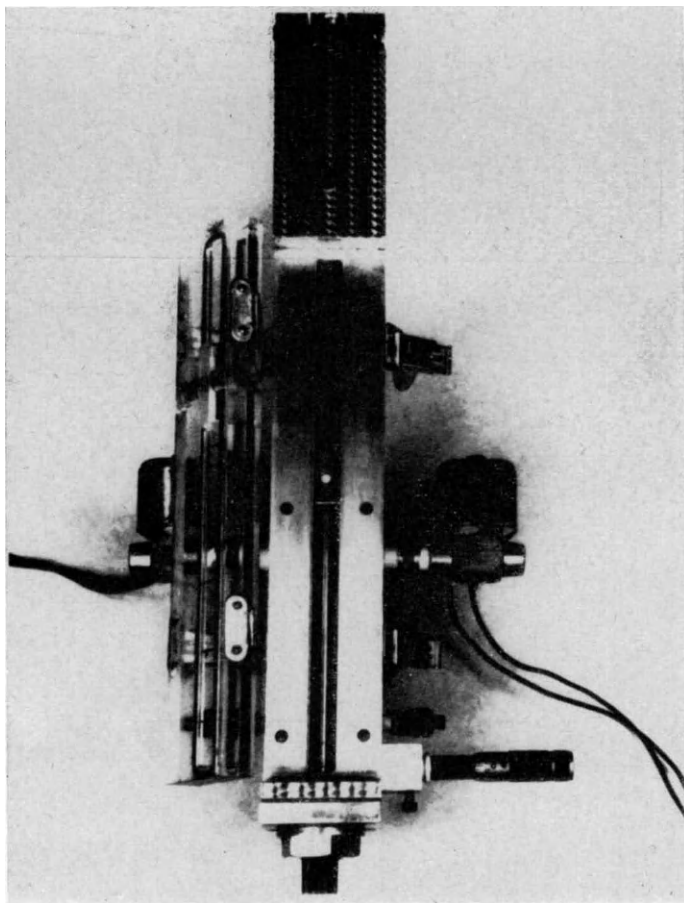
FIG. 16. Front view of gas dilatometer with door open.

by strain [15]. The apparatus (Fig. 16) consists of a movable piston in a dilatometer, which allows straining of a propellant sample while simultaneously measuring the pressure within the dilatometer. The pressure change precisely measures the volume change of the propellant when the apparatus and sample are maintained at constant temperature. These studies indicated that the volume change was due to formation of vacuoles around the solid filler particles as the propellant was strained. The formation of vacuoles and releasing of the binder

from the filler is termed blanching. Blanching is a detrimental irreversible process which, in extreme cases, can have serious effects on the ballistic and mechanical properties of a propellant grain resulting in catastrophic failure of the motor. This phenomenon is illustrated in Fig. 17 for a steel ball enclosed in a polyurethane binder.

2a Polyurethane binder containing steel spheres in jig of Instron machine. No strain applied.

2b Formation of small bubbles above surface of sphere when critical stress, σ', has been reached.

$\sigma' = \frac{E}{2} + 8 \, psi$

(independent of material)
    E = Modulus of binder.

2c Blanching (dewetting) at stresses above σ'. Occurs only in "unbonded" spheres.
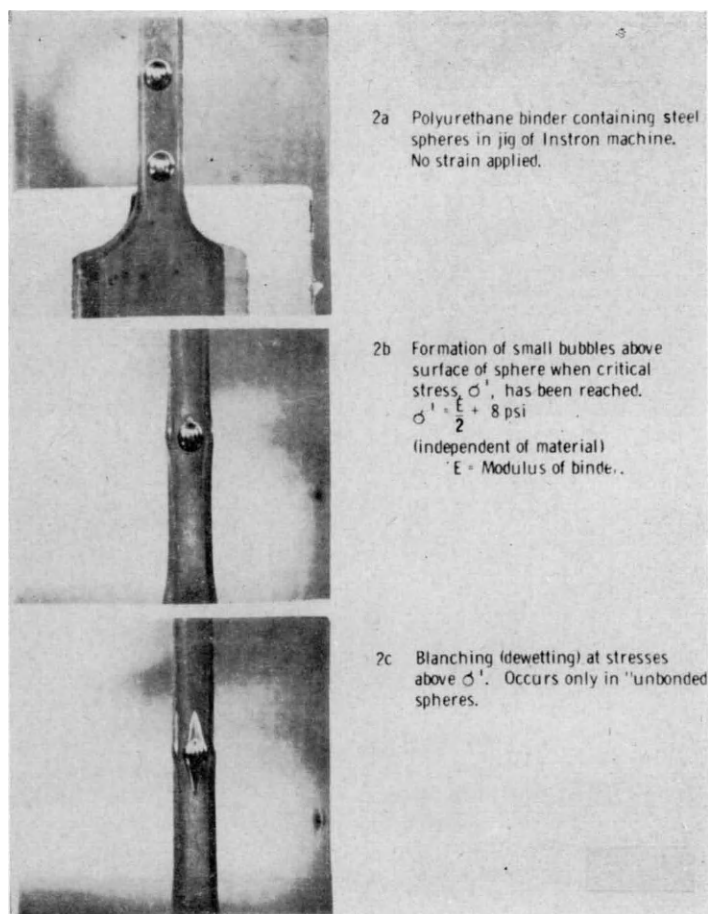
FIG. 17. Formation of cavities and blanching around spherical particle.

Initially the first step in blanching was believed to result from "dewetting", i.e. release of the binder from the solid oxidizer in the propellant to form vacuoles containing loose filler particles. However, careful study showed that the first sign of a void occurred at a critical stress [16], which, for noncrystallized binders, is close to the value of Young's modulus. Because of stress concentrations around the filler particles, the stress level at which the first voids will appear is always lower than the critical stress for void formation in the unfilled

polymer, for example,

$$\sigma' = \left(\frac{E}{2} + 8\right) \text{ psi for spheres}$$

$$\sigma' = \text{critical stress}$$

$$E = \text{Young's modulus}$$
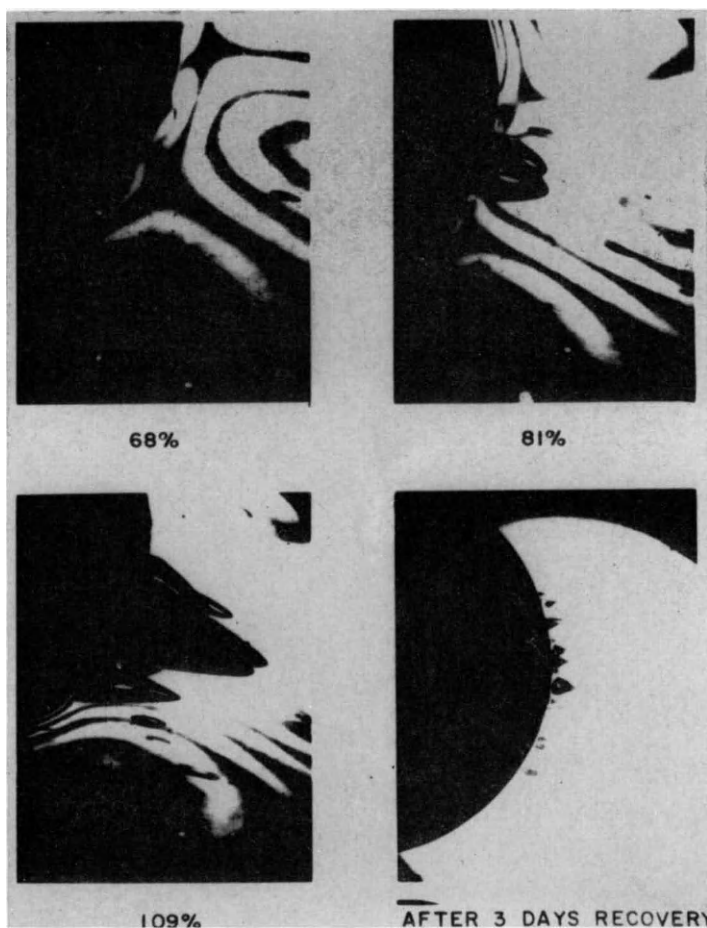
FIG. 18. Photoelastic strain patterns and binder void formation around a $\frac{1}{4}$ in. steel ball bonded with bonding agent to a polyurethane rubber. Magnification 17×.

It was observed that the initial void occurs completely within the polymer phase and not on the surface of the solid. This is illustrated in Fig. 18 which shows the voids and birefringence pattern around a steel ball contained in a polyurethane rubber. When the strain is released, it is seen that the voids are entirely in the polymer. Theoretical calculations of the stress pattern around a spherical filler particle indicate that the points of maximum stress should occur

a short distance from the particle surface (Fig. 19). The calculated strain pattern shows a reasonably close resemblance to the birefringence pattern in Fig. 18.

When the number of particles increase, the stress patterns around each particle begin to interact. The situation is then more complicated, but basically unchanged. Figure 20 illustrates the sequence of events in a densely packed system. The first void is formed in the polymer between particles after the critical

(LOADING VERTICAL)
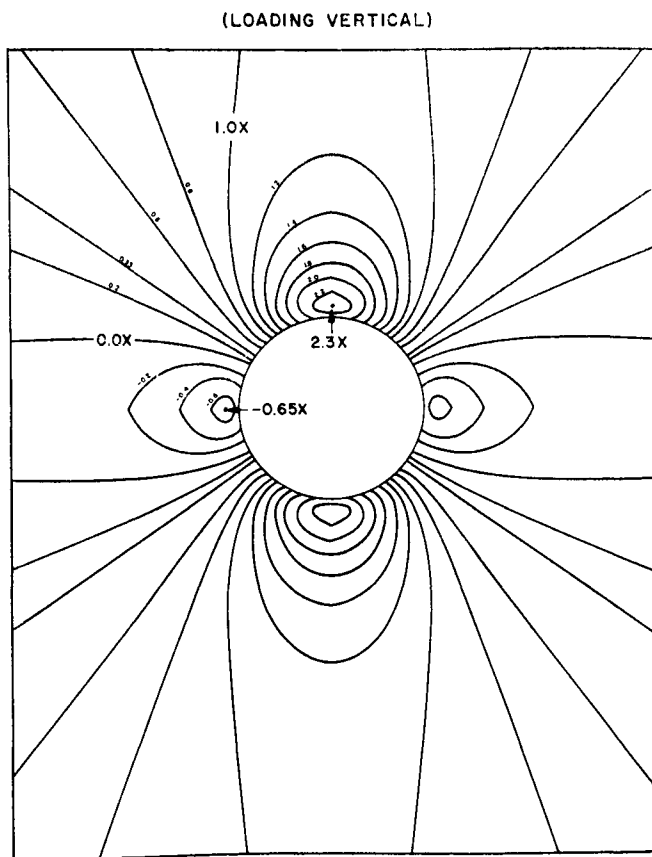
FIG. 19. Binder stresses around filler particle.

stress is reached. The shape of the void indicates strongly that the void is entirely within the binder and does not contact the particle surface. The void propagates, by tearing as the strain increases, and eventually reaches the particle surface. When the void reaches the surface, the polymer tears rapidly away from the particle, creating a large vacuole. This sudden withdrawal of the binder from the solid (blanching) occurs at a stress level somewhat higher than σ'. A similar process occurs on the other side of the particle.

The shape of the stress-strain curve for a solid propellant can be explained by using this sequence of events. Figure 21 shows the shape of a stress-strain curve

for a polyurethane binder with five steel balls. When the binder is stressed, the first void occurs at a critical stress of 225 psi. When the void tears to the surface of a steel ball, the stress decreases abruptly and then rises again. The behavior is repeated for each steel ball. This results in a saw-tooth pattern with five teeth (one for each ball). The stress does not rise above the blanching stress until the binder has been torn from all five of the balls.

An analogous situation is thought to occur in a solid propellant, but the saw-tooth pattern is not discernible because the large number of particles produces a smooth stress–strain curve.

(Polystyrene spheres in PU binder)
Magnified 250X

A
No strain.

B
Approximately 10% strain.
Appearance of bubbles (tears) in binder phase (curvature of bubbles shows that they don't reach the filler-surface.

C
"Break through" to filler surface has occurred. (beginning of blanching)
Strain approximately 50%

D
Several hundred % strain.
Blanching almost complete.
Magnified 50 times.

FIG. 20. Sequence of binder-filler separation in highly loaded elastomers.

With the understanding of the fundamental processes which occur comes the ability to modify the tear process and alter the mechanical response of the composite. This understanding may ultimately result in the elimination of catastrophic blanching. Certainly the hindering of the voids, formed in the binder phase, from reaching the filler surface is a step in the right direction. A practical way to change the mechanical response is to create a boundary layer which has a higher modulus from the bulk of the polymer phase and which prevents tear of the voids to the particle surface. This has been achieved by use of a "bonding agent".

The "bonding agent" is a surface active agent which will adsorb on the surface of the filler particles and carries functional groups by which it can be polymerized and chemically bonded into the polymer phase. The photomicrographs in Fig. 22 shows the difference in formation of vacuoles around the particles in the case of bonding and non-bonding and bond. Table 7 gives the effect of bonding agent on propellant mechanical properties.

I   Unfilled Polyurethane

II   Above Filled with 5 Steel Balls 0.34 in.
                  f = first blanching from sphere
                  s = second blanching

III   Above Binder loaded with 50 Vol % Glass Beads
     (400 Mesh)

Temp. = 77°F $\dot{\varepsilon} = 0.74 \text{ min}^{-1}$
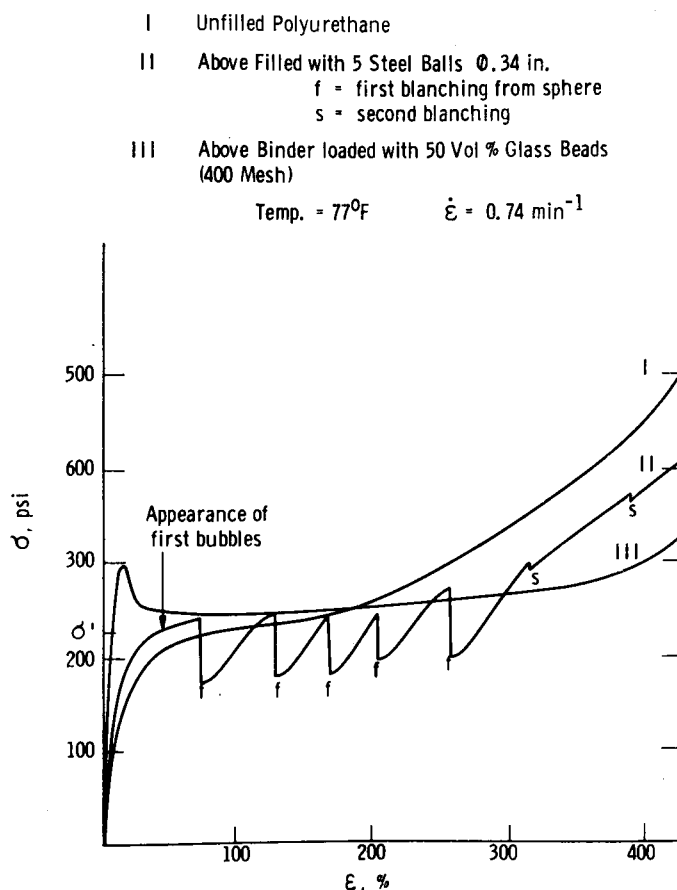
FIG. 21. Tensile curves.

This promises to be a significant method for tailoring the mechanical behavior of solid propellants with either polyurethane or polybutadiene binders.

A solid propellant is subject to aging depending on its storage conditions. Figure 23 shows the effect of storage time and temperature upon polyurethane propellant. The general aging behavior for polyurethanes is a decrease in modulus and tensile strength and an increase in elongation with time. Aging of polybutadienes results in increasing modulus and tensile strength and decreasing elongation. Methods of increasing the shelf life of propellants have been similar
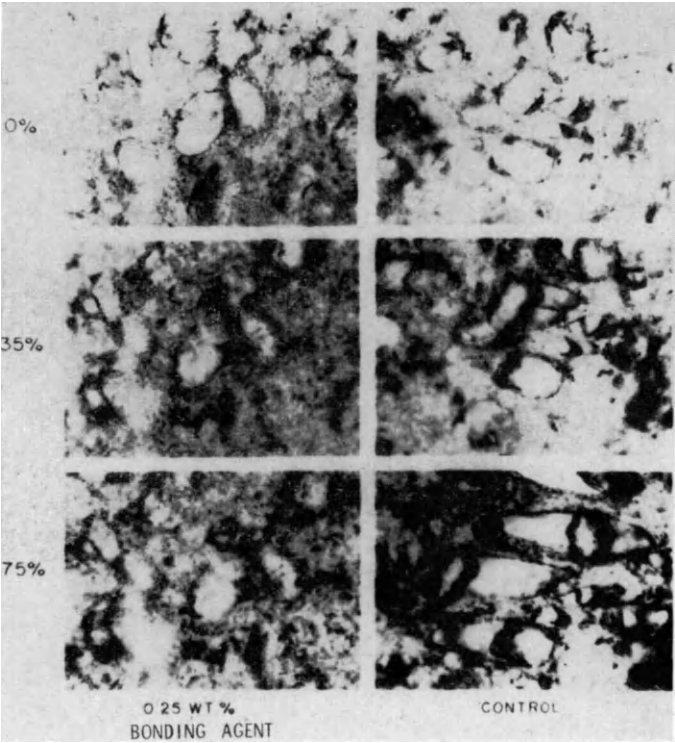
FIG. 22. Photomicrographs of polyurethane propellants under different strains.
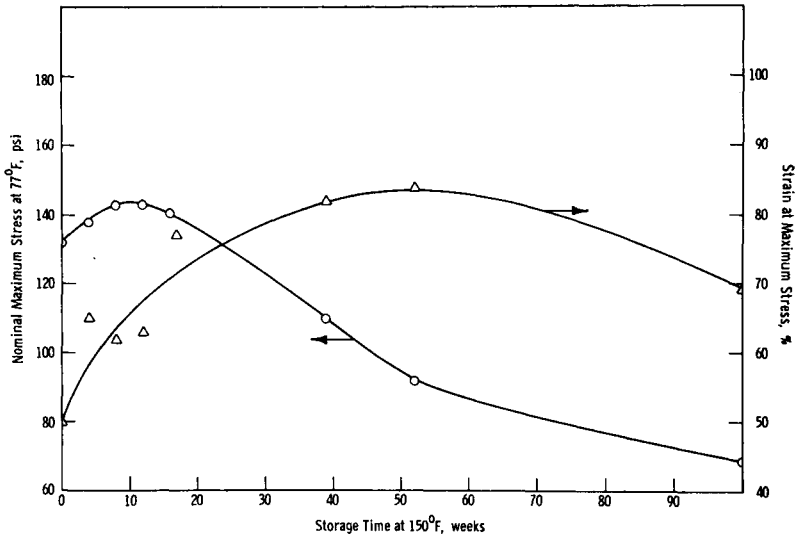
FIG. 23. Effect of storage at 150°F on the mechanical behavior of a polyurethane propellant.

TABLE 7. EFFECT OF A BONDING AGENT (0.3wt.%) ON THE MECHANICAL PROPERTIES OF POLYURETHANE

Temperature °F	Mechanical properties									
	No bonding agent					With bonding agent				
	S_{nm} psi	S_b psi	γ_m %	γ_b %	E psi	S_{nm} psi	S_b psi	γ_m %	γ_b %	E psi
−75	340	239	28	63	2900	710	710	63	63	4000
−40	194	167	40	58	780	432	432	97	97	900
0	122	105	43	57	410	295	295	89	89	630
77	72	72	32	32	325	220	220	67	67	500
180	180	45	26	26	270	78	78	28	28	290

to those used by the polymer industry. These involve using the highest permissible crosslink density and incorporation of inhibitors of phenol or amine type.

4. SUMMARY AND CONCLUSIONS

Both the binder and filler from which solid propellants are formulated play major roles in controlling the ballistic and mechanical properties. The organic elastomeric binder has the dual function of furnishing most of the gas producing elements and of being the continuous matrix which binds the composite mass together into a grain with useful mechanical properties for case-bonded motors. The solid filler particles are generally of three types which perform separate functions. The oxidizer is the source of oxygen which exothermally oxidizes the binder and metallic fuels to yield the propulsive gases. The metallic fuels are a substantial source of thermal energy, and metallic oxides or salts are used as combustion accelerators to control the burning rate.

In preceding discussions general polymer chemistry principles were applied to the binder elastomers. It was emphasized that approaching the ideal elastomeric network in the binder structure is necessary to achieve the optimum mechanical properties of the highly filled solid propellants. To achieve this objective and still retain the other necessary polymer properties is difficult. Only a few of the commercially produced polymers are useful as binders because of requirements imposed by techniques of preparing and using case-bonded solid rocket motors. Some of these required properties are as follows: The polymer must be a good gas producer when burned with oxidizers, but must be stable in intimate contact with the oxidizer until ignited. It must be initially a fluid prepolymer which remains fluid when highly filled with granular materials. It must have chemically reactive functional groups which do not react with the filler materials, but can be crosslinked or chain extended during the propellant cure without yielding side reaction products which result in propellant porosity or interfere with the cure process. It must form a strong adhesive bond with chamber metals and insulating materials.

The most widely used polymers are the polyurethanes formed from the reaction of diol prepolymers and isocyanates, the polybutadiene derivatives formed from carboxyterminated polybutadienes prepolymers and aziridines, and double base binders which cure through a swelling process. These polymers partially fulfill, to a greater or lesser degree, most of the properties required for a solid propellant binder. Current research, using principles discussed here, is expected to result in considerable improvement in the polymers available for solid propellant binders.

REFERENCES

[1] SUMMERFIELD, M., *Solid Propellant Rocket Research*, Academic Press, 1 (1960).
[2] "Research on physical and chemical principles affecting high temperature materials for rocket nozzles", *Union Carbide Research Institute Quarterly Reports* (1963, 1964).
[3] ALTMAN, D. and CARTER, J., "High temperature equilibria", *High Speed Aerodynamic and Jet Propulsion*, 2, Ed. B. LEWIS, Princeton University Press (1960).
[4] DEKKER, A. O., *Jet Propulsion*, 26, 572 (1956).
[5] NAEGELI, C., TYABI, A., CONRAD, L. and LITWAN, F., *Helv. Chim. Acta*, 21, 1100 (1938).
[6] COOPER, PEARSON and DARKE, *Ind. Chemist*, 36, 121 (1960).
[7] FLORY, P. J., *Principles of Polymer Chemistry*, Cornell University Press, Ithaca, N.Y. 92–93 (1953).
[8] *ibid*, 348–354.
[9] FLORY, P. J., *Chem. Review*, 39, 137 (1946).
[10] EILERS, H., *Kolloid Z.*, 97, 313 (1941).
[11] LANDEL, R. F. and SMITH, T. L., *J. Am. Rocket Soc.*, 31, 599 (1951).
[12] MILLOWAY, W. T. and WIEGAND, J. H., *J. Appl. Polymer Sci.*, 7, 1325 (1963).
[13] WILLIAMS, M. L., LANDEL, R. F. and FERRY, J. D., *J. Am. Chem. Soc.*, 77, 3701 (1955).
[14] SMITH, T. L., *Trans. Soc. of Rheology*, 3, 133 (1959).
[15] FARRIS, R. J., *J. Appl. Polymer Sci.*, 8, 25 (1964).
[16] BRUENNER, R. S. and OBERTH, A. E., "Tear phenomena around solid inclusions in castable elastomers", *Society of Rheology 2nd Winter Meeting*, Santa Barbara, Calif. (1965).

INTERRELATIONS BETWEEN COMBUSTION
PHENOMENA AND MECHANICAL PROPERTIES
IN SOLID PROPELLANT ROCKET MOTORS*

M. Summerfield and K. H. Parker

Guggenheim Aerospace Propulsion Laboratories
Princeton University, Princeton, N.J.

Abstract—For the successful design of a solid propellant grain it is necessary to know not only the intricate mechanical properties of the solid propellant but also the static and dynamic combustion phenomena that determine the environment in which the grain must exist. On an even broader basis, there are numerous points of interaction between combustion and structural mechanics in solid propellant rockets. The most obvious interaction is that the grain configuration determines the mass combustion rate and hence the steady-state pressure, while the pressure in turn determines the stress and strain distribution, and hence the choice of configuration. This paper is focused on equally important, but less obvious structural implications of combustion research. For example, through research on the physicochemical basis of ignition, it is possible to predict (under certain conditions) the starting pressure transient. This is important since too rapid a stress development in a viscoelastic medium at low temperature can induce structural failure. In the field of combustion oscillation and combustion instability, the propellant grain as an elastic medium modifies the natural frequencies and also serves as a damping mechanism to reduce the instability. In the area of steady-state combustion, physical additives such as fusible or combustible wires serve on the one hand to modify significantly the burning rate of the propellant, and on the other hand to modify significantly the strength of the grain. Current research on the effects of the composition and the physical state of the propellant on both the combustion characteristics and the structural properties is reviewed.

1. INTRODUCTION

The problem of designing a solid propellant grain is basically the problem of finding the optimum compromise between the many considerations which determine its acceptability. Two of the primary factors that enter into this compromise are the internal ballistic characteristics and the structural integrity of the rocket motor grain. The problem of finding the optimum compromise between just these two factors is complicated; the choices of propellant formulation, of propellant configuration, of operating pressure, etc., frequently have opposing effects on the overall performance objectives as a result of separate effects on the internal ballistics and on the structural characteristics. More important than this, it is known that, in some cases, the combustion characteristics affect the structural integrity and the structural characteristics affect the

ballistic performance. These interactions compound the problem in seeking the optimum compromise.

If this design is to be carried out on a rational basis, it is imperative that the interrelations between combustion phenomena and structural mechanics in solid propellant rocket motors be recognized and understood. Without such understanding grain design is reduced to inefficient and costly empirical development—an approach which is inconsistent with the refined and the large rocket motors of today.

The problem is not a simple one. To the internal ballistics engineer a solid propellant grain is a material which is capable of undergoing an incredibly complex and poorly understood series of reactions which release large amounts of energy. To the structural engineer it is a material of a complicated shape subjected to ill-defined loads, and possessing complex and continually varying physical properties. In spite of the complexity, however, great progress has been made in both fields and some progress has been made in the study of the interaction of these two fields. It is the purpose of this paper to describe this progress by examining some of these interrelations, reviewing some of them broadly and others in more detail.

The topics and the order in which they are treated are the following: First, the well-known effects of geometry upon the combustion and the structural properties of a grain are discussed briefly in Section 2. The effects of propellant composition, especially oxidizer loading and particle size distribution, are discussed in rather more depth in Section 3. Also included at the end of Section 3 is a discussion of wire embedded propellants—an interesting class of propellant, of current importance. Section 4 is a similar discussion of the effects of the physical state of the propellant: the temperature, the state of cure, and the strain level. Section 5 deals with some of the special interactions between ballistic characteristics and structural integrity encountered during the ignition transient. And, finally, the interactions between the structural properties and oscillatory combustion are surveyed in Section 6.

2. THE EFFECTS OF COMBUSTION PROPERTIES AND MECHANICAL PROPERTIES ON GRAIN DESIGN

The interplay between internal ballistics and structural analysis in the geometric design of a solid propellant grain is well known. A great deal of effort has been expended over the years to obtain this knowledge and even greater efforts have been made in finding ways to apply this understanding to the efficient and effective design of practical rocket motors. The result of these efforts is that today, with the use of time-proven design techniques coupled with the capabilities of modern computers, the fundamental design of a solid propellant grain has been almost automated.

The philosophy of design is simple: given certain mission specifications, find the design which best satisfies these conditions and which simultaneously optimizes all of the factors which determine its acceptability, especially the cost

and the reliability. Because of the ability of the computer quickly to calculate and compare vast amounts of data, it is now possible to approach the ultimate goal of full optimization more closely than could be done with the old, intuitive approach to design. The calculation and comparison of two "acceptable" designs, based upon two different classes of geometries, can now be accomplished in minutes rather than months.

The technique of design, as discussed and outlined in considerable detail for a general design program in ref. [1] and [2], is also rather simple, although it should be added that the actual programs represent years of experience and effort. As outlined in Fig. 1 the ballistic requirements are determined from the
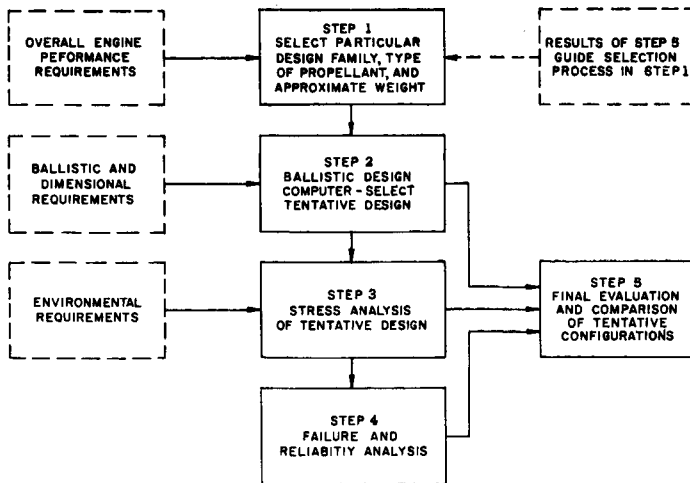
FIG. 1. Outline of a typical grain design program (adapted from Billheimer and Wiegand [1].

mission specifications. All other constraints, such as the external envelope or the maximum weight, are established. A class of grain geometries is chosen, and using the best data available for the internal ballistics—the burning rate, the internal pressure field and the nozzle processes—the geometry which satisfies the ballistic requirements is selected by iteration. If this class of geometries cannot provide the required ballistic performance, or if the stresses calculated for the grain are prohibitive, or if the calculated design requires costly fabrication techniques, or if for any reason the designer feels that a better design should exist, a new class of geometries is chosen and a new design is calculated. New designs can be calculated until the designer is satisfied that he has found the best possible design.

Obviously the process of design is not and cannot be wholly automatic. It remains to the ingenuity of the designer to formulate the class of geometries best suited for the particular rocket being designed if he is to find the optimum design. More important, it is the designer who must mentally balance the myriad of considerations to decide which design is truly optimum.

The problems confronting the designer of a large rocket motor offer a good example of some of these problems. For instance, the designer must choose between a standard star shaped grain design and a design using a circular cylinder with uninhibited ends, both of which fully satisfy the ballistic requirements. The circular port design is sturdy, easily fabricated and essentially sliverless but it creates problems of insulation for the unprotected casing. The star design, on the other hand, requires little or no insulation but offers a lower structural integrity and an increased sliver. So the decision between design families must be made by balancing these unrelated advantages and disadvantages in some meaningful way. These decisions can be similarly difficult even within a particular family of designs. For example, the design of the fillets in a star or a wagon wheel geometry is a similar trade-off between minimizing both the stress multiplier and the sliver while simultaneously maintaining an acceptable degree of progressivity. Likewise, there must be a compromise between maximum volume loading and maximum storage capabilities in the selection of the number of star points. It is these considerations and comparisons which, defying simple numerical evaluation, confront the designer today.

3. EFFECTS OF COMPOSITION VARIABLES ON COMBUSTION CHARACTERISTICS AND MECHANICAL PROPERTIES

For optimum design procedures it is necessary to know the influence of each of the design parameters upon the entire system. Just like the geometry, the composition of the grain can have a strong influence upon both the internal ballistics and the mechanics of the rocket motor. The nature of these effects will be discussed in general in the first part of this section. The second part will deal in greater detail with one of the more interesting classes of propellant compositions—propellants with embedded wires.

This discussion is primarily directed to the composite solid propellants, typically ammonium perchlorate and aluminum particles combined with an elastomeric fuel as a binder. However, the plasticized nitrocellulose based propellants behave like elastomers, so that the discussion of elastomers pertains equally well to the so-called double base propellants and much of the discussion of filled elastomers pertains to the commonly used composite double base propellants.

Because of the heterogeneous nature of a composite solid propellant, a great many parameters are needed to fully describe its composition. Obviously essential parameters are the loading fraction and the chemical composition of each of the components—the binder, the oxidizer, and the metal or other additives. The distribution of particle sizes of both the oxidizer and the metal additives have also been found to be important composition parameters. The influence of these particular parameters has been recognized and they are generally reported in the description of a propellant, but some of the parameters which are needed for a complete description of a propellant are seldom reported. Among these are the distributions of particle shapes—particularly important

in the questions of dewetting and of microscopic flame structure—and the temperature of cure—potentially important in the analysis of thermal stresses in the propellant. Adding to the complexity, there are many classes of propellants, such as the above-mentioned wire embedded propellants, which require further parameters for their description.

This study is confined to the effects of the principal composition variables upon the mechanical and ballistic properties of a propellant: the chemical compositions of the components, the loading fraction of each component, and the particle size distributions of the solid additives. As an example, the effects of the loading fraction and the particle size distribution of the oxidizer are discussed in some detail. The effects of the other variables are only summarized.

Effects of Oxidizer Loading Fraction and Particle Size Distribution

In order to discuss the effect of a composition variable on the combustion and mechanical properties of a propellant, it is necessary to be able to characterize these properties. For the purposes of design, almost all of the important properties of the combustion of a grain can be reported in terms of a few parameters. Perhaps the most convenient of these are:

(1) the burning rate, r, generally reported at 1000 psi.
(2) the pressure dependence of the burning rate, usually expressed as the exponent, n, of an empirically fitted power law, $r = cp^n$.
(3) the theoretical specific impulse, I_{sp}, generally calculated at a standardized chamber pressure of 1000 psi with the gases expanded to atmospheric pressure under equilibrium conditions.
(4) the density of the propellant, ρ_p, and
(5) the adiabatic flame temperature, T_f, at 1000 psi.

It is much more difficult to characterize fully the mechanical properties of a composite solid propellant. However, some of the most important mechanical parameters are:

(1) the equilibrium modulus, E
(2) the glass transition temperature, T_g
(3) the dynamic modulus, $E^* \equiv E' + iE''$
    where $E' =$ storage modulus
          $E'' =$ loss modulus
(4) the Poisson ratio, v, conveniently defined in terms of logarithmic or Hencky strains.
(5) the propellant failure boundary, generally presented as

$$\sigma_b \frac{T_s}{T} \text{ versus } \epsilon \text{ at } \sigma_b \text{ (see below)}$$

This is by no means a complete set of parameters sufficient to describe the mechanical behavior of a propellant in its entirety. However, most of the important structural properties of the grain can be described in terms of these parameters and their behavior will certainly serve to illustrate some of the basic trends.

A. Combustion Properties.

The most successful theory of composite solid propellant combustion to date is the granular diffusion theory proposed by Summerfield [3]. Simply stated, this theory is based upon a model of a gas phase reaction sustained by energy transfer from the reaction zone which pyrolyzes the fuel and oxidizer components of the propellant. According to the model the pyrolyzed gases form discrete pockets upon leaving the surface, the size of these pockets being directly related to the size of the solid particles in the propellant. The burning rate is thus controlled by the rate of the reaction between these pockets of fuel and oxidizer gases. This reaction is in turn controlled by the rate of diffusion between particles and the rate of the elementary chemical reactions. The theory is outlined in Fig. 2.

LOW PRESSURE EXTREME (HOMOGENEOUS)   HIGH PRESSURE EXTREME (HETEROGENEOUS)

GAS PHASE CHEMISTRY CONTROLLING   DIFFUSIONAL MIXING CONTROLLING

$\dot{m} \sim p$ $\dot{m} \sim p^{1/3}$

GENERAL CASE

$$\frac{1}{r} = \frac{a}{p} + \frac{b}{p^{2/3}}$$

a (REACTION TIME PARAMETER) = FUNCTION OF OXIDIZER LOADING FRACTION

b (DIFFUSION TIME PARAMETER) = FUNCTION OF OXIDIZER PARTICLE SIZE
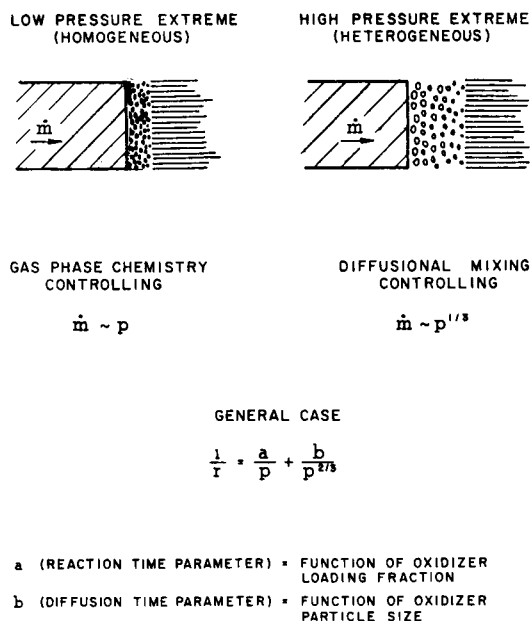
FIG. 2. The development of granular diffusion theory for the combustion of composite solid propellant.

Using this model and some further assumptions, Summerfield solved for the burning rate as a function of pressure for the two limiting cases: (a) high pressure —where the rate of chemical reaction is very high and the rate of diffusion becomes the controlling factor, and (b) low pressure—where the diffusion is relatively fast and the rate of chemical reaction becomes the controlling factor. Assuming that the burning rate at intermediate pressures can be expressed as a linear average of these limiting solutions, the granular diffusion theory predicts a burning rate-pressure law of the form:

$$\frac{1}{r} = \frac{a}{p} + \frac{b}{p^{2/3}} \tag{1}$$

where a and b are constants. The constant a in eqn. (1) is called the "reaction time parameter" and depends primarily upon the properties of the reaction. It is very sensitive to the flame temperature and hence to the fuel-oxidizer mixture ratio in the propellant. The constant b is called the "diffusion time parameter" and depends both on the properties of the gases and the size of the oxidizer particles. Detailed analysis of these parameters [3] shows that the burning rate at a given pressure should increase with increasing oxidizer loadings and with decreasing oxidizer particle sizes.

POLYSTYRENE-AMMONIUM PERCHLORATE COMPOSITE PROPELLANTS

SYMBOL	% AP	PARTICLE SIZE	a	b
O	75%	120μ	365	39.0
▽	80%	120μ	160	27.0
△	75%	16μ	400	19.8
□	80%	16μ	245	17.3

$$\frac{1}{r} = \frac{a}{p} + \frac{b}{p^{1/3}}$$

$$\frac{PRESSURE}{BURNING\ RATE} = \frac{PSIA}{IN/SEC}$$
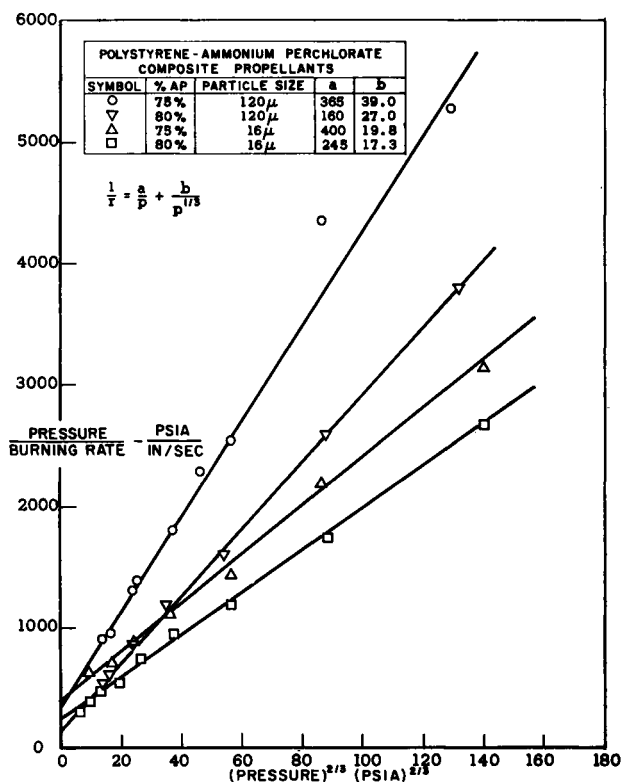
FIG. 3. Burning rate data plotted to test validity of granular diffusion theory, r/p vs. $p^{2/3}$ (from Sutherland [3]).

Some of the assumptions in the model which lead to the burning rate law in eqn. (1) are difficult if not impossible to verify directly. Therefore, the success of the theory must be judged primarily on its agreement with experimental results. The most convenient way to check this burning rate law is to plot experimental burning rates measured at different pressures on a p/r versus $p^{2/3}$ graph. According to eqn. (1) such a plot should be linear with slope b and intercept a. Such a plot is shown in Fig. 3 for four AP-polystyrene propellants with different oxidizer loadings and particle size distributions. The close agreement between theory and experiment is typical.

6

Although a great wealth of experimental burning rate data for all types of propellants has been amassed, very few systematic studies have been published on the effects of oxidizer concentration and particle size distribution. Two of the published studies are by Summerfield, Sutherland *et al.* [3] and by Adams, Newman and Robins [4]. Some typical results of these studies are shown in Fig. 4 through 7.

The propellants used by Adams, Newman and Robins (pressed mixtures of ammonium perchlorate and polystyrene particles) are structurally dissimilar to commercially used propellants. However, comparison with the results obtained
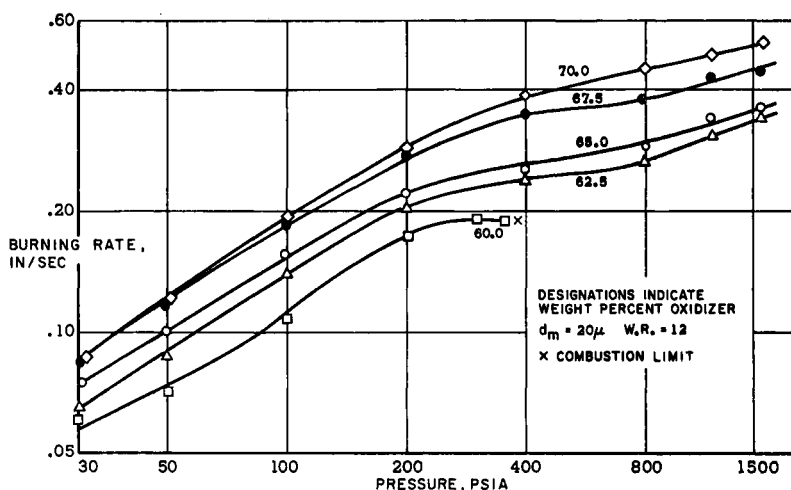
FIG. 4. Oxidizer loading effects on burning rate of polysulfide–AP propellant (from Bastress [3]).

by Summerfield *et al.* for their cast ammonium perchlorate–polystyrene copolymer propellants shows that the burning rate behavior of pressed composites and cast composite propellants are broadly similar. Reference to Figs. 4 and 5 and other data reported by Summerfield *et al.* and by Adams, Newman and Robins shows that, up to stoichiometry, the burning rate increases with increasing oxidizer loading. This is in qualitative agreement with the predictions of the granular diffusion theory.

The effects of particle size of the oxidizer were also studied by Summerfield *et al.* [3], by Bastress [3], and by Adams, Newman and Robins [4]. Some of the results of these studies are shown in Figs. 6 and 7 for several average oxidizer particle sizes. In general, it is found that decreasing the particle size increases the burning rate at a given pressure. In certain pressure ranges the particle size also influences the pressure dependence of the burning rate. Again, these observations are in qualitative agreement with the granular diffusion theory of solid propellant combustion.

As opposed to the burning rate and the pressure dependence, the variation of the specific impulse, the propellant density, and the adiabatic flame temperature

with oxidizer concentration is quite straightforward. The theoretical density varies linearly with the volume per cent of oxidizer, and both the specific impulse and the adiabatic flame temperature can be calculated from standard thermodynamic relationships. The typical variation of these parameters with oxidizer
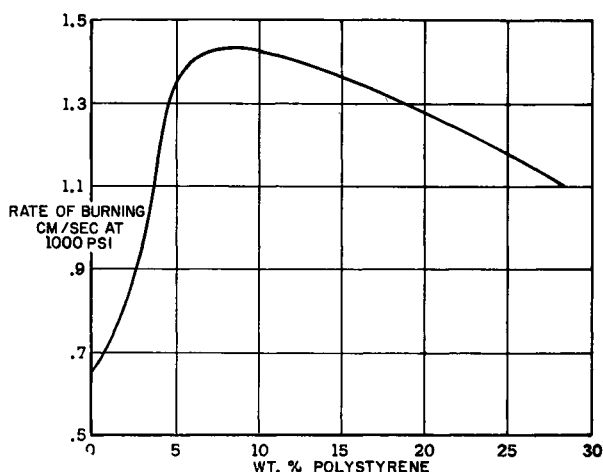
FIG. 5. Oxidizer loading effects on burning rate of pressed polystyrene–AP propellant, (from Adams, Newman and Robins [4]).
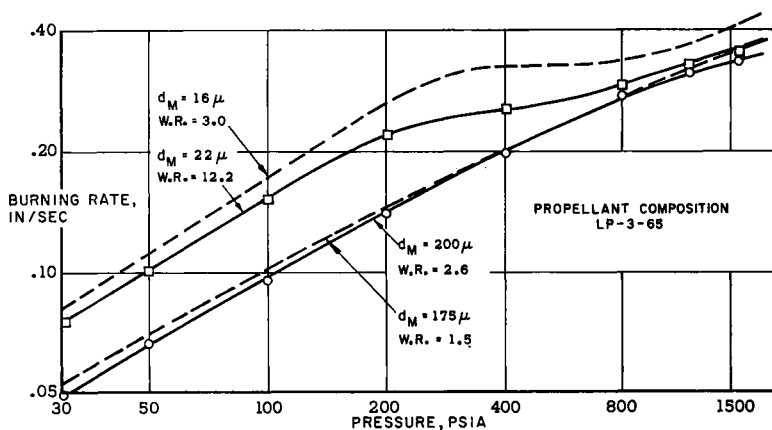
FIG. 6. Oxidizer particle size effects on burning rate of polysulfide–AP propellant (from Bastress [3]).

loading is seen in Fig. 8 for a non-metallized PBAA-AP propellant. These curves were calculated using a general computer program for calculating the thermodynamic properties of rocket motors developed by NASA [5]. Because of the great importance of the specific impulse in the performance of a rocket in almost every mission, the maximum in the specific impulse, a little to the fuel-rich side of stoichiometry, indicates that the oxidizer loading fraction of future

propellants will be increased closer and closer to stoichiometry. This increased loading is dictated by the desire for greater ballistic performance in spite of the difficulties which accompany such an increase in loading fraction.

The particle size distribution has no direct effect upon either the density or the theoretical thermodynamic quantities, I_{sp} and T_f, which depend only upon the chemical concentrations. However, as the loading fraction of solids is increased, simple geometric loading considerations impose certain requirements on the
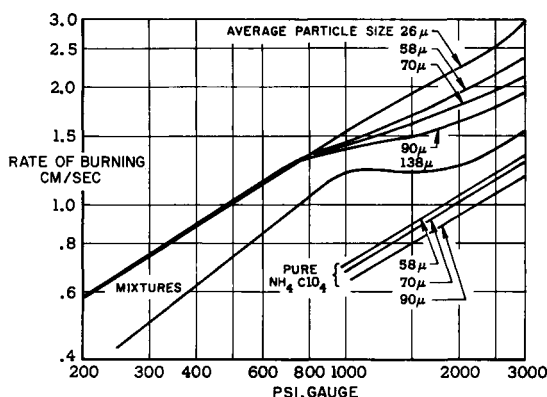
FIG. 7. Oxidizer particle size effects on burning rate of pressed polystyrene–AP propellant (from Adams, Newman and Robins [4]).

particle size distributions. For example, in the non-metallized PBAA-AP propellant of Fig. 8 the maximum weight fraction of unimodal, spherical oxidizer particles which can be included without introducing voids is 86 per cent —less than stoichiometric. For this reason bimodal or even trimodal particle size distributions are used in practical propellant formulations.

B. Mechanical Properties.

The mechanical behavior of a composite solid propellant is currently explained on the following microscopic basis. (See, for example, Ref. [6]). The propellant behaves like an elastomer (the plastic binder) filled with small, rigid particles (the metal and oxidizer particles). For small stresses the elastomer adheres to the particles and the overall modulus of the material is increased. As the stress increases, the bond between the elastomer and the filler begins to fail,* lowering the modulus of the material. Finally, as the stress is increased, the failure of the elastomer-filler bonds, or as it is generally called, the dewetting is complete and the material behaves like a polymeric foam. The dewetting is thought to be irreversible although there is evidence that some of the adhesive bonds will reform slowly upon the release of the stress.

---

* There is some recent evidence that initial failure occurs in the elastomer itself rather than at the elastomer-filler bond. (See the paper by A. Durelli presented at this conference.) If this mechanism of dewetting is shown to be true, certain modifications of the following discussion would be required.

(1) *Equilibrium Modulus.*

The variation of the equilibrium modulus of filled elastomers with the volume fraction of filler was reported for several different materials by Smith and Landel [7], and more recently for a polyurethane–NaCl system by Schwarzl [8] and for a propellant system by Martin [9]. The data reported by Smith and Landel
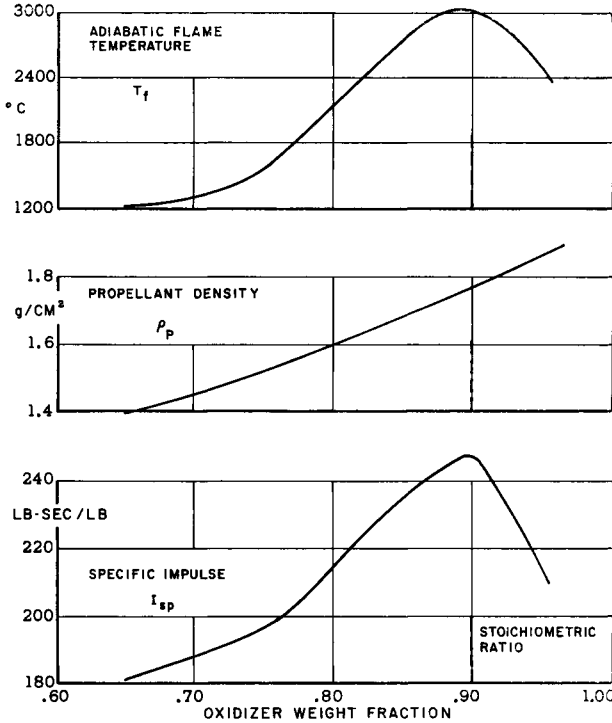
FIG. 8. Effect of oxidizer loading upon T_f, ρ_p, and I_{sp} for PBAA–AP propellant.

(Fig. 9) were measured under dynamic conditions, in creep tests, and from the initial slope of stress–strain curves. They observe that the experimental data for the elastic modulus are correlated very well by a curve of the Eilers–Van Dyck form;

$$\frac{E}{E_0} = \left(1 + \frac{1}{1 + \left(\dfrac{\phi}{\phi_{max}}\right)}\right)^2 \tag{2}$$

where ϕ is the volume fraction of filler, E_0 is the modulus of the elastomer alone, and k and ϕ_{max} can be considered to be positive empirical constants. As pointed out by Landel, eqn. (2) is a special case of the van der Poel equation which holds in the glassy region also. Furthermore, from the analogy between viscosity-filler effects and modulus-filler effects, ϕ_{max} is expected to be the maximum value of ϕ attainable because of packing considerations, and $2k$ is expected to be

about 2.5, the Einstein viscosity coefficient. All of this indicates that the higher the oxidizer loading fraction the more rigid is the propellant. Clearly, this must break down as the maximum loading fraction is approached and voids are introduced into the binder-filler matrix.

No effect of particle size on the equilibrium modulus has been reported, at least for particle sizes and loading fractions in the range of interest for composite propellants, although Schwarzl [8] reports modulus measurements of a lightly loaded polyurethane–NaCl system for six sizes of particles (33μ–480μ). These measurements indicate that there is an effect of particle size upon the modulus. Theoretically, eqn. (2) is independent of filler particle size but shows a slight
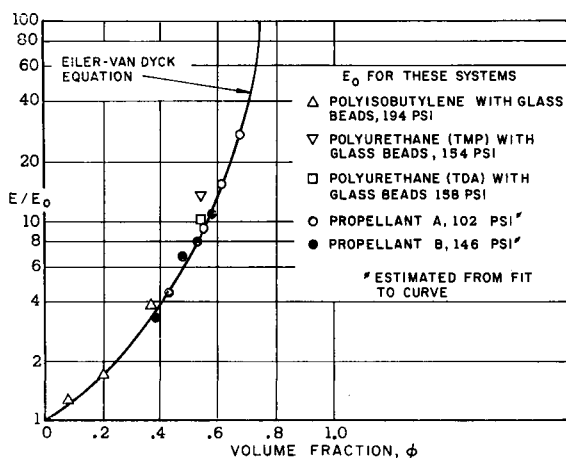
FIG. 9. Dependence of relative modulus on volume fraction of filler, (from Landel and Smith [7]).

dependence upon the particle size distribution through the term ϕ_{max}. For a unimodal distribution of spherical particles $\phi_{max} = 0.74$ and it increases as the distribution becomes wider [39]. Thus, until the maximum loading fraction is approached, a propellant with uniform particles is more rigid than one with the same loading fraction but with a broad size distribution of particles.

(2) Glass Transition Temperature.

The glass transition temperature in polymers is roughly analogous to the critical temperature of gases; both temperatures mark a change in the physical properties of the material, and therefore both serve as convient reference temperatures in the development of theoretical descriptions of these properties. Extensive investigations have shown that it is not the absolute temperature T but the temperature above the glass transition temperature, $T - T_g$, which determines the mechanical behavior of elastomers and filled elastomers. Thus, in any analytic or systematic study of the mechanical properties of propellants, the glass transition temperature is a very important parameter.

Landel and Smith [7] report the variation of the glass transition temperature T_g with volume per cent of filler ϕ for two different binders, polyurethane and polyisobutylene. Their results are shown in Fig. 10 where it appears that the increase in T_g is linear with ϕ. However, Schwarzl [8] reports that there is no change in the glass transition temperature of his polyurethane–NaCl system as the filler fraction is varied. It thus appears that different systems exhibit different behaviors and that nothing definitive can now be said about the effect of filler fraction upon the glass transition temperature.
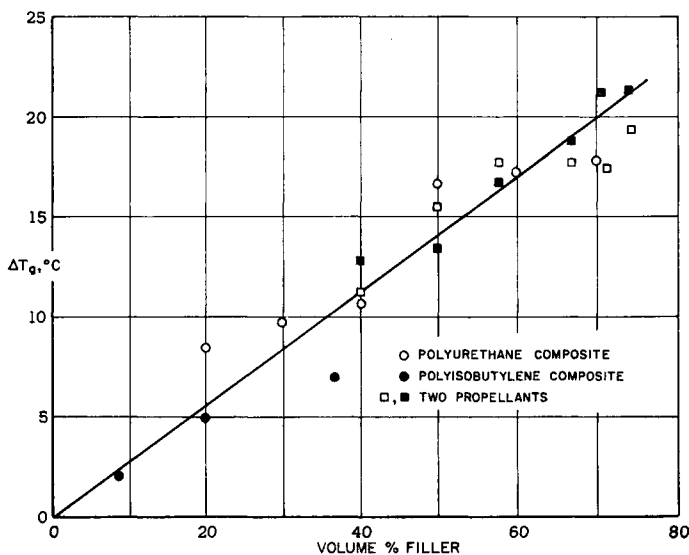
FIG. 10. Increase in glass temperature produced by fillers (from Landel and Smith [7]).

(3) Dynamic Modulus.

Landel [10] studied the time dependent mechanical properties of an uncross-linked polymer—polyisobutylene (PIB)—containing a non-reinforcing, non-interacting filler—glass beads with a mean diameter of $40\,\mu$. Although composite propellants are highly cross-linked and highly filled with reinforcing ammonium perchlorate and aluminum particles, the behavior of this simple PIB–glass beads system should give some indication of the mechanical behavior of composite propellants.

Using classical theory to account for density changes, Landel defines a reduced storage modulus G_c' and a reduced loss modulus G_c'' from the experimentally determined G' and G'' through the reduction formulas;

$$\frac{1}{G_c'} = \frac{1}{G_g} + \left(\frac{1}{G'} - \frac{1}{G_g}\right)\frac{T\rho}{T_0\rho_0}$$

$$\frac{1}{G_c''} = \frac{1}{G''}\frac{T\rho}{T_0\rho_0}$$

(3)

where ρ and ρ_0 are the densities of the system at the temperature of measurement T and at the standard temperature T_0, and G_g is the glass modulus or the maximum modulus exhibited by the system. Also, to account for the change in the glass transition temperature, as discussed previously, the experiments were conducted at the same value of $T-T_g$. These reduced moduli are plotted against a reduced frequency ωa_T in Fig. 11, where a_T is the Williams–Landel–Ferry "temperature shift factor" [11]. As discussed briefly below and more fully in reference [11], the use of this reduced frequency should compensate for the effects of temperature on the response time of the various systems. Thus plotted, Fig. 11 illustrates the effects of filler alone; the effects of temperature and density
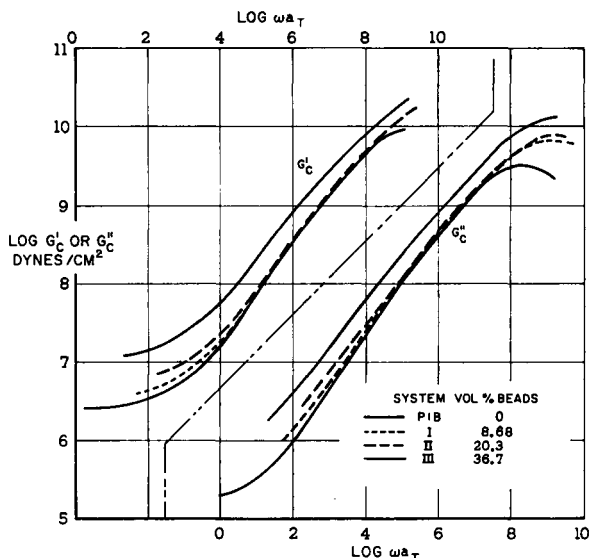
FIG. 11. Reduced storage modulus and reduced loss modulus for systems of varying filler fraction (from Landel [10]).

are accounted for in the definition of the reduced variables. As seen, both moduli of this system increase with increasing filler fraction for all but the very highest portion of the frequency spectrum.

If both the equilibrium and the dynamic modulus of a filled elastomer vary in the same way with the volume fraction of filler, then eqn. (2) should be valid for the dynamic modulus also. To check this possibility the reduced storage and loss moduli presented in Fig. 11 are divided by a correction factor, F,

$$F = \left(1 + \frac{1}{1 - \left(\dfrac{\phi}{\phi_{max}} \right)} \right)^2 \qquad (4)$$

where $2k$ is taken as 2.5, the Einstein viscosity coefficient, and ϕ_{max}, the maximum allowable volume fraction of particles, is taken to be 0.83. The results shown in Fig. 12, show that the effect of the volume fraction of particles in the low frequency or rubbery region is predicted extremely well by eqn. (2); for

reduced frequencies less than 10^5 sec^{-1} the curves for all four systems coalesce into a single curve to within a tenth of a log unit. As the frequency is increased the dispersion of the curves increases indicating that eqn. (2) is no longer valid. This is not surprising, since at high frequencies the modulus of the elastomer approaches that of the filler, invalidating the assumption in the derivation of eqn. (2) of relatively rigid filler particles. Further analysis shows that at high frequencies the dynamic modulus is affected in a complex way by the filler fraction; in fact, it can be shown that, unlike their behavior at low frequencies, the storage and the loss moduli have different dependencies upon the filler fraction at high frequencies.
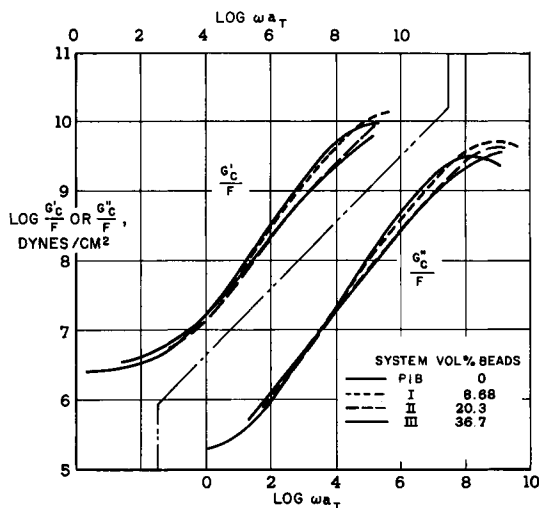
FIG. 12. Reduced storage modulus and reduced loss modulus divided by Eiler-van Dyck factor for systems of varying filler fraction (adapted from Landel [10]).

(4) *Poisson Ratio.*

In discussing the dilatational behavior of a material, it is most convenient to define Poisson's ratio, ν, in terms of the logarithmic or Hencky strains

$$\nu = - \frac{d \ln \left(\dfrac{W}{W_0} \right)}{d \ln \left(\dfrac{L}{L_0} \right)} \tag{5}$$

Unlike the classically-defined Poisson ratio based upon small deformation theory, the Poisson ratio, thus defined, is independent of the extension. It also provides a very convenient relationship between the Poisson ratio and the volume change. For example, for samples of square cross-section:

$$\frac{d \ln \left(\dfrac{V}{V_0} \right)}{d \ln \left(\dfrac{L}{L_0} \right)} = 1 + 2 \frac{d \ln \left(\dfrac{W}{W_0} \right)}{d \ln \left(\dfrac{L}{L_0} \right)} = 1 - 2\nu \tag{6}$$

Thus, $\nu = \frac{1}{2}$ would indicate no volume change with strain regardless of extension.

Smith [12] has conducted a systematic study of the dilatational behavior of a filled elastomer as a function of filler fraction. The experiments were conducted on a polyvinyl chloride–dioctyl sebacate rubber filled with varying concentrations of glass beads. The glass beads were essentially spherical and size distributions with the mean diameters between 40 and 140 μ were used. A dilatometer was used to measure the volume of the samples as a function of elongation. The data for a single test temperature have been taken from his measurements of composites with varying volume fractions of filler and plotted in Fig. 13. As
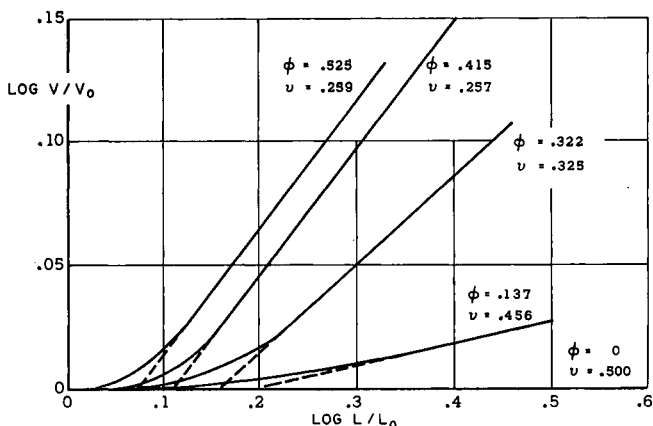
FIG. 13. Volume increase during the extension of a composite propellant with varying filler fractions (from Smith [12]).

indicated by the discussion in the introduction of this section, these curves can be divided into three sections. In the region of small deformations, no volume increase is observed as the specimen is extended. In the second section dewetting begins and the volume of the specimen increases at a progressively increasing rate as the deformation and the degree of dewetting increases. In the final section dewetting is thought to be complete and the logarithmic volume increases linearly with the logarithmic strain.

Smith also observed that it is possible to estimate the yield strain of the binder-filler bond from measurements like those shown in Fig. 13.* Consider a unit cube of elastomer filled with uniform, spherical, relatively rigid particles, where the volume fraction of the filler is ϕ. Assume that the spheres lie with their centers in a cubic close-packed array, and consider a line through the centers of particles in a row parallel to the axis of elongation. The length of the line is unity and the fraction of the line occupied by spheres is $(\phi/\phi_{max})^{1/3}$, where

---

* As mentioned in the footnote on page 84, this discussion must be altered if it is found that dewetting initiates in the binder rather than at the binder-filler bond. However, in this case this discussion is still valid if "local yield strain of the elastomer" is substituted for "yield strain of the binder-filler bond".

ϕ_{max} is the maximum volume fraction of particles allowed by close packing consideration ($\phi_{max} = 0.74$ for uniform spheres). If the cube is strained, the following relationship is obtained

$$\epsilon = \epsilon' \left[1 - \left(\frac{\phi}{\phi_{max}} \right)^{1/3} \right] \tag{7}$$

where ϵ is the overall strain and ϵ' is the strain in the binder between two adjacent spheres. If dewetting occurs at some critical value, ϵ'_c, which is independent of the filler fraction, then from equation (6) the experimentally observed yield strain, ϵ_c, would be given by the equation

$$\epsilon_c = \epsilon'_c \left[1 - \left(\frac{\phi}{\phi_{max}} \right)^{1/3} \right] \tag{8}$$
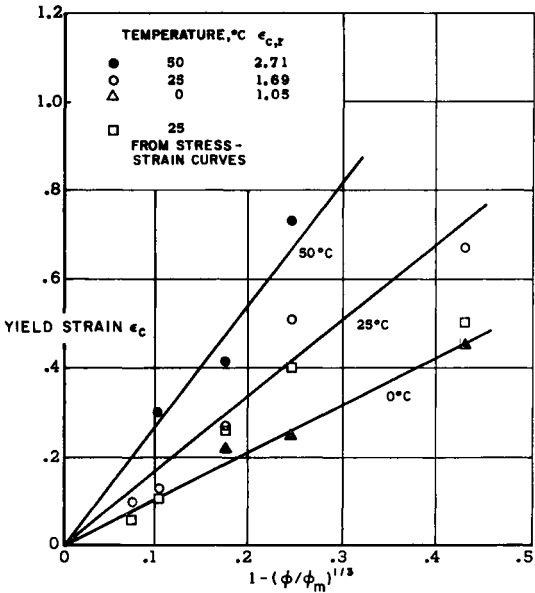
FIG. 14. Variation of yield strain with filler fraction (from Smith [13]).

The yield strain, obtained by extrapolating the linear portion of curves like those in Fig. 13, is plotted against $[1 - (\phi/\phi_m)^{1/3}]$ in Fig. 14. There is considerable scatter but eqn. (8) appears to be qualitatively justified. From the slopes in Fig. 8, and the stress–strain curves for the unfilled binder, Smith obtained stresses at bond failure of 550, 470 and 430 psi at 0°, 25° and 50°C respectively. Despite the sparsity of data these results suggest that the filler-binder bond in this system is relatively insensitive to temperature.

(5) *The Propellant Failure Boundary.*

The concept of a failure envelope for elastomers was developed by Smith [13]. He observed that in certain elastomeric materials the temperature reduced stress at failure, $\sigma_b T_s/T$, plotted against the failure strain, ϵ_b, for different

temperatures and rates of strain seemed to define a curve, or failure boundary. By the discussion of the preceding section, a propellant just prior to failure is almost certainly fully dewetted. In this dewetted condition the physical properties of a filled elastomer are almost completely determined by the properties of the elastomer alone, so it is reasonable to expect that filled elastomers such as composite propellants should also exhibit failure boundaries. And, in fact, they do, as seen in Fig. 15 for a typical propellant. A very extensive study undertaken at the Stanford Research Institute [14] has shown that these failure boundaries are dependent to some extent upon the stress–strain path by which the propellant
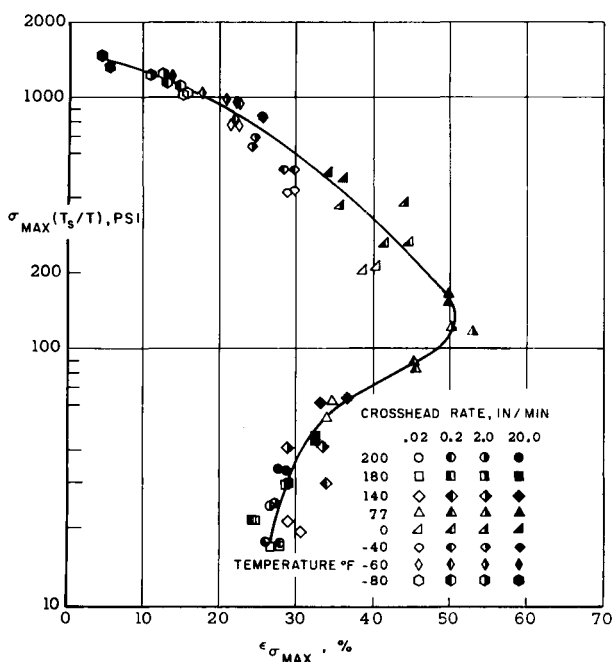
FIG. 15. Propellant failure boundary (from Kruse [16]).

reaches the failure boundary. Nevertheless, the uniaxial failure boundary still provides a very convenient basis of comparison of the ultimate properties of propellants.

The view of a binder dominated failure boundary indicates that the fraction and the size distribution of the oxidizer particles should have only a small influence on the failure boundary through their influence upon the number and size of the vacuoles formed by dewetting. Some preliminary data obtained by Kelley [15] support this prediction; for the three propellants he tested, there was a slight effect of filler fraction. Only for one propellant shown in Fig. 16, was the variation with filler fraction systematic. There are no data to indicate the effect of the particle size distribution of the filler.

The usefulness of the uniaxial failure boundary is limited by the fact that failure in real rocket motors is the result of complex multiaxial-stresses and

strains. For the positive prediction of failure, it is therefore necessary to know the failure properties of a propellant under multiaxial loadings, or, as it is generally called, the failure surface. A great deal of work has been devoted to the development of the topology of the failure surface of propellants; see, for instance, [16]. However, little or nothing can be said about the effects of the filler on this failure surface.
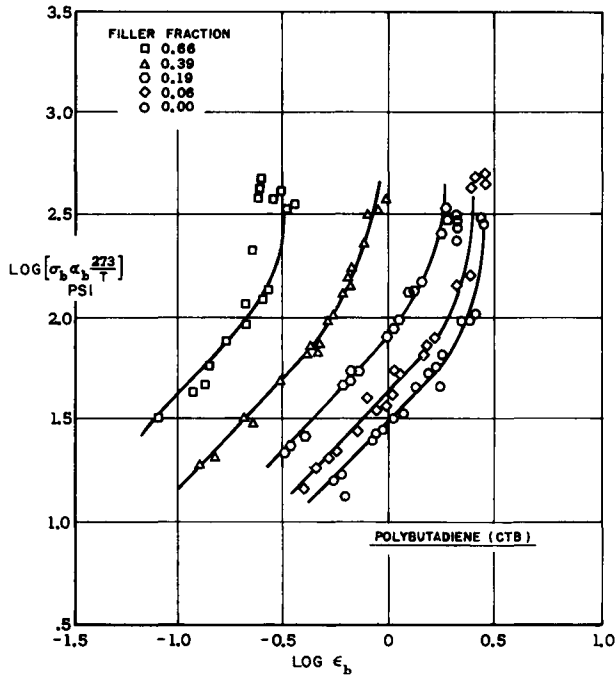
FIG. 16. Propellant failure boundary for several filler fractions (from Kelley [15]).

Effects of Other Composition Variables

The effects of the oxidizer particles discussed above and the effects of the other composition variables are outlined in Table 1. In referring to this table, it should be remembered that general statements of trends can be made only within a family of propellants. What is true for ammonium perchlorate propellants may not be true for propellants based on ammoniun nitrate, and trends observed in simple binder-oxidizer propellants may not be at all typical of catalyzed or metallized propellants. Therefore, this table must be considered indicative of general trends and not all definitive.

Effects of Embedded Wires

One of the most interesting possibilities in solid propellant design has been the inclusion of metallic fibers in the propellants. It has been found experimentally that overall burning rates can be increased several-fold simply by embedding these fibers into the propellant. Fibers of many configurations

TABLE 1. EFFECTS OF COMPOSITION VARIABLES ON COMBUSTION PROPERTIES
AND ON MECHANICAL PROPERTIES

I Effect of percent oxidizer on:

  A. Combustion properties
- 1. r_{1000}—maximum near stoichiometric mixture ratio [3] [4] [34][†]
- 2. n—strong effect but not predictable [3] [4] [34]
- 3. I_{sp}—maximum near stoichiometric mixture ratio on fuel-rich side
- 4. ρ_p—increases linearly with volume fraction of oxidizer
- 5. T_f—maximum near stoichiometric mixture ratio

  B. Mechanical properties
- 1. E_e—increases sharply with volume fraction of filler, ϕ [7] [10]
- 2. E^*—increases with ϕ [7] [10]
- 3. T_g—increases linearly with ϕ [7] [10]
- 4. ν—decreases with ϕ in dewetted condition [12] [14]
- 5. failure boundary—effect observed but uncertain [15]

II Effect of particle size distribution on:

  A. Combustion properties
- 1. r_{1000}—increases for smaller particle sizes [3] [4] [34]
- 2. n—slight effect, not predictable [3] [4] [34]
- 3. I_{sp}—no effect
- 4. ρ_p—no direct effect; distribution determines the maximum possible loading, ϕ_{max}
- 5. T_f—no effect

  B. Mechanical properties
- 1. E_e—slight theoretical dependence upon ϕ which depends upon distribution of particle sizes
- 2. E^*—slight theoretical dependence upon ϕ
- 3. T_g—uncertain
- 4. ν—uncertain
- 5. failure boundary—uncertain [8]

III Effect of percent of metals (Al, Mg, Be, . . .) on:

  A. Combustion properties
- 1. r_{1000}—effect varies widely with nature of the particular metal and its physical characteristics
- 2. n—effect varies widely with nature of the metal
- 3. I_{sp}—sharp maximum near the stoichiometric ratio of binder-oxidizer-metal [38]
- 4. ρ_p—increases with increasing percent metal
- 5. T_f—maximum near stoichiometric composition [38]

  B. Mechanical properties[‡]

† Numbers in brackets refer to cited references.

‡ The effect of metal particles is the same as the effect of oxidizer particles (see I and II above) except for the nature of the binder-filler bond for different metals [36]

TABLE 1—*continued*

IV. Effect of binder composition on:
    A. Combustion properties
        1. r_{1000}—broad effect, strongly affected by catalysts [3] [4]
        2. n—broad effect [3] [4]
        3. I_{sp}—different binders lead to different stoichiometries [38]
        4. ρ_p—varies linearly with density of binder
        5. T_f—different binders lead to different stoichiometries [38]

    B. Mechanical properties
        1. E_e—modulus depends linearly upon modulus of the unfilled
               binder [7] [10] [37]
        2. E^*—modulus depends linearly upon modulus of the unfilled
               binder [7] [10]
        3. T_g—varies linearly with the T_g of the unfilled binder [7] [10]
        4. ν—varies widely with the strength of the adhesive bond
               between binder and filler [12] [35]
        5. failure boundary—varies with the ultimate properties of the
               binder [13] [15] [22]

(continuous wires, staples and foils) have been tried and surprisingly small wire loadings, generally only a few per cent, have been found to be sufficient to cause large increases in burning rate. The method is doubly appealing for future use since metals such as aluminum are almost universally used in current propellant formulations, so that these burning rate increases can be obtained with an almost negligible loss in the specific impulse. Here, then, is a potentially powerful tool for the rocket designer, a means of varying the burning rate substantially without altering any of the other combustion characteristics.

The challenge of wire embedded grains to the analyst of propellant structures and properties is obvious and complex [17]. The addition of wires adds another degree of difficulty to the already difficult problem of "filled elastomers". In the case of continuous wires or oriented staples, the problem becomes strongly anisotropic. In general, it has been found that very long or continuous wires tend to strengthen the grain, while short wires tend to weaken the grain. Quantitatively, the strength of the grain certainly must depend upon the bond between the elastomer and the embedded fibers, which in turn depend strongly upon the materials, the processing techniques, and the stress history of the material.

The most widely used model for the combustion of wire embedded propellants is a thermal one. According to this model, the wires, having a far greater thermal conductivity than the propellant, conducts heat from the hot combustion gases into the interior of the propellant. The propellant adjacent to the wires is heated and burns at an appropriately increased rate. This more rapid burning along the wires causes a local distortion or "coning" of the propellant surface which finally results in a large overall increase in the burning surface area. According to this model, it is this increase in burning surface area which causes the observed increase in the mass burning rate. For certain fiber materials and for fibers which are not closely bonded to the surrounding propellant, other models seem to be

more appropriate [18]. However, for a wide range of materials and conditions, the thermal model of burning rate enhancement has proved to be consistent with experimental observations.

Because of the insulative nature of solid propellants and the small wire loadings which are generally used, direct interactions between the temperature fields of two wires should occur only infrequently. Therefore, most of the properties of wire embedded burning can be predicted from the analysis of the burning around a single wire.

Consider, then, the quasi-steady burning of a semi-infinite propellant with a single wire embedded in it parallel to the direction of burning, Fig. 17. Analysis
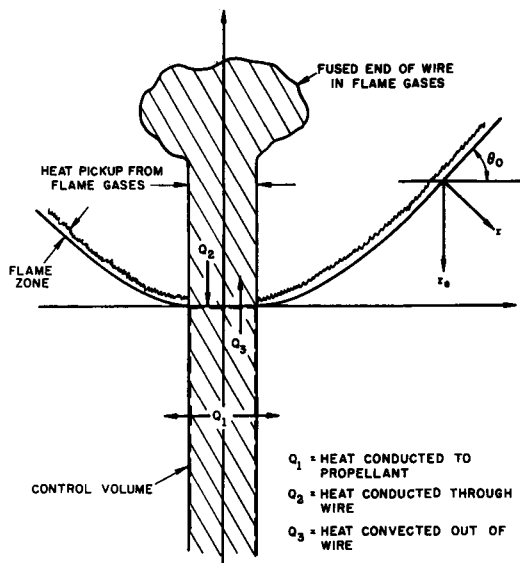
FIG. 17. Thermal model of wire embedded burning, showing the geometry and defining a control volume in the wire.

shows that the burning surface of the propellant not in the direct temperature field of the wire is wedge-shaped in the two dimensional case, or approximately conical in the axisymmetric case. In either case this burning surface is at an angle θ_0 from a plane normal to the wire, where

$$\cos \theta_0 = \frac{r}{r_e} \tag{9}$$

r being the normal burning rate of the propellant and r_e the enhanced burning rate of the propellant.

A heat balance in a control volume defined by the position of the wire embedded in the propellant yields the following relationship, Fig. 17

$$Q_1 = Q_2 - Q_3 \tag{10}$$

where Q_1 is the heat conducted into the propellant; Q_2 heat conducted into the control volume through the wire; and Q_3 heat convected out of the control

volume. The exact form of each of these terms is very complicated and many assumptions must be made before they can be written in analytical form. However, this equation combined with a little intuition results in some interesting predictions.

Consider, for example, the effect of wire diameter d in the axisymmetric case. The dependence of Q_1 and Q_3 upon the wire diameter is relatively simple. Under similar conditions the amount of heat conducted to the propellant will depend upon the area of the wire in contact with the propellant; i.e. $Q_1 \sim d$. Similarly the heat convected out of the control volume will depend upon the cross-sectional area of the wire; $Q_3 \sim d^2$.

The dependence of Q_2 is undoubtedly much more complex. The heat conducted through the wire will depend upon the amount of heat picked up by the portion of the wire extending into the gas phase. The amount of heat pickup will depend upon the state of the exposed wire—continuous, molten, burning, etc.—which can depend upon the diameter in a very complex way. However, assuming that the exposed portion of the wire is essentially continuous, it is reasonable to assume that for very small wires the amount of heat will depend upon the thermal resistivity of the wire; i.e. $Q_2 \sim d^2$, for small d, whereas for large wires it probably depends upon the area of the wire exposed to the hot gases; $Q_2 \sim d$, for large d.

Substituting these dependencies into the heat balance equation, one sees that for small diameter wires the right side of the equation depends upon the square of the wire diameter, while the left side varies linearly with diameter. Thus, as the diameter approaches zero, the right-hand side will approach zero more quickly than the left-hand side. This says that for small diameter wires the amount of heat conducted into the propellant, and hence the enhancement of the burning rate, decreases with decreasing diameter. On the other hand, for large diameter wires $Q_2 \sim d$ and $Q_3 \sim d^2$. Thus, as the diameter increases the convective loss, Q_3, will increase faster than the heat supplied through conduction, Q_2, indicating that for large diameter wires, Q_1 and likewise the enhancement of the burning rate will decrease with increasing diameter. (In fact, in accordance with intuition, if the wires are large enough they will act like heat sinks, inhibiting rather than enhancing the burning rate.)

This behavior at small and large diameters indicates that there should be a wire diameter at which the enhancement of the burning rate is a maximum. A computer analysis conducted by Caveny and Glick [19] for the burning rate along a fiber of rectangular cross section also predicted just such a maximum, Fig. 18.

All of the above discussion pertains to a quasi-steady, single wire process. The transients, both in the development of a steady process in each individual wire and in the development of the burning surface between the wires, have been neglected. However, Caveny and Glick report a transient period of only a few milliseconds duration in their calculations for a typical single fiber of rectangular cross section. Similarly, the steady, or in the case of staples, the quasi-steady, burning surface between the wires should be accomplished in fractions of

7

seconds. The development of the burning surface for an array of parallel, continuous wires is represented in Fig. 19.

As mentioned above, if the wires are oriented, both the burning rate and the mechanical properties of the propellant are anisotropic. This anisotropy intro-
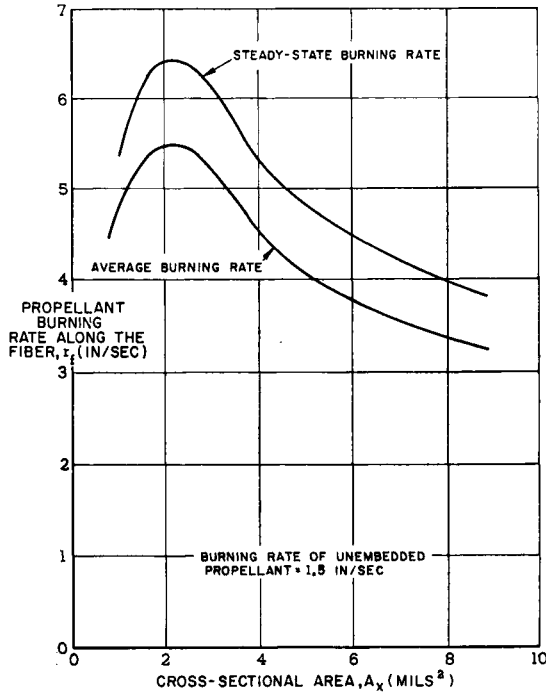
Fig. 18. Effect of varying the cross-sectional area on the propellant burning rate along the fiber (from Caveny and Glick [19]).

duces many complications into the design and evaluation of the grain—the geometric design, the calculation of stress distributions, and the prediction of failure properties. However, once these problems are surmounted, the extra degree of freedom offered by the possibility of wire orientation may lead to new and better designs.

4. EFFECTS OF STATE VARIABLES ON COMBUSTION CHARACTERISTICS AND MECHANICAL PROPERTIES

The influence of propellant composition on the combustion and mechanical properties of a solid propellant rocket motor are discussed in the previous section. This section is devoted to a discussion of the influence of the physical state of the propellant. The primary state variables which are discussed are the temperature and the degree of cure of the binder. Finally, the provocative possibility of a direct effect of strain upon the burning rate is discussed at the end of this section.

Effects of Temperature

The effect of temperature on the combustion characteristics of a propellant is confined to a slight influence on the burning rate. The thermodynamic parameters, such as I_{sp} and T_f, vary with the temperature of the grain, but since the variation of sensible enthalpy is negligible compared to the great quantities of chemical enthalpy released during the burning process, the net effect is small. Similarly, because of the thermal variations experienced during processing and curing, the thermal expansion, and hence the density variation with temperature, is necessarily small in any practical propellant. The thermal effect on the burning
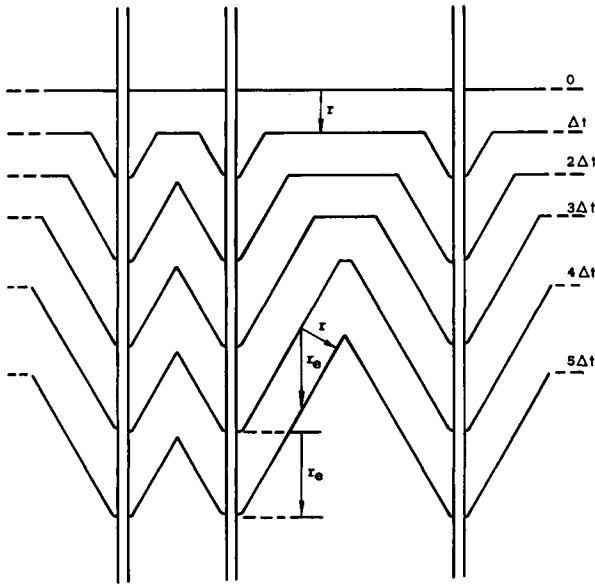
Fig. 19. Development of the steady state burning surface for an array of long, parallel wires.

rate, while more pronounced, is still relatively small. For most composite propellants the reported increase in burning rate over a wide range of temperatures is of the order of 0.1 to 0.2 per cent per °F [20]. It may be twice this much for typical double base propellants.

The effects of temperature on the structural properties of elastomeric materials are pronounced. Almost every facet of the mechanical behavior of these materials —stress–strain relationships, creep compliance, dynamic response, dilatational behavior, and the ultimate tensile properties—exhibits a well-defined variation with temperature. It was observed very early that there was a reciprocity between the temperature and the rate at which strain was applied, low strain rates corresponding to high temperatures and high rates to low temperatures. This analogy was made quantitative on a semi-empirical basis by Williams, Landel and Ferry [11]. They found that the ratio a_T of any relaxation time at a test

TABLE 2. EFFECTS OF PHYSICAL STATE ON COMBUSTION PROPERTIES AND ON
MECHANICAL PROPERTIES

1. Effect of initial temperature on:
   A. Combustion properties
      1. r_{1000}—$\dfrac{d \ln r}{dt} \approx 0.1\%$ [20]
      2. n—little effect [20]
      3. I_{sp}—little effect, the increase in sensible enthalpy is negligible compared to the chemical enthalpy of the propellant
      4. ρ_p—negligible variation
      5. T_f—little effect, generally determined by dissociation reactions which are independent of initial temperature

   B. Mechanical properties
      1. E_e—proportional to absolute temperature
      2. E^*—proportional to absolute temperature on a WLF reduced time scale, t/a_T [7] [11]
      3. T_g—no effect
      4. ν—depends upon temperature in some complicated way [35]
      5. failure boundary—represents the effect of the temperature on the ultimate properties

II Effect of state of cure of the binder on:
   A. Combustion properties
      1. r_{1000}—little or no effect [3]
      2. n—little or no effect [3]
      3. I_{sp}—no effect
      4. ρ_p—little effect
      5. T_f—no effect

   B. Mechanical properties
      1. E_e—varies inversely with molecular weight between cross-links, M_c [15] [22]
      2. E^*—varies inversely with M_c [15] [22]
      3. T_g—uncertain
      4. ν—complex dependence upon "strain energy" (area under the stress-strain curve) [35]
      5. failure boundary—the strain maxima, $\varepsilon_b^{1/2} \sim M_{c\mathrm{max}}$ [15] [22] [23]

temperature T to the relaxation time at some standard temperature T_s could be evaluated by the semi-empirical equation,

$$\log a_T = -\frac{C_1 (T - T_s)}{C_2 + (T - T_s)} \tag{11}$$

where C_1 and C_2 are empirically chosen constants and T_s is generally chosen to be about 50°C above the glass transition temperature T_g. The ratio a_T is generally called the temperature shift factor.

Even though solid propellants are highly filled elastomers, the principle of time-temperature equivalency seems to be valid. The technique of temperature

shifting [7] has had excellent success in superimposing many different types of data obtained at various strain rates and temperatures, although there is evidence that a vertical as well as a horizontal shift is necessary for some propellants [21].
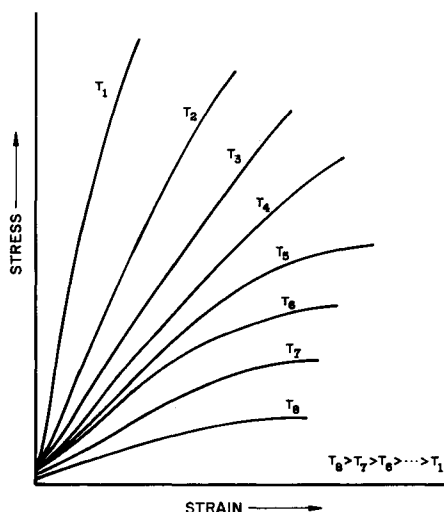
FIG. 20. Effect of temperature on stress-strain behavior of composite solid propellants (from Kruse [16]).
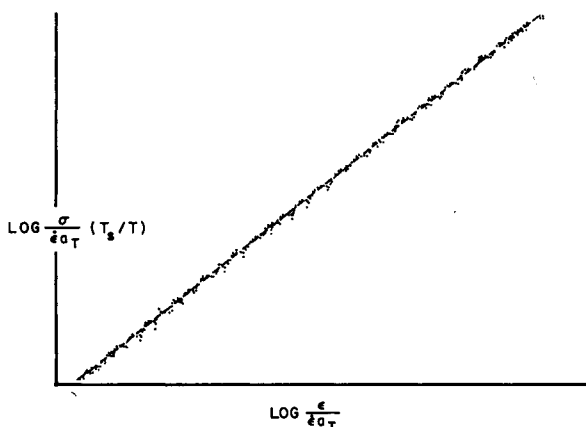
FIG. 21. Master stress-strain curve obtained from constant strain rate tests (from Kruse [16]).

In spite of the fact that the theoretical basis for this temperature shifted superposition is derived from the theory of small deformations, the strain rate and temperature effects on the ultimate properties of propellants are very successfully reduced with the same temperature shift factor.

As an example of the temperature-rate superposition, Fig. 20 shows the stress–strain curves for a typical propellant at various temperatures. Figure 21 shows the single curve obtained from the stress–strain data by plotting the reduced

stress, $\sigma/\dot{\epsilon}a_T\,T_s/T$, versus the reduced strain, $\epsilon/\dot{\epsilon}a_T$, where a_T is determined from eqn. (11). The value of this technique is obvious; the physical properties at any temperature and any strain rate can be determined from a single experiment conducted at any convenient temperature and strain rate.

Effects of Degree of Cure of Binder

The combustion of a propellant is essentially independent of the physical state of the binder. The specific impulse and flame temperature depend only upon the chemical composition not the physical state of the binder. And, similarly, the density is little affected. It is not surprising, therefore, that the burning rate of a propellant is also only slightly dependent upon the degree of
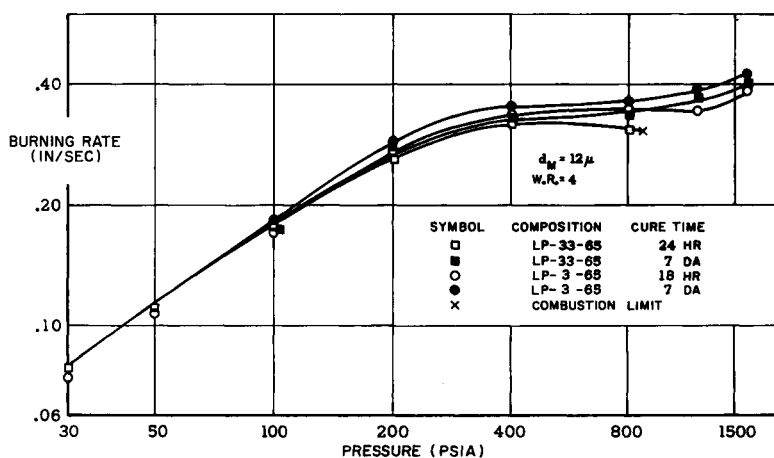
FIG. 22. Degree of polymerization effects on burning rate of polysulfide–AP propellant, (from Bastress [3]).

cure of the binder. Bastress [3] measured the burning rate of several propellants at various stages of cure. The results for one of his propellants are shown in Fig. 22.

The structural properties, naturally, are strongly affected by the physical state of the binder, the structurally most important component in the composite system. Questions about the state of cure, sol fraction, degree of crosslinking, etc., are of prime importance in a mechanical properties analysis.

In an extremely interesting study, Kelley conducted ultimate property tests on propellant systems for which the degree of cross-linking—as measured by the average molecular weight between cross-links, M_c—had been determined by using rather novel equilibrium swollen state tensile and compression techniques [15]. As expected, his data indicate that the equilibrium modulus E_e varies inversely with M_c. Figure 16 shows the failure envelopes obtained by Kelley for one of his propellants.

Kelley also plotted his failure envelopes in a log $\sigma_b 273/T$ versus log $E_e\epsilon_b$ scale, following the suggestion of Smith that failure envelopes should be compared at

equivalent cross-link densities by shifting the logarithmic strain axis by the logarithmic of the equilibrium modulus [22]. As seen in Fig. 23, the failure envelopes reduced in this way do superimpose quite well. However, it is also pointed out by Kelley that the vertical shift suggested by Landel [23] would also superimpose the failure envelopes. The vertical shift proposed by Landel, however, has the disadvantage that it does not superimpose the maximum strains, ϵ_{bmax}, as does the horizontal shift proposed by Smith [15].
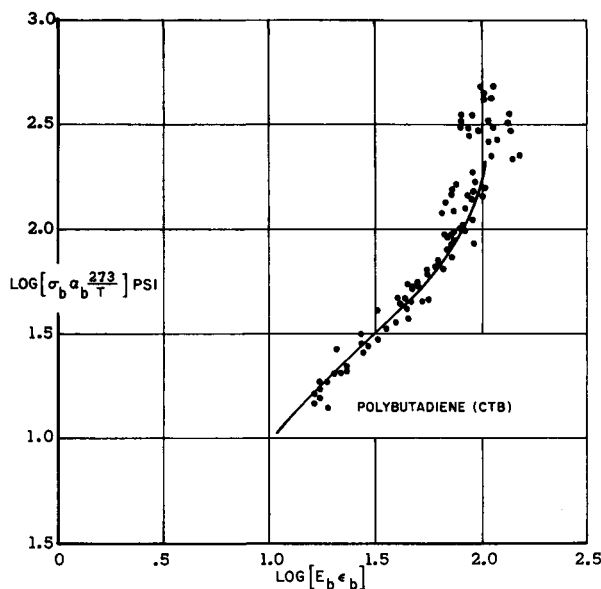
FIG. 23. Superimposed failure boundary (from Kelley [15]).

The final state property to be discussed is the strain level and its effect on the burning rate of the propellant. The results of the few investigations of this effect which have been reported are interesting but generally inconclusive. As a result very little can be said definitely about the effect of strain except that the effect does seem to exist for some propellants and some strain levels.

Coy [24] reported a 1.5 per cent increase in burning rate for each per cent strain in a polyurethane–AP propellant. Tests conducted at Atlantic Research Corporation at strains on the order of 100 per cent also showed a definite increase in burning rate [25]. And, finally, in a more extensive study, Saylak [25] measured the burning rate of four propellants at different strain levels. The results for each of these propellants are shown in Fig. 24. The magnitude of the effect, typically a one to two per cent increase in burning rate for each per cent of strain, indicates that this is a phenomenon worthy of further attention.

Any detailed study of this effect would be difficult because the combustion processes are confined to a region very near the surface where edge-effects are

certain to complicate the actual stress distribution. Furthermore, the thickness of the preheat region of the combustion zone, typically 10–50 μ, is on the order of the diameter of the oxidizer particles, so that within the combustion zone it is not proper to consider the propellant to be homogeneous. Phenomenologically, however, it is reasonable to expect that the dewetting caused by the strain is the agent through which the interaction exists. From the discussion of dewetting above, it is suggested that a critical test of this hypothesis is to compare the
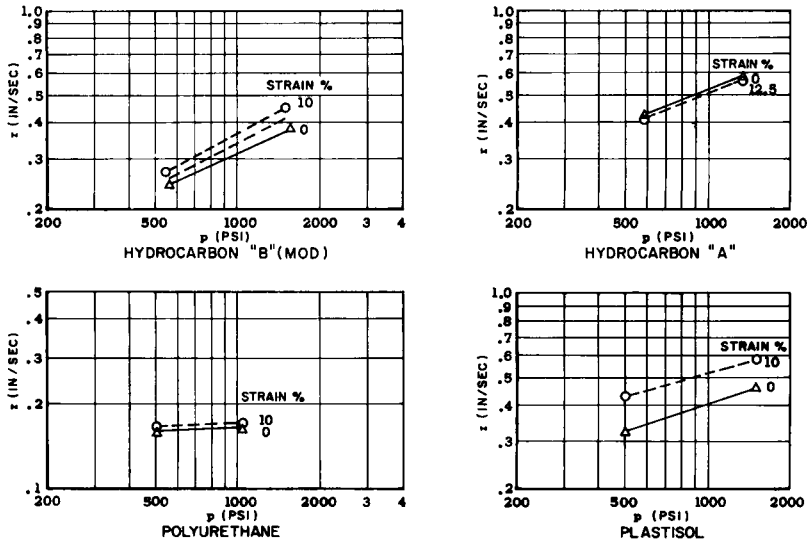
FIG. 24. Effect of strain on the linear burning rate of a typical composite propellant (from Saylak [25]).

effect of strain to the level of dewetting. If such a relationship exists, the strain level at which no effect on the burning rate is observed should correspond to the strain level below which there is no dewetting. If this hypothesis is true, the burning rate should also be dependent upon the history of the propellant; a propellant which has been recently strained should be partially dewetted even in the unstrained state.

5. THE PRESSURE TRANSIENT AT IGNITION AND ITS RELATION TO THE "IGNITION SHOCK"

Each of the above sections deals with the interactions between the combustion and the physical structure of a propellant during periods of steady burning. Equally, or possibly more, important are these interactions during periods of transition—during the ignition transient or in periods of actual or potential instability. The ignition transient is discussed in this section, while some of the interrelations between mechanical properties and oscillatory combustion are examined in Section 4.

The pressure transient at ignition is of critical importance in the design of solid propellant rocket motors. Because of the viscoelastic nature of solid propellants, both the stress and the rate at which this stress is applied are highly important to the structural performance of the grain. Thus, both the high rates of pressurization and the commonly observed possibility of the pressure overshooting its design level during the ignition transient place stringent requirements on the structural design of a grain. It is essential, therefore, in the design of an ignition system and in the design of the grain itself to understand the pressure transient at ignition as fully as possible.
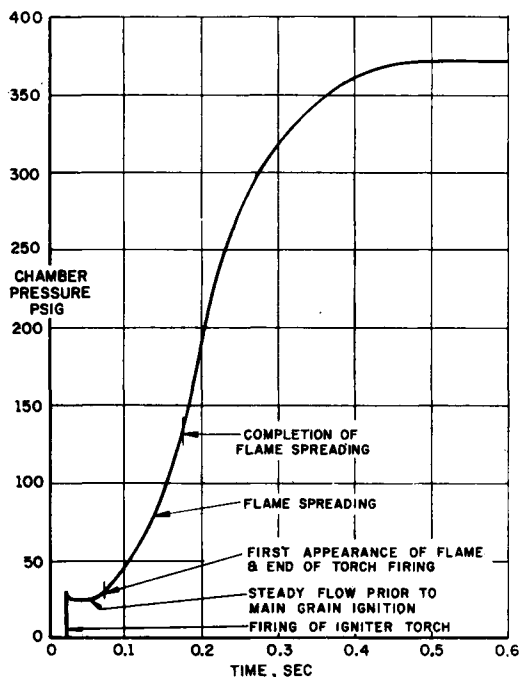
FIG. 25. Pressure transient during ignition of test motor [26].

For the purposes of analysing the ignition processes, it is convenient to divide the ignition transient into three intervals.* These intervals are: the "ignition lag" —the interval between the firing of the igniter and the first ignition of the grain surface; the "flame spreading" interval—the interval between this first ignition and the moment when the ignition flame has spread over the entire surface; and the "chamber filling" interval—the interval during which the equilibrium chamber pressure is finally attained. The relationship between these intervals for a small ignition test motor is shown in Fig. 25.

In general the characteristics of the igniter can have a strong effect upon all the phases of the igniter transient. However, in an effort to explore the effects of the individual phenomena, it is assumed that the igniter behaves "nicely" for

* This discussion is based primarily upon work reported in Ref. [26].

the present. That is, it is assumed that the igniter serves its function of igniting a certain portion of the propellant surface without otherwise affecting the ignition process. Some of the igniter effects observed in real rocket motors are discussed below.

Throughout the ignition interval the integral equation of mass continuity must be satisfied.

$$\dot{m}_{\text{igniter}} + \dot{m}_{\text{propellant}} = \dot{m}_{\text{nozzle}} + \dot{m}_{\text{chamber}} \tag{12}$$

If some reasonable assumptions are made—a power law relation between the burning rate and the pressure, negligible variation in the gas properties through the chamber, a choked nozzle, etc.—this equation can be written as a first order differential equation for the chamber pressure:

$$\dot{m}_{\text{igniter}} + S\rho_p b p_c^n = \frac{A_t p_c}{c^*} + \frac{V_c}{RT_c}\frac{dp_c}{dt} \tag{13}$$

where:

S = instantaneous area of propellant burning
p_c = instantaneous chamber pressure
T_c = chamber gas temperature, taken constant
ρ_p = density of propellant
b, n = constants in the burning rate law, $r = bp_c^n$
A_t = throat area
V_c = chamber volume
c^* = characteristic exhaust velocity
R = gas constant for the chamber gases

It can be shown from this equation that the maximum rate of pressure rise at any pressure level occurs at maximum S; that is, in the chamber filling interval. Since the maximum rate of pressure rise is a convenient parameter for use in a structural analysis, it is informative to look in detail at the chamber filling interval.

Under the condition of negligible igniter flow, the mass continuity equation becomes a Bernoulli equation with the solution:

$$p_c = p_{c_{\text{eq}}} \left[1 - P_0\, e^{-\left(\frac{(1-n)c^*\Gamma^2}{L^*}\right)t} \right]^{\frac{1}{1-n}} \tag{14}$$

where $(p)_{\text{eq}}$ is the equilibrium chamber pressure; P_0 a function of the initial conditions; $L^*\ V_c/A_t$, a characteristic length; and

$$\Gamma^2 = \text{a function of } \gamma;\ \sqrt{\gamma\left(\frac{2}{\gamma+1}\right)^{\frac{\gamma+1}{\gamma-1}}}$$

Analysis of this solution shows that during the chamber filling interval a plot of the function $\ln[1 - p_c^{(1-n)}(p_c)_{\text{eq}}^{(n-1)}]$ versus t is linear. This observation provides a very convenient method for deducing the time of flame spreading in a rocket

motor from the experimental record of the chamber pressure. Such a plot is shown in Fig. 26 for a small test motor; graph (a) is the experimental pressure trace, graph (b) is a plot of the above function, and graph (c) is a plot of the area burning obtained from the experimental pressure record and numerical solution of the mass continuity equation. As can be seen, this graphical method provides a distinct resolution of the time of flame spreading.
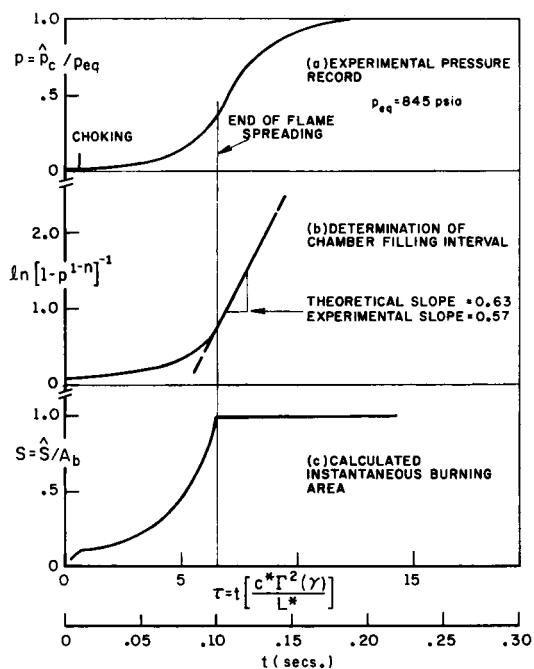
FIG. 26. Determination of flame spreading interval for an experimental pressure trace [26].

Further analysis of this solution shows that the maximum rate of pressure rise during the chamber filling interval can be written quite simply;

$$\left(\frac{dp_c}{dt}\right)_{max} = \frac{p_{c_{eq}} c^* \Gamma^2}{L^*}(1 - n)n^{\frac{n}{1-n}} \tag{15}$$

Barring igniter effects this surprisingly simple expression represents the maximum rate of pressure rise which can occur during the ignition transient. Substituting values for a typical rocket motor, a maximum rate of pressure rise of the order of 2×10^5 psi/sec is predicted during the chamber filling interval.

This expression for the maximum rate of pressure rise depends quite strongly upon the burning rate exponent n as seen in Fig. 27. It is largest for small n and decreases, in fact approaches zero, as n approaches one. At first it seems contradictory, that the propellant whose burning rate exhibits the least dependence upon pressure should have the greatest rate of pressure rise. However, since the propellant with the least pressure dependence has the greatest burning rate at

pressures lower than the equilibrium pressure, the predicted dependence of the pressure rise upon the burning rate exponent is reasonable.

All of the above discussion is for the special case of negligible igniter effects during the ignition transient. This, of course, is frequently untrue; the igniter

$$(dp_c/dt)_{MAX} = \frac{P_{c_{eq}} c^* \Gamma(\gamma)^2}{L^*} (1-n)n^{n/1-n}$$

$P_{c_{eq}} = 1000 \text{ PSI}$

$c^* = 5000 \text{ FT/SEC}$

$L^* = 5 \text{ FT}$

$\gamma = 1.2$

$(dp_c/dt)_{MAX}$ PSI/SEC
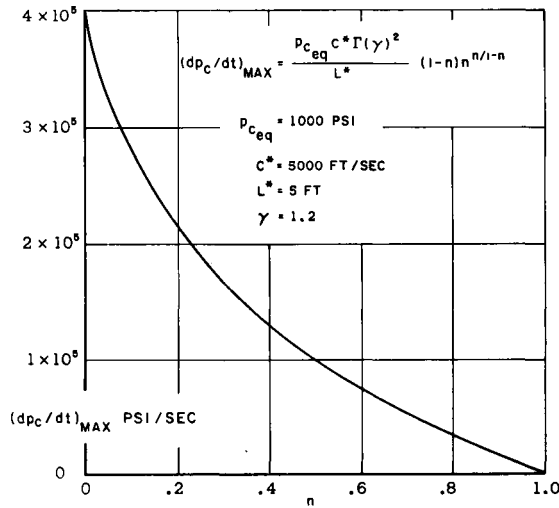
FIG. 27. Variation of the maximum rate of pressure rise during the ignition transient with the burning rate exponent.
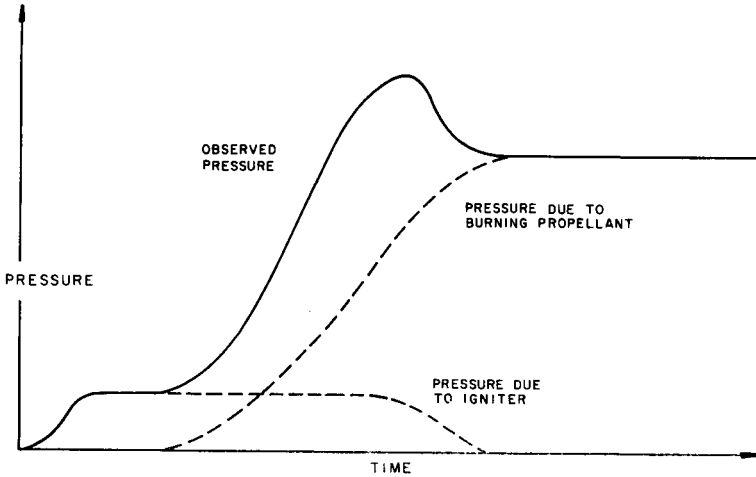
FIG. 28. Pressure overshoot due to an "oversize" igniter.

has several effects upon the combustion processes during ignition. If the igniter continues to generate gases throughout the flame spreading and the chamber filling intervals, the mass continuity equation shows that the rate of pressure rise is increased. If the igniter flow continues even beyond this, an artificially high chamber pressure results. The pressure overshoot frequently observed in rocket motors can thus be the result of an "oversize" igniter [Fig. 28].

Interestingly, an igniter which is "undersized" can also cause a pressure overshoot. The mechanism of such an overshoot is generally described in the following way. Prior to ignition of the propellant surface, the igniter serves to heat the propellant. If the heat flux from the igniter is low enough there is a considerable ignition delay and a relatively large depth of propellant is heated. Because of this preheating of the subsurface propellant, the burning rate immediately after ignition is greater than the normal burning rate. Clearly, if the depth of preheating by the igniter is great enough—this is, if the heat flux from the igniter is low enough—this increase in the burning rate will prevail long enough to cause an overshoot in the chamber pressure. This behavior is described pictorally in Fig. 29.
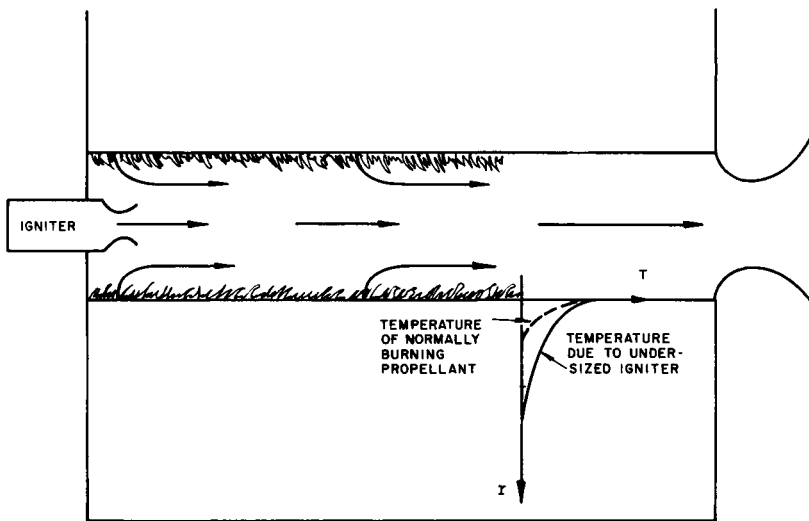
FIG. 29. Explanation of mechanism of pressure overshoot due to an "undersized" igniter.

6. THE INTERRELATION BETWEEN OSCILLATORY COMBUSTION AND THE STRUCTURAL PROPERTIES OF THE PROPELLANT

Combustion instability is present to some degree in almost every solid propellant rocket motor. The potential of instability results from the great amounts of energy released by the combustion process, the acoustic nature of the combustion chamber, and the changing geometry of the port as the burning progresses. As the geometry of the combustion chamber varies continuously, it is almost certain that some of the acoustic modes are amplified in their interaction with the complex combustion process. It is the responsibility of the design engineer to control the severity and duration of the instabilities through the proper design of the propellant—its configuration and formulation.

Because of the complex, "noisy" flow patterns in the interior of a rocket motor, there is always a large source of initial perturbations for any potential instability. With this wealth of sources small scale oscillations are almost certainly

present even in "stable" motors—neutrally stable modes, unstable modes which are quickly damped by non-linear effects, and even stable modes with very small attenuation factors. These small scale oscillations place further requirements on the physical properties of the grain on both the large and the small scale. Overall grain integrity under these dynamic loadings is of primary importance, of course, but for high combustion efficiency it is also important that the propellant does not shatter locally, breaking into fragments which are injected into the combustion chamber.
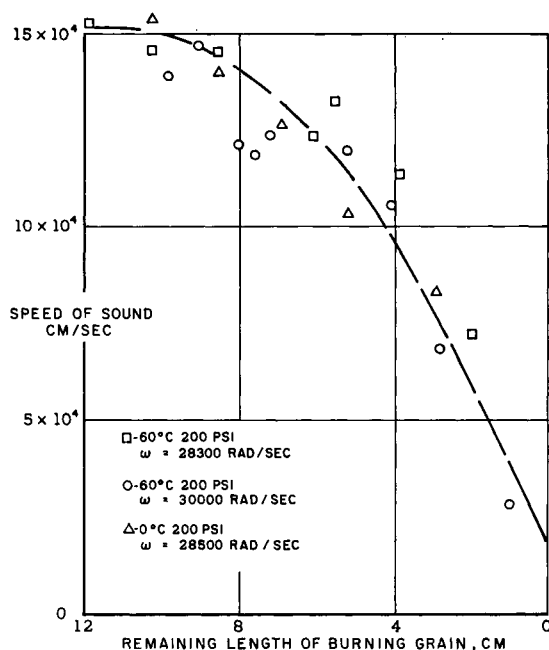
FIG. 30. Variation of propellant sound speed with time under conditions of dynamic loading (adapted from Ryan and Coates [27]).

Another effect of these small-scale oscillations is their influence upon the physical properties of the propellant. The possibility of this interaction has been almost completely neglected, but a recent experimental study has shown that the influence may be remarkably strong [27]. In this study an end-burning grain was fired in a constant oscillation frequency T-burner while the pressure in the gas and in the solid were measured. From the analysis of the amplitude and phase of the acoustic oscillations it was determined that the physical properties of the propellant had changed markedly over the course of the run. Figure 30 shows the temporal variation of the measured speed of sound in the propellant. The data shown in this figure actually represent three separate experiments all conducted under different conditions. However, the differences between the test conditions are so slight that all of the data tabulated in Ref. [27] are included in Fig. 30 to indicate qualitatively the magnitude of the effect. As can be seen,

the effect of the dynamic loading on the sound speed in the propellant is large; the sound speed decreases more than 50 per cent in the course of a 10 sec firing at normal stress amplitude variations of less than 50 psi.

Confidence in these reported results is limited by the validity of the assumptions by which the physical properties are calculated from their experimental pressure data. For instance, in the analysis of the acoustics it is assumed that there is a velocity node at the gas-propellant interface. Some objections to this *a priori* assumption have been raised [28], as is discussed briefly below. However, environmental studies involving cyclic loading indicate that under many conditions the propellant properties do indeed change when subjected to dynamic loadings [29]. And, even if these tests are merely indicative, the implications for long duration solid propellant boosters are obvious.

The above discussion deals with the effect of combustion instability upon the grain. Equally important, but frequently neglected, is the effect of the propellant upon the instability characteristics of a rocket motor. As is discussed, the bulk properties of the grain may have a significant effect upon the acoustic behavior of the combustion chamber and therefore have a direct influence upon the stability–instability behavior of the rocket.

The major portion of the energy release during the combustion of solid propellants occurs in the gas phase very near the burning surface. The thickness of this "flame zone", generally measured in microns, is very small compared to the wavelengths of typical acoustic modes which are comparable to the physical dimensions of the combustion chamber. It is, therefore, both convenient and consistent to consider the combustion zone to be of infinitesimal thickness and to be located right at the surface of the propellant. This is the commonly made "collapsed flame zone" assumption. It should be recognized that some propellant formulations, notably those with metal additives, exhibit a more widely distributed heat release. In fact, the well known ability of aluminum powder to suppress instabilities when added to some propellants in relatively small quantities may be the result of the more widely distributed heat release which results. Attempts have been made to analyze the effect of distributed heat sources upon instability [30], but for this generalized discussion it remains informative to retain the concept of a collapsed flame zone.

Since nearly all the energy in the rocket motor system is released through chemical reaction in the flame zone, it is reasonable that the greatest interaction between the combustion and the acoustic modes occurs when the flame zone lies in a region of maximum pressure fluctuation; that is, at or near an antinode in the pressure wave. Just this behavior was reported in some of the earlier instability experiments [31] where it was shown that instability occurred only when propellant was placed near the pressure wave antinodes in an acoustic resonator. The acoustic nature of the entire rocket—combustion gases, propellant, liner, casing, etc.,—therefore, becomes of primary interest.

Although the velocity of sound in many solid propellants is comparable to the sound velocity in the combustion gases, the far greater density of the solid results in a very low ratio of energy transfer to the propellant from an incident

acoustic wave in the gas phase. Because of this small ratio of energy transfer, it is tempting to make the simplifying assumption of an incompressible boundary condition at the propellant surface. However, McClure, Hart and Bird [28] have shown that this assumption often leads to erroneous predictions about the natural modes of the complex acoustic system.

As an example, they consider the simple problem of a one-dimensional, two-medium, rigid ended cavity where the "solid" and the "gas" support only scalar wave notion [28] (Fig. 31). Straightforward solution of the scalar wave
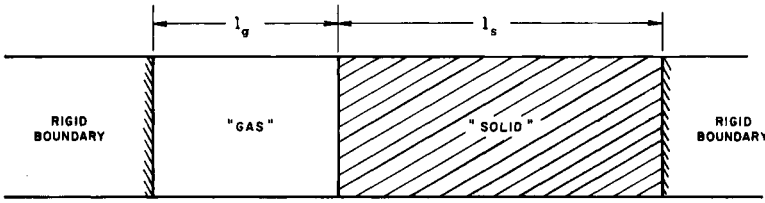
FIG. 31. One-dimensional, two-medium, rigid-ended acoustic cavity.

equation shows that the normal modes ω_n of the system are given by the characteristic equation;

$$\tan\left(\frac{l_g\omega_n}{c_g}\right) + \frac{\rho_g c_g}{\rho_s c_s}\tan\left(\frac{l_s\omega_n}{c_s}\right) = 0 \tag{16}$$

where ρ is the density; c the velocity of sound; and l the length of the corresponding region (total cavity length $= l_g + l_s$). The subscript 'g' refers to "gas"; 's' refers to "solid".

Because of the discrepancy in density between the propellant and the gas, the parameter $\rho_g c_g/\rho_s c_s$ is very small in general. Thus, the equation for the normal modes of the system has two limiting forms of solution:

$$\tan\left(\frac{l_g\omega_n}{c_g}\right) \to 0 \tag{17}$$

and

$$\tan\left(\frac{l_s\omega_n}{c_s}\right) \to 0$$

It is now observed that the first equation approaches the equation for the natural modes of the gas cavity under the boundary condition of no velocity at the gas–solid interface. Similarly, the second equation approaches the equation for the natural modes in the solid under the boundary condition of no pressure variation at the gas–solid interface. In the terminology of McClure, Hart and Bird, these are referred to as the "gas quasi-modes" and the "solid quasi-modes" respectively.

A representative case, calculated in Ref. [28], is shown in Fig. 32. The solid lines represent the first and second modes for the system, and the dashed lines represent the quasi-modes of the gas and of the solid. As can be seen, the gas

quasi-modes are followed closely by the normal modes of the system except in regions where the gas and solid quasi-modes intersect. This is reasonable since near the intersections the propellant surface is required to behave like a rigid surface if the gas quasi-modes are to be followed and like a free surface if the solid quasi-modes are to be followed. Because of these forbidden regions, the observed frequencies in the cavity, instead of varying continuously as the gas cavity volume increases, should exhibit an intermittent behavior as the web thickness varies. Extending this analysis to cylindrical geometries, analogous results are calculated for the radial and the tangential modes. The intermittency predicted in this way is in good qualitative agreement with the intermittent instability observed experimentally in rocket motors [32].
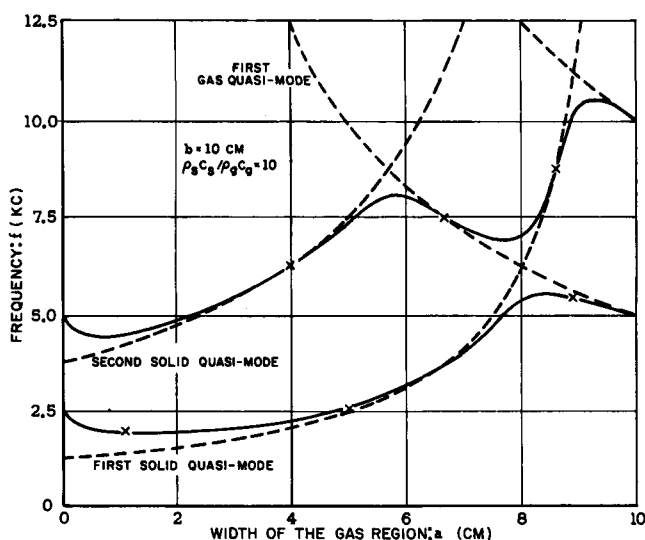
FIG. 32. Normal modes and "quasi-modes" of a one-dimensional, two-medium cavity as the width of the gas region varies (from McClure, Hart and Bird [28]).

Other strong evidence for the participation of the propellant in the acoustical behavior of a rocket motor is reported by Angelus [33] who studied the instability characteristics of several rocket motors which were identical except for the nature of the interface between the motor casing and the exterior of the cylindrical grain—some grains were bonded tightly to the case and others were only loosely fitted. He observed that the instability characteristics of the two types of motors were quite different. This difference is almost impossible to explain on this basis of an acoustical behavior controlled solely by the nature of the gas cavity, whereas the lack of any difference would be difficult to explain on this basis of the two medium nature of the cavity.

The following physical explanation of the unsuspected importance of the viscoelastic motion of the solid is offered [28]. To the initial oscillations originating in the gas phase the solid boundary does indeed appear to be rigid because of the far greater inertia of the solid. However, for appropriate geometries of the

solid, the pressure wave which is generated in the solid is reflected from the outer boundary in such a way that it interferes with the pressure wave then at the surface. In fact, if the phase shift is exactly 180°, the cancellation of the pressure wave is exact and the gas–solid interface behaves like a free boundary rather than a rigid boundary. For these geometries the natural modes of the system are very similar to the solid quasi-modes. Otherwise, the solid boundary does behave like a rigid boundary and the gas quasi-modes determine the natural modes of the system.

Here, then, is an area of interaction between combustion and structural properties which might be fruitfully explored. If both the dilatational and the shear elastic moduli of the propellant could be determined, it would be possible to determine the natural acoustic modes of the system. Knowing these "potentially dangerous" modes, it might be possible to suppress them. Or, conversely, if the frequencies at which the combustion process will support instabilities are known, it may be possible for the designer to eliminate the natural acoustic modes of these frequencies—perhaps by judiciously hardening or softening the propellant formulation.

7. SUMMARY

To summarize, it is necessary to return to the discussion of solid propellant rocket design, for it is only in this discussion that the cohesiveness of this study can be seen. The many subjects and the diverse discussions are bound together by a single purpose—the optimization of design. As indicated in the introduction, design is merely the attempt to find the optimum compromise between all of the possibilities.

In the most general terms design optimization involves the consideration of three factors: performance, reliability, and cost. But, in specific terms, the questions and the complexity are multiplied many times. Does the increased ease of fabrication warrant the resulting loss in performance? Will the structural advantages gained by using larger fillets outweigh the disadvantage of a larger sliver? Will the greater stresses due to a higher operating pressure be tolerable in view of the greater combustion efficiency? And so on, until each possibility has been recognized and evaluated.

This then is a necessary step in the rational design of a rocket motor—to recognize and to evaluate the full effect of each design variable. This study has dealt with some of the aspects of two of the many areas which must be considered in the overall design, combustion and structural integrity. It was seen in Section 3, for instance, that some composition variables, such as the oxidizer loading or the form and degree of wire embedding, have a strong effect on both the combustion and the mechanical properties of a grain. Similarly, other variables, such as the state of cure of the binder discussed in Section 4, can affect some properties strongly and others not at all. In Section 5 it was seen that the ignition transient, which can have a significant effect upon the structural integrity of a grain, is a function of the combustion parameters, and this interrelation is

discussed in some detail. Finally, the many interrelations between the structural properties and combustion instability phenomena were surveyed in Section 6 in the hope that this discussion, like all of the others, might aid in the development of more effective designs and more effective design practices.

Acknowledgments—It is a pleasure to acknowledge the helpful discussions and the assistance of Dr. A. Gordon, Mr. L. Kurylko and Dr. J. Wenograd.

REFERENCES

[1] BILLHEIMER, J. S. and WIEGAND, J. H., "Integrated solid rocket design procedure utilizing computers" (unclassified), *Bulletin of the Interagency Solid Propulsion Meeting*, Vol. III (conf.), p. 11, July 1963.

[2] ROSSINI, R. A. and THREEWIT, T. R., "An automatic design-selection and optimization program for solid rocket systems" (unclassified), *ibid*, p. 37.

[3] SUMMERFIELD, M., SUTHERLAND, G. S., WEBB, M. J., TABACK, H. J. and HALL, K. P., "Burning mechanism of ammonium perchlorate propellants", *Solid Propellant Rocket Research* (Ed. M. Summerfield), pp. 141–182, Academic Press, New York, 1960. See also: E. K. Bastress, "Modifications of the burning rates of ammonium perchlorate solid propellants by particle size control", Ph.D. Thesis, Princeton University, January 1961.

[4] ADAMS, G. K., NEWMAN, B. H. and ROBINS, A. B., "The combustion of propellants based upon ammonium perchlorate", *8th Symposium on Combustion*, Williams and Wilkins, Baltimore, 1962, p. 693.

[5] GORDON, S. and ZILEZNIK, F. J., "A general IBM 704 or 7090 computer program for computation of chemical equilibrium compositions, rocket performance, and Chapman–Jouguet detonations" (Supplement I), NASA TN D-1737, October 1963.

[6] BLATZ, P. J., "Studies of the mechanical behavior of ammonium perchlorate particles, a glass-bead filled polyurethane binder, and a typical continuum binder", *Bulletin of the 2nd Meeting, ICRPG Working Group on Mechanical Behavior*, Vol. I (conf.), October 1963.

[7] LANDEL, R. F. and SMITH, T. L., "Viscoelastic properties of rubberlike composite propellants and filled elastomers", *ARS Journal* 31, 599 (May 1961).

[8] SCHWARZL, F. W., "Mechanical properties of highly filled elastomers", I (1962), II (1963), III (1964), ONR Technical Reports, 1, 2, 3, Contract N-62558-2822, -3243, -3581, and -3884.

[9] MARTIN, D. L., "Effect of filler concentration on the viscoelastic response of a filler polymer system", *Bulletin of the 3rd Meeting, ICRPG Working Group on Mechanical Behavior*, Vol. I, p. 303, October 1964.

[10] LANDEL, R. F., "The dynamic mechanical properties of a model filled system: polyisobutylene-glass beads", *Trans. Soc. Rheology*, 2, 53, 1958.

[11] WILLIAMS, M. L., LANDEL, R. F. and FERRY, J. D., *J. Am. Chem. Soc.*, 77, 3701 (1955).

[12] SMITH, T. L., "Volume changes and dewetting in glass bead–polyvinyl chloride elastomeric composites under large deformations", *Trans. Soc. Rheology*, 3, 113 (1959).

[13] SMITH, T. L., "Ultimate tensile properties of elastomers: I. Characterization by a time and temperature independent failure envelope", *J. Polymer Sci.*, Part A, I, 3597 (1963).

[14] FISHMAN, N. and RINDE, J. A., "Solid propellant mechanical properties investigations", Stanford Research Institute Quarterly Progress Reports, SRI Project No. PRU-4673 (1963-4).

[15] KELLEY, F. N., Personal discussions, March 1965.

[16] KRUSE, R. B., "Laboratory characterization of solid propellant mechanical properties", AIAA Preprint No. 65-147 (1965).

[17] GOLDBERG, R. S. and CHU, H. N., "Fiber mechanics of reinforced structures", *Bulletin of the 3rd Meeting, ICRPG Working Group on Mechanical Behavior*, Vol. I, p. 91, October 1964.

[18] SMITH, H. M., "Studies on the mechanism of combustion of high burning rate composite modified double base propellants" (conf.), see *AIAA Bulletin*, Vol. I, December 1964, p. 600.

[19] CAVENY, L. H. and GLICK, R. L., "Mechanical models for burning of composite propellant with embedded metallic fibers", Thiokol, Control No. U–64–332A, May 1964.

[20] *SPIA Solid Propellant Manual* (conf.).

[21] MILLOWAY, W. T. and WIEGAND, J. H., "Failure criteria for some polyurethane propellants", *Bulletin of the 20th Meeting, JANAF Physical Properties Panel*, SPIA Publication No. PP14u, p. 323, November 1961.

[22] SMITH, T. L., "Ultimate tensile properties of elastomers, II. Comparison of failure envelopes for unfilled vulcanizates", *J. Appl. Phys.*, **35**, 27, January 1964.

[23] LANDEL, R. F., CIT Abstracts on Mechanical Properties of Propellants, January 1965.

[24] COY, J., Jet Propulsion Laboratory Quarterly Summary Report 38-4, WASA Contract No. NASW-6, July 1961 (conf.).

[25] SAYLAK, D., "The effect of strain on the burning rate of solid (unconf.) propellants", *Bulletin of the 2nd Meeting, ICRPG Working Group on Mechanical Behavior*, Vol. I (conf.), October 1963, p. 395.

[26] PARKER, K. H., WENOGRAD, J. and SUMMERFIELD, M., "The ignition transient in solid propellant rocket motors", AIAA Preprint No. 64–126, January 1964.

[27] RYAN, N. W. and COATES, R. L., "Acoustic instability: Influence of and on the solid phase", *AIAA Journal*, **2**, 1130, June 1964.

[28] McCLURE, F. T., HART, R. W. and BIRD, J. F., "Solid propellant rocket motors as acoustic oscillators", *Progress in Astronautics and Rocketry*, Vol. I, Academic Press, 1960, p. 295.

[29] TORMEY, J. F. and BIRTTON, S. C., "Effect of cyclic loading on solid propellant grain structures", *AIAA Journal*, **1**, 1763 (1963).

[30] CHENG, S. I., "Combustion instability in solid rockets using propellants with reactive additives", *Solid Propellant Rocket Research* (Ed. M. Summerfield), Academic Press, 1960, p. 393.

[31] PRICE, E. W. and SOFFERIS, J. W., "Combustion instability in solid propellant rocket motors", *Jet Propulsion Laboratories*, Vol. 28, 1958, p. 190.

[32] BROWNLEE, W. G., "Nonlinear axial combustion instability in solid propellant motors", *AIAA Journal*, **2**, 275 (1964).

[33] ANGELUS, T. A., "Unstable burning phenomena in double-base propellants", *Solid Propellant Rocket Research* (Ed. M. Summerfield), Academic Press, 1960, p. 527.

[34] SUMMERFIELD, M. Princeton University, unpublished data.

[35] FISHMAN, N. and RINDE, J. A., "Development of a dilatational equation-of-state", *Bulletin of the 3rd Meeting, ICRPG Working Group on Mechanical Behavior*, Vol. I, October 1964, p. 267.

[36] SVOB, G. J., COLODNY, P. C., WADDLE, L. A. and LEFFERDINK, T. B., "Volume changes in polyurethane propellants subjected to small strains", *Bulletin of the JANAF–ARPA–NASA Panel on the Physical Properties of Solid Propellants*, 1961.

[37] ICRPG: *Solid Propellant Mechanical Behavior Manual*, CPIA Publication No. 21, September 1963.

[38] BARRERE, M., JAUMOTTE, A., FRAEIJS DE VEUBEKE, B. and VANDENKERCKHOVE, *Rocket Propulsion*, Elsevier, Paris, 1960.

[39] ORR, C. and DOLLAVALLE, J. M., *Fine Particle Measurement*, The Macmillan Co., New York, N.Y., 1959.

THE CHEMISTRY OF SOLID PROPELLANT COMBUSTION: NITRATE ESTER OR DOUBLE BASE SYSTEMS*

G. K. ADAMS

Explosives Research and Development Establishment,
Waltham Abbey, Essex, England

Abstract—During the last decade there has been a great increase in the scale of application of solid propellants in rocketry and a corresponding increase in our empirical knowledge of the internal ballistics of solid propellants. Superficially, it would appear that our understanding of the detailed mechanism of their combustion has failed to keep pace.

In this lecture an attempt will be made to review the current state of knowledge in this field and to place it in perspective in relation to the general field of combustion chemistry. We shall discuss the broad trends in research on flame propagation during the last ten years and examine their relevance to problems of solid propellant burning. At the beginning of this period there was a tendency to regard the combustion of all solids and liquids as a gasphase flame coupled to the surface of the condensed phase by heat and mass transfer processes. The successes and failures of this simple picture will be examined with reference to nitric ester propellants.

1. INTRODUCTION

The chemistry of propellant combustion has occupied the attention of scientists for many years. The burning of a solid propellant provides a striking example of the conversion of chemical energy into heat and energy of motion. Moreover, we have learned to control the rate of conversion of chemical energy. In physically homogeneous, or monopropellant, systems, this control is basically a problem in chemical kinetics, an application of the principle that substances undergo chemical change at a rate which is determined by the forces of interaction between atoms and the frequency and energy of collision processes between molecules. The science of the chemistry of propellant combustion is part of the more general field of flame chemistry. This has largely been concerned with the reaction of relatively simple fuel molecules with molecular oxygen. Even so, we still have a long way to go in understanding the detailed nature of the elementary chemical reactions which occur in such flames and which determine the speed of flame propagation. In solid propellant combustion we are usually concerned with the reactions of oxygen atoms chemically combined with other atoms in relatively complex molecules. The detailed chemistry of the combustion process is very different from hydrocarbon–oxygen systems although the physico-chemical principles involved are the same.

It is interesting to consider the broad trends in the development of combustion research. We can distinguish three phases. In the first we find the experimental study of the relation between the speed of flame propagation and the chemical composition of the combustible, together with the influence of environmental factors such as pressure and initial temperature. This leads to a recognition of the importance of the rate of chemical reaction and its dependence on the chemical nature of the reacting substances together with the temperature and pressure in the flame.

We then see the development of the theory of flame propagation, the progressive understanding of the quantitative relation between the speed of movement of the wave of chemical reaction and the rate of the processes which control that reaction. Once the difficulties in the formulation of this type of problem were overcome, and the advent of modern computing techniques made it possible to solve the resulting set of simultaneous differential equations for reaction schemes of an arbitrary degree of complexity, it became apparent that the major problem was to identify the elementary chemical reaction steps and to obtain quantitative data on their chemical kinetic properties. Thus we find evidence in the literature of an intensive experimental study of the structure of the reaction zone in flames and of the kinetics of elementary reactions of the type we should expect to occur in flames.

This suggests a suitable order of presentation of the subject of this lecture. We shall restrict the scope to that of the mechanism of combustion of double base solid propellants, since it is with these that the chemistry has a predominant effect on the internal ballistic properties. Furthermore, although our knowledge of the chemical mechanism is far from complete, the chemistry is essentially that of the combustion of nitrate esters and the reactions of nitrogen oxides, both of which have been studied more intensively than the inorganic perchlorates which are the major constituents of composite solid propellants.

2. THE INTERNAL BALLISTIC PROPERTIES
OF SOLID PROPELLANTS

The characteristic property of a useful propellant explosive is that under a given set of environmental conditions it has a unique burning rate. The burning surface regresses in the direction normal to itself at a steady rate, determined by the composition of the propellant and the external conditions, giving a flow of gaseous combustion products away and normal to the surface. It is not a difficult experiment to measure this rate in laboratory equipment and to determine its variation with composition and with the initial temperature of the propellant sample and with the external gas pressure [1]. Under rocket chamber conditions other factors, such as gas flow parallel to the surface, can influence the burning rate but we shall here only consider these first three factors. The earlier solid rocket propellants were derived from gun propellants of the cordite type: nitrocellulose plasticized with nitroglycerine and organic coolants and chemical stabilizers. At gun pressures the mass burning rate varies with very nearly the

first power of the pressure and at a fixed pressure depends mainly upon the thermochemical energy or calorimetric value of the composition. It was fortunate from the point of view of the application to rocket propulsion that the burning rate varies more slowly with pressure at pressures of 5000 psi and below. Figure 1 shows the linear burning rate plotted against the pressure on a log–log scale for Cordite S.C. This composition has been used for many years as a ballistic standard, its rate-pressure behavior has been measured by a variety of experimental techniques and is known accurately.
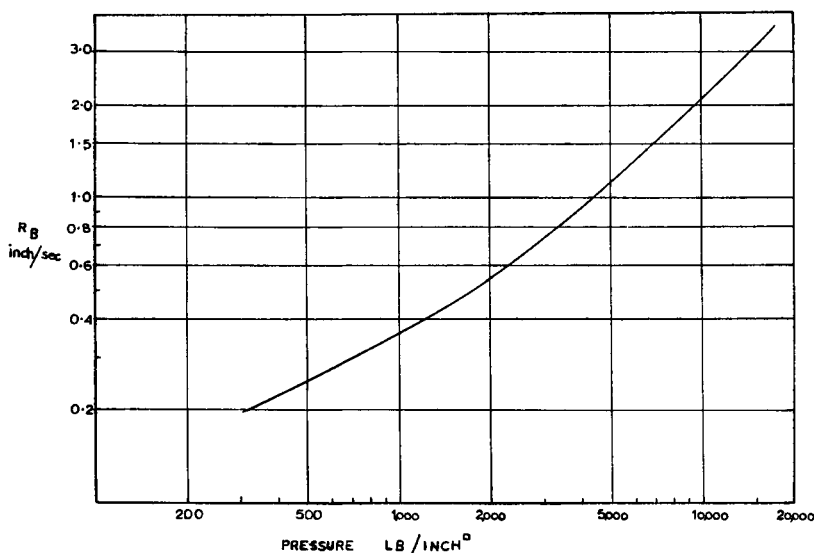
FIG. 1. Burning rate as a function of combustion pressure for Cordite S.C.

The burning rate can be represented in terms of the now standard exponential formula $r = cp^n$ with n taking different values over different ranges of pressure. For S.C. Cordite, n varies from 0.5 below 2000 psi to a value of 1 above 10,000 psi. Most double base propellants of this simple type show a qualitatively similar behavior although as the burning rate is increased by raising the calorimetric level, the pressure exponent tends to increase to the value of unity at lower pressures [5]. We now know that this ballistic property, essential for rocket propellants, is in fact not typical of organic explosives as a class. The great majority have pressure exponents of burning rate close to unity at all pressures. We also find that comparing the burning rates of a wide range of explosive compounds at a fixed pressure they are not only a function of the calorimetric level but are also dependent upon the chemical structure of the explosive molecule (Fig. 2).

The calorimetric level of explosives is known not to be a good indication of the flame temperature in low pressure combustion where the extent of chemical reaction to final products near the burning surface is incomplete. However, if we compare the burning rates of some simple nitrate esters with their experimentally

measured flame temperature, the latter is still not the only factor in determining rate. The structure of the parent molecule or the detailed mechanism of reaction of its decomposition products must play an important part in determining the rate of burning. The conventional representation of the combustion of nitrate ester propellants is in terms of three formally simple and consecutive reactions: decomposition to aldehydes and nitrogen dioxide followed by oxidation first by nitrogen dioxide and then by nitric oxide [2], for example,

$$\begin{array}{l} CH_2ONO_2 \\ \mid \qquad\qquad \rightarrow 2CH_2O + 2NO_2 \rightarrow CO + CO_2 + H_2O + H_2 \rightarrow 2CO_2 + 2H_2O + N_2 \\ CH_2ONO_2 \qquad\qquad\qquad\qquad +2NO \end{array}$$
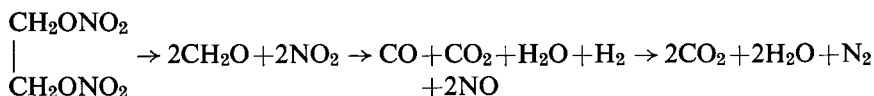
As we shall demonstrate, this simple sequence of chemical reaction steps, although adequate in this particular example of ethylene glycol dinitrate, cannot be representative of nitrate ester combustion in general.

Nitrocellulose appears to have special ballistic properties in that it not only burns at some rate three times that of the liquid ester component of a double base propellant (at equal calorimetric level) but also in that it lowers the pressure exponent of a mixture of the two components over a considerable range of concentration. It also confers the property of susceptibility to catalysis of rate of burning at low pressures by metallic compounds.

Two recent papers [6, 7] have given examples of the effect of the addition of various lead compounds to double base propellants. The addition of a few per cent of lead oxide or salts of aliphatic acids to compositions of low calorimetric value, and therefore relatively low burning rate, can increase the rate at low pressures by factors of three or more. The increase in burning rate diminishes with increasing combustion pressure so that the overall result is to give regions of very low pressure exponent (Fig. 3). At higher pressure, and with compositions of high energy and burning rate, the catalysis by these lead compounds is small but a similar effect can be induced by more thermally stable lead compounds such as salts of aromatic acids (Fig. 4).

Finely divided carbon black has a synergistic effect with lead compounds in that it enables the catalysis to persist at higher pressures [7]. Some other finely divided, thermally stable, pigments are reported to show a similar effect [7] (Fig. 5).

The effect of additions of lead compounds to the burning rate of the liquid component of the propellant is relatively small. It cannot be said to be completely specific to nitrocellulose since it is promoted by non-explosive polymers such as cellulose acetate and, to a lesser extent polymethyl methacrylate and acrylate. The monomers of these materials do not promote the catalytic effect of lead. It appears that a condensed phase surface above some minimum temperature is necessary. In a subsequent section we shall discuss other evidence on the cause of this effect of lead compounds.

Although we may now have access to a considerable volume of empirical ballistic data on solid propellant compositions, data which are essential for the development and application of solid propellants, this has not, of itself, led to
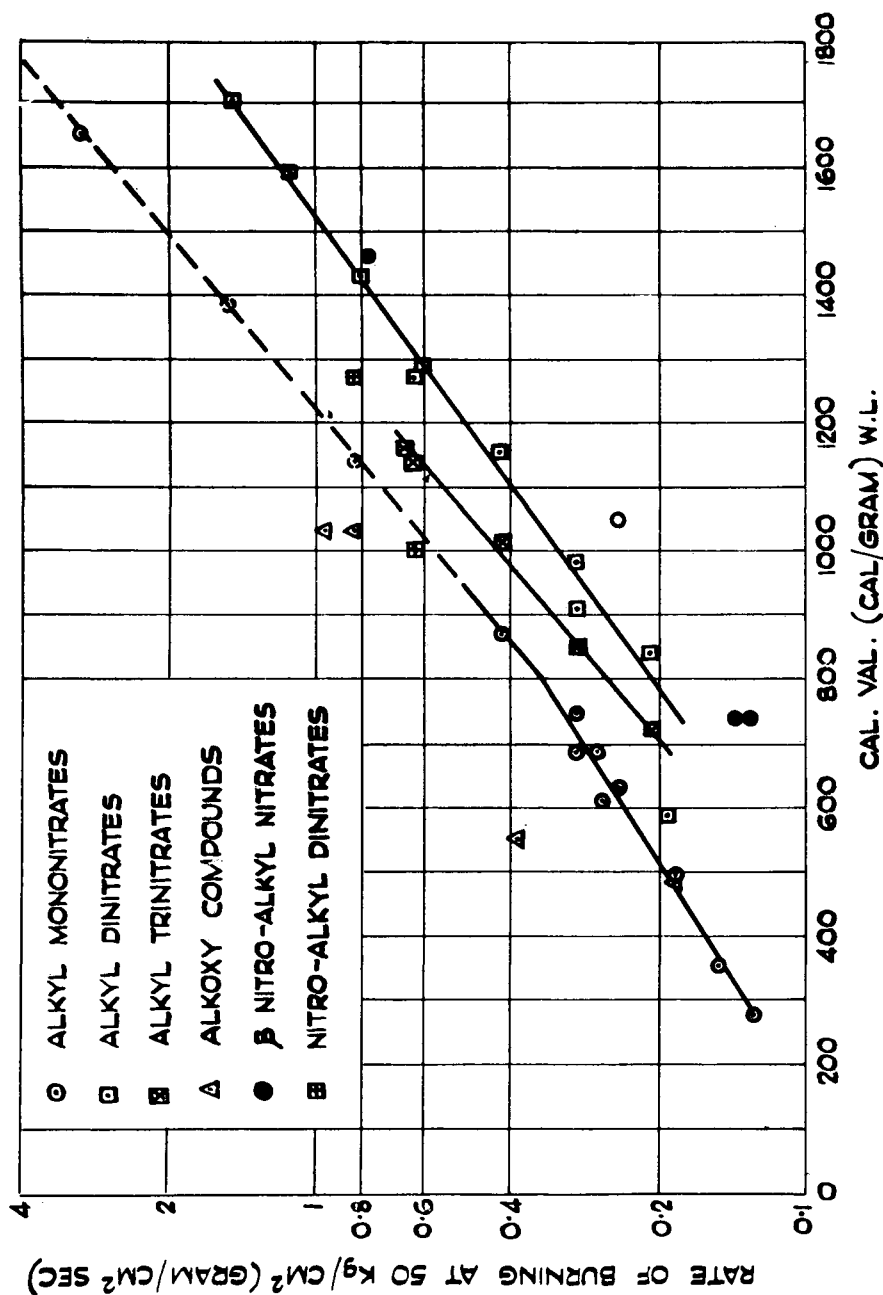
Fig. 2. Burning rate at 50 kg/cm² for nitrate esters as a function of calorimetric value.
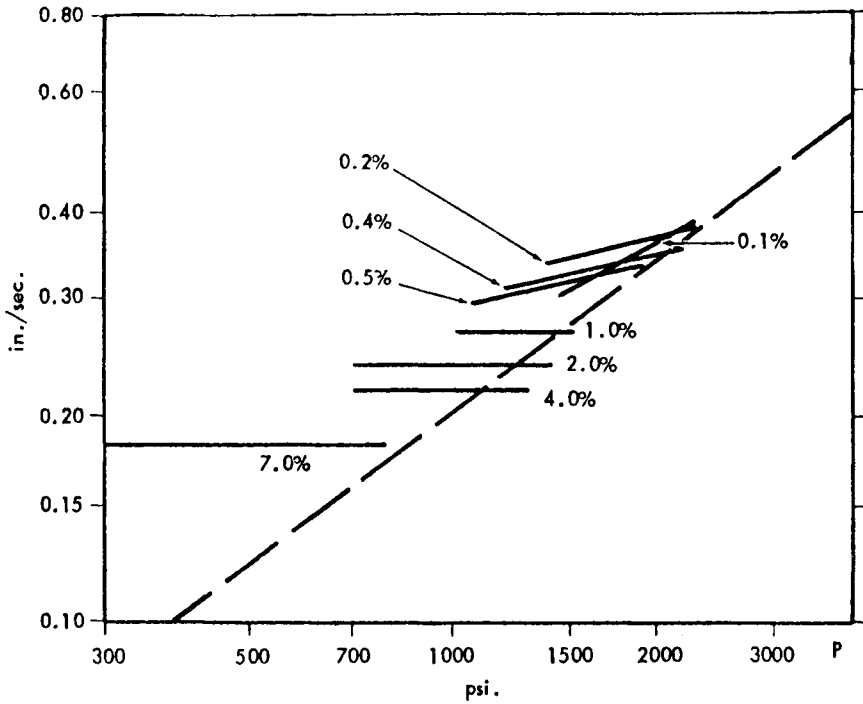
FIG. 3. Burning rate as a function of pressure for double base propellants containing x wt. % of lead stearate. Dashed curve is the unmodified propellant cal. val. = 800 cal/g. (After Preckel [6].)
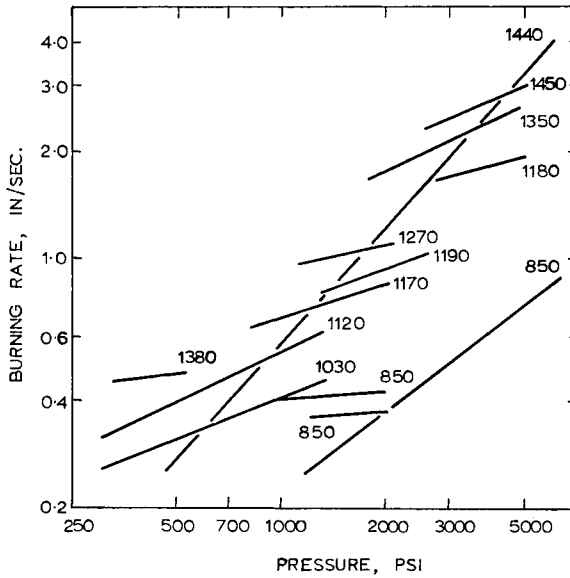
FIG. 4. Plateau ballistics with aromatic lead compounds. Numbers signify cal. val. (cal/g.) (After Preckel [7].)

any improved understanding of the mechanism of the combustion process. It will provide a proof, in the original sense of the word, of any views of the mechanism which we can obtain in other ways. A prerequisite of such tests is an understanding of the theory of the propagation of a flame supported by the pyrolysis or vaporization of a condensed phase and which, even in the simplest conception, involves a sequence of chemical reactions in the gas phase.
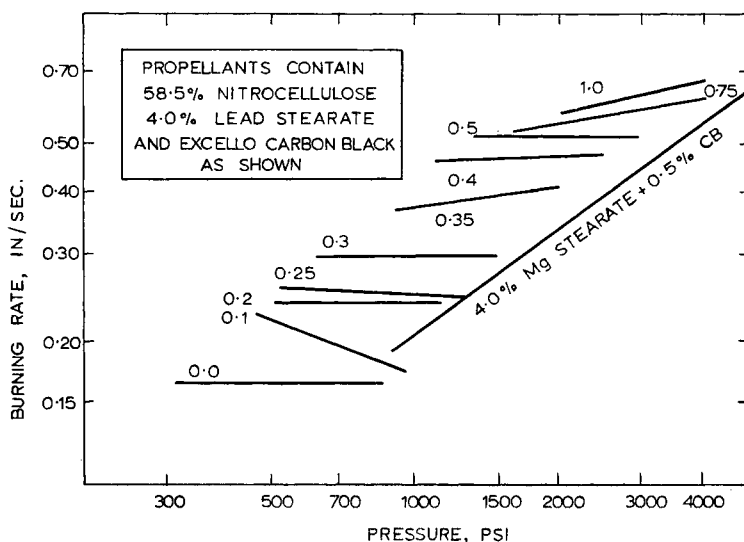
FIG. 5. Effect of carbon black on plateau ballistics. (After Preckel [7].)

3. THE THEORY OF THE BURNING
OF HOMOGENEOUS PROPELLANTS

The theory of steady laminar flame propagation in a gas undergoing a single exothermic chemical reaction is now well understood [8–10]. The problem is essentially that of determining the value of the mass flux which enables the temperature and concentration distributions to satisfy the boundary conditions imposed in the unreacted and the completely reacted regions of the flame.

The spatial variation of temperature and reactant concentrations are determined by the solution of the differential equations of mass and energy conservation together with the diffusion equations for the reacting species. For plane, one-dimensional flow these can be written as:

$$\text{Mass conservation: } M\frac{dG_i}{dx} = -w_i \tag{1}$$

where M is the total mass flux, MG_i the fractional mass flux for component I, x the space coordinate, and w_i the net rate of loss of component I due to chemical change. It is assumed that w_i can be specified in terms of chemical reaction rates which are functions of the local concentrations and temperature.

$$\text{Diffusion: } MG_i = MY_i - \rho D_i \frac{\mathrm{d}Y_i}{\mathrm{d}x} \tag{2}$$

where ρ is the mass density and Y_i is the mass fractional concentration of component I of mass diffusivity D_i.

$$\text{Energy conservation: } \frac{\mathrm{d}}{\mathrm{d}x}\left[M \sum G_i h_i - \lambda \frac{\mathrm{d}T}{\mathrm{d}x}\right] = 0 \tag{3}$$

where h_i, the component enthalpies per unit mass, are defined by

$$h_i = \Delta hf_i + \int^{T} c_p \mathrm{d}T \tag{4}$$

Δhf_i is the standard heat of formation of species I. The summation in eqn. (3) is taken over all components of the system and λ is defined as the bulk thermal conductivity.

If there is no heat loss from the combustion products and the system tends to a state of chemical equilibrium, the derivatives vanish at the hot boundary downstream of the flame. The total enthalpy then tends to a constant value and equation (3) can be integrated to give the upstream temperature gradient in terms of the local component mass fluxes and enthalpies.

$$\lambda \frac{\mathrm{d}T}{\mathrm{d}x} = M\sum G_i h_i - M \left(\sum G_i h_i\right)_{\text{hot boundary}} \tag{3a}$$

Since the space variable appears only as a differential, it is possible to eliminate it from the equations and to use the temperature as the independent variable. If the Lewis numbers are unity, $\rho D_i = \lambda/\bar{c}_p$, and if the enthalpy tends to a constant value at the hot boundary, it is well known that equations (2) and (3) can be combined and integrated to give the result that the local enthalpy remains constant from the hot through to the cold boundary. This result can also be expressed in terms of an implicit relation between the concentrations of the initial and intermediate reactants and the local temperature:

$$\sum Y_i(\Delta hf_i - \Delta hf_m) = \int_{T}^{T_m} c_p \mathrm{d}T \tag{5}$$

where Δhf_m is the standard heat of formation of the final product species, T_m is the temperature reached at the hot boundary where $Y_m = 1$, and c_p has been assumed independent of composition. The important feature of these relations between the temperature and reactant concentrations and between the temperature gradient, temperature and the component mass fluxes is the fact that they have been obtained by specifying only the hot boundary conditions; they are independent of the conditions to be imposed at the upstream boundary.

If we take the case of a single reaction step, $A \to B$, unit Lewis number, and constant heat capacity, the problem reduces to the integration of a single first

order equation for the variable G_a and the temperature T.
Thus combining

$$M \frac{dG_a}{dT} = - \frac{w_a}{dT/dx} \tag{1}$$

and

$$\lambda \frac{dT}{dx} = M(\Delta hf_a - \Delta hf_b)G_a - M\bar{c}_p(T_b - T) \tag{3b}$$

we obtain

$$\frac{dG_a}{dT} = \frac{\lambda w_a}{M^2[\bar{c}_p(T_b - T) - (\Delta hf_a - \Delta hf_b)G_a]} \tag{6}$$

where w_a can be expressed as a known function of temperature since a dependence on the reactant concentration Y_a can be eliminated by using the relation (5) which becomes:

$$(\Delta hf_a - \Delta hf_b)\, Y_a = \bar{c}_p\, (T_b - T) \tag{5a}$$

The integral curves for equation (6) which pass through the point $T = T_b$, $G_a = 0$ have been obtained by Hirschfelder, Curtiss and Campbell [8], and are illustrated in Fig. 6. The curves intersect the line $G_a = 1$ at a temperature, T_1,
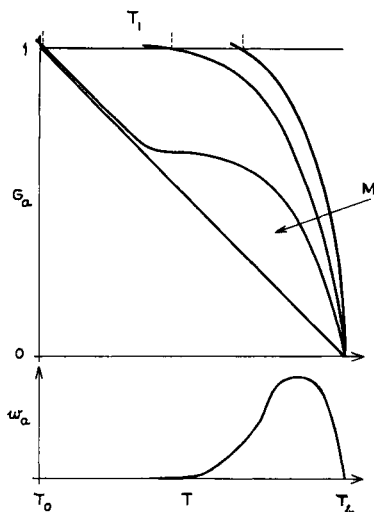
FIG. 6. G_a–T curves for varying mass flux values, M. (After Hirschfelder, Curtiss and Campbell [8].)

which decreases as the value of the total mass flux, M, increases. This temperature can be regarded as the cold boundary condition which is necessary to determine a unique flame speed. If the chemical reaction term remains finite and positive with decreasing temperature, the integral curve cannot cross the line defined by setting the denominator of the R.H.S. of (6) equal to zero and intersects the $G_a = 1$ line no matter how large is the value of the total mass flux. The

rate of heat loss at the upstream boundary can be determined by setting $G_a = 1$ and $T = T_1$ in the energy flux equation (3b):

$$\frac{\lambda}{M}\left(\frac{\mathrm{d}T}{\mathrm{d}x}\right)_1 = (\Delta h f_a - \Delta h f_b) - \bar{c}_p\,(T_b - T_1) \tag{7}$$

The concept of a flameholder abstracting heat at the cold boundary of the flame was introduced by Hirschfelder [8] to resolve the problem which results from an attempt to allow $\mathrm{d}T/\mathrm{d}x$ to vanish at the cold boundary while allowing the reaction rate to remain finite. He points out that the temperature dependence of the reaction rate function is normally such that the flame speed is insensitive to the values assigned to the cold boundary conditions so that the empirical association of a unique steady flame speed with a given inflammable gas at a given initial temperature is not contraverted.
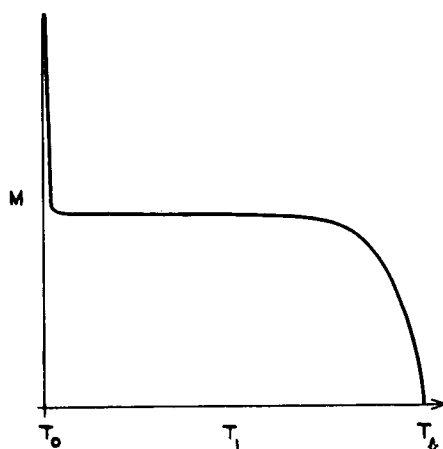
FIG. 7. M as function of cold boundary temperature, T_1. (After Hirschfelder, Curtiss and Campbell [8].)

The degree of dependence of the mass flux through a steady flame on the upstream boundary condition is a crucial point in the understanding of combustion supported by a condensed phase and involving a sequence of reactions. The relation of the mass flux to the cold boundary conditions at a constant final flame temperature is shown schematically in Fig. 7. The left hand region illustrates the fact that provided the reaction rate is everywhere finite and there is no heat loss downstream of the cold boundary, the reaction will still go to completion at very large values of the mass flux. In the middle portion of the curve the mass flux is very insensitive to variations in the upstream boundary condition. As T_1 approaches T_b the mass flux falls to zero as an increasing proportion of the area under the reaction rate curve is cut off by the upstream boundary.

Let us apply this result to the simple $A \to B$ reaction supported by evaporation from a condensed phase. The concentration-temperature relation for species A

in the gas phase is determined by the final flame temperature and the enthalpy difference between the two gas phase species. If the required mass evaporation rate is much less than the kinetic vacuum evaporation rate, an equilibrium condition will hold at the interface which provides a second relation between the fractional concentration and the temperature:

$$(Y_a)_s P = P_a^* \exp\left(\frac{-L}{RT_s}\right) \tag{8}$$

where P_a^* is a constant reference vapor pressure, P is the total pressure and L the heat of evaporation at T_s.

From (5a) and (8) the surface temperature, T_s, is determined by the equation:

$$(\Delta h f_a - \Delta h f_b) P_a^* \exp\left(\frac{-L}{RT_s}\right) = P \bar{c}_p (T_b - T_s) \tag{9}$$

It is independent of the mass flux but increases with increasing pressure. The fractional concentration of the gaseous reactant at the surface, $(Y_a)_s$, is always less than unity and decreases with increasing pressure.

We may also conclude that, so long as T_s is in a temperature region where the rate of the gas phase reaction is small compared to its maximum value, the mass burning rate is almost independent of T_s or, at a fixed flame temperature, the heat of evaporation, L. The mass flux for the gaseous flame supported by a condensed phase, its pressure exponent and its dependence on flame temperature will be the same as that of the flame propagating through the gaseous reactant at the same flame temperature.

If the mass flux is comparable with the kinetic evaporation rate or if the gasification process is a surface pyrolysis, the surface temperature is determined by the mass flux rate through an equation of the form:

$$M = k \exp\left(\frac{-E}{RT_s}\right) \tag{10}$$

In this case, the surface temperature at constant pressure will vary with the mass flux and, if the mass flux for the gas phase reaction increases with pressure, the surface temperature will also increase with pressure. $(Y_a)_s$ is again less than unity and is a function of M. At high pressures where T_s approaches the final flame temperature, the mass flux tends to a constant value determined by the rate of the surface reaction at $T_s = T_b$.

Spalding [11] has used this variation of the surface temperature with pressure to develop a theory of inflammability limits for the burning of solid or liquid monopropellants based upon radiative heat loss from the surface of the condensed phase to the surroundings. If the heat absorbed by the surface is small compared with that radiated, then the final flame temperature will be less than the adiabatic value T'_b by the amount

$$T'_b - T_b = \sigma\epsilon \frac{T_s^4}{M\bar{c}_p} \tag{11}$$

where σ is Stefan's constant and ϵ is the emissivity. This equation expresses the fact that the change in the heat flux in the burnt gases must equal the rate of loss of heat by radiation.

Spalding defines a dimensionless heat loss intensity:

$$Q = \frac{\sigma\epsilon(T'_b)^3}{\bar{c}_p M} \tag{12}$$

He shows that if this exceeds a critical value, no steady value of the mass flux is obtained. Thus if M decreases with decreasing pressure, there will be a lower pressure limit for steady burning. An upper pressure limit may exist for a gaseous flame supported by an equilibrium evaporation process if the exothermic reaction does not occur in the condensed phase. Although upper pressure limits for some monopropellant systems have been observed experimentally [12, 13], this explanation seems an unlikely one because chemical reaction rates do not in fact vanish in a condensed phase.

The dependence of the steady state mass flux upon the boundary conditions for a single step reaction can be used to examine the behavior of a combustion process involving a number of consecutive reaction steps. If each reaction rate is assumed to depend upon a different power of reactant concentration, the mass flux satisfying given boundary conditions for each step in the sequence will vary in a different way with pressure. The steady mass flux for each step can easily be shown to vary as $P^{n/2}$ where n is the order of the chemical reaction. With suitable assumptions as to the reactive magnitudes of each reaction rate at a given pressure and temperature, we can consider the overall reaction to consist of a series of reaction zones located at different distances from the propellant surface and occurring at different temperature levels in the flame. The total mass flux is the same for each zone so that the boundary conditions at their junctions must satisfy this condition.

When the junction boundary conditions have been determined, the steady state mass flux is also determined. Several authors have used this method to determine the variation of burning rate with pressure for a hypothetical combustion model involving a sequence of reactions of increasing reaction order. Early treatments [2, 3, 4] assume that diffusion in the gas phase could be neglected. A more recent paper by Vilyunov [14] attempts to solve the diffusion equation but makes the arbitrary assumption that the mass fractional concentration of gaseous reactant at the surface of the condensed phase is equal to unity irrespective of the value of the surface temperature. We have seen that this is not generally true because the concentration–temperature relation is determined by the downstream boundary conditions in the gas phase.

Let us consider a solid A undergoing an exothermic, zero order, reaction to give a gas phase product B which then is converted to a stable product D in two stages of first and second order respectively:

$$A \underset{\text{zero order}}{\overset{k_A}{\rightarrow}} B \underset{\text{first order}}{\overset{k_B}{\rightarrow}} C \underset{\text{second order}}{\overset{k_C}{\rightarrow}} D$$
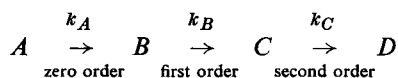
The mass rates of each successive reaction are proportional to P^0, P^1, and P^2 respectively, and at a given temperature there will be a pressure below which each successive rate will be negligibly small compared with that of the preceding rate. We assume that each reaction commences only when the preceding one has gone effectively to completion. Then in the first reaction zone $G_a + G_b = 1$, $G_c = G_d = 0$; in the second $G_b + G_c = 1$, $G_a = G_d = 0$; in the third $G_c + G_d = 1$, $G_a = G_b = 0$.

If the overall process is adiabatic and leads to a final temperature T_d, the energy flux equation can be integrated to obtain:

$$M \sum_a^d G_i (\Delta hf_i - \Delta hf_d) - \frac{\lambda dT}{dx} = M\bar{c}_p (T_d - T) \qquad (13)$$

Using the mass flux fraction relations for the first reaction zone, we find that in this zone:

$$MG_a (\Delta hf_a - \Delta hf_b) + M (\Delta hf_b - \Delta hf_d) - \frac{\lambda dT}{dx} = M\bar{c}_p (T_d - T) \qquad (14)$$

There is a minimum surface temperature T'_s defined by setting the temperature gradient in the gas phase adjacent to the surface equal to zero in (14) and putting $G_a = 0$, to give

$$(\Delta hf_b - \Delta hf_d) = \bar{c}_p(T_d - T'_s) \qquad (15)$$

If we use this relation to eliminate T_d, equation 14 becomes:

$$MG_a(\Delta hf_a - \Delta hf_b) - \frac{\lambda dT}{dx} = M\bar{c}_p(T'_s - T) \qquad (16)$$

The differential equation for G_a as a function of T is then:

$$\frac{dG_a}{dT} = \frac{\lambda w_a}{M^2 [\bar{c}_p(T'_s - T) - G_a(\Delta hf_a - \Delta hf_b)]} \qquad (17)$$

This equation is to be integrated from the cold boundary where $G_a = 1$ to the propellant surface where $T = T_s$, $G_a = 0$. Using the thermochemical relation defining the initial temperature T_0:

$$\bar{c}_p(T'_s - T_0) = \Delta hf_a - \Delta hf_b \qquad (18)$$

we may write (17) as:

$$(T'_s - T) \, dG_a - (T'_s - T_0) \, G_a dG_a = \frac{\lambda w_a}{M^2 \bar{c}_p} \, dT \qquad (17a)$$

The LHS of equation (17a) can also be expressed as:

$$(T'_s - T_s)dG_a + (T_s - T)dG_a - (T'_s - T_0)G_a dG_a \qquad (17b)$$

If E_a/RT_s is large and we restrict the solutions to those which cross the $G_a = 1$ line nearly horizontally, G_a becomes close to unity for small values of $T_s - T$

9

so that the second term is small compared with the last term. A first approximation to the solution passing through $G_a = 0$, $T = T_s$ is given by

$$\frac{G_a^2(T_s' - T_0)}{2} - (T_s' - T_s)G_a = \frac{1}{M^2\bar{c}_p} \int\limits_T^{T_s} \lambda w_a dT \qquad (19)$$

and an approximate value of the mass flux is found by putting $G_a = 1$ in this equation. We assume that $w_a = \rho_a k_a \exp - (E_a/RT)$ and that the term on the right-hand side can be written as

$$\frac{\lambda_a \rho_a k_a}{M^2 \bar{c}_p} \int\limits_T^{T_s} \exp\left(\frac{-E_a}{RT}\right) dT$$

This integral is insensitive to the value of the lower limit, T, and we can obtain a first approximation for the mass flux as:

$$M^2 = \frac{2\lambda_a \rho_a k_a}{\bar{c}_p(2T_s - T_s' - T_0)} \frac{RT_s^2}{E_a} \exp\left(\frac{-E_a}{RT_s}\right) \qquad (20)$$

This is identical with that given by Vilyunov. Better approximations can be obtained by writing the integral on the R.H.S. of (19) in terms of a series involving powers of RT_s/E_a and by correcting for the term $(T_s - T)dG_a$ in (17b). These do not differ by more than 10 per cent from the first approximation for values of $E/RT_s > 20$.

The differential equation for G_b in the second stage of the flame is obtained by a similar procedure as

$$\frac{dG_b}{dT} = \frac{\lambda w_b}{M^2 [\bar{c}_p(T_c' - T) - G_b(\Delta hf_b - \Delta hf_c)]} \qquad (21)$$

where T_c' is the adiabatic flame temperature for the reactions $A \to B \to C$.

Strictly, for a first order gas phase reaction, G_b and Y_b cannot become zero at any temperature below the maximum final flame temperature, T_d. If the reaction rate is strongly temperature dependent, the G_b versus temperature curves decrease from a value close to unity to a value close to zero over a small temperature range. In these conditions it is possible to define a temperature T_c greater than T_c' but less than T_d at which G_b and Y_b effectively vanish and G_c becomes equal to unity.

The variation of M^2 with the boundary conditions can be found as for the first zone, by integrating equation (21) from $G_b = 0$, $T = T_c$ to give the approximate equation:

$$\frac{G_b(T_c' - T_s')}{2} - (T_c' - T_c)G_b = \frac{1}{M^2\bar{c}_p} \int\limits_T^{T_c} \lambda w_b dT \qquad (22)$$

where were have again neglected the term $(T_c - T)dG_b$ on the assumption that

G_b becomes near to unity at a value of T close to T_c. Inserting the boundary condition $G_b = 1$ at $T = T_s$ we obtain:

$$\frac{M^2 \bar{c}_p (2T_c - T'_c - T'_s)}{2} = \int_{T_s}^{T_c} \lambda w_b dT \tag{23}$$

The dependence of M^2 on T_s arises from the R.H.S. of this equation. The integral can vary with T_s through the lower limit of integration and through λw_b if this is a function of both T and T_s. Differentiating M^2 with respect to T_s we obtain

$$\frac{\bar{c}_p (2T_c - T'_c - T'_s)}{2} \frac{d(M^2)}{dT_s} = -\lambda w_b(T_s) + \int_{T_s}^{T_c} \frac{\partial(\lambda w_b)}{\partial T_s} dT \tag{24}$$

The first term on the R.H.S. of this equation depends on the reaction rate at the solid surface boundary, if $w_b(T_s) \ll w_b(T_c)$, it gives rise to a negligible decrease in M with increasing T_s. Since $\lambda w_b = \lambda \rho Y_b k_b \exp -(E_b/RT)$, it can have a partial derivative with respect to T_s only if the gas composition is a function of T_s. If we neglect any small dependence of $\lambda \rho$ on composition, this depends upon whether Y_b is a function of T_s.

We have seen that, for a single gas phase reaction step, the reactant concentration depends only on the downstream boundary conditions. This is still true for a multiple gas phase reaction steps. The relation between the reactant concentration and the temperature in the second reaction zone where $Y_a = 0$ is, for Lewis numbers of unity:

$$Y_b(\Delta hf_b - \Delta hf_a) + Y_c(\Delta hf_c - \Delta hf_a) = \bar{c}_p(T_d - T) \tag{25}$$

If we assume that T_b tends to zero at T_c and that, because of the temperature coefficient of w_b and w_c, the B and C reaction zones occupy small temperature intervals at T_c and T_d respectively, we can put $G_b = 1$ throughout most of the region between T_s and T_c and $G_c = 1 - G_b$ throughout this region. The diffusion equations for $d Y_b/dx$ and $d Y_c/dx$ can be combined to give:

$$\frac{d Y_c}{d Y_b} = \frac{Y_c - G_c}{Y_b - G_b} \tag{26}$$

where $G_b = 1$ and $G_c = 0$, this can be integrated to give

$$Y_c = C(Y_b - 1) \tag{27}$$

The constant of integration C can be determined from the condition that $Y_b = 0$ at T_c. Then from (25)

$$Y_c(T_c) = \frac{\bar{c}_p(T_d - T_c)}{(\Delta hf_c - \Delta hf_a)} \tag{28}$$

and, for $T < T_c$,

$$Y_c = \frac{\bar{c}_p(T_d - T_c)}{\Delta hf_c - \Delta hf_a}(1 - Y_b) \tag{29}$$

Substituting this relation and the equality $\Delta hf_b - \Delta hf_a = \bar{c}_p(T_d - T'_s)$ in equation 25, we obtain

$$Y_b = \frac{T_b - T}{T_b - T'_s} \tag{30}$$

The reactant concentration is therefore still independent of the down-stream boundary, T_s. Similarly Y_c can be shown to be independent of T_c in the region between T_c and T_d.

The variation of the mass flux with the downstream boundary condition is therefore similar to that of the single flame. It is almost independent of the value of T_s as long as T_s does not approach T'_s. When this occurs, we can no longer
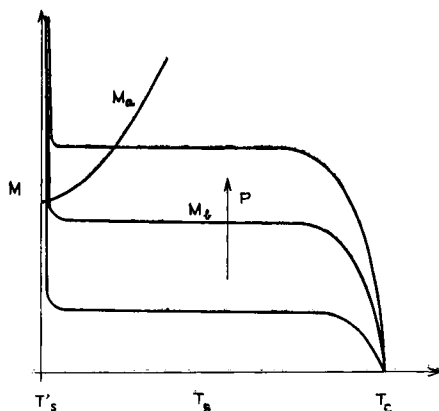
FIG. 8. Variation of mass flux and surface temperature of condensed phase with pressure for zero order–first order coupled system.

neglect the term $(T_c - T)dG_b$ in the solution of equation (21). The exact solution for M^2 indicates that it tends to infinity as $T_s \to T'_s$ in the same way as the single step flame illustrated in Fig. 7. The way in which the lower boundary condition and the mass flux are determined by the combustion pressure is illustrated in Fig. 8, where the mass fluxes for the solid phase and the first order gas phase reactions are plotted as functions of the surface temperature T_s. The mass flux for the coupled system, and the value of T_s, is determined by the intersection of the two curves. The solid phase curve is independent of the pressure but the curves for the first order gas reaction are shifted vertically upwards as the pressure increases, M_b being proportional to the square root of the pressures. Below a certain pressure, P^*, the intersection lies on the nearly vertical section of the M_b curve where $T_s \to T'_s$. The burning rate is effectively that of the adiabatic solid phase reaction. Above P^* the intersections occur on the section of the curve which is nearly parallel to the T_s axis, the burning rate is then determined by the gas phase reaction and will increase with the square root of the pressure. Because of the sharpness of the bend in the gas phase mass flux curve, the transition between the two conditions occurs over a narrow interval of burning

rate. A similar set of curves can be drawn for the conjunction of the two gas phase reactions.

The variation of burning rate with pressure for this type of consecutive reaction scheme corresponds to a series of regions in which the pressure exponent is constant and identical to that of one particular step in the reaction sequence This conclusion is quite different from that reached by Vilyunov who assumed that the fractional concentration of the gas phase reactant at the surface of the condensed phase was unity. He wrote the variation of concentration with temperature as $Y_b = (T_c - T)/(T_c - T_s)$. The reaction rate w_b is then a function of T_s. For a zero order solid phase decomposition and a first order gas phase reaction he calculated that the pressure exponent would increase continuously with the pressure and burning rate and was actually greater than that of the gas phase flame. Although his results agree roughly with the experimental behavior of simple double base propellants, his assumption is inconsistent with the correct solution of the diffusion equation derived in this paper and it is clear that a simple series of consecutive reactions of increasing reaction order is not an adequate model. If we require the pressure exponent to increase continuously, then we must either assume that the reaction order of the rate controlling step increases continuously or that effective heat of reaction associated with that step increases with pressure.

4. CHEMICAL REACTIONS IN THE BURNING OF NITRATE ESTER PROPELLANTS

If we are to try to interpret the burning rate properties in terms of the rates and exothermicities of elementary chemical reactions, we need to identify these and to devise methods for determining the variation of rate with temperature and reactant concentration. For the complex decomposition and oxidation system involved in the combustion of even the simplest nitrate ester this is a formidable problem. In the last fifteen years there have been improvements in techniques of chemical identification and quantitative estimation which may make this objective possible, but it will be many years before it is achieved. At present much of the data that we have refers to the net result of a sequence of elementary reaction steps. Any one product of the reaction may be formed by several competing reaction sequences. This is particularly true at high temperatures where difference in the rates of elementary reactions caused by differences in activation energy become smaller.

For the purposes of this lecture it will be desirable to present a somewhat over-simplified picture of the mechanism of reaction but to draw attention to reactions which can be of importance in determining the flame properties even though they occur to a relatively minor extent. The primary process in the decomposition of organic nitrates is without doubt the splitting of the RO–NO$_2$ bond with an activation energy of approximately 40 kcal mole. When compared at a temperature of 200°C, the rates of decomposition increase with the complexity of the compound over a range of about 10^{-4} to 10^{-2} sec^{-1}, increasing with increasing

complexity and being somewhat greater in the liquid phase than in the gas phase. Experimental activation energies for liquid phase decompositions are frequently quoted in the range 40–50 kcal/mole, the value increasing with increasing temperature. It appears that the decomposition is catalyzed by the retention of decomposition products. As the temperature and the rate of decomposition increases, the steady concentration of volatile products in the condensed phase increases, causing the apparent activation energy to exceed the true value for the primary step. The observed products of the decomposition depend upon the structure of the nitrate ester. Ethylene glycol dinitrate gives formaldehyde and nitrogen dioxide:

$$\begin{array}{l} CH_2ONO_2 \\ | \qquad\qquad \to 2CH_2O + 2NO_2 \\ CH_2ONO_2 \end{array}$$
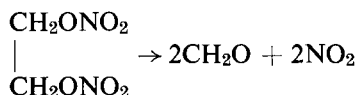
The breaking of one $O—NO_2$ bond gives a free radical which can decompose, probably without further activation, to formaldehyde and nitrogen dioxide:

$$\begin{array}{ll} CH_2O. & CH_2O \\ | \qquad\quad \to & \\ CH_2O–NO_2 & CH_2O \quad NO_2 \end{array}$$
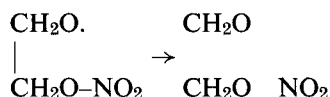
The rate of oxidation of formaldehyde by nitrogen dioxide has been studied [15] and is known to have an activation energy of about half that of the decomposition of the nitrate ester. In the pressure and temperature range of importance for rocket propellants it will be a slow reaction compared to the decomposition of the nitrate ester. Thus at 1000°K and a reactant partial pressure of 50 atm the life time of nitrogen dioxide will be about 300 times longer than that of the nitrate ester molecule.

Ethyl nitrate decomposes at about the same rate as the glycol dinitrate but the products formed are much more complex [16]. A major product is ethyl nitrite. The ethoxy radical produced by the breaking of the $O–NO_2$ bond cannot rearrange intramolecularly to give stable products. Its decomposition to an aldehyde will give yet another free radical or atom and will require some energy of activation. Thus the alkoxy radical can be destroyed only by reaction with another free radical or with nitrogen oxides, thus

$$CH_3CH_2O–NO_2$$

$$\cdot CH_3 + CH_2O \longleftarrow CH_3CH_2O\cdot + NO_2$$

$$NO \qquad CH_3CHO + HONO$$

$$\tfrac{1}{2}CH_3CHO \qquad CH_3CHO + HNO$$

$$+ \tfrac{1}{2}CH_3CH_2OH \qquad \text{or } CH_3CH_2O–NO$$
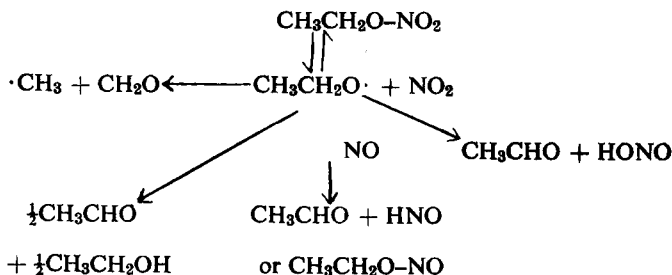
These reactions of alkoxy radicals with other radicals and with nitrogen oxides require little or no energy of activation and are therefore fast compared with the decomposition of the nitrate ester. The rate constants have recently [18] been reinvestigated and fall within the range $10^{10}-10^{11}$ mole^{-1} cc sec^{-1}. The reaction half life of the alkoxy radical in the presence of nitrogen oxides will be of the order of 10^{-6} P^{-1} sec atm^{-1} compared with 10^{-3} sec at 500°C for the nitrate ester.

The sequence of reactions in the ethyl nitrate flame has been studied by Hicks [19]. At a pressure of 35 mm Hg the flame is some 6 mm thick so that the variation of chemical composition with distance can be determined by gas sampling techniques. Figure 9 shows the results obtained. These show that the rate determining process is the decomposition of nitrate, the nitrogen dioxide being removed so rapidly by reactions with radicals that its concentration is too small to be estimated. The presence of the ethoxy radical can be inferred from the formation of ethyl nitrite, acetaldehyde and ethanol. In the high temperature zone of the flame we find a range of products containing one carbon atom which indicates that at higher temperatures the ethoxy radical pyrolyses rapidly to a methyl radical and a molecule of formaldehyde. This decomposition has an energy of activation of between 10 and 20 kcal/mole and would be expected to be significant relative to the other reactions of the radical in the hotter regions of the flame. The methyl radical reacts with nitrogen dioxide in the following reactions:

$$CH_3 + NO_2 \rightarrow CH_3O + NO$$

$$CH_3 + NO_2 \xrightarrow{M} CH_3NO_2$$
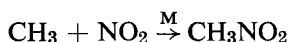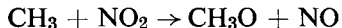
M being a third body which removes the energy of formation of the nitromethane. The methyl radical is most probably responsible for the rapid disappearance of ethyl nitrite which should be relatively stable compared with the nitrate at these temperatures. It is known [20] that a rapid exchange reaction can occur:

$$CH_3CH_2ONO + \cdot CH_3 \rightarrow CH_3CH_2O\cdot + CH_3NO$$
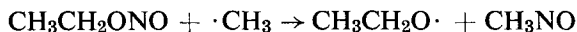
The nitrosomethane formed in this reaction was not detected but it is known to be unstable at these temperatures and to be the source of minor amounts of hydrogen cyanide,

$$CH_3NO \rightarrow H_2O + HCN$$
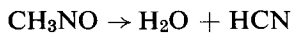
and of nitrogen-containing polymers which are produced in the combustion of nitrate esters [21].

When ethyl nitrate is burned at atmospheric pressure, the final products show a similar pattern, but some 35 per cent of the nitric oxide is reduced to nitrogen and there is considerable decomposition of the aldehyde and alcohols formed in the primary reaction. The measured flame temperature is increased by some 300°C.
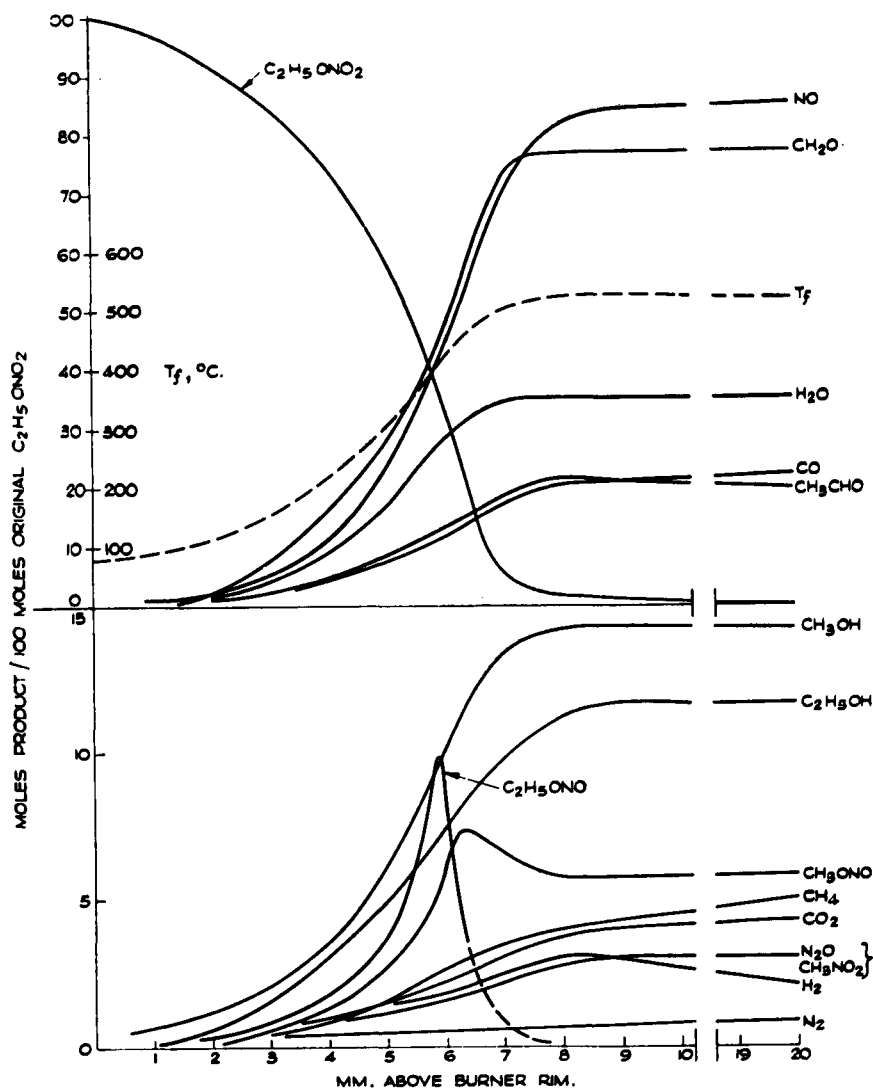
FIG. 9. Spatial variation of composition and temperature through ethyl nitrate flame at 35 mm Hg. (After Hicks [19].)

The flame temperature in nitric ester combustion is very sensitive to the degree of reduction of nitric oxide. The thermal decomposition of this molecule or the reaction with fuel molecules should be slow below 2000°C, but in fact significant amounts of nitrogen are almost always produced in the primary decomposition zones of nitrate esters burning at atmospheric pressure. The primary step in this reduction of nitric oxide appears to be the abstraction of a hydrogen atom from alkoxy radicals and molecules containing a reactive hydrogen to form the transient molecule HNO. It has been shown that methyl nitrite can sustain

combustion at flame temperatures of about 1000°K and at atmospheric pressure. The composition profiles have been studied by Powling [22], who found that the rate of reduction of nitric oxide was linked with the rate of pyrolysis of the primary decomposition products, formaldehyde and methanol:

$$CH_3ONO \rightarrow \tfrac{1}{2}CH_2O + \tfrac{1}{2}CH_3OH + NO$$
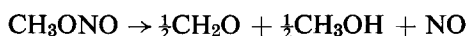
This reaction is almost thermally neutral and extensive reduction of nitric oxide is essential for the propagation of a flame in this system. About half of the
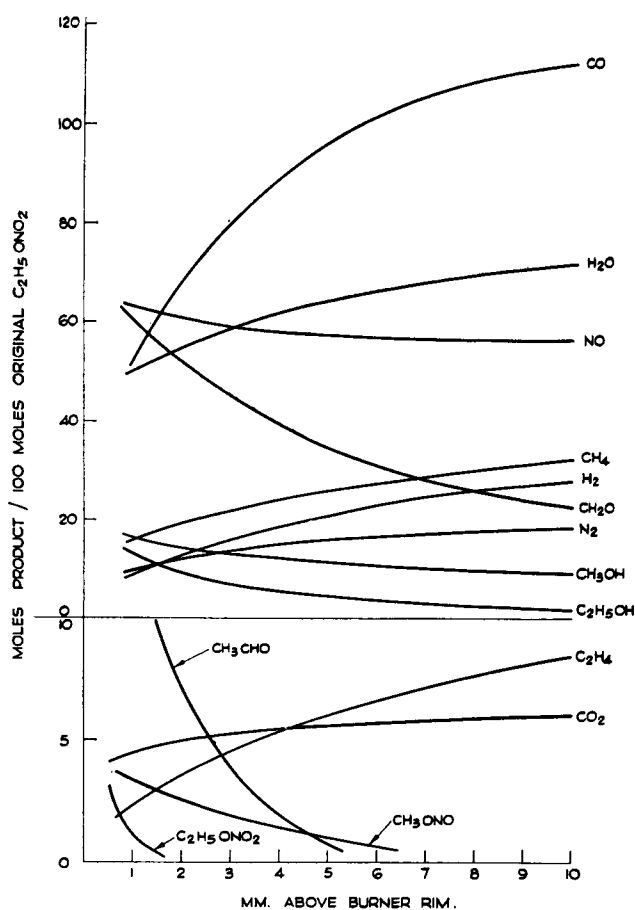
FIG. 10. Spatial variation of composition through ethyl nitrate flame at atmospheric pressure.

available nitric oxide is reduced to nitrogen; the reduction ceases when the formaldehyde and methanol have been completely oxidized or pyrolyzed (Fig. 11). It seems probable that in this flame the three reactions are linked by a common factor, the availability of reactive hydrogen from the methoxyl ($CH_3O\cdot$) or formyl ($\cdot CHO$) radicals or as free hydrogen atoms.
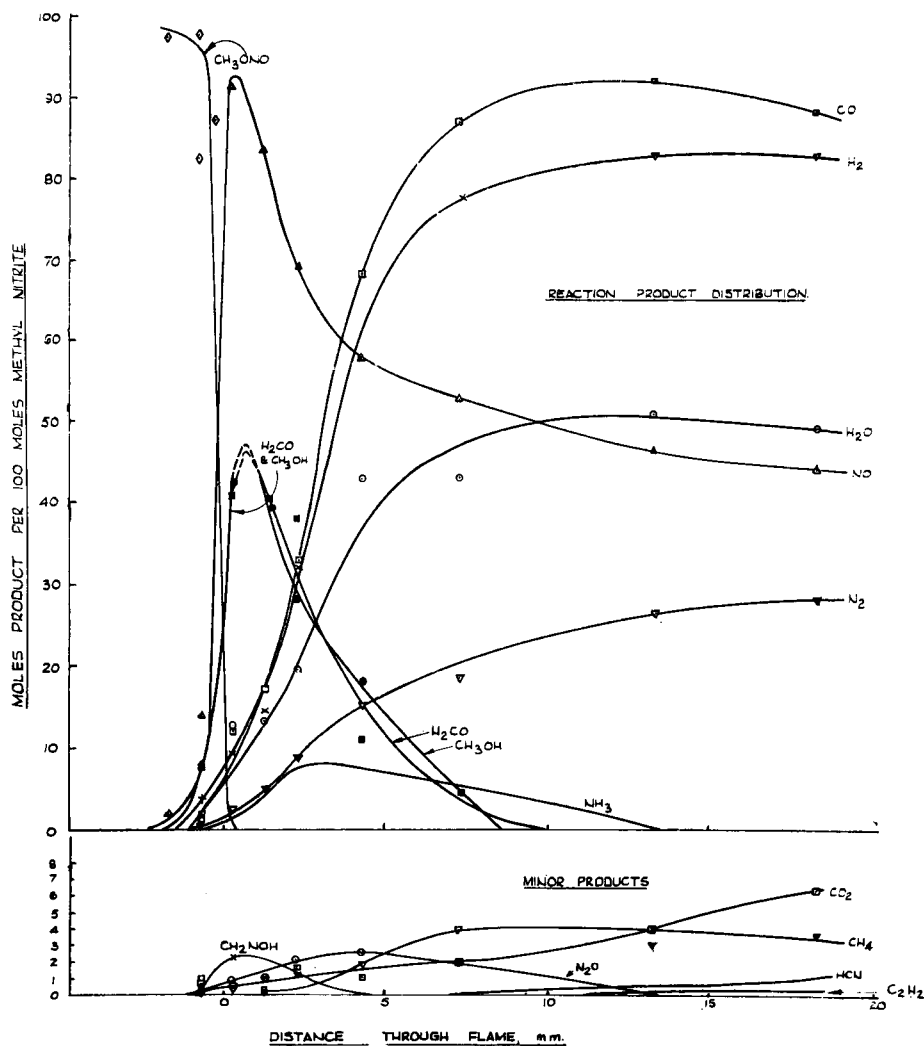
FIG. 11. Spatial variation of composition through methyl nitrite flame at atmospheric pressure. (After Powling [22].)

These reactions are relatively slow in the ethyl nitrate flame at pressures of 50 mm Hg and below. The rate determining step can be identified with the primary decomposition of the nitrate ester. The evidence for this is that the activation energy derived from the variation of flame speed with flame temperature is 38 kcal/mole, a value very close to the strength of the $O–NO_2$ bond. Furthermore the same value is found from the heat release profile obtained by differentiating the temperature–distance curve (Fig. 12). The ethyl nitrate concentration is seen to be a linear function of the temperature in the flame and to vanish at the maximum flame temperature. This not only confirms its identity as the rate-determining reactant but also indicates the degree of applicability

to such complex systems of the theoretical relationship obtained by setting the Lewis number equal to unity. When this concentration temperature relationship is used to determine the specific rate constant from the heat release distribution, the activation energy over the major portion of the heat release region is again 38 kcal/mole.

At pressures below 150 mm Hg, the flame speed is independent of pressure. This suggests that the decomposition reaction is controlled by the rate of collisional activation. At higher pressures the flame speed decreases with increasing pressure indicating a transition to first order unimolecular decomposition kinetics. The flame speed in the vapor has not been determined over a sufficient pressure range to enable the pressure exponent to be determined with

RATE PARAMETER v. TEMPERATURE
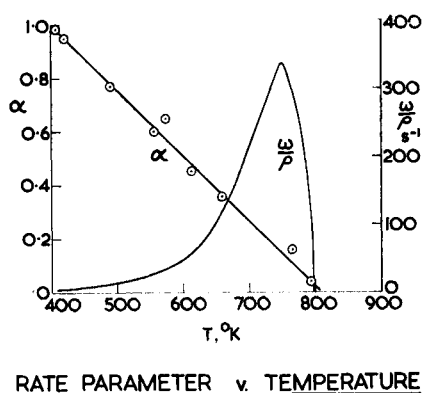
FIG. 12. Ethyl nitrate mass fraction α and decomposition rate ω/ϱ as function of temperature in flame. (After Hicks [19].)

any precision. Above one atmosphere pressure the flame can be stabilized on the surface of the liquid and the burning rate can be determined over a wide pressure range but the observed pressure exponent is nearer to unity than to the value of one-half expected for a first order reaction. However, the flame temperature is also found to be increasing with pressue due to the reduction of increasing amounts of nitric oxide. It appears that the reaction of nitric oxide with molecules such as those of aldehydes becomes increasingly important as the pressure is raised. The burning rate of liquid ethylene glycol dinitrite, which decomposes into formaldehyde and nitric oxide, is almost identical with that of ethyl nitrate in the pressure range 500 to 1000 psi. This tends to confirm the suggestion that this type of reaction is important in determining the burning rate and pressure exponent at high pressures.

The composition profiles of a number of other liquid nitric flames at atmospheric pressure have been studied by Powling [23–25]. Of particular interest are the dinitrates where spectrophotometric measurements have shown that

nitrogen dioxide is a major intermediate product. The dinitrate decomposes to produce equal amounts of aldehyde and nitrogen dioxide:

$$\begin{array}{l} R\text{--}CHONO_2 \\ | \qquad\qquad\qquad \rightarrow 2RCHO + 2NO_2 \\ R\text{--}CHONO_2 \end{array}$$
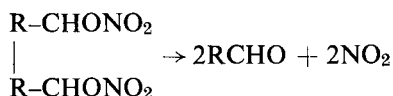
This reaction is about thermally neutral and the rate determining reaction in the flame is the oxidation reaction between nitrogen dioxide and the aldehyde
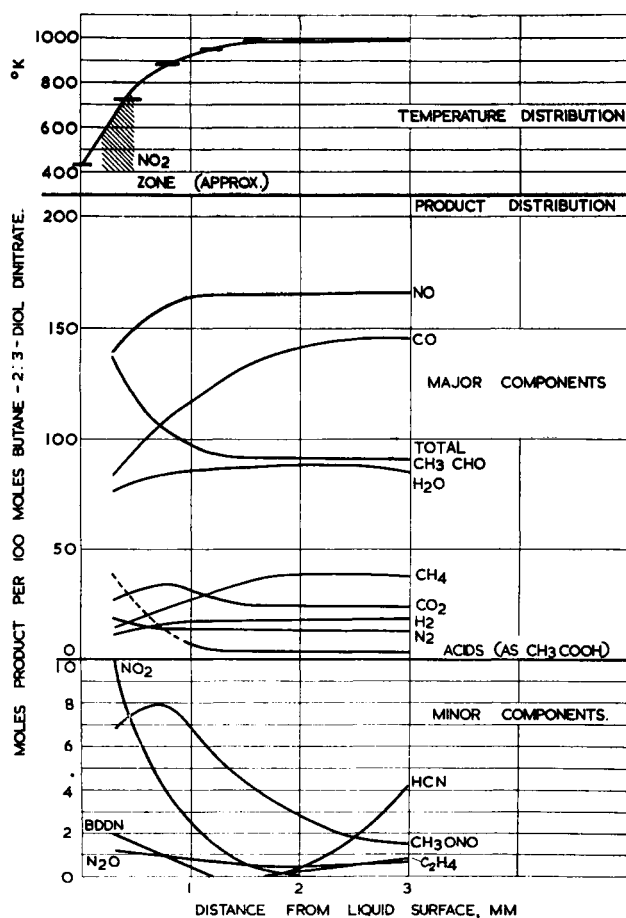
FIG. 13. Spatial variation of composition through butane-2,3-diol dinitrate flame. (After Powling [25].)

(Fig. 13). This is confirmed by the fact that the flame speeds for the combustion of dinitrates are identical with those of mixtures of nitrogen dioxide and the appropriate aldehyde. Figure 14 shows both the large difference between the flame speeds of different nitric esters at similar flame temperatures and pressures, and also the similarity between the speeds for the dinitrates and for mixtures

of nitrogen dioxide with the appropriate aldehyde. The equivalent flame speed of liquid ethylene glycol dinitrate (calculated with respect to the flame products so that, for identical products, we are comparing the mass burning rates) is identical with that of a formaldehyde-nitrogen dioxide mixture extrapolated
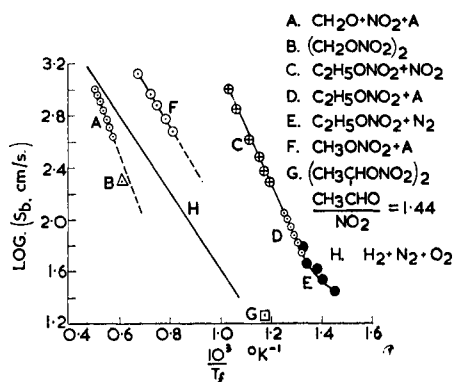
FIG. 14. Flame speed measured with respect to the products of combustion as a function of flame temperature for various nitrate esters and nitrogen dioxide mixtures.

to the same flame temperature. Similarly the flame consumption rate of 2,3-butane-diol dinitrate is identical with that of its primary decomposition products, acetaldehyde and nitrogen dioxide

$$
\begin{array}{ccc}
CH_3 & CH_3 & \\
| & | & \\
CHONO_2 & CHO & NO_2 \\
| & \rightarrow & + \\
CHONO_2 & CHO & NO_2 \\
| & | & \\
CH_3 & CH_3 & \\
\end{array}
$$
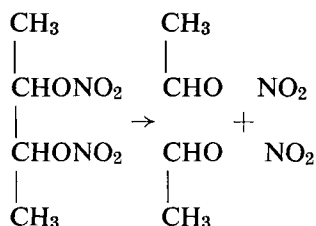
We may conclude that at low pressures the burning rate of the mononitrate is controlled by the rate of decomposition of the nitric ester molecule which is slow compared with the oxidation of the resulting free radical. With the dinitrates, the rate controlling process is the oxidation of the aldehyde. The decomposition of the nitrate ester is relatively fast and is completed well below the final flame temperature.

At pressures above one atmosphere the properties of these flames are liable to be influenced by the reduction of nitric oxide to nitrogen which takes place within the primary reaction zone. This reaction is quite distinct from the visible flame reaction which is observed some distance from the primary zone at high pressure and which can be identified with the reaction of nitric oxide with the stable products carbon monoxide and hydrogen. It is clearly associated with reaction of the nitric oxide with free radicals produced in the decomposition of the nitrate ester and with intermediate products such as formaldehyde. The extent to which the reaction occurs depends upon the structure of the nitrate

ester and its decomposition products and, unlike the visible flame, becomes more obvious as the energy of the system is reduced. Table 1 gives the percentage of reduction for a range of nitrate ester propellants at atmospheric pressure.

TABLE 1

Composition	Cal. val. cal/g	% NO Reduced
Methyl nitrate	1640	10
Ethylene glycol dinitrate	1740	4
Ethylene glycol mononitrate	920	50
Ethylene glycol dinitrate (70%) + Triacetin 30%	860	25
Ethyl nitrate	870	35
2-Methoxy ethyl nitrate	510	55
Isopropyl nitrate	515	10
Nitrocellulose (12.2% N)	912	15
Double base propellant	767	26

In some, although not all systems, the amount of reduction increases continuously in the range 1 to 40 atm pressure and the measured flame temperature increases as much as two-fold.

We know very little about the detailed kinetics of reduction reactions of nitric oxide. At low temperatures and pressures, and in the liquid phase, one type of reaction is known to involve the reaction of two molecules of nitric oxide with an unstable nitroso compound [26]:

$$R\cdot + NO \rightleftharpoons R-NO$$

$$R-NO + 2NO \rightarrow R\cdot + N_2 + NO_3$$

$$NO_3 + NO \rightarrow 2NO_2$$
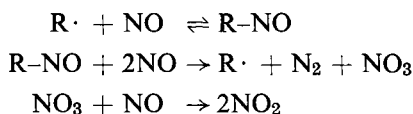
The rate of consumption of NO is second order in the nitric oxide concentration and may have a negative temperature coefficient due to the first equilibrium being displaced to the left by increasing temperature. This type of reaction is likely to be unimportant in the high temperature regions of the flame but may be significant where the primary decomposition and oxidation reactions occur in the condensed phase.

In the flame the formation of HNO by hydrogen abstraction from radicals and molecules with a weak C–H bond is likely to be more important. HNO can then lead to nitrogen formation through the relatively unstable nitrous oxide

$$2HNO \rightarrow H_2O + N_2O$$
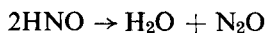
or, at high temperatures,

$$HNO + NO \rightarrow N_2O + OH$$

$$N_2O + NO \rightarrow N_2 + NO_2$$
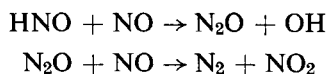
The detailed mechanisms of the decomposition and combustion of the two main components of double base propellants, nitrocellulose and nitroglycerine are less well understood than those of the simple nitrates. Wolfram *et al.* have

made an extensive study of the products of ignition of nitrocellulose at sub-atmospheric pressures [27]. As one would expect from the possible variations in the individual chain segments in partially nitrated cellulose and the number of ways in which each segment can break down, the products form a complex mixture of partially denitrated and depolymerized fragments together with simple carbonyl compounds formed by oxidative pyrolysis of the glucopyranose rings. The gaseous products contain considerable fractions of molecular nitrogen and nitrous oxide. These are formed even in the slow isothermal decomposition of nitrocellulose so that the state of the intermediate decomposition products must favour ready reduction of the nitrogen oxides initially produced. When formed in a polymer chain, free radicals are restrained from undergoing mutual disproportionation reactions by reason of their immobility and may therefore be more readily available for reaction with nitrogen oxides.

Nitrogen dioxide has not been observed as a major intermediate in the combustion of double base propellants which tends to confirm the supposition that the mechanism is more nearly that corresponding to the mononitrates (rapid reduction of nitrogen dioxide by free radicals) than to that of the dinitrates.

The rate of pyrolysis of nitrocellulose has been reinvestigated in recent years by Phillips, Orlick and Steinberger by a spectrophotometric technique using thin films of nitrocellulose [28]. Their rate constants and temperature dependence can be used to estimate the temperature at which the primary decomposition reaches completion, a temperature which should correspond to the measured surface temperature.

From Section 3 the mass flux and the temperature are approximately related by the equation

$$M^2 = \frac{2\rho\lambda k}{\bar{c}_p(2T_s - T_s' - T_0)} \; \frac{RT^2}{E} \exp\left(\frac{-E}{RT_s}\right) \tag{20}$$

If we insert a measured value of the mass burning rate and the values of k and E given in reference [28], we can calculate a value for the surface temperature The heat release of the solid phase reaction and therefore the adiabatic surface temperature T_s' are not known but the calculation is relatively insensitive to the possible variation in these parameters We shall assume $T_s' - T_0$ equal to 250°C corresponding to a heat reaction in the solid phase of ~ 90 cal/g; if we had assumed zero heat of reaction the surface temperature, T_s, would be $\sim 10°$ higher.

At atmospheric pressure the burning rate of a nitrocellulose strand is quoted by Powling [29] as 4.5×10^{-2} cm/sec. We use the values:

$$k = 3.54 \times 10^{18} \text{ sec}^{-1}$$
$$E = 45 \times 10^3 \text{ cal/mole}$$
$$R = 1.9866 \text{ cal/deg mole}$$
$$T_0 = 300°K$$

and $\qquad\qquad \lambda/\bar{c}_p = 5 \times 10^{-4} \text{ cm}^2/\text{sec}$

The last value is estimated from the known thermal diffusivities of organic liquids in an appropriate temperature range.

Solving equation (20) for T_s we obtain a value of 585°K which is not very different from the experimental value of $\sim 600°$ K measured by Powling [29] using an infrared emission technique. At first sight these values appear surprisingly low in comparison with the temperature of the ethyl nitrate decomposition flame ($\sim 800°$K). The difference arises not so much from the faster decomposition rate of the nitrocellulose at similar temperatures as from the higher density and thermal diffusivity of the condensed phase reaction zone. The measured gas temperature close to the burning surface is $\sim 870°$K at atmospheric pressure. The heat released in combustion at atmospheric pressure is a fraction of the thermochemical energy of the reaction to products in chemical equilibrium and is of the order of 200 cal/g. Since the calculated surface temperature is insensitive to the heat release assumed for the solid phase reaction, we cannot make any statement on the latter quantity other than that it cannot exceed a value of about 100 cal/g at atmospheric pressure. It may seem odd that a reduction in the assumed heat release in the solid phase leads to a slightly higher calculated surface temperature for a given mass flux. This arises because a decrease in the exothermicity increases the temperature gradient in the reaction zone and therefore decreases the thickness of the reaction zone. This must be compensated by a higher volumetric reaction rate and therefore by a higher surface temperature.

At higher pressures where the burning rate is greater than at atmospheric pressure, the surface temperature must increase. There are no reliable experimental measurements of the rate of increase of surface temperature with pressure.

The calculated surface temperature at a pressure of 600 psi where the burning rate is ten times its value at atmospheric pressure is 667°K, which is still considerably less than experimental values of the gas temperature of 1300°K adjacent to the surface at this pressure. Measurement of the temperature profile by the insertion of fine thermocouples into propellant strands so that they are overtaken by the combustion zone indicate that there is a further rapid temperature rise just upstream of the propellant surface. The rate of rise of temperature is too great at high pressures for the thermocouple method to give a reliable indication of the heat release profile or the surface temperature, but it is clear that a major proportion of the heat release takes place in the gas phase close to the solid surface. The amount of heat release in the gas phase is found to increase considerably with increasing pressure above atmospheric. This is associated with the reduction of increasing amounts of nitric oxide. What is not clear is what proportion of this heat release is effective in increasing the burning rate of the propellant and whether the rapid rise of gas temperature close to the solid surface is due to reduction of some fraction of the nitric oxide or to the reduction of nitrogen dioxide formed by the initial pyrolysis of the nitrate ester. The thermochemistry of the decomposition of nitrocellulose indicates that some reduction of nitric oxide is essential if the heat of decomposition is to reach values of 200 cal/g, but this amount depends very much on the extent of degradation of the glucopyranose ring structure.

Strictly the concept of a uniform regression of a surface at a uniform temperature is an over-simplification of the burning of double base propellants in this pressure range. It can be observed visually that the burning surface exhibits a wave-like mode of consumption. It appears as if glowing filaments of carbonaceous material periodically move over the surface consuming a thin layer of propellant. Ciné photography of the propellant surface shows that a smooth area on this surface appears to darken and to roughen. This area is then consumed by a wave of combustion which moves across the surface and leaves behind a network of carbon filaments which are blown off the surface by the steady evolution of gas. The edge or periphery of the surface wave is delineated by a glowing filament of carbonaceous product. This effect is related to the "foam" reaction observed by Crawford and Huggett [33] and to the intermittent nature of the burning of cordite first reported by Huffington [34].

The consumption of the reacting surface layer leaves a smooth surface which subsequently repeats this sequence. It seems probable that the overall, average rate of burning is the result of two components: a steady rate analogous to the burning of a liquid propellant and a surface or condensed phase reactive wave moving laterally across the surface. The enhanced temperature of the carbonaceous filaments appears to be due to their combustion in nitric oxide but it is not completely certain whether they are the cause or effect of the surface wave process. The fact that the burning rate of nitrocellulose and compositions containing it is some twice as fast as that of nitric esters of similar flame temperature with which the surface mode is not observed, suggests that it makes a substantial contribution to the average burning rate. We know that the production of a solid carbonaceous residue does not of itself cause high burning rates even though its formation would tend to increase the exothermicity of the solid phase decomposition as against the formation of simple gaseous products. This can be demonstrated by adding traces of flame-retardants such as phosphates which can be seen to promote the formation of carbonaceous products but inhibit their oxidation. These additives depress the burning rate by a factor of two. This suggests that the burning of the carbonaceous residue in nitric oxide can have a significant effect on the burning rate.

This reaction of a carbonaceous residue with nitric oxide has been suggested [31] as a possible cause of the " platonization " effect of lead compounds described by Preckel [6, 7]. The addition of lead compounds to cellulose esters can be observed to promote the formation of solid carbonaceous residues on pyrolysis as do many other inorganic compounds. Lead also catalyzes the oxidation of this carbonaceous residue by nitric oxide [32]. Visual and photographic observation on the burning of propellant strands show that additions of lead compounds increase the number and extent of the incandescent regions on the burning surface which are associated with the formation of carbonaceous products and that these "hot spots" disappear when the pressure is increased to values at which the catalysis of the burning rate vanishes. There appears to be a correlation between the occurrence of incandescent regions on the propellant surface and the promotion of the burning rate.

10

Qualitatively it is easier to understand why a strongly exothermic, hetero-geneous reaction on the propellant surface should increase the burning rate than to explain why this effect vanishes with increasing pressure. There is some evi-dence that an active agent in the action of lead compounds is lead oxide produced by their pyrolysis. When lead oxide itself is added to the propellant composition it has been observed that the smaller the amount of added oxide the higher is the pressure at which the rate promoting effect vanishes. This conforms with the observation that the more stable aromatic lead salts are more effective in pro-moting the burning rate at high pressure than the easily pyrolyzed aliphatic lead compounds [7]. It appears that lead oxide can catalyze some rate-promoting reaction but can also eliminate, as the combustion pressure is increased, some intermediate responsible for this reaction. If the intermediate is supposed to be a carbonaceous residue, the effect might be explained on the basis of a lead catalyzed reduction of nitric oxide on a carbonaceous product, coupled with the destructive oxidation of such a product by lead oxide [31].

It is, however, difficult to see why the oxidation of a carbonaceous residue by lead oxide should be inactive in promoting the burning rate when oxidation by nitric oxide is assumed to be effective. Both reactions will be strongly exo-thermic and an increase in pressure should favour the reaction with the gas phase species rather than that with the solid oxide. There appears to be no evidence of any major change in the gaseous products of combustion on addition of lead compounds although there is an indication of a slight increase in the amount of nitrogen formed and a consequent small increase in the temperature of the products of the primary reaction zone. On the other hand, it has been observed that lead tetramethyl added to ethyl nitrate decreases the burning rate [35] and completely inhibits the formation of nitrogen in the products of combustion at atmospheric pressure, resulting in a fall in the measured flame temperature of some 200°C.

We must conclude that the action of lead compounds in nitrate ester combustion is no less complex than is their role in hydrocarbon combustion.

REFERENCES

[1] CRAWFORD, B. L., HUGGETT, C., DANIELS, F. and WILFONG, R. E., "Direct determination of the burning rates of propellant powders", *Analyt. Chem.*, **19**, 630 (1947).

[2] PARR, R. G. and CRAWFORD, B. L., "A physical theory of burning of double base rocket propellants", *J. Phys. Chem.*, **54**, 929 (1950).

[3] BOYS, S. F. and CORNER, J., "The structure of the reaction zone in a flame", *Proc. Roy. Soc.* **197A**, 90 (1949).

[4] RICE, O. K. and GINELL, R., "Theory of burning of double base rocket powders", *J. Phys. Chem.*, **54**, 885 (1950).

[5] GECKLER, R. D., "The mechanism of combustion of solid propellants", *Selected Combustion Problems*, Butterworths, London, 289 (1954).

[6] PRECKEL, R. F., "Plateau ballistics in nitrocellulose propellants", *A.R.S.J.*, **31**, 1286 (1961).

[7] PRECKEL, R. F., *A.I.A.A. Preprint* No. 64–113 (1964).

[8] HIRSCHFELDER, J. O., CURTISS, C. F. and CAMPBELL, D. E., "The theory of flames and detonations", *Fourth Symposium on Combustion*, Williams Wilkins, Baltimore, 190 (1953).

[9] VON KARMAN, T. and PENNER, S. S., "Fundamental approach to laminar flame propagation", *Selected Combustion Problems*, Butterworths, London, 5 (1954).

[10] SPALDING, D. B., "One-dimensional laminar flame theory for temperature-explicit reaction rates", *Combustion and Flame*, **1**, 293 (1957).

[11] SPALDING, D. B., "Theory of burning of solid and liquid propellants", *Combustion and Flame*, **4**, 59 (1960).

[12] ADAMS, G. K. and STOCKS, G. W., "The combustion of hydrazine", *Fourth Symposium on Combustion*, Williams Wilkins, Baltimore, 239 (1953).

[13] LEVY, J. B. and FRIEDMAN, R., "Further studies of pure ammonium perchlorate deflagration", *Eighth Symposium on Combustion*, Williams Wilkins, Baltimore, 663 (1962).

[14] VILYUNOV, V. N., "A mathematical theory for the combustion of solids", *Proc. Academy of Sciences U.S.S.R.*, **196**, 136 (1961).

[15] POLLARD, F. H. and WYATT, R. M. H., "Reactions between formaldehyde and nitrogen dioxide", *Trans. Farad. Soc.*, **45**, 760 (1949).

[16] LEVY, J., "The thermal decomposition of nitrate esters", *J.A.C.S.*, **76**, 3254 and 3790 (1954).

[17] POLLARD, F. H., MARSHALL, H. S. B. and PEDLER, A. E., "The thermal decomposition of ethyl nitrate", *Trans. Farad. Soc.*, **52**, 59 (1956).

[18] BAKER, G. and SHAW, R., "Reactions of methoxyl, ethoxyl and t-butoxyl with nitric oxide and with nitrogen dioxide", submitted to *J. Chem. Soc.* (1965).

[19] HICKS, J. A., "The low pressure decomposition flame of ethyl nitrate", *Eighth Symposium on Combustion*, Williams Wilkins, Baltimore, 487 (1962).

[20] BROMBERGER, B. and PHILLIPS, L., "The abstraction of nitric oxide from alkyl nitrites by methyl radicals", *J. Chem. Soc.*, **1048**, 5302 (1961).

[21] NEEDHAM, D. P. and POWLING, J., "The decomposition flame of ethyl nitrate", *Proc. Roy. Soc.*, A**232**, 337 (1955).

[22] ARDEN, E. A. and POWLING, J., "The methyl nitrite decomposition flame", *Combustion and Flame*, **2**, 55 (1958).

[23] POWLING, J. and SMITH, W. A. W., "Flame decomposition of the propyl nitrates", *Combustion and Flame*, **1**, 308 (1957).

[24] POWLING, J., SMITH, W. A. W. and THYNNE, J., "The flame decomposition of some substituted ethyl nitrates", *Combustion and Flame*, **4**, 201 (1960).

[25] POWLING, J. and SMITH, W. A. W., "The combustion of the butane 2,3 and 1,4 diol dinitrates", *Combustion and Flame*, **2**, 157 (1958).

[26] CHRISTIE, M. I., COLLINS, J. M. and VOISEY, M. A., "Reaction of acetyl radicals with nitric oxide", *Trans. Farad. Soc.*, **61**, 462 (1965).

[27] WOLFRAM, M. L. *et alia* "Controlled thermal decomposition of cellulose nitrate", *J.A.C.S.*, **77**, 6573 (1955); **78**, 4695 (1956); **80**, 946 (1958).

[28] PHILLIPS, R. W., ORLICK, C. A. and STEINBERGER, R., "Kinetics of the thermal decomposition of nitrocellulose", *J. Phys. Chem.*, **59**, 1034 (1955).

[29] POWLING, J. and SMITH, W. A. W., "Measurement of temperatures of propellant compositions by infrared emission", *Combustion and Flame*, **6**, 173 (1962).

[30] HELLER, C. A. and GORDON, A. S., "Structure of the gas phase combustion region of a solid double base propellant", *J. Phys. Chem.*, **59**, 773 (1955).

[31] HICKS, J. A., POWLING, J. and WATTS, H., Unpublished *E.R.D.E. Report*.

[32] WATTS, H., "The oxidation of charcoal by nitric oxide and the effect of some additives", *Trans. Farad. Soc.*, **54**, 93 (1958).

[33] CRAWFORD, B. O., HUGGETT, C. and McBRADY, J. J., "Mechanism of the burning of double base propellants", *J. Phys, Chem.*, **54**, 863 (1950).

[34] HUFFINGTON, J. D., "The unsteady burning of cordite", *Trans. Farad. Soc.*, **50**, 942 (1954).

[35] ADAMS, G. K. and SCRIVENER, J., "Flame propagation in methyl and ethyl nitrate", *Fifth Symposium on Combustion*, Reinhold, New York (1955).

A MOLECULAR THEORY FOR VISCOELASTIC
BEHAVIOR OF AMORPHOUS POLYMERS

A. V. Tobolsky and J. J. Aklonis

Frick Chemical Laboratory,
Princeton University
Princeton, New Jersey

Abstract—The relaxation modulus for N.B.S. polyisobutylene has been interpreted as a sum of two Rouse functions each arising from a different molecular mechanism. One is associated with torsional vibrations and internal rotation. The other is associated with an entangled network of gaussian segments. Each Rouse function is characterized by three parameters, which can be obtained from the experimental relaxation modulus.

In 1952 the complete relaxation modulus $E_r(t)$ for polyisobutylene was analyzed [1] in terms of an idealized distribution of mechanical relaxation times $\bar{H}(\tau)$, as is shown in Fig. 1 for 25°C. When plotted in the form log $\bar{H}(\tau)$ versus
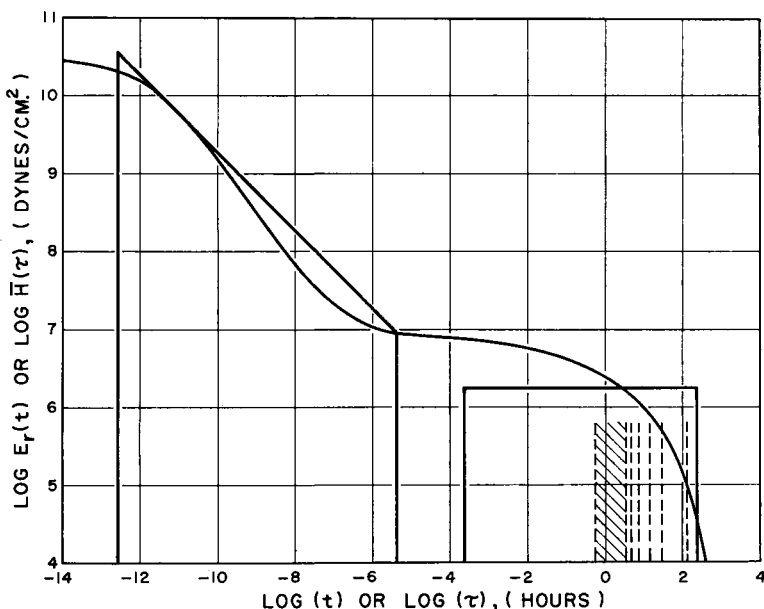
FIG. 1. Master curve for N.B.S. polyisobutylene at 25°C with "wedge", "box", and the discrete distributions of relaxation times in rubbery flow region.

log (τ), one obtains a "wedge" representing the shorter relaxation times, which is independent of molecular weight (at high molecular weights), and a "box" representing the longer relaxation times, which is translated along the log time

149

axis with increasing molecular weight. To what extent can theory explain these empirical results?

In 1953 and 1954 two similar mathematical treatments [2, 3] were given which provided a degree of theoretical understanding for the problem of the mechanical relaxation time distribution. The theories were basically designed to treat the viscoelastic behavior of a polymer molecule in dilute solution.

The simplest mechanical analogue corresponding to these theoretical treatments is a linear array of z balls of mass m, each separated at equilibrium by a distance a, and connected by springs of force constant c. The entire array is immersed in a liquid, and the friction constant of the balls moving through the liquid is f.

The equation of motion of the jth ball is [3]:

$$m\ddot{x}_j + f\dot{x}_j + c(2x_j - x_{j+1} - x_{j-1}) = 0 \qquad (j = 1, 2, 3, \ldots, z) \qquad (1)$$

where x_j represents the displacement of the jth mass from its position of equilibrium, and similarly for x_{j-1} and x_{j+1}.

It is easily shown that the relaxation times arising from the z equations shown in (1) are [2, 3]:

$$\tau_p = \frac{f}{4c \sin^2(\pi p/z)} \approx \frac{fz^2}{4\pi^2 cp^2} \qquad (p = 1, 2, 3, \ldots, z) \qquad (2)$$

Suppose we had N parallel linear arrays of this type, separated by a lattice spacing b. The tensile relaxation modulus of this array is:

$$E_r(t) = \frac{ca}{zb^2} \sum_{p=1}^{z} e^{-t/\tau_p} \qquad (3)$$

$$\tau_p = \frac{fz^2}{4\pi^2 cp^2}; \quad \tau_{max} = \frac{fz^2}{4\pi^2 c}; \quad \tau_{min} = \frac{f}{4\pi^2 c} \qquad (p = 1, 2, 3, \ldots, z)$$

Equation (3) corresponds to the Rouse–Bueche theory for N macromolecules in solution per c.c., each composed of z gaussian segments. The force constant c of the gaussian segment is taken to be $3kT/\sigma^2$, arising from the theory of rubber elasticity. The quantity σ^2 is the mean square length of the gaussian segment. The quantitities a and b are defined by

$$b^2 a = 1/Nz = \text{volume per segment.} \qquad (4)$$

With these correlations, eqn. (3) becomes

$$E_r(t) = \frac{3NkTa^2}{\sigma^2} \sum_{p=1}^{z} e^{-t/\tau_p} \qquad (5)$$

$$\tau_p = \frac{fz^2\sigma^2}{12\pi^2 kTp^2} \qquad (p = 1, 2, 3, \ldots) \qquad (6)$$

This corresponds exactly to the Rouse–Bueche theory if (a^2/σ^2) equals unity. That a factor of this kind should indeed modify the ideal equation of state for rubber elasticity has been proposed for a long time [4].

In order to make eqn. (5) applicable to undiluted polymer, it was suggested that any given segment can be regarded as moving in a "liquid" composed of other segments [3, 5, 6]. Also it was suggested, in order to explain the observed facts, that the friction factor in eqn. (6) be made to vary with the 2.4 power of z for values of p smaller than p_{ent}. The quantity p_{ent} relates to the smallest mode of motion which is affected by entanglement.

Nevertheless, eqns. (5) and (6), even after modification, cannot explain the observed experimental facts. It is clear that no elastic modulus larger than 10^8 to 10^9 dynes/cm² can be explained by rubber elasticity theory [7]. Recently, it has been argued that the Rouse–Bueche theory cannot explain the experimental facts when the elastic modulus is in excess of 10^7 dynes/cm² [8].

We propose that the facts can be reasonably explained by considering eqn. (3) anew. We shall designate the function in eqn. (3) as the Rouse function $R(t)$. (For simplicity in notation we shall designate b^2/a equal to a'.)

$$\sum_{p=1}^{z} \left(\frac{c}{za'}\right) e^{-t/\tau_p} = \frac{c}{a'} \sum_{p=1}^{z} \frac{1}{z} e^{-t/\tau_p} \equiv R(t) \tag{7}$$

The Rouse function can be completely defined by

$$\left(\tau_{min}, \frac{c}{a'}, z\right) \quad \text{or} \quad \left(\tau_{max}, \frac{c}{za'}, z\right).$$

We believe that the observed relaxation modulus of a linear amorphous polymer consists of a sum of two independent Rouse functions, $R_1(t)$ and $R_2(t)$ arising from two quite different physical mechanisms.

$$E_r(t) = R_1\left(\frac{c_1}{a_1'}, \tau_1, z_1\right) + R_2\left(\frac{c_2}{z_2 a_2'}, \tau_m, z_2\right). \tag{8}$$

$R_1(t)$ arises from the relaxation times associated with the torsional motion (internal rotations) along the chain. We are here considering the lattice elements of the array described by eqn. (3) to be torsional oscillators capable of occasionally surmounting the energy barrier for internal rotation. The quantity $c_1 a_1'$ is the tensile modulus E_1 of the ploymer in the glassy state, under conditions of time and temperature such that no internal rotation occurs. We are considering not gaussian segments but pairs or triads of bonds along the chain. The quantity c_1 relates to the force constant for torsion, a' is related to the length of two or three bonds and z_1 is very large. More appropriately, we should replace eqn. (1) by an analogous equation for angular motion, whereupon c_1 would be replaced by a torque constant T, and a_1 would be replaced by the volume per segment, v.

$R_2(t)$ on the other hand arises from the relaxation and slippage processes of the macromolecules at high enough temperatures and long enough times so that we can consider these as an entangled network of gaussian segments. The quantity c_2/a_2' corresponds to the rubbery plateau modulus E_2; $c_2/z_2 a_2'$ and τ_m correspond to the values E_m and τ_m obtained from Procedure X [9].

In short, $R_1(t)$ and $R_2(t)$ correspond respectively to the contribution to $E_r(t)$ of the "wedge" and the "box". Although they arise from different physical

mechanisms, their temperature dependence is the same inasmuch as they are affected by similar segmental motions. An idealized model of our theoretical conception is shown in Fig. 4.

It is indeed very easy to fit an observed relaxation modulus by eqn. (8). The parameters of $R_2(t)$ are completely defined by experimental quantities.

$$\tau_m = \tau_m \text{ (from Procedure X)} = 1.16 \times 10^2 \text{ hours}$$

$$\frac{c_2}{z_2 a_2} = E_m \text{ (from Procedure X)} = 3.0 \times 10^5 \text{ dynes/cm}^2 \tag{9}$$

$$z_2 = \frac{E_2}{E_m} = 20$$

We can regard $R_1(t)$ as follows:

$$R_1(t) = E_1 \sum_{p=1}^{z_1} \frac{1}{z_1} \exp\left(\frac{-tp^2}{z_1^2 \tau_1}\right) \tag{10}$$

$$E_1 = \frac{c_1}{a_1}$$

For z_1 sufficiently large we can replace the sum in eqn. (10) by an integral, which simplifies to the tabulated incomplete gamma function.

$$R_1(t) = \frac{E_1 \tau_{\min}^{1/2}}{2} t^{-1/2} \left[\Gamma_{t/\tau_1}\left(\tfrac{1}{2}\right) - \Gamma_{t/\tau_1 z_1^2}\left(\tfrac{1}{2}\right)\right] \tag{11}$$

In eqn. (11) $\Gamma_x(\tfrac{1}{2})$ is the incomplete gamma function of the argument $\tfrac{1}{2}$.

We have graphed $R_1(t)$ in the form $\log R_1(t)/E_1$ versus $\log (t/\tau_1)$ in Fig. 2, for $z_1 = 3.55 \times 10^3$, and for z_1 approaches infinity. By sliding this tabulated
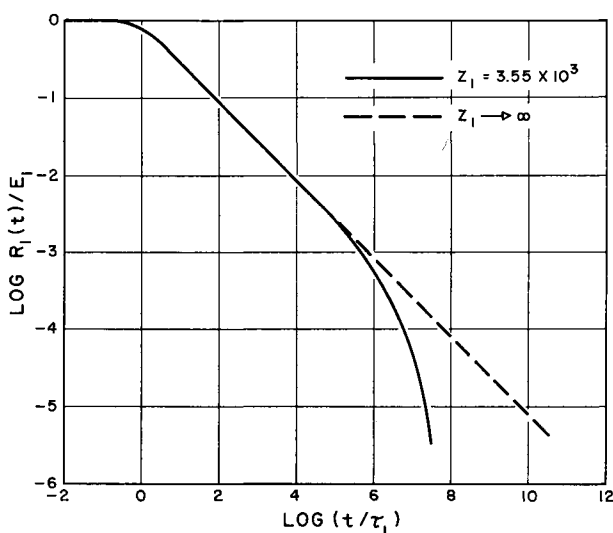
FIG. 2. Log $R_1(t)/E_1$ versus log $(t/\tau_1$ for $z_1 = 3.55 \times 10^3$ and z_1 approaches infinity.

function over a plot of the experimental values of $\log E_r(t)/E_1$ versus $\log (t)$ in the transition region, one can readily select the value of τ_1 that gives the best fit to the experimental data.

However, eqn. (11) is actually identical with the result obtained long ago by using the "wedge" distribution of relaxation times. To make the identification complete we identify E_1, τ_1 and z_1 with the constants M, τ_1 and τ_2 which were previously used to define the wedge distribution at 25°C.

$$E_1 = 2M/\tau_1{}^{1/2} = 10^{10.5} \text{ dynes/cm}^2$$
$$\tau_1 \equiv \tau_1 \qquad = 10^{-12.5} \text{ hours} \qquad (12)$$
$$z_1 = (\tau_2/\tau_1)^{1/2} = 3.55 \times 10^3$$

We have therefore used eqn. (11) and the parameters given by (12) to define $R_1(t)$. The choice of $z_1 = 3.55 \times 10^3$ was used to make present results identical
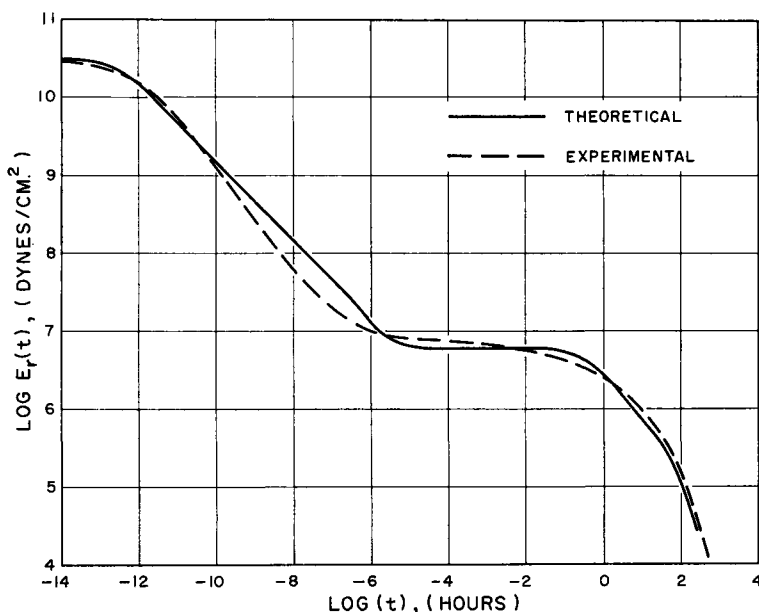
FIG. 3. Theoretical and experimental master curves for N.B.S. polyisobutylene at 25°C.

with previous results. However, a good fit of the data could be obtained with any sufficiently large value of z_1, preferably larger than 10^3, and even with a value of z_1 of about 10^8. We point this out lest too much physical significance be attached to the actual value of z_1 we selected. Its physical meaning is the number of torsional oscillators in the linear arrays which we associate with our macromolecular system. We merely know that z_1 is very large, and that $R_1(t) + R_2(t)$ can be made to fit the observed relaxation of stress data with any reasonable choice of z_1.

In Fig. 3 we show the experimental values of $E_r(t)$ versus the theoretical value given by eqn. (8). The parameters given in eqns. (9) and (12) were utilized

in computing $R_1(t)$ and $R_2(t)$. The fit between theory and experiment is reasonably good, but not excellent. The fit in the rubbery flow region, where $R_2/t)$ is utilized would be much better if N.B.S. polyisobutylene were monodisperse, which it is not. In subsequent papers we shall show that $R_2(t)$ fits data for monodisperse polystyrene in the rubbery flow region quite well.
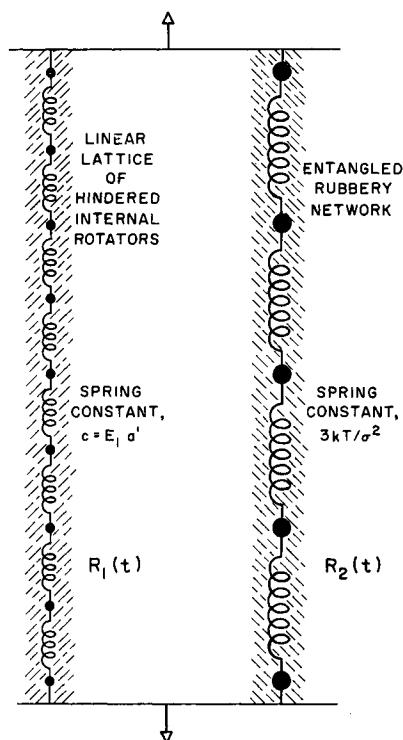
FIG. 4. Idealized model showing mechanisms by which $R_1(t)$ and $R_2(t)$ contribute to $E_r(t)$.

In Fig. 1 we have plotted the discrete relaxation time spectrum associated with $R_2(t)$ for comparison with the empirical "box" function, which is a continuous distribution. The relaxation spectrum associated with $R_1(t)$ is essentially a continuous function since z_1 is so large. It is identical with the wedge which had been previously postulated on a purely empirical basis [1].

The quantity E_1 has been associated with a force constant for torsional vibrations; the quantity τ_1 would be associated with the relaxation time for an elementary process of internal rotation. Interpreted in this manner the numerical values shown in eqn. (12) are quite reasonable.

The treatment of the relaxation time distribution for the transition region presented here is consistent with a more general treatment previously given for one-, two-, and three-dimensional lattices [10]. It was postulated that for such

lattices each normal mode frequency is correlated with a relaxation time inversely proportional to the square of the frequency. This gives a slope of $-\frac{1}{2}$ for the log $E_r(t)$ versus log t curve for a linear lattice. It gives a much narrower distribution of relaxation times and hence a much steeper slope for three-dimensional lattices. It was in fact shown that for rosin, which was considered as a good experimental model for a three-dimensional quasi-lattice, the viscoelastic properties are nearly those of a Maxwell body [11].

In some polymers the negative slope in the transition region is larger than $\frac{1}{2}$. This may be an indication that the linear lattice model (for the internal rotations) is somewhat modified by intermolecular interactions between segments of neighboring molecules. This would provide a higher dimensional aspect to the relaxation problem and give negative slopes larger than $\frac{1}{2}$.

COMPLIANCE CURVES

From the theory of linear viscoelasticity, the shear compliance can be computed from the stress relaxation modulus. In Fig. 5 we show the computed shear
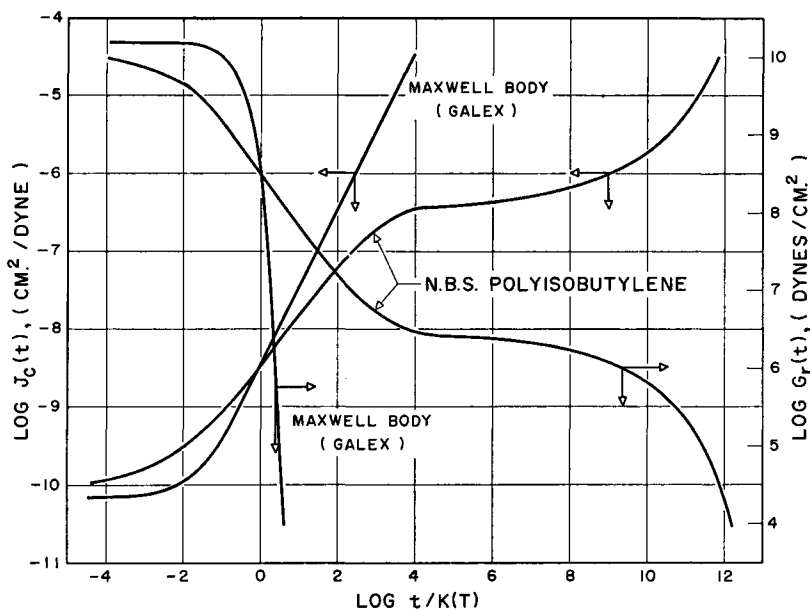
FIG. 5. Computed shear compliances and shear relaxation modulus vs. $t/K(T)$ for two materials.

compliance and shear relaxation modulus versus $t/K(T)$ for N.B.S. polyisobutylene and for aromatized rosin (Galex). The latter substance is shown as an ideal Maxwell body. The quantity $K(T)$ is the characteristic relaxation time, that is the time at any temperature required for $3G_r(t)$ to attain a value of 10^9 dynes/cm^2.

REFERENCES

[1] TOBOLSKY, A. V., *J. Am. Chem. Soc.*, **74**, 3786 (1952).
[2] ROUSE, P. E., *J. Chem. Phys.*, **21**, 1272 (1953).
[3] BUECHE, F., *J. Chem. Phys.*, **22**, 603 (1954).
[4] TOBOLSKY, A. V., CARLSON, D. and INDICTOR, N., *J. Polymer Sci.*, **54**, 175 (1961).
[5] BUECHE, F., *J. Appl. Phys.*, **26**, 738 (1955); *J. Chem. Phys.*, **25**, 599 (1956).
[6] FERRY, J. D., LANDEL, R. F. and WILLIAMS, M. L., *J. Appl. Phys.*, **26**, 359 (1955).
[7] TOBOLSKY, A. V., *Structure and Properties of Polymers*, p. 173, John Wiley, New York (1960).
[8] WILLIAMS, M. L., *J. Polymer Sci.*, **62**, S7 (1962).
[9] TOBOLSKY, A. V. and MURAKAMI, K., *J. Polymer Sci.*, **40**, 443 (1959).
[10] TOBOLSKY, A. V., *J. Chem. Phys.*, **37**, 1575 (1962).
[11] TOBOLSKY, A. V. and TAYLOR, R. B., *J. Phys. Chem.*, **67**, 2439 (1963).

CONTINUUM THEORY OF
NONLINEAR VISCOELASTICITY

A. C. Eringen and R. A. Grot

Purdue University, Lafayette, Indiana

Abstract—An assessment of the recent developments in the field of nonlinear continuum mechanics is presented with the view of developing a systematic approach to the formulation of nonlinear theories of viscoelastic materials. Contact is provided with various types of approximations useful in the treatment of engineering problems involving solid propellant material.

1. INTRODUCTION

Solid materials that possess fluid characteristics are called viscoelastic materials. These materials possess a certain amount of rigidity that is characteristic of solid bodies; at the same time they flow and dissipate energy by frictional losses as some fluids. The elastic solid and viscous fluids occupy the two extremes of the spectrum of viscoelastic materials. Characteristic to any dissipative process is heat generation by internal friction. Consequently, thermal phenomena are inherent and coupled with the mechanical deformations and flow. Without further complicating the state of affairs with chemical or electromagnetic phenomena, it is not difficult to see that viscoelastic materials represent a very general model of *thermomechanical* materials. The study of thermoviscoelastic materials can be said to be equivalent to the study of real materials exhibiting mechanical and thermal behavior.

The theories of viscoelasticity initiated by Maxwell [1], Meyer [2–4], Boltzmann [5] and studied by Voigt [6–9], Kelvin [10], Duhem [11–12], Natanson [13–15], Zaremba [16–18] and others at the turn of the century remained in a slow "creep" for nearly half a century. With the advances of technology and demands from the solid propellant industry, the theoretical workers have been shaken up from their long sleep. While the early theories were mostly confined to linear approximations and were not organized within the axiomatic disciplines of present developments, nevertheless they had far-reaching physical implications. The profound significance of the theory and its universal character have been demonstrated by Vito Volterra [19] in connection with the problems of heredity. He has made extensions and applications of the theory to electromagnetic phenomena, biological phenomena and living organisms.

From 1900 to 1950 we find studies of more limited nature in the molecular models of viscoelasticity and some phenomenological linear theories mostly concerned with one-dimensional models, creep and relaxation experiments and thermal transition of the viscoelastic properties of various high polymers.

Several review articles and books on these early developments exist. To cite just a few, we have the volumes edited by Eirich [20] and Staverman and Schwarzl [21].

The modern theory of viscoelasticity has its profound roots in the early works of Zaremba [16–18] and the Cosserat [22] brothers' book entitled *Theory of Deformable Bodies* where the basic principles of mechanics of continua were established. Unnoticed until the 1950's new developments took place in England and in this country by a small group of investigators. The status of various nonlinear theories up to 1962 was presented in a book by Eringen [23]. In the space available, it is impossible to mention and discuss the evolution of the theory, the rediscovery and/or reorganization of its various fundamental principles. We hope many active investigators in this field will forgive us for not being able to reference their work properly.

It is with this expedience that we limit this article to the developments of the last few years—especially those which treated thermal phenomena. In order to reach those not familiar with the modern theories of continuum mechanics, many simplifying assumptions are made at judicious spots. The engineer will be relieved to know that such assumptions should be adequate for his needs. It should be pointed out that they are not necessary for a general development of the theory, and ample reference is made to sources which remove some of these limitations.

We believe that it is appropriate in an article of this type to say something about the overall philosophy and direction of the recent work. It appears that the trend once again is towards more and more generalizations and complete characterization of all materials. The futility of such a desire, clearly demonstrated in the extensive works of Jaumann [24] and Lohr [25], has not been rediscovered as yet. It is not difficult to criticize the usefulness of such generalities even for those who are not concerned with applications. However, on the constructive side, we see a sound and profound school of physics, or more properly engineering science, arising. This school has concerned itself with the intimate ties among seemingly separate properties of materials. We are forced to accept the fact that it is no longer possible to explain many physical phenomena with just Newton's laws or just the basic laws of thermodynamics or the laws of electricity and magnetism alone. The superposition of these laws is not possible either. In fact, some of these basic principles will have to be reformulated. Moreover, contrary to the view of classical physicists, Hooke's Law, Fourier's Law, Ohm's Law, etc., are not laws of nature but are approximations to more complete constitutive equations. We have definite signs that the theory of continuous media as an axiomatized and rigorously organized scientific discipline when nourished by rational experiments could well be the long-desired unified source for the formulation of all macroscopic physical phenomena. In as short a time as one decade, we have already encountered serious works on the formulation of the material properties of continuous media, subject to severe physical and chemical effects (including motion, heat, E-M fields, chemical reactions, diffusion). These studies are truly interdisciplinary in character and are not bias

and fashionably marked as such. By the same token, they often appear in a format incomprehensible not only to engineers but also to physicists, mathematicians and engineering scientists trained in this field. This unfortunate situation will no doubt be ironed out soon. The far-reaching implications of this work will then reach the enrichening and useful circles of engineers. Once the trivial generality and wasteful pedanticism is overcome, a rich harvest will follow.

Without further excursion into the philosophical implications of these novel approaches, we now would like to proceed to lay down the fundamental ideas underlying the theories of nonlinear viscoelasticity. We choose to proceed from simple ideas towards the modern developments, ending with some suggestions useful to engineers in their work.

2. ELEMENTARY THEORIES

A thin metallic wire clamped at one end and set into free oscillations by means of a circular disk attached to the other end comes to rest in time whether the oscillation takes place in air or in vacuum. This elementary observation led several mathematical physicists of the late nineteenth century to the discovery of the phenomena of internal friction in materials. Two main approaches to this subject matter are based on the following two simple mechanical models:

(a) Kelvin–Voigt solid.

(b) Maxwell solid.

(a) *Kelvin–Voigt solid.* This model consists of a spring and a dashpot adjoined in parallel so that the force t applied to the system is given by a linear combination of an elastic and a viscous stress, i.e.

$$t = Ee + c\dot{e} \qquad (2.1)$$

where e is the strain in the spring and E and c are respectively the elastic and viscous moduli. A dot represents the time rate.

This form of the internal friction was proposed and developed by O. E. Meyer [2–4], Voigt [6–9], Duhem [11–12], Kelvin [10], Strutt [26], H. J. Jeffereys [27], Gerasimov [28] and others at the turn of the century. Subsequent developments of this idea were pursued in the direction of adjoining many spring elements in parallel so that (2.1) is modified to include higher order rates of strain, three-dimensional effects and nonlinear deformations and rates. Thus, for example, for a three-dimensional elastic solid we may write

$$t_{kl} = E_{klmn} \tilde{e}_{mn} + \sum_{n=1}^{N} {}_n B_{klrs} \left(\frac{\partial}{\partial t}\right)^n \tilde{e}_{rs} \qquad (2.2)$$

where t_{kl}, $\tilde{e}_{mn}$ are respectively the stress and infinitesimal strain tensors and E_{klmn} and ${}_n B_{klrs}$ are the elastic and viscous moduli which must be determined experimentally. Repeated indices indicate summation over the range (1, 2, 3). In

the theory underlying (2.1) or (2.2) we see that the elastic and viscous stresses are additive, i.e.

$$\mathbf{t} = \mathbf{f}(\tilde{\mathbf{e}}) + \boldsymbol{\varphi}\,(\dot{\tilde{\mathbf{e}}}) \tag{2.3}$$

where $\mathbf{f}$ and $\boldsymbol{\varphi}$ are linear tensor functions of the tensor variables $\tilde{\mathbf{e}}$ and $\dot{\tilde{\mathbf{e}}}$. When bodies are subjected to large strains and deformation rates, can we keep the form (2.3) with $\mathbf{f}$ and $\boldsymbol{\varphi}$ now being nonlinear? The answer is no, and we give the correct form of (2.3) and its generalizations in Section 5 of the present paper.

(b) *Maxwell solid.* In this case the spring and dashpot are connected in series form. The applied force t is calculated from

$$\dot{e} = \frac{1}{k}t + \frac{1}{E}\dot{t} \tag{2.4}$$

where k is a material constant. This model was proposed by Maxwell [1] and developed by Natanson [13–15] and Zaremba [16–18]. Again the nonlinear generalization of (2.4) in the form

$$\dot{\mathbf{e}} = \mathbf{f}(\mathbf{t}) + \boldsymbol{\varphi}\,(\dot{\mathbf{t}}) \tag{2.5}$$

is meaningless.

A combined three-dimensional linear theory may be expressed in the general form

$$\sum_{n=0}^{M} {}_{n}A_{klrs}\left(\frac{\partial}{\partial t}\right)^{n} t_{rs} = \sum_{n=0}^{N} {}_{n}B_{klrs}\left(\frac{\partial}{\partial t}\right)^{n} \tilde{e}_{rs} \tag{2.6}$$

where ${}_{n}\mathbf{A}$ and ${}_{n}\mathbf{B}$ are material constants. A large literature on theories of the form (2.6) exists. Among early proponents of these combined theories we mention the works of Alfrey [29–30]. An account on the subject is to be found in Zener [31], Staverman and Schwarzl [21] and in Freudenthal and Geiringer [32, ch. III].

For large strains and deformation rates, constitutive equations (2.5) and (2.6) are not admissible on physical grounds. Proper forms of the corresponding generalizations must be found.

(c) *Boltzmann–Volterra superposition theory.* Boltzmann [5] and Volterra [19, 33] proposed linear theories which assume that the stress depends on the entire past history of strain. For such materials, in the linear range of strains, the stress constitutive equations are usually expressed in the form

$$t_{kl} = E_{klrs}\,\tilde{e}_{rs} + \int_{-\infty}^{t} K_{klrs}(t-\tau)\tilde{e}_{rs}(\tau)\,d\tau \tag{2.7}$$

where $\mathbf{E}$ and $\mathbf{K}$ are elastic and hereditary moduli. Materials whose behavior is governed by the previous history of strain are called *hereditary materials* or *materials with memory.*

The relation of the Boltzmann superposition theory (2.7) to the general linear rate theory (2.6) can be established easily (cf. Eringen [34]).

The viscoelastic moduli appearing in the above equations are found to be highly sensitive to thermal changes. Thus a discussion of viscoelasticity without thermal effects is liable to remain incomplete. For one-dimensional models various approximations exist (cf. Eirich [20]). The complete determination of viscoelastic moduli of various polymeric materials at different range of temperature and frequencies has only been achieved for special one-dimensional models. Statistical mechanical models have also been proposed; however, these are adequate only for simple one-dimensional situations.

Within the framework of the foregoing sketch of various linear theories, several important questions are induced:

(i) What are the physically acceptable nonlinear forms of these linear constitutive equations?

(ii) How are we to incorporate the thermal effects?

Indeed these questions are adequate to shake the complete foundations of continuum thermomechanics. In the light of advances made during the past ten years, we are now able to organize our subject matter on a firm foundation. Nevertheless, the complete answer to the problem of thermal effects is as yet to come.

We begin our study with the establishment of basic principles of continuum thermomechanics by briefly presenting in Section 3 the basic principles of mechanics and thermodynamics and in Section 4 some of the fundamental axioms of constitutive theory. For a detailed treatment of either, reference can be made to Eringen [23, 35]. These basic principles together with the constitutive axioms are adequate for the establishment of nonlinear theories of thermomechanical materials. This is shown to be the case in Section 5 where a detailed treatment is presented for the non-heat-conducting Kelvin–Voigt solid. In Section 6 we present a nonlinear theory of viscoelasticity for the so-called Maxwell material. Section 7 deals with non-thermal materials involving higher order strain rates. The nonlinear generalization of the Boltzmann-Volterra superposition theory leads to functional constitutive equations; this is the topic of Section 8. The inclusion of heat conduction into these various theories is discussed in Sections 9–12. Section 13 contains what the authors consider useful approximate formulae for practical applications of these theories.

3. EQUATIONS OF BALANCE FOR NON-POLAR CONTINUA

A material body $\mathscr{B}$ consists of a collection of mass points having continuous mass density ρ at all points of the body at all times. A material in the undeformed state is located by its rectangular coordinates X_K ($K = 1, 2, 3$) or the position vector $\mathbf{X}$ referred to an origin O at time $t = 0$. At any other time under the influence of external effects the body may deform and move to new places. The motion carries $\mathbf{X}$ to a new place $\mathbf{x}$ at time t, i.e. the motion of the material point

11

X may be described by

$$\mathbf{x} = \mathbf{x}(\mathbf{X}, t) \quad \text{or} \quad \mathbf{X} = \mathbf{X}(\mathbf{x}, t) \tag{3.1}$$

We assume that the body does not split or intermingle except possibly at some singular surfaces, lines and points. This expresses the principle of indestructibility of matter and mathematically requires that

$$J = \frac{\rho_0}{\rho} = \det\left(\frac{\partial x_k}{\partial X_K}\right) \neq 0 \tag{3.2}$$

where ρ_0 is the mass density in the undeformed state.

A non-polar continuum is a body which cannot be influenced by couple stress and body couple. For such bodies the internal state of stress is fully described by a symmetric stress tensor.

The basic equations of balance for non-polar continua are [23]:
Balance of mass:

$$\dot{\rho} + \rho v_{k,\,k} = 0 \qquad \text{in } \mho \tag{3.3}$$

Balance of momentum:

$$t_{kl,\,k} + \rho(f_l - \dot{v}_l) = 0 \qquad \text{in } \mho \tag{3.4}$$

Balance of moment of momentum:

$$t_{kl} = t_{lk} \qquad \text{in } \mho \tag{3.5}$$

Balance of energy:

$$\rho\dot{\epsilon} = t_{kl}v_{l,\,k} + q_{k,\,k} + \rho h \qquad \text{in } \mho \tag{3.6}$$

Entropy inequality:

$$\rho\gamma = \rho\dot{\eta} - \rho\frac{h}{\theta} - \mathrm{div}\left(\frac{\mathbf{q}}{\theta}\right) \geq 0 \qquad \text{in } \mho \tag{3.7}$$

all valid within the volume $\mho$ of the body where

$$v_k \equiv \text{velocity} = \left.\frac{\partial x_k}{\partial t}\right|_{\mathbf{X}}$$

$t_{kl} \equiv$ stress tensor

$f_l \equiv$ body force per unit mass

$\epsilon \equiv$ internal energy density per unit mass

$q_k \equiv$ heat vector directed outward from the surface $\mathscr{S}$ of the body

$h \equiv$ energy source per unit mass

$\theta \equiv$ temperature

$\eta \equiv$ entropy per unit mass

Repeated indices indicate summation over the range (1, 2, 3) and an index after a comma indicates partial derivative, e.g.

$$v_{l,\,k} \equiv \frac{\partial v_l}{\partial x_k}$$

We also employ a superposed dot to indicate the material derivative, e.g.

$$\dot{v}_l \equiv a_l \equiv \frac{Dv_l}{Dt} \equiv \frac{\partial v_l}{\partial t}\bigg|_{\mathbf{x}} + v_{l,\,k}\,v_k$$

If the body is being traversed by a moving discontinuity surface $\sigma(t)$ (having velocity $\mathbf{u}$ directed along its normal $\mathbf{n}$), the equations (3.3) to (3.7) would be valid only in $\mathcal{V} - \sigma(t)$. On the discontinuity surface these equations are replaced by the jump conditions

$$[\rho(\mathbf{v} - \mathbf{u})] \cdot \mathbf{n} = 0 \qquad\qquad \text{on } \sigma(t) \qquad (3.8)$$

$$[\rho v_l(\mathbf{v} - \mathbf{u})] \cdot \mathbf{n} - [t_{kl}]n_k = 0 \qquad \text{on } \sigma(t) \qquad (3.9)$$

$$[\rho(\epsilon + \tfrac{1}{2}\mathbf{v}\cdot\mathbf{v})(\mathbf{v} - \mathbf{u})] \cdot \mathbf{n} - [t_{kl}v_l + q_k]n_k = 0 \quad \text{on } \sigma(t) \qquad (3.10)$$

$$\left[\rho\eta(\mathbf{v} - \mathbf{u}) - \frac{\mathbf{q}}{\theta}\right]\cdot\mathbf{n} \geq 0 \qquad \text{on } \sigma(t) \qquad (3.11)$$

where bold-face brackets indicate the difference in the value of its content taken from the front of the surface (the side of the positive normal) and the back side. Note also that there is no jump condition corresponding to (3.5).

By considering that the discontinuity surface $\sigma(t)$ coincides with the surface $\mathcal{S}$ of the body, from (3.8) to (3.11) we obtain the boundary conditions to be satisfied on $\mathcal{S}$. In this case we have $\mathbf{u} \equiv \mathbf{v}$ and we have

$$t_{kl}n_k = t_{(n)l} \qquad \text{on } \mathcal{S} \qquad (3.12)$$

$$\mathbf{q}\cdot\mathbf{n} = q(\mathbf{n}) \qquad \text{on } \mathcal{S} \qquad (3.13)$$

where $t_{(n)l}$ and $q_{(n)}$ are respectively the surface traction and the normal component of the surface heat vector to be prescribed on the surface of the body $\mathcal{S}$. Other boundary conditions replacing these are possible. For example, the displacement vector and temperature may be prescribed on $\mathcal{S}$ instead of (3.12) and (3.13). Among the many possibilities, those that are mathematically acceptable are decided on the basis of uniqueness theorems. We do not delve into this matter any further here.

We note that the jump conditions (3.8) to (3.11) are important in the treatment of shock wave phenomena and propagations of discontinuities in a continuous material body. The system of partial differential equations (3.3) to (3.6) is essential in the treatment of all problems in continuum mechanics. They must, of course, be supplemented by additional equations characterizing the material. In the following sections, we develop equations characteristic to different types of viscoelastic solids starting from simple cases and moving towards more complicated ones.

4. CONSTITUTIVE EQUATIONS

Balance eqns. (3.3) to (3.7) given in Section 3 are valid for any type of media irrespective of its constitutions. These equations, however, are not sufficient to determine the motion of any continuum since the number of unknowns (which is 14 in the present case, namely ρ, v_k, t_{kl}, q_k and ϵ) exceeds the number

of equations, namely, five. Since the basic axioms of motion and thermo-
dynamics are fully employed, the necessary equations supplementing (3.3) to
(3.7) must be derived on other grounds. These equations must of necessity
reflect the character of the medium. This is often popularly described by such
vague terminology as fluids, solids, gases, porous solids, electromagnets, etc.
The present article is concerned with the description of solids which have fluid
characteristics. Such solids deform and change their shapes under the effect of
external loads and at the same time through some internal friction mechanism
dissipate energy and produce heat. For an elastic solid and viscous fluid the
constitutive equations for stress are respectively expressed in the general forms,
cf. [23, ch. 5].

$$t_{kl} = f_{kl}(x_{r,S}) \qquad \text{elastic solid} \qquad (4.1)$$

$$t_{kl} = f_{kl}(\dot{x}_{r,S}) \qquad \text{viscous fluid} \qquad (4.2)$$

For a viscoelastic solid the combined feature of both media may be obtained by
use of the principle of unification [23, p. 138] in the form

$$t_{kl} = f_{kl}(x_{r,S}, \quad \dot{x}_{r,S}) \qquad \text{viscoelastic material} \qquad (4.3)$$

But materials may exhibit dependence on higher order time rates of $x_{r,S}$. A
very large class of viscoelastic materials is characterized by a combined feature
of stress, heat, internal energy and entropy functions being expressed in terms
of the past history of the deformation gradient, temperature and temperature
gradients. According to the *axiom of casuality* [35], the deformation gradients
and temperature histories are self-evident *observable* effects which cause stress,
heat, internal energy and entropy changes. Mathematically

$$t_{kl} = f_{kl}[x_r, \kappa(t'), \theta(t'), \theta, \kappa(t'); \mathbf{X}, t] \qquad (4.4)$$

$$q_k = g_k[x_r, \kappa(t'), \theta(t'), \theta, \kappa(t'); \mathbf{X}, t] \qquad (4.5)$$

$$\epsilon = e[x_r, \kappa(t'), \theta(t'), \theta, \kappa(t'); \mathbf{X}, t] \qquad (4.6)$$

$$\eta = n[x_r, \kappa(t'), \theta(t'), \theta, \kappa(t'); \mathbf{X}, t] \qquad (4.7)$$

where f_{kl}, g_k, are respectively tensor-valued and vector-valued functionals and
e and n are scalar-valued functionals of the argument functions x_r, $\kappa(t')$, $\theta(t')$,
$\theta, _r(t')$ at all times $t' \leq t$. In addition they are functions of $\mathbf{X}$ and t. The depend-
ence on $\mathbf{X}$ is required for inhomogeneous materials. The domains of the argument
functions and smoothness conditions are presently unspecified. Note that when
t' is allowed to take only the value t, equation (4.4) gives the stress constitutive
equation of thermo-elastic solid. If, on the other hand, $\theta(t') = \theta, \kappa(t') \equiv 0$
and $x_r, \kappa(t')$ can be approximated by

$$x_r, \kappa(t') = x_r, \kappa(t) + (t' - t)\dot{x}_r, \kappa(t)$$

and consequently the functional f_{kl} by

$$t_{kl} = f_{kl}(x_r, \kappa, \dot{x}_r, \kappa; \mathbf{X}, t)$$

we see that we obtain the viscoelastic material described by (4.3). Constitutive equation (4.5) gives the heat conduction law and (4.6) and (4.7) are the general equations of state. It should be observed that the functionals **f**, **g**, e and n contain the same constitutive variables at the start. This is known as the *axiom of equipresence* [23, p. 137]. By use of other axioms of constitutive theory and the principle of entropy some of these functionals are restricted and others can be shown to be independent of some constitutive variables. Among these axioms we cite the *axioms of objectivity*, *material invariance*, and the *axiom of memory*. For a thorough discussion of these axioms we refer the reader to Eringen [23, ch. 5] and Eringen [35] in the latter of which a general unified theory of thermomechanical materials is studied in detail. For our present purposes, a short discussion is presented below.

The axiom of objectivity states that the constitutive equations must be form-invariant with respect to rigid motions of the spatial frame of reference and any arbitrary shift of time. Let $\bar{x}$ and x be two spatial frames of reference that can be made to coincide with each other by a rigid motion and a time shift. Then we must have

$$\bar{x}_k(\mathbf{X}, \bar{t}) = Q_{kl}(t)\, x_l\,(\mathbf{X}, t) + b_k\,(t) \tag{4.8}$$

where $\mathbf{Q}(t)$ is a proper orthogonal transformation (a rigid rotation) and $\mathbf{b}(t)$ is a translation and $\bar{t}$ is obtained from t by a constant shift a of time, i.e.

$$\mathbf{Q}\mathbf{Q}^T = \mathbf{Q}^T\mathbf{Q} = \mathbf{I}, \quad \det \mathbf{Q} = +1, \quad \bar{t} = t - a \tag{4.9}$$

where $\mathbf{I}$ is a unit tensor and $\mathbf{Q}^T \equiv$ transpose of $\mathbf{Q}$. According to the axiom of objectivity, equations (4.4) to (4.7) must be form-invariant for all rotations $\mathbf{Q}$, for all translations $\mathbf{b}$ and for all time shifts a. As we can see, these conditions place severe restrictions on the constitutive functionals **f**, **g**, e and n. Functionals obeying the above restrictions for all $\mathbf{Q}$ are called *spatially hemitropic*. If we include the reflection of the coordinate axes (in which det $\mathbf{Q} = -1$) to the group $\{\mathbf{Q}\}$ then these functionals become *spatially isotropic*. In this latter case, $\{\mathbf{Q}\}$ is the full orthogonal group of transformations. The form-invariance with respect to all translations $\mathbf{b}$ implies *spatial homogeneity* and with respect to a implies a shift of origin of time. The important consequence of the axiom of objectivity will be seen in the following articles.

The axiom of material invariance requires that we take care of the material symmetry requirements properly. This can be expressed by the form-invariance of the constitutive functionals with respect to some rotations $\{\mathbf{S}\}$ and translations $\{\mathbf{B}\}$ of the material frame of reference $\mathbf{X}$. The group $\{\mathbf{S}\}$ depends on the number of symmetry axes for the material properties and $\{\mathbf{B}\}$ depends on the conditions of inhomogeneity. For homogeneous materials the dependence on $\{\mathbf{B}\}$ disappears, and for isotropic materials $\{\mathbf{S}\}$ is the full group of orthogonal transformations of the material axes, i.e. the constitutive functionals are form-invariant under all conceivable rotations and reflections of the material frame of reference.

Axiom of memory is a statement of smoothness on the constitutive functionals. Most materials possess short memory so that the deformations and thermal changes in distant past do not affect the present conditions. This is often expressed as the principle of heredity—Volterra [19], Straneo [36]—or principle of fading memory—Coleman and Noll [37, 38]. We will also use the terminology of principle of *smooth memory* for certain special conditions of smoothness [35]. Since this latter case is encountered often in what follows we give a short account of the axiom of smooth memory. Suppose that the functions $x_{k, K}(t')$, $\theta(t')$ and $\theta_{, K}(t')$ possess terminating Taylor series expansions of the forms

$$x_{k,K}(t') = x_{k,K}(t) + (t'-t)\dot{x}_{k,K}(t) + \frac{(t'-t)^2}{2!}\ddot{x}_{k,K}(t) + \ldots + \frac{(t'-t)^M}{M!} x_{k,K}^{(M)}$$

$$\theta(t') = \theta(t) + (t' - t)\dot{\theta}(t) + \ldots + \frac{(t'-t)^N}{N!} \theta^{(N)}(t) \qquad (4.10)$$

$$\theta_{,K}(t') = \theta_{,K}(t) + (t'-t)\dot{\theta}_{,K}(t) + \ldots + \frac{(t'-t)^P}{P!}\theta_{,k}^{(P)}(t)$$

If the constitutive functionals (such as f_{kl}) are smooth enough to allow representation of the form

$$t_{kl} = f_{kl}(x_{k, K}, \dot{x}_{k, K}, \ldots, x_{k, K}^{(M)}; \quad \theta, \dot{\theta}, \ldots, \theta^{(N)};$$
$$\theta_{, K}, \dot{\theta}_{, K}, \ldots, \theta_{,K}^{(P)}; \quad \mathbf{X}, t) \qquad (4.11)$$

then we say that the material obeys the axiom of smooth memory. The degree of smoothness depends on the order of the highest time rates present. We thus can see that under the hypothesis of the smooth memory the constitutive functionals become functions of various order time rates of $x_{k, K}$, θ and $\theta_{, K}$. In the following articles we apply these axioms to obtain the restricted forms of the constitutive equations of various types of viscoelastic materials. For a thorough exposition of these axioms and a detailed study of simple and non-simple thermomechanical materials the reader is referred to Eringen [35].

5. NONLINEAR KELVIN–VOIGT SOLID

In this section we present a derivation of the constitutive equations of the Kelvin–Voigt type of viscoelastic materials under the assumption that the phenomena of heat conduction is absent. Nevertheless, the constitutive coefficients can be considered temperature dependent.

The fundamental physical idea underlying the linear equations (2.1) of the Kelvin–Voigt solid is that the stress is dependent on the strain and strain rate. Since all strain measures are deducible from the deformation gradients $x_{k, K}$ in nonlinear elasticity, the starting point is to assume that the stress is a function of the deformation gradients. In nonlinear fluid dynamics it is a function of the material time rate of the deformation gradients. Consequently, a physically reasonable generalization of the linear theory of the Kelvin–Voigt solid (neglect-

ing heat conduction) may be obtained by a constitutive assumption similar to the form (4.3), i.e.

$$t_{kl} = f_{kl}(x_k, K, \dot{x}_k, K, \theta, \mathbf{X}, \mathbf{x}, t) \tag{5.1}$$

For a complete description of the material, additional constitutive equations are needed for the internal energy density ϵ, the entropy η and the heat flux $\mathbf{q}$. Following the principle of equipresence* we consider these quantities to be functions of the same list of variables appearing in (4.3). Thus

$$t_{kl} = f_{kl}(x_k, K, \dot{x}_k, K; \theta, \mathbf{X}, \mathbf{x}, t) \tag{5.2}$$

$$q_k = g_k(x_k, K, \dot{x}_k, K; \theta, \mathbf{X}, \mathbf{x}, t) \tag{5.3}$$

$$\epsilon = e(x_k, K, \dot{x}_k, K; \theta, \mathbf{X}, \mathbf{x}, t) \tag{5.4}$$

$$\eta = \eta(x_k, K, \dot{x}_k, K; \theta, \mathbf{X}, \mathbf{x}, t) \tag{5.5}$$

These equations must now be restricted by the axioms of the constitutive theory and the Clausius–Duhem inequality (3.7).

A. Consequence of Axiom of Objectivity

According to this axiom (5.2) to (5.5) must be form-invariant when the spatial frame $\mathbf{x}$ moves rigidly and the origin of time is changed, e.g.

$$f(\mathbf{x}, K, \dot{\mathbf{x}}, K; \theta, \mathbf{X}, \mathbf{x}, t) = f(\bar{\mathbf{x}}, K, \dot{\bar{\mathbf{x}}}, K, \theta, \mathbf{X}, \bar{\mathbf{x}}, \bar{t}) \tag{5.6}$$

where $\bar{\mathbf{x}}(\mathbf{X}, \bar{t})$ and $\bar{t}$ are related to $\mathbf{x}(\mathbf{X}, t)$ and t by (4.8) and (4.9), i.e.

$$\bar{\mathbf{x}}(\mathbf{X}, \bar{t}) = \mathbf{Q}(t)\mathbf{x}(\mathbf{X}, t) + \mathbf{b}(t) \tag{5.7}$$

$$\bar{t} = t - a \tag{5.8}$$

$$\mathbf{Q}\mathbf{Q}^T = \mathbf{Q}^T\mathbf{Q} = \mathbf{I}, \det \mathbf{Q} = +1 \tag{5.9}$$

We consider three special changes:

(a) *The rigid translation of frame* $\mathbf{x}$. For this case we take

$$\mathbf{Q}(t) = \mathbf{I}, \quad a = 0, \quad \mathbf{b}(t) = -\mathbf{x}(\mathbf{X}, t)$$

This means that the spatial frame $\mathbf{x}$ is translated so that the material point $\mathbf{X}$ at time t remains at the origin. From (5.7) it follows that

$$\bar{\mathbf{x}} = \mathbf{x} - \mathbf{x} = 0; \quad \bar{t} = t$$

From (5.6) it follows that

$$f(\mathbf{x}, K, \dot{\mathbf{x}}, K, \theta, \mathbf{X}, \mathbf{x}, t) = f(\mathbf{x}, K, \dot{\mathbf{x}}, K, \theta, \mathbf{X}, 0, t)$$

Hence the *response function* $\mathbf{f}$ is independent of $\mathbf{x}$.

---

* For a discussion of the principle of equipresence see Eringen [23, p. 137]. The basic idea was first employed by Koh and Eringen [39] in their work on thermoviscoelasticity. These authors did not, however, consider the thermodynamic functions ϵ and η to be a function of $\dot{x}_{k,K} \equiv Dx_{k,K}/Dt$ as the stress $\mathbf{t}$ and heat flux $\mathbf{q}$. Coleman and Mizel [40] went further and considered ϵ and η to depend on $x_{k,K}$. The dependence of the internal energy and entropy on the time rate of the deformation gradients will appear strange to the majority of scientists and engineers trained in classical thermodynamis. As it turns out the dependence of ϵ and η on $x_{k,K}$ drops out on the ground of other physical principles, namely the second law of thermodynamics. However, the basic idea used by these authors has other important implications, cf. the article by Eringen [35] and also appendix.

(b) *Shift of time.* We select

$$\mathbf{Q}(t) = \mathbf{I}, \quad \mathbf{b}(t) = 0, \quad a = t$$

This gives

$$\bar{\mathbf{x}}(\mathbf{X}, \bar{t}) = \mathbf{x}(\mathbf{X}, t), \quad \bar{t} = t - t = 0$$

From (5.6) it then follows that $\mathbf{f}$ is independent of time so that

$$\mathbf{t} = \mathbf{f}(\mathbf{x}, _K, \dot{\mathbf{x}}, _K; \quad \theta, \mathbf{X}) \tag{5.10}$$

(c) *Rigid rotations of the frame* $\mathbf{x}$. Now take $\mathbf{b} = 0$, $a = 0$ and $\mathbf{Q}(t)$ subject to $(5.9)_1$ otherwise being arbitrary. In this case the stress $\mathbf{t}$ transforms as

$$\bar{\mathbf{t}} = \mathbf{Q}\mathbf{t}\mathbf{Q}^T$$

Using (5.10) we get

$$\mathbf{Q}\mathbf{f}(\mathbf{x}, _K, \dot{\mathbf{x}}, _K; \quad \theta, \mathbf{X})\, \mathbf{Q}^T = \mathbf{f}(\mathbf{Q}, \mathbf{x} _K, \mathbf{Q}\dot{\mathbf{x}}, _K + \dot{\mathbf{Q}}\mathbf{x}, _K; \quad \theta, \mathbf{X}) \tag{5.11}$$

These conditions place restrictions on the form of $\mathbf{f}$. We can always select a rigid rotation $\mathbf{Q}$ such that at time t, $Q_{kl} = \delta_{kl}$ and $\dot{Q}_{kl} = - w_{kl}$ where

$$w_{kl} = \tfrac{1}{2}\,(v_{k,\,l} - v_{l,\,k}) \tag{5.12}$$

is the spin tensor. The identity (5.11) now reads

$$\mathbf{f}(x_k, _K, \dot{x}_k, _K, \theta, \mathbf{X}) = \mathbf{f}(x_k, _K, d_{kl}\, x_l, _K; \quad \theta, \mathbf{X})$$

where we used the identity

$$\dot{x}_k, _K = v_{k,\,l}\, x_l, _K \tag{5.13}$$

and the deformation rate tensor $\mathbf{d}$ is defined by

$$d_{kl} = \tfrac{1}{2}\,(v_{k,\,l} + v_{l,\,k}) \tag{5.14}$$

The above equation for $\mathbf{f}$ is equivalent to

$$\mathbf{f} = \mathbf{f}\,(x_k, _K, \dot{C}_{KL}; \quad \theta, \mathbf{X}) \tag{5.15}$$

where

$$\begin{aligned} C_{KL} &= x_k, _K\, x_k, _L \\ \dot{C}_{KL} &= 2d_{kl}\, x_k, _K\, x_l, _L \end{aligned} \tag{5.16}$$

are respectively the Green deformation tensor and its rate tensor. Now form

$$F_{KL} = f_{kl}(x_k, _K, \dot{\mathbf{C}}; \quad \theta, \mathbf{X})\, x_k, _K\, x_l, _L \tag{5.17}$$

Here F_{KL} are invariant under the rigid motion of the spatial frame of reference $\mathbf{x}$, and they are functions of three vectors $\mathbf{x}, _K$. According to a theorem of Cauchy* it can be expressed as functions of the inner products of these vectors two at a time and the triple scalar product given below

$$C_{KL} = x_k, _K\, x_k, _L, \quad \det x_k, _K = (\det C_{KL})^{1/2} \tag{5.18}$$

Thus†

$$F_{KL} = F_{KL}\,(C_{MN}, \dot{C}_{MN}, \theta, \mathbf{X}) \tag{5.19}$$

---

* Cf. Weyl [41, p. 53]; see also Eringen [23, p. 149].

† The dependence on C_{KL} implies that on $\det C_{KL}$. Hence it is not explicitly shown in (5.19). However, it is important to remember this point in polynomial or other approximations of F_{KL}.

Inverting (5.17) we now have

$$t_{kl} = F_{KL}(\mathbf{C}, \dot{\mathbf{C}}; \ \theta, \mathbf{X}) X_{K, k} X_{L, l} \tag{5.20}$$

A more convenient form is obtained if we write

$$F_{KL} = j T_{MN} C_{MK} C_{NL}, \quad j \equiv \det X^K_{,k} = \frac{1}{\sqrt{\det C_{KL}}} > 0 \tag{5.21}$$

Equation (5.20) now reads

$$t_{kl} = j T_{KL}(\mathbf{C}, \dot{\mathbf{C}}; \ \theta, \mathbf{X}) x_{k, K} x_{l, L} \tag{5.22}$$

The stress constitutive equation (5.22) so obtained obeys the axiom of objectivity. It is the most general equation of this theory. It is valid for anisotropic and inhomogeneous viscoelastic solids of the Kelvin–Voigt type. A similar treatment of the equations (5.3) to (5.5) result in

$$q_k = j Q_K(\mathbf{C}, \dot{\mathbf{C}}; \ \theta, \mathbf{X}) x_{k, K} \tag{5.23}$$

$$\epsilon = E(\mathbf{C}, \dot{\mathbf{C}}; \ \theta, \mathbf{X}) \tag{5.24}$$

$$\eta = N(\mathbf{C}, \dot{\mathbf{C}}; \ \theta, \mathbf{X}) \tag{5.25}$$

where Q_K is a vector function and E and N are scalar functions of the tensor variables $\mathbf{C}$ and $\dot{\mathbf{C}}$ and θ and $\mathbf{X}$.

Response functions are further restricted by the second law of thermodynamics and axiom of material invariance emanating from material symmetry conditions.

B. *Consequence of the Second Law of Thermodynamics*

.Constitutive equations (5.22) to (5.25) are subject to the Clausius–Duhem inequality (3.7). We first eliminate ph between the equation of energy balance (3.6) and entropy inequality (3.7). This gives

$$\rho\left(\dot{\eta} - \frac{\dot{\epsilon}}{\theta}\right) + \frac{1}{\theta} t_{kl} v_{l, k} + \frac{1}{\theta^2} q_k \theta_{, k} \geq 0 \tag{5.26}$$

This inequality will be used repeatedly to determine the thermodynamically admissible forms of the constitutive equations. Another convenient form of (5.26) is

$$-\frac{\rho}{\theta}(\dot{\Psi} + \eta\dot{\theta}) + \frac{1}{\theta} t_{kl} v_{l, k} + \frac{1}{\theta^2} q_k \theta_{, k} \geq 0 \tag{5.27}$$

where

$$\Psi(\mathbf{C}, \dot{\mathbf{C}}, \theta, \mathbf{X}) \equiv \epsilon - \theta\eta \tag{5.28}$$

is the *Helmholtz free energy* function. Upon substituting (5.22), (5.23) and (5.28) into (5.27) we get

$$-\frac{\rho_0}{\theta}\left(\eta + \frac{\partial\Psi}{\partial\theta}\right)\dot{\theta} + \frac{1}{2\theta}\left(T_{KL} - 2\rho_0\frac{\partial\Psi}{\partial C_{KL}}\right)\dot{C}_{KL} - \frac{\rho_0}{\theta}\frac{\partial\Psi}{\partial\dot{C}_{KL}}\ddot{C}_{KL} + \frac{1}{\theta^2} Q_K\theta_{, K} \geq 0 \tag{5.29}$$

where we employed (5.16) and the conservation of mass, $\rho = \rho_0 j$.

Inequality (5.29) is postulated to be valid for all independent variations of $\dot{\theta}$, $\ddot{C}_{KL}$, $\dot{C}_{KL}$ and $\theta, {}_L$. Since the coefficients of $\dot{\theta}$, $\ddot{C}_{KL}$ and $\theta, {}_L$ and other terms in (5.24) are independent of $\dot{\theta}$, $\ddot{C}_{KL}$ and $\theta, {}_L$, we immediately deduce that the necessary and sufficient condition for (5.29) to be valid for all possible values of $\dot{\theta}$, $\ddot{C}_{KL}$ and $\theta, {}_L$ is

$$\eta = -\frac{\partial \Psi}{\partial \theta}, \quad \frac{\partial \Psi}{\partial \dot{C}_{KL}} = 0, \qquad Q_K = 0 \tag{5.30}$$

Consequently, $\Psi = \Psi(\mathbf{C}; \theta, \mathbf{X})$ and (5.29) reduces to

$$\frac{1}{2\theta}\left(T_{KL} - 2\rho_0 \frac{\partial \Psi}{\partial C_{KL}}\right)\dot{C}_{KL} \geq 0 \tag{5.31}$$

Independence of Ψ from $\dot{\mathbf{C}}$ suggests that we decompose T_{KL} into two parts

$$T_{KL} = {}_ET_{KL}(\mathbf{C}; \theta, \mathbf{X}) + {}_DT_{KL}(\mathbf{C}, \dot{\mathbf{C}}, \theta, \mathbf{X}) \tag{5.32}$$

where

$$_ET_{KL} = 2\rho_0 \frac{\partial \Psi}{\partial C_{KL}} \tag{5.33}$$

and (5.28) becomes

$$\frac{1}{2\theta} {}_DT_{KL}\dot{C}_{KL} \geq 0 \tag{5.34}$$

Thus we have shown that *the necessary and sufficient conditions for the satisfaction of the local Clausius–Duhem inequality* are (5.30) and (5.32) to (5.34). The constitutive equations are now reduced to

$$t_{kl} = 2\rho \frac{\partial \Psi}{\partial C_{KL}} x_{k,\,K} x_{l,\,L} + {}_jT_{KL}(\mathbf{C}, \dot{\mathbf{C}}; \theta, \mathbf{X}) x_{k,\,K} x_{l,\,L} \tag{5.35}$$

$$q_k = 0 \tag{5.36}$$

$$\epsilon = \Psi(\mathbf{C}; \theta, \mathbf{X}) - \theta \frac{\partial \Psi}{\partial \theta} \tag{5.37}$$

$$\eta = -\frac{\partial \Psi}{\partial \theta} \tag{5.38}$$

where $_DT$ is subject to

$$\frac{1}{2\theta} {}_DT_{KL}\dot{C}_{KL} \geq 0 \tag{5.39}$$

for all independent variations of $\dot{\mathbf{C}}$. Inequality (5.39) in particular implies that

$$_DT_{KL}(\mathbf{C}, 0; \theta, \mathbf{X}) = 0 \tag{5.40}$$

The proof of this follows from using (5.39) and the continuity of $_DT_{KL}$. For if we set all $\dot{C}_{KL} = 0$ except $\dot{C}_{11}$, then from (5.39) we must have $_DT_{11}\dot{C}_{11}/2\theta \geq 0$. If $\dot{C}_{11} > 0$, then $_DT_{11} > 0$; if $\dot{C}_{11} < 0$, then $_DT_{11} < 0$. Thus $_DT_{11} = 0$ when $\dot{C}_{11} = 0$. The argument is the same for other components of $_DT_{KL}$.

Several remarks are in order:

(i) The stress tensor is decomposed into a *purely elastic* part $_ET$ and a *dissipative* part $_DT$. The dissipative energy according to (5.39) must be non-negative.

(ii) Equation (5.40) states that the dissipative part contains no purely elastic effect.

(iii) The heat flux must vanish (eqn. 5.36). This, of course, is the consequence of not including the temperature gradient $\theta_{,k}$ as a constitutive variable. This restriction which is equivalent to neglecting the heat conduction will be removed in Section 10.

(iv) The internal energy and entropy according to (5.37) and (5.38) depend only on $\mathbf{C}$, θ and $\mathbf{X}$ and not on the rate of strain $\dot{\mathbf{C}}$. We are, therefore, in a safe condition again. This situation is certainly correct on intuitive grounds and the contrary would be argued strenuously by the classical thermodynamicists. Nevertheless, these *a priori* arguments have now found a solid foundation. In fact, as we shall see later in more general type of dissipative materials, we may have to retain the dependence of internal energy and entropy on the past histories of deformation and temperature gradients.

C. *Material Symmetry Restrictions*

The forms of Ψ and $_DT$ further depend on the material symmetry. The material symmetry is expressed in the form of invariance of response function to a group of transformations $\{S\}$ which is capable of describing the symmetry conditions. Out of infinitely many such transformation groups, twelve particular transformations are adequate for the description of material symmetries in thirty-two known crystal classes. An account on the subject for elastic materials is to be found in Green and Adkins [42, ch. I]. In the literature there does not seem to exist a similar reduction for the viscoelastic crystal classes involving $_DT_{KL}$. For the homogeneous solid the dependence of Ψ and $_DT$ on $\mathbf{X}$ disappear and for the isotropic solids the form of Ψ and $_DT_{KL}$ are well known from various sources, see, for instance, [23, pp. 145 and 356]. For the isotropic solid both Ψ and $_DT$ are form-invariant under the full group of orthogonal transformations of the material frame $\mathbf{X}$. This means that Ψ is a function of the strain invariants and $_DT$ is an isotropic tensor function of $\mathbf{C}$. Since any two sets of invariants are related to each other (cf. [23, p. 31]) we can write

$$\Psi = \Psi(I, I_2, I_3; \quad \theta) \tag{5.41}$$

I_1, I_2, I_3 being any set of invariants. In particular, the invariants of the inverse Cauchy deformation tensor

$$c^{-1}_{kl} \equiv x_{k,K}\, x_{l,K} \tag{5.42}$$

defined by

$$\begin{aligned}
I_1 &= c^{-1}_{kk} = \operatorname{tr} \mathbf{c}^{-1}\\
I_2 &= c^{-1}_{kl}\, c^{-1}_{lk} = \operatorname{tr} \mathbf{c}^{-2}\\
I_3 &= c^{-1}_{kl}\, c^{-1}_{lm}\, c^{-1}_{mk} = \operatorname{tr} \mathbf{c}^{-3}
\end{aligned} \tag{5.43}$$

are found suitable in many instances. The Cauchy c deformation tensor

$$c_{kl} = X_{K,\,k}\,X_{K,\,l} \tag{5.44}$$

can also be used.

Substituting (5.41) into (5.35) and using the chain rule of differentiation we obtain

$$\mathbf{t} = c_0\mathbf{I} + a_1\mathbf{c}^{-1} + a_2\mathbf{c}^{-2} + {}_D\mathbf{t}\,(\mathbf{c}^{-1},\,\mathbf{d},\,\theta) \tag{5.45}$$

where

$$a_0 = \frac{\rho}{3}\,(I_1^3 + 2I_3 - 3I_1\,I_2)\,\frac{\partial\Psi}{\partial I_3}$$

$$a_1 = 2\rho\,\frac{\partial\Psi}{\partial I_1} - \rho\,(I_1^2 - I_2\,)\frac{\partial\Psi}{\partial I_3} \tag{5.46}$$

$$a_2 = 2\rho\,\frac{\partial\Psi}{\partial I_2} + 2\rho I_1\,\frac{\partial\Psi}{\partial I_3}$$

and ${}_D\mathbf{t}$ is a function of $\mathbf{c}^{-1}$, $\mathbf{d}$ and θ only. In this derivation the Cayley–Hamilton theorem is used which states any 3×3 matrix must $\mathbf{A}$ satisfy its characteristic equation, i.e.

$$\mathbf{A}^3 - \mathbf{A}^2\,\mathrm{tr}\,\mathbf{A} + \tfrac{1}{2}\,\mathbf{A}[(\mathrm{tr}\,\mathbf{A})^2 - \mathrm{tr}\,\mathbf{A}^2] - \mathbf{I}\,\det\mathbf{A} \tag{5.47}$$

If we assume that ${}_D\mathbf{t}$ is a polynomial in the arguments $\mathbf{c}^{-1}$ and $\mathbf{d}$, a simplification is possible by use of well-known techniques of reduction of matrix polynomials. The result is (cf. [23] p. 354, where $\mathbf{c}$ is used instead of $\mathbf{c}^{-1}$

$$\begin{aligned}
{}_D\mathbf{t} &= a_{00}\mathbf{I} + a_{10}\mathbf{c}^{-1} + a_{20}\mathbf{c}^{-2} + a_{01}\mathbf{d} + a_{02}\mathbf{d}^2 \\
&\quad + a_{11}(\mathbf{c}^{-1}\mathbf{d} + \mathbf{d}\mathbf{c}^{-1}) + a_{12}\,(\mathbf{c}^{-1}\mathbf{d}^2 + \mathbf{d}^2\mathbf{c}^{-1}) \\
&\quad + a_{21}\,(\mathbf{c}^{-2}\mathbf{d} + \mathbf{d}\mathbf{c}^{-2}) + a_{22}(\mathbf{c}^{-2}\mathbf{d}^2 + \mathbf{d}^2\mathbf{c}^{-2})
\end{aligned} \tag{5.48}$$

where $a_\kappa\lambda$ are scalar invariants in

$$I_1, I_2, I_3, \quad \mathrm{tr}\,\mathbf{d}, \quad \mathrm{tr}\,\mathbf{d}^2, \quad \mathrm{tr}\,\mathbf{d}^3, \quad \mathrm{tr}\,\mathbf{c}^{-1}\mathbf{d}, \quad \mathrm{tr}\,\mathbf{c}^{-1}\mathbf{d}^2, \quad \mathrm{tr}\,\mathbf{c}^{-2}\mathbf{d}, \quad \mathrm{tr}\,\mathbf{c}^{-2}\mathbf{d}^2 \tag{5.49}$$

and

$$a_{00} = a_{10} = a_{20} = 0 \text{ when } \mathbf{d} = 0 \tag{5.50}$$

6. NONLINEAR MAXWELL SOLID

Here we present an account of a nonlinear generalization of the Maxwell solid whose linear one-dimensional description was given by (2.4). We assume that the heat conduction is negligible and obtain a stress constitutive equation for a homogeneous isotropic solid.

Following Noll [43] the stress constitutive equations of such solids can be expressed in the general form

$$\dot{\mathbf{t}} = \mathbf{f}(\mathbf{l},\,\mathbf{t}) \tag{6.1}$$

where

$$\mathbf{l} = \|\,v_{k,\,l}\,\|$$

and where $\mathbf{f}$ is a symmetric second order tensor function of two second order tensors, the velocity gradients $v_{k,\,l}$ and the stress tensor t_{kl}. A dot superposed

on **t** indicates material time derivative, i.e.

$$\dot{t}_{kl} = \frac{\partial t_{kl}}{\partial t} + t_{kl,\, m}\, v_m \tag{6.2}$$

in rectangular coordinates. The axioms of constitutive theory place restrictions on the form of (6.1). In particular according to the axiom of objectivity in a frame of reference $\bar{x}$ differing from x by a rigid motion the form of (6.1) should remain the same, i.e.

$$\ddot{\bar{t}} = \mathbf{f}\,(\bar{\mathbf{l}},\, \bar{\mathbf{t}}) \tag{6.3}$$

where $\bar{\mathbf{t}}$ and $\bar{\mathbf{l}}$ are related to **t** and **l** by

$$\bar{\mathbf{t}} = \mathbf{Q}\mathbf{t}\mathbf{Q}^T, \quad \bar{\mathbf{l}} = \mathbf{Q}\mathbf{l}\mathbf{Q}^T + \dot{\mathbf{Q}}\mathbf{Q}^T \tag{6.4}$$

with $\mathbf{Q}(t)$ being any arbitrary time dependent rotation of the spatial frame x satisfying the condition (5.9). Substituting (6.4) into (6.3) we get

$$\mathbf{Q}f(\mathbf{l},\mathbf{t})\mathbf{Q}^T + \dot{\mathbf{Q}}\mathbf{t}\mathbf{Q}^T + \mathbf{Q}\mathbf{t}\dot{\mathbf{Q}}^T = \mathbf{f}(\mathbf{Q}\mathbf{l}\mathbf{Q}^T + \dot{\mathbf{Q}}\mathbf{Q}^T, \mathbf{Q}\mathbf{t}\mathbf{Q}^T) \tag{6.5}$$

a relation which must be valid for all $\mathbf{Q}(t)$ subject to (5.9). In particular by choosing at any arbitrary point x and instant t a rigidly rotating frame such that $Q_{kl} = \delta_{kl}$, $\dot{Q}_{kl} = -w_{kl}$ where

$$w_{kl} = \tfrac{1}{2}(v_{k,\, l} - v_{l,\, k}) \tag{6.6}$$

is the vorticity tensor, (6.5) can be reduced to

$$\mathbf{f}(\mathbf{l},\, \mathbf{t}) + \mathbf{t}\mathbf{w} - \mathbf{w}\mathbf{t} = \mathbf{f}(\mathbf{d},\, \mathbf{t}) \tag{6.7}$$

Often for the left side of (6.7) a new notation is introduced

$$\overset{\circ}{\mathbf{t}} = \dot{\mathbf{t}} + \mathbf{t}\mathbf{w} - \mathbf{w}\mathbf{t} \tag{6.8}$$

Thus the stress constitutive equations obeying the axiom of objectivity must have the form

$$\overset{\circ}{\mathbf{t}} = \mathbf{f}(\mathbf{d},\, \mathbf{t}) \tag{6.9}$$

where $\overset{\circ}{\mathbf{t}}$ defined in accordance with (6.8) is called *stress flux*. Unfortunately there exist many different admissible forms for the stress flux. For various other forms and a discussion of the stress flux, see Eringen [23, arts. 35, 72, 93]. However, the choice of any one form suffices for the exact theory since others are deducible from the one chosen. Nevertheless, differences occur in approximate theories or polynomial expressions of the constitutive equations.

Presently no thermodynamic theory exists which further restricts the form of (6.9).

If we assume that **f** in (6.9) is expressible as a matrix polynomial in **d** and **t** and use the Cayley–Hamilton theorem repeatedly and remember that **f** is an isotropic function, we obtain the following specific form

$$\begin{aligned}
\overset{\circ}{\mathbf{t}} = {} & a_{00}\mathbf{I} + a_{10}\mathbf{d} + a_{20}\mathbf{d}^2 + a_{01}\mathbf{t} + a_{02}\mathbf{t}^2 \\
& + a_{11}(\mathbf{d}\mathbf{t} + \mathbf{t}\mathbf{d}) + a_{12}(\mathbf{d}\mathbf{t}^2 + \mathbf{t}^2\mathbf{d}) \\
& + a_{21}(\mathbf{d}^2\mathbf{t} + \mathbf{t}\mathbf{d}^2) + a_{22}(\mathbf{d}^2\mathbf{t}^2 + \mathbf{t}^2\mathbf{d}^2)
\end{aligned} \tag{6.10}$$

where $a_{\kappa\lambda}$ are functions of the following ten invariants

$$\text{tr } \mathbf{d}, \quad \text{tr } \mathbf{d}^2, \quad \text{tr } \mathbf{d}^3, \quad \text{tr } \mathbf{t}, \quad \text{tr } \mathbf{t}^2, \quad \text{tr } \mathbf{t}^3, \quad \text{tr } \mathbf{dt}, \quad \text{tr } \mathbf{dt}^2, \quad \text{tr } \mathbf{d}^2\mathbf{t}, \quad \text{tr } \mathbf{d}^2\mathbf{t}^2 \quad (6.11)$$

Further progress is possible on the ground of various order approximations. For example, theories linear in $\mathbf{t}$ or $\mathbf{d}$ further simplify (6.10). Decisions could be made to retain only up to certain order terms. Theories linear in $\mathbf{d}$ apply to materials with very short memory. For such materials no characteristic time constant exists. A theory of this type was introduced by Truesdell [44] under the name hypoelasticity.

In Section 13 we give a few forms that may be useful from the engineering viewpoint.

7. GENERAL STRAIN RATE DEPENDENT MATERIALS

In the two previous sections nonlinear extensions of Kelvin–Voigt and Maxwell solids were presented. These theories generalized the concept of Kelvin–Voigt and Maxwell solids to include large elastic strains or stresses and strain rates. Such theories have limited applicability to physical situations which involve rapid changes in the strain rate. This deficiency can be partly alleviated by assuming that the stress is dependent on higher order strain rates. In its full generality a theory of strain rate dependent materials is highly complicated. It is, however, an instructive introduction to the form of viscoelastic theories which are required to satisfy the second law of thermodynamics.

Generalizing eqn. (2.2) (again neglecting the phenomenon of heat conduction), it is assumed that the stress is a function of the temperature and the first ν rates of deformation gradients.

$$t_{kl} = f_{kl} \left(\mathbf{x}, \, _K, \, \dot{\mathbf{x}}, \, _K, \, \ldots, \, \mathbf{x}_{,K}^{(\nu)}; \quad \theta, \mathbf{X} \right) \quad (7.1)$$

The principle of equipresence requires that the internal energy, the entropy, and the heat flux are determined by constitutive equations of the form:

$$q_k = g_k \left(\mathbf{x}, \, _K, \, \dot{\mathbf{x}}, \, _K, \, \ldots, \, \mathbf{x}_{,K}^{(\nu)}; \quad \theta, \mathbf{X} \right) \quad (7.2)$$

$$\epsilon = e \left(\mathbf{x}, \, _K, \, \dot{\mathbf{x}}, \, _K, \, \ldots, \, \mathbf{x}_{,K}^{(\nu)}; \quad \theta, \mathbf{X} \right) \quad (7.3)$$

$$\eta = n \left(\mathbf{x}, \, _K, \, \dot{\mathbf{x}}, \, _K, \, \ldots, \, \mathbf{x}_{,K}^{(\nu)}; \quad \theta, \mathbf{X} \right) \quad (7.4)$$

It can be shown that the requirement that f_{kl}, e, n, and g_k are objective tensors leads to the following functional forms of these constitutive equations (see Eringen [23] p. 349, or Green and Rivlin [45])

$$t_{kl} = j x_{k, \, K} \, x_{l, \, L} \, T_{KL} \left(\theta, \, C_{KL}, \, C_{KL}^{(1)}, \, \ldots, \, C_{KL}^{(\nu)}; \quad \theta, \mathbf{X} \right) \quad (7.5)$$

$$q_k = j x_{k, \, K} \, Q_K \left(\theta, \, C_{KL}, \, C_{KL}^{(1)}, \, \ldots, \, C_{KL}^{(\nu)}; \quad \theta, \mathbf{X} \right) \quad (7.6)$$

$$\epsilon = e \left(\theta, \, C_{KL}, \, C_{KL}^{(1)}, \, \ldots, \, C_{KL}^{(\nu)}; \quad \theta, \mathbf{X} \right) \quad (7.7)$$

$$\eta = n \left(\theta, \, C_{KL}, \, C_{KL}^{(1)}, \, \ldots, \, C_{KL}^{(\nu)}; \quad \theta, \mathbf{X} \right) \quad (7.8)$$

where
$$C_{KL}^{(1)} \equiv \frac{DC_{KL}}{Dt}, \ldots, C_{KL}^{(v)} \equiv \frac{D^v C_{KL}}{Dt^v} \tag{7.9}$$

The substitution of (7.5) to (7.8) into (5.26) leads to

$$-\frac{\rho_0}{\theta}\left(\frac{\partial \psi}{\partial \theta} + \eta\right)\theta + \frac{1}{\theta}\left(\frac{1}{2}T_{KL} - \rho_0\frac{\partial \Psi}{\partial C_{KL}}\right)C_{KL}^{(1)} \tag{7.10}$$

$$-\frac{1}{\theta}\sum_{\beta=1}^{v}\rho_0\frac{\partial \Psi}{\partial C_{KL}^{(\beta)}}C_{KL}^{(\beta+1)} + \frac{1}{\theta^2}Q_L\theta,\; L \geq 0$$

By repetition of the argument used in Section 5 (5.30) one can deduce that (7.5) to (7.8) are equivalent to

$$t_{kl} = 2\rho\frac{\partial \Psi}{\partial C_{KL}}x_{k,\,K}\,x_{l,\,L} + j_DT_{KL}\,x_{k,\,K}\,x_{l,\,L} \tag{7.11}$$

$$Q_K = 0 \tag{7.12}$$

$$\epsilon = \Psi - \theta\frac{\partial \Psi}{\partial \theta} \tag{7.13}$$

$$\eta = -\frac{\partial \Psi}{\partial \theta} \tag{7.14}$$

where Ψ and $_DT$ subject to

$$\frac{\partial \Psi}{\partial C_{KL}^{(v)}} = 0 \tag{7.15}$$

$$_DT_{\,KL}\dot{C}_{KL} - 2\rho_0\sum_{\beta=1}^{v-1}\frac{\partial \Psi}{\partial C_{KL}^{(\beta)}}C_{KL}^{(\beta+1)} \geq 0 \tag{7.16}$$

Here $_DT$ is a function of $\mathbf{C}, \dot{\mathbf{C}}, \ldots, \mathbf{C}^{(v)}, \theta$ and $\mathbf{X}$, i.e.

$$_DT = {}_DT(\mathbf{C}, \dot{\mathbf{C}}, \ldots, \mathbf{C}^{(v)};\; \theta, \mathbf{X}) \tag{7.17}$$

It is quite simple to show that the inequality (7.16) implies that

$$_DT_{KL} = 0$$
$$\frac{\partial \Psi}{\partial C_{KL}^{(\beta)}} = 0 \quad \text{when} \quad C_{KL}^{(1)} = \ldots C_{KL}^{(v)} = 0 \tag{7.18}$$
$$(\beta = 1, \ldots, v)$$

If $_DT_{KL}$ and Ψ are polynomials in the strain rates, (7.18) implies that $_DT_{KL}$ must be at least linear in the strain rates and Ψ has no linear term in the strain rates. This fact is extremely useful in determining approximate theories.

Here we see for the first time that the thermodynamic state function Ψ is rate dependent. This, of course, is strange in light of our previous practice. Nevertheless if we assume that the Clausius–Duhem inequality must be valid for all independent processes and reject the principle of equipresence, then the existence of linear viscoelastic materials will have to be denied.

Since the physical fact of the existence of such materials cannot be denied,

either we accept these axioms as enunciated or else we use the Clausius–Duhem inequality as a restriction on the motion rather than on the material. For a discussion of this point the reader is referred to the appendix.

Due to the nature of the constitutive equations of general strain rate dependent materials, it is extremely difficult to draw any specific conclusions without making some simplifying assumption. In many physical situations, the strains are large and the strain rates are small (for example the creep and relaxation of polymers). In such cases it is justifiable to describe the material by a stress constitutive equation that is linear in the strain rates. In conjunction with the above remarks, the stress and free energy have constitutive equations of the form:

$$\Psi = \Psi^0(\theta, C_{KL}) + \frac{1}{4\rho_0} \sum_{\beta,\gamma=1}^{\nu-1} F_{KL,MN}^{(\beta,\gamma)} C_{KL}^{(\beta)} C_{MN}^{(\gamma)} \tag{7.19}$$

$$_D T_{KL} = \sum_{\beta=1}^{\nu} G_{KL,MN}^{(\beta)} C_{MN}^{(\beta)} \tag{7.20}$$

where $F_{KL,MN}^{(\beta,\gamma)}$ and $G_{KL,MN}^{(\beta)}$ are functions of (θ, C_{KL}) and satisfy

$$F_{KL,MN}^{(\beta,\gamma)} = F_{LK,MN}^{(\beta,\gamma)} = F_{KL,NM}^{(\beta,\gamma)} = F_{MN,KL}^{(\gamma,\beta)}$$

$$G_{KL,MN}^{(\beta)} = G_{LK,MN}^{(\beta)} = G_{KL,NM}^{(\beta)} \tag{7.21}$$

Inequality (7.16) specializes to

$$\sum_{\beta=1}^{\nu} G_{KL,MN}^{(\beta)} C_{KL}^{(1)} C_{MN}^{(\beta)} - \sum_{\beta,\gamma=1}^{\nu-1} F_{KL,MN}^{(\beta,\gamma)} C_{KL}^{(\beta+1)} C_{MN}^{(\gamma)} \geq 0 \tag{7.22}$$

It is possible to deduce that a necessary and sufficient condition that (7.22) is satisfied is that

$$G_{KL,MN}^{(\nu-\beta)} = F_{MN,KL}^{(\nu-\beta-1,1)}$$

$$F_{MN,KL}^{(\nu-\beta-1,\gamma+1)} = 0; \qquad \gamma = \beta+1, \ldots, \nu-\beta-2 \tag{7.23}$$

$$F_{MN,KL}^{(\nu-\beta,\gamma)} = -F_{MN,KL}^{(\nu-\beta-1,\gamma+1)}; \qquad \gamma = 1, \ldots, \beta$$

where $\beta = 0, 1, \ldots, \beta'$ and β' is the largest non-negative integer such that $2\beta' + 1 < \nu$; and the following inequality must hold:

$$\sum_{\beta=1}^{\nu-\beta'-1} G_{KL,MN}^{(\beta)} C_{KL}^{(1)} C_{MN}^{(\beta)} - \sum_{\beta=1}^{\nu-\beta'-2} \sum_{\gamma=1}^{\nu-\beta'-1} F_{KL,MN}^{(\beta,\gamma)} C_{KL}^{(\beta+1)} C_{MN}^{(\gamma)} \geq 0 \tag{7.24}$$

If it is assumed that the material is isotropic, the constitutive equations (7.19–20) reduce to:

$$\Psi = \Psi^0(\theta, I_1, I_2, I_3) + \frac{1}{4\rho} \sum_{\beta=1}^{\nu-1} f_{kl,mn}^{(\beta,\gamma)} A_{kl}^{\beta} A_{mn}^{\gamma}$$

$$_D t_{kl} = \sum_{\beta=1}^{\nu} \delta_{kl,mn}^{(\beta)} A_{mn}^{\beta}$$

$$\tag{7.25}$$

where $f_{kl,mn}^{(\beta,\gamma)}$ and $\delta_{kl,mn}^{(\beta)}$ have the form:

$$
\begin{aligned}
f_{kl,mn}^{(\beta,\gamma)} =\; & a_{\beta,\gamma}^1 \,\delta_{kl}\,\delta_{mn} + a_{\beta,\gamma}^2 \,(\delta_{km}\,\delta_{ln} + \delta_{kn}\,\delta_{lm}) \\
& + a_{\beta,\gamma}^3 \, c_{kl}^{-1}\,\delta_{mn} + a_{\beta,\gamma}^4 \,\delta_{kl}\, c_{mn}^{-1} \\
& + a_{\beta,\gamma}^5 \,(c_{km}^{-1}\,\delta_{ln} + c_{kn}^{-1}\,\delta_{lm} + c_{lm}^{-1}\,\delta_{kn} + c_{ln}^{-1}\,\delta_{km}) \\
& + a_{\beta,\gamma}^6 (c_{kq}^{-1}c_{mq}^{-1}\delta_{ln} + c_{lq}^{-1}c_{mq}^{-1}\delta_{kn} + c_{kq}^{-1}c_{nq}^{-1}\delta_{lm} + c_{lq}^{-1}c_{nq}^{-1}\delta_{km}) \\
& + a_{\beta,\gamma}^7 \, c_{kl}^{-1}c_{mn}^{-1} + a_{\beta,\gamma}^8 \,\delta_{kl}c_{mq}^{-1}c_{qn}^{-1} + a_{\beta,\gamma}^9 \, c_{kq}^{-1}c_{l}^{-1}q\,\delta_{mn} \qquad (7.26)\\
& + a_{\beta,\gamma}^{10} c_{kl}^{-1}c_{mq}^{-1}c_{nq}^{-1} + a_{\beta,\gamma}^{11} c_{kq}^{-1}c_{l}^{-1}q\,c_{mn}^{-1} \\
& + a_{\beta,\gamma}^{12} c_{kq}^{-1}c_{l}^{-1}q\,c_{mp}^{-1}c_{pn}^{-1}
\end{aligned}
$$

where (7.21) implies

$$
\begin{array}{llll}
a_{\beta,\gamma}^1 = a_{\gamma,\beta}^1; & a_{\beta,\gamma}^2 = a_{\gamma,\beta}^2; & a_{\beta,\gamma}^3 = a_{\gamma,\beta}^4 & \\
a_{\beta,\gamma}^5 = a_{\gamma,\beta}^5; & a_{\beta,\gamma}^6 = a_{\gamma,\beta}^6; & a_{\beta,\gamma}^7 = a_{\gamma,\beta}^7 & (7.27)\\
a_{\beta,\gamma}^8 = a_{\gamma,\beta}^9; & a_{\beta,\gamma}^{10} = a_{\gamma,\beta}^{11}; & a_{\beta,\gamma}^{12} = a_{\gamma,\beta}^{12} &
\end{array}
$$

$$
\begin{aligned}
\delta_{kl,mn}^{(\beta)} =\; & \beta_\beta^1 \delta_{kl}\delta_{mn} + \beta_\beta^2(\delta_{km}\delta_{ln} + \delta_{kn}\delta_{lm}) + \beta_\beta^3 c_{kl}^{-1}\delta_{mn} \\
& + \beta_\beta^4 \delta_{kl}c_{mn}^{-1} + \beta_\beta^5(c_{km}^{-1}\delta_{ln} + c_{kn}^{-1}\delta_{lm} + c_{lm}^{-1}\delta_{kn} + c_{ln}^{-1}\delta_{km}) \\
& + \beta_\beta^6(c_{kq}^{-1}c_{mq}^{-1}\delta_{ln} + c_{lq}^{-1}c_{mq}^{-1}\delta_{kn} + c_{kq}^{-1}c_{nq}^{-1}\delta_{lm} + c_{lq}^{-1}c_{nq}^{-1}\delta_{km}) \\
& + \beta_\beta^7 c_{kl}^{-1}c_{mn}^{-1} + \beta_\beta^8 \delta_{kl}c_{mq}^{-1}c_{qn}^{-1} + \beta_\beta^9 c_{kq}^{-1}c_{ql}^{-1}\delta_{mn} \qquad (7.28)\\
& + \beta_\beta^{10} c_{kl}^{-1}c_{mq}^{-1}c_{nq}^{-1} + \beta_\beta^{11} c_{kq}^{-1}c_{lq}^{-1}c_{mn}^{-1} + \beta_\beta^{12} c_{kq}^{-1}c_{lq}^{-1}c_{mp}^{-1}c_{np}^{-1}
\end{aligned}
$$

The scalars $a_{\beta,\gamma}^1, \ldots, a_{\beta,\gamma}^{12}$, and $\beta_\beta^1, \ldots, \beta_\beta^{12}$ are functions of θ, I_1, I_2, I_3.

The tensor A^β can be implicitly defined by

$$
C_{KL}^{(\beta)} = x_{k,K}\, x_{l,L}\, A_{kl}^\beta \qquad (7.29)
$$

An explicit expression for A^β can be derived by a repeated use of (5.13) and (5.18). It is not difficult to show that A^β are objective. (See for example Eringen [23] p. 341).

In terms of $f_{kl,mn}^{(\beta,\gamma)}$ and $\delta_{kl,mn}^{(\beta)}$ the restrictions (7.23) and (7.24) become:

$$
\begin{aligned}
\delta_{kl,mn}^{(\nu-\beta)} &= f_{mn,kl}^{(\nu-\beta-1,1)} \\
f_{mn,kl}^{(\nu-\beta-1,\gamma+1)} &= 0; \qquad \gamma = \beta+1, \ldots, \nu-\beta-2 \qquad (7.30)\\
f_{mn,kl}^{(\nu-\beta,\gamma)} &= -f_{mn,kl}^{(\nu-\beta-1,\gamma+1)}; \qquad \gamma = 1, \ldots, \beta
\end{aligned}
$$

where $\beta = 0, 1, \ldots, \beta'$ and β' is the largest non-negative integer such that $2\beta' + 1 < \nu$

$$
\sum_{\beta=1}^{\nu-\beta'-1} \delta_{kl,mn}^{(\beta)} A_{kl}^1 A_{mn}^\beta - \sum_{\beta=1}^{\nu-\beta'-2} \sum_{\gamma=1}^{\nu-\beta'-1} f_{kl,mn}^{(\beta,\gamma)} A_{kl}^{\beta+1} A_{mn}^\gamma \geq 0 \qquad (7.31)
$$

12

For concreteness we list the results of this analysis for certain lower order rate theories:

Case I: $\nu = 2$

For an anisotropic second order rate theory the free energy and the disipative part of the stress tensor are given by:

$$\Psi = \Psi^0(\theta, C_{KL}) + \frac{1}{4\rho_0} F^{(1,1)}_{KL,MN} C^{(1)}_{KL} C^{(1)}_{MN} \tag{7.32}$$

$$_D T_{KL} = G^{(1)}_{KL,MN} C^{(1)}_{MN} + F^{(1,1)}_{KL,MN} C^{(2)}_{MN} \tag{7.33}$$

where $G^{(1)}_{KL,MN}$ must satisfy the inequality

$$G^{(1)}_{KL,MN} C^{(1)}_{KL} C^{(1)}_{MN} \geq 0 \tag{7.34}$$

To within linear terms in the strain rates, the stress relations are:

$$T_{KL} \approx 2\rho_0 \frac{\partial \Psi^0}{\partial C_{KL}} + _D T_{KL} \tag{7.35}$$

For an isotropic material

$$\Psi = \Psi^0(\theta, I_1, I_2, I_3) + \frac{1}{4\rho} f^{(1,1)}_{kl,mn} A^1_{kl} A^1_{mn} \tag{7.36}$$

$$_D t_{kl} = \delta^{(1)}_{kl,mn} A^1_{mn} + f^{(1,1)}_{kl,mn} A^2_{mn} \tag{7.37}$$

where $\delta^{(1)}_{kl,mn}$ must satisfy the inequality

$$\delta^{(1)}_{kl,mn} A^1_{kl} A^1_{mn} \geq 0$$

The restrictions (7.21) and (7.29) should be noted.

Case II: $\nu = 3$

The free energy and the dissipative stress tensor for an anisotropic material have the form:

$$\Psi = \Psi^0(\theta, C_{KL}) + \frac{1}{4\rho_0} [F^{(1,1)}_{KL,MN} C^{(1)}_{KL} C^{(1)}_{MN} + 2 F^{(1,2)}_{KL,MN} C^{(1)}_{KL} C^{(2)}_{MN}] \tag{7.38}$$

$$_D T_{KL} = G^{(1)}_{KL,MN} C^{(1)}_{MN} + G^{(2)}_{KL,MN} C^{(2)}_{MN} + F^{(1,2)}_{KL,MN} C^{(3)}_{MN} \tag{7.39}$$

where

$$G^{(1)}_{KL,MN} C^{(1)}_{KL} C^{(1)}_{MN} + G^{(2)}_{KL,MN} C^{(1)}_{KL} C^{(2)}_{MN} - F^{(1,1)}_{KL,MN} C^{(2)}_{KL} C^{(1)}_{MN}$$
$$- F^{(1,2)}_{KL,MN} C^{(2)}_{KL} C^{(2)}_{MN} \geq 0 \tag{7.40}$$

For an isotropic material, these reduce to:

$$\Psi = \Psi^0(\theta, I_1, I_2, I_3) + \frac{1}{4\rho} [f^{(1,1)}_{kl,mn} A^1_{kl} A^1_{mn} + 2f^{(1,2)}_{kl,mn} A^1_{kl} A^2_{mn}] \tag{7.41}$$

$$_Dt_{kl} = \delta^{(1)}_{kl,mn} A^1_{mn} + \delta^{(2)}_{kl,mn} A^2_{mn} + f^{(1,2)}_{kl,mn} A^3_{mn} \qquad (7.42)$$

where (7.31) becomes:

$$\delta^{(1)}_{kl,mn} A^1_{kl} A^1_{mn} + \delta^{(2)}_{kl,mn} A^1_{kl} A^2_{mn} - f^{(1,1)}_{kl,mn} A^2_{kl} A^1_{mn}$$
$$- f^{(1,2)}_{kl,mn} A^2_{kl} A^2_{mn} \geq 0 \qquad (7.43)$$

Again restrictions (7.21) and (7.29) should be noted.

Case III: $\nu = 4$

The free energy and dissipative stress tensor assume the form for an aniso-tropic material:

$$\Psi = \Psi^0(\theta, C_{KL}) + \frac{1}{4\rho_0} [F^{(1,1)}_{KL,MN} C^{(1)}_{KL} C^{(1)}_{MN} + 2F^{(1,2)}_{KL,MN} C^{(1)}_{KL} C^{(2)}_{MN}$$
$$- 2F^{(2,2)}_{KL,MN} C^{(3)}_{KL} C^{(1)}_{MN} + F^{(2,2)}_{KL,MN} C^{(2)}_{KL} C^{(2)}_{MN}] \qquad (7.44)$$

$$_DT_{KL} = G^{(1)}_{KL,MN} C^{(1)}_{MN} + G^{(2)}_{KL,MN} C^{(2)}_{MN} + F^{(1,2)}_{KL,MN} C^{(3)}_{MN}$$
$$- F^{(2,2)}_{KL,MN} C^{(4)}_{MN} \qquad (7.45)$$

where the following inequality must hold

$$G^{(1)}_{KL,MN} C^{(1)}_{KL} C^{(1)}_{MN} + G^{(2)}_{KL,MN} C^{(1)}_{KL} C^{(2)}_{MN}$$
$$- F^{(1,1)}_{KL,MN} C^{(2)}_{KL} C^{(1)}_{MN} - F^{(1,2)}_{KL,MN} C^{(2)}_{KL} C^{(2)}_{MN} \geq 0 \qquad (7.46)$$

For an isotropic material these equations become

$$\Psi = \Psi^0(\theta, I_1, I_2, I_3) + \frac{1}{4\rho} [f^{(1,1)}_{kl,mn} A^1_{kl} A^1_{mn} + 2f^{(1,2)}_{kl,mn} A^1_{kl} A^2_{mn}$$
$$- 2f^{(2,2)}_{kl,mn} A^3_{kl} A^1_{mn} + f^{(2,2)}_{kl,mn} A^2_{kl} A^2_{mn}] \qquad (7.47)$$

$$_Dt_{kl} = \delta^{(1)}_{kl,mn} A^1_{mn} + \delta^{(2)}_{kl,mn} A^2_{mn} + f^{(1,2)}_{kl,mn} A^3_{mn} - f^{(2,2)}_{kl,mn} A^4_{mn} \qquad (7.48)$$

and the inequality (7.31) becomes:

$$\delta^{(1)}_{kl,mn} A^1_{kl} A^1_{mn} + \delta^{(2)}_{kl,mn} A^1_{kl} A^2_{mn} - f^{(1,1)}_{kl,mn} A^2_{kl} A^1_{mn} - f^{(1,2)}_{kl,mn} A^2_{kl} A^2_{mn} \geq 0 \qquad (7.49)$$

8. FUNCTIONAL CONSTITUTIVE EQUATIONS

The generalization of the Boltzmann–Volterra hereditary materials to large deformations leads naturally to the concept of functional constitutive equations. The materials described by these theories possess continuous relaxation. The mechanical aspects of such theories have been developed by Green and Rivlin [45, 46], Noll [47], Green, Rivlin and Spencer [48], and Coleman and Noll [37, 38]. The thermodynamics of materials with continuous memory has been treated by Coleman [49, 50]. A presentation of this work up to 1961 is given by Eringen [23], ch. 10. It is impossible to present a general and thorough dis-cussion of the various theories that have functional constitutive equations in an

article of this type. In this section a specialized version of the class of materials classified as "simple materials" will be outlined.

The integral in the linear Boltzmann–Volterra equation (2.7) can be approximated by a linear function of the strain of the material at $(N + 1)$ times τ_K:

$$\tau_N = t > \tau_{N-1}, \ldots, > \tau_0 = 0 \ (N \text{ sufficiently large}).$$

It is also reasonable to assume that the stress depends on the temperature at these $(N + 1)$ times. For large deformations these ideas are generalized by assuming that the stress constitutive equation can be approximated by an arbitrary function of the temperature and the strain at $(N + 1)$ times.

$$t_{kl} = f_{kl} \left[x_{k, R} (\tau_K), \theta (\tau_K) \right], \quad K = 0, \ldots, N \tag{8.1}$$

By letting $N \to \infty$, the constitutive equation (8.1) becomes a functional equation (see Volterra [19], and Green and Rivlin [46]).

$$t_{kl} = \overset{t}{\underset{\tau = 0}{f_{kl}}} \left[\mathbf{x}, _K (\tau), \theta (\tau) \right] \tag{8.2}$$

If it is assumed that the memory functional is of finite duration T,* the invariance of (8.2) under time shift, according to the axiom of objectivity, implies that

$$t_{kl} = \overset{T}{\underset{\tau = 0}{f_{kl}}} \left[\theta(t - \tau), \quad x_{k, K} (t - \tau) \right] \tag{8.3}$$

The requirement that (8.3) be invariant under arbitrary rigid motions implies that (8.3) has the form (see Green and Rivlin [46], and Noll [47])

$$t_{kl} = j x_{k, K} \, x_{l, L} \, \overset{T}{\underset{\tau = 0}{T_{KL}}} \left[C_{KL}(t - \tau), \theta(t - \tau), \mathbf{x} \right] \tag{8.4}$$

By envoking the principle of equipresence, the constitutive equations for the internal energy, the entropy and the heat flux must be functionals of the form (neglecting heat conduction)

$$\epsilon = \overset{T}{\underset{\tau = 0}{\epsilon}} \left[C_{KL}(t - \tau), \theta(t - \tau), \mathbf{x} \right] \tag{8.5}$$

$$\eta = \overset{T}{\underset{\tau = 0}{\eta}} \left[C_{KL}(t - \tau), \theta(t - \tau), \mathbf{x} \right] \tag{8.6}$$

$$q_k = j x_{k, K} \, \overset{T}{\underset{\tau = 0}{Q_K}} \left[C_{KL}(t - \tau), \theta(t - \tau), \mathbf{x} \right] \tag{8.7}$$

The functionals (8.4) to (8.7) must still satisfy the requirement of non-negative entropy production (5.26):

$$\rho_0 \left(\dot{\eta} - \frac{1}{\theta} \dot{\epsilon} \right) + \frac{1}{2} \frac{T_{KL} \dot{C}_{KL}}{\theta} + \frac{1}{\theta^2} Q_K \theta, _K \geq 0 \tag{8.8}$$

---

* A more general assumption is that of fading memory introduced by Coleman and Noll [37, 38].

Within the present theory, it is obvious that (8.8) implies that

$$Q_K = 0 \tag{8.9}$$

With the proper smoothness conditions on the functionals (8.4) and (8.7) it is possible to deduce necessary and sufficient conditions for the satisfaction of (8.8) (see Coleman [49]). Such results require the concept of functional differentiation which is a little too technical for presentation here. We will by-pass this by making a few more assumptions. It is convenient to rewrite (8.4) and (8.7) in terms of difference histories:

$$t_{kl} = j x_{k, K} \, x_{l, L} \, T_{KL} \, [\overset{T}{\underset{\tau=0}{\tilde{C}^t_{KL}}}(\tau), \, \tilde{\theta}^t(\tau); \, C_{KL}(t), \, \theta(t)] \tag{8.10}$$

$$\epsilon = e \, [\overset{T}{\underset{\tau=0}{\tilde{C}^t_{KL}}}(\tau), \, \tilde{\theta}^t(\tau); C_{KL}(t), \, \theta(t)] \tag{8.11}$$

$$\eta = n \, [\overset{T}{\underset{\tau=0}{\tilde{C}^t_{KL}}}(\tau), \, \tilde{\theta}^t(\tau); C_{KL}(t), \, \theta(t)] \tag{8.12}$$

where

$$\begin{aligned} \tilde{\theta}^t(\tau) &\equiv \theta(t - \tau) - \theta(t) \\ \tilde{C}^t_{KL}(\tau) &\equiv C_{KL}(t - \tau) - C_{KL}(t) \end{aligned} \tag{8.13}$$

For simplicity, we assume that (8.10) to (8.12) possess no memory of the temperature. (There is no difficulty in relaxing this assumption. See Coleman [49].) Thus we assume (8.10) to (8.12) reduce to:

$$t_{kl} = j x_{k, K} \, x_{l, L} \, T_{KL} \, [\overset{T}{\underset{\tau=0}{\tilde{C}^t_{KL}}}(\tau); C_{KL}(t), \, \theta(t)] \tag{8.14}$$

$$\epsilon = e \, [\overset{T}{\underset{\tau=0}{\tilde{C}^t_{KL}}}(\tau); C_{KL}(t), \, \theta(t)] \tag{8.15}$$

$$\eta = n \, [\overset{T}{\underset{\tau=0}{\tilde{C}^t_{KL}}}(\tau); C_{KL}(t), \, \theta(t)] \tag{8.16}$$

From (8.14) to (8.16) and (8.8), it is easily deduced that (as in the previous sections):

$$\eta = - \frac{\partial \Psi}{\partial \theta} \tag{8.17}$$

$$\Psi = \epsilon - \eta \theta$$

Under the proper smoothness conditions the response functionals can be expanded in a "power" series (see Green and Rivlin [46] and Coleman and Noll [38]). In particular, a second order approximation to the free energy is:

$$\begin{aligned} \Psi = \Psi^0 \, [\theta(t), \, C_{KL}(t)] &+ \int_0^T F_{KL}(s) \, \tilde{C}_{KL}(s) \, ds \\ &+ \int_0^T \int_0^T F_{KL, \, MN}(s_1, s_2) \, \tilde{C}^t_{KL}(s_1) \, \tilde{C}^t_{MN}(s_2) \, ds_1 \, ds_2 \end{aligned} \tag{8.18}$$

$$F_{KL}(s) = F_{LK}(s)$$

$$F_{KL,\ MN}(s_1, s_2) = F_{MN,\ KL}(s_2, s_1) \tag{8.19}$$

$$F_{KL,\ MN}(s_1, s_2) = F_{LK,\ MN}(s_1, s_2) = F_{KL,\ NM}(s_1, s_2)$$

The approximation (8.18) is the generalization of the linear rate theories presented in Section 7 to the case of continuous memory. In general Ψ^0, $F_{KL}(s)$ and $F_{KL,\ MN}(s_1, s_2)$ are nonlinear functions of $\theta(t)$, $C_{KL}(t)$. For the following presentation we shall treat (8.18) as exact. It is simple to prove that

$$
\dot{\Psi} = \frac{\partial \Psi}{\partial \theta}\, \dot{\theta} + \left\{ \frac{\partial \Psi}{\partial C_{KL}} - \int_0^T F_{KL}(s)\, ds - 2 \int_0^T \int_0^T F_{KL,\ MN}(s_2, s_1)\, ds_2\, \tilde{C}^t_{MN}(s_1)\, ds_1 \right\} \dot{C}_{KL}
$$

$$
- \int_0^T F_{KL}(s)\, \frac{d}{ds} C_{KL}(t - s)\, ds \tag{8.20}
$$

$$
- 2 \int_0^T \int_0^T F_{KL,\ MN}(s_1, s_2)\, \tilde{C}^t_{KL}(s_1)\, \frac{d}{ds_2} C_{MN}(t - s_2)\, ds_1\, ds_2
$$

Substituting (8.20) into (8.8), using (8.9) and (8.13), one obtains:

$$
\frac{1}{2} \left\{ T_{KL} - 2\rho_0 \frac{\partial \Psi}{\partial C_{KL}} + 2\rho_0 \int_0^T F_{KL}(s)\, ds \right.
$$

$$
\left. - 4\rho_0 \int_0^T \int_0^T F_{KL,\ MN}(s_2, s_1)\, ds_2\, \tilde{C}^t_{MN}(s_1)\, ds_1 \right\} \dot{C}_{KL} \tag{8.21}
$$

$$
+ \rho_0 \int_0^T F_{KL}(s)\, \frac{d}{ds} C_{KL}(t - s)\, ds
$$

$$
+ 2\rho_0 \int_0^T \int_0^T F_{KL,\ MN}(s_1, s_2)\, \tilde{C}_{KL}(s_1)\, \frac{d}{ds_2} C_{MN}(t - s_2)\, ds_1\, ds_2 \geq 0
$$

It can be shown that necessary and sufficient conditions* for (8.21) to be valid for all independent processes are that

$$
T_{KL} = 2\rho_0 \frac{\partial \Psi}{\partial C_{KL}} - 2\rho_0 \int_0^T F_{KL}(s)\, ds - 4\rho_0 \int_0^T \int_0^T F_{KL,\ MN}(s_1, s_2)\, \tilde{C}^t_{MN}(s_1)\, ds_1\, ds_2
$$

and $\tag{8.22}$

$$
\int_0^T F_{KL}(s)\, \frac{d}{ds} C_{KL}(t - s)\, ds
$$

$$
+ 2 \int_0^T \int_0^T F_{KL,\ MN}(s_1\, s_2)\, \tilde{C}_{KL}(s_1)\, \frac{d}{ds_2} C_{MN}(t - s_2)\, ds_1\, ds_2 \geq 0 \tag{8.23}
$$

* It can be shown that for any history $C_{KL}(\tau)$, there exists a sufficiently near history $C_{KL}(\tau)$ such that $\dot{C}_{KL}(t)$ is arbitrary. See Coleman [49].

The inequality (8.23) implies that

$$F_{KL}(s) = 0 \tag{8.24}$$

and

$$\int_0^T \int_0^T \phi_{KL,\,MN}(s_1, s_2)\, \dot{C}_{KL}^t(s_1)\, \dot{C}_{MN}^t(s_2)\, ds_1\, ds_2 \geq 0 \tag{8.25}$$

where we have used $(8.13)_2$ and the definitions:

$$\phi_{KL,\,MN}(s_1, s_2) = \int_{s_1}^T F_{KL,\,MN}(s_3, s_2)\, ds_3 \tag{8.26}$$

$$\dot{C}_{MN}^t(s) \equiv \frac{d}{d\tau}\, C_{MN}(\tau)\, \Big|_{\tau = t - s} \tag{8.27}$$

If one introduces the notations

$$\phi_{KL,\,MN}(s) = \phi_{KL,\,MN}(0, s) \tag{8.28}$$

$$\Psi_{KL,\,MN}(s) = \int_s^T \phi_{KL,\,MN}(s_1)\, ds_1 \tag{8.29}$$

the constitutive equations for the stress become

$$T_{KL} = 2\rho_0 \frac{\partial \Psi}{\partial C_{KL}} + 4\rho_0 \int_0^T \Psi_{KL,\,MN}(s)\, \dot{C}_{MN}^t(s)\, ds \tag{8.30}$$

For practical purposes, (8.30) can be approximated by (for slow motions)

$$T_{KL} \approx 2\rho_0 \frac{\partial \Psi^0}{\partial C_{KL}} + 4\rho_0 \int_0^T \Psi_{KL,\,MN}(s)\, \dot{C}_{MN}^t(s)\, ds \tag{8.31}$$

and $(8.17)_1$ by

$$\eta \approx -\frac{\partial \Psi^0}{\partial \theta} \tag{8.32}$$

9. THERMAL PHENOMENA IN VISCOELASTIC MATERIALS

In the previous sections the thermal effects such as heat conduction have been neglected in the formulation of visco-elastic materials. For either slow deformations and motions or in very short rapid motions of materials the heat conduction can be neglected on the ground that in the former temperature rise too slowly while in the latter there is no time for the heat conduction to take place. The effect of heat conduction cannot be ignored for the intermediary cases where appreciable thermal changes occur during the motion. Without the inclusion of the temperature gradient into constitutive equations we have seen that heat conduction is not permissible on the grounds of the second law of

thermodynamics even though the material constants are affected by the local temperature.

Heat conduction phenomena, classically, has been treated by use of the Fourier's law

$$q_k = K\theta, _k \qquad (9.1)$$

Nevertheless for rapid temperature changes and motions, (9.1) is no longer adequate; and new equations must be found to replace it. Inclusion of the temperature gradient into constitutive equations is in fact adequate as a starting point for the development of theory of thermo-viscoelasticity. In fact, no other new principles are needed for such a theory. However, in the application of the axioms of constitutive theory and the Clausius–Duhem inequality, care must be exercised. A theory including various order rates of deformation gradients and temperature gradients is highly complicated. Foundations of thermomechanical materials including spatial and time histories of deformation and temperature were recently laid down by Eringen [35]. Various parts of this work in simpler form will be reproduced below. For simplicity we begin our work with a Kelvin–Voigt material. Afterwards we give a more general theory including higher order time rates of the strain tensor. The last article is devoted to materials having functional constitutive equations, a generalization of the Boltzmann–Volterra theory of linear isothermal viscoelasticity.

10. THERMOELASTIC KELVIN–VOIGT SOLIDS

The inclusion of the effect of heat conduction in the theory of Kelvin–Voigt materials was first made by Koh and Eringen [39]. Coleman and Mizel [40] subsequently treated the same problem.* According to the principle of equipresence, it is assumed that the constitutive equations have the form†

$$t_{kl} = f_{kl} (\mathbf{x}, _K, \dot{\mathbf{x}}, _K, \theta, _k; \quad \theta, \mathbf{X}) \qquad (10.1)$$

$$q_k = g_k(\mathbf{x}, _K, \dot{\mathbf{x}}, _K, \theta, _k; \quad \theta, \mathbf{X}) \qquad (10.2)$$

$$\epsilon = e (\mathbf{x}, _K, \dot{\mathbf{x}}, _K, \theta, _k; \quad \theta, \mathbf{X}) \qquad (10.3)$$

$$\eta = n (\mathbf{x}, _K, \dot{\mathbf{x}}, _K, \theta, _k; \quad \theta, \mathbf{X}) \qquad (10.4)$$

The axiom of objectivity can be shown to lead to

$$t_{kl} = jT_{KL} (\mathbf{C}, \dot{\mathbf{C}}, \theta, _K; \quad \theta, \mathbf{X}) x_{k}, _K x_{l}, _L \qquad (10.5)$$

$$q_k = jQ_K (\mathbf{C}, \dot{\mathbf{C}}, \theta, _K; \quad \theta, \mathbf{X}) x_{k}, _K \qquad (10.6)$$

$$\epsilon = E (\mathbf{C}, \dot{\mathbf{C}}, \theta, _K; \quad \theta, \mathbf{X}) \qquad (10.7)$$

$$\eta = N (\mathbf{C}, \dot{\mathbf{C}}, \theta, _K; \quad \theta, \mathbf{X}) \qquad (10.8)$$

---

* Koh and Eringen assumed that the stress $\mathbf{t}$ and heat $\mathbf{q}$ are functions of $\mathbf{x}, _K$, $\dot{\mathbf{x}}, _K$, $\theta, _k$ and θ. They considered internal energy ϵ and entropy η as functions of $\mathbf{x}, _K$ and θ only. This was their interpretation of the principle of equipresence. Coleman and Mizel consider ϵ and η also being dependent on the same variable as the stress. For the present theory, as we shall see below (eqns. 10.10), Koh–Eringen hypothesis turns out to be the case.

† For the origin of such equations see Eringen [35].

Upon substituting these expressions into (5.27) we obtain

$$-\frac{\rho_0}{\theta}\left(\frac{\partial\Psi}{\partial\theta}+\eta\right)\dot\theta+\frac{1}{2\theta}\left(T_{KL}-2\rho_0\frac{\partial\Psi}{\partial C_{KL}}\right)\dot C_{KL}$$
$$-\frac{\rho_0}{\theta}\frac{\partial\Psi}{\partial\dot C_{KL}}\ddot C_{KL}-\frac{\rho_0}{\theta}\frac{\partial\Psi}{\partial\theta,_K}\dot\theta,_K+\frac{1}{\theta^2}Q_K\theta,_K\geq0 \tag{10.9}$$

This inequality is to be satisfied for all independent variations of $\dot\theta$, $\dot C$, C, $\dot\theta,_K$. Since it is linear in $\dot\theta$, $\ddot C$ and $\dot\theta,_K$, we immediately see that this is possible if and only if

$$\eta=-\frac{\partial\Psi}{\partial\theta}$$

$$\frac{\partial\Psi}{\partial\dot C_{KL}}=0 \tag{10.10}$$

$$\frac{\partial\Psi}{\partial\theta,_K}=0$$

and

$$\frac{1}{2\theta}\left(T_{KL}-2\rho_0\frac{\partial\Psi}{\partial C_{KL}}\right)\dot C_{KL}+\frac{1}{\theta_2}Q_K\theta,_K\geq0 \tag{10.11}$$

Hence we proved that

$$\Psi=\Psi(\mathbf{C};\quad\theta,\mathbf{X}) \tag{10.12}$$

Next (10.11) suggests that we decompose T_{KL} into two parts as

$$T_{KL}=T_{KL}(\mathbf{C},\theta,\mathbf{X})+{}_DT_{KL}(\mathbf{C},\dot{\mathbf{C}},\theta,\mathbf{X}) \tag{10.13}$$

It then follows from (10.11) that

$${}_ET_{KL}=2\rho_0\frac{\partial\Psi}{\partial C_{MN}} \tag{10.14}$$

$$\frac{1}{2\theta}{}_DT_{KL}\dot C_{KL}+\frac{1}{\theta^2}Q_K\theta,_K\geq0 \tag{10.15}$$

This last inequality, on account of continuity conditions on ${}_DT$ and $\mathbf{Q}_K$, implies that

$${}_DT_{KL}(\mathbf{C},0,0;\quad\theta,\mathbf{X})=0 \tag{10.16}$$

$$Q_K(\mathbf{C},0,0;\quad\theta,\mathbf{X})=0 \tag{10.17}$$

Collecting the results, we have found that the constitutive equations (10.5) to (10.8) are reducible to

$$t_{kl}=2\rho\frac{\partial\Psi}{\partial C_{KL}}x_{k,K}x_{l,L}+j{}_DT_{KL}x_{k,K}x_{l,L} \tag{10.18}$$

$$q_k=jQ_Kx_{k,K} \tag{10.19}$$

$$\epsilon=\Psi-\theta\frac{\partial\Psi}{\partial\theta} \tag{10.20}$$

$$\eta = -\frac{\partial \Psi}{\partial \theta} \tag{10.21}$$

where $\Psi = \Psi(\mathbf{C}; \quad \theta, \mathbf{X})$ and $_D T(\mathbf{C}, \dot{\mathbf{C}}, \theta, _K; \quad \theta, \mathbf{X})$ and $Q_K(\mathbf{C}, \dot{\mathbf{C}}, \theta, _K; \quad \theta, \mathbf{X})$ are subject to

$$\frac{1}{2\theta} \, _D T_{KL} \, \dot{C}_{KL} + \frac{1}{\theta^2} Q_K \, \theta, _K \geq 0 \tag{10.22}$$

$$_D T_{KL} (\mathbf{C}, 0, 0; \quad \theta, \mathbf{X}) = 0 \tag{10.23}$$

$$Q_K (\mathbf{C}, 0, 0; \quad \theta, \mathbf{X}) = 0 \tag{10.24}$$

The last two expressions are, of course, contained in (10.22).

There is no difficulty in applying material symmetry restrictions to (10.18) and (10.21); however, such expressions become extremely long. In many situations the strain rates and temperature gradients are small even though the strains are large. In this case it is reasonable to approximate $_D\mathbf{T}$ and $\mathbf{Q}$ by equations that are linear in $\dot{C}_{KL}$ and $\theta, _K$. That is:

$$_D T_{KL} = G_{KLMN} \, \dot{C}_{MN} + H_{KLM} \, \theta, _M \tag{10.25}$$

$$Q_K = K_{KL} \, \theta, _L + J_{KLM} \, \dot{C}_{LM} \tag{10.26}$$

where G_{KLMN}, H_{KLM}, K_{KL} and J_{KLM} are functions of θ, C_{KL}.

For homogeneous materials the dependence on $\mathbf{X}$ disappears. For isotropic materials further simplifications occur. In this case the constitutive equations take the form

$$t_{kl} = a_0 \, \delta_{kl} + a_1 \, c^{-1}_{kl} + a_2 \, c^{-1}_{km} \, c^{-1}_{ml} + \beta_{klmn} \, d_{mn} \tag{10.27}$$

$$q_k = (\kappa_0 \delta_{kl} + \kappa_1 c^{-1}_{kl} + \kappa_2 \, c^{-1}_{km} \, c^{-1}_{ml}) \, \theta, _l \tag{10.28}$$

where $a_0, a_1, a_2, \kappa_0, \kappa_1, \kappa_2$ are functions of the invariants I_1, I_2, I_3 of c^{-1} and β_{klmn} have the form (7.28).

Large strains but small deformation rates, equations (10.27) and (10.28), should give an adequate basis for the isotropic thermoviscoelastic materials. The first three terms in (10.27) are due to purely elastic deformations and the term containing $\mathbf{d}$ is due to flow and dissipation of energy. Heat conduction equation (10.28) generalizes that of Fourier (9.1) for the deforming solid. For small thermal gradients again an adequate basis for the heat conduction is established.

11. HIGHER ORDER RATE DEPENDENT THERMAL MATERIALS

The pattern set in Section 10 for the treatment of thermo-elastic materials of Kelvin–Voigt type is valid for materials whose behavior is influenced by the higher order time rates of the deformation gradients. Excluding the possible dependence on the higher order time rates of the temperature gradients [35], we

begin our treatment with the constitutive equations of the form

$$t_{kl} = f_{kl}(\mathbf{x}, {}_K, \dot{\mathbf{x}}, {}_K, \ldots, \mathbf{x}^{(v)}_{,K}, \theta, {}_k; \quad \theta, \mathbf{X}) \tag{11.1}$$

$$q_k = g_k(\mathbf{x}, {}_K, \dot{\mathbf{x}}, {}_K, \ldots, \mathbf{x}^{(v)}_{,K}, \theta, {}_k; \quad \theta, \mathbf{X}) \tag{11.2}$$

$$\epsilon = e(\mathbf{x}, {}_K, \dot{\mathbf{x}}, {}_K, \ldots, \mathbf{x}^{(v)}_{,K}, \theta, {}_k; \quad \theta, \mathbf{X}) \tag{11.3}$$

$$\eta = n(\mathbf{x}, {}_K, \dot{\mathbf{x}}, {}_K, \ldots, \mathbf{x}^{(v)}_{,K}, \theta, {}_k; \quad \theta, \mathbf{X}) \tag{11.4}$$

The axiom of objectivity requires that these equations have the objective forms ([35, eq. 3.14]).

$$t_{kl} = j T_{KL}(\mathbf{C}, \dot{\mathbf{C}}, \ldots, \mathbf{C}^{(v)}, \theta_{,K}; \quad \theta, \mathbf{X}) x_{k, K} x_{l, L} \tag{11.5}$$

$$q_k = j Q_K(\mathbf{C}, \dot{\mathbf{C}}, \ldots, \mathbf{C}^{(v)}, \theta, {}_K; \quad \theta, \mathbf{X}) x_{k, K} \tag{11.6}$$

$$\epsilon = E(\mathbf{C}, \dot{\mathbf{C}}, \ldots, \mathbf{C}^{(v)}, \theta, {}_K; \quad \theta, \mathbf{X}) \tag{11.7}$$

$$\eta = N(\mathbf{C}, \dot{\mathbf{C}}, \ldots, \mathbf{C}^{(v)}, \theta, {}_K; \quad \theta, \mathbf{X}) \tag{11.8}$$

The Clausius–Duhem inequality requires that

$$-\frac{\rho_0}{\theta}\left(\frac{\partial \Psi}{\partial \theta} + \eta\right)\theta + \frac{1}{2\theta}\left(T_{KL} - 2\rho_0 \frac{\partial \Psi}{\partial C_{KL}}\right)\dot{C}_{KL}$$
$$-\frac{\rho_0}{\theta}\sum_{\beta=1}^{v}\frac{\partial \Psi}{\partial C^{(\beta)}_{KL}}C^{(\beta+1)}_{KL} - \frac{\rho_0}{\theta}\frac{\partial \Psi}{\partial \theta, {}_K}\theta, {}_K + \frac{1}{\theta^2}Q_K\theta, {}_K \geq 0 \tag{11.9}$$

for all independent processes. It can be shown that (11.9) implies that the free energy Ψ must be of the form

$$\Psi = \Psi(\mathbf{C}, \dot{\mathbf{C}}, \ldots, \mathbf{C}^{(v-1)}; \quad \theta, \mathbf{X}) \tag{11.10}$$

and the following inequality hold

$$\frac{1}{2\theta}{}_DT_{KL}\dot{C}_{KL} - \frac{\rho_0}{\theta}\sum_{\beta=1}^{v-1}\frac{\partial \Psi}{\partial C^{(\beta)}_{KL}}C^{(\beta+1)}_{KL} + \frac{1}{\theta^2}Q_K\theta, {}_K \geq 0 \tag{11.11}$$

where

$$_DT_{KL} = T_{KL} - 2\rho_0\frac{\partial \Psi}{\partial C_{KL}} \tag{11.12}$$

If one assumes that only the linear terms in rates and thermal gradient are important, $_DT$ and $\mathbf{Q}$ will have the forms

$$_DT_{KL} = \sum_{\beta=1}^{v}{}_\beta G_{KLMN}C^{(\beta)}_{MN} + H_{KLM}\theta, {}_M \tag{11.13}$$

$$Q_K = K_{KL}\theta, {}_L + \sum_{\beta=1}^{v}{}_\beta J_{KMN}C^{(\beta)}_{MN} \tag{11.14}$$

and Ψ has the form (7.19).

The conclusions arrived at in Section 7 still hold. In addition (11.11) implies that

$$_\beta J_{KMN} = 0, \quad \beta = v - \beta', \ldots, v \tag{11.15}$$

For an isotropic solid it can be shown that

$$t_{kl} = a_0 \, \delta_{kl} + a_1 \, c^{-1}_{\ kl} + a_2 \, c^{-1}_{\ km} \, c^{-1}_{\ ml} + \sum_{\kappa}^{\nu} \beta^{(\kappa)}_{klmn} \, A^{(\kappa)}_{mn} \qquad (11.16)$$

$$q_k = (\kappa_0 \, \delta_{kl} + \kappa_1 \, c^{-1}_{\ kl} + \kappa_2 \, c^{-1}_{\ km} \, c^{-1}_{\ ml}) \, \theta,_l \qquad (11.17)$$

where a_λ, κ_λ and $\beta^{(\kappa)}_{klmn}$ are functions of the invariants of c^{-1}.

The materials characterized by (11.16) and (11.17) are homogeneous, isotropic and linearly dependent on the rates of the deformation rate tensor. The only difference from Kelvin–Voigt solid here is the presence of higher order rates $A^{(\kappa)}$, $\kappa > 1$.

12. FUNCTIONAL THEORY OF THERMO-VISCOELASTICITY

In the Boltzmann–Volterra theory of linear viscoelasticity the stress is dependent linearly on the history of strain (eqn. 2.7) For a nonlinear theory that includes the deformation as well as temperature histories the constitutive equations must be expressed as functionals on the deformation and temperature histories. A general theory of this type was given by Eringen [35]. For simple materials the theory begins with constitutive equations of the form

$$t_{kl} = f_{kl} \, [\mathbf{x}, \kappa \, (t - \tau), \theta, \kappa \, (t - \tau), \theta \, (t - \tau); \quad \theta, \mathbf{X}] \qquad (12.1)$$

$$q_k = g_k \, [\mathbf{x}, \kappa \, (t - \tau), \theta, \kappa \, (t - \tau), \theta \, (t - \tau); \quad \theta, \mathbf{X}] \qquad (12.2)$$

$$\epsilon = e \, [\mathbf{x}, \kappa \, (t - \tau), \theta, \kappa \, (t - \tau), \theta \, (t - \tau); \quad \theta, \mathbf{X}] \qquad (12.3)$$

$$\eta = n \, [\mathbf{x}, \kappa \, (t - \tau), \theta, \kappa \, (t - \tau), \theta \, (t - \tau); \quad \theta, \mathbf{X}] \qquad (12.4)$$

where f_{kl}, g_k, e and n are functionals of the deformation, temperature gradient and temperature histories in the range of times $\tau = 0$ to $\tau = T$ prior to the present time t, and functions of temperature θ and material point $\mathbf{X}$. For the homogeneous materials, of course, the dependence on $\mathbf{X}$ disappears. According to this theory the stress, heat, energy and entropy at time t and material point $\mathbf{X}$ is fully determined by the history of deformation gradients, temperature gradients and temperature. The time range T is an indication how far past must be considered. Clearly for most materials histories into the distant past do not affect the present situations. This is known as the *axiom of fading memory* or *axiom of heredity*. This situation is usually taken care of by using exponentially decaying kernel functions in the kernel of the Boltzmann–Volterra theory. The principle was known to Boltzmann [5], Volterra [19, 33] and Straneo [36]. The nonlinear form of a fading memory hypothesis was recently introduced by Coleman and Noll [37]. A discussion and generalization of this hypothesis is given by Eringen [35]. Since the concept of fading memory basically is a smoothness hypothesis on the constitutive functionals and involves much detailed technicality, we omit a discussion of it here. The reader should consult the above references in this regard.

The axiom of objectivity applied to (12.1) to (12.4) shows that these equations are reducible to the following forms:

$$t_{kl} = jT_{KL} [\mathbf{C}(t-\tau), \theta, \kappa(t-\tau), \theta(t-\tau); \quad \theta, \mathbf{X}] x_{k,K} x_{l,L} \quad (12.5)$$

$$q_k = jQ_K [\mathbf{C}(t-\tau), \theta_{,K}(t-\tau), \theta(t-\tau); \quad \theta, \mathbf{X}] x_{k,K} \quad (12.6)$$

$$\epsilon = E[\mathbf{C}(t-\tau), \theta, \kappa(t-\tau), \theta(t-\tau); \quad \theta, \mathbf{X}] \quad (12.7)$$

$$\eta = N[\mathbf{C}(t-\tau), \theta, \kappa(t-\tau), \theta(t-\tau); \quad \theta, \mathbf{X}] \quad (12.8)$$

In this generality the theory of heat conduction in a material with continuous memory has not been fully developed. Eringen [51] has developed a linear theory within the framework of irreversible processes. A general scheme for the non-linear theory is included in Eringen [35]. However, the thermodynamic treatment has not been fully carried out for the general case. Coleman [49, 50] has treated a theory in which the material has no memory of the temperature gradient, i.e.

$$t_{kl} = jT_{KL} [\mathbf{C}(t-\tau), \theta(t-\tau); \quad \theta, \kappa] x_{k,K} x_{l,L} \quad (12.9)$$

$$q_k = jQ_K [\mathbf{C}(t-\tau), \theta(t-\tau); \quad \theta, \kappa] x_{k,K} \quad (12.10)$$

$$\epsilon = E[\mathbf{C}(t-\tau), \theta(t-\tau); \quad \theta, \kappa] \quad (12.11)$$

$$\eta = N[\mathbf{C}(t-\tau), \theta(t-\tau); \quad \theta, \kappa] \quad (12.12)$$

In this special case the second law of thermodynamics leads to the conclusions that t, ϵ and η are independent of θ, κ. The conclusions arrived at in Section 8 for the material with linear memory for t, ϵ, η and Ψ remain valid under the assumptions made in that section. To a first order approximation the heat flux becomes

$$Q_K = \kappa_{KL}\, \theta,_L + \int_0^T M_{KLM}(s)\, \tilde{C}^t_{LM}(s)\, ds \quad (12.13)$$

or equivalently

$$Q_K = \kappa_{KL}\, \theta,_L + \int_0^T N_{KLM}(s)\, \dot{C}^t_{LM}(s)\, ds \quad (12.14)$$

where

$$N_{KLM} = \int_0^s M_{KLM}(\tau)\, d\tau \quad (12.15)$$

The inequality (8.25) is now replaced by

$$\rho_0 \int_0^T \int_0^T \phi_{KLMN}(s_1, s_2)\, \dot{C}^t_{KL}(s_1)\, \dot{C}^t_{MN}(s_2)\, ds_1\, ds_2$$

$$+ \frac{1}{\theta} \kappa_{KL}\, \theta,_K\, \theta,_L + \frac{1}{\theta} \int_0^T N_{KLM}\, \dot{C}^t_{LM}(s)\, \theta,_K(t)\, ds \quad (12.16)$$

13. APPROXIMATE FORMULAE
FOR ENGINEERING APPLICATION

The theories of viscoelasticity presented in the previous sections have one common feature—they describe materials by constitutive relations which are lengthy and involved. The application of these theories to practical engineering problems entails the solution of complicated nonlinear boundary value problems. Excluding some special simple problems (mostly one-dimensional) an exact solution to the field equations is impossible. Fortunately for a great variety of practical situations, an approximation is often more than adequate. There are several schemes, depending on the order of magnitude of the strains, rotations, or strain rates, for producing approximate equations. It is not our intention to dwell on the distinctions between these schemes. A brief indication of the technique should suffice.

The solution to any physical problem in continuum mechanics requires the solving of a system of equations which consists of balance and constitutive equations under some boundary and initial conditions. These and various approximations to them are discussed in the following subsections.

In the formulation of boundary value problems in nonlinear continuum mechanics, both the Eulerian and the Lagrangian descriptions find important uses. The Eulerian description has the intrinsic difficulty that the location of the boundary surface is part of the problem. Since a boundary is by definition a material surface, it is a fixed surface in the Lagrangian description. Hence, the Lagrangian description often produces simpler expressions for the boundary conditions than the Eulerian one. However, the differential equations in the latter case are more complicated. In the following subsections both the Eulerian and the Lagrangian forms of the balance equations, boundary conditions, kinematical relations, and constitutive equations are presented.

A. *Balance Equations*

The Eulerian form of the system of balance equations was listed in Section 3, equations (3.3) to (3.6). The Lagrangian description can be derived from these (see [23] or [52] for the details).

Eulerian Description

Balance of mass:

$$\dot{\rho} + \rho\, v_{k,k} = 0 \tag{13.1}$$

Balance of momentum:

$$t_{kl,k} + \rho(f_l - a_l) = 0 \tag{13.2}$$

Balance of moment of momentum:

$$t_{kl} = t_{lk} \tag{13.3}$$

Balance of energy:

$$\rho \dot{\epsilon} = t_{kl} v_{l,k} + q_{k,k} + \rho h \qquad (13.4)$$

Lagrangian Description

Balance of mass:

$$\rho = \rho_0 j \qquad (13.5)$$

Balance of momentum

$$(T_{KL} x_{l,L})_{,K} + \rho_0(f_l - a_l) = 0 \qquad (13.6)$$

Balance of moment of momentum:

$$T_{KL} = T_{LK} \qquad (13.7)$$

Balance of energy

$$\rho_0 \dot{\epsilon} = \tfrac{1}{2} T_{KL} \dot{C}_{KL} + Q_{K,K} + \rho_0 h \qquad (13.8)$$

where

$$j \equiv \det X_{K,k} \qquad (13.9)$$

$$t_{kl} = j T_{KL} x_{k,K} x_{l,L} \qquad (13.10)$$

$$q_k = j x_{k,K} Q_K \qquad (13.11)$$

and ρ_0 is the density of the material in the undeformed state.

B. *Boundary Conditions*

A brief discussion of the type of boundary conditions which can occur in various situations was presented at the end of Section 3. Various combinations which prescribe the temperature or heat flux and the displacement or stress on portions of the boundary are typical. Here we shall only discuss briefly the form of the stress and heat flux boundary conditions.

Eulerian Description

The stress and heat flux are prescribed on the boundary surface, $\mathscr{S}$, with equation $s(\mathbf{x}, t) = 0$, by

$$t_{lk} n_l = t_{(n)k} \qquad \text{on } \mathscr{S} \qquad (13.12)$$

$$q_k n_k = q_{(n)} \qquad \text{on } \mathscr{S} \qquad (13.13)$$

where n_k is the exterior normal to $\mathscr{S}$ and where $t_{(n)k}$ and $q_{(n)}$ are respectively the surface traction and normal component of the surface heat vector. Note that the equation for the boundary surface is determined in this case from the requirements that $\mathscr{S}$ be a material surface and at $t = 0$ that it coincide with the initial boundary of the body, $b(\mathbf{x}) = 0$. That is

$$\frac{\partial s}{\partial t} + s_{,k} v^k = 0 \qquad (13.14)$$

$$s(\mathbf{x}, 0) = b(\mathbf{x}) \tag{13.15}$$

Lagrangian Description

In the Lagrangian description the surface of the body remains fixed. The stress and heat flux are respectively prescribed by:

$$T_{KL}N_K x_{l,L} = t_{(n)l} \frac{\sqrt{C^{-1}_{KL}N_K N_L}}{j} \tag{13.16}$$

$$Q_K N_K = q_{(n)} \frac{\sqrt{C^{-1}_{KL}N_K N_L}}{j} \tag{13.17}$$

where N_K is the exterior normal to the surface $b(\mathbf{x}) = 0$. The factor on the right side of (13.16) and (13.17) is due to the area change caused by the deformation.

C. *Kinematical Relations*

The necessary kinematical relations for the solution of a boundary value problem are the relations between the various strain tensors and the displacement vector and the relations for the velocity and acceleration in terms of the displacement.

Eulerian Description

The Eulerian strain tensor is defined by

$$2e_{kl} = \delta_{kl} - c_{kl} \tag{13.18}$$

where

$$c_{kl} = \delta_{KL} X_{K,k} X_{L,l} \tag{13.19}$$

In terms of the Eulerian components of the displacement vector, $\mathbf{u}$, e_{kl} can be expressed by

$$2e_{kl} = u_{k,l} + u_{l,k} - u_{m,k} u_{m,l} \tag{13.20}$$

The velocity v_l is defined by

$$v_l = \frac{\partial x_l}{\partial t} \bigg|_{X_K} = \text{const.} \tag{13.21}$$

The acceleration a_l is determined from

$$a_l \equiv \frac{\partial v_l}{\partial t} \bigg|_{X_K} = \text{const.} = \frac{\partial v_l}{\partial t} + v_{l,k} v_k \tag{13.22}$$

Lagrangian Description

The Lagrangian strain tensor is defined by

$$2E_{KL} = C_{KL} - \delta_{KL} \tag{13.23}$$

where

$$C_{KL} = \delta_{kl} x_{k,K} x_{l,L} \tag{13.24}$$

In terms of the Lagrangian components of the displacement vector E_{KL} is given by

$$2E_{KL} = U_{K,\,L} + U_{L,\,K} + U_{M,\,K}\, U_{M,\,L} \tag{13.25}$$

Often approximations are made in terms of the displacement gradients. For this the following expression is convenient

$$x_{k,\,K} = \delta_{kM}\,(\delta_{Mk} + U_{M,\,K}) \tag{13.26}$$

where the convention of Section 3 is employed.

D. Constitutive Theories

In this section we will present approximations to the theories of the previous sections by expanding the constitutive equations in power series in strains and strain rates. From these it is not difficult to derive expansions in terms of the displacement gradients and/or the rotations. (For more details, see [23], pp. 47, 268 or [52], p. 303.)

(a) Kelvin–Voigt Solid

Approximations to the nonlinear Kelvin–Voigt solid presented in Section 5 can be obtained by expanding (5.28) and (5.35) in a power series in **E**. The results for the following cases are:

(i) Anisotropic solid

(1) Linear approximation

$$\Psi(\theta, E_{KL}) = \Psi^0(\theta) + A_{KL}(\theta)\, E_{KL} + \tfrac{1}{2} A_{KLMN}(\theta)\, E_{KL}E_{MN} \tag{13.27}$$
$$_E T_{KL}(\theta, E_{KL}) = \rho_0[A_{KL}(\theta) + A_{KLMN}(\theta)\, E_{MN}] \tag{13.28}$$
$$_D T_{KL}(\theta, \dot{E}_{KL}) = G^{(1)}_{KLMN}(\theta)\, \dot{E}_{MN} \tag{13.29}$$

(2) Second order approximations

$$\Psi(\theta, E_{KL}) = \Psi^0(\theta) + A_{KL}(\theta)\, E_{KL} + \tfrac{1}{2} A_{KLMN}(\theta)\, E_{KL}E_{MN}$$
$$+ \tfrac{1}{3} A_{KLMNRS}(\theta)\, E_{KL}\, E_{MN}\, E_{RS} \tag{13.30}$$

$$_E T_{KL}(\theta, E_{KL}) = \rho_0[A_{KL}(\theta) + A_{KLMN}(\theta)\, E_{MN} + A_{KLMNRS}(\theta)\, E_{MN}\, E_{RS}] \tag{13.31}$$

$$_D T_{KL}(\theta, E_{KL}, \dot{E}_{KL}) = G^{(1)}_{KLMN}(\theta)\, \dot{E}_{MN} + G^{(2)}_{KLMNRS}(\theta)\, \dot{E}_{MN}\, E_{RS}$$
$$+ G^{(3)}_{KLMNRS}(\theta)\, \dot{E}_{MN}\, \dot{E}_{RS} \tag{13.32}$$

If the reference state is unstressed, $A_{KL}(\theta) = 0$. Note that a linear (slow) rate theory which still allows "large" strains can be obtained from (13.32) by setting $G^{(3)}_{KLMNRS}(\theta) = 0$.

(ii) Isotropic solid

For the isotropic solid we present two expansions: one in terms of the Lagrangian strain tensor and one in terms of the Eulerian strain tensor.

Lagrangian Description

(1) Linear

$$\Psi(\theta, \mathbf{E}) = \Psi^0(\theta) + a_1 \operatorname{tr} \mathbf{E} + a_2 \operatorname{tr} \mathbf{E}^2 + a_3 (\operatorname{tr} \mathbf{E})^2 \tag{13.33}$$

$$_E\mathbf{T}(\theta, \mathbf{E}) = \rho_0(a_1 + 2a_3 \operatorname{tr} \mathbf{E}) \mathbf{I} + 2\rho_0 a_2 \mathbf{E} \tag{13.34}$$

$$_D\mathbf{T}(\theta, \dot{\mathbf{E}}) = \gamma_1 \operatorname{tr} \dot{\mathbf{E}}\mathbf{I} + \gamma_2 \dot{\mathbf{E}} \tag{13.35}$$

where $a_1, a_2, a_3, \gamma_1, \gamma_2$ are functions of θ.

(2) Second order

$$\Psi(\theta, \mathbf{E}) = \Psi^0(\theta) + a_1 \operatorname{tr} \mathbf{E} + a_2 \operatorname{tr} \mathbf{E}^2 + a_3 (\operatorname{tr} \mathbf{E})^2 + a_4 \operatorname{tr} \mathbf{E}^3$$
$$+ a_5 \operatorname{tr} \mathbf{E} \operatorname{tr} \mathbf{E}^2 + a_6 (\operatorname{tr} \mathbf{E})^3 \tag{13.36}$$

$$_E\mathbf{T}(\theta, \mathbf{E}) = \rho_0[a_1 + 2a_3 \operatorname{tr} \mathbf{E} + a_5 \operatorname{tr} \mathbf{E}^2 + 3 a_6 (\operatorname{tr} \mathbf{E})^2] \mathbf{I}$$
$$+ 2\rho_0 (a_2 + a_5 \operatorname{tr} \mathbf{E}) \mathbf{E} + 3\rho_0 a_4 \mathbf{E}^2 \tag{13.37}$$

$$_D\mathbf{T}(\theta, \mathbf{E}, \dot{\mathbf{E}}) = [\gamma_1 \operatorname{tr} \dot{\mathbf{E}} + \gamma_3 (\operatorname{tr} \dot{\mathbf{E}})^2 + \gamma_4 \operatorname{tr} \mathbf{E} \operatorname{tr} \dot{\mathbf{E}} + \gamma_5 \operatorname{tr} \dot{\mathbf{E}}^2 + \gamma_6 \operatorname{tr} (\mathbf{E}\dot{\mathbf{E}})] \mathbf{I}$$
$$+ \gamma_7 (\operatorname{tr} \dot{\mathbf{E}})\mathbf{E} + (\gamma_2 + \gamma_8 \operatorname{tr} \mathbf{E} + \gamma_9 \operatorname{tr} \dot{\mathbf{E}}) \dot{\mathbf{E}} + \gamma_{10} (\mathbf{E}\dot{\mathbf{E}} + \dot{\mathbf{E}} \mathbf{E}) + \gamma_{11} \dot{\mathbf{E}}^2 \tag{13.38}$$

where $\gamma_1, \ldots, \gamma_{11}$ and $a_1, \ldots, a_6$ are functions of θ. If the references state is stress free, $a_1 = 0$.

Eulerian Description

(1) Linear

$$\Psi(\theta, \mathbf{e}) = \Psi^0(\theta) + \beta_1 \operatorname{tr} \mathbf{e} + \beta_2 \operatorname{tr} \mathbf{e}^2 + \beta_3 (\operatorname{tr} \mathbf{e})^2 \tag{13.39}$$

$$_E\mathbf{t}(\theta, \mathbf{e}) = \rho(\mathbf{I} - 2\mathbf{e}) [(\beta_1 + 2\beta_3 \operatorname{tr} \mathbf{e}) \mathbf{I} + 2\beta_2 \mathbf{e}]$$
$$\approx \rho (\beta_1 + 2\beta_3 \operatorname{tr} \mathbf{e}) + 2\rho (\beta_2 - \beta_1) \mathbf{e} \tag{13.40}$$

$$_D\mathbf{t}(\theta, \mathbf{d}) = \delta_1 (\operatorname{tr} \mathbf{d}) \mathbf{I} + \delta_2 \mathbf{d} \tag{13.41}$$

where $\beta_1, \beta_2, \beta_3, \delta_1, \delta_2$ are functions of θ.

(2) Second order

$$\Psi(\theta, \mathbf{e}) = \Psi^0(\theta) + \beta_1 \operatorname{tr} \mathbf{e} + \beta_2 \operatorname{tr} \mathbf{e}^2 + \beta_3 (\operatorname{tr} \mathbf{e})^2 + \beta_4 \operatorname{tr} \mathbf{e}^3$$
$$+ \beta_5 (\operatorname{tr} \mathbf{e}) (\operatorname{tr} \mathbf{e}^2) + \beta_6 (\operatorname{tr} \mathbf{e})^3 \tag{13.42}$$

$$_E\mathbf{t}(,\theta \, \mathbf{e}) = \rho(\mathbf{I} - 2\mathbf{e}) \{[\beta_1 + 2\beta_3 \operatorname{tr} \mathbf{e} + \beta_5 \operatorname{tr} \mathbf{e}^2 + 3\beta_6 (\operatorname{tr} \mathbf{e})^2] \mathbf{I}$$
$$+ 2 [\beta_2 + \beta_5 \operatorname{tr} \mathbf{e}] \mathbf{e} + 3\beta_4 \mathbf{e}^2\}$$
$$\approx \rho [\beta_1 + 2\beta_3 \operatorname{tr} \mathbf{e} + \beta_5 \operatorname{tr} \mathbf{e}^2 + 3\beta_6 (\operatorname{tr} \mathbf{e})^2] \mathbf{I}$$
$$+ 2\rho [\beta_2 - \beta_1 + (\beta_5 - 2\beta_3) \operatorname{tr} \mathbf{e}] \mathbf{e} + \rho(3\beta_4 - 2\beta_2) \mathbf{e}^2 \tag{13.43}$$

$$_D\mathbf{t}(,\theta \, \mathbf{e}, \mathbf{d}) = [\delta_1 \operatorname{tr} \mathbf{d} + \delta_3 (\operatorname{tr} \mathbf{d})^2 + \delta_4 (\operatorname{tr} \mathbf{d}) (\operatorname{tr} \mathbf{e})$$
$$+ \delta_5 \operatorname{tr} \mathbf{d}^2 + \delta_6 \operatorname{tr} (\mathbf{e} \mathbf{d})] \mathbf{I} + \delta_7 (\operatorname{tr} \mathbf{d}) \mathbf{e}$$
$$+ (\delta_2 + \delta_8 \operatorname{tr} \mathbf{e} + \delta_9 \operatorname{tr} \mathbf{d}) \mathbf{d} + \delta_{10} (\mathbf{e} \mathbf{d} + \mathbf{d} \mathbf{e})$$
$$+ \delta_{11} \mathbf{d}^2 \tag{13.44}$$

where $\beta_1, \ldots, \beta_6$ and $\delta_1, \ldots, \delta_{11}$ are functions of θ.

(b) *Maxwellian Solid*

The theory of a Maxwellian solid presented in Section 6 is of necessity isotropic. It is possible to construct an anisotropic theory for such a material if one adopts a different starting point. We will, however, be content with the theory outlined in Section 6 and present approximations for that theory.

(1) Linear approximation

$$\hat{t} = (\alpha_1 \operatorname{tr} \mathbf{d} + \alpha_2 \operatorname{tr} \mathbf{t}) \, \mathbf{I} + \alpha_3 \, \mathbf{d} + \alpha_4 \mathbf{t} \tag{13.45}$$

(2) Second order

$$
\begin{aligned}
\hat{t} = {} & [\alpha_1 \operatorname{tr} \mathbf{d} + \alpha_2 \operatorname{tr} \mathbf{t} + \alpha_5 \, (\operatorname{tr} \mathbf{d})^2 + \alpha_6 \, (\operatorname{tr} \mathbf{t})^2 + \alpha_7 \, (\operatorname{tr} \mathbf{t}) \, (\operatorname{tr} \mathbf{d}) \\
& + \alpha_8 \operatorname{tr} \mathbf{dt} + \alpha_9 \operatorname{tr} \mathbf{t}^2 + \alpha_{10} \operatorname{tr} \mathbf{d}^2] \, \mathbf{I} \\
& + (\alpha_3 + \alpha_{11} \operatorname{tr} \mathbf{d} + \alpha_{12} \operatorname{tr} \mathbf{t}) \, \mathbf{d} \\
& + (\alpha_4 + \alpha_{13} \operatorname{tr} \mathbf{d} + \alpha_{14} \operatorname{tr} \mathbf{t}) \, \mathbf{t} + \alpha_{15} \, \mathbf{t}^2 \\
& + \alpha_{16} \, \mathbf{d}^2 + \alpha_{17} \, (\mathbf{dt} + \mathbf{td})
\end{aligned} \tag{13.46}
$$

A "slow" rate theory which still allows "large" stresses can be obtained from (13.25) by setting $\alpha_5 = \alpha_{10} = \alpha_{11} = \alpha_{16} = 0$.

(c) *General Strain Rate Dependent Materials* (*Linear Rate Approximations*)

In Section 7 a linear rate theory was developed for an arbitrary strain. We now present approximations to this theory:

(i) *Anisotropic solid*

(1) Linear

$$
\begin{aligned}
\Psi = {} & \Psi^0(\theta) + A_{KL}(\theta) \, E_{KL} + \tfrac{1}{2} A_{KLMN}(\theta) \, E_{KL} \, E_{MN} \\
& + \frac{1}{4\rho_0} \sum_{\beta, \gamma = 1}^{\nu - 1} F_{KLMN}^{(\beta, \gamma)}(\theta) \, E_{KL}^{(\beta)} \, E_{MN}^{(\gamma)}
\end{aligned} \tag{13.47}
$$

$$_E T_{KL}(\theta, E_{KL}) \approx \rho_0 [A_{KL}(\theta) + A_{KLMN}(\theta) \, E_{MN}] \tag{13.48}$$

$$_D T_{KL}(\theta, E_{KL}^{(\beta)}) = \sum_{\beta = 1}^{\nu} G_{KLMN}^{(\beta)}(\theta) \, E_{KL}^{(\beta)} \tag{13.49}$$

(2) Linear strain theory

$$
\begin{aligned}
\Psi = {} & \Psi^0(\theta) + A_{KL}(\theta) \, E_{KL} + \tfrac{1}{2} A_{KLMN}(\theta) \, E_{KL} \, E_{MN} \\
& + \frac{1}{4\rho_0} \sum_{\beta, \gamma = 1}^{\nu - 1} [F_{KLMN}^{(\beta, \gamma)}(\theta) + F_{KLMNRS}^{(\beta, \gamma)}(\theta) \, E_{RS}] \, E_{KL}^{(\beta)} \, E_{MN}^{(\gamma)}
\end{aligned} \tag{13.50}
$$

$$_E T_{KL} \approx \rho_0 [A_{KL}(\theta) + A_{KLMN}(\theta) \, E_{MN}] \tag{13.51}$$

$$_D T_{KL} \approx \sum_{\beta = 1}^{\nu} [G_{KLMN}^{(\beta)}(\theta) + G_{KLMNRS}^{(\beta)}(\theta) \, E_{RS}] \, E_{MN}^{(\beta)} \tag{13.52}$$

(3) Second order strain theory

$$\Psi = \Psi^0(\theta) + A_{KL}(\theta)\, E_{KL} + \tfrac{1}{2} A_{KLMN}(\theta)\, E_{KL} E_{MN}$$

$$+ \tfrac{1}{3} A_{KLMNRS}\, E_{KL} E_{MN} E_{RS} \tag{13.53}$$

$$+ \frac{1}{4\rho_0} \sum_{\beta,\,\gamma=1}^{\nu=1} [F^{(\beta,\gamma)}_{KLM\,N}(\theta) + F^{(\beta,\gamma)}_{KLM\,NRS}(\theta)\, E_{RS} + F^{(\beta,\gamma)}_{KLM\,NRSUV}(\theta)\, E_{RS} E_{UV}]$$

$$E^{(\beta)}_{KL} E^{(\gamma)}_{MN}$$

$$_E T_{KL} \approx \rho_0 [A_{KL}(\theta) + A_{KLMN}(\theta)\, E_{MN} + A_{KLMNRS}\, E_{MN} E_{RS}] \tag{13.54}$$

$$_D T_{KL} = \sum_{\beta=1}^{\nu} [G^{(\beta)}_{KLMN}(\theta) + G^{(\beta)}_{KLMNRS}(\theta)\, E_{RS}$$

$$+ G^{(\beta)}_{KLMNRSUV}(\theta)\, E_{RS} E_{UV}]\, E^{(\beta)}_{MN} \tag{13.55}$$

(ii) *Isotropic solid*

The forms of the constitutive equations for an isotropic solid can be obtained from (7.26) and (7.28) by expanding $\alpha^\delta_{\beta,\gamma}$ and β^δ_γ in a power series in the invariants of **e** and by replacing c^{-1} by **e**. This will give the Eulerian description. The Lagrangian description of an isotropic material can be obtained from (7.26) and (7.28) by noting that the form of $F_{KL,\,MN}(\theta, \mathbf{E})$ is that of $f_{kl,\,mn}(\theta, \mathbf{c}^{-1})$ with $\mathbf{c}^{-1}$ replaced by **E**. We list only the results for a second order strain theory which is linear in the strain rates. The linear and linear strain theories are easily derived from this approximation.

Lagrangian Description

$$\Psi = \Psi^0(\theta) + a_1 \operatorname{tr} \mathbf{E} + a_2 \operatorname{tr} \mathbf{E}^2 + a_3 (\operatorname{tr} \mathbf{E})^2 + a_4 \operatorname{tr} \mathbf{E}^3 + a_5 \operatorname{tr} \mathbf{E} \operatorname{tr} \mathbf{E}^2 + a_6 (\operatorname{tr} \mathbf{E})^3$$

$$+ \frac{1}{4\rho_0} \sum_{\beta,\gamma=1}^{N-1} \left\{ \left[\underset{0}{\overset{1}{a}}_{(\beta,\,\gamma)} + \underset{1}{\overset{1}{a}}_{(\beta,\,\gamma)} \operatorname{tr} \mathbf{E} + \underset{2}{\overset{1}{a}}_{(\beta,\gamma)} (\operatorname{tr} \mathbf{E})^2 + \underset{3}{\overset{1}{a}}_{(\beta,\,\gamma)} \operatorname{tr} \mathbf{E}^2 \right] \operatorname{tr} \mathbf{E}^{(\beta)} \operatorname{tr} \mathbf{E}^{(\gamma)} \right.$$

$$+ 2 \left[\underset{0}{\overset{2}{a}}_{(\beta,\,\gamma)} + \underset{1}{\overset{2}{a}}_{(\beta,\,\gamma)} \operatorname{tr} \mathbf{E} + \underset{2}{\overset{2}{a}}_{(\beta,\,\gamma)} (\operatorname{tr} \mathbf{E})^2 + \underset{3}{\overset{2}{a}}_{(\beta,\,\gamma)} \operatorname{tr} \mathbf{E}^2 \right] \operatorname{tr} (\mathbf{E}^{(\beta)} \mathbf{E}^{(\gamma)})$$

$$+ \left[\underset{0}{\overset{3}{a}}_{(\beta,\gamma)} + \underset{1}{\overset{3}{a}}_{(\beta,\gamma)} \operatorname{tr} \mathbf{E} \right] \operatorname{tr} (\mathbf{E}\mathbf{E}^{(\beta)}) \operatorname{tr} \mathbf{E}^{(\gamma)} + \left[\underset{0}{\overset{4}{a}}_{(\beta,\gamma)} + \underset{1}{\overset{4}{a}}_{(\beta,\gamma)} \operatorname{tr} \mathbf{E} \right] \operatorname{tr} (\mathbf{E}\mathbf{E}^{(\gamma)}) \operatorname{tr} \mathbf{E}^{(\beta)}$$

$$+ 2 \left[\underset{0}{\overset{5}{a}}_{(\beta,\,\gamma)} + \underset{1}{\overset{5}{a}}_{(\beta,\,\gamma)} \operatorname{tr} \mathbf{E} \right] [\operatorname{tr} (\mathbf{E}^{(\beta)} \mathbf{E}\, \mathbf{E}^{(\gamma)}) + \operatorname{tr} (\mathbf{E}^{(\gamma)} \mathbf{E}\, \mathbf{E}^{(\beta)})]$$

$$+ 2 \underset{0}{\overset{6}{a}}_{(\beta,\,\gamma)} [\operatorname{tr} (\mathbf{E}^{(\beta)} \mathbf{E}^2 \mathbf{E}^{(\gamma)}) + \operatorname{tr} (\mathbf{E}^{(\gamma)} \mathbf{E}^2 \mathbf{E}^{(\beta)})] + \underset{0}{\overset{7}{a}}_{(\beta,\,\gamma)} [\operatorname{tr} (\mathbf{E}\mathbf{E}^{(\beta)}) \operatorname{tr} (\mathbf{E}\mathbf{E}^{(\gamma)})]$$

$$+ \underset{0}{\overset{8}{a}}_{(\beta,\,\gamma)} [\operatorname{tr} (\mathbf{E}^{(\beta)}) \operatorname{tr} (\mathbf{E}^2 \mathbf{E}^{(\gamma)})] + \underset{0}{\overset{9}{a}}_{(\beta,\,\gamma)} [\operatorname{tr} (\mathbf{E}^2 \mathbf{E}^{(\beta)}) \operatorname{tr} \mathbf{E}^{(\gamma)}] \right\} \tag{13.56}$$

$$\mathbf{T} \approx {}_E \mathbf{T} + \sum_{\gamma=1}^{N} \left\{ \left[\underset{0}{\overset{1}{\beta}}_\gamma + \underset{1}{\overset{1}{\beta}}_\gamma \operatorname{tr} \mathbf{E} + \underset{2}{\overset{1}{\beta}}_\gamma (\operatorname{tr} \mathbf{E})^2 + \underset{3}{\overset{1}{\beta}}_\gamma \operatorname{tr} \mathbf{E}^2 \right] [\operatorname{tr} \mathbf{E}^{(\gamma)}]\, \mathbf{I} \right.$$

$$+2\left[\underset{0}{\overset{2}{\beta_\gamma}}+\underset{1}{\overset{2}{\beta_\gamma}}\,\text{tr }\mathbf{E}+\underset{2}{\overset{2}{\beta_\gamma}}\,(\text{tr }\mathbf{E})^2+\underset{3}{\overset{2}{\beta_\gamma}}\,\text{tr }\mathbf{E}^2\right]\mathbf{E}^{(\gamma)}+\left[\underset{0}{\overset{3}{\beta_\gamma}}+\underset{1}{\overset{3}{\beta_\gamma}}\,\text{tr }\mathbf{E}\right]\,[\text{tr }\mathbf{E}^{(\gamma)}\mid\mathbf{E}$$

$$+\left[\underset{0}{\overset{4}{\beta_\gamma}}+\underset{1}{\overset{4}{\beta_\gamma}}\,\text{tr }\mathbf{E}\right]\,[\text{tr }(\mathbf{E}^{(\gamma)}\mathbf{E})]\,\mathbf{I}+2\left[\underset{0}{\overset{5}{\beta_\gamma}}+\underset{1}{\overset{5}{\beta_\gamma}}\,\text{tr }\mathbf{E}\right]\,[\mathbf{E}\,\mathbf{E}^{(\gamma)}+\mathbf{E}^{(\gamma)}\mathbf{E}]$$

$$+2\underset{0}{\overset{6}{\beta_\gamma}}\,[\mathbf{E}^2\mathbf{E}^{(\gamma)}+\mathbf{E}^{(\gamma)}\mathbf{E}^2]+\underset{0}{\overset{7}{\beta_\gamma}}\,\text{tr }[\mathbf{E}\,\mathbf{E}^{(\gamma)}]\,\mathbf{E}$$

$$+\underset{0}{\overset{8}{\beta_\gamma}}\,\text{tr }[\mathbf{E}^2\mathbf{E}^{(\gamma)}]\,\mathbf{I}+\underset{0}{\overset{9}{\beta_\gamma}}\,[\text{tr }\mathbf{E}^{(\gamma)}]\,\mathbf{E}^2\bigg\} \tag{13.57}$$

where $_E\mathbf{T}$ is given by (13.37).

Eulerian Description

$$\Psi=\Psi^0(\theta)+\beta_1\,\text{tr }\mathbf{e}+\beta_2\,\text{tr }\mathbf{e}^2+\beta_3\,(\text{tr }\mathbf{e})^2+\beta_4\,\text{tr }\mathbf{e}^3+\beta_5\,\text{tr }\mathbf{e}\,\text{tr }\mathbf{e}^2+\beta_6\,(\text{tr }\mathbf{e})^3$$

$$+\frac{1}{4\rho_0}\sum_{\beta,\gamma=1}^{N-1}\bigg\{\left[\underset{0}{\overset{1}{\epsilon_{(\beta,\,\gamma)}}}+\underset{1}{\overset{1}{\epsilon_{(\beta,\,\gamma)}}}\,\text{tr }\mathbf{e}+\underset{2}{\overset{1}{\epsilon_{(\beta,\,\gamma)}}}\,(\text{tr }\mathbf{e})^2+\underset{3}{\overset{1}{\epsilon_{(\beta,\,\gamma)}}}\,\text{tr }\mathbf{e}^2\right]\,\text{tr }\mathbf{A}^{(\beta)}\,\text{tr }\mathbf{A}^{(\gamma)}$$

$$+2\left[\underset{0}{\overset{2}{\epsilon_{(\beta,\,\gamma)}}}+\underset{1}{\overset{2}{\epsilon_{(\beta,\,\gamma)}}}\,\text{tr }\mathbf{e}+\underset{2}{\overset{2}{\epsilon_{(\beta,\,\gamma)}}}\,(\text{tr }\mathbf{e})^2+\underset{3}{\overset{3}{\epsilon_{(\beta,\,\gamma)}}}\,\text{tr }\mathbf{e}^2\right]\,\text{tr }(\mathbf{A}^{(\beta)}\mathbf{A}^{(\gamma)})$$

$$+\left[\underset{0}{\overset{3}{\epsilon_{(\beta,\,\gamma)}}}+\underset{1}{\overset{3}{\epsilon_{(\beta,\,\gamma)}}}\,\text{tr }\mathbf{e}\right]\,\text{tr }(\mathbf{e}\mathbf{A}^{(\beta)})\,\text{tr }\mathbf{A}^{(\gamma)}+\left[\underset{0}{\overset{4}{\epsilon_{(\beta,\,\gamma)}}}+\underset{1}{\overset{4}{\epsilon_{(\beta,\,\gamma)}}}\,\text{tr }\mathbf{e}\right]\,\text{tr }(\mathbf{e}\mathbf{A}^{(\gamma)})\,\text{tr }\mathbf{A}^{(\beta)}$$

$$+2\left[\underset{0}{\overset{5}{\epsilon_{(\beta,\,\gamma)}}}+\underset{1}{\overset{5}{\epsilon_{(\beta,\,\gamma)}}}\,\text{tr }\mathbf{e}\right]\,[\text{tr }(\mathbf{A}^{(\beta)}\,\mathbf{e}\,\mathbf{A}^{(\gamma)})+\text{tr }(\mathbf{A}^{(\gamma)}\,\mathbf{e}\,\mathbf{A}^{(\beta)})]$$

$$+2\underset{0}{\overset{6}{\epsilon_{(\beta,\,\gamma)}}}\,[\text{tr }(\mathbf{A}^{(\beta)}\,\mathbf{e}^2\mathbf{A}^{(\gamma)})+\text{tr }(\mathbf{A}^{(\gamma)}\,\mathbf{e}^2\mathbf{A}^{(\beta)})]+\underset{0}{\overset{7}{\epsilon_{(\beta,\,\gamma)}}}\,[\text{tr }(\mathbf{e}\mathbf{A}^{(\beta)})\,\text{tr }(\mathbf{e}\mathbf{A}^{(\gamma)})]$$

$$+\underset{0}{\overset{8}{\epsilon_{(\beta,\,\gamma)}}}\,[\text{tr }\mathbf{A}^{(\beta)}\,\text{tr }(\mathbf{e}^2\mathbf{A}^{(\gamma)})]+\underset{0}{\overset{9}{\epsilon_{(\beta,\,\gamma)}}}\,[\text{tr }(\mathbf{e}^2\mathbf{A}^{(\beta)})\,\text{tr }\mathbf{A}^{(\gamma)}]\bigg\} \tag{13.58}$$

$$\mathbf{t}\approx{_E}\mathbf{t}+\sum_{\beta,\gamma=1}^{N-1}\bigg\{\left[\underset{0}{\overset{1}{\delta_\gamma}}+\underset{1}{\overset{1}{\delta_\gamma}}\,\text{tr }\mathbf{e}+\underset{2}{\overset{1}{\delta_\gamma}}\,(\text{tr }\mathbf{e})^2+\underset{3}{\overset{1}{\delta_\gamma}}\,\text{tr }\mathbf{e}^2\right]\,[\text{tr }\mathbf{A}^{(\gamma)}]\,\mathbf{I}$$

$$+2\left[\underset{0}{\overset{2}{\delta_\gamma}}+\underset{1}{\overset{2}{\delta_\gamma}}\,\text{tr }\mathbf{e}+\underset{2}{\overset{2}{\delta_\gamma}}\,(\text{tr }\mathbf{e})^2+\underset{3}{\overset{2}{\delta_\gamma}}\,\text{tr }\mathbf{e}^2\right]\,\mathbf{A}^{(\gamma)}+\left[\underset{0}{\overset{3}{\delta_\gamma}}+\underset{1}{\overset{3}{\delta_\gamma}}\,\text{tr }\mathbf{e}\right]\,[\text{tr }\mathbf{A}^{(\gamma)}]\,\mathbf{e}$$

$$+\left[\underset{0}{\overset{4}{\delta_\gamma}}+\underset{1}{\overset{4}{\delta_\gamma}}\,\text{tr }\mathbf{e}\right]\,[\text{tr }(\mathbf{A}^{(\gamma)}\mathbf{e})]\,\mathbf{I}+2\left[\underset{0}{\overset{5}{\delta_r}}+\underset{1}{\overset{5}{\delta_\gamma}}\,\,\text{tr }\mathbf{e}\right]\,[\mathbf{e}\mathbf{A}^{(\gamma)}+\mathbf{A}^{(\gamma)}\mathbf{e}]$$

$$+2\underset{0}{\overset{6}{\delta_\gamma}}[\mathbf{e}^2\mathbf{A}^{(\gamma)}+\mathbf{A}^{(\gamma)}\mathbf{e}^2]+\underset{0}{\overset{7}{\delta_\gamma}}\,\text{tr }(\mathbf{e}\mathbf{A}^{(}{}_\gamma^{)})\,\mathbf{e}$$

$$+\underset{0}{\overset{8}{\delta_\gamma}}\,[\text{tr }(\mathbf{e}^2\mathbf{A}^{(\gamma)})]\,\mathbf{I}+\underset{0}{\overset{9}{\delta_\gamma}}\,[\text{tr }\mathbf{A}^{(\gamma)}]\,\mathbf{e}^2\bigg\} \tag{13.59}$$

where $_E\mathbf{t}$ is given by (13.43).

The restrictions (7.21), (7.23), (7.27) and (7.30) should be noted.

(d) *Functional Constitutive Equations (Linear History)*

The approximations to the theory presented in Section 8 are obtained by expanding $\Psi^0(\theta, \mathbf{E})$, $F_{KL, MN}$ and $\Psi_{KL, MN}$ in a power series in $\mathbf{E}$, the coefficients now being functions of s. These approximations can be obtained by comparison with the results previously derived in this section. We list only a second order strain approximation from which a linear or linear strain approximation is easily deduced.

(i) *Anisotropic solid*

$$\Psi = \Psi^0(\theta) + A_{KL}(\theta)E_{KL} + \tfrac{1}{2}A_{KLMN}(\theta)E_{KL}E_{MN} + \tfrac{1}{3}A_{KLMNRS}(\theta)E_{KL}E_{MN}E_{RS}$$

$$+ \tfrac{1}{2}\int_0^T \int_0^T [\overset{1}{F}_{KLMN}(\theta, s_1, s_2) + \overset{2}{F}_{KLMNRS}(\theta, s_1, s_2)\, E_{RS}(t)$$

$$+ \overset{3}{F}_{KLMNRSUV}(\theta, s_1, s_2)\, E_{RS}(t)\, E_{UV}(t)]\, \tilde{E}^t_{KL}(s_1)\, \tilde{E}^t_{MN}(s_2)\, ds_1\, ds_2 \qquad (13.60)$$

$$T_{KL} \approx \rho_0[A_{KL}(\theta) + A_{KLMN}(\theta)\, E_{MN} + A_{KLMNRS}(\theta)\, E_{MN}\, E_{RS}]$$

$$+ \rho_0 \int_0^T [\overset{1}{\Psi}_{KLMN}(\theta, s_1) + \overset{2}{\Psi}_{KLMNRS}(\theta, s_1)\, E_{RS}(t)$$

$$+ \overset{3}{\Psi}_{KLMNRSUT}(\theta, s_1)\, E_{RS}(t)\, E_{UT}(t)]\, \dot{E}_{KL}\,(t - s_1)\, ds_1 \qquad (13.61)$$

where $\overset{1}{F}_{KLMN}$ etc. and $\overset{1}{\Psi}_{KLMN}$ etc. are related by (8.26), (8.28) and (8.29).

(ii) *Isotropic solid*

For an isotropic solid, the free energy can be approximated by

$$\Psi = \Psi^0(\theta) + a_1 \operatorname{tr} \mathbf{E} + a_2 \operatorname{tr} \mathbf{E}^2 + a_3(\operatorname{tr} \mathbf{E})^2 + a_4 \operatorname{tr} \mathbf{E}^3 + a_5 \operatorname{tr} \mathbf{E} \operatorname{tr} \mathbf{E}^2 + a_6(\operatorname{tr} \mathbf{E})^3$$

$$+ \tfrac{1}{2}\int_0^T \int_0^T \{[f_1(s_1, s_2) + f_2(s_1, s_2) \operatorname{tr} \mathbf{E} + f_3(s_1, s_2)(\operatorname{tr} \mathbf{E})^2 + f_4(s_1, s_2) \operatorname{tr} \mathbf{E}^2]\operatorname{tr}\tilde{\mathbf{E}}^t(s_1)\operatorname{tr}\tilde{\mathbf{E}}^t(s_2)$$

$$+ 2[f_5(s_1, s_2) + f_6(s_1, s_2) \operatorname{tr} \mathbf{E} + f_7(s_1, s_2)(\operatorname{tr} \mathbf{E})^2 + f_8(s_1, s_2) \operatorname{tr} \mathbf{E}^2]\operatorname{tr}[\tilde{\mathbf{E}}^t(s_1)\,\tilde{\mathbf{E}}^t(s_2)]$$

$$+ [f_9(s_1, s_2) + f_{10}(s_1, s_2) \operatorname{tr} \mathbf{E}]\operatorname{tr}[\mathbf{E}\,\tilde{\mathbf{E}}^t(s_1)]\operatorname{tr}\tilde{\mathbf{E}}^t(s_2)$$

$$+ [f_{11}(s_1, s_2) + f_{12}(s_1, s_2) \operatorname{tr} \mathbf{E}]\operatorname{tr}[\mathbf{E}\,\tilde{\mathbf{E}}^t(s_2)]\operatorname{tr}\tilde{\mathbf{E}}^t(s_1)$$

$$+ 2[f_{13}(s_1, s_2) + f_{14}(s_1, s_2) \operatorname{tr} \mathbf{E}]\,[\operatorname{tr}(\tilde{\mathbf{E}}^t(s_1)\mathbf{E}\,\tilde{\mathbf{E}}^t(s_2)) + \operatorname{tr}(\tilde{\mathbf{E}}^t(s_2)\mathbf{E}\,\tilde{\mathbf{E}}^t(s_2))]$$

$$+ 2f_{15}(s_1, s_2)\,[\operatorname{tr}(\tilde{\mathbf{E}}^t(s_1)\,\mathbf{E}^2\,\tilde{\mathbf{E}}^t(s_2)) + \operatorname{tr}(\tilde{\mathbf{E}}^t(s_2)\,\mathbf{E}^2\,\tilde{\mathbf{E}}^t(s_1))]$$

$$+ f_{16}(s_1, s_2)\,[\operatorname{tr}(\mathbf{E}\,\tilde{\mathbf{E}}^t(s_1))]\,[\operatorname{tr}(\mathbf{E}\,\tilde{\mathbf{E}}^t(s_2))]$$

$$+ f_{17}(s_1, s_2)\,[\operatorname{tr}\tilde{\mathbf{E}}^t(s_1)]\,[\operatorname{tr}(\mathbf{E}^2\,\tilde{\mathbf{E}}^t(s_2)]$$

$$+ f_{18}(s_1, s_2)\,[\operatorname{tr}\tilde{\mathbf{E}}^t(s_2)]\,[\operatorname{tr}(\mathbf{E}^2\,\tilde{\mathbf{E}}^t(s_1)]\}\, ds_1\, ds_2 \qquad (13.62)$$

$$\mathbf{T} \approx {}_E\mathbf{T} + \int_0^T \{[\Psi_1(s) + \Psi_2(s) \operatorname{tr} \mathbf{E} + \Psi_3(s) (\operatorname{tr} \mathbf{E})^2 + \Psi_4(s) \operatorname{tr} \mathbf{E}^2] [\operatorname{tr} \dot{\mathbf{E}}(t-s)] \mathbf{I}$$

$$+ 2[\Psi_5(s) + \Psi_6(s) \operatorname{tr} \mathbf{E} + \Psi_7(s) (\operatorname{tr} \mathbf{E})^2 + \Psi_8(s) \operatorname{tr} \mathbf{E}^2] \dot{\mathbf{E}}(t-s)$$

$$+ [\Psi_9(s) + \Psi_{10}(s) \operatorname{tr} \mathbf{E}] [\operatorname{tr} \dot{\mathbf{E}}(t-s)]\mathbf{E} + [\Psi_{11}(s) + \Psi_{12}(s) \operatorname{tr} \mathbf{E}] [\operatorname{tr} (\dot{\mathbf{E}}(t-s)\mathbf{E})] \mathbf{I}$$

$$+ 2[\Psi_{13}(s) + \Psi_{14}(s) \operatorname{tr} \mathbf{E}][\mathbf{E} \dot{\mathbf{E}}(t-s) + \dot{\mathbf{E}}(t-s) \mathbf{E}]$$

$$+ 2\Psi_{15}(s)[\mathbf{E}^2\dot{\mathbf{E}}(t-s) + \dot{\mathbf{E}}(t-s)\mathbf{E}^2] + \Psi_{16}(s)[\operatorname{tr} \mathbf{E} \dot{\mathbf{E}}(t-s)]\mathbf{E}$$

$$+ \Psi_{17}(s) [\operatorname{tr} \mathbf{E}^2\dot{\mathbf{E}}(t-s)] \mathbf{I} + \Psi_{18} [\operatorname{tr} \dot{\mathbf{E}}(t-s) \mathbf{E}^2] \qquad (13.63)$$

The f_i's are restricted by

$$f_i(s_1, s_2) = f_i(s_2, s_1) \qquad i = 1, \ldots, 8; \quad 13, \ldots, 16$$

$$f_9(s_1, s_2) = f_{11}(s_2, s_1); \quad f_{10}(s_1, s_2) = f_{12}(s_2, s_1); \quad f_{17}(s_1, s_2) = f_{18}(s_2, s_1)$$

and Ψ_i is related to f_i by (8.26), (8.28) and (8.29).

(e) Thermal Phenomena (Linear Dissipation)

The approximations for the free energy and the elastic part of the stress tensor found previously in this section are still valid in this case. One need only find how the strain affects heat flow and how the temperature gradients affect the dissipative part of the stress tensor. This can be obtained from equations (7.25) and (7.26) by expanding H_{KLM} and $_\beta J_{KLM}$ in a series in E_{KL}. This is straightforward enough not to warrant any illustration. For the isotropic case the stress tensor has no linear terms in $\theta_{,k}$; thus the previous formulae hold. The heat flux reduces for a second order strain theory to

$$q_k = \{[K_{00} + K_{01} \operatorname{tr} \mathbf{e} + K_{02} \operatorname{tr} \mathbf{e}^2 + K_{03}(\operatorname{tr} \mathbf{e})^2]\delta_{kl} + (K_{10} + K_{11} \operatorname{tr} \mathbf{e})e_{kl} + K_{20}e_{km}e_{ml}\}\theta_{,l}$$

APPENDIX ON THERMODYNAMICS

The thermodynamical practice used in this paper has the form introduced by Coleman and Mizel [40]. The main departure of this work from the ones used by Eringen [23, art. 49] and Koh and Eringen [39] is the consideration of energy ϵ and entropy η as an integral part of the constitutive theory which must not violate the axiom of equipresence at the start. This means that ϵ and η may depend on the rate variable (e.g. strain rates) just as the stress. The Clausius-Duhem inequality can then be used with this beginning to determine the restrictions on the response functions. If one accepts this practice then the use of the second law of thermodynamics in various classical cases of viscoelasticity leads to known results. Energy and entropy assume their usual forms and become independent of the rate variables. For more general theories of viscoelasticity treated in Sections 7, 8, 11 and 12 one can show, however, that a dilemma can result if ϵ and η are not dependent on the same constitutive variables. In particular suppose that ϵ and η are independent of strain rates and depend on θ and $\mathbf{C}$, i.e.

$$\epsilon = e(\mathbf{C}, \theta), \qquad \eta = n(\mathbf{C}, \theta) \qquad (A.1)$$

but stress depends on various order rates of $\mathbf{C}$ also (cf. Section 7).

$$t_{kl} = T_{KL}(\mathbf{C}, \dot{\mathbf{C}}, \ddot{\mathbf{C}}, \ldots ; \quad \theta, \mathbf{X}) x_{k,K} x_{l,L} \qquad (A.2)$$

In addition assume that the Clausius–Duhem inequality is postulated to be valid for *all independent processes*. From this inequality it then follows that

$$\eta = -\left.\frac{\partial \Psi(\mathbf{C}, \theta)}{\partial \theta}\right|\mathbf{C} \qquad (A.3)$$

and

$$_D T_{KL}\, \dot{C}_{KL} \geq 0 \qquad (A.4)$$

where

$$_D T_{KL} \equiv T_{KL} - 2\rho_0 \frac{\partial \Psi}{\partial C_{KL}} \qquad (A.5)$$

Inequality (A. 4), on account of the continuity of $_D T$ in $\dot{\mathbf{C}}$, implies that

$$_D T = 0 \text{ whenever } \dot{\mathbf{C}} = 0$$

This means that stress cannot depend linearly on the higher order rates of $\mathbf{C}$ other than the first. This rules out the existence of viscoelastic solids characterized by stress constitutive equations linear in rates of C higher than the first. A similar conclusion can be drawn for the Boltzmann–Volterra theory of linear viscoelasticity, see Section 8.

The above arguments compel us to either

(i) abandon the hypothesis that the Clausius–Duhem inequality is valid for all independent processes and assume that it is a restriction on the types of motion rather than material, or

(ii) accept the hypothesis that ϵ and η may depend on rate variables contained in stress and heat.

Inclusion of ϵ and η into the class of constitutive functions on a same footing as the stress and heat flow has an aesthetic appeal and it has not so far contradicted known results of physical theories. Nevertheless, the ultimate choice of the above alternatives must be settled on physical grounds.

REFERENCES

[1] MAXWELL, J. C., *Phil. Mag.* (4), **35**, 129 (1868).
[2] MEYER, O. E., *J. reine angew. Math.*, **78**, 130 (1874).
[3] MEYER, O. E., *Ann. d. Physik*, **1**, 108 (1874).
[4] MEYER, O. E., *J. reine angew. Math.*, **80**, 315 (1875).
[5] BOLTZMANN, L., *Sitzgsber. Akad. Wiss. Wien*, **70**, 275 (1874).
[6] VOIGT, W., *Göttinger Abh.*, **36**, 1 (1889).
[7] VOIGT, W., *Ann. d. Physik*, (2), **47**, 671 (1892).
[8] VOIGT, W., *Göttinger Abh.*, **38**, 2 (1892).
[9] VOIGT, W., *Lehrbuch der Kristallphysik*, Leipzig and Berlin, Teubner, (1910).
[10] LORD KELVIN, *Encyl. Brit.* 3, 27 (1875).
[11] DUHEM, P., *C.R. Acad. Sci., Paris*, **136**, 281, 343, 592, 733, 858, 1032 (1903).
[12] DUHEM, P., *Ann. Ecole Normale* (3), **21**, 99 (1904).
[13] NATANSON, L., *Phil. Mag.* (6), **2**, 342 (1901).

[14] NATANSON, L., *Bull. Int. Acad. Sci. Cracovie*, 95 (1901).
[15] NATANSON, L., *Z. Physik Chem.*, **38**, 690 (1901).
[16] ZAREMBA, S., *Bull. Int. Acad. Sci. Cracovie*, 380 (1903).
[17] ZAREMBA, S., *Bull. Int. Acad. Sci. Cracovie*, 594, 614 (1903).
[18] ZAREMBA, S., *Mem. Sci. Math.*, Gauthier-Villars, **82** (1937).
[19] VOLTERRA, V., *Theory of Functionals and of Integral and Integro-Differential Equations*, Blackie (1930).
[20] EIRICH, F., *Rheology*, Academic Press, New York, Vol. I (1956), Vol. II (1958).
[21] STAVERMAN, A. J., and SCHWARZL, F. *Die Physik der Hochpolymeren*, Vol. IV, edited by H. A. Stuart, Springer-Verlag, Berlin (1956).
[22] COSSERAT, E. and F., *Theorie des corps deformables*, Paris; in O.D. Chwolson *Traite di physique*, Hermann et Cie, Paris (1909).
[23] ERINGEN, A. C., *Nonlinear Theory of Continuous Media*, McGraw-Hill, New York (1962).
[24] JAUMANN, G., *Denkschr. Akad. Wiss. Wien*, **95**, 461 (1918).
[25] LOHR, E., *Denkschr. Akad. Wiss. Wien*, **93**, 339 (1917).
[26] STRUTT, M. *Ann. d. Physik* (4), **87**, 153 (1928).
[27] JEFFEREYS, H. J., *The Earth*, Cambridge (1929).
[28] GERASIMOV, A. N., *Prikl. Math. Mech.* (2), **2**, 379, 467 (1938).
[29] ALFREY, T., *Quart. Appl. Math.*, **2**, 113 (1944).
[30] ALFREY, T., *Quart. Appl. Math.*, **3**, 143 (1943).
[31] ZENER, C., *Elasticity and Anelasticity*, University of Chicago Press (1948).
[32] FREUDENTHAL, A. M. and GEIRINGER, H. *Handbuch der Physik*, Vol. VI, p. 229, Springer-Verlag (1958).
[33] VOLTERRA, V., *R. Acc. dei Lincei Rend.*, I, Series 6, 25 (1925).
[34] ERINGEN, A. C., *J. Appl. Mech.*, **22**, 4, 563 (1955).
[35] ERINGEN, A. C., "A unified theory of thermomechanical materials", ONR Report No. 30, 1965 to appear in *Int. J. Eng. Sci.*
[36] STRANEO, P., *R. Acc. dei Lincei Rend.*, I, Series 6, 29 (1925).
[37] COLEMAN, B. D. and NOLL, W., *Arch. Rat. Mech. Anal.*, **6**, 355 (1960).
[38] COLEMAN, B. D. and NOLL, W., *Rev. Mod. Phys.*, **33**, 239, 1961.
[39] KOH, S. and ERINGEN, A. C., *Int. J. Eng. Sci.*, **1**, 199 (1963).
[40] COLEMAN, B. and MIZEL, V., *J. Chem. Phys.*, **40**, 1116 (1964).
[41] WEYL, H., *Classical Groups*, Princeton University Press, Princeton, New Jersey (1946).
[42] GREEN, A. E. and ADKINS, J. E., *Large Elastic Deformations*, Oxford (1960).
[43] NOLL, W., *J. Rat. Mech. Anal.*, **4**, 3 (1955).
[44] TRUESDELL, C., *J. Rat. Mech. Anal.*, **4**, 83 (1955).
[45] GREEN, A. E. and RIVLIN, R. S., *Arch. Rat. Mech. Anal.*, **4**, 387 (1960).
[46] GREEN, A. E. and RIVLIN, R. S., *Arch. Rat. Mech. Anal.*, **1**, 1 (1957).
[47] NOLL, W., *Arch. Rat. Mech. Anal.*, **2**, 197 (1958).
[48] GREEN, A. E., RIVLIN, R. S. and SPENCER, A. J. M., *Arch. Rat. Mech. Anal.*, **3**, 82 (1959).
[49] COLEMAN, B. D., *Arch. Rat. Mech. Anal.*, **17**, 1 (1964).
[50] COLEMAN, B. D., *Arch. Rat. Mech. Anal.*, **17**, 230 (1964).
[51] ERINGEN, A. C., *Phys. Rev.*, **117**, 1174 (1960).
[52] TRUESDELL, C. and TOUPIN, R., "The classical field theories", *Handbuch der Physik*, Vol. III/1, Springer-Verlag (1960).

ON ANISOTROPIC LINEAR VISCOELASTIC SOLIDS*

L. S. SHU and E. T. ONAT**

Division of Engineering,
Brown University, Providence, R.I.

Abstract—The requirement that the work done to deform a virgin element be non-negative implies restrictions on the relaxation moduli of an anisotropic linear viscoelastic solid. The present paper is devoted to a study of these restrictions.

It is shown that if the work is non-negative, then the tensor of relaxation moduli is fully symmetric at time zero and it can be represented by certain Fourier–Stieltjes integrals. Conversely, if the relaxation moduli are representable by the same Fourier–Stieltjes integrals, then the work done is non-negative. It is also shown, by means of a counter example, that the requirement of non-negative work is not sufficient to ensure the full symmetry of the tensor of relaxation moduli for all times.

1. INTRODUCTION

We shall be concerned with anisotropic linear viscoelastic solids characterized by the constitutive relations:†

$$\sigma_{ij}(t) = \int_0^t G_{ijkl}(t - \tau)\dot{\epsilon}_{kl}(\tau)\,\mathrm{d}\tau, \qquad i, j, k, l = 1, 2, 3 \tag{1}$$

where $\sigma_{ij}(t)$ and $\epsilon_{ij}(t)$ denote the components of stress and infinitesimal strain tensors respectively and the dot denotes differentiation with respect to time t. The relaxation moduli $G_{ijkl}(t)$ have the following symmetry properties on account of symmetry of stress and strain tensors:

$$G_{jikl}(t) = G_{ijkl}(t) = G_{ijlk}(t). \tag{2}$$

We observe from (1) that $G_{ijkl}(t)$ need only be defined for non-negative values of their argument t. We shall assume that $G_{ijkl}(t)$ are bounded and continuous on the interval $0 \le t < \infty$.

It may be noted that the constitutive relations (1) contain the tacit assumption that the solid is in the unstressed and unstrained virgin state for $t < 0$.

We now consider the work done to deform an element from its virgin state during the time interval $0 \le t \le T$,

$$W = \int_0^T \sigma_{ij}(t)\dot{\epsilon}_{ij}(t)\mathrm{d}t. \tag{3}$$

** Now at the Department of Engineering and Applied Science, Yale University.

† The usual summation convention is used throughout the paper.

By using (1), (3) can be written in the following form:

$$W = \int\limits_0^T \int\limits_0^t G_{ijkl}(t - \tau)\dot{\epsilon}_{kl}(\tau)\dot{\epsilon}_{ij}(t)\mathrm{d}\tau\mathrm{d}t. \tag{4}$$

For future convenience, we extend the range of definition of $G_{ijkl}(t)$ to negative values of their argument in the following manner:

$$G_{klij}(-t) = G_{ijkl}(t). \tag{5}$$

With this extension, $G_{ijkl}(t)$ become bounded and continuous for all real t except at $t = 0$ where a simple jump discontinuity may occur in the event when

$$G_{ijkl}(0) \neq G_{klij}(0). \tag{6}$$

By using (5), (4) can be written in the following symmetrical form:

$$2W = \int\limits_0^T \int\limits_0^T G_{ijkl}(t - \tau)\dot{\epsilon}_{ij}(t)\dot{\epsilon}_{kl}(\tau)\mathrm{d}t\mathrm{d}\tau. \tag{7}$$

In the present paper, we shall be interested in viscoelastic solids for which W is positive semi-definite, i.e. W is non-negative for all arbitrary piecewise continuous $\dot{\epsilon}_{ij}(t)$ and for all T. Following König and Meixner [1] we may call the solids having the above property dissipative.

The requirement of positive semi-definiteness of work density W has an important place in the theory of elasticity. Udeschini [2] has shown that if W is positive semi-definite, the fourth order tensor of elastic moduli must be fully symmetric and therefore there must exist a strain energy function. Recently in his work on stable materials, Drucker [3] has emphasized the importance of this and similar requirements in mechanics of continua. The bearing that this requirement may have on thermodynamics has been discussed by Coleman [4]. König and Meixner [1] investigated, in the case of uniaxial stress, the restrictions which the requirement of non-negative work places on the relaxation modulus and they noted that the main result concerning such restrictions had already been obtained by Bochner in his work on the theory of probability [5]. In their work on uniqueness in viscoelasticity, Breuer and Onat [6] noted independently that Bochner's Theorem provides restrictions on the relaxation moduli which define a dissipative isotropic viscoelastic solid.

Recently, Gurtin and Herrera [7] studied dissipative anisotropic linear viscoelastic solids. They showed that the positive semi-definiteness of work density implies

$$G_{ijkl}(0) = G_{klij}(0) \tag{8}$$

and that $G_{ijkl}(0)$ is positive semi-definite.* They also showed that if $G_{ijkl}(\infty)$ exist, the positive semi-definiteness of work density implies

---

* A fourth order tensor C_{ijkl} is said to be positive semi-definite if and only if $C_{ijkl}\gamma_{ij}\gamma_{kl} \geq 0$ for any real γ_{ij} ($\gamma_{ij} = \gamma_{ji}$).

$$G_{ijkl}(\infty) = G_{klij}(\infty) \tag{9}$$

and that $G_{ijkl}(\infty)$ is positive semi-definite.

Furthermore, they observed that the tensor of dynamic viscosities

$$K_{ijkl}(\omega) = \int_0^\infty \cos \omega t \, G_{ijkl}(t)dt \tag{10}$$

is positive semi-definite whenever W is positive semi-definite.

In our present work, after having established (8) by a method different from that used in [7], we observe that H. Cramér's Theorem [8] on stationary random processes constitutes the main tool for the study of implications of the requirement that W is positive semi-definite. This theorem, when adapted to the present case, states that W is positive semi-definite if and only if $G_{ijkl}(t)$ are representable by certain Fourier–Stieltjes integrals. In Section 2 we give a statement and proof of the theorem without using the language and tools of probability. In Section 3 we discuss the various implications of the theorem. In particular, we show that the following symmetry property (i.e. the Onsager's Reciprocal Relations [9])

$$G_{ijkl}(t) = G_{klij}(t)$$

does not necessarily hold on the interval $0 < t < \infty$.

2. MAIN THEOREM ON DISSIPATIVE ANISOTROPIC LINEAR VISCOELASTIC SOLIDS

In this section we proceed to state and prove the following theorem, which constitutes the central part of this paper.

THEOREM. Consider a linear viscoelastic solid characterized by the relaxation moduli $G_{ijkl}(t)$ which have the symmetry properties (2) and are assumed to be bounded and continuous on the interval $0 \le t < \infty$. Extend the domain of definition of $G_{ijkl}(t)$ by (5) to negative values of t. The theorem states that if the work density W (as defined in (4) or (7)) is positive semi-definite, then

(a) $G_{ijkl}(0) = G_{klij}(0)$. \hfill (11)

(b) The relaxation moduli are given, for all real t, by the Fourier–Stieltjes integrals of the form

$$G_{ijkl}(t) = \int_{-\infty}^\infty e^{itx}dF_{ijkl}(x) \tag{12}$$

where $F_{ijkl}(x)$ are functions of bounded variation on the interval $-\infty < x < \infty$, which may be assumed to be everywhere continuous to the right.

(c) Denote by ΔF_{ijkl} the difference $F_{ijkl}(\beta) - F_{ijkl}(\alpha)$ of $F_{ijkl}(x)$ on the real interval $\alpha \le x \le \beta$; the form

$$H(z_{ij}) = z_{ij}\bar{z}_{kl}\Delta F_{ijkl} \tag{13}$$

is, for any $z_{ij}(z_{ij} = z_{ji})$ and for any (α, β), non-negative.*

Conversely, if the relaxation moduli are given, for all real t, by the Fourier–Stieltjes integrals of the form (12) where $F_{ijkl}(x)$ are of bounded variation on the interval $-\infty < x < \infty$ and everywhere continuous to the right and moreover the form (13) is, for any $z_{ij}(z_{ij} = z_{ji})$ and for any (α, β), non-negative, then $G_{ijkl}(t)$ are continuous on the interval $-\infty < t < \infty$ and W is positive semi-definite.

Proof: The proof of part (a) of the theorem is motivated by Udeschini's paper [2] where he showed that in the classical theory of elasticity, the positive semi-definiteness of work density implies the full symmetry of the tensor of elastic moduli.

In the viscoelastic case, the work density is defined by (4) where the domain of integration for the integral is the triangular region Ω_1 in a (τ, t) plane defined by the inequality $0 \leq \tau \leq t \leq T$.

Let us decompose $G_{ijkl}(t)$ into symmetric and antisymmetric parts, i.e.

$$G_{ijkl}(t) = S_{ijkl}(t) + E_{ijkl}(t) \text{ for } t \geq 0 \tag{14}$$

where

$$S_{ijkl}(t) = S_{klij}(t),$$
$$E_{ijkl}(t) = -E_{klij}(t). \tag{15}$$

Now since $G_{ijkl}(t)$ are continuous functions for $t \geq 0$, so are $S_{jkl}{}^{(t)}$ and $E_{ijkl}(t)$. It is clear from (15) that $E_{ijkl}(t) \equiv 0$ when $\{i, j\} = \{k, l\}$ so that we need only to prove (11) for $\{i, j\} \neq \{k, l\}$.

To show, for example, that $G_{1122}(0) = G_{2211}(0)$, we choose a particular strain history for which

$$\dot{\epsilon}_{11}(t) \neq 0, \qquad \dot{\epsilon}_{22}(t) \neq 0$$

and the remaining components of $\dot{\epsilon}_{ij}(t) \equiv 0$ for $0 \leq t \leq T$.

By (4), (14) and (15), we have then

$$W = \int_{\Omega_1} S_{1111}(t - \tau)\dot{\epsilon}_{11}(t)\dot{\epsilon}_{11}(\tau)dtd\tau + \int_{\Omega_1} S_{2222}(t - \tau)\dot{\epsilon}_{22}(t)\dot{\epsilon}_{22}(\tau)dtd\tau$$

$$+ \int_{\Omega_1} S_{1122}(t - \tau)\dot{\epsilon}_{11}(t)\dot{\epsilon}_{22}(\tau)dtd\tau + \int_{\Omega_1} E_{1122}(t - \tau)\dot{\epsilon}_{11}(t)\dot{\epsilon}_{22}(\tau)dtd\tau$$

$$+ \int_{\Omega_1} S_{1122}(t - \tau)\dot{\epsilon}_{22}(t)\dot{\epsilon}_{11}(\tau)dtd\tau - \int_{\Omega_1} E_{1122}(t - \tau)\dot{\epsilon}_{22}(t)\dot{\epsilon}_{11}(\tau)dtd\tau. \tag{16}$$

---

* A quantity with a bar on top denotes the complex conjugate of the relevant quantity. Since $G_{ijkl}(t)$ are real-valued functions, $F_{ijkl}(x) = X_{ijkl}(x) + iY_{ijkl}(x)$ are subject to the following restriction

$$\int_{-\infty}^{\infty} \sin tx \, dX_{ijkl}(x) + \int_{-\infty}^{\infty} \cos tx \, dY_{ijkl}(x) = 0.$$

From the fact that the form (13) is non-negative for any z_{ij} and for any (α, β), it can be shown that $F_{ijkl}(x)$ is real, bounded and non-decreasing on $-\infty < x < \infty$ when $\{i, j\} = \{k, l\}$ where the notation $\{i, j\}$ indicates the set of two numbers with no question of order involved; thus $\{i, j\} = \{j, i\}$. For example, $F_{1313}(x) = F_{1331}(x)$ is real, bounded and non-decreasing.

Further, suppose that

$$\dot{\epsilon}_{11}(t) = \lambda \qquad \text{for } 0 < t < T$$
$$\dot{\epsilon}_{22}(t) = \mu \qquad 0 < t < T/2$$
$$= -\mu \qquad T/2 < t < T$$

where λ, μ are real constants.

Then (16) can be written as

$$W = \lambda^2 \int_{\Omega_1} S_{1111}(t - \tau) dt d\tau + \mu^2 \, [2 \int_{\Omega_1} S_{2222}(t - \tau) dt d\tau$$
$$- \int_{\Omega_3} S_{2222}(t - \tau) dt d\tau] + 2\lambda\mu \int_{\Omega_3} E_{1122}(t - \tau) dt d\tau \qquad (17)$$

where Ω_2 is the triangular region in the (τ, t) plane defined by the inequalities

$$0 \le \tau \le t \le T/2$$

and Ω_3 is the square region in the (τ, t) plane defined by the inequalities

$$T/2 \le t \le T, \qquad 0 \le \tau \le T/2.$$

Now, since W is non-negative, we must have in view of (17),

$$\Delta \equiv [\int_{\Omega_3} E_{1122}(t - \tau) dt d\tau]^2 - [\int_{\Omega_1} S_{1111}(t - \tau) dt d\tau]$$
$$[2 \int_{\Omega_2} S_{2222}(t - \tau) dt d\tau - \int_{\Omega_3} S_{2222}(t - \tau) dt d\tau] \le 0. \qquad (18)$$

We wish to show that Δ will be positive for small values of T if $E_{1122}(0) \ne 0$. For this purpose, we approximate the continuous functions $E_{1122}(t)$, $S_{1111}(t)$ and $S_{2222}(t)$ by Bernstein polynomials [10] on the interval $0 \le t \le T_1$ where T_1 is a fixed number. An important feature of the Bernstein polynomial is that it coincides with the function it approximates at the end points of the interval. Thus, we have for example,

$$E_{1122}(t) = E_{1122}(0) + E_1 t + E_2 t^2 + \ldots + E_n t^n + E(t) \qquad (19)$$

where the first $n + 1$ terms constitute the approximating polynomial for $E_{1122}(t)$. We now choose n in (19) in such a way that the error term $E(t)$ satisfies the inequality

$$| E(t) | < \frac{E_{1122}(0)}{N} \text{ on } 0 \le t \le T_1 \qquad (20)$$

where N is a positive number.

Then by integrating (19) term by term over Ω_3, keeping in mind that the same polynomial is used on $[0, T]$ for all $T \le T_1$, we obtain*

$$\int_{\Omega_3} E_{1122}(t - \tau) dt d\tau = [E_{1122}(0) + a_1] \frac{T^2}{4} + 0(T^3) \text{ as } T \to 0 \qquad (21)$$

---

* $\phi = 0(\Psi)$ as $\Psi \to 0$ if and only if $\phi/\Psi < M$ as $\Psi \to 0$, where M is independent of Ψ.

where
$$|\alpha_1| < \frac{E_{1122}(0)}{N}.$$

By similar approximations involving the maximum error shown in (20), we have for $T \to 0$

$$\int_{\Omega_1} S_{1111}(t - \tau)\mathrm{d}t\mathrm{d}\tau = [S_{1111}(0) + \alpha_2]\frac{T^2}{2} + 0(T^3) \qquad (22)$$

and

$$2\int_{\Omega_2} S_{2222}(t - \tau)\mathrm{d}t\mathrm{d}\tau - \int_{\Omega_3} S_{2222}(t - \tau)\mathrm{d}t\mathrm{d}\tau = \alpha_3\frac{T^2}{4} + 0(T^3) \qquad (23)$$

where

$$|\alpha_2| < \frac{E_{1122}(0)}{N},$$

$$|\alpha_3| < 2\frac{E_{1122}(0)}{N}.$$

In view of (21), (22) and (23), Δ in (18) becomes

$$\Delta = [(E_{1122}(0) + \alpha_1)^2 - 2(S_{1111}(0) + \alpha_2)\alpha_3]\frac{T^4}{16} + 0(T^5).$$

We now observe that when N is large and hence α_1, α_2 and α_3 are small $E_{1122(0)}^2$ is the dominant term in the above square bracket. Thus, for small values of T, Δ will be positive if $E_{1122}(0) \neq 0$. This would violate the inequality (18). Therefore, we must have $E_{1122}(0) = 0$ and hence $G_{1122}(0) = G_{2211}(0)$.

Since the same procedure is applicable to the remaining $G_{ijkl}(0)$ with $\{i, j\} \neq \{k, l\}$, the assertion (a) of the theorem is proved. Therefore, in view of the remark associated with (6), $G_{ijkl}(t)$ are continuous on the whole real line.

A proof of the parts (b) and (c) of the theorem which is based on Cramér's work, [8], [11], but does not employ the tools and language of probability theory is given in the appendix.

The proof of the converse theorem is as follows: Since by hypothesis $F_{ijkl}(x)$ are of bounded variation on the interval $-\infty < x < \infty$, then the improper integrals in (12) converge uniformly to $G_{ijkl}(t)$ for all real t. Therefore, $G_{ijkl}(t)$ are continuous functions of t. Furthermore, substituting (12) into (7), we have

$$2W = \int_0^T \int_0^T [\int_{-\infty}^{\infty} e^{i(t-\tau)x}\mathrm{d}F_{ijkl}(x)]\dot{\epsilon}_{ij}(t)\dot{\epsilon}_{kl}(\tau)\mathrm{d}t\mathrm{d}\tau \qquad (24)$$

and since the order of integration can be interchanged by the uniform convergence of the improper integral in (24), (24) becomes

$$2W = \int_{-\infty}^{\infty} z_{ij}(x)\bar{z}_{kl}(x)\mathrm{d}F_{ijkl}(x) \qquad (25)$$

where

$$z_{ij}(x) \equiv \int_0^T e^{itx}\dot{\epsilon}_{ij}(t)\mathrm{d}t.$$

Now, it follows from our hypothesis concerning the form (13) that W in (25) is positive semi-definite. The proof of the converse theorem is thus complete.

As noted in the introduction, Gurtin and Herrera proved in [7] that $G_{ijkl}(0)$ is positive semi-definite and that whenever $G_{ijkl}(\infty)$ exist, $G_{ijkl}(\infty) = G_{klij}(\infty)$ and $G_{ijkl}(\infty)$ is positive semi-definite. It can easily be seen that the present theorem implies the above results. For instance, we have from (12) that

$$G_{ijkl}(0) = F_{ijkl}(\infty) - F_{ijkl}(-\infty) = \Delta F_{ijkl}$$

where ΔF_{ijkl} are real. But the fact that ΔF_{ijkl} are real implies, in view of (13), that ΔF_{ijkl} and hence $G_{ijkl}(0)$ are positive semi-definite.

3. AN APPLICATION OF THE THEOREM

Let us consider the case where $F_{ijkl}(x)$ possess continuous first order derivatives $F'_{ijkl}(x)$. The relaxation moduli then become, according to (12), the Fourier transforms of $F'_{ijkl}(x)$:

$$G_{ijkl}(t) = \int_{-\infty}^{\infty} e^{itx} F'_{ijkl}(x) dx. \tag{26}$$

Moreover, by the Mean Value Theorem of Differential Calculus, the assertion (c) of the theorem in Section 2 becomes

$$z_{ij} \bar{z}_{kl} F'_{ijkl}(x) \geq 0 \tag{27}$$

for any $z_{ij}(z_{ij} = z_{ji})$ and for any real x.

It is well known from Matrix Theory that (27) is equivalent to the following six inequalities [12]:

$$F'_{1111}(x) \geq 0, \ \det. \begin{bmatrix} F'_{1111}(x) & F'_{1122}(x) \\ F'_{2211}(x) & F'_{2222}(x) \end{bmatrix} \geq 0, \ldots,$$

$$\det. \begin{bmatrix} F'_{1111}(x) & F'_{1122}(x) & \ldots & F'_{1112}(x) \\ F'_{2211}(x) & F'_{2222}(x) & \ldots & F'_{2212}(x) \\ \cdot & \cdot & \cdots & \cdot \\ \cdot & \cdot & \cdots & \cdot \\ \cdot & \cdot & \cdots & \cdot \\ F'_{1211}(x) & F'_{1222}(x) & \ldots & F'_{1212}(x) \end{bmatrix} \geq 0 \tag{28}$$

for all real x.

Notice that the determinants in (28) are all real-valued for all real x even though $F'_{ijkl}(x)$ may be complex-valued for $\{i,j\} \neq \{k,l\}$.

The earlier referred result of Gurtin and Herrera [7] concerning with the dynamic viscosities (10) is a consequence of (27). But the positive semi-definiteness of $K_{ijkl}(\omega)$ does not in general imply that W is positive semi-definite. Of

14

course, when $G_{ijkl}(t) = G_{klij}(t)$ for all t, the positive semi-definiteness of $K_{ijkl}(\omega)$ is equivalent to (27).

We now inquire whether W being positive semi-definite implies the full symmetry expressed by the equations:

$$G_{ijkl}(t) = G_{klij}(t),$$

for $t > 0$.

We have already proved that at $t = 0$, the above relations hold. We wish now to construct a set of relaxation moduli for which W is positive semi-definite but the above symmetry relations do not hold.

We consider an anisotropic linear viscoelastic solid which has the following relaxation moduli:

$$
\begin{aligned}
G_{1111}(t) &= Ae^{-a|t|}, & -\infty < t < \infty, \\
G_{2222}(t) &= Be^{-b|t|}, & -\infty < t < \infty, \\
G_{1122}(t) &= Ee^{-mt}, & t \geq 0, \\
G_{2211}(t) &= Ee^{-nt}, & t \geq 0,
\end{aligned}
\tag{29}
$$

the remaining components of $G_{ijkl}(t)$ being zero for all t. Furthermore, A, B, E, a, b, m and n are all positive constants.

Note that we have, according to (5),

$$
\begin{aligned}
G_{1122}(t) &= Ee^{nt} & t \leq 0 \\
G_{2211}(t) &= Ee^{mt} & t \leq 0
\end{aligned}
$$

and that (11) holds.

By inversion of (26), we have

$$
F'_{1111}(x) = \frac{1}{2\pi} \int_{-\infty}^{\infty} e^{-itx} G_{1111}(t)\,\mathrm{d}t = \frac{1}{2\pi} \frac{2Aa}{(a^2 + x^2)},
$$

$$
F'_{2222}(x) = \frac{1}{2\pi} \int_{-\infty}^{\infty} e^{-itx} G_{2222}(t)\,\mathrm{d}t = \frac{1}{2\pi} \frac{2Bb}{(b^2 + x^2)},
$$

$$
F'_{1122}(x) = \frac{1}{2\pi} \int_{-\infty}^{\infty} e^{-itx} G_{1122}(t)\,\mathrm{d}t = \frac{1}{2\pi} \frac{E(m + n)}{(n - ix)(m + ix)},
$$

$$
F'_{2211}(x) = \frac{1}{2\pi} \int_{-\infty}^{\infty} e^{-itx} G_{2211}(t)\,\mathrm{d}t = \frac{1}{2\pi} \frac{E(m + n)}{(n + ix)(m - ix)},
$$

and the inequalities (28) become

$$Aa \geq 0 \tag{30a}$$

and

$$\frac{4ABab}{(a^2 + x^2)(b^2 + x^2)} - \frac{E^2(m + n)^2}{(m^2 + x^2)(n^2 + x^2)} \geq 0 \tag{30b}$$

for all real x.

It can be shown that it is possible to choose the constants A, B, E, a, b, m and n in such a way that (30b) holds for all real x.* Thus, we have just constructed an anisotropic linear viscoelastic solid for which W is positive semi-definite and yet the Onsager's Reciprocal Relations $G_{ijkl}(t) = G_{klij}(t)$ are not satisfied for $t > 0$. Therefore, we conclude that the condition of positive semi-definiteness of work density alone is not sufficient to ensure the validity of the Onsager's Reciprocal Relations for the relaxation moduli. However, as we now show, the inequality (30b) implies that the difference of the relaxation times associated with the two relaxation moduli $G_{1122}(t)$ and $G_{2211}(t)$ must be smaller than a given quantity.

For this purpose, we consider (30b) for $x = 0$. We have then

$$\frac{4AB}{ab} - \frac{E^2(m + n)^2}{m^2 n^2} \geq 0. \tag{31}$$

Taking the square root of (31), we obtain

$$2\sqrt{\frac{AB}{ab}} - E(\tau_m + \tau_n) \geq 0 \tag{32}$$

where $\tau_m = 1/m$ and $\tau_n = 1/n$ are the relaxation times associated with $G_{1122}(t)$ and $G_{2211}(t)$, respectively.

For definiteness, assume that $\tau_m > \tau_n$; then by (32) and by the fact that τ_m and τ_n are positive numbers, we have

$$\tau_m - \tau_n < \frac{2}{E}\sqrt{\frac{AB}{ab}} \tag{33}$$

which shows that in this simple example the difference of the two relaxation times cannot differ from each other more than a given quantity.

APPENDIX

The proof of parts (b) and (c) of the theorem is as follows: By hypothesis and the result of part (a), $G_{ijkl}(t)$ are bounded and continuous on the interval $-\infty < t < \infty$.

We first observe that the hypothesis that W is positive semi-definite will also imply, in view of (5),

---

* For example, we can choose $a = m$ and $b = n$, then (30b) reduces to
$$4ABab - E^2(a + b)^2 \geq 0.$$
It is then easy to choose A, B, E, a and b such that the above inequality is satisfied.

$$\int_0^T \int_0^T G_{ijkl}(t - \tau)\phi_{ij}(t)\bar{\phi}_{kl}(\tau)dtd\tau \geqslant 0 \tag{34}$$

Where $\phi_{ij}(t)$, $(\phi_{ij}(t) = \phi_{ji}(t))$ are complex-valued functions whose real and imaginary parts are piecewise continuous functions of t.

This can be done without loss of generality since the imaginary part of the integral in (34) is zero due to (5).

Now, let us define, for any real x and any $A > 1$,

$$g_{ijkl}(x, A) = \frac{1}{2\pi A} \int_0^A \int_0^A G_{ijkl}(t - \tau)e^{-ix(t-\tau)}dtd\tau. \tag{35}$$

It is obvious that,

$$\bar{g}_{ijkl}(x, A) = g_{klij}(x, A). \tag{36}$$

It is known from [11] that a necessary and sufficient condition for the representation of the bounded and continuous functions $G_{ijkl}(t)$ in the form of (12) where $F_{ijkl}(x)$ is real, bounded and non-decreasing is that $g_{ijkl}(x, A)$ is real and non-negative for all real x and all $A > 1$. Moreover, $F_{ijkl}(x)$ in (12) is of bounded variation on the interval $-\infty < x < \infty$ if, and only if, for all $A > 1$,

$$\int_{-\infty}^{\infty} |g_{ijkl}(x, A)| \, dx < \text{constant}. \tag{37}$$

Now, let us choose a particular $\phi_{ij}(t) = e^{-itx}$ (where x is any real number)* and the remaining components $\phi_{kl}(t) \equiv 0$ for $\{k, l\} \neq \{i, j\}$.

Inequality (34) then becomes

$$\int_0^T \int_0^T G_{i\underset{\sim}{j}ij}(t - \tau) e^{-ix(t-\tau)}dtd\tau \geq 0\dagger$$

for all T, which in turn implies that $g_{i\underset{\sim}{j}ij}(x, A)$ is real and non-negative for all real x and for all $A > 1$. Therefore, $G_{i\underset{\sim}{j}ij}(t)$ can be represented, for all real t, as follows:

$$G_{i\underset{\sim}{j}ij}(t) = \int_{-\infty}^{\infty} e^{itx}dF_{i\underset{\sim}{j}ij}(x) \tag{38}$$

Where $F_{i\underset{\sim}{j}ij}(x)$ is real, bounded and non-decreasing for all real x on the interval $-\infty < x < \infty$. Furthermore, since $F_{i\underset{\sim}{j}ij}(x)$ is real, bounded and non-decreasing for all real x on the interval $-\infty < x < \infty$, it is of bounded variation on the same interval [13]. Then by (37), for all $A > 1$,

$$\int_{-\infty}^{\infty} g_{i\underset{\sim}{j}ij}(x, A) \, dx < \text{constant}. \tag{39}$$

---

* i and j can be any integers from 1 to 3; once chosen, they remain fixed.

† "not summed on repeated indices" is implied by a bar below the index. Thus, $G_{i\underset{\sim}{j}ij}(t) = G_{1212}(t)$ or $G_{1111}(t)$, etc.

On the other hand, let us choose

$$\phi_{ij}(t) = \phi_{ji}(t) = -\beta_1 e^{-itx}, \qquad \phi_{kl}(t) = \phi_{lk}(t) = \beta_2 e^{-itx},$$

($\{i,j\} \neq \{k,l\}$; $\beta_1 = 1$ when $i = j$, $\beta_1 = \frac{1}{2}$ when $i \neq j$; $\beta_2 = 1$ when $k = l$, $\beta_2 = \frac{1}{2}$ when $k \neq l$) and the remaining "ϕ-components" are all zero, then (34) becomes

$$\int_0^T \int_0^T G_{ijkl}(t-\tau) e^{-ix(t-\tau)} dt d\tau + \int_0^T \int_0^T G_{klij}(t-\tau) e^{-ix(t-\tau)} dt d\tau$$

$$\leq \int_0^T \int_0^T G_{ijij}(t-\tau) e^{-ix(t-\tau)} dt d\tau + \int_0^T \int_0^T G_{klkl}(t-\tau) e^{-ix(t-\tau)} dt d\tau. \qquad (40)$$

In particular, for $T = A > 1$, we have, by dividing (40) by $2\pi A$ and by the definition of $g_{ijkl}(x, A)$ in (35),

$$g_{ijkl}(x, A) + g_{klij}(x, A) \leq g_{ijij}(x, A) + g_{klkl}(x, A)$$

or, by (36),

$$g_{ijkl}(x, A) + \bar{g}_{ijkl}(x, A) \leq g_{ijij}(x, A) + g_{klkl}(x, A) \qquad (41)$$

for all real x and all $A > 1$.
Let

$$g_{ijkl}(x, A) = \text{Re}\,[g_{ijkl}(x, A)] + i\,\text{Im}\,[g_{ijkl}(x, A)], \qquad (42)$$

then (41) can be written as

$$2\text{Re}\,[g_{ijkl}(x, A)] \leq g_{ijij}(x, A) + g_{klkl}(x, A). \qquad (43)$$

On the other hand, if we let*

$$\phi_{ij}(t) = \phi_{ji}(t) = \beta_1 e^{-itx}, \qquad \phi_{kl}(t) = \phi_{lk}(t) = \beta_2 e^{-itx} \quad (\{i,j\} \neq \{k,l\})$$

and the remaining "ϕ-components" are zero, we obtain by similar steps,

$$2\,\text{Re}\,[g_{ijkl}(x, A)] \geq -[g_{ijij}(x, A) + g_{klkl}(x, A)].$$

We combine the above inequality with (43) to obtain

$$\left|\,\text{Re}\,[g_{ijkl}(x, A)]\,\right| \leq \frac{1}{2}[g_{ijij}(x, A) + g_{klkl}(x, A)] \qquad (44)$$

for all real x and all $A > 1$.
Furthermore, by choosing

$$\phi_{ij}(t) = \phi_{ji}(t) = \beta_1 i e^{-itx}, \qquad \phi_{kl}(t) = \phi_{lk}(t) = \pm \beta_2 e^{-itx}$$

($\{i,j\} \neq \{k,l\}$) with the remaining "ϕ-components" identically zero, we arrive by similar steps at the following inequality:

$$\left|\,\text{Im}\,[g_{ijkl}(x, A)]\,\right| \leq \frac{1}{2}[g_{ijij}(x, A) + g_{klkl}(x, A)] \qquad (45)$$

for all real x and all $A > 1$.

---

* β_1 and β_2 are defined as before.

Thus, it follows from (42), (44) and (45) that

$$\left| g_{ijkl}(x, A) \right| \leq \left| \operatorname{Re}(g_{ijkl}(x, A)] \right| + \left| \operatorname{Im}[g_{ijkl}(x, A)] \right|$$
$$\leq g_{ijij}(x, A) + g_{klkl}(x, A) \tag{46}$$

for all real x and all $A > 1$. Hence by (39) and (46),

$$\int_{-\infty}^{\infty} \left| g_{ijkl}(x, A) \right| dx < \text{constant, for all } A > 1,$$

which is exactly (37). Therefore, we have the representation of the form (12) for $G_{ijkl}(t)$, with $F_{ijkl}(x)$ being of bounded variation for x on the interval $-\infty < x < \infty$.

Obviously, we may always assume that the functions $F_{ijkl}(x)$ are everywhere continuous to the right, since a modification of $F_{ijkl}(x)$ in a countable set of points does not affect the values of the integral in (12).

It remains to prove that the form $H(z_{ij})$ defined in (13) is always real and non-negative for any z_{ij} and for any (α, β). For this purpose, let us put $\phi_{ij}(t) = z_{ij}\phi(t)$ for all i and j where z_{ij} are arbitrary complex numbers and $\phi(t)$ is an arbitrary complex-valued function of t. Then (34) becomes

$$z_{ij}\bar{z}_{kl} \int_0^T \int_0^T G_{ijkl}(t - \tau)\phi(t)\bar{\phi}(\tau)dtd\tau \geq 0 \tag{47}$$

for all T.

Notice that in the above inequality $\phi(t)$ is defined only for $t \geq 0$. We can extend its domain of definition to negative values of t by

$$\phi(-t) = \bar{\phi}(t). \tag{48}$$

Then (47) implies

$$H_T(z_{ij}) = z_{ij}\bar{z}_{kl} \int_{-T}^T \int_{-T}^T G_{ijkl}(t - \tau)\phi(t)\bar{\phi}(\tau)dtd\tau \geq 0. \tag{49}$$

Thus $H_T(z_{ij})$ is real and non-negative for any z_{ij} and for any non-trivial function $\phi(t)$ and any $T > 0$.

Now substitute (12) into (49) to obtain

$$H_T(z_{ij}) = z_{ij}\bar{z}_{kl} \int_{-\infty}^{\infty} \left| \int_{-T}^T e^{itx}\phi(t)dt \right|^2 dF_{ijkl}(x) \geq 0 \tag{50}$$

Now, following Cramèr [8], we choose the following function which satisfies (48)

$$\phi(t) = \frac{e^{-it\alpha} - e^{-it\beta}}{2\pi i t}$$

where $\alpha < \beta$ are two real numbers. It is then easily seen from (50) that

$$\lim_{T \to \infty} H_T(z_{ij}) = H(z_{ij})$$

Since $H_T(z_{ij})$ is real and non-negative, the same holds true for $H(z_{ij})$. This completes the proof.

REFERENCES

[1] KÖNIG, H. and MEIXNER, J., "Lineare Systeme und Lineare Transformationen", *Math. Nach.*, **19**, 256 (1958).

[2] UDESCHINI, P., "Sull' Energia di Deformazione", *Rendiconti Real Istituto Lombardo di Sci. E. Lett.*, **76** (7 of Series III), 25–34 (1942/43).

[3] DRUCKER, D. C., "A definition of stable inelastic material", *J. Appl. Mech.*, **101**—106 (1959).

[4] COLEMAN, B. D., "Thermodynamics of materials with memory", *Arch. Rational Mech. Anal.*, **17**, 1–46 (1964).

[5] LOÈVE, M., *Probability Theory*, Von Nostrand (1955).

[6] BREUER, S. and ONAT, E. T., "On uniqueness in linear viscoelasticity", *Quarterly of Applied Mathematics*, **19**, 355 (1962).

[7] GURTIN, M. E. and HERRERA, I. "On dissipative inequalities and linear viscoelasticity", Brown University, Nonr 562 (25), Technical Report No. 27, June 1964.

[8] CRAMÈR, H., "On the theory of stationary random processes", *Annals of Mathematics*, Series 2, **41**, 215 (1940).

[9] DEGROOT, S. R., *Thermodynamics of Irreversible Processes*, North-Holland Publishing Company (1952).

[10] NATANSON, I. P., *Theory of Functions of a Real Variable*, vol. 1, Frederick Ungar Publishing Company, p. 108 (1955).

[11] CRAMÈR, H., "On the representation of a function by certain Fourier integrals", *Transactions of American Math. Soc.*, **46**, 191 (1939).

[12] See, for example, BECKENBACH, E. F. and BELLMAN, R., *Inequalities*, Springer-Verlag (1961).

[13] APOSTOL, T. M., *Mathematical Analysis*, Addison-Wesley Publishing Company, 187 (1960).

THERMODYNAMICS AND MECHANICS OF MIXTURES OF VISCOELASTIC SUBSTANCES

RAY M. BOWEN

Department of Mechanics
Johns Hopkins University
Baltimore, Maryland

Abstract—An entropy inequality is formulated which is valid for all mixtures of non-polar chemically reacting materials. An especially interesting feature of this formulation is that each material in the mixture is allowed to have a temperature field distinct from that of the other materials. Restricting the development to the case of no chemical reactions, I propose that for a mixture of N materials the values of the partial stresses, partial internal energies, partial entropies, partial heat fluxes, momentum supplies, and internal energy supplies are given by functions of the N temperatures, N temperature gradients, N deformation gradients, N velocity gradients, and N velocities. Using the entropy inequality, I derive a set of necessary and sufficient conditions that the above constitutive assumptions must obey. Two of these conditions are that the partial internal energy of the αth material in the mixture is dependent only on its own entropy and deformation gradient and that the equilibrium value of the partial stress on the αth material is related to its internal energy through the classical Kirchhoff relation. Also, I prove that in an appropriately defined state of equilibrium the partial heat fluxes, momentum supplies, internal energy supplies, and the dissipative part of the partial stresses must vanish. Reduced forms of the constitutive functions which satisfy the axiom of material indifference and certain special material symmetries are also presented.

217

RECENT WORK IN ELASTIC STABILITY

J. L. ERICKSEN

Department of Mechanics
Johns Hopkins University
Baltimore, Maryland

Abstract—The first part of the lecture will cover observations bearing on the question of when elasticity theory might reasonably be used to explore stability problems in cases where viscous or thermal effects may play an important role. The remainder will be devoted to description of some of what has been learned about formulations of and comparisons between the various criteria for elastic stability.

PROBLEMS IN NONLINEAR VISCOELASTICITY

SEVERINO L. KOH

Purdue University
Lafayette, Indiana

Abstract—Interest in the behavior of nonlinear viscoelastic materials has remained unabated since it was aroused some two decades ago with the observation of certain "nonlinear" effects in some simple experiments. A wealth of nonlinear theories characterizing materials exhibiting such effects has since been recorded in the literature. Many interesting problems dealing with these materials have been formulated and solved.

A brief review is given of the various nonlinear constitutive relations proposed by different investigators, including an enumeration of the other fundamental equations needed in the analysis of specific problems. Some significant mathematical problems are discussed including steady flow of nonlinear viscoelastic fluids, periodic motion, wave propagation, thermomechanical coupled effects and other problems.

1. INTRODUCTION

Not quite two decades ago, several experimental investigators in fluid dynamics [1, 2] aroused the interest of other workers in the field of continuum mechanics with the publication of some curious results—curious in the sense that so-called "normal stress effects" were observed in some new experiments which cannot be justified in the flow of the classical Newtonian fluid. These observations of abnormal behavior of fluids—rather, *normal* behavior of *abnormal* substances, as Weissenberg [2] called these materials, provided the *prima facie* evidence for the existence of nonlinear fluids (fluids which are characterized by nonlinear constitutive equations).

To be sure, this was not the first time that investigators had wondered about nonlinear materials. (For instance, see Reiner [3], Rivlin [4], and Doyle and Ericksen [5].) Nevertheless, it was these dramatic experimental results that provided the impetus and generated wider interest in the study of non-linear fluids. It is only natural that such interest should exceed the bounds of fluid dynamics and propagate into the realm of viscoelasticity.

A review of the foundations underlying the theory of non-linear viscoelastic materials is given by Eringen [6, p. 336]. This has been expanded by Eringen and Grot [7] to include recent results. As indicated in these articles, the rational approach to nonlinear viscoelasticity has now been developed. However, the technical literature is significantly wanting in experimental evidence to prove or disprove the veracity of the theory. Yet this is to be expected: an intriguing experimental discovery is made and theoretical explanations naturally follow; as theories develop, further experimentation becomes necessary.

An activity that plays an indispensable role in the development of fundamental theories and in subsequent experimentation is the application of the

221

untested theory to practical problems. The analytical study of these problems, especially if the results may be shown to be consistent with earlier proven theories, gives added credence to the new theory. What is equally important is the fact that these analyses of specific problems provide the needed guidelines for meaningful experimental work.

During the last few years, several significant problems in nonlinear visco-elasticity have been formulated and solved. We here attempt to survey these analyses, discuss the methods used and evaluate the theoretical results obtained. It is not possible to discuss all these problems in the details the author would have desired. Such would have rendered this paper entirely too voluminous.

We briefly discuss the general method of analysis employed in nonlinear viscoelasticity (Section 2) including for completeness a short discussion on the basic equations needed in such analysis. In Section 3 we discuss several representative problems on purely mechanical behavior. The vast majority of the problems solved in nonlinear viscoelasticity falls within this subject; we include discussions on steady flow of viscoelastic fluids, extension problems, periodic motion, wave propagation and other dynamical problems. In Section 4, we consider coupled effects in these materials, but confine most of the discussion to thermomechanical effects. We conclude with a brief note on further problems that still exist.

2. METHOD OF ANALYSIS

2.1. Basic Equations

The equations which are derived from the fundamental axioms of continuum physics, such as the principles of conservation of mass, momentum, moment of momentum, and energy, must be satisfied in nonlinear viscoelasticity in the same manner that these so-called field equations are satisfied in other continuous media.* For convenient reference, we enumerate below those equations which are pertinent in the analysis of problems in nonlinear viscoelasticity. For simplicity and unless otherwise specified, we will refer points to a fixed rectangular frame and use rectangular Cartesian coordinates X_K: (X_1, X_2, X_3) for material points (coordinates of particles in some prescribed undistorted or natural configuration of the body under study, particularly meaningful in discussions of solids) and x_k: (x_1, x_2, x_3) for spatial points (coordinates of the same material particles at some deformed configuration of the body).

The well-known *continuity equation* is expressible in the form

$$\dot{\rho} + \rho v_{k, k} = 0 \qquad (2.1)$$

where ρ is the mass density and v_k are the velocity components. The superposed dot ($\cdot$) denotes a material derivative and the comma (,) preceding a subscript denotes partial differentiation with respect to the spatial coordinates if the subscript is a lower case letter, such as k in eqn. (2.1) above, or with respect to the

---

* A comprehensive discussion of these basic equations is presented by Eringen [6].

material coordinates if the subscript is an upper case letter. Repeated indices (e.g. k above) indicates summation over the range (1, 2, 3).

The *equations of motion* are given by

$$t_{mk,\,m} + \rho f_k = \rho a_k \tag{2.2}$$

and

$$t_{mk} = t_{km} \tag{2.3}$$

where t_{mk}; f_k; and $a_k \equiv \dot{v}_k$ are respectively the components of the stress tensor, the body force and the acceleration.

In addition to the above field equations, certain *constitutive equations* are needed in the analysis of the behavior of a particular medium under study. These constitutive equations define *ideal* media and frequently only approximate the characteristics of the *real* material being considered. Consistent with the physical observation that bodies of different materials generally exhibit different responses to the same environmental conditions, mechanical or otherwise, these equations are different for different materials, not only in the values of the material moduli but generally in form as well. Eringen [6] discusses the theory of constitutive equations in some detail. A paper [7] published in the present proceedings presents some of the more recent constitutive theories of nonlinear viscoelasticity. To cite examples and to provide materials for reference in our succeeding discussions, we list below three general types of nonlinear viscoelastic continua. In these examples, thermal or other non-mechanical effects are not taken into account.

Hygrosteric materials [8].—These materials are nonlinear generalizations of the classical Maxwell material and may be characterized by the following constitutive equation.

$$\overset{*}{\bar{t}} + \bar{t}w - w\bar{t} = a_1 I + a_2 d + a_3 d^2 + a_4 \bar{t} + a_5 \bar{t}^2 + a_6(\bar{t}d + d\bar{t})$$
$$+ a_7(\bar{t}^2 d + d\bar{t}^2) + a_8(\bar{t}d^2 + d^2\bar{t}) + a_9(\bar{t}^2 d^2 + d^2\bar{t}^2) \tag{2.4}$$

where $\bar{t}$, w and d are respectively the extra stress (also called the deviatoric stress), the spin and the deformation rate matrices defined according to

$$\bar{t}: \qquad \bar{t}_{km} \equiv \bar{p}\delta_{km} + t_{km}$$
$$w: \qquad 2w_{km} \equiv v_{k,\,m} - v_{m,\,k} \tag{2.5}$$
$$d: \qquad 2d_{km} \equiv v_{k,\,m} + v_{m,\,k}$$

and $a_1, a_2, \ldots, a_9$ are in general polynomials in the joint scalar invariants of $\bar{t}$ and d. In (2.5), $\bar{p} = -\frac{1}{3}\,\text{tr}\,t = -\frac{1}{3}\,t_{mm}$ is the mean hydrostatic pressure and δ_{km} is the Kronecker delta.

Rivlin–Ericksen materials [9]. These materials which include as special case a nonlinear generalization of the Voigt–Kelvin viscoelastic materials are defined by the following constitutive equation.

$$t = f(,c^{-1}\,a_1, a_2, \ldots, a_n) \tag{2.6}$$

where $\mathbf{f}$ denotes some general tensor functions of the deformation tensor $\mathbf{c}^{-1}$ and the n acceleration tensors $\mathbf{a}_1$, $\mathbf{a}_2$, . . . , $\mathbf{a}_n$ frequently referred to as the Rivlin–Ericksen tensors. These second order kinematic tensors are defined according to

$$\mathbf{c}^{-1}: \qquad c_{km}^{-1} \equiv x_{k,\ M}\ x_{m,\ M}$$
$$\mathbf{a}_1: \quad (a_1)_{km} \equiv 2d_{km} \equiv v_{k,\ m} + v_{m,\ k} \qquad\qquad (2.7)$$
$$\mathbf{a}_n: \quad (a_n)_{km} \equiv (\dot{a}_{n-1})_{km} + (a_{n-1})_{kp}v_{p,\ m} + (a_{n-1})_{pm}v_{p,\ k}$$

where the subscripts n and $n-1$ in $(2.7)_3$ denote the order, respectively the nth and $(n-1)$th orders, of the Rivlin–Ericksen tensors. It might be mentioned here that for the case $\mathbf{a}_2$, . . . , $\mathbf{a}_n$ all identically zero, we have the equation for a general nonlinear Voigt–Kelvin material.

Simple materials [10].—Materials characterized by a dependence of the stress tensor $\mathbf{t}$ at time t on the history of the motion of the body up to that time t have been called *simple* and are defined by the following constitutive equation

$$\mathbf{t}(t) = \mathscr{F}_{\tau-0}^{\infty} [\mathbf{c}_t(t-\tau)] \qquad\qquad (2.8)$$

where $\mathscr{F}$ is some general isotropic functional of the deformation tensor function $\mathbf{c}_t(t-\tau)$ taken with respect to the configuration at time t. In other words, the constitutive functional $\mathscr{F}$ is determined by the history of $\mathbf{c}_t$ and satisfies certain isotropy conditions, $\mathbf{c}_t$ being defined by

$$\mathbf{c}_t(t-\tau): \quad c_{km} \equiv \chi_{\mu,\ k}\ \chi_{\mu,\ m} \qquad\qquad (2.9)$$

where $\chi_{\mu,\ k}$ is the deformation gradient at time τ at the spatial point $\chi \equiv (\chi_\mu) \equiv (\chi_1, \chi_2, \chi_3)$ taken with respect to the configuration at time t.

In addition to the three classes of materials defined above there are several other types of nonclassical viscoelastic materials that have been studied by various authors. We take particular note of a generalization proposed by Oldroyd [11], not only due to the simplicity of the theory, but also due to the fact that this study was among the earlier attempts in the rational development of a general viscoelasticity theory employing now familiar invariance principles. These materials, which we shall refer to as the *Oldroyd materials*, are defined by constitutive equations of the form

$$\left(1 + \lambda \frac{\delta}{\delta t}\right) \bar{\mathbf{t}} = 2\,\mu \left(1 + \nu \frac{\delta}{\delta t}\right) \mathbf{d} \qquad\qquad (2.10)$$

where λ, μ and ν are scalar material constants and $\bar{\mathbf{t}}$ and $\mathbf{d}$ are respectively the extra stress and deformation rate tensors defined in (2.5)) The operator $\delta/\delta t$ denotes a convected derivative, the derivative $\delta \bar{\mathbf{t}}/\delta t$ sometimes referred to as the *Oldroyd stress rate*, may be expressed in curvilinear coordinates in terms of either

the covariant tensor components $\bar{t}_{km}$ of $\bar{t}$ or the contravariant components $\bar{t}^{km}$ or mixed components $\bar{t}^{k}_{m}$ according to

$$\frac{\delta \bar{t}_{km}}{\delta t} \equiv \dot{\bar{t}}_{km} + v^{a}_{;k} \bar{t}_{am} + v^{a}_{;m} \bar{t}_{ka}$$

$$\frac{\delta \bar{t}^{km}}{\delta t} \equiv \dot{\bar{t}}^{km} - v^{k}_{;a} \bar{t}^{am} - v^{m}_{;a} \bar{t}^{ka} \qquad (2.11)$$

$$\frac{\delta \bar{t}^{k}_{m}}{\delta t} \equiv \dot{\bar{t}}^{k}_{m} - v^{k}_{;a} \bar{t}^{a}_{m} + v^{a}_{;m} \bar{t}^{k}_{a}$$

where the semi-colon (;) preceding a subscript denotes covariant partial differentiation. The convected derivative $\delta \mathbf{d}/\delta t$ is analogously defined.

Equation (2.10) is a generalization of the equation characterizing a colloidal suspension model of Hookean elastic spherical particles suspended in a Newtonian viscous fluid. The Oldroyd material behaves more like a Maxwell medium as ν approaches zero and reduces to a Newtonian fluid of viscosity μ as λ and ν tend to equality.

The basic field equations (2.1) to (2.3) and a suitable constitutive equation such as those exemplified by (2.4), (2.6) (2.8) and (2.10) form a complete set of equations for the analysis of a mechanical problem. The explicit solution of the problem will of course require the satisfaction of the necessary boundary and initial conditions dictated by the physical situation under consideration.

In cases where non-mechanical effects are significant, it will be necessary to take into account other additional physical concepts, e.g. the principle of conservation of energy and other thermodynamical concepts in considering thermal effects and the principle of conservation of charge in an electromagnetic system. Furthermore, for nonlinear materials, the coupled mechanical and non-mechanical properties of the media must be properly incorporated into the constitutive equations. Obviously these additional considerations further complicate the problem. Thus, although the fundamental equations necessary for the consideration of nonlinear coupled effects have been established (for instance, see refs. [12–15]), only a very insignificant number of problems of these types have been analyzed. In view of the fact that these additional considerations are not pertinent to the discussion of the bulk of the problems presented in the succeeding sections, we shall postpone until later further consideration of non-mechanical effects.

Finally, it must be remarked that although the theory of nonlinear viscoelasticity now appears to be well-founded, no existence and uniqueness theorems have been developed in nonlinear viscoelasticity. We recognize the difficulty of the task and draw whatever little comfort we can from the knowledge that in spite of the comparatively long history of classical viscoelasticity it is only recently that such theorems have been discovered in this much older field. (For instance, see refs. [16–19].)

15

2.2. *General Approach*

The constitutive equations that define nonlinear viscoelastic materials are more complicated than those of linear materials* introducing into the analyses of problems certain characteristic complexities. Many mathematical techniques developed for the analysis of problems pertaining to linear viscoelastic materials are no longer directly applicable to nonlinear viscoelasticity problems. To cite an example, the principle of superposition is invalid in nonlinear viscoelasticity. More significantly, a counterpart to as powerful an analytical tool as the correspondence principle of linear viscoelasticity has not been discovered in nonlinear viscoelasticity.

Instead, many of the problems solved in nonlinear viscoelasticity employ the semi-inverse method widely used in finite elasticity and other branches of applied mechanics. By this method, general forms of the independent field variables of the constitutive equations are prescribed, consistent with given boundary and initial conditions. To illustrate, if the motion of the medium is assumed, it is possible to determine corresponding expressions for the kinematic variables, e.g. c^{-1}, d, a_1. a_2, . . . , according to the definitions given in Section 2.1. With the application of the constitutive equations, expressions for the dependent variables (e.g. t in eqn. (2.6) for the Rivlin–Ericksen material) are obtained. These expressions are then substituted into the field equations (2.1) to (2.3). In certain cases (for example, the rectilinear flow of a Rivlin–Ericksen fluid [20]), the dynamical equations are automatically satisfied and the problem is completely solved. Usually this is not the case. Then it remains to solve these equations subject to the prescribed boundary and initial conditions.

For a large class of simple problems, the partial differential equations that form the set of dynamical equations are solved exactly using standard mathematical techniques, for example, refs. [8, 20, 21]. However, for more complex physical problems, solutions to the differential equations are not apparent nor readily obtained. In these cases, one may resort to some approximation methods.

One approach is to replace the general constitutive theory by an approximate theory. For example, eqn. (2.8) may be approximated by a second-order theory simplified further by an assumption of incompressibility [22]:

$$t = -p\mathbf{I} + a_1\mathbf{a} + a_2\mathbf{a}_1^2 + a_3\mathbf{a}_2 \qquad (2.12)$$

where p is the undetermined hydrostatic pressure and a_1 and a_2 are respectively the Rivlin–Ericksen tensors. The dynamical equations for the specific problem can then be formulated; these are generally simpler and more amenable to solution than those which would have resulted were the general nonlinear constitutive theory used. These simplified equations are solved "exactly", yielding some approximate results to the problem, second-order results in the above example. (For instance, see Ting [23].)

---

* The constitutive formulation of simple materials (2.8) appears to be rather simple. However, in actual situations, even in such simple cases as viscometric flows, the equations for these materials assume forms which are certainly more complicated than those for linear viscoelastic materials.

The determination of higher order effects would, of course, necessitate the consideration of a higher order constitutive theory which would expectedly require the consideration of a more complicated set of equations. In this case and in problems where even a low order approximate constitutive theory does not yield easily solved equations, one may have to employ some further approximating methods (e.g. perturbation). For instance, see Koh and Eringen [12] and Langlois [24].

2.3. *Exact Solution—Couette Flow of Two Oldroyd Viscoelastic Fluids*

In general, the basic differential equations that must be solved in a problem on the deformation or flow of a nonlinear viscoelastic material are not readily reduced to forms amenable to known mathematical analysis, and closed-form solutions are generally unavailable. However, there exist some simple but significant problems which may be solved exactly without much difficulty. To illustrate the general approach employed in solving these problems, we discuss here the Couette flow of two types of Oldroyd viscoelastic fluids [11]. The choice of these particular problems is made not only to demonstrate the simplicity of the analysis, but more significantly to emphasize in a simple example how two seemingly similar materials may exhibit entirely different responses to identical physical situations.

The Oldroyd materials are characterized by equations of the general form (2.10). Of the many possible explicit forms that one may select from this general class of equations, let us consider the following two equations defining two ideal incompressible materials which we will identify respectively as fluid I and fluid II:

$$\text{I:} \quad \bar{t}_{km} + \lambda \left(\frac{\partial \bar{t}_{km}}{\partial t} + v^j \bar{t}_{km;j} + v^j_{;k} \bar{t}_{jm} + v^j_{;m} \bar{t}_{kj} \right)$$
$$= 2\mu d_{km} + 2\mu\tau \left(\frac{\partial d_{km}}{\partial t} + v^j d_{km;j} + v^j_{;k} d_{jm} + v^j_{;m} d_{kj} \right) \tag{2.13}$$

and

$$\text{II:} \quad \bar{t}^{km} + \lambda \left(\frac{\partial \bar{t}^{km}}{\partial t} + v^j \bar{t}^{km}_{;j} - v^k_{;j} \bar{t}^{jm} - v^m_{;j} \bar{t}^{kj} \right)$$
$$= 2\mu d^{km} + 2\mu\tau \left(\frac{\partial d^{km}}{\partial t} + v^j d^{km}_{;j} - v^k_{;j} d^{jm} - v^m_{;j} d^{kj} \right) \tag{2.14}$$

The Couette flow is a two-dimensional steady flow of a fluid between two vertical coaxial circular cylinders and may be described in a Cartesian system by the following velocity field:

$$\mathbf{v} = (v_k) = (v^k) = [-y\omega(r), \, x\omega(r), \, 0] \tag{2.15}$$

where the z-axis is taken to be in the direction of the axis of the cylinders. Using (2.15) in the definition (2.5)$_3$, we obtain the components of the deformation rate

tensor in the rectangular Cartesian system

$$\mathbf{d} = [d_{km}] = [d^{km}] = \frac{d\omega}{dr} \begin{bmatrix} -\dfrac{xy}{r} & \dfrac{x^2 - y^2}{2r} & 0 \\[2mm] \dfrac{x^2 - y^2}{2r} & \dfrac{xy}{r} & 0 \\[2mm] 0 & 0 & 0 \end{bmatrix} \qquad (2.16)$$

The rectangular components of the extra stress tensor are also expressible in terms of the physical components of this tensor in the cylindrical coordinate system $(r,\ \theta,\ z)$ according to the following

$$\bar{\mathbf{t}} = [\bar{t}_{km}] = [\bar{t}^{km}]$$

$$= \frac{1}{r^2} \begin{bmatrix} x^2\bar{t}_{rr} + y^2\bar{t}_{\theta\theta} - 2xy\bar{t}_{r\theta} & xy(\bar{t}_{rr} - \bar{t}_{\theta\theta}) + (x^2 - y^2)\bar{t}_{r\theta} & 0 \\[2mm] xy(\bar{t}_{rr} - \bar{t}_{\theta\theta}) + (x^2 - y^2)\bar{t}_{r\theta} & y^2\bar{t}_{rr} + x^2\bar{t}_{\theta\theta} + 2xy\bar{t}_{r\theta} & 0 \\[2mm] 0 & 0 & r^2\bar{t}_{zz} \end{bmatrix}$$

$$(2.17)$$

It must be remarked that here the components $\bar{t}_{xz}$ and $\bar{t}_{yz}$ are taken to be identically zero. (Noll [8] makes a similar assumption in his analysis of the Couette flow of a special type of hygrosteric materials; however, Rivlin [20] and Coleman and Noll [21] show that these components are indeed zero for Rivlin–Ericksen and simple fluids in a flow defined by (2.15) above).

If the rectangular system is rotated so that at the point of the fluid under consideration the x-axis coincides with the radial axis, $x = r$ and $y = 0$. The physical components of the deformation rate and stress tensors in the cylindrical system are then given by

$$\mathbf{d} = \tfrac{1}{2}r\frac{d\omega}{dr} \begin{bmatrix} 0 & 1 & 0 \\ 1 & 0 & 0 \\ 0 & 0 & 0 \end{bmatrix}; \qquad \bar{\mathbf{t}} = \begin{bmatrix} \bar{t}_{rr} & \bar{t}_{r\theta} & 0 \\ \bar{t}_{r\theta} & \bar{t}_{\theta\theta} & 0 \\ 0 & 0 & \bar{t}_{zz} \end{bmatrix} \qquad (2.18)$$

Using (2.18) in the constitutive equations (2.13) and (2.14), we obtain respectively for fluids I and II the following equations

(I) $\quad \bar{t}_{rr} + 2\lambda r \dfrac{d\omega}{dr} \bar{t}_{r\theta} = 2\mu\tau r^2 \left(\dfrac{d\omega}{dr}\right)^2$

$$(2.19)$$

$\quad \bar{t}_{r\theta} + \lambda r \dfrac{d\omega}{dr} \bar{t}_{\theta\theta} = \mu r \dfrac{d\omega}{dr}$

$\quad \bar{t}_{\theta\theta} = \bar{t}_{zz} = 0$

(II) $\quad \bar{t}_{\theta\theta} - 2\lambda r \dfrac{d\omega}{dr} \bar{t}_{r\theta} = -2\mu\tau r^2 \left(\dfrac{d\omega}{dr}\right)^2$

$$(2.20)$$

$\quad \bar{t}_{r\theta} - \lambda r \dfrac{d\omega}{dr} \bar{t}_{rr} = \mu r \dfrac{d\omega}{dr}$

$\quad \bar{t}_{rr} = \bar{t}_{zz} = 0$

Equation (2.1) reduces to the condition of incompressibility for the given velocity field. Equation (2.3) is automatically satisfied as seen in (2.17). Finally, from (2.2) we have the equations of motion which are conveniently expressed as follows:

$$\frac{\partial \bar{t}_{rr}}{\partial r} + \frac{\bar{t}_{rr} - \bar{t}_{\theta\theta}}{r} = \frac{\partial \bar{p}}{\partial r} - \rho r \omega^2$$

$$\frac{\partial \bar{t}_{r\theta}}{\partial r} + \frac{2\bar{t}_{r\theta}}{r} = 0 \qquad (2.21)$$

$$\frac{\partial \bar{t}_{zz}}{\partial z} = \frac{\partial \bar{p}}{\partial z} + \rho g$$

where z is measured positive upwards and g is the acceleration of gravity. The system of equations (2.21) with (2.19) for fluid I, or (2.21) with (2.20) for fluid II, is then solved for the unknown functions of r, namely $\bar{t}_{rr}$, $\bar{t}_{\theta\theta}$, $\bar{t}_{zz}$, $\bar{t}_{r\theta}$, ω and $\bar{p}$. It is easily seen that the *exact* solutions of these two sets of equations are:

(I) $\quad \bar{t}_{rr} = -8\mu(\lambda - \tau) b^2 r^{-4}; \quad \bar{t}_{\theta\theta} = \bar{t}_{zz} = 0; \quad \bar{t}_{r\theta} = 2\mu b r^{-2}$

$\qquad \omega = a - b r^{-2}; \quad \bar{p} = \rho \left(\frac{1}{2} a^2 r^2 - 2ab \log r - \frac{1}{2} b^2 r^{-2} \right)$

$$- 6\mu(\lambda - \tau) b^2 r^{-4} - g\rho z + c \qquad (2.22)$$

(II) $\quad \bar{t}_{rr} = \bar{t}_{zz} = 0; \quad \bar{t}_{\theta\theta} = 8\mu(\lambda - \tau) b^2 r^{-4}; \quad \bar{t}_{r\theta} = 2\mu b r^{-2}$

$\qquad \omega = a - b r^{-2}; \quad \bar{p} = \rho(\frac{1}{2} a^2 r^2 - 2ab \log r - \frac{1}{2} b^2 r^{-2})$

$$+ 2\mu(\lambda - \tau) b^2 r^{-4} - g\rho z + c \qquad (2.23)$$

where a, b, and c are constants, with

$$b = r_1^2 r_2^2 (r_2^2 - r_1^2)^{-1} (\omega_2 - \omega_1)$$

and r_2, ω_2 are respectively the radius and angular velocity of the external cylinder, and r_1, ω_1 correspond to those of the internal cylinder. The boundary conditions imposed are such that at the bounding cylinders, ω takes on the values of the constant angular velocities of these cylinders.

To demonstrate an interesting result of this analysis, we consider the special case of stationary external cylinder, i.e. $\omega_2 = 0$. Furthermore, if the fluids are sufficiently viscous such that for $(\lambda > \tau)$, the factor $\mu(\lambda - \tau)$ is large compared to ρr_2^2, the expressions for $\bar{p}$ in (2.22) and (2.23) are respectively approximated by the following quantitities:

(I) $\qquad\qquad\qquad \bar{p} = -6\mu(\lambda - \tau) b^2 r^{-4} + A$

$$\qquad\qquad (2.24)$$

(II) $\qquad\qquad\qquad \bar{p} = 2\mu(\lambda - \tau) b^2 r^{-4} + A$

Therefore, the normal stress in the z-direction required to maintain the motion steady and two-dimensional is

$$t_{zz} = -\bar{p} + \bar{t}_{zz} \simeq 6\mu(\lambda - \tau) b^2 r^{-4} + A \qquad (2.25)$$

in fluid I, and

$$t_{zz} = -\bar{p} + \bar{t}_{zz} \simeq -2\mu(\lambda - \tau) b^2 r^{-4} + A \qquad (2.25)_2$$

in fluid II, where in both cases A is a negative constant. Clearly, since the normal pressure necessary to maintain the prescribed two-dimensional steady flow increases with r for fluid I and decreases with r for fluid II, we would expect the two fluids to behave differently were these constraining normal forces suddenly removed and the fluid given a free horizontal surface: fluid I would tend to rise near the stationary external cylinder and fall near the inner cylinder, while fluid II would have the opposite tendency of rising near the inner cylinder and falling near the outer cylinder. These theoretical considerations form what appears to be a basis for explaining the interesting results of the now well-known Weissenberg experiments [2].

2.4. *Approximate Solution—Slow Viscoelastic Flow*

Exact solutions have been found to only a limited number of classes of problems in nonlinear viscoelasticity where the constitutive equations used in the analysis are *exact* (in the sense that no approximation has been introduced in the general constitutive theory). To obtain closed-form solutions to certain specific problems, some investigators (e.g. Koh and Eringen [12; p. 218], Ting [23] and Markovitz and Coleman [25]) found it necessary to consider constitutive equations which are approximations of more general theories.

This is a reasonable procedure since in numerous practical problems low order approximations may suffice in the theoretical consideration of the observed nonlinear effects or in the prediction of other nonclassical behavior. Apart from this approximation introduced in the constitutive equations, the analysis of the problem under consideration may proceed as discussed in the preceding section. With the application of some standard mathematical methods, an exact solution to the "approximate" basic equations is obtained.

There are, however, problems where the governing differential equations are not tractable in spite of the use of an approximate constitutive theory. In these cases further approximation may be the only obvious recourse. Koh and Eringen [12] (p. 219) in their analysis of a problem dealing with a heat-conducting, second order hygrosteric material applied a simple perturbation method, the zeroth order of the solution reducing conveniently to the case of the non-heat-conducting fluid analyzed by Noll [8]. To demonstrate how similar methods may be applied to other problems in nonlinear viscoelasticity, we present here a discussion of a formulation for slow nonlinear viscoelastic flows. We make free use of the results derived by Langlois [26].

Although the method is equally applicable to other types of materials, we consider for our example the Rivlin–Ericksen viscoelastic fluid. The constitutive equation for this material is given by (2.6) with the exception that the dependence of the stress tensor $\mathbf{t}$ on the deformation tensor $\mathbf{c}^{-1}$ is suspended for the fluid. (It must be realized that this is a physical postulate and not a mathematical approximation.) Thus, the constitutive equation for the incompressible fluid may be expressed as follows:

$$\mathbf{t} = -p\mathbf{I} + \mathbf{f}(\mathbf{a}_1, \mathbf{a}_2, \ldots, \mathbf{a}_n) \qquad (2.26)$$

where p is the hydrostatic pressure, and $\mathbf{a}_1, \mathbf{a}_2, \ldots, \mathbf{a}_n$ are the Rivlin–Ericksen tensors defined in (2.7). Furthermore, under appropriate hypothesis (viz., the stress is expressible as a polynomial in the gradients of velocity, acceleration, $\ldots, (n-1)$th acceleration), the stress matrix may then be expressed as a matrix polynomial in the matrices $\mathbf{a}_1, \mathbf{a}_2, \ldots, \mathbf{a}_n$, with coefficients which are polynomials in the joint scalar invariants of these matrices. Thus, (2.26) specializes to the form

$$\mathbf{t} = -p\mathbf{I} + [a_1 + a_2 \operatorname{tr} \mathbf{a}_1^2 + a_3 \operatorname{tr} \mathbf{a}_2] \mathbf{a}_1 + a_4 \mathbf{a}_1^2 + a_5 \mathbf{a}_2$$
$$+ a_6 \mathbf{a}_3 + a_7(\mathbf{a}_1 \mathbf{a}_2 + \mathbf{a}_2 \mathbf{a}_1) + \text{higher order terms} \qquad (2.27)$$

where $a_1, a_2, \ldots, a_7$ are constants, and $\operatorname{tr} \mathbf{a}_1^2$ and $\operatorname{tr} \mathbf{a}_2$ are respectively the traces of $\mathbf{a}_1^2$ and $\mathbf{a}_2$. In (2.27) only the third order terms are shown. The term $\mathbf{a}_1^3$ is not explicitly indicated since by the Cayley–Hamilton theorem this term is expressible in terms of $\mathbf{a}_1$, $\mathbf{a}_1^2$ and their respective traces together with $\det \mathbf{a}_1$. For the incompressible case, we have, of course, $\operatorname{tr} \mathbf{a}_1 = 0$ also.

We consider the case of the Rivlin–Ericksen fluid in a steady state flow, slow enough to allow assumption of the following forms for velocity and pressure

$$v_i = \epsilon v_i^{(1)} + \epsilon^2 v_i^{(2)} + \epsilon^3 v_i^{(3)} + \cdots \qquad (2.28)$$

$$p = \text{constant} + \epsilon\, p^{(1)} + \epsilon^2 p^{(2)} + \epsilon^3 p^{(3)} + \cdots \qquad (2.29)$$

where ϵ is a small dimensionless constant. Using (2.28) in (2.7), we obtain the following expressions for the Rivlin–Ericksen tensors:

$$\begin{aligned}
\mathbf{a}_1 &= \epsilon \mathbf{A} + \epsilon^2 \mathbf{D} + \epsilon^3 \mathbf{F} + 0(\epsilon^4) \\
\mathbf{a}_2 &= \epsilon^2 \mathbf{B} + \epsilon^3 \mathbf{E} + 0(\epsilon^4) \\
\mathbf{a}_3 &= \epsilon^3 \mathbf{C} + 0(\epsilon^4) \\
\mathbf{a}_j &= 0(\epsilon^4) \quad \text{for } j > 3
\end{aligned} \qquad (2.30)$$

where $\mathbf{A}, \mathbf{B}, \mathbf{C}, \mathbf{D}, \mathbf{E}$ and $\mathbf{F}$ are 3×3 matrices defined respectively as follows:

$$\begin{aligned}
\mathbf{A} &\equiv [A_{ij}] \equiv [v_{i,j}^{(1)} + v_{j,i}^{(1)}] \\
\mathbf{B} &\equiv [B_{ij}] \equiv [v_m^{(1)} A_{ij,m} + A_{im} v_{m,j}^{(1)} + A_{mj} v_{m,i}^{(1)}] \\
\mathbf{C} &\equiv [C_{ij}] \equiv [v_m^{(1)} B_{ij,m} + B_{im} v_{m,j}^{(1)} + B_{mj} v_{m,i}^{(1)}] \\
\mathbf{D} &\equiv [D_{ij}] \equiv [v_{i,j}^{(2)} + v_{j,i}^{(2)}] \\
\mathbf{E} &\equiv [E_{ij}] \equiv [v_m^{(1)} D_{ij,m} + v_m^{(2)} A_{ij,m} + D_{im} v_{m,j}^{(1)} \\
&\qquad\qquad + A_{im} v_{m,j}^{(2)} + D_{mj} v_{m,i}^{(1)} + A_{mj} v_{m,i}^{(2)}] \\
\mathbf{F} &\equiv [F_{ij}] \equiv [v_{i,j}^{(3)} + v_{j,i}^{(3)}]
\end{aligned} \qquad (2.31)$$

Using (2.29) and (2.30) in (2.27), we obtain the following expression for stress:

$$\begin{aligned}
\mathbf{t} = {}& \epsilon[-p^{(1)}\mathbf{I} + \mu\mathbf{A}] + \epsilon^2[-p^{(2)}\mathbf{I} - \mu\mathbf{D} + \lambda\mathbf{A}^2 + \nu\mathbf{B}] \\
&+ \epsilon^3[-p^{(3)}\mathbf{I} + \mu\mathbf{F} + \lambda(\mathbf{AD} + \mathbf{DA}) + \nu\mathbf{E} \\
&+ a(\operatorname{tr}\mathbf{B})\mathbf{A} + \beta(\mathbf{AB} + \mathbf{BA}) + \gamma\mathbf{C}] + 0(\epsilon^4)
\end{aligned} \qquad (2.32)$$

where $\lambda, \mu, \nu, a, \beta, \gamma$ are the material constants of the fluid and are related to the constants of (2.27). For instance, μ in (2.32) is equal to a_1 in (2.27).

We now substitute (2.32) and (2.28) into the field equations (2.1) and (2.2) to obtain the equations of motion. To illustrate, we give below the pertinent equations for a third-order approximation.

Such an analysis, for that matter an analysis in any degree of approximation, starts with the first-order approximate equations. By the procedure indicated above, neglecting the inertia terms and considering the body forces equal to zero, we have the following first-order equations which are in fact the equations for a Newtonian fluid in slow steady flow:

$$v_{i,i}^{(1)} = 0$$
$$p_{,i}^{(1)} - \mu v_{i,jj}^{(1)} = 0 \tag{2.33}$$

Similarly, we have the second-order corrections

$$v_{i,i}^{(2)} = 0$$
$$p_{,i}^{(2)} - \mu v_{i,jj}^{(2)} = \lambda(A_{im}A_{mj})_{,j} + \nu B_{ij,j} \tag{2.34}$$

and those for the third-order approximation

$$v_{i,i}^{(3)} = 0$$
$$p_{,i}^{(3)} - \mu v_{i,jj}^{(3)} = \lambda(A_{ik}D_{kj} + D_{ik}A_{kj})_{,j} \tag{2.35}$$
$$+ \nu E_{ij,j} + \alpha(B_{kk}A_{ij})_{,j} + \beta(A_{ik}B_{kj} + B_{ik}A_{kj})_{,j} + \gamma C_{ij,j}$$

The application of the above equations in a specific problem is quite simple. Equations (2.33) are solved for $v_i^{(1)}$ and $p^{(1)}$ satisfying exactly the boundary conditions of the given problem. These results are used in (2.34), which may then be solved for $v_i^{(2)}$ and $p^{(2)}$ satisfying corresponding homogeneous boundary conditions. Finally, using the calculated values of $v_i^{(1)}$ and $v_i^{(2)}$, one solves (2.35) for the third-order flow field $v_i^{(3)}$ and $p^{(3)}$ subject to appropriate homogeneous boundary conditions. By (2.28), (2.29) and (2.32), one is able to calculate the stress field to a third-degree of approximation.

No particular difficulty is encountered in the analysis since each system of dynamical equations, (2.33), (2.34) or (2.35), is linear at each stage of the analysis. System (2.33) corresponds to the classical case, while (2.34) and (2.35) are similar except that nonhomogeneous terms involving the solution(s) of the preceding system(s) are present in these succeeding systems.

Should it be desired or necessary to extend the analysis to higher degrees of approximation,* no difficulty is anticipated. However, one should be reminded that a higher order of approximation involves a larger number of material constants, viz., one in the first order approximation, three in the second order, six in the third order, fourteen in the fourth order [27], etc.

The above equations have been determined for a rectangular Cartesian frame of reference. Langlois [28] has recently derived the corresponding expressions in curvilinear coordinates.

---

* Langlois and Rivlin [27] found it necessary to apply a fourth-order approximation in their analysis of secondary flows in non-circular tubes since the third order theory failed to predict these phenomena.

Finally, it must be remarked that these approximation methods lack the elegance of other mathematical techniques which yield closed-form solutions. There are also inherent assumptions in the approximate analysis that render the solution rather restrictive. For example, in the discussions presented above the flow is assumed to be slow, in a steady state and with inertia terms negligible. Nevertheless, an approximate solution to an intricate problem for which no exact solution is available will have to suffice until better solutions are obtained.

3. MECHANICAL BEHAVIOR
OF NONLINEAR VISCOELASTIC MATERIALS

With the exception of a few, the problems solved in nonlinear viscoelasticity consider the behavior of the material only under purely mechanical influences. Although it has been recognized for a long time now that viscoelastic materials are quite sensitive to certain nonmechanical environmental changes, such as thermal variations, as indicated by the volume of experimental and theoretical work published on these topics in linear viscoelasticity, it is only during the past few years that investigators have begun to study these important coupled effects for nonlinear materials.

The discussions in this section will be limited to purely mechanical situations. In the next section, we will include in our consideration non-mechanical effects as well. In order to keep this paper within reasonable length, discussions in these sections will be confined to the more significant results available in the literature.

3.1. Steady Shear Flow of Viscoelastic Fluids

The Rivlin–Ericksen viscoelastic fluid is characterized by a constitutive equation of the form (2.26) which assumes that the fluid is incompressible. In its general form, the stress tensor is a function of n kinematic tensor variables, the Rivlin–Ericksen tensors. Under certain assumptions, it is possible to express this constitutive function as a polynomial in the n variables with coefficients which are polynomials in the joint scalar invariants of these variables. Without further elaboration, one can see that such a general theory as this can prove unwieldy when applied to specific problems even when one *assumes* the dependence of stress on only a few of these variables. It is, therefore, significant when Rivlin [20] noted that for certain types of steady laminar flow the kinematic variables a_i are identically zero for $i > 2$. Thus, in these cases, the stress matrix is expressible as a polynomial in only the first two Rivlin–Ericksen matrices. Explicitly, for these cases the constitutive equation assumes the form

$$\mathbf{t} = p\mathbf{I} + a_1\mathbf{a}_1 + a_2\mathbf{a}_2 + a_3\mathbf{a}_1^2 + a_4\mathbf{a}_2^2 + a_5(\mathbf{a}_1\mathbf{a}_2 + \mathbf{a}_2\mathbf{a}_1)$$
$$+ a_6(\mathbf{a}_1^2\mathbf{a}_2 + \mathbf{a}_2\mathbf{a}_1^2) + a_7(\mathbf{a}_1\mathbf{a}_2^2 + \mathbf{a}_2^2\mathbf{a}_1) + a_8(\mathbf{a}_1^2\mathbf{a}_2^2 + \mathbf{a}_2^2\mathbf{a}_1^2) \quad (3.1)$$

where $a_1, a_2, \ldots, a_8$ are in general polynomials in the scalar invariants tr $\mathbf{a}_1^2$, tr $\mathbf{a}_1^3$, tr $\mathbf{a}_2^2$, tr $\mathbf{a}_2^3$, tr $\mathbf{a}_1\mathbf{a}_2$, tr $\mathbf{a}_1^2\mathbf{a}_2$, tr $\mathbf{a}_1\mathbf{a}_2^2$ and tr $\mathbf{a}_2^2\mathbf{a}_1^2$. (For a compressible material,

the constitutive coefficients should also depend on tr $\mathbf{a}_1$ and tr $\mathbf{a}_2$. However, on the assumption of incompressibility, tr $\mathbf{a}_1 = 0$ and tr $\mathbf{a}_2 = $ tr $\mathbf{a}_1^2$.)

To illustrate the reduction of (2.26) to (3.1) for a special case, let us consider the helical flow of the fluid between two coaxial cylinders of radii r_1 and $r_2(r_1 > r_2)$. These cylinders are assumed to rotate about their common axis at constant angular velocities Ω_1 and Ω_2, respectively. A constant pressure gradient p_0 also exists in the fluid in the direction of the axis of the cylinders. Each particle of the fluid moves along a helical path about this axis and its velocity is given by

$$v_x = -\omega y, \quad v_y = \omega x \quad \text{and} \quad v_z = u \tag{3.2}$$

where ω is the angular velocity about the cylinder axis and u is the velocity component parallel to this axis, both ω and u being functions of only the radial distance r from the axis. The exact solution to the problem is obtained by the method indicated in Section 2.3. We now proceed to show this.

Substituting (3.2) in (2.7), we obtain

$$\mathbf{a}_1 = \begin{bmatrix} -2\dfrac{xy}{r}\omega' & \dfrac{x^2 - y^2}{r}\omega' & \dfrac{x}{r}u' \\[2mm] \dfrac{x^2 - y^2}{r}\omega' & 2\dfrac{xy}{r}\omega' & \dfrac{y}{r}u' \\[2mm] \dfrac{x}{r}u' & \dfrac{y}{r}u' & 0 \end{bmatrix}$$

$$\mathbf{a}_2 = \begin{bmatrix} 2x^2(\omega'^2 + u'^2/r^2) & 2xy(\omega'^2 + u'^2/r^2) & 0 \\[2mm] 2xy(\omega'^2 + u'^2/r^2) & 2y^2(\omega'^2 + u'^2/r^2) & 0 \\[2mm] 0 & 0 & 0 \end{bmatrix} \tag{3.3}$$

$$\mathbf{a}_i = 0 \text{ for } i > 2$$

where $\omega' \equiv d\omega/dr$ and $u' \equiv du/dr$. By a suitable choice of rectangular coordinates at the point of the fluid (see Section 2.3), matrices (3.3) may be expressed as

$$\mathbf{a}_1 = \begin{bmatrix} 0 & r\omega' & u' \\ r\omega' & 0 & 0 \\ u' & 0 & 0 \end{bmatrix}; \quad \mathbf{a}_2 = 2(r^2\omega'^2 + u'^2)\begin{bmatrix} 1 & 0 & 0 \\ 0 & 0 & 0 \\ 0 & 0 & 0 \end{bmatrix} \tag{3.4}$$

Substituting (3.4) in the constitutive equation (3.1), we obtain the following expressions for the stress components in terms of ω' and u'.

$$\begin{aligned} t_{rr} &= -p + (2a_2 + a_3)\kappa^2 + 4(a_4 + a_6)\kappa^4 + 8a_8\kappa^6 \\ t_{\theta\theta} &= +p + a_3 r^2\omega'^2; \quad t_{zz} = -p + a_3 u'^2 \\ t_{\theta z} &= a_3 \, r\omega'u' \\ t_{rz} &= u'[a_1 + 2a_5\kappa^2 + 4a_7\kappa^4] \\ t_{r\theta} &= r\omega'[a_1 + 2a_5\kappa^2 + 4a_7\kappa^4] \end{aligned} \tag{3.5}$$

where the hydrostatic pressure p is a function of r and z only and $\kappa^2 = r^2\omega'^2 + u'^2$.

On the other hand, the dynamical equations for this case (with the assumption of zero body forces) take the form

$$\frac{\partial t_{rr}}{\partial r} + \frac{t_{rr} - t_{\theta\theta}}{r} = -\rho r \omega^2$$

$$\frac{\partial t_{r\theta}}{\partial r} + \frac{2}{r} t_{r\theta} = 0 \qquad\qquad (3.6)$$

$$\frac{\partial t_{rz}}{\partial r} + \frac{1}{r} \frac{\partial t_{r\theta}}{\partial r} + \frac{\partial t_{zz}}{\partial z} = 0$$

An elementary analysis of system $(3.6)_{2,\ 3}$, making use of pertinent expressions of (3.5) and the assumption that pressure gradient p_0 exists, yields the following system of first-order differential equations in u and ω subject to the boundary conditions: at $r = r_1$, $u = 0$ and $\omega = \Omega_1$; at $r = r_2$, $u = 0$ and $\omega = \Omega_2$.

$$u'[a_1 + 2a_5\kappa^2 + 4a_7\kappa^4] = \tfrac{1}{2} p_0 r + \frac{A}{r}$$

$$\omega'[a_1 + 2a_5\kappa^2 + 4a_7\kappa^4] = \frac{B}{r^3} \qquad\qquad (3.7)$$

where A and B are constants of integration. From (3.5) and $(3.6)_1$ we also have

$$\frac{\partial p}{\partial r} = \rho r \omega^2 + \frac{\partial}{\partial r} [(2a_2 + a_3)\kappa^2 + 4(a_4 + a_6)\kappa^4 + 8a_8\kappa^6]$$

$$+ \frac{1}{r}[2a_2\kappa^2 + a_3 u'^2 + 4(a_4 + a_6)\kappa^4 + 8a_8\kappa^6] \qquad\qquad (3.8)$$

which integrates to

$$p = (2a_2 + a_3)\kappa^2 + 4(a_4 + a_6)\kappa^4 + 8a_8\kappa^6 + \int^r \rho r \omega^2 dr$$

$$+ \int^r \frac{1}{r} [2a_2\kappa^2 + a_3 u'^2 + 4(a_4 + a_6)\kappa^4 + 8a_8\kappa^6]dr + p_0 z + C \quad (3.9)$$

where C is a constant of integration. Solving (3.7) and (3.9) and using the results in (3.5), we obtain explicit expressions for the stress components.

It is interesting to note that this analysis covers two simpler problems, viz., longitudinal flow between two coaxial cylinders (characterized by the analysis above for $\omega = 0$) and Couette flow (for $u = 0$). By the same method of analysis, Rivlin [20] also determined the solutions for rectilinear laminar flow and for torsional flow between two parallel discs.

The case of shearing of a viscoelastic fluid between a cone and a plate was analyzed by Markovitz and Williamson [29]. In spherical coordinates (r, θ, ϕ) and with the assumption of laminar flow with the conical surfaces $\theta = $ constant as surfaces of constant velocity, the velocity is given by

$$v_r = 0, \qquad v_\theta = 0, \qquad v_\phi = r\omega \qquad\qquad (3.10)$$

where the angular velocity ω is a function of θ but not of r or ϕ. As in the earlier

cases considered by Rivlin, all $\mathbf{a}_i$ are identically zero for $i > 2$, and the constitutive equation for the Rivlin–Ericksen fluid simplifies to (3.1).

The stress components for the cone and plate case are given by

$$t_{rr} = -p$$
$$t_{\theta\theta} = -p + \mu^2[(2a_2 + a_3) + 4\mu^2(a_4 + a_6) + 8\mu^4 a_8]$$
$$t_{\phi\phi} = -p + a_3\mu^2 \tag{3.11}$$
$$t_{\theta\phi} = \mu[a_1 + 2a_5\mu^2 + 4a_7\mu^2]$$
$$t_{r\theta} = t_{r\phi} = 0$$

where μ is the rate of shear, a quantity which is independent of r but dependent on the angular velocity of the cone with respect to the plate and the colatitude θ.

As before, the expressions for the stress obtained from the constitutive equations are substituted in the equations of motion to obtain the basic differential equations of the problem. An analysis of these equations yields a logarithmic dependence of the normal stress on the distance from the axis of rotation, a result supported by experiments with polyisobutylene solutions.

In evaluating several rheological theories that may be applied to the analysis of the flow of specimens in various types of viscometers, Markovitz [30] made the observation that seemingly different types of shear flows may indeed be related to the simple shearing of an infinitesimal cube of the viscoelastic material. In particular, with respect to an orthogonal coordinate system (x_1, x_2, x_3) so chosen that x_2 is the direction of the motion of the particle and $x_3 = $ constant is a surface of constant velocity, the stress field may be expressed in the following form for Rivlin–Ericksen materials.

$$t_{11} = -p$$
$$t_{22} = -p + a_3\dot{\gamma}^2$$
$$t_{33} = -p + \dot{\gamma}^2[(2a_2 + a_3) + 4(a_4 + a_6)\dot{\gamma}^2 + 8a_3\dot{\gamma}^4] \tag{3.12}$$
$$t_{23} = \dot{\gamma}[a_1 + 2a_5\dot{\gamma}^2 + 4a_7\dot{\gamma}^4]$$
$$t_{12} = t_{13} = 0$$

where $\dot{\gamma}$ is the rate of shear. That this is the case is readily seen from the two problems discussed above:

(i) *Couette flow* is derivable from the helical flow by simply letting u, the longitudinal component of velocity, equal to zero. Applying this to (3.5); and equating θ to x_2, the direction of the motion of the fluid particles; and r to x_3, since $r = $ constant is a surface of constant velocity; we obtain an expression of the form (3.12). In this case $\dot{\gamma} = r\omega'$.

(ii) *Longitudinal flow between two coaxial cylinders* is also derivable from the helical flow. This is done by considering ω, the angular velocity in the helical flow, equal to zero. The stress components for this case are also obtainable

from (3.5) and may be expressed in the form (3.12) by proper identification of the variables: $\omega = 0$; $z = x_2$; and $r = x_3$. The rate of shear $\dot{\gamma} = u'$.

(iii) *Cone and plate flow* of a Rivlin–Ericksen fluid yields a stress field given by (3.11). It is readily seen that these equations for stress are indeed of the form (3.12).

The other two problems analyzed by Rivlin [20], namely, the rectilinear laminar shear flow and the torsional flow between two parallel discs, are also characterized by stress fields reducible to the form (3.12).

A most significant result with practical applications to viscometry is obtained from (3.12). In terms of the extra stress components, we have from (3.12)

$$
\begin{aligned}
\bar{t}_{11} &= t_{11} + \bar{p} = -\tfrac{1}{3}\dot{\gamma}^2 A \\
\bar{t}_{22} &= t_{22} + \bar{p} = -\tfrac{1}{3}\dot{\gamma}^2(A - 3a_3) \\
\bar{t}_{33} &= t_{33} + \bar{p} = \tfrac{1}{3}\dot{\gamma}^2(2A - 3a_3) \\
\bar{t}_{23} &= t_{23} = \dot{\gamma}(a_1 + 2a_5\dot{\gamma}^2 + 4a_7\dot{\gamma}^4) \\
\bar{t}_{12} &= \bar{t}_{13} = 0
\end{aligned}
\tag{3.13}
$$

where $A \equiv 2a_2 + 2a_3 + 4(a_4 + a_6)\dot{\gamma}^2 + 8a_3\dot{\gamma}^4$. It must be noted that $\bar{p}$ in (3.13) is the mean pressure used in (2.5) and is different from the undetermined hydrostatic pressure p in (3.12). Since the constitutive coefficients a_i are each some polynomials in the invariants of the tensors a_1 and a_2 which are in turn expressible in terms of the rate of shear $\dot{\gamma}$, the extra stress components are then functions of the rate of shear only. Thus, (3.13) may be written as

$$
\begin{aligned}
\bar{t}_{11} &= t_{11} + \bar{p} = -\nu_1 \\
\bar{t}_{22} &= t_{22} + \bar{p} = -\nu_2 \\
\bar{t}_{33} &= t_{33} + \bar{p} = -\nu_3 \\
\bar{t}_{23} &= t_{23} = \dot{\gamma}\nu_4 \\
\bar{t}_{12} &= \bar{t}_{13} = 0
\end{aligned}
\tag{3.14}
$$

where ν_i are functions of $\dot{\gamma}^2$. In addition, by the definition of the mean pressure $\bar{p} = \tfrac{1}{3}t_{mm}$ or equivalently $\bar{t}_{mm} = 0$, we have

$$
\nu_1 + \nu_2 + \nu_3 = 0
\tag{3.15}
$$

Therefore, for each Rivlin–Ericksen material, instead of the eight constitutive functions $a_i(\dot{\gamma}^2)$ required by Rivlin [20] to characterize the behavior of the fluid in certain viscometers, only three *material* functions are really necessary, namely: any two of the three normal stress functions ν_1, ν_2, ν_3, plus the shear stress function ν_4. As may be deduced from Markovitz's results [30] and explicitly stated by Ericksen [31], the normal stress functions (or the difference between any two) are even functions of the rate of shear, while the shear stress function ν_4 is an odd function of the same variable.

It is remarkable that these results obtained explicitly for Rivlin–Ericksen fluids should apply equally to other materials defined by entirely different forms

of constitutive equations. In particular, Coleman and Noll [21, 32] demon-strated that this is the case of incompressible simple fluids. These materials are characterized by constitutive equations of the form

$$\bar{t}(t) = \mathop{\mathscr{F}}_{\tau = \infty}^{\infty} [c_t(t - \tau)] \tag{3.16}$$

(Cf. eqn. (2.8) given in Section 2.) For the class of steady flows considered above and a few others such as Poiseuille and channel flows, Coleman and Noll showed that in some suitable orthogonal coordinate system the deformation tensor function $c_t(t - \tau)$ assumes the form

$$c_t(t - \tau) = I - \tau a_1 + \tfrac{1}{2}\tau^2 a_2 \tag{3.17}$$

where a_1 and a_2 are respectively the first and second Rivlin–Ericksen tensors. In the cases considered, since a_1 and a_2 are independent of τ and t, the functional $\mathscr{F}$ of (3.16) reduces to a function f of the two tensors a_1 and a_2. Thus,

$$\bar{t} = f(a_1, \quad a_2) \tag{3.18}$$

By the application of certain invariance principles of constitutive theory, (3.18) may be expressed in the form

$$\bar{t}^* = f(A,B) \tag{3.19}$$

where the physical components of A and B are given by

$$A = \kappa \begin{bmatrix} 0 & 1 & 0 \\ 1 & 0 & 0 \\ 0 & 0 & 0 \end{bmatrix}; \quad B = \kappa^2 \begin{bmatrix} 1 & 0 & 0 \\ 0 & 0 & 0 \\ 0 & 0 & 0 \end{bmatrix} \tag{3.20}$$

where κ is the rate of shear ($\dot{\gamma}$) or some simple functions of this rate. Without much difficulty, it can be shown that only the stress components $\bar{t}_{13}$ and $\bar{t}_{23}$ are zero and that the other components are functions of κ alone. On the basis of this and the fact that $\bar{t}_{mm} = 0$, the extra stress components may be expressed in terms of three independent functions of κ:

$$\bar{t}_{11} - \bar{t}_{33} = \sigma_1(\kappa); \quad \bar{t}_{22} - \bar{t}_{33} = \sigma_2(\kappa); \quad \bar{t}_{12} = \sigma_3(\kappa) \tag{3.21}$$

where σ_1 and σ_2 determine the normal stress effects and σ_3 is the shear stress.

Coleman and Noll then proceeded to show that the normal stress functions σ_1 and σ_2 are even functions in κ while the shear stress function σ_3 is odd. If these functions are known for a material under consideration, the state of stress in the fluid in the flow described above are, of course, determined. Furthermore, with the use of the dynamical equations and the prescribed boundary conditions, one can obtain expressions for other relevant quantities (e.g. velocity field) in terms of these three independent functions. For example, for the helical flow of the simple fluid [32] the velocity field given by

$$v = [0, r\omega(r), \quad u(r)] \tag{3.22}$$

is completely determined from

$$u(r) = \int_{r_1}^{r} \frac{\sigma_3^{-1}[a(\xi)]}{a(\xi)} \left(-\tfrac{1}{2}a\xi + b\xi^{-1}\right) d\xi \tag{3.23}$$

$$\omega(r) = \frac{M}{2\pi} \int_{r_1}^{r} \frac{\sigma_3^{-1}[a(\xi)]}{\xi^2 a(\xi)} \, d\xi + \Omega_1$$

where σ_3^{-1} is the inverse function of σ_3; M is the torque per unit height of the fluid required to maintain relative motion of the bounding coaxial cylinders; a is the applied force per unit volume in the axial direction; b is a constant determined from the boundary condition; and a is a function defined by

$$a^2(r) = \left(\frac{M}{2\pi r^2}\right)^2 + \left(\frac{b}{r} - \frac{ar}{2}\right)^2 \tag{3.24}$$

and Ω_1 is the angular velocity of the inner cylinder (the radius of which is r_1). Thus, it is seen that the velocity field is fully determined once the material function σ_3 of the particular fluid is known.

In terms of the three material functions the extra stress for the helical flow of the simple fluid is given by

$$t_{rr} = \tfrac{1}{3}[2\sigma_1(\kappa) - \sigma_2(\kappa)]$$

$$t_{\theta\theta} = -\tfrac{1}{3}\,\sigma_1(\kappa) + \frac{-(u')^2 + 2(r\omega')^2}{3\kappa^2}\,\sigma_2(\kappa)$$

$$t_{zz} = -\tfrac{1}{3}\,\sigma_1(\kappa) + \frac{2(u')^2 - (r\omega')^2}{3\kappa^2}\,\sigma_2(\kappa)$$

$$t_{r\theta} = \frac{r\omega'}{\kappa}\,\sigma_3(\kappa) \tag{3.25}$$

$$t_{rz} = \frac{u'}{\kappa}\,\sigma_3(\kappa)$$

$$t_{\theta z} = \frac{r\omega' u'}{\kappa^2}\,\sigma_2(\kappa)$$

where for the above helical case $\kappa = [u'^2 + (r\omega')^2]^{1/2}$; $u' \equiv du/dr$; $\omega' \equiv d\omega/dr$.

It must be remarked that the three material functions σ_1, σ_2, σ_3 are not entirely different from those proposed earlier by Markovitz. In fact, these material functions are related according to

$$\sigma_1(\kappa) = \nu_1(\kappa) - \nu_3(\kappa)$$
$$\sigma_2(\kappa) = \nu_1(\kappa) - \nu_2(\kappa) \tag{3.26}$$
$$\sigma_3(\kappa) = \kappa\nu_4(\kappa)$$

where ν_1, ν_2, ν_3, ν_4 are the functions used in (3.14) and σ_1, σ_2, σ_3 are the expressions introduced in (3.21).

It must also be remarked that although Markovitz [30] and later Coleman

and Noll [21, 32] were able to express results for the above cases in terms of three scalar material functions while Rivlin [20] required a knowledge of eight scalar functions characterizing the material, the Rivlin formulation possesses the explicitness which the functional form of the simple fluids lacks. In other words, should it be acceptable to disregard acceleration gradients of order higher than the first, to within an undetermined hydrostatic pressure the incompressible Rivlin–Ericksen material is explicitly defined by eight material functions for *all* cases of material deformation and flow. (See eqn. (3.1).) On the other hand, the three material functions defining the simple fluids are only valid for the flows discussed in this section; these functions cannot predict the behavior of the simple fluids under other situations. For example, for the steady extension of these fluids material functions other than the above three (σ_1, σ_2, σ_3) are needed to describe material behavior. (See Section 3.2 below).

Finally, note is made of the studies by other investigators on the steady shear flow of nonlinear viscoelastic materials. Noll [8] presented some results on the flow of certain types of hygrosteric materials. Sharma [33] discussed three steady flows of a nonlinear viscoelastic fluid which is a generalization of the linear Maxwell material. Ericksen [31] analyzed the problem of flow of the Rivlin–Ericksen fluid between coaxial cones. Criminale, Ericksen and Filbey [34] considered the laminar shear flow of the same fluid and based calculations on a simplified constitutive equation peculiar to these problems using also three material scalar functions slightly different from those used by Markovitz and Coleman and Noll. Further work on allied topics involving simple fluids was conducted by Coleman [35, 36], who attempted a generalization of these types of flows under a class he calls *viscometric flows*. Noll [37] further generalized this class of flows in a treatment of simple fluids undergoing motions with constant stretch characterized by a constant tensor. He proved that viscometric flows form a subclass of these motions. Other non-viscometric flows belong to this general class of motions; among these is the steady extension of simple fluids discussed below.

3.2. Steady Extension of Simple Fluids

To demonstrate a simple case of steady non-viscometric flow, we discuss here the steady extension of incompressible simple fluids (Coleman and Noll [38]). This problem is of particular interest in that it is not equivalent to a simple shearing flow as the problems discussed in the preceding section. Furthermore, this case shows that in general the behavior of the simple fluid depends on different material functions for different physical situations. This is also a case where none of the Rivlin–Ericksen tensors of finite orders vanishes; therefore, unlike the cases considered in the preceding section, the theory of simple fluids for the present case does not reduce to the theory of Rivlin–Ericksen fluids.

The fluid is said to undergo steady extension if in a fixed Cartesian coordinate system x_i the velocity of the material point is given by

$$v_i = a_i x_i \tag{3.27}$$

where underscored indices indicate a suspension of the summation convention and a_i are constants such that $a_1 + a_2 + a_3 = 0$. Thus the flow characterized by this velocity field is isochoric.

The constitutive equation of simple fluids is given in (2.8) which for the incompressible case such as this is expressible in the form

$$t_{ij} = -p\delta_{ij} + \overset{\infty}{\underset{\tau=0}{\mathscr{F}_{ij}}} [c_{(t)mn}(t - \tau)] \tag{3.28}$$

where p is the arbitrary hydrostatic pressure. The motion of the fluid is expressible in terms of the following relation between the position χ_i of the material point at time $t - \tau$ to its position x_i at time t:

$$\chi_i = x_i e^{-a_i \tau} \tag{3.29}$$

Thus, the deformation tensor $c_{(t)mn}$ is given by

$$C_{(t)ij}(t - \tau) = e^{-2a_i \tau}\delta_{ij} \tag{3.30}$$

From (3.30), (3.28), and the application of the principle of objectivity and a representation theorem for isotropic functions of symmetric matrices, the stress matrix is given by

$$[t_{ij}] = \begin{bmatrix} t_{11} & 0 & 0 \\ 0 & t_{22} & 0 \\ 0 & 0 & t_{33} \end{bmatrix} \tag{3.31}$$

with the differences of the diagonal elements represented in the form

$$\begin{aligned} t_{11} - t_{22} &= (a_1 - a_2)g + (a_1^2 - a_2^2)h \\ t_{11} - t_{33} &= (a_1 - a_3)g + (a_1^2 - a_3^2)h \end{aligned} \tag{3.32}$$

where $g = g(\text{II}, \text{III})$ and $h = h(\text{II}, \text{III})$ are material functions of $\text{II} = \sum_i a_i^2$ and $\text{III} = \sum_i a_i^3$, and depend in form on the particular fluid under consideration.

The dynamical equations are given by

$$(t_{\underline{i}\underline{i}} - p\psi)_{,\underline{i}} = \rho(a_i)^2 x_{\underline{i}} \quad (i = 1, 2, 3) \tag{3.33}$$

where ψ is the assumed body force potential. A solution of (3.33) subject to (3.32) is given by

$$t_{\underline{i}\underline{i}} = \tfrac{1}{2}\rho(a_m x_m)^2 + \rho\psi + a_i g + a_i^2 h + f(t) \tag{3.34}$$

where $f(t)$ is an arbitrary function of time.

To demonstrate the application of these results, we consider the case of a circular cylinder with radius $R = R(t)$ and length $L = L(t)$. We assume that the axis of the cylinder is the x_1-axis and that $a_2 = a_3$. Thus, we have $a_1 = a$; $a_2 = a_3 = -\tfrac{1}{2}a$. If we assume further that the body forces are zero and adjust the arbitrary function $f(t)$ such that the mean of t_{rr} vanishes along each generator

16

of the cylindrical boundary, we have the following normal stresses

$$t_{rr}(R,\ \theta,\ z) = \tfrac{1}{2}\rho a^2(z^2 - \tfrac{1}{3}L^2)$$

$$t_{zz}(r,\ \theta,\ 0) = \tfrac{1}{2}\rho a^2(\tfrac{1}{4}r^2 - \tfrac{1}{3}L^2) + \tfrac{3}{2}ag + \tfrac{3}{4}a^2h \qquad (3.35)$$

$$t_{zz}(r,\ \theta,\ L) = \tfrac{1}{2}\rho a^2(\tfrac{1}{4}r^2 + \tfrac{2}{3}L^2) + \tfrac{3}{2}ag + \tfrac{3}{4}a^2h$$

with the first of (3.35) being the normal stress at the cylindrical surface $r = R$, and the remaining two being those at the ends of the cylinder: respectively planes $z = 0$ and $z = L$.

It follows from $(3.35)_1$ that normal tractions must be applied to the cylindrical surface to maintain steady extension. Otherwise, the cylinder will tend to bulge for $0 < z < L/\sqrt{3}$ and to contract for $L/\sqrt{3} < z \leqslant L$.

3.3. Hydrostatic Extension of a Hygrosteric Body

The vast majority of problems solved in nonlinear viscoelasticity employs a condition of incompressibility of the material. This condition may be postulated initially or may result from the specific motion the body is restricted to undergo. In either case, the analysis is greatly simplified. However, there are deformations of the body which will not allow this simplification. An example is the problem discussed below.

A body is under homogeneous stress if the stress at any point x in that body is a function of time t only, i.e. the stress is independent of x_i. Such a state of stress is exemplified by the case of hydrostatic extension (or compression) as characterized by the following velocity and extra stress fields.

$$\mathbf{v} = (\mathbf{x} - \mathbf{x}_0)h; \quad \bar{\mathbf{t}} = q\mathbf{I} \qquad (3.36)$$

where $h = h(t)$ and $q = q(t)$ are functions of time, and $\mathbf{x}_0$ is some fixed point in space. Hydrostatic extension requires that $h(t) > 0$, while the compression case has $h(t) < 0$. Noll [8] derived the basic equations for hygrosteric materials in homogeneous stress. We here present some of his results for the hydrostatic extension (or compression) of a special class of hygrosteric materials, the linear fluent body. Such a body is characterized by a constitutive equation of the form

$$\dot{\bar{\mathbf{t}}} + \bar{\mathbf{t}}\mathbf{w} - \mathbf{w}\bar{\mathbf{t}} = (\lambda_1 + \nu_5\ \mathrm{tr}\ \mathbf{d})\,\bar{\mathbf{t}} + (\mu_1 + \nu_2\ \mathrm{tr}\ \bar{\mathbf{t}})\mathbf{d}$$
$$+ \nu_3(\bar{\mathbf{t}}\mathbf{d} + \mathbf{d}\bar{\mathbf{t}}) + [\mu_2\ \mathrm{tr}\ \mathbf{d} + \lambda_2\ \mathrm{tr}\ \bar{\mathbf{t}} + \nu_1\ \mathrm{tr}\ (\mathbf{d}\bar{\mathbf{t}}) + \nu_4\ (\mathrm{tr}\ \bar{\mathbf{t}})\ (\mathrm{tr}\ \mathbf{d})]\mathbf{I} \quad (3.37)$$

derivable from the more general expression (2.4) for hygrosteric materials. In (3.37), the material constants λ_i, μ_i and ν_i are related to the constitutive coefficients α_i of (2.4). For the linear fluent body under consideration, $\lambda_1 \neq 0$ and $3\lambda_2 + \lambda_1 \neq 0$.

Since the stress is independent of x_i, $t_{mk,\ m} = 0$. Thus, the equations of motion (2.2) imply that for zero body forces the motion is accelerationless,* and for the case under consideration we have

$$h(t) = (t + t_0)^{-1} \qquad (3.38)$$

* See Eringen [6] and Noll [8] for details.

over the range

$$0 \leqslant t < \infty \qquad \text{if } t_0 > 0 \text{ (extension)}$$
$$0 \leqslant t < |t_0| \qquad \text{if } t_0 < 0 \text{ (compression)}$$

where $t_0 \equiv h^{-1}(0)$.

For the velocity field given by (3.36) and (3.38), the continuity equation (2.1) assumes the form

$$\dot{\rho} + 3\rho(t + t_0)^{-1} = 0 \tag{3.39}$$

which integrates into

$$\rho = \rho_0(t + t_0)^{-3} \tag{3.40}$$

Using (3.36) and (3.38) in (2.5), we calculate expressions for **d, w** and the various pertinent invariants. With these expressions substituted into the constitutive equation (3.37), we get the differential equation for $q(t)$:

$$\dot{q} = [3\lambda_2 + \lambda_1 + \beta(t + t_0)^{-1}]q + \mu(t + t_0)^{-1} \tag{3.41}$$

where $\beta \equiv 3(\nu_1 + \nu_2 + 2\nu_4 + \nu_5) + 2\nu_3$ and $\mu \equiv 3\mu_2 + \mu_1$. For initial value $q(0) \equiv q_0$, (3.41) integrates to

$$q = q_0 \left(\frac{t}{t_0} + 1\right)^{\beta} \exp\left(-\frac{t}{\tau_p}\right) + \frac{\mu}{t + t_0} g(t) \tag{3.42}$$

where

$$\tau_p \equiv -(3\lambda_2 + \lambda_1)^{-1} > 0$$

$$g(t) \equiv \int_0^t \left(\frac{t + t_0}{u + u_0}\right)^{\beta + 1} \exp\left(\frac{u - t}{\tau_p}\right) du \tag{3.43}$$

Eringen [6] expressed $g(t)$ in (3.43) in terms of incomplete gamma functions and calculated the variation of q with t. He showed how the extra stress builds up in time for several values of β and $t_0 (3\lambda_2 + \lambda_1)$ and demonstrated that the hydrostatic extension of the linear fluent body exhibits a yieldlike phenomenon of instability as time varies from zero.

3.4. *Periodic Motion, Wave Propagation and Other Dynamical Problems*

The analysis of boundary value problems for nonsteady motion of nonlinear viscoelastic materials is more complicated than the treatment of corresponding steady flow problems. However, in recent years several *exact* solutions have been determined for these dynamical problems albeit most of these solutions are for materials characterized by some *approximate* constitutive theory in the manner discussed in the last paragraph of Section 2.2 above.

Coleman and Noll [39], however, obtained some interesting results in an analysis of the periodic shearing flow of an incompressible simple fluid without applying any approximation in either the constitutive theory or in the analysis.

The simple fluid is defined by a constitutive equation similar to (3.16). The velocity field defining this periodic motion is given by

$$v_i = [0, v(x_1, t), 0] \tag{3.44}$$

where v is periodic in t with period θ, i.e.

$$v(x_1, t + \theta) = v(x_1, t) \tag{3.45}$$

for all x_1 and t.

It can be shown that for the velocity field (3.44), the position χ_i of the material point at time τ is related to its position x_i at time t according to

$$
\begin{aligned}
\chi_1(\tau) &= x_1 \\
\chi_2(\tau) &= x_2 - u_{(t)}(x_1, t - \tau) \\
\chi_3(\tau) &= x_3
\end{aligned}
\tag{3.46}
$$

where

$$u_{(t)}(x_1, r) = \int_0^r v(x_1, t - \tau)\, d\tau \tag{3.47}$$

Using (3.46) in (2.9), we calculate the deformation tensor

$$[\mathbf{c}_t(t - r)] = \begin{bmatrix} 1 + \lambda^2_{(t)}(r) & \lambda_{(t)}(r) & 0 \\ \lambda_{(t)}(r) & 1 & 0 \\ 0 & 0 & 1 \end{bmatrix} \tag{3.48}$$

where

$$\lambda_{(t)}(r) = \frac{\partial u_{(t)}(x_1, r)}{\partial x_1}; \qquad \lambda_{(t+\theta)}(r) = \lambda_{(t)}(r) \tag{3.49}$$

Thus, $\mathbf{c}_t(t - r)$ is expressible in the form

$$\mathbf{c}_t(t - r) = \mathbf{I} + \mathbf{E}_t(r) + \mathbf{G}_t(r) \tag{3.50}$$

where

$$\mathbf{E}_t(r) \equiv \lambda_{(t)}(r) \begin{bmatrix} 0 & 1 & 0 \\ 1 & 0 & 0 \\ 0 & 0 & 0 \end{bmatrix}; \qquad \mathbf{G}_t(r) \equiv \lambda^2_{(t)}(r) \begin{bmatrix} 1 & 0 & 0 \\ 0 & 0 & 0 \\ 0 & 0 & 0 \end{bmatrix}$$

By substituting (3.50) in the constitutive equation (3.16), we note that the extra stress $\bar{\mathbf{t}}$ is a functional expressible in terms of $\mathbf{E}_t(r)$ and $\mathbf{G}_t(r)$ and that $\bar{\mathbf{t}}$ is dependent on $\lambda_{(t)}(r)$ solely. An application of the principle of objectivity also yields

$$\bar{\mathbf{t}} = \begin{bmatrix} \bar{t}_{11} & \bar{t}_{12} & 0 \\ \bar{t}_{12} & \bar{t}_{22} & 0 \\ 0 & 0 & \bar{t}_{33} \end{bmatrix} \tag{3.51}$$

where the trace of $\bar{\mathbf{t}}$ is zero.

Analogous to the corresponding steady flow problem, the stress solution is expressible in terms of three material functionals according to

$$\hat{t}_{12}(t) = \underset{r=0}{\overset{\infty}{\mathscr{G}}} [\lambda_{(t)}(r)]$$

$$\hat{t}_{11}(t) - \hat{t}_{33}(t) = \underset{r=0}{\overset{\infty}{\mathscr{H}_1}} [\lambda_{(t)}(r)]$$

$$\hat{t}_{22}(t) - \hat{t}_{33}(t) = \underset{r=0}{\overset{\infty}{\mathscr{H}_2}} [\lambda_{(t)}(r)] \tag{3.52}$$

As with the steady case, it can be shown by an application of the principle of objectivity that $\mathscr{G}$ is an odd functional, while $\mathscr{H}_1$ and $\mathscr{H}_2$ are both even.

An interesting result follows if one imposes a further assumption on v such that

$$v(x_1, t) = - v(x_1, t + \theta/2) \tag{3.53}$$

This assumption which is commonly observed in experiments implies that the absolute value of v has a period that is one half the minimum period of v. It then follows from (3.53) and (3.49) that

$$\lambda_{(t)}(r) = - \lambda_{(t+\theta/2)}(r) \tag{3.54}$$

Thus, using the fact that $\mathscr{G}$ is odd while $\mathscr{H}_i$ ($i = 1, 2$) are even, we have

$$\underset{r=0}{\overset{\infty}{\mathscr{G}}}[\lambda_{(t+\theta/2)}(r)] = \underset{r=0}{\overset{\infty}{\mathscr{G}}}[- \lambda_{(t)}(r)] = - \underset{r=0}{\overset{\infty}{\mathscr{G}}}[\lambda_{(t)}(r)]$$

$$\underset{r=0}{\overset{\infty}{\mathscr{H}_i}}[\lambda_{(t+\theta/2)}(r)] = \underset{r=0}{\overset{\infty}{\mathscr{H}_i}}[- \lambda_{(t)}(r)] = \underset{r=0}{\overset{\infty}{\mathscr{H}_i}}[\lambda_{(t)}(r)] \tag{3.55}$$

Consequently, we have

$$\hat{t}_{12}(t + \theta/2) = - \hat{t}_{12}(t)$$

$$\hat{t}_{ii}(t + \theta/2) = \hat{t}_{ii}(t), \quad i = 1, 2, 3 \tag{3.56}$$

In other words, if the velocity has the property (3.53), $\hat{t}_{12}$ behaves similarly, and the normal extra stresses $\hat{t}_{11}$, $\hat{t}_{22}$ and $\hat{t}_{33}$ will oscillate with a frequency that is twice that of the velocity and displacement fields.

The nonsteady flow of simple fluids is further treated by Markovitz and Coleman [25], with the analysis particularly pertaining to an incompressible second order fluid such as that characterized by a constitutive equation of the form (2.12). It was shown that for a helical flow defined in cylindrical coordinates by a velocity field of physical components given by

$$v^r = 0, \qquad v^\theta = rw(r, t), \qquad v^z = u(r, t) \tag{3.57}$$

the dynamical equations (2.2) reduce to the following two uncoupled linear third-order partial differential equations in w and u:

$$\frac{\partial}{\partial r}\left[r^3\left(\alpha_1 \frac{\partial w}{\partial r} + \alpha_3 \frac{\partial^2 w}{\partial r \partial t}\right)\right] = \rho r^3 \frac{\partial w}{\partial t}$$

$$\frac{\partial}{\partial r}\left[r\left(\alpha_1 \frac{\partial u}{\partial r} + \alpha_3 \frac{\partial^2 u}{\partial r \partial t}\right)\right] + r\lambda(t) = \rho r \frac{\partial u}{\partial t} \tag{3.58}$$

where a_1 and a_2 are the material constants given in (2.12) and $\lambda(t)$ is the gradient of a potential ϕ in the axial direction expressible as a sum of the z-components (in axial direction) of the body force $\mathbf{f}$ and the pressure gradient, i.e.

$$\lambda(t) = -\frac{\partial \phi}{\partial z} = f^z - \frac{\partial p}{\partial z} \qquad (3.59)$$

The basic differential equations (3.58) are directly applicable to several special situations. We present here the analysis for a sinusoidal Poiseuille flow defined by

$$u(r, t) = \mathrm{Re}[U_0(r) + U_1(r)e^{i\omega t}] \qquad (3.60)$$

where $U_0(r)$ and $U_1(r)$ are complex functions of r, $i \equiv \sqrt{-1}$, and Re signifies the real part of the bracketed expression. For the case under consideration, $w = 0$, and eqn. (3.58)$_2$ remains to be solved. By this equation $\lambda(t)$ must also be a sinusoidal function of t expressible in the form

$$\lambda(t) = \lambda_0 + \lambda_1 \,\mathrm{Re}\,[e^{i\omega t}] \qquad (3.61)$$

where λ_0 and λ_1 are real constants. Substituting (3.60) and (3.61) in (3.58)$_2$, one obtains the ordinary differential equation

$$a_1 \frac{d}{dr}\left(r \frac{dU_0}{dr}\right) + r\lambda_0 = \left\{ i\omega\rho r U_1 - [a_1 + i\omega a_3] \frac{d}{dr}\left(r \frac{dU_1}{dr}\right) - r\lambda_1 \right\} e^{i\omega t} \qquad (3.62)$$

Since the left-hand side of this equation is independent of t, so must the right-hand side be also. This is possible only if the coeficient of $\exp(i\omega t)$ is zero, i.e.

$$(a_1 + i\omega a_3) \frac{d}{dr}\left(r \frac{dU_1}{dr}\right) - i\omega\rho r U_1 + r\lambda_1 = 0 \qquad (3.63)$$

From (3.62), eqn. (3.63) also implies that

$$a_1 \frac{d}{dr}\left(r \frac{dU_0}{dr}\right) + r\lambda_0 = 0 \qquad (3.64)$$

Thus, solving (3.63) and (3.64), we obtain

$$U_1 = aJ_0(ar) + b Y_0(ar) + \frac{\lambda_1}{i\omega\rho}$$

$$U_0 = -\frac{\lambda_0 r^2}{4a_1} + c \ln r + d \qquad (3.65)$$

where

$$a^2 = -\frac{i\omega\rho}{a_1 + i\omega a_3} \qquad (3.66)$$

J_0 and Y_0 are respectively the Bessel functions of the first and second kinds of order zero; and a, b, c, d are integration constants to be determined from the boundary conditions.

A special boundary value problem considered is that of the fluid flowing

between two infinitely long coaxial cylinders of radii R_1 and R_2, with one cylinder (that of radius R_1) stationary while the other oscillates longitudinally with velocity

$$V(t) = V_1 \cos \omega t$$

V_1 being a real constant. It is also assumed that $\lambda(t)$ is zero, i.e. $\lambda_0 = \lambda_1 = 0$. The boundary conditions for this problem are then

$$u(R_1, t) = V_1 \cos \omega t \text{ and } u(R_2, t) = 0 \tag{3.67}$$

or equivalently

$$U_0(R_1) = U_0(R_2) = 0$$
$$U_1(R_2) = 0; \qquad U_1(R_1) = V_1 \tag{3.68}$$

Solution (3.65) under these boundary conditions (3.68) takes the form

$$U_0 = 0$$

$$U_1(r) = \frac{V_1[Y_0(aR_2)J_0(ar) - J_0(aR_2)Y_0(ar)]}{Y_0(aR_2)J_0(aR_1) - J_0(aR_2)Y_0(aR_1)} \tag{3.69}$$

With this solution, Markovitz and Coleman derived approximate expressions for the velocity and stress for the case where the gap between the two cylinders is small. They also considered other cases including a sinusoidal Poiseuille flow between two stationary coaxial cylinders and the sinusoidal Couette flow of the fluid between two oscillating cylinders.

Ting [23] investigated several interesting initial value problems pertaining to second-order fluids of the type considered above. In particular, Ting analyzed the generation of flows between two infinite parallel planes by a constant tangential surface force, the formation of flows through straight channels and pipes by a constant pressure gradient, and the decay of such flows when the pressure gradient is suddenly removed. He used the same partial differential equation (3.58)$_2$ as Markovitz and Coleman [25] employed in their later work. However, some physical discrepancy has arisen between these two investigations: Ting uses a constitutive equation of the form given by (3.16) and so do Markovitz and Coleman. However, Ting's analysis hinges on the fact that both material constants α_1 and α_3 are positive; whereas Markovitz and Coleman maintain that α_3 is negative, a contention for which they appear to have the support of some experimental evidence. Nevertheless, the elegant analysis presented by Ting deserves consideration and should not be dismissed lightly until further experimentation proves conclusively that his assumptions are indeed not sustained by the physical aspect of the problem.

The problem of wave propagation in nonlinear viscoelastic media has not been studied to any great extent.* Markovitz and Coleman [25] treated the case of the Rayleigh problem of sinusoidal oscillation of a flat plate bounding a semi-infinite body of the second-order incompressible simple fluid. The fluid is

---

* During the last stages of the preparation of this paper, several interesting investigations on this subject were reported in the literature. Special attention is called to the contributions of Varley [40] and Coleman, Gurtin and Herrera [41].

considered to occupy the half-space $x_1 > 0$ with the plane boundary oscillating sinusoidally in the x_2-direction such that velocity of points at $x_1 = 0$ is given by

$$\mathbf{v} = [0, V \cos \omega t, 0] \tag{3.70}$$

where V is a constant. For zero body force and vanishing pressure gradient in the direction of fluid motion, the differential equation is given by

$$\alpha_1 \frac{\partial^2 v}{\partial x_1^2} + \alpha_3 \frac{\partial^3 v}{\partial x_1^2 \partial t} = \rho \frac{\partial v}{\partial t} \tag{3.71}$$

where $v = v(x_1, t)$ is the velocity component in the x_2-direction. A solution of (3.71) satisfying boundary conditions

$$v(0, t) = V \cos \omega t; \qquad v(\infty, t) \text{ finite} \tag{3.72}$$

is given by

$$v(x_1, t) = V e^{-ax_1} \cos (\omega t - bx_1) \tag{3.73}$$

where a and b are real and positive and are defined as follows

$$a = \sqrt{\frac{\omega \rho [(a_1^2 + \omega^2 a_3^2)^{1/2} + \omega a_3]}{2(a_1^2 + \omega^2 a_3^2)}}; \qquad b = \sqrt{\frac{\omega \rho [(a_1^2 + \omega^2 a_3^2)^{1/2} - \omega a_3]}{2(a_1^2 + \omega^2 a_3^2)}} \tag{3.74}$$

Thus, it is seen that at any imposed frequency, the fluid can support a shear wave with amplitude approaching zero exponentially with increasing distance from the oscillating bounding plate.

A similar problem was treated by Niiler and Pipkin [42] for several types of fluids which they showed to reduce to the Rivlin–Ericksen type of constitutive equation such as (2.26). The basic equation to be solved is expressible in the form

$$\frac{\partial \bar{t}_{12}}{\partial x_1} = \rho \frac{\partial v}{\partial t} \tag{3.75}$$

where $\bar{t}_{12}$ is the pertinent extra shear stress which depends only on x_1 and t. However, since the constitutive equation (2.26) carries the dependence of $\bar{t}_{12}$ on the Rivlin–Ericksen kinematic tensors to as high an order as desired, one does not obtain an explicit expression for (3.75) in terms of the velocity. By expanding the velocity in powers of a parameter proportional to the square root of the frequency, Niiler and Pipkin were able to obtain for a specified order of approximation a solution that is an asymptotic approximation to the differential equation.

With regard to studies on wave propagation, one should probably mention also the work of Pipkin and Rivlin [43] on small deformations superposed on large deformations in materials with fading memory, a general nonlinear viscoelastic material characterized by Green, Rivlin and Spencer [44]. The basic equations derived in the Pipkin–Rivlin paper have applications in problems dealing with wave propagation in finitely deformed viscoelastic media; however, no attempts have been made to make such applications.

An interesting problem that has attracted the attention of some investigators

is the occurrence of secondary flows in fluids flowing through tubes of arbitrary cross section. (For example, see Green and Rivlin [45].) Pipkin [46] recently investigated such a flow of a Rivlin–Ericksen fluid under a sinusoidally alternating pressure gradient. He employed an approximation similar to that proposed by Langlois and Rivlin [27]. (Also see Section 2.4). He observed that a transverse flow is induced by the alternating pressure gradient; however, to the degree of approximation considered, he found that this secondary flow is steady. More significantly, it was noted that while the Langlois–Rivlin analysis predicts the onset of secondary flow in a third order of approximation, such transverse flows are present in the corresponding first order of approximation for the alternating primary flow. This would imply that secondary flows may be detected more readily in alternating flows than in steady motion.

On the subject of stability of motion of nonlinear viscoelastic media, only a few short papers have been published. Datta [47] considered the case of a second-order incompressible fluid with constitutive equation (2.12). He employed a common stability method of analysis of superposing a small disturbance on a steady flow, in his case the Couette flow. Assuming the usual exponential form for the infinitesimal disturbance velocity components and pressure, the linearized disturbance equation was solved. Genensky [48] also made some stability studies for a simplified Rivlin–Ericksen fluid. Finally, it must be mentioned that the results of Pipkin and Rivlin [43] certainly have applications in the study of stability of flows of Green–Rivlin–Spencer materials. However, such applications have not been undertaken.

4. COUPLED EFFECTS IN NONLINEAR VISCOELASTICITY

4.1. Thermomechanical Effects

It is a well-known fact that viscoelastic materials are highly sensitive to thermal changes. Experimental evidence to this is recorded in many publications. (For instance, see Ferry [49].) The theories proposed to account for these observations are also plentiful; however, these theories are mostly empirical laws characterizing specific materials under the restrictive conditions of the tests or simple extensions to the linear theory of viscoelasticity with modifications introduced to incorporate thermal effects, usually through temperature-dependent moduli.

Such theories are either too restrictive or, worse yet, they do not properly characterize the coupled thermomechanical behavior of nonlinear materials in the light of the invariance principles of constitutive theory. A rational formulation of a thermomechanical theory that includes nonlinear effects and also reduces by suitable linearization to the classical theories was proposed by Koh and Eringen [50]. (Also see [12]). This theory presents a complete set of equations necessary for the analysis of the behavior of nonlinear heat-conducting viscoelastic materials. It postulates a constitutive theory composed of two sets of equations, specifically:

$$t = t(c^{-1}, d, b)$$
$$h = h(c^{-1}, d, b)$$

$$(4.1)$$

where $\mathbf{t}$ the stress tensor, is considered a function of three variables: $\mathbf{c}^{-1}$ the deformation tensor defined by (2.7), $\mathbf{d}$ the deformation rate tensor given by (2.5), and $\mathbf{b}$ the temperature gradient bi-vector defined by

$$\mathbf{b}: b_{ij} \equiv e_{ijk}\theta_{,k} \qquad (4.2)$$

where θ is the temperature and e_{ijk} is the permutation symbol. The second equation of (4.1) relates the heat flux bi-vector $\mathbf{h}$ to the same independent variables $\mathbf{c}^{-1}$, $\mathbf{d}$, $\mathbf{b}$ of (4.1)$_1$. Here $\mathbf{h}$ is defined by

$$\mathbf{h}: h_{ij} \equiv e_{ijk}q_k \qquad (4.3)$$

where q_k is the heat flux vector. The dependence of $\mathbf{t}$ and $\mathbf{h}$ on the density and temperature is also implied.

In addition to these constitutive equations and the field equations (2.1), (2.2) and (2.3) given in Section 2, we must also satisfy in the analysis of the thermo-mechanical problem the principle of conservation of energy which is expressible in the form

$$\rho\dot{\epsilon} = t_{mk}d_{km} - q_{k,\,k} + \rho r \qquad (4.4)$$

where ϵ is the specific internal energy and r is the supply of energy.

With the application of a caloric equation of state, it was shown that (4.4) reduces to a heat conduction equation which for the incompressible case simplifies to

$$\rho\kappa\dot{\theta} = t_{km}d_{mk} - q_{k,\,k} + \rho r \qquad (4.5)$$

where κ is the specific heat.

This theory provides the mechanism whereby thermomechanical coupling may be introduced into other purely mechanical theories. Such modifications are indicated for hygrosteric materials and for a particular subclass of Rivlin–Ericksen viscoelastic fluids.

The Koh–Eringen theory is the first attempt at the complete characterization of nonlinear thermoviscoelastic materials. Other theories on nonlinear thermo-mechanical materials have since been presented. (Cf. Eringen and Grot [7].)

Since all these theories are quite recent, with none dated before 1962, very little has been done to apply them to practical problems. Koh and Eringen [12] considered the case of rectilinear laminar flow of three special classes of thermo-viscoelastic media. We briefly present here the analysis as it pertains to a thermo-fluent body, a modification of Noll's non-heat conducting hygrosteric material.

The fluid is characterized by the following constitutive equations

$$\dot{\mathbf{t}} + \bar{\mathbf{t}}\mathbf{w} - \mathbf{w}\bar{\mathbf{t}} = a_1\mathbf{I} + a_2\bar{\mathbf{t}} + a_3\mathbf{d} + a_4(\bar{\mathbf{t}}\mathbf{d} + \mathbf{d}\bar{\mathbf{t}}) + a_5(\mathbf{d}\mathbf{b} - \mathbf{b}\mathbf{d})$$
$$+ a_6(\mathbf{t}\mathbf{b} - \mathbf{b}\bar{\mathbf{t}}) + a_7(\bar{\mathbf{t}}\mathbf{d}\mathbf{b} - \mathbf{b}\mathbf{d}\bar{\mathbf{t}}) + a_8(\mathbf{d}\bar{\mathbf{t}}\mathbf{b} - \mathbf{b}\bar{\mathbf{t}}\mathbf{d}) + a_9(\mathbf{d}\mathbf{b}\bar{\mathbf{t}} - \bar{\mathbf{t}}\mathbf{b}\mathbf{d}) \quad (4.6)$$

and

$$\mathbf{h} = \beta_1\mathbf{b} + \beta_2(\bar{\mathbf{t}}\mathbf{d} - \mathbf{d}\bar{\mathbf{t}}) + \beta_3(\mathbf{b}\mathbf{d} + \mathbf{d}\mathbf{b})$$
$$+ \beta_4(\mathbf{b}\bar{\mathbf{t}} + \bar{\mathbf{t}}\mathbf{b}) + \beta_5(\bar{\mathbf{t}}\mathbf{d}\mathbf{b} + \mathbf{b}\mathbf{d}\bar{\mathbf{t}}) + \beta_6(\mathbf{d}\bar{\mathbf{t}}\mathbf{b} + \mathbf{b}\bar{\mathbf{t}}\mathbf{d}) \qquad (4.7)$$

where $\bar{\mathbf{t}}$, $\mathbf{w}$, $\mathbf{d}$ are defined by (2.5), and α_i and β_i are constitutive coefficients which are polynomials in the invariants $\mathrm{tr}\,\bar{\mathbf{t}}$, $\mathrm{tr}\,\mathbf{d}$ and $\mathrm{tr}\,\bar{\mathbf{t}}\mathbf{d}$. Explicitly, we have

$$
\begin{aligned}
\alpha_1 &= \alpha_{11}\,\mathrm{tr}\,\dot{\bar{\mathbf{t}}} + \alpha_{12}\,\mathrm{tr}\,\mathbf{d} + \alpha_{13}\,\mathrm{tr}\,\bar{\mathbf{t}}\mathbf{d} + \alpha_{14}\,\mathrm{tr}\,\bar{\mathbf{t}}\,\mathrm{tr}\,\mathbf{d} \\
\alpha_2 &= \alpha_{21} + \alpha_{22}\,\mathrm{tr}\,\mathbf{d} \\
\alpha_3 &= \alpha_{31} + \alpha_{32}\,\mathrm{tr}\,\bar{\mathbf{t}} \\
\alpha_5 &= \alpha_{51} + \alpha_{52}\,\mathrm{tr}\,\bar{\mathbf{t}} \\
\alpha_6 &= \alpha_{61} + \alpha_{62}\,\mathrm{tr}\,\mathbf{d} \\
\beta_1 &= \beta_{11} + \beta_{12}\,\mathrm{tr}\,\bar{\mathbf{t}} + \beta_{13}\,\mathrm{tr}\,\mathbf{d} + \beta_{14}\,\mathrm{tr}\,\bar{\mathbf{t}}\mathbf{d} + \beta_{15}\,\mathrm{tr}\,\bar{\mathbf{t}}\,\mathrm{tr}\,\mathbf{d} \\
\beta_3 &= \beta_{31} + \beta_{32}\,\mathrm{tr}\,\bar{\mathbf{t}} \\
\beta_4 &= \beta_{41} + \beta_{42}\,\mathrm{tr}\,\mathbf{d}
\end{aligned}
\tag{4.8}
$$

where α_{ij}, β_{ij}, α_4, α_7, α_8, α_9, β_5 and β_6 are constants.

The fluid is considered to flow between two parallel plates maintained at two different temperatures. One of these plates is assumed to be stationary with a constant temperature Θ_1; while the other located at a distance D from the first has a constant temperature Θ_2 and moves with a constant velocity V in a direction parallel to the plates. This direction will be called the x_1-direction, with x_2 in the direction perpendicular to the plates: $x_2 = 0$ defines the stationary plate and $x_2 = D$ the moving plate.

The problem presupposes the existence of the following velocity and temperature profiles in the thermo-fluent body.

$$
\begin{aligned}
\mathbf{v} &= \{v, 0, 0\}; \qquad v = v(x_2) \\
\theta &= \Theta_1 + \psi(x_2)
\end{aligned}
\tag{4.9}
$$

where $v(x_2)$ and $\psi(x_2)$ are functions to be determined.

Using the notation $s_1 \equiv t_{11}$; $s_2 \equiv t_{22}$; $s_3 \equiv t_{33}$; $s_4 \equiv t_{12}$; $s_5 \equiv t_{13}$; $s_6 \equiv t_{23}$ and substituting (4.9) in (4.6) and (4.7), we obtain from the stress flux equation the following:

$$
\begin{aligned}
- v' s_4 &= \mu_1 S + \mu_2 v' s_4 + \mu_3 s_1 + \mu_6 v' s_4 + 2\mu_9 \psi' s_5 + \mu_{11} v' \psi' s_6 \\
v' s_4 &= \mu_1 S + \mu_2 v' s_4 + \mu_3 s_2 + \mu_6 v' s_4 - \mu_{12} v' \psi' s_6 \\
0 &= \mu_1 S + \mu_2 v' s_4 + \mu_3 s_3 - 2\mu_9 \psi' s_5 - \mu_{10} v' \psi' s_6 \\
\tfrac{1}{2} v'(s_1 - s_2) &= \mu_3 s_4 + \tfrac{1}{2}\mu_4 v' + \tfrac{1}{2}\mu_5 v' S + \tfrac{1}{2}\mu_6 v'(s_1 + s_2) + \mu_9 \psi' s_6 \\
&\quad + \tfrac{1}{2}\mu_{11} v' \psi' s_5 - \tfrac{1}{2}\mu_{12} v' \psi' s_5 \\
- \tfrac{1}{2} v' s_6 &= \mu_3 s_5 + \tfrac{1}{2}\mu_6 v' s_6 + \mu_9 \psi'(s_3 - s_1) - \tfrac{1}{2}\mu_{10} v' \psi' s_4 - \tfrac{1}{2}\mu_{11} v' \psi' s_4 \\
\tfrac{1}{2} v' s_5 &= \mu_3 s_6 + \tfrac{1}{2}\mu_6 v' s_5 - \tfrac{1}{2}\mu_7 v' \psi' - \tfrac{1}{2}\mu_8 v' \psi' S \\
&\quad - \mu_9 \psi' s_4 - \tfrac{1}{2}\mu_{10} v' \psi' s_2 - \tfrac{1}{2}\mu_{11} v' \psi' s_1 - \tfrac{1}{2}\mu_{12} v' \psi' s_3
\end{aligned}
\tag{4.10}
$$

and from the heat flux equation the following equations

$$
\begin{aligned}
q_1 &= -\tfrac{1}{2}\lambda_4 v' s_5 - \tfrac{1}{2}\lambda_5 v' \psi' - \tfrac{1}{2}\lambda_6 v' \psi' S - \lambda_7 \psi' s_4 - \tfrac{1}{2}\lambda_8 v' \psi' s_2 - \tfrac{1}{2}\lambda v' \psi' s_1 \\
q_2 &= \lambda_1 \psi' + \lambda_2 \psi' S + \lambda_3 v' s_4 + \tfrac{1}{2}\lambda_4 v' s_6 + \lambda_7 \psi'(s_1 + s_3) + \tfrac{1}{2}\lambda_8 v' \psi' s_4 + \tfrac{1}{2}\lambda_9 v' \psi' s_4 \\
q_3 &= \tfrac{1}{2}\lambda_4 v'(s_1 - s_2) - \lambda_7 \psi s_6 - \lambda_9 v' \psi' s_5
\end{aligned}
\tag{4.11}
$$

where $v' \equiv dv/dx_2$; $\psi' \equiv d\psi/dx_2$; and μ_i and λ_i are constants; and

$$S \equiv \text{tr } \mathbf{s} = s_1 + s_2 + s_3 \tag{4.12}$$

From the heat conduction equation (4.5), we have

$$
\begin{aligned}
v's_4 = \frac{d}{dy}\Bigg\{ \lambda_1\psi' + v's_4 \Bigg[\lambda_3 + \tfrac{1}{2}(\lambda_8 + \lambda_9)\psi' \\
- \frac{(2\mu_2 + \mu_6 + 1)}{\mu_3} - \frac{(\mu_3\lambda_2 - 2\mu_1\lambda_7)(3\mu_2 + 2\mu_6)}{\mu_3(3\mu_1 + \mu_3)}\psi' \Bigg] \\
+ v's_6 \Bigg[\tfrac{1}{2}\lambda_4 - \frac{(\mu_{11} - \mu_{10})}{\mu_3}\psi' - \frac{(\mu_3\lambda_2 - 2\mu_1\lambda_7)(\mu_{11} - \mu_{12} - \mu_{10})}{\mu_3(3\mu_1 + \mu_3)}(\psi')^2 \Bigg] \Bigg\}
\end{aligned}
\tag{4.13}
$$

where we have considered the energy supply r to be equal to zero.

We propose an approximate solution to the problem with the extra stress components expressible in the form

$$s_\alpha(v', \psi') \equiv \overset{0}{s}_\alpha(v') + \psi'\overset{1}{s}_\alpha(v') + (\psi')^2\overset{2}{s}_\alpha(v') + \ldots \tag{4.14}$$

$$(\alpha = 1, 2, \ldots, 6)$$

where $\overset{0}{s}_\alpha, \overset{1}{s}_\alpha, \ldots,$ are functions of v' only. For the case of $(\psi')^2 \ll \psi'$, we assume

$$s_\alpha(v', \psi') \cong \overset{0}{s}_\alpha(v') + \psi'\overset{1}{s}_\alpha(v') \tag{4.15}$$

Substituting (4.15) in (4.10) and using the fact that ψ' is arbitrary, we obtain two sets of simultaneous equations, one set in terms of $\overset{0}{s}_\alpha$ and the other in terms of $\overset{0}{s}_\alpha$ and $\overset{1}{s}_\alpha$. Solving these equations we obtain explicit expressions for the extra stress components:

$$s_1 = \frac{\mu_4(\nu_2 + \mu_2 + \mu_6 + 1)}{2\mu_3^2} \left[\frac{(v')^2}{1 + \nu_1(v')^2} \right]$$

$$s_2 = \frac{\mu_4(\nu_2 + \mu_2 + \mu_6 - 1)}{2\mu_3^2} \left[\frac{(v')^2}{1 + \nu_1(v')^2} \right]$$

$$s_3 = \frac{\mu_4(\nu_2 + \mu_2)}{2\mu_3^2} \left[\frac{(v')^2}{1 + \nu_1(v')^2} \right]$$

$$s_4 = -\frac{\mu_4}{2\mu_3} \frac{v'}{1 + \nu_1(v')^2} \tag{4.16}$$

$$s_5 = \left(\frac{\nu_8}{\nu_5} \left[1 - \frac{1}{1 + \nu_5(v')^2} \right] + \frac{\nu_3}{\mu_3} v's_4 \left[\nu_9 + \frac{\nu_{10}}{1 + \nu_5(v')^2} \right] \right)\psi'$$

$$s_6 = \left(\tfrac{1}{2}\frac{\mu_7}{\mu_3} v' \left[\frac{1}{1 + \nu_5(v')^2} \right] + \frac{\nu_7}{\nu_5} s_4 \left(1 + \frac{\nu_5\nu_6 - \nu_7}{\nu_7[1 + \nu_5(v')^2]} \right) \right)\psi'$$

where ν_i are material constants expressible in terms of μ_i.

We note that for the isothermal case, i.e. $\psi' = 0$, the solution reduces to that obtained by Noll [8]. For the case of zero body force in the direction of the flow, v' is a constant and the flow is a simple shear flow. Using this fact in $(4.16)_6$ together with the pertinent equation of motion, we obtain a parabolic temperature profile.

4.2. *Other Coupled Effects*

If work on coupled effects in nonlinear thermoviscoelastic materials is meager, rational studies on other coupled effects in nonlinear viscoelastic materials are positively nil.

Several investigators have made attempts at the analysis of the motion of viscoelastic materials in the presence of electromagnetic fields, for example, Agarwal and Jain [51]. However, effects are assumed uncoupled in the constitutive equations. While this is true in the classical, linear theories, it is no longer valid in the nonlinear case. Neither would a simple superposition of effects be suitable in the nonlinear theory.

The basic theory for such effects would not be difficult to formulate in the light of many recent results on coupled effects in nonlinear materials. (For instance, see refs. [13, 14, 15]). However, until such rational theories are introduced for viscoelastic materials, the actual analysis of specific problems in this field will have to wait.

5. CONCLUSIONS

In spite of the relative novelty of the theories proposed on nonlinear viscoelasticity, a significant number of practical problems have been analyzed. This is particularly true in the analytical study of the steady flow of viscoelastic media. Important results have been obtained and useful guidelines have been set for experimentalists in nonlinear materials to apply. Dynamical problems have also been considered by several investigators; however, it is only recently that interest has started to develop in the study of wave propagations in nonlinear viscoelastic materials. Very little has been done in the study of coupled effects in these media. Some results have been obtained on the behavior of heat-conducting viscoelastic materials, but no significant problems have been solved to study other coupled effects. Finally, although the constitutive theory of nonlinear viscoelasticity is now reasonably well-set, theorems on the uniqueness and existence of solutions for initial and boundary value problems are still unavailable.

REFERENCES

[1] GARNER, F. H. and NISSAN, A. H., "Rheological properties of high-viscosity solutions of long molecules", *Nature*, **158**, 634–635 (1946).

[2] WEISSENBERG, K., "Abnormal substances and abnormal phenomena of flow", *Proc. Int. Congr. Rheol.*, I-29, I-46 (1948).

[3] REINER, M., "Slippage in a non-Newtonian liquid", *J. Rheol.*, **2**, 337–350 (1931).

[4] RIVLIN, R. S., "Hydrodynamics of non-Newtonian fluids", *Nature*, **160**, 611–613 (1947).

[5] DOYLE, T. C. and ERICKSEN, J. L., "Nonlinear elasticity", *Advances in Appl. Mechs.*, **4**, 53–115 (1956).

[6] ERINGEN, A. C., *Nonlinear Theory of Continuous Media*, McGraw-Hill (1962).

[7] ERINGEN, A. C. and GROT, R. A., "Continuum theory of nonlinear viscoelasticity", This volume, p. 157.

[8] NOLL, W., "On the continuity of the solid and the fluid states", *J. Rational Mech. Anal.*, **4**, 3–81 (1955).

[9] RIVLIN, R. S. and ERICKSEN, J. L., "Stress-deformation relations for isotropic materials", *ibid.*, **4**, 323–425 (1955).

[10] NOLL, W., "A mathematical theory of the mechanical behavior of continuous media", *Arch. Rational Mech. Anal.*, **2**, 197–226 (1958).

[11] OLDROYD, J. G., "On the formulation of rheological equations of state", *Proc. Royal. Soc. Lond.*, A–**200**, 523–541 (1950).

[12] KOH, S. L. and ERINGEN, A. C., "On the foundations of nonlinear thermo-viscoelasticity", *Int. J. Eng. Sci.*, **1**, 199–229 (1963).

[13] JORDAN, N. F. and ERINGEN, A. C., "On the static nonlinear theory of electromagnetic thermoelastic solids", *ibid.*, **2**, 59–96 (1964).

[14] ERINGEN, A. C. and INGRAM, J. D., "A continuum theory of chemically reacting media-I", *ibid.*, **3**, 197–212 (1965).

[15] DIXON, R. C. and ERINGEN, A. C., "A dynamical theory of polar elastic dielectrics-I", *ibid.*, **3**, 359–378 (1965).

[16] GURTIN, M. E. and STERNBERG, E., "On the linear theory of viscoelasticity", *Arch. Rational Mech. Anal.*, **11**, 291–356 (1962).

[17] ONAT, E. T. and BREUER, S., "On uniqueness in linear viscoelasticity", *Prog. Appl. Mech.*, *Prager Anniversary Volume*, Macmillan, N.Y. (1963).

[18] EDELSTEIN, W. S. and GURTIN, M. E., "Uniqueness thorems in the linear theory of aniso-tropic viscoelastic solids", *Arch. Rational Mech. Anal.*, **17**, 47–60 (1964).

[19] ODEH, F. and TADJBAKHSH, I., "Uniqueness in the linear theory of viscoelasticity", *ibid.*, **18**, 244–250 (1965).

[20] RIVLIN, R. S., "Solution of some problems in the exact theory of viscoelasticity", *J. Rational Mech. Anal.*, **5**, 179–188 (1956).

[21] COLEMAN, B. D. and NOLL, W., "On certain steady flows of general fluids", *Arch. Rational Mech. Anal.*, **3**, 289–303 (1959).

[22] COLEMAN, B. D. and NOLL, W., "An approximation theorem for functionals with applica-tions in continuum mechanics", *ibid.*, **6**, 355–370 (1960).

[23] TING, T. W., "Certain non-steady flows of second-order fluids", *ibid.*, **14**, 1–26 (1963).

[24] LANGLOIS, W. E., "Steady flow of a slightly viscoelastic fluid between rotating spheres", *Quart. Appl. Math.*, **21**, 61–71 (1963).

[25] MARKOVITZ, H. and COLEMAN, B. D., "Nonsteady helical flow of second-order fluids", *Phys. of Fluids*, **7**, 833–841 (1964).

[26] LANGLOIS, W. E., "A recursive approach to the theory of slow, steady-state viscoelastic flow", *Trans. Soc. Rheol.*, **7**, 75–99 (1963).

[27] LANGLOIS, W. E. and RIVLIN, R. S., "Slow steady-state flow of viscoelastic fluids through non-circular tubes", *Rend. Matematica di Roma*, **22**, 169 (1963).

[28] LANGLOIS, W. E., "The recursive theory of slow viscoelastic flow applied to three basic problems of hydrodynamic", *Trans. Soc. Rheol.*, **8**, 33–60 (1964).

[29] MARKOVITZ, H. and WILLIAMSON, R. B., "Normal stress effect in polyisobutylene solutions. I. Measurements in a cone and plate instrument", *ibid.*, **1**, 25–36 (1957).

[30] MARKOVITZ, H., "Normal stress effect in polyisobutylene solutions. II. Classification and application of rheological theories", *ibid.*, **1**, 37–52 (1957).

[31] ERICKSEN, J. L., "The behavior of certain viscoelastic materials in laminar shearing motions", *Viscoelasticity: Phenomenological Aspects*, BERGEN, J. T., Ed., Academic Press, pp 77–91 (1960).

[32] COLEMAN, B. D. and NOLL, W., "Helical flow of general fluids", *J. Appl. Physics*, **30**, 1508–1512 (1959).

[33] SHARMA, S. K., "Viscoelastic steady flow", *Z.A.M.M.*, **39**, 313–322 (1959).

[34] CRIMINALE, W. O., Jr., ERICKSEN, J. L. and FILBEY, G. L., Jr., "Steady flow of non-Newtonian fluids", *Arch. Rational Mech. Anal.*, **1**, 410–417 (1958).

[35] COLEMAN, B. D., "Substantially stagnant motions", *Trans. Soc. Rheol.*, **6**, 293–300 (1962).

[36] COLEMAN, B. D., "Kinematical concepts with applications in the mechanics and thermodynamics of incompressible viscoelastic fluids", *Arch. Rational Mech. Anal.*, **9**, 273–300 (1962).

[37] NOLL, W., "Motions with constant stretch history", *ibid.*, **11**, 97–105 (1962).

[38] COLEMAN, B. D. and NOLL, W., "Steady extension of incompressible simple fluids", *Phys. of Fluids*, **5**, 840–843 (1962).

[39] COLEMAN, B. D. and NOLL, W., "Recent results in the continuum theory of viscoelastic fluids", *Annals N. Y. Acad. Sci.*, **89**, 672–714 (1961).

[40] VARLEY, E., "Acceleration fronts in viscoelastic materials", *Arch. Rational Mech. Anal.*, **19**, 215–225 (1965).

[41] COLEMAN, B. D., GURTIN, M. E. and HERRERA, R. I., "Waves in materials with memory", *ibid.*, **19**, 1–19, 239–298 (1965).

[42] NIILER, P. O. and PIPKIN, A. C., "Finite amplitude shear waves in some non-Newtonian fluids", *Int. J. Eng. Sci.*, **2**, 305–315 (1964).

[43] PIPKIN, A. C. and RIVLIN, R. S., "Small deformations superposed on large deformations in materials with fading memory", *Arch. Rational Mech. Anal.*, **8**, 297–308 (1961).

[44] GREEN, A. E., RIVLIN, R. S. and SPENCER, A. J. M., "The mechanics of non-linear materials with memory", *ibid.*, **1**, 1–21 (1957); **3**, 82–90 (1959); **4**, 387–404 (1960).

[45] GREEN, A. E. and RIVLIN, R. S., "Steady flow of non-Newtonian fluids through tubes", *Quart. Appl. Math.*, **14**, 299–308 (1956).

[46] PIPKIN, A. C., "Alternating flow of non-Newtonian fluids in tubes of arbitrary cross-section", *Arch. Rational Mech. Anal.*, **15**, 1–13 (1964).

[47] DATTA, S. K., "Note on the stability of an elastico-viscous liquid in Couette flow", *Phys. of Fluids*, **7**, 1915–1919 (1964).

[48] GENENSKY, S. M., "A general theorem concerning the stability of a particular non-Newtonian fluid", *Quart. Appl. Math.*, **18**, 245–250 (1960).

[49] FERRY, J. D., *Viscoelastic Properties of Polymers*, Wiley and Sons (1961).

[50] KOH, S. L. and ERINGEN, A. C., "On the foundations of nonlinear thermo-viscoelasticity", *ONR Tech. Rept.* 20, Purdue University School of Aero. and Eng. Sci. (1962).

[51] AGARWAL, J. P. and JAIN, M. K., "On the motion of viscoelastic electrically conducting liquid in the presence of a magnetic fluid", *ZAMP*, **13**, 152–160 (1962).

THE SOLUTION OF BOUNDARY VALUE
PROBLEMS IN LINEAR VISCOELASTICITY

S. C. HUNTER

Mathematics Department, University of Strathclyde
Glasgow, Scotland

Abstract—Methods for the solution of boundary value problems in linear viscoelasticity
are surveyed and applied to a number of physical problems.

1. INTRODUCTION

Although the subject of viscoelasticity dates back to the mid nineteenth century, it is only within the last decade that attempts have been made to solve boundary value problems in which stress, strain and displacement fields are functions of space and time. The purpose of the present paper is to review the types of problem that have proved soluble and the methods and techniques that have been developed.

In the theory of infinitesimal elasticity, problems are classified as dynamic or static according to whether or not the solution depends on time. For viscoelasticity, where the viscoelastic effects are of any significance at all, there are no real static problems for self evident reasons; however, in many problems it is permissible to neglect the acceleration terms in the equations of motion, in which circumstances the problems are usually known as "quasi-static" or "quasi-stationary". The only truly static problems of viscoelasticity are problems of classical elasticity obtained in the equilibrium limit of complete stress relaxation.

In classical elasticity, static problems are divided into one of two types. In the simpler problems either the external load or alternatively the external displacement is everywhere specified on the bounding surfaces. The more complicated problems are those with mixed boundary conditions, where over part of the surface the load is specified, while over the complementary surface the displacement is given. The classification of viscoelastic problems is more involved. The viscoelastic analogues of the simpler elastic problems possess solutions expressible directly in terms of the associated elastic problem, and the difficulties of solution are no more than for the elastic problem. However, mixed boundary value problems of viscoelasticity are subdivided into two further classes. In the simpler of these two classes, the loading history is known for all time over a fixed boundary area, while the displacement history is known for the (fixed) complementary boundary area. An example of such a problem is the indentation of a half space by a flat circular punch (Section 3.3). This type of problem also possesses a solution expressible directly in terms of the corresponding elastic

17   257

solution and the difficulties of solution are again no more than that of the elastic problem.

There remain the "essentially" viscoelastic problems which are of the mixed boundary type, but where the position of the line delineating the complementary regions varies with time. For such problems, for example the progressive indentation of a half space by a rigid sphere or cone (Section 4), there are boundary areas where for part of the history the loading is specified while for the remainder of the history the displacement is defined. For problems of this type there is no viscoelastic–elastic correspondence principle and solutions of these problems entail features for which there is no elastic analogue. Mathematically these problems are the most interesting of the quasi-static type in that the inherent difficulties are due to the viscoelastic nature of the solid.

Quasi-static viscoelastic problems for which a viscoelastic–elastic correspondence principle may be invoked may be regarded as completely solved in terms of the associated elastic problem, and there are a number of examples in the literature. These problems are discussed in Section 3. On the other hand few "essentially" viscoelastic problems have been examined; in the present article the spherical indenter problem is solved by a new method (Section 4) and reference is made to the other solved problems.

Most published research on dynamic problems of viscoelasticity (Section 5) has been concerned primarily with the simpler wave propagation problems involving only one space variable, i.e. either rectilinear or spherical wave propagation. Much of this work is based on the use of steady state eigenfunctions for which displacement, stress and strain are everywhere proportional to $\exp(i\omega t)$ where t is the time variable. Solutions to transient problems are then obtained by a Fourier synthesis of the steady state eigenfunctions.

Lockett [1] recently discovered the possibility of viscoelastic waves propagating in three dimensions with different directions of attenuation and propagation (Section 5.2). The novel features of these waves suggest that they are most likely to occur in dynamic problems which are "essentially" viscoelastic, i.e. in problems for which there is no dynamic correspondence principle.

Section 5.3 deals with the general solution of free vibration problems from a new viewpoint; finally in Section 5.4 and 5.5 we give a brief review of other solved problems in dynamic viscoelasticity.

Throughout this paper an attempt has been made to express results in terms of observable viscoelastic properties (e.g. complex moduli, loss angle) rather than in terms of the parameters of the somewhat artificial spring and dashpot models, whose utility is limited by the experimental fact that most real materials exhibit viscoelastic behaviour characterized by a relaxation spectrum spread over many decades (typically from 10^{-5} to 10^3 sec). To this end it has been necessary to employ some of the more common physical approximations.

No attempt has been made to include the study of thermo-viscoelasticity in this review. Thermo-viscoelasticity is complicated by the problem that the mechanical properties of most viscoelastic solids are highly susceptible to temperature variation, in contrast to the relatively insensitive behavior of the

elastic constants of metals. Further by their very nature, viscoelastic solids necessarily generate heat during deformation, and a full analysis of the equations governing the propagation of temperature, stress and strain in the most general case entail thermodynamic problems which as yet are not fully understood. In an earlier paper [2] the author has indicated a possible approach to these difficulties for the "thermo-rheologically simple" solid defined by Schwarzl and Staverman [3].

The basic equations of a thermo-rheologically simple solid in the absence of internally generated heat and thermodynamic coupling effects are given by Morland and Lee [4], who apply the equations to the quasistatic problem of an incompressible long cylinder subject to radial temperature gradient and internal pressure. Similar equations are derived by Muki and Sternberg [5] who discuss transient stress problems in plane slabs and spheres subject to temperature variation. More recently Rogers and Lee [6] have solved the quasi-static thermo-viscoelastic problem for a sphere with an internally ablating cavity. To date the complexities of the basic equations have prevented the solution of any dynamic thermoviscoelastic problems, although an exhaustive study of quasi-static thermal stress problems has been recently published by Sternberg [7].

2. BASIC EQUATIONS

The constitutive equations for the isothermal deformation of a linear visco-elastic solid may be taken in either of the forms

$$\sigma_{ij} = \delta_{ij} \int_{-\infty}^{t} \Gamma(t - t')\, \dot{\Delta}(t')\, dt' + 2 \int_{-\infty}^{t} G(t - t')\, \dot{\epsilon}'_{ij}(t')\, dt' \tag{2.1}$$

$$\epsilon_{ij} = (\delta_{ij}/9) \int_{-\infty}^{t} \Gamma^{-1}(t - t')\, \dot{\Sigma}(t')\, dt' + \tfrac{1}{2} \int_{-\infty}^{t} G^{-1}(t - t')\, \dot{\sigma}'_{ij}(t')\, dt' \tag{2.2}$$

In these equations σ_{ij} denotes stress and ϵ_{ij} denotes infinitesimal strain i.e.

$$\epsilon_{ij} = \tfrac{1}{2} \left[\frac{\partial u_i}{\partial x_j} + \frac{\partial u_j}{\partial x_i} \right]$$

where u_i is the displacement field. Also δ_{ij} is the Kronecker delta

$$\delta_{ij} = \begin{cases} 1 & (i = j) \\ 0 & (i \neq j) \end{cases}$$

while in cartesian tensor notation

$$\Delta = \epsilon_{ii} \qquad \qquad \Sigma = \sigma_{ii}$$
$$\epsilon'_{ij} = \epsilon_{ij} - \tfrac{1}{3}\Delta\delta_{ij} \qquad \sigma'_{ij} = \sigma_{ij} - \tfrac{1}{3}\Sigma\delta_{ij}$$

and the fluxion dot denotes differentiation with respect to time. Finally the pairs of functions $\Gamma(t)$, $\Gamma^{-1}(t)$ and $G(t)$, $G^{-1}(t)$ are experimental functions defined by

creep and relaxation tests in uniform dilatation and pure shear

i.e.
$$\text{for } \Delta = \Delta_0\, H(t) \qquad \Sigma = 3\Delta_0\, \Gamma(t)$$
$$\text{for } \Sigma = \Sigma_0\, H(t) \qquad \Delta = \tfrac{1}{3}\Sigma_0\, \Gamma^{-1}(t)$$
$$\text{for } \epsilon_{ij} = \epsilon_{ij}^0\, H(t) \qquad \sigma_{ij} = 2\,\epsilon_{ij}^0\, G(t) \qquad [i \neq j]$$
$$\text{for } \sigma_{ij} = \sigma_{ij}^0\, H(t) \qquad \epsilon_{ij} = \tfrac{1}{2}\,\sigma_{ij}^0 G^{-1}(t) \qquad [i \neq j)$$

In these equations $H(t)$ is the Heaviside step function

$$H(t) = \begin{cases} 1 & t \geq 0 \\ 0 & t < 0 \end{cases}$$

while the Δ_0, ϵ_{ij}^0 etc., are constant amplitudes.

The notation $\Gamma(t)$, $\Gamma^{-1}(t)$ is not meant to imply that Γ and Γ^{-1} are reciprocal functions (although for sufficiently small t, this is true) but to discriminate between relaxation and creep. However, Γ and Γ^{-1} are related, and as will be seen subsequently, the S-multiplied Laplace transforms of Γ and Γ^{-1} are reciprocal functions. Similar remarks apply to G and G^{-1}.

It is assumed that both the shear and dilatational behaviour may be modelled by a mechanical analogue comprising a distribution, possibly continuous, of springs and dashpots in series and parallel. (The model is surprisingly close to the current molecular physics models of elastomers and linear polymers, e.g. see Marvin and Oser [8], Rouse [9], Bueche [10]. Under these circumstances $G(t)$ and $G^{-1}(t)$ may be written as

$$G = G_0(1 - \phi(t)) \qquad G^{-1} = G_0^{-1}(1 + \psi(t))$$

where G_0 is the instantaneous or dynamic shear modulus while ϕ and ψ are monotonically increasing functions of time which admit the integral representations

$$\phi = \int_0^\infty g(\tau)\,(1 - e^{-t/\tau})\,d\tau$$

$$\psi = \int_0^\infty f(\tau)\,(1 - e^{-t/\tau})\,d\tau$$

in which the relaxation spectrum $g(\tau)$ and retardation (or creep) spectrum $f(\tau)$ are positive. $\phi(t)$ also satisfies the inequality

$$\phi(\infty) \leq 1$$

and in the limiting case of equality, ψ is further supplemented by a linear creep term. A more extensive discussion is given by the author [11], and, with different notations, in numerous other articles (e.g. see Alfrey [12], Gross [13].) Similar remarks apply to $\Gamma(t)$ and $\Gamma^{-1}(t)$.

With the assumptions outlined above the constitutive equations (2.1), (2.2) may be expressed in the form (e.g. see Hunter [11])

$$\bar{\sigma}_{ij}(S) = \lambda(S)\,\bar{\Delta}(S)\,\delta_{ij} + 2\mu(S)\,\bar{\epsilon}_{ij}(S) \qquad (2.3)$$

obtained from subjecting (2.1) and (2.2) to a Laplace transform and assuming that at some time in the finite past the solid was stress free and in mechanical equilibrium. In equation (2.3) the field quantities $\bar{\sigma}_{ij}$ and $\bar{\epsilon}_{ij}$ are the Laplace transforms of σ_{ij} and ϵ_{ij}

$$\bar{\sigma}_{ij}(x_k, S) = \int_0^\infty e^{-St} \sigma_{ij}(x_k, t) \, dt \quad \text{etc.}$$

while $\lambda(S)$ and $\mu(S)$ are defined by

$$\left.\begin{array}{c} \lambda(S) = K(S) - \tfrac{2}{3}\mu(S) \\[2mm] \mu(S) = S \int_0^\infty G(t) \, e^{-St} \, dt \\[2mm] K(S) = S \int_0^\infty \Gamma(t) \, e^{-St} \, dt \end{array}\right\} \qquad (2.4)$$

Finally the self-consistency of eqns. (2.1) and (2.2) require the auxiliary relations

$$\left[S \int_0^\infty G^{-1}(t) \, e^{-St} \, dt \right]^{-1} = S \int_0^\infty G(t) \, e^{-St} \, dt \qquad (2.5)$$

and similarly for Γ.

In eqn. (2.3), $\bar{\sigma}_{ij}$ and $\bar{\epsilon}_{ij}$ are usually functions of both the transform parameter S and the space variables x_i. On the other hand the transform moduli $\lambda(S)$ and $\mu(S)$ are functions solely of the complex variable S, analytic in the entire S-plane cut along the negative real axis.

The formal analogy between (2.3) and the corresponding equation for elastic solids

$$\sigma_{ij} = \lambda \Delta \, \delta_{ij} + 2\mu \, \epsilon_{ij}$$

where λ, μ are the Lamé constants, has proved very fruitful in the solution of viscoelastic problems. This correspondence is discussed more fully in Section 3 in connection with the simpler quasi-static viscoelastic problems.

In terms of $\lambda(S)$ and $\mu(S)$ it is possible to construct a transform Young's modulus and Poisson's ratio from the usual formulae of elasticity theory:

$$E(S) = 2\mu(S) \, [1 + \nu(S)], \quad \nu(S) = \tfrac{1}{2}\lambda(S)/[\lambda(S) + \mu(S)]$$

and it is sometimes more convenient to work with E and ν in place of λ and μ.

Experimental information on the mechanical properties of solids is usually expressed in terms of the complex moduli measured in steady state oscillatory tests, in which small samples are subjected to uniform shear or tensile strains*

$$\gamma = \gamma_0 \, e^{i\omega t} \qquad \epsilon = \epsilon_0 \, e^{i\omega t}$$

---

* Strictly the ensuing formulae should read $\gamma = \text{Re} \, \gamma_0 \, e^{i\omega t}$ etc. where Re stands for real part. Conventionally, as here, the Re is omitted.

The corresponding steady state stresses are

$$\tau = 2\mu(i\omega)\,\gamma_0\,e^{i\omega t} \qquad \sigma = E(i\omega)\,\epsilon_0\,e^{i\omega t}$$

where the complex moduli are given by substituting $S = i\omega$ in the transform moduli (e.g. see Hunter [11].)

i.e. $$E(i\omega) = [E(S)]_{s=i\omega} \quad \text{etc.}$$

For some calculations, particularly in wave propagation theory, it is more convenient to work with the complex moduli rather than the transform moduli.

As is implied by the notation, the complex moduli are complex numbers

$$E(i\omega) = E_1(\omega) + i\,E_2(\omega) \quad \text{etc.}$$

where E_1 is a real even function of ω and E_2 a real odd function. The "loss" angle is defined by

$$\tan \varDelta(\omega) = \frac{E_2}{E_1}, \qquad \omega > 0, \qquad 0 < \varDelta < \frac{\pi}{2}$$

and in general there are different loss angles associated with the different moduli.

Information on the dilatational behaviour of solids is at best scanty and for many materials non-existent. In principle the dilatational behaviour is determined from the shear and tensile behaviour, e.g. in terms of complex moduli

$$[9\,K(i\omega)]^{-1} + [3\,\mu(i\omega)]^{-1} = [E(i\omega)]^{-1} \tag{2.6}$$

but the accuracy of most experimental data, particularly at low circular frequencies ω is inadequate to discriminate between (2.6) and the incompressible approximation

$$E(i\omega) = 3\,\mu(i\omega)$$

In view of this, and because of the mathematical simplifications entailed, we make frequent use of the approximation that similar viscoelastic response obtains for both shear and dilatational behaviour, i.e. it is assumed that $\lambda(S)$, $\mu(S)$, $E(S)$, $K(S)$ are all essentially the same function of S with different multiplicative constants λ_0, μ_0, E_0, K_0 denoting the instantaneous or high frequency elastic moduli. In this approximation $\nu(S)$ is independent of S and given by

$$\nu(S) = \nu_0 = \tfrac{1}{2}\lambda_0/(\lambda_0 + \mu_0) \tag{2.7}$$

and the same loss angle $\varDelta(\omega)$ is associated with every complex modulus.

In the solution of boundary value problems the constitutive equations (2.1) [or (2.2) or (2.3)] are supplemented by the equations of motion

$$\frac{\partial \sigma_{ij}}{\partial x_j} + \rho\,B_i = \rho\,\frac{\partial^2 u_i}{\partial t^2} \tag{2.8}$$

where ρ is density and B_i the body force. For quasi-static problems, the inertial term is neglected.

In writing down the equations of this section and in their subsequent appli-

cation to boundary value problems, all the usual geometrical assumptions of infinitesimal elasticity theory are implied. These include the assumptions of small strains, small displacements, boundary conditions applied to unperturbed surfaces and neglect of convective terms in the acceleration.

The extensive body of existence and uniqueness theorems in classical elasticity has been extended by Gurtin and Sternberg [14] to the equations of linear viscoelasticity. In the following the uniqueness and existence of solutions is taken for granted, and we are predominantly concerned with the methods and techniques of solution.

3. SOLUTION OF QUASI-STATIC PROBLEMS VIA CORRESPONDING ELASTIC SOLUTION

3.1. *The Correspondence Principle*

For quasi-static problems, eqns. (2.8) are approximated by

$$\frac{\partial \sigma_{ij}}{\partial x_j} + \rho B_i = 0 \tag{3.1}$$

or on multiplying by e^{-St} and integrating over $-\infty < t < \infty$*

$$\frac{\partial \bar{\sigma}_{ij}}{\partial x_j} + \rho \bar{B}_i = 0 \tag{3.2}$$

For the simpler quasi-static viscoelastic problems the boundary (or boundaries) $\mathscr{S}$ are divided into a fixed region(s) $\mathscr{S}_1$ and a complementary region(s) $\mathscr{S}_2 = \mathscr{S} - \mathscr{S}_1$. On $\mathscr{S}_1$ the external loading F_i is prescribed

$$\sigma_{ij} n_j = F_i(x, t) \qquad x \text{ on } \mathscr{S}_1 \tag{3.3}$$

while on $\mathscr{S}_2$ the surface displacements U_i are prescribed

$$u_i = U_i(x, t) \qquad x \text{ on } \mathscr{S}_2 \tag{3.4}$$

Since F_i and U_i are prescribed for all t, the time variable may be removed by a Laplace transform and the boundary conditions taken in the form

$$\bar{\sigma}_{ij} n_j = \bar{F}_i \qquad x \text{ on } \mathscr{S}_1 \tag{3.5}$$

$$\bar{u}_i = \bar{U}_i \qquad x \text{ on } \mathscr{S}_2 \tag{3.6}$$

where

$$\bar{F}_i = \int_{0^-}^{\infty} F_i(x, t) e^{-St} dt \quad \text{etc.}$$

Equations (2.3), (3.2), (3.5), (3.6) and the transform of the strain-displacement relation

$$\bar{\epsilon}_{ij} = \frac{1}{2} \left[\frac{\partial \bar{u}_i}{\partial x_j} + \frac{\partial \bar{u}_j}{\partial x_i} \right]$$

---

* Usually the integration range is $0^- < t < \infty$, the solid being assumed undisturbed prior to $t = 0$. The notation 0^- takes account of any possible step function discontinuities at $t = 0$.

define a fictitious elastic problem in which the elastic constants, body forces, external forces and external displacements are functions of the transform parameter S. If this associated elastic problem can be solved to yield $\bar{\sigma}_{ij}$ and/or $\bar{u}_i$ throughout the body then a subsequent Laplace inversion gives σ_{ij} and/or u_i for the viscoelastic problem (Lee [15, 16, 17], Lee, Radok and Woodward [18]).

The general correspondence principle discussed above is most easily utilized when the dependence of B_i, F_i and U_i on x and t is separable in the sense*

$$\left.\begin{array}{l} B_i = \beta_i^0 \, \beta_i \, (t) \, B_i^{(0)}(x) \\[4pt] F_i = \pi_i^0 \, \pi_i \, (t) \, F_i^{(0)}(x) \\[4pt] U_i = \chi_i^0 \, \chi_i \, (t) \, U_i^{(0)}(x) \end{array}\right\} \qquad (3.7)$$

where β_i^0, π_i^0, χ_i^0 are constants and where the associated static elastic problem is defined by

$$B_i = \beta_i^0 \, B_i^{(0)}(x), \quad F_i = \pi_i^0 F_i^{(0)}(x), \quad U_i = \chi_i^0 \, U_i^{(0)}(x).$$

If the solution of this elastic problem is given by

$$u_i \, (x, t) = \xi_i \, (\rho \beta_i^0, \, x_i^0, \, \pi_i^0, \, \lambda, \, \mu, \, x)$$

then for the viscoelastic problem, the transform of u_i is given by

$$\bar{u}_i(x, S) = \xi_i \, (\rho \, \beta_i^0 \, \bar{\beta}_i, \, \pi_i^0 \, \bar{\pi}_i, \, \chi_i^0 \, \bar{\chi}_i, \, \lambda(S), \, \mu(S), \, x)$$

whose inversion yields $u_i(x, t)$. Since the functions $\beta_i(t)$, $\pi_i(t)$, $\chi_i(t)$ are arbitrary, it is evident that one elastic solution yields the solution to a wide class of viscoelastic problems.

Although the use of the correspondence principle yields a formal solution to a viscoelastic problem, there remains the difficult problem of inverting the resultant transforms. In many cases it may be unnecessary to invert the transforms for all x, if for example the predominant interest is the value of displacement (or stress) at some fixed point; in other cases the quantity of major interest may be an integral property of the solution (e.g. the total load required to indent a half space) in which case it is usually easier to evaluate the relevant integral before inversion.

A number of simplifications occur in the general theory of the correspondence principle if body forces are neglected and if the constant Poisson's ratio model of eqn. (2.7) is adopted. In particular if $\mathscr{S}_1$ is a stress free surface, then the boundary value problem may be formulated entirely in terms of displacements and independent of the transform moduli. In consequence the displacement field at any given time is identical with the displacement field of the corresponding elastic problem, subject to the same boundary conditions. A less useful result concerns examples where $\mathscr{S}_2$ vanishes and the external loading is everywhere specified; here the resultant viscoelastic stress field is identical with the stress field of the corresponding elastic problem. In both cases the viscoelastic proper-

---

* In eqns. (3.7) the summation convention is not used.

ties reappear in evaluating respectively the stress and displacement/strain fields
   The use of the correspondence principle is illustrated below in three elementary examples.

3.2. Torsional Oscillations of a Cylinder

In the theory of elasticity, the displacement field of a twisted solid cylinder with a stress free cylindrical surface (Love [19]) is given by

$$u_\theta = \theta r \frac{z}{l} \qquad u_r = u_z = 0 \tag{3.8}$$

where u_r, u_θ, u_z are components of displacement in cylindrical polar coordinates, l is the length of the cylinder and θ the angle of twist at $z = l$. For the analogous quasi-static viscoelastic problem with prescribed displacement

$$u_\theta = \begin{cases} r\theta & z = l \\ 0 & z = 0 \end{cases}$$

and a stress free cylindrical surface, the displacement field is given by (3.8) with the modification that θ is now dependent on time.
   The only non-vanishing strain component is

$$\epsilon_{\theta z} = \tfrac{1}{2}\theta(t)\frac{r}{l}$$

so that the only non-vanishing transformed stress is

$$\bar\tau_{\theta z} = \mu(S)\,\bar\theta(S)\,\frac{r}{l}$$

and the total (transformed) couple required to maintain θ is

$$\bar{M} = 2\pi \int_0^a \bar\tau_{\theta z}\, r^2\, dr = \frac{\pi a^4}{2l}\,\mu(S)\,\bar\theta(S) \tag{3.9}$$

Equation (3.9) may be inverted in either of the forms

$$M(t) = \frac{\pi a^4}{2l} \int_{-\infty}^{t} \theta(t')\, G(t - t')\, dt'$$

$$\theta(t) = \left(\frac{\pi a^4}{2l}\right)^{-1} \int_{-\infty}^{t} \dot{M}(t')\, G^{-1}(t - t')\, dt'$$

which provides a complete solution for either prescribed $\theta(t)$ or $M(t)$.
   Of more interest is the problem of free torsional oscillations for which

$$M = -I\,\ddot\theta \tag{3.10}$$

where I is the moment of inertia of the suspended mass. If initially

$$\theta = \theta_0, \qquad \dot\theta = 0, \qquad t = 0,$$

the transform of (3.10) yields

$$\bar M = S^2\bar\theta - S\theta_0.$$

Substituting this result in (3.9) and solving for $\bar\theta$ gives

$$\frac{\bar\theta}{\theta_0} = S\left[S^2 + \frac{\pi a^4}{2l}\,\mu(S)\right]^{-1}$$

or by the inversion theorem

$$\frac{\theta}{\theta_0} = (2\pi i)^{-1}\int\limits_{c-i\infty}^{c+i\infty} Se^{St}\left[S^2 + \frac{\pi a^4}{2l}\,\mu(S)\right]^{-1}\mathrm{d}S \qquad (3.11)$$

which can be evaluated completely only with detailed specification of $\mu(S)$. However, the major contribution to the Laplace inversion arises from two simple poles which correspond to the poles

$$S = \pm\,i\omega_0 \qquad \omega_0^2 = \frac{\pi a^4}{2l}\,\mu_0$$

in the corresponding elastic problem.

For the present problem we assume the denominator of (3.11) to vanish for

$$S_1 = i\omega - \delta \qquad (3.12)$$

so that

$$-\,\omega^2 + \delta^2 - 2i\omega\delta + \frac{\pi a^4}{2l}\,\mu(i\omega - \delta) = 0 \qquad (3.13)$$

To proceed further requires the introduction of some physical approximations concerning the real and imaginary parts of $\mu(i\omega)$. For most real materials exhibiting significant viscoelastic behaviour the relaxation and retardation spectra are smooth functions of τ spread over many decades of τ; under these circumstances it may be shown that μ_1 and μ_2 are related by

$$\frac{\mathrm{d}\mu_1(\omega)}{\mathrm{d}(\log\omega)} \simeq \left(\frac{2}{\pi}\right)\mu_2(\omega) = \left(\frac{2}{\pi}\right)\mu_1(\omega)\tan\Delta \qquad (3.14)$$

(e.g. see Ferry and Williams [20], Ferry and Fitzgerald [21]. Also for these values of ω where the viscoelasticity is significant, $\tan\Delta$ is commonly a slowly varying function of frequency, so that

$$\mu_2'(\omega) \ll \mu_1'(\omega)$$

provided

$$\tan\Delta \ll 1$$

an inequality valid for many materials.

Introducing these approximations into (3.13) and expanding $\mu(i\omega - \delta)$ by

Taylor's theorem* under the assumption $\delta \ll \omega$, yields to first order in $\tan \Delta$ and δ.

$$- \omega^2 - 2i\omega\delta + \frac{\pi a^4}{2l} \mu_1(\omega) (1 + i \tan \Delta) = 0$$

so that ω is the single positive root of

$$\omega^2 = \frac{\pi a^4}{2l} \mu_1(\omega) \tag{3.15}$$

and δ is given by

$$\delta = \frac{\pi a^4}{4l} \mu_1(\omega) \tan \Delta = \tfrac{1}{2}\omega \tan \Delta \tag{3.16}$$

which justifies the initial assumption $\delta \ll \omega$.

In the same approximation a second simple pole is located at

$$S_2 = - i\omega - \delta$$

with ω, δ given by (3.15), (3.16).

From a well-known theorem the residue of the right-hand side of (3.11) at $S = S_1$ is given by

$$R_1 = S_1 \left[2S_1 + \frac{\pi a^4}{2l} \mu'(S_1) \right]^{-1} e^{S_1 t}$$

with a similar formula for S_2. Evaluating these residues with the help of the physical approximations already introduced and retaining first order terms in $\tan \Delta$ leads finally to

$$\frac{\theta(t)}{\theta_0} = (1 + \pi^{-1} \tan \Delta) \exp \left[- \tfrac{1}{2}(\omega \tan \Delta) t \right] \cos(\omega t) \tag{3.17}$$

with ω given by (3.15).

It is apparent that the solution obtained does not quite satisfy the initial boundary conditions; this is a consequence of neglecting other singularities of the integrand in (3.11) which contribute to the Laplace inversion. These remaining singularities give rise to an additional sum of exponentially decaying transients which for the most general case of a continuous spectrum $g(\tau)$ may be written as an integral

$$- \int_0^\infty q(\tau) e^{-t/\tau} d\tau \tag{3.18}$$

with $q(\tau) > 0$. While in general it is not possible to proceed further without detailed specification of $\mu(S)$, an approximate estimate of the supplementary term can be made by replacing (3.18) with a single exponential with amplitude and decay constant chosen to satisfy the initial conditions correctly to first

---

* The expansion is valid since μ is analytic everywhere except on the negative real axis.

order in tan Δ. In this approximation (3.18) becomes

$$- \frac{\tan \Delta}{\pi} \exp[- \pi\omega \, t/2] \qquad (3.19)$$

which sensibly vanishes for $\omega t > 2$. Then for sufficiently large t the free motion of the cylinder is given by (3.17).

In the practical application of this result, the observed circular frequency of the damped oscillation determines μ_1 (from eqn. (3.15)), and the observed damping constant then yields tan Δ.

3.3. *Impact of a Flat Circular Punch on a Half Space*

An important problem in polymer physics is the assessment of mechanical properties by various testing devices. From an experimental viewpoint one of the simplest apparatus to use in the laboratory is the sclerescope, in which a rigid ball is bounced on the surface of the specimen and measurements are taken of the energy loss and (less frequently) of impact duration.

Unfortunately while the apparatus is simple to use, the interpretation of the resulting data is difficult. Although a complete solution of the relevant boundary value problem has been obtained (Section 4), the resulting ordinary integro-differential equations for the motion of the ball are non-linear; it has only been possible to obtain a solution under highly restrictive conditions (Hunter [22]). In view of this it is of some value to analyse the simpler problem of the impact of a flat circular cylinder, for which a general solution is possible.

The solution of the problem of the normal indentation of an elastic half space by a flat ended rigid circular punch of radius a gives a pressure distribution

$$p(r) = \begin{cases} \dfrac{4\mu a}{1 - \nu} \times (a^2 - r^2)^{-1/2} & r < a \\ 0 & r > a \end{cases}$$

where x is the depth of penetration (Boussinesq [23]). The solution is singular at $r = a$ and for this reason is hardly realistic near the edge of the punch. In practice the local deformation and normal pressure will differ from the Boussinesq solution near $r = a$. In what follows, these deviations are neglected on the grounds that the important quantity is the total load given by

$$F = 2\pi \int_0^a pr \, \mathrm{d}r = \frac{8\pi a}{1 - \nu} \mu x \qquad (3.20)$$

rather than the detailed pressure distribution.

For the viscoelastic problem eqn. (3.20) is replaced by

$$F = \frac{8\pi a}{1 - \nu} \, \mu(S)\bar{x} \qquad (3.21)$$

on the assumption of a constant Poisson's ratio. Given $F(t)$ or $x(t)$ eqn. (3.21) then determines x or F. However, for the impact problem F is given by Newton's

law
$$F = -m\ddot{x},$$

where m is the indenter mass, or on taking a Laplace transform

$$\bar{F} = -m(S^2\,\bar{x} - V) \qquad (3.22)$$

where V is the initial impact velocity at $t = 0$, $x = 0$. Solving (3.21) and (3.22) for $\bar{x}$ gives

$$\bar{x} = V\left[S^2 + \frac{8\pi a}{m(1-\nu)}\,\mu(S)\right]^{-1} \qquad (3.23)$$

which is an equation very similar to that found in the torsional oscillation problem of Section 3.2. Making use of the same physical approximation as previously, the inversion of (3.23) gives

$$x = \frac{V}{\omega}\left(1 + \frac{\tan \varDelta}{\pi}\right)\exp[-\tfrac{1}{2}(\omega \tan \varDelta)\,t]\sin(\omega t - \tfrac{1}{2}\tan \varDelta)$$
$$+ \frac{V \tan \varDelta}{2\omega}\exp\frac{-2\omega t}{\pi} \qquad (3.24)$$

where ω is the solution of $\dfrac{m(1-\nu)}{8\pi a}\,\omega^2 = \mu_1(\omega)$.

The impact terminates at a time given by $\ddot{x} = 0$ with solution

$$\omega t = x - \tfrac{1}{2}\left[1 + \left(\frac{2}{\pi e}\right)^2\right]\tan \varDelta + 0\,(\tan^2 \varDelta)$$

when the indenter velocity is

$$-V\left[1 - \gamma \tan \varDelta\right]$$

where

$$\gamma = \tfrac{1}{2}\pi - \pi^{-1}\left[1 + e^{-2}\right] = 1.205$$

so that the coefficient of restitution is

$$e = 1 - 1.2\tan \varDelta$$

and the energy absorbed by the solid

$$\epsilon = 1.2\,mV^2\tan \varDelta$$

which completes the solution to the impact problem.

3.4. *Internal Radial Creep of a Rocket Filling under Centrifugal Forces*

As a final example of the use of the correspondence principle we examine the problem of a cylindrical rocket filling $b \le r \le a$, bonded at $r = a$ to a rigid wall, and rotated at angular velocity $\varOmega$. Assuming zero axial strain the radial displacement for the elastic problem is given by

$$u = Ar^{-1} + Br - \frac{\rho\varOmega^2}{8(\lambda + 2\mu)}\,r^3$$

where A and B are disposable constants determined by the boundary conditions. If the latter are taken to be

$$u = 0 \qquad r = a$$

$$\sigma_r = 0 \qquad r = b$$

the solution to the elastic problem yields a stress field independent of the elastic constants except for v. Thus for a solid of constant Poisson's ratio, the viscoelastic stress field is identical with the elastic problem. The most severe tensile stress occurs in the circumferential direction at $r = b$ with value

$$(\sigma_\theta)_{r=b} = \frac{\rho\Omega^2(1 - 2v)(a^2 - b^2)}{4(1 - v)[b^2 + (1 - 2v)a^2]}$$

so that tensile cracking will initiate at the inner surface.

The internal radial displacement for the elastic problem is given by

$$u(b) = \frac{\rho\Omega^2(1 - 2v)b(a^2 - b^2)^2}{8\mu[b^2 + (1 - 2v)a^2]}$$

so that for the viscoelastic problem

$$u(b) = \frac{\rho(1 - 2v)b(a^2 - b^2)^2}{8[b^2 + (1 - 2v)a^2]} \int_{-\infty}^{t} \frac{d\Omega^2(t')}{dt'} G^{-1}(t - t')\, dt' \qquad (3.25)$$

which determines the radial creep directly in terms of the shear creep function.

So far the problems discussed have been such that either the stress or displacement field is the same as for the elastic problem. Under these circumstances either μ^{-1} is a common factor in the displacement field (as in 3.25) or μ is a common factor in the stress field. In both cases it is possible to invert the Laplace transform of the displacement field or stress field directly in terms of hereditary integrals as in (3.25). A more complicated version of the rocket filling problem where direct inversion is no longer possible, is obtained by modifying the external boundary condition by assuming the filling to be bonded to a thin elastic shell. The modified boundary condition, obtained from equilibrium considerations of the thin shell, is

$$\sigma_r + Eh\frac{u}{a^2} = 0 \qquad r = a$$

where E and h are respectively Young's modulus and thickness of the (elastic) casing. The resulting algebra is involved and only the formula for the internal radial displacement is given. We find for the viscoelastic problem

$$\bar{u}(b, S) = \rho b(a^2 - b^2)\frac{\bar{\Omega}^2}{8\mu(S)} \qquad \times$$

$$\frac{Eh(1 - 2v)(a^2 - b^2) + 2\mu a[(3 - 2v)a^2 + (1 - 2v)b^2]}{Eh[(1 - 2v)a^2 + b^2] + 2\mu a(a^2 - b^2)} \qquad (3.26)$$

where $\mu \equiv \mu(S)$ and ν refer to the filling. In the limit of infinite reinforcement ($Eh \to \infty$), (3.26) reduces to (3.25). However, for finite Eh, the inversion of (3.26) is not possible without a detailed knowledge of $\mu(S)$, although in the limit of an incompressible filling ($\nu = \frac{1}{2}$), (3.26) simplifies to

$$\bar{u}(b, S) = \tfrac{1}{4}\rho\, ba^2 \overline{\Omega}^2 \left[\mu(S) + \frac{Ehb^2}{2a(a^2 - b^2)}\right]^{-1}$$

which may be formally inverted in the form

$$u(b) = \tfrac{1}{4}\rho\, ba^2 \int\limits_{-\infty}^{t} \frac{d[\Omega^2(t')]}{dt'}\, Q(t - t')\, dt'$$

where Q is the shear creep function of a hypothetical solid whose relaxation behaviour in shear is given by $G(t) + Eh\, b^2/2a(a^2 - b^2)$, i.e. a solid with dynamic modulus larger than the real solid but with identical relaxation characteristics.

A different class of case-bonded cylinder problems have been studied by Freudenthal and Shinozuka [24] who evaluate the shrinkage stresses occasioned by a uniform temperature change throughout the filling.

4. SOLUTION OF QUASI-STATIC PROBLEMS IN THE ABSENCE OF A CORRESPONDENCE PRINCIPLE— THE SPHERICAL INDENTER PROBLEM

Mixed boundary value problems with time variable boundary regions are not susceptible to solution by the correspondence principle because of the impossibility of obtaining Laplace transforms of the boundary conditions. Of the few examples of this type to be solved the problem of the indentation of a half space by a rigid spherical ball is of direct physical interest in connection with Brinell tests and the sclerescope rebound tests discussed previously.

The problem is defined by the boundary conditions

$$z = 0 \qquad u_z = a(t) - \frac{1}{2R}\,(x^2 + y^2)\,H(t) \qquad r \le r_1(t) \qquad (4.1)$$

$$z = 0 \qquad \sigma_z = 0 \qquad\qquad\qquad\qquad r > r_1(t) \qquad (4.2)$$

$$z = 0 \qquad \tau_{rz} = 0 \qquad\qquad\qquad\qquad\qquad\qquad (4.3)$$

where $z = 0$ is the surface of the half space, $r^2 = x^2 + y^2$, R is the radius of the indenter, $a(t)$ is the depth of penetration and $r_1(t)$ the radius of the contact circle. The principal quantities of interest are the stress distribution under the ball and the relation between $a(t)$ and $r_1(t)$.

The spherical indenter problem was first solved for monotonically increasing $r_1(t)$ by Lee and Radok [25], who showed that an assumed normal surface stress distribution (eqn. 4.10) was compatible with the boundary conditions (4.1) and (4.2). The Lee and Radok solution fails for decreasing $r_1(t)$ and a complete

solution for the case where r_1 increases from zero monotonically to a single maximum and subsequently decreases to zero was given by the author [22] using dual integral equation techniques. More recently Graham [26] has recovered the author's results by more direct methods. In the present account Graham's solution is given.

The starting point for Graham's solution may be taken as the Boussinesq formula for the normal surface displacement of an elastic solid subjected to a normal point load P at $x'y'$

viz. $$u_z = \frac{(1 - \nu)P}{2\pi\mu} [(x - x')^2 + (y - y')^2]^{-1/2} \tag{4.4}$$

Generalizing (4.4) to the case of a viscoelastic half space subject to time variable distributed load $P(x, y, t)$ gives

$$u_z = \frac{(1 - \nu)}{2\pi} G^{-1} * d \iint\limits_{\Omega_m} dx'\, dy'\, P(x', y', t')\, [(x - x')^2 + (y - y')^2]^{-1/2} \tag{4.5}$$

where again we have adopted the constant Poisson's ratio model and where we have utilized the notation of Gurtin and Sternberg [14]:

$$\alpha * d\beta = \int_{-\infty}^{t} \alpha(t - t')\, \dot\beta(t')\, dt' \equiv \int_{-\infty}^{t} \alpha(t - t')\, d\beta(t')$$

In (4.5) the surface integral is taken over the maximum region Ω_m enclosing all points $x'\, y'$ for which $P(x', y', t')$ is non-zero for any time t' in the range $-\infty < t' < t$.

For given $P(x, y, t)$ eqn. (4.5) presents the solution for the normal surface displacement and such a problem comes within the class that can be solved by the correspondence principle. On the other hand, for the indentation problem, eqn. (4.5) is to be considered as an integral equation for P, subject to the condition that for $r < r_1$ the surface displacement u_z is given by (4.1), while for $r > r_1$, P vanishes.

For monotonically increasing $r_1(t)$, Ω_m is $\Omega(t) = \pi r_1^2(t)$ and the orders of space and time integration in (4.5) may be interchanged to give

$$u_z = \frac{(1 - \nu)}{2\pi} \iint\limits_{\Omega(t)} dx'\, dy'\, [(x - x')^2 + (y - y')^2]^{-1/2}\, G^{-1} * dP \tag{4.6}$$

It is evident that $G^{-1} * dP$ is given by

$$G^{-1} * dP = q[x, y, r_1] \tag{4.7}$$

where q is the unique solution of the corresponding elastic problem defined by

$$\frac{1}{-} (x^2 + y^2) = \frac{(1 - \nu)}{2\pi} \iint\limits_{\Omega} dx'\, dy'\, [(x - x')^2 + (y - y')]^{-1/2}\, q(x, y, r_1)$$

$$\tag{4.8}$$

with

$$q = 0 \qquad r > r_1$$

The solution to the latter problem is known [23] and given by

$$q = \frac{4}{\pi (1 - \nu) R} [r_1^2 - r^2]^{1/2} \tag{4.9}$$

so that inverting (4.7)

$$P(x, y, t) = G * dq \equiv \frac{4}{\pi(1 - \nu)R} \int_0^t G(t - t') \frac{d}{dt'} (r_1^2(t') - r^2)^{1/2} \, dt' \tag{4.10}$$

in which for fixed r, the lower limit of the integral is given by t'' where t'' is the unique solution of

$$r_1(t'') = r$$

The total load on the indenter is given by

$$F = 2\pi \int_0^{r_1} r P \, dr$$

which is most conveniently evaluated by interchanging the order of the two integrations (see Hunter [22]) to give

$$F = \frac{8}{3R(1 - \nu)} \int_0^t G(t - t') \frac{d}{dt'} r_1^3(t') \, dt' \tag{4.11}$$

Also on substituting from (4.9) into (4.8) we find the relation

$$a(t) = r_1^2(t)/R \tag{4.12}$$

which is the same as for the elastic problem.*

The above solution is valid for monotonically increasing $r_1(t)$. For the case where $r_1(t)$ increases monotonically to a maximum value at $t = t_m$ and then decreases monotonically to zero, the solution given is valid for $t \leq t_m$. For $t > t_m$ the solution fails because it is no longer permissible to replace Ω_m in (4.5) by $\Omega(t)$. To obtain the solution of (4.5) for $t > t_m$, we introduce the function $t_1(t)$ defined by the relations

$$
\left.
\begin{array}{ll}
t \leq t_m. & t_1(t) = t \\
t \geq t_m. & r_1(t_1) = r_1(t) \qquad t_1 < t_m
\end{array}
\right\} \tag{4.13}
$$

i.e. t_1 is the time prior to t_m for which the radius of the contact circle is identical with the current value.

---

* In fact for $\nu = $ constant, the entire displacement field is the same as for the elastic problem for monotonically increasing $r_1(t)$.

18

Graham's solution is obtained using the identity (for x, y in $\Omega(t)$)

$$R^{-1}[r_1^2 - \tfrac{1}{2}(x^2 + y^2)] = \frac{(1-\nu)}{2\pi} G^{-1*} \, \mathrm{d} \iint_{\Omega_m} \mathrm{d}x' \, \mathrm{d}y' \, G^* \, \mathrm{d}q \, [(x-x')^2 + (y-y')^2]^{-1/2}$$

(4.14)

which is obtainable from the fundamental identity

$$\beta(t) = G^{-1*} \, \mathrm{d} \, [G^* \, \mathrm{d}\beta]$$

[cf. 2.5] together with (4.8), (4.9) and (4.12). Writing out (4.14) in full and re-arranging the orders of integration leads to

$$R^{-1}[r_1^2 - \tfrac{1}{2}(x^2 + y^2)] - \frac{(1-\nu)}{2\pi} \qquad \times$$

$$\int_0^t G^{-1}(t - \theta) \, \mathrm{d} \int_{t_1(\theta)}^{\theta} G(\theta - t') \, \mathrm{d} \iint_{\Omega_m} \frac{q \, \mathrm{d}x' \, \mathrm{d}y'}{[(x - x')^2 + (y - y')^2]^{1/2}}$$

$$= \frac{(1-\nu)}{2\pi} \int_0^t G^{-1}(t - \theta) \, \mathrm{d} \iint_{\Omega_m} \mathrm{d}x' \, \mathrm{d}y' \left[\int_0^{t_1(\theta)} \frac{G(\theta - t') \, \mathrm{d}q(x', y', t')}{[(x - x')^2 + (y - y')^2]^{1/2}} \right]$$

(4.15)

where we have introduced $t_1(t)$. In the outer integral on the left-hand side the limit 0 may be replaced by t_m since for $t < t_m$ the limits $t_1(\theta)$ and θ on the subsequent integral are identical. Also evaluating the surface integral on the left-hand side with the help of (4.8) reduces (4.15) to

$$R^{-1}[r_1^2 - \int_{t_m}^t G^{-1}(t - \theta) \frac{\mathrm{d}}{\mathrm{d}\theta} \int_{t_1(\theta)}^{\theta} G(\theta - t') \frac{\mathrm{d}}{\mathrm{d}t'} [r_1^2(t')] \, \mathrm{d}t' - \tfrac{1}{2}(x^2 + y^2)]$$

$$= \frac{(1-\nu)}{2\pi} G^{-1*} \, \mathrm{d} \iint_{\Omega_m} \mathrm{d}x' \, \mathrm{d}y' \, [(x - x')^2 + (y - y')^2]^{-1/2} \times$$

$$\int_0^{t_1(\theta)} G(\theta - t') \, \mathrm{d}q \, (x', y', t')$$

On comparing this result with the original integral equation (4.5), it is seen that a pressure distribution

$$P(x, y, t) = \frac{4}{\pi(1-\nu)R} \int_0^{t_1(t)} G(t - t') \frac{\mathrm{d}}{\mathrm{d}t'} [r_1^2(t') - r^2] \, \mathrm{d}t'$$

(4.16)

is consistent with the imposed boundary conditions provided $a(t)$ is given by

$$Ra(t) = r_1^2(t) - \int_{t_m}^t G^{-1}(t - \theta) \int_{t_1(\theta)}^{\theta} G(\theta - t') \frac{\mathrm{d}}{\mathrm{d}t'} (r_1^2(t')) \, \mathrm{d}t'$$

(4.17)

For $t > t_m$ eqn. (4.16) replaces (4.10) and (4.17) replaces (4.12). Equation (4.16) differs from (4.10) only in that $t_1(t)$ replaces t in the upper limit of the integral, so that for $t > t_m$ the total force is given by a formula similar to (4.11) but with the upper limit of the integral again replaced by $t_1(t)$.

Equations (4.11) [together with its modified form for $t > t_1$], (4.12) and (4.17) supplemented by Newton's law of motion

$$F = - m\ddot{a}$$

are the non-linear integro-differential equations for the analysis of the sclerescope test discussed previously. A solution of these equations was obtained by the author [22] for the limiting case of a nearly elastic solid. In contrast, the solution (3.24) of the parallel problem for the flat ended cylinder is of wider validity.

With the aid of the methods used in the above analysis, Graham also obtains a solution to the indentation problem for a rigid cone and a viscoelastic half space, and to the general Hertz problem for the contact of two viscoelastic solids, each with different principal radii of curvature.

A second Hertz-type problem of direct physical interest is the rolling contact of a cylinder or sphere on a viscoelastic half space. The physical interest stems from experimental evidence on the variation of the coefficient of rolling friction with velocity for viscoelastic materials; for high and low velocity the coefficient of friction is small and possesses a maximum at an intermediate value. An analysis of the rolling cylinder problem for a standard linear solid has been given by the author [27]. The theory predicts coefficients of friction in qualitative agreement with the experimental evidence. The analysis is based on eqn. (4.5) together with the "steady state" assumption that time enters the problem only through a reduced spatial coordinate $x - vt$, where v is the rolling velocity.

Few mixed boundary problems of the type considered in this section appear to have been solved, and no systematic methods of solution have been developed. In conclusion we mention a novel variant of this type of problem in which the boundary changes by ablation, as for example in the case of a spinning rocket filling burning internally (Corneliussen, Kamowitz, Lee and Radok [28]. The similar problem of an internally ablating sphere is solved by Rogers and Lee [6]

5. DYNAMIC PROBLEMS AND WAVE PROPAGATION

5.1. *Tensile Waves in Slender Rods*

The most completely studied field in dynamic viscoelasticity is the propagation of mechanical disturbances along filaments. Since almost all of the important features associated with wave propagation occur in this one dimensional case, the latter will be discussed in detail.

With neglect of body forces, the basic equations governing the propagation of tensile waves along slender rods are the equation of motion

$$\frac{\partial \sigma}{\partial x} = \rho \frac{\partial^2 u}{\partial t^2} \tag{5.1}$$

the strain–displacement relation

$$\epsilon = \frac{\partial u}{\partial x} \qquad (5.2)$$

and the constitutive equation. For present purposes this may be taken in either of the forms

$$\bar{\sigma}(x, S) = E(S)\, \bar{\epsilon}(x, S), \qquad \bar{\sigma}(x, \omega) = E(i\omega)\, \bar{\epsilon}(x, \omega) \qquad (5.3)$$

where $E(S)$ is the transform Young's modulus and $E(i\omega)$ the corresponding complex modulus. In eqns. (5.3) the bar notation implies either a Laplace or Fourier transform:

$$\bar{\sigma}(x, S) = \int_0^\infty \sigma(x, t)\, e^{-St}\, dt$$

$$\bar{\epsilon}(x, \omega) = \int_{-\infty}^\infty \epsilon(x, t)\, e^{i\omega t}\, dt \text{ etc.}$$

Much of the early work on one-dimensional wave propagation utilized Laplace transform methods and was directed towards finding analytical solutions for the propagation of disturbances along viscoelastic solids characterized by simple expressions for $E(S)$, i.e. standard linear solid, Maxwell solid, Kelvin solid, etc. (Lee and Kanter [29], Lee and Morrison [30], Berry and Hunter [31].) Because real solids are characterized by a wide spectrum of relaxation times, the detailed consequences of this earlier work are of little practical value; however, two important results emerge from these studies. The first concerns the speed of propagation of the wave front which is independent of the viscoelastic properties and given by (Berry [32])

$$C_0 = \left(\frac{E_D}{\rho}\right)^{1/2}$$

where

$$E_D = E_1(\infty)$$

is the instantaneous Young's modulus. Secondly, the solutions of problems for finite rods are expressible in terms of solutions of associated problems for semi-infinite rods. In particular suppose that as a consequence of a given input condition at the end $x = 0$ of a semi-infinite rod $0 < x < \infty$, the stress distribution is given by $\sigma_1(x, t)$. Then the stress distribution in a finite rod, subject to the same boundary conditions at $x = 0$, but with $x = l$ stress free, is given by the formulae (Lee and Kanter [29])

$$0 \le t < l/C_0 \qquad \sigma = \sigma_1(x, t)$$
$$l/C_0 \le t < 2l/C_0 \qquad \sigma = \sigma_1(x, t) - \sigma_1(2l - x, t)$$
$$2l/C_0 \le t < 3l/C_0 \qquad \sigma = \sigma_1(x, t) - \sigma_1(2l - x, t)$$
$$+ \sigma_1(2l + x, t) \text{ etc.}$$

where, without loss of generality, we assume $\sigma_1(x, t) \equiv 0$ for $t < 0$, and where

the time intervals l/C_0 correspond to the time taken for a single passage of the wave front along the bar. The corresponding velocity (and displacement) distributions are of the form

$$0 \le t < \ l/C_0 \quad v = v_1(x, t)$$

$$l/C_0 \le t < 2l/C_0 \quad v = v_1(x, t) + v_1(2l - x, t)$$

$$2l/C_0 \le t < 3l/C_0 \quad v = v_1(x, t) + v_1(2l - x, t) + v_1(2l + x, t)$$

so that the surface velocity at $x = l$ during the first reflection of a pulse generated at $x = 0$ is just twice that occurring at $x = l$ in a semi-infinite rod.*

Similar formulae may be derived for the case where $x = l$ is a fixed end. For the most general problem where both $x = 0$ and $x = l$ are subject to time dependent boundary conditions, the stress and velocity distributions are expressible in terms of the solutions of two semi-infinite rod problems.

Excepting the immediately preceding theorems, the Laplace transform method is of little help for predicting the dispersion and attenuation of waves in real materials. On the other hand the solution of dynamic problems using Fourier transform methods leads to a basic set of experimentally observable eigenfunctions. Measurement of the eigenfunction characteristics then provides the directly relevant viscoelastic data required to evaluate the inverse Fourier transforms for the solution of transient wave problems.

The basic set of eigenfunctions are harmonic in time and of the form

$$\left.\begin{aligned} u(x, t) &= u_0(x, \omega)\, e^{i\omega t} \\ \sigma(x, t) &= \sigma_0(x, \omega)\, e^{i\omega t} \\ \epsilon(x, t) &= \epsilon_0(x, \omega)\, e^{i\omega t} \end{aligned}\right\} \tag{5.4}$$

On substituting these expressions into (5.1), (5.2) and the second of (5.3), there results a single differential equation satisfied by u_0, σ_0 and ϵ_0,

$$\left[\frac{d}{dx^2} - \lambda^2(\omega)\right] (u_0, \sigma_0, \epsilon_0) = 0 \tag{5.5}$$

where $\lambda(\omega)$ is a complex function of the real variable ω,

$$\lambda(\omega) = \lambda_1(\omega) + i\lambda_2(\omega) \tag{5.6}$$

in which $\lambda_1(\omega)$ is a positive even function,

$$\lambda_1(\omega) = \left[\frac{\rho}{|E(i\omega)|}\right]^{1/2} \omega \sin \frac{\Delta}{2} \tag{5.7}$$

and $\lambda_2(\omega)$ an odd function ($\lambda_2 > 0$ for $\omega > 0$),

$$\lambda_2(\omega) = \left[\frac{\rho}{|E(i\omega)|}\right]^{1/2} \omega \cos \frac{\Delta}{2} \tag{5.8}$$

---

* It is assumed that the width of the pulse arriving at $x = l$ is less than $2l/C_0$.

Finally $\Delta(\omega)$ is the "loss angle" defined by

$$\tan \Delta(\omega) = \frac{E_2(\omega)}{E_1(\omega)} \qquad \left(-\frac{\pi}{2} < \Delta < \frac{\pi}{2} \right) \tag{5.9}$$

The solution of (5.5) for $u_0(x)$ (say) is

$$u_0(x) = A(\omega)\, e^{\lambda x} + B(\omega)\, e^{-\lambda x}$$

where A and B are disposable constants determined by boundary conditions. For problems concerned with wave propagation along semi-infinite bars $0 < x < \infty$, A must vanish and the basic eigenfunction $e^{-\lambda x}$ may be written in the form

$$e^{-\alpha(\omega)x + i\omega(t - x/C(\omega))} \tag{5.10}$$

which is a spatially attenuated harmonic wave progressing in the positive x direction with phase velocity

$$C(\omega) = C(-\omega) = \left| \frac{E(i\omega)}{\rho} \right|^{1/2} \sec \frac{\Delta}{2} \tag{5.11}$$

and attenuation

$$\alpha(\omega) = \alpha(-\omega) = \frac{\omega \tan(\Delta/2)}{C(\omega)} \tag{5.12}$$

The general solution to the transient wave problem in a semi-infinite bar may now be written as the Fourier integral

$$u(x, t) = \int_{-\infty}^{\infty} B(\omega)\, e^{-\alpha x + i\omega(t - x/C)}\, d\omega \tag{5.13}$$

where $B(\omega)$ is determined by impact conditions obtaining at $x = 0$. For example if $u(0, t)$ is prescribed, eqn. (5.13) yields

$$u(0, t) = \int_{-\infty}^{\infty} B(\omega)\, e^{i\omega t}\, d\omega$$

so that $B(\omega)$ is determined by the inversion theorem for Fourier integrals

$$B(\omega) = (2)\pi^{-1} \int_{-\infty}^{\infty} u(0, t)\, e^{-i\omega t}\, dt.$$

More commonly the prescribed boundary conditions at $x = 0$ are for $\sigma(0, t)$. The case

$$\sigma(0, t) = -P_0 \delta(t) \tag{5.14}$$

where δ is the Dirac delta function is of particular importance in the analysis of bar response under explosive loading condition. Further the solution of the problem specified by (5.14) provides a set of "Green's" functions for the general solution of the semi-infinite bar problem with arbitrarily prescribed $\sigma(0, t)$. For, if for a semi-infinite bar, the solution of the problem defined by (5.14) leads to a

stress distribution

$$\sigma(x, t) = - P_0\, \sigma_1(x, t),$$

the solution for arbitrary input loading $\sigma(0, t)$ is given by the convolution integral

$$\sigma(x, t) = \int_{-\infty}^{\infty} \sigma(0, t')\, \sigma_1(x, t - t')\, dt'$$

which result follows from the linear nature of the governing equations.

A complete solution of the problem defined by (5.14) may be obtained as follows. The general solution for $u(x, t)$ may be written

$$u(x, t) = \int_{-\infty}^{\infty} B(\omega)\, e^{i\omega(t - x/C) - \alpha x}\, d\omega \tag{5.15}$$

where B is to be determined. Corresponding formulae for velocity, strain and stress are respectively

$$v(x, t) = \int_{-\infty}^{\infty} i\omega\, B(\omega)\, e^{i\omega(t - x/C) - \alpha x}\, d\omega \tag{5.16}$$

$$\epsilon(x, t) = - \int_{-\infty}^{\infty} (\alpha + i\omega/C)\, B(\omega)\, e^{i\omega(t - x/C) - \alpha x}\, d\omega \tag{5.17}$$

$$\sigma(x, t) = - \int_{-\infty}^{\infty} E(i\omega)\, (\alpha + i\omega/C)\, B(\omega)\, e^{i\omega(t - x/C) - \alpha x}\, d\omega \tag{5.18}$$

where in the last of these integrals, use has been made of the second of (5.3). For $x = 0$, (5.18) reduces to

$$\sigma(0, t) = - \int_{-\infty}^{\infty} E(i\omega)\, (\alpha + i\omega/C)\, B(\omega)\, e^{i\omega t}\, d\omega$$

On comparing this result with (5.14) we find

$$B(\omega) = \frac{P_0/2\pi}{E(i\omega)\, [\alpha + i\omega/C]} \tag{5.19}$$

where use has been made of the result that the spectrum of a delta function is $(2\pi)^{-1}$, independent of ω. Substitution from (5.19) into (5.15)–(5.18) now gives displacement, velocity, strain and stress.

The stress distribution is

$$\sigma(x, t) = - (P_0/2\pi) \int_{-\infty}^{\infty} e^{i\omega(t - x/C) - \alpha x}\, d\omega$$

which could have been deduced immediately. Of more interest from an experi-

mental viewpoint is the formula for velocity which becomes

$$v(x, t) = \frac{P_0}{2\pi\rho} \int_{-\infty}^{\infty} \left[1 - i \tan \frac{\varDelta}{2}\right] [C(\omega)]^{-1} e^{i\omega(t-x/C)-\alpha x} \, d\omega \qquad (5.20)$$

where use has been made of eqns. (5.9), (5.11) and (5.12). We return to (5.20) subsequently in connection with experimental evidence on the response of polyethylene bars subject to explosive loading conditions.

Evaluation of integrals of the type (5.20) requires knowledge of $C(\omega)$ and $\alpha(\omega)$ for $0 < \omega < \infty$. While in principle the information is derivable from a knowledge of $E_1(\omega)$, direct measurements of α and C are of more help in suggesting possible approximations for evaluating the Fourier integrals.

As indicated previously the steady state eigenfunctions (5.10) are experimentally realizable in an experiment in which one end of a long filament is oscillated at constant amplitude and circular frequency ω. The filament is taken sufficiently long for the attenuation to be sensibly complete (i.e. the length l is chosen to satisfy the inequality $\alpha l \gg 1$), and sufficient time is allowed to elapse in order to establish a steady state. Values of $C(\omega)$ and $\alpha(\omega)$ may then be derived from comparisons of displacement amplitude at various points along the filament. (The experiment also serves to check the basic hypothesis that the material behaves linearly.)

The experiment was undertaken by Hillier and Kolsky [33] and Hillier [34] who found that for polyethylene at 10°C, the attenuation was a linear function of ω over a frequency range 1 kc/s $< \omega/2\pi <$ 16 kc/s. The corresponding phase velocity increased rapidly from 3.5×10^4 cms/sec at low frequencies to 10^5 cm/sec at 2 kc/s and then remained sensibly constant from 2 kc/s to 16 kc/s. Thus over a large frequency range $C(\omega) = C_0 =$ constant and $\alpha = k \mid \omega \mid$ where k is a constant; from equation (5.12) this implies that over the same frequency range $\mid \tan (\varDelta/2) \mid$ is constant, confirming a physical assumption adopted freely throughout the present paper. Similar behaviour was found in neoprene and a particular nylon.

In subsequent experiments Kolsky [35] examined the velocity profiles of transient pulses generated by explosive detonation at one end of polyethylene and perspex bars. Measurements were taken of the velocity–time pulse at the end of the bar remote from the explosion, using a condenser microphone technique. Since during the first reflection of the incident pulse at the stress free end, the velocity is just twice that obtaining at the same distance along a semi-infinite bar, comparison of the observed velocity profiles for different bar lengths yields experimental information which may be compared directly with the predictions of eqn. (5.20).

Kolsky found in his experiments that the propagating velocity pulse dispersed and attenuated according to a "similarity" formula

$$v(x, t) = x^{-1} f(t'/x) \qquad (5.21)$$

where f is a function specifying pulse shape and t' is time measured from an

origin which propagates with the pulse (e.g. measured with origin at the maximum value of v). Thus the amplitude of the pulse attenuates as x^{-1} while concurrently the pulse width increases proportionally to x.

Equation (5.21) may be compared with the integral (5.20) which is obtained on the assumption that the explosive loading condition is adequately modelled by the boundary condition (5.14). Since the duration of detonation is of the order of a microsecond, while the experimental pulse shapes extend over a hundred or so microseconds, the error involved in this assumption is negligible.

Comparison of (5.21) and (5.20) show that there is no possibility of evaluating the Fourier integral by a stationary phase approximation since the latter necessarily leads to amplitude attenuation of the form $x^{-1/2} e^{-\Gamma x}$ where Γ is a constant. However, the integral may be evaluated explicitly if we adopt the viscoelastic model suggested by the earlier experiments.
i.e.

$$C(\omega) \simeq C_0 \qquad a(\omega) = k \mid \omega \mid \tag{5.22}$$

where

$$k = C_0^{-1} \tan \left(\frac{\Delta}{2}\right) \tag{5.23}$$

and where in (5.23), the positive value of $\tan (\Delta/2)$ is implied. ($\tan \Delta$ is an odd function of ω. In evaluating the Fourier integrals, this must be taken into account even for the "constant" $\tan \Delta$ model used here.) With the approximations (5.22), the integral (5.20) may be evaluated explicitly to yield

$$v(x, t) = \left(\frac{P_0}{\pi \rho C_0}\right) \frac{kx + \tan (\Delta/2) [t - x/C_0]}{k^2 x^2 + (t - x/C_0)^2} \equiv \left(\frac{P_0 k}{\pi \rho}\right) \frac{t}{k^2 x^2 + (t - x/C_0)^2} \tag{5.24}$$

The first of these expressions may be written in the form

$$v(x, t) = \left(\frac{P_0}{\pi \rho C_0 kx}\right) \frac{1 + \tau \tan (\Delta/2)}{1 + \tau^2} \tag{5.25}$$

where τ is the dimensionless time variable

$$\tau = \frac{t - x/C_0}{kx}$$

Equation (5.25), which is precisely of the form (5.21) with $t' = t - x/C_0$, is a slightly asymmetric pulse centred around $\tau = 0$; the expression is compared with Kolsky's experimental pulse obtained after 50 cm of travel in polyethylene in Fig. 1. Here the theoretical and experimental pulses have been plotted in the form (v/v_{max}) as a function of τ and have been matched along the time scale by the choice of coincident maxima. In the comparison the adopted values of $C_0 = 9.5 \times 10^4$ cm/sec and $\tan (\Delta/2) = 0.081$ are obtained from Kolsky's earlier experiments in conjunction with the formulae (5.22) and (5.23).

Although the agreement is tolerably good, the asymmetry of the experimental pulse is only partly explained by the present theory. In fact, in a previous
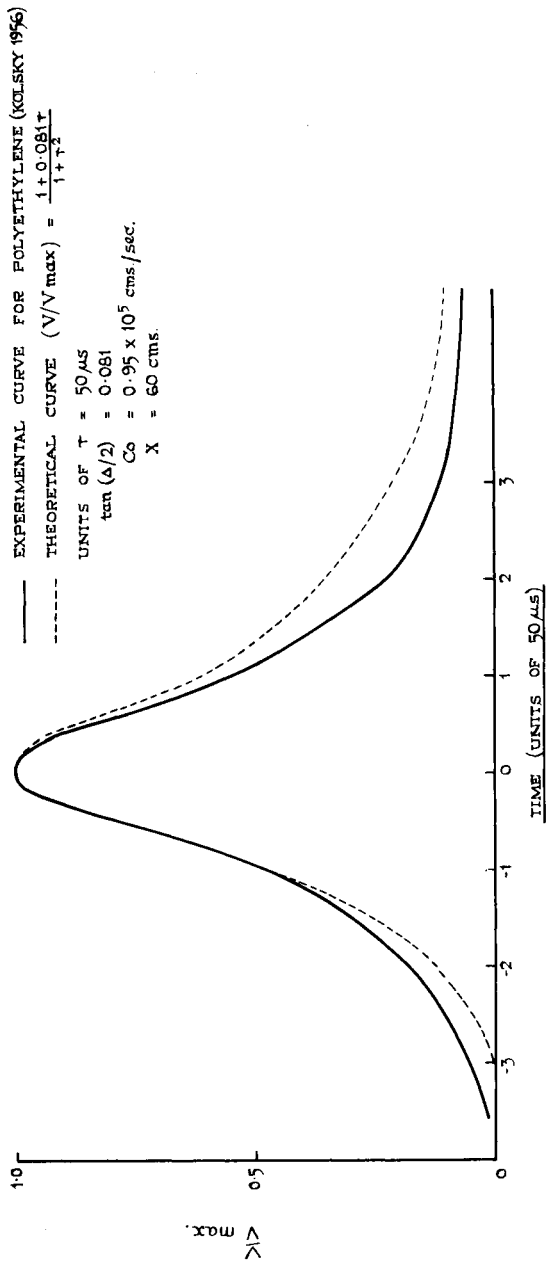
FIG. 1. Velocity profiles after 60 cm travel in polyethylene.

calculation by the author [11], the term $\tau \tan (\Delta/2)$ appearing in (5.25) was omitted because the boundary conditions of the problem were assumed (falsely) to be equivalent to

$$v(0, t) = v_0 \delta(t) \tag{5.26}$$

and this leads to the completely symmetric pulse

$$v(x, t) = \frac{v_0}{\pi k x} (1 + \tau^2)^{-1}$$

in place of (5.25). However, while the modified calculation presented here gives reasonably good results for polyethylene, with the much smaller value of $\tan (\Delta/2)$ for perspex [$\tan (\Delta/2) = 0.02$], the theory fails to predict the asymmetry of the experimental pulses found by Kolsky.

Much improved agreement between theory and experiment is obtained if account is taken of the variation of C with ω within the periodic term in the Fourier integral (5.20). Details of the revised calculation, which is based on a model which retains the assumption of constant $\tan \Delta$, but makes use of eqn. (3.14), are to be found in the papers of Kolsky [35] and the author [11]. In both papers the boundary conditions are taken as (5.26) rather than the more correct form (5.14); however, for reasons explained above this leads to negligible errors for the perspex case, and the revised calculation leads to almost exact agreement between theory and experiment.

The theory of the present section is applicable with slight modification to the propagation of plane shear and dilatational waves. The essential modifications are that phase velocity, attenuation and loss angle are defined by a different complex modulus. For shear waves the relevant modulus is $\mu(i\omega)$, for dilatational waves the modulus is $\lambda(i\omega) + 2\mu(i\omega)$.

5.2. Periodic Eigenfunctions in Three Dimensions

Basic plane wave eigenfunctions for the propagation of mechanical disturbances in elastic solids are of the form

$$\mathbf{u} = - i \mathbf{k} \, \phi_0 \, e^{i\omega (t - \mathbf{k} \cdot \mathbf{r}/C_1)} \tag{5.27}$$

$$\mathbf{u} = - i(\mathbf{k} \times \mathbf{A}_0) \, e^{i\omega (t - \mathbf{k} \cdot \mathbf{r}/C_2)} \tag{5.28}$$

where $\mathbf{k}$ is an arbitrary unit vector C_1 and C_2 are the dilatational and shear wave velocities

$$C_1^2 = \frac{\lambda + 2\mu}{\rho} \qquad C_2^2 = \frac{\mu}{\rho}$$

and where ϕ_0 and $\mathbf{A}_0$ are constants.

Equations (5.27) and (5.28) derive respectively from

$$\mathbf{u} = \text{grad } \phi \qquad \mathbf{u} = \text{curl } \mathbf{A}$$

where ϕ and $\mathbf{A}$ are scalar and vector potentials satisfying the wave equations

$$C_1^2 \, \nabla^2 \phi = \ddot{\phi} \qquad C_2^2 \, \nabla^2 \mathbf{A} = \ddot{\mathbf{A}}$$

The solution for viscoelastic solids is more complicated. If we assume generally that

$$\mathbf{u} = \operatorname{grad} \phi + \operatorname{curl} \mathbf{A} \tag{5.29}$$

and seek solutions of the equations of motion and constitutive equations which are periodic in time
i.e.

$$\phi = \phi_1(\mathbf{r}) \, e^{i\omega t} \qquad \mathbf{A} = \mathbf{A}_1(\mathbf{r}) \, e^{i\omega t} \tag{5.30}$$

we easily derive

$$\nabla^2 \phi_1 + \frac{\rho \omega^2}{\lambda(i\omega) + 2\mu(i\omega)} \, \phi_1 = 0$$

$$\nabla^2 \mathbf{A}_1 + \frac{\rho \omega^2}{\mu(i\omega)} \, \mathbf{A}_1 = 0.$$

Fundamental solutions of these equations are

$$\phi = \phi_0 \, e^{-i\mathbf{P} \cdot \mathbf{r}} \qquad \mathbf{A} = \mathbf{A}_0 \, e^{-i\mathbf{Q} \cdot \mathbf{r}} \tag{5.31}$$

where $\mathbf{P}$ and $\mathbf{Q}$ are complex vectors*

$$\mathbf{P} = \mathbf{p}_1 + i\mathbf{p}_2 \qquad \mathbf{Q} = \mathbf{q}_1 + i\mathbf{q}_2 \tag{5.32}$$

satisfying the algebraic equations

$$[\lambda(i\omega) + 2\mu(i\omega)] \, \mathbf{P}^2 = \rho\omega^2, \qquad \mu(i\omega) \, \mathbf{Q}^2 = \rho\omega^2 \tag{5.33}$$

A detailed analysis is now given for $\mathbf{Q}$. From the second of (5.33) we have, on equating real and imaginary parts,

$$\mu_1(\omega)(\mathbf{q}_1^2 - \mathbf{q}_2^2) + 2\mu_2(\omega)(\mathbf{q}_1 . \mathbf{q}_2) = \rho\omega^2$$

$$\mu_2(\omega)(\mathbf{q}_1^2 - \mathbf{q}_2^2) = \mu_1(\omega)(\mathbf{q}_1 . \mathbf{q}_2)$$

These equations are sufficient to determine $|\mathbf{q}_1|$ and $|\mathbf{q}^2|$ if the angle β between $\mathbf{q}_1$ and $\mathbf{q}_2$ is given. Writing

$$\mathbf{q}_1 = \frac{\omega}{CA(\omega)} \, \mathbf{k}_1, \qquad \mathbf{q}_2 = a_s(\omega) \, \mathbf{k}_2 \tag{5.34}$$

where C_s and a_s are respectively the phase velocity and attenuation coefficient for shear waves, and where $\mathbf{k}_1$ and $\mathbf{k}_2$ are arbitrary unit vectors satisfying

$$\mathbf{k}_1 . \mathbf{k}_2 = \cos \beta, \tag{5.35}$$

we obtain for $\omega > 0$

$$C_s^2(\omega) = \frac{2 \, | \mu(i\omega) | \cos \beta}{\rho \sin \Delta_s} \, G(\Delta_s, \beta) \tag{5.36}$$

$$a_s(\omega) = \frac{\omega}{C_S(\omega)} \, G(\Delta_s, \beta) \tag{5.37}$$

---

* P_1 and P_2 do not necessarily lie in the same direction. However, as may be verified directly complex vectors obey the usual rules of vector analysis e.g. $\mathbf{P} \times \mathbf{P} = 0$. $\mathbf{P}.(\mathbf{P} \times \mathbf{A}_0) = 0$.

where G is the function

$$G(\Delta_s, \beta) = (1 + \cot^2 \Delta \cos^2 \beta)^{1/2} - \cot \Delta_s \cos \beta \qquad (5.38)$$

and where Δ_s is the loss angle

$$\tan [\Delta_s(\omega)] = \frac{\mu_2(\omega)}{\mu_1(\omega)}.$$

For negative ω, a_S and C_S are defined by the equations

$$a_s(\omega) = a_s(-\omega), \qquad C_s(\omega) = C_s(-\omega).$$

In the derivation of (5.36) and (5.37) the quantity $\cos \beta$ is restricted to be positive so that

$$|\beta| \leqslant \pi/2$$

With C_s and a_s given by (5.36) and (5.37), the fundamental shear wave eigenfunction derived from $\mathbf{u} = \mathrm{curl}\ \mathbf{A}$ is

$$\mathbf{u} = \left[\frac{i\omega}{C_s}\ \mathbf{k}_1 + a_s\mathbf{k}_2\right] \times \mathbf{A}_0\ e^{i\omega(t-\mathbf{k}\cdot\mathbf{r}/C_s)-\alpha_s\mathbf{k}_2\cdot\mathbf{r}} \qquad (5.39)$$

where $\mathbf{A}_0$ is an arbitrary vector and the unit vectors $\mathbf{k}_1$ and $\mathbf{k}_2$ are arbitrary subject only to the restriction

$$\mathbf{k}_1 \cdot \mathbf{k}_2 = \cos \beta > 0.$$

For the particular limiting case $\beta = 0$, $\mathbf{k}_1 = \mathbf{k}_2$ and the eigenfunctions simplify to

$$u_y, u_z = e^{i\omega(t-x/C_s)-\alpha_s x}$$

where we have assumed $\mathbf{k}_1$ to lie in the positive x direction.

Also for $\beta = 0$, the formulae for C_s and a simplify considerably:

$$C_s = \left|\frac{\mu(i\omega)}{\rho}\right|^{1/2} \sec \frac{\Delta_s}{2}, \qquad a_s = \frac{\omega\tan(\Delta_s/2)}{C_s}$$

which differ from (5.11) and (5.12) only in the substitution of $\mu(i\omega)$ for $E(i\omega)$. Thus the theory of the propagation of "simple" shear waves with $\mathbf{k}_1 = \mathbf{k}_2$ is similar to the theory developed in Section 5.1 for the propagation of tensile waves in rods. However, β need not vanish and the general steady state viscoelastic shear wave is one for which the directions of attenuation and propagation are different.

The analysis for dilatational waves closely follows the theory developed for shear waves. The final form assumed by the displacement eigenfunction is

$$\mathbf{u} = \frac{i\omega}{C_d}\ \mathbf{k}_1 + a_d\mathbf{k}_2)\ \phi_0\ e^{i\omega(t-\mathbf{k}^1\cdot\mathbf{r}/C_d)-\alpha_d(\mathbf{k}_2\cdot\mathbf{r})} \qquad (5.40)$$

where a_d and C_d are defined analogous to a_s and C_s but with $\mu(i\omega)$ replaced by $\lambda(i\omega) + 2\mu(i\omega)$.

The discovery of periodic waves in three dimensions, with different directions of propagation and attenuation, was made by Lockett [1], on whose work the

preceding analysis is based. Lockett's paper contains the solution of a number of scattering problems in which incident waves of the simple type (i.e. $\mathbf{k}_1 = \mathbf{k}_2$) are reflected and refracted at plane boundaries. As in elasticity theory the scattering of an incident shear or dilatational wave generally entails reflected and refracted waves of both types. Under certain circumstances the reflected and refracted waves are also simple, but in general the solution of the scattering problem requires non-simple waves.

Excluding the problems considered by Lockett, no use appears to have been made of the non-simple eigenfunctions (5.39) and (5.40). This is not surprising since for $\mathbf{k}_1 \neq \mathbf{k}_2$ the functions have no elastic analogue and this suggests that the functions could only appear in problems for which there is no correspondence principle, i.e. mixed boundary value problems of the type discussed in Section 4 in a quasi-static context.* This intuitive result is confirmed immediately below in discussion on the form of the dynamic correspondence principle.

There exists a correspondence principle for dynamic viscoelastic problems provided the boundary conditions conform to the restrictions discussed in Section 3.1. Under these circumstances the dynamic viscoelastic problem is defined by the equation†

$$[\lambda(i\omega) + \mu(i\omega)] \text{ grad div } \bar{\mathbf{u}} + \mu(i\omega) \; \nabla^2\bar{\mathbf{u}} + \rho\omega^2\bar{\mathbf{u}} = 0 \qquad (5.41)$$

together with the boundary conditions

$$\bar{\mathbf{u}} \text{ prescribed on } \mathscr{S}_1 \qquad (5.42)$$

$$\bar{\sigma}_{ij}n_j \text{ prescribed on } \mathscr{S}_2 = \mathscr{S} - \mathscr{S}_1 \qquad (5.43)$$

where the bars denote Fourier transforms. As in the quasi-static case the essential point is that the boundary conditions can be prescribed for the transformed displacement and stress if and only if $\mathscr{S}_1$ and $\mathscr{S}_2$ are fixed in time. With this limitation, the viscoelastic solution may be derived from the corresponding elastic solution which is defined by the same equations (5.41), (5.42) and (5.43) but with $\lambda(i\omega)$ and $\mu(i\omega)$ replaced by the Lamé constants λ and μ. If now the solution of eqns. (5.41)–(5.43) yields the Fourier transform of the elastic displacement in the form

$$\bar{\mathbf{u}} = \bar{\mathbf{u}} \, [\mathbf{r}, \, \omega, \, \lambda, \, \mu]$$

then the corresponding displacement transform for the solution to the viscoelastic problem is given by

$$\bar{\mathbf{u}} = \bar{\mathbf{u}} \, [\mathbf{r}, \, \omega, \, \lambda(i\omega), \, \mu(i\omega)]$$

which completes formally the solution to the viscoelastic problem.

The theory for the dynamic correspondence principle may also be formulated in terms of Laplace transforms.

---

* Excluding Lockett's scattering problems no such dynamic problems appear to have been solved.

† For brevity we omit consideration of body forces; by comparison with Section 3.1 the reader will have no difficulty in generalizing the present results.

If in the above theory we write for the elastic solution

$$\bar{\mathbf{u}} = \operatorname{grad} \bar{\Phi} + \operatorname{curl} \bar{\mathbf{A}}$$

then ϕ and $\bar{\mathbf{A}}$ satisfy the equations

$$\nabla^2 \phi + \frac{\rho\omega^2}{\lambda + 2\mu}\, \phi = 0, \qquad \nabla^2 \mathbf{A} + \frac{\rho\omega^2}{\mu}\, \bar{\mathbf{A}} = 0$$

A complete set of eigenfunctions for the first of these equations are the plane harmonic waves

$$e^{-i(\mathbf{k}.\mathbf{r})\omega/C_d^0}$$

where C_d^0 is the elastic dilatational wave velocity

$$C_d^0 = \frac{\lambda + 2\mu}{\rho} \tag{5.44}$$

and $\mathbf{k}$ is an arbitrary unit vector. It follows that the general solution for ϕ can be written

$$\phi = \sum_{\mathbf{k}} \phi(\mathbf{k},\, \omega)\, e^{-i(\mathbf{k}.\mathbf{r})\omega/C_d^0}$$

and that ϕ is given by

$$\phi = \sum_{\mathbf{k},\, \omega} \phi(\mathbf{k},\, \omega)\, e^{i\omega(t - (\mathbf{k}.\mathbf{r})/C_d)} \tag{5.45}$$

The transition to the viscoelastic problem is given by substituting $\lambda(i\omega)$ and $\mu(i\omega)$ for λ and μ in (5.45). Now λ and μ appear in $\phi\,(\mathbf{k},\, \omega)$ but the effect of the substitution here merely entails the appearance of a new function ϕ of $\mathbf{k}$ and ω. For the exponential term appearing in (5.45) λ and μ appear in the definition of C_d^0 [cf. eqn. (5.44)] which is now to be replaced by the complex quantity

$$\left[\frac{\lambda(i\omega) + 2\mu(i\omega)}{\rho} \right]^{1/2}$$

By analogy with the analysis of Section 5.1

$$\left[\frac{\rho}{\lambda(i\omega) + 2\mu(i\omega)} \right]^{1/2} = [C_d(\omega)]^{-1} - i\, \frac{a_d(\omega)}{\omega}$$

where

$$C_d(\omega) = \frac{|\,\lambda(i\omega) + 2\mu(i\omega)\,|^{1/2}}{\rho} \sec \frac{\Delta_d}{2}$$

$$a_d(\omega) = \frac{\omega}{C_d(\omega)} \tan \frac{\Delta_d}{2}$$

$$\tan \Delta_d = \frac{\lambda_2(\omega) + 2\mu_2(\omega)}{\lambda_1(\omega) + 2\mu_1(\omega)}$$

Thus for viscoelastic problems for which a correspondence principle may be

invoked, the scalar potential may be written

$$\phi = \sum_{\mathbf{k},\,\omega} \phi(\mathbf{k},\,\omega)\, e^{i\omega(t-\mathbf{k}.\mathbf{r}/C_d)-\alpha_d(\mathbf{k}.\mathbf{r})}$$

which contains only the "simple" dilatatonal waves for which $\mathbf{k}_1 = \mathbf{k}_2 \equiv \mathbf{k}$. Again a similar argument for the vector potential leads to the result that only simple shear waves appear in the solution to the viscoelastic problem. Thus the more general Lockett waves in which the direction of attenuation and propagation are different will only enter problems for which no correspondence principle exists.

5.3. Free Vibrations of a Viscoelastic Solid

Among the more important applications of linear viscoelasticity theory are problems concerning the free vibrations of solids. Free vibration problems are defined by the condition that external forces, where they exist, do no work. Thus the boundary conditions are of the type

$$\left. \begin{array}{ll} \mathbf{u} = 0 & \mathbf{r} \text{ on } \mathscr{S}_1 \\[2mm] \sigma_{ij} n_j = 0 & \mathbf{r} \text{ on } \mathscr{S}_2 \equiv \mathscr{S} - \mathscr{S}_1 \end{array} \right\} \tag{5.46}$$

where $\mathscr{S}_1$ and $\mathscr{S}_2$ are time independent.

For a body of given geometry the free vibration problem is completely specified by supplementing the external boundary conditions by initial conditions which prescribe $\mathbf{u}(\mathbf{r}, 0)$ and $\dot{\mathbf{u}}(\mathbf{r}, 0)$.

Although the form of the boundary conditions suggests a direct application to the correspondence principle, we adopt a slightly different procedure which takes account of the physical content of the problem, and leads directly to harmonic vibrations which are exponentially damped in time. A reasonably complete theory of free vibrations is possible for a solid with constant Poisson's ratio. No comparable theory exists for the case where the viscoelastic behaviour in shear and dilatational is different.

We assume that the analogue elastic problem has been solved. The elastic problem is defined by the boundary conditions (5.46) and the equation of motion,

$$\mu_0[\, \nabla^2 \mathbf{u} + (1 - 2\sigma)^{-1} \operatorname{grad} (\operatorname{div} \mathbf{u})] = \rho \, \frac{\partial^2 \mathbf{u}}{\partial t^2} \tag{5.47}$$

The existence of a complete elastic solution means that all periodic solutions of (5.47) of the type

$$\mathbf{u} = \mathbf{u}^e(\omega, \mathbf{r})\, e^{i\omega t}$$

are known. We note for future reference that with the boundary conditions (5.46), these solutions are orthogonal in the sense

$$\int_{v} \mathbf{u}^e(\omega, \mathbf{r}).\mathbf{u}^e(\omega', \mathbf{r})\, d^3x = 0 \qquad \omega \neq \omega'$$

where v denotes the volume of the body enclosed by $\mathscr{S}$. With suitable normaliza-

tion conditions therefore

$$\int_v \mathbf{u}^e(\omega, \mathbf{r}).\mathbf{u}^e(\omega', \mathbf{r})\, d^3x = \delta\omega\omega'$$

Further the eigenfunctions $\mathbf{u}(\omega, \mathbf{r})$ are a complete set of functions so that it is possible to solve the problem of arbitrary specified initial displacement and velocity by standard methods. Thus the general solution of the elastic problem may be written

$$\mathbf{u} = \sum_\omega [A(\omega)\cos \omega t + B(\omega)\, \omega^{-1} \sin \omega t]\, \mathbf{u}^e(\omega, \mathbf{r}) \tag{5.48}$$

where

$$\sum_\omega A(\omega)\, \mathbf{u}^e(\omega, \mathbf{r}) = \mathbf{u}(\mathbf{r}, 0)$$

$$\sum_\omega B(\omega)\, \mathbf{u}^e(\omega, \mathbf{r}) = \dot{\mathbf{u}}(\mathbf{r}, 0)$$

or on using the orthogonality relations

$$A(\omega) = \int_v \mathbf{u}(\mathbf{r}, 0).\mathbf{u}^e(\omega, \mathbf{r})\, d^3x$$

$$B(\omega) = \int_v \dot{\mathbf{u}}(\mathbf{r}, 0).\mathbf{u}^e(\omega, \mathbf{r})\, d^3x$$

The spectrum of values for ω may be either continuous or discrete depending on the problem.

The corresponding viscoelastic problem is defined by the equation of motion

$$\mu(S)[\, \nabla^2\bar{\mathbf{u}} + (1 - 2\sigma)^{-1}\, \text{grad (div } \bar{\mathbf{u}})] = \rho\, \overline{\frac{\partial^2\mathbf{u}}{\partial t^2}} \tag{5.49}$$

where the bar denotes a Laplace transform. We assume solutions of this equation of the form

$$\mathbf{u} = \mathbf{u}^e(\omega, \mathbf{r}) f(t) \tag{5.50}$$

where the $\mathbf{u}^e(\omega, \mathbf{r})$ are the elastic eigenfunctions and $f(t)$ is to be determined. We note immediately that (5.50) satisfies the external boundary conditions. Also, from (5.47), $\mathbf{u}^e$ satisfies

$$\mu_0[\, \nabla^2\mathbf{u}^e(\omega, \mathbf{r}) + (1 - 2\sigma)^{-1}\, \text{grad div } \mathbf{u}^e(\omega, \mathbf{r})] = -\, \rho\omega^2\mathbf{u}^e(\omega, \mathbf{r}) \tag{5.51}$$

Substituting (5.50) into (5.49) and making use of (5.51) now leads to the result

$$-\frac{\mu(S)}{\mu_0}\, \omega^2 \bar{f}(S) = \overline{\frac{\partial^2 f}{\partial t^2}}$$

$$= S^2 \bar{f}(S) - f'(0) - Sf(0)$$

i.e.

$$\bar{f}(S) = \frac{f'(0) + Sf(0)}{(S^2 + \omega^2\mu(S)/\mu_0)} \tag{5.52}$$

whose inversion yields the desired function $f(t)$.

19

Laplace transforms of the type (5.52) were encountered previously in Sections 3.2 and 3.3 in an entirely different context. Making use of the same approximations as before gives

$$f(t) = f(0)\ \xi(\omega,\,t) + \dot{f}(0)\ \eta(\omega,\,t) \tag{5.53}$$

where

$$\xi(\omega,\,t) = \Omega^{-1}[(1 + \pi^{-1}\tan\varDelta)\exp[-\tfrac{1}{2}(\Omega\tan\varDelta)t]\sin(\Omega t - \tfrac{1}{2}\tan\varDelta)$$
$$+ \tfrac{1}{2}\tan\varDelta\exp[-2\Omega t/\pi]] \tag{5.54}$$

$$\eta(\omega,\,t) = (1 + \pi^{-1}\tan\varDelta)\exp[-\tfrac{1}{2}(\Omega\tan\varDelta)t]\cos(\Omega t)$$
$$+ \pi^{-1}\tan\varDelta\exp[-2\pi\Omega t] \tag{5.55}$$

Here $\tan\varDelta(\Omega)$ is the loss angle in shear for frequency Ω, while Ω is the solution of the equation

$$\frac{\Omega^2}{\omega^2} = \frac{\mu_1(\Omega)}{\mu_0} \tag{5 56}$$

To first order in $\tan\varDelta$ the functions ξ and η satisfy the initial conditions

$$\left.\begin{array}{ll} \xi(\omega,\,0) = 0 & \dot{\xi}(\omega,\,0) = 1 \\ \eta(\omega,\,0) = 1 & \dot{\eta}(\omega,\,0) = 0 \end{array}\right\} \tag{5.57}$$

so that these functions are the exact analogues of the functions $\cos(\omega t)$, $\omega^{-1}\sin(\omega t)$ which appear in the elastic problem [eqn. (5.48)]. Thus finally the solution of the general viscoelastic free vibration problem may be written

$$\mathbf{u} = \sum_\omega [A(\omega)\ \eta(\omega,\,t) + B(\omega)\ \xi(\omega,\,t)]\ \mathbf{u}^e(\omega,\,\mathbf{r})$$

where the $A(\omega)$, $B(\omega)$ are determined by the initial conditions exactly as in the elastic problem.

The exponentially decaying form of both η and ξ confirms the physical expectations of the behaviour of a free vibrating viscoelastic solid.

The theory given above is incomplete only in the sense that the expressions for η and ξ are approximations. In principle η and ξ can be determined precisely for a specified $\mu(S)$.

The assumption of a constant Poisson's ratio is imperative in the above analysis. If this assumption is abandoned, we are compelled to breakdown $\mathbf{u}$ into na irrotational and equivoluminal part. Further, the viscoelastic problem involves coupling between these two components, which is absent in the corresponding elastic problem. No theory of these more complex vibrations has been given.

Frequently vibration problems are described by approximate equations of motion, quite different to eqn. (5.49). For example in elasticity theory the transverse motion of a beam is usually described by the equations

$$Q = \frac{\partial M}{\partial x} \qquad M = EI\frac{\partial^2 y}{\partial x^2}$$

$$\frac{\partial Q}{\partial x} = -\rho A\frac{\partial^2 y}{\partial t^2}$$

Here y is the transverse displacement, Q the transverse shear force, M the bending moment, E Young's modulus, A the cross-sectional area and I the second moment of area about the neutral section.

For a viscoelastic solid, the second of these equations is modified to read

$$\overline{M} = E(S) I \frac{\partial^2 \bar{y}}{\partial x^2}$$

The use of approximate equations does not affect the general method given above. In fact, usually in these approximate equations, only one elastic modulus occurs and the validity or otherwise of the constant Poisson's ratio model is no longer a relevant question. As an illustration we consider in detail the free vibration of a cantilever beam for which the boundary conditions are

$$\left. \begin{array}{ll} y = \dfrac{\partial y}{\partial x} = 0 & x = 0 \\[3mm] \dfrac{\partial^2 y}{\partial x^2} = \dfrac{\partial^3 y}{\partial x^3} = 0 & x = l \end{array} \right\} \tag{5.58}$$

The elastic eigenfunctions are solutions of

$$\frac{d^4 y}{dx^4} = \frac{\rho A}{E_0 I} \omega^2 y$$

subject to eqns. (5.58). The functions are (Rayleigh [36])

$$y_m = a_m \left[\cos \frac{mx}{l} - \cosh \frac{mx}{l} \right] + \beta_m \left[\sin \frac{mx}{l} - \sinh \frac{mx}{l} \right]$$

where

$$a_m = - (2/l)^{1/2} \frac{\cos m + \cosh m}{\sin m \sinh m}$$

$$\beta_m = (2/l)^{1/2} \frac{\sin m - \sinh m}{\sin m \sinh m}$$

and

$$m^4 = \frac{\rho A \omega^2 l^4}{E_0 I} \tag{5.59}$$

The absolute magnitude of a_m and β_m have been chosen so that the y_m form a set of normalized orthogonal functions. In this example the eigenvalues are discrete and given by the positive real roots of the transcendental equation

$$\cos m \cosh m + 1 = 0$$

In ascending magnitude these roots are (Rayleigh—*loc. cit.*)

$$m_1 = 1.875 \qquad m_2 = 4.694 \qquad m_3 = 7.855 \tag{5.60}$$

and satisfy the equation

$$\Sigma m_1^{-4} = \tfrac{1}{12} \tag{5.61}$$

We consider a problem in which the beam is initially displaced but with zero velocity
i.e.

$$y(x, 0) = \gamma \left[\frac{lx^2}{2} - \frac{x^3}{6} \right] \tag{5.62}$$

which is the static deflexion of an elastic beam under terminal load. Since at $t = 0$, $\dot{y}(0, x) = 0$, the functions $\xi(\omega, t)$ do not appear, and we have for the dynamic viscoelastic problem

$$y(x, t) = \sum_m A_m \, \eta(\omega, t) \, y_m(x) \tag{5.63}$$

in which the η functions are defined by (5.55) and (5.56) with the slight modification that μ is replaced by E. Thus tan $\varDelta$ now refers to the loss angle for tensile oscillations while eqn. (5.56) becomes

$$\frac{\Omega^2}{\omega^2} = \frac{E_1(\Omega)}{E_0} \tag{5.64}$$

From (5.59) and (5.64) Ω is the solution of*

$$\Omega^2 = \frac{m^4 I \, E_1(\Omega)}{\rho A} \tag{5.65}$$

and for each value of m there is a corresponding value of Ω.

Finally, the A_m are given by

$$A_m = \int_0^l \gamma(lx^2/2 - x^3/6) \, y_m(x) \, \mathrm{d}x = 2 \sqrt{2} \gamma l^{7/2} \, m^{-4} \tag{5.66}$$

which result is most simply obtained by remembering that $y_m(x)$ satisfies

$$\frac{\mathrm{d}^4 y_m}{\mathrm{d}x^4} = \frac{m^4}{l^4} \, y_m \tag{5.67}$$

while $y(x, 0)$ satisfies

$$\frac{\mathrm{d}^4 y \, (x, 0)}{\mathrm{d}x^4} = 0 \tag{5.68}$$

The result then follows from multiplying (5.67) by $y(x, 0)$, (5.68) by y_m, subtracting, integrating over $0 < x < l$ and remembering the boundary conditions satisfied by both y_m and $y(x, 0)$.

Since the coefficients A_m vary as m^{-4} while the first few values of m are given by (5.60), it is clear that the expansion (5.63) is entirely dominated by the first term. In turn the time dependence of this first term is dominated by the damped harmonic component in (5.56) so that experimental observations of the fre-

---

* Clearly the quantity E_0 (or μ_0) always drops out of the calculation in any particular application and is replaced by the pertinent parameters of the problem as in (5.65).

quency and attenuation of the motion of a vibrating reed provide a method for determining $E_1(\Omega)$ and tan $\Delta(\Omega)$.

The vibrating reed problem was first considered, from a rather different viewpoint, by Bland and Lee [37].

5.4. *Other Problems Dependent on one Space Coordinate*

A number of dynamic problems which depend on a single space coordinate have been discussed in the literature. The theory of the propagation of torsional waves along cylinders and thick walled cylindrical shells has been given by Berry [38]. In cylindrical polar coordinates r, θ, z, these waves are defined by the displacement field

$$u_\theta = rf(z, t), \qquad u_r = u_z = 0$$

The only non-vanishing component of strain is

$$\epsilon_{\theta z} = \tfrac{1}{2}r \frac{\partial f}{\partial z}$$

so that the constitutive equation may be written

$$\overline{\tau_{\theta z}} = \mu(i\omega)\, r \frac{\overline{\partial f}}{\partial z} \tag{5.69}$$

where the bar denotes a Fourier transform with respect to time. Combining (5.69) with the equation of motion

$$\frac{\partial \tau_{\theta z}}{\partial z} = \rho \frac{\partial^2 u_\theta}{\partial t^2}$$

yields

$$\mu(i\omega) \frac{\partial^2 \bar{f}}{\partial z^2} = -\rho\omega^2 \bar{f}$$

so that the theory of torsional waves is essentially identical with the theory of Section 5.1.

The theory of spherically symmetric waves generated by transient pressure on the surface of an internal cavity has been considered by a number of authors (Bland [39], Berry [38], Lockett [44] and Chao and Auchenbach [40]). Of these papers the one by Lockett uses a realistic viscoelastic model and considers the response of the medium to pressure pulses with finite rise times.

Naghdi and Orthwein [41] have studied the behaviour of shallow shells of revolution under axisymmetric dynamic loads.

5.5. *Problems in Two and Three Dimensions*

Few solutions have been given for dynamic problems involving two and three space coordinates. For the simple boundary value problems for which the correspondence principle may be invoked, it is always possible to write down formal solutions in terms of Fourier integrals or inverse Laplace transforms. In

general, the subsequent inversion of those transforms is a more difficult task.

For certain types of problems considerable simplifications are possible in the theory of the correspondence principle with the adoption of the constant Poisson's ratio model. Chao and Auchenbach [40] have shown that under otherwise quite general conditions, the use of this approximation yields the viscoelastic solution directly in terms of integrals of the corresponding elastic solution. Chao and Auchenbach apply their results to the spherically symmetric problem and to the problem of a half space subject to transient point loading on the free surface.

The theory of the vibrations of thin elastic and viscoelastic plates has been given by Zorski [42].

Finally, Miklowitz [43] has given detailed solutions to two plane strain problems for a Maxwell solid. In the first problem the internal surface of a cylindrical cavity is subject to a transient line load. The second problem concerns the scattering of an incident dilatational wave by a cylindrical cavity. Interesting features of both problems are the Rayleigh waves circulating around the cavity surface.

REFERENCES

[1] LOCKETT, F. J., *J. Mech. Phys. Sol.*, **10**, 53 (1962).
[2] HUNTER, S. C., *J. Mech. Phys. Sol.*, **9**, 39 (1961).
[3] SCHWARZL, F. and STAVERMAN, A. J., *J. Appl. Phys.*, **23**, 838 (1952).
[4] MORLAND, L. W. and LEE, E. H., *Trans. Soc. Rheology*, vol. **IV**, 233 (1960).
[5] MUKI, R. and STERNBERG, E., *J. Appl. Mechanics*, (paper 60 WA–126) (1961).
[6] ROGERS, T. G. and LEE, E. H., Brown University Report NORD 18594/6 (1962).
[7] STERNBERG, E., *High Temperature Structures and Materials*, Editors, A. M. FREUDENTHAL, B. A. BOLEY and H. LIEBOWITZ, Pergamon Press, 348 (1964).
[8] MARVIN, R. S. and OSER, H., *J. of Research*, National Bureau of Standards, **66B**, 171 (1962).
[9] ROUSE, P. E., *J. Chem. Phys.*, **21**, 1272 (1953).
[10] BUECHE, F., *J. Chem. Phys.*, **22**, 603 (1954).
[11] HUNTER, S. C., *Progress in Solid Mechanics*, vol. I, Editors, R. HILL and I. N. SNEDDON (North Holland, Amsterdam) (1960).
[12] ALFREY, T., *Mechanical Behaviour of High Polymers*, Interscience Publishers, New York (1948).
[13] GROSS, B., *The Mathematical Structures of the Theory of Viscoelasticity*, Hermann et Cie, Paris (1953).
[14] GURTIN, M. E. and STERNBERG, E., *Archive for Rational Mechanics and Analysis*, **11**, 291 (1962).
[15] LEE, E. H., *Q. App. Maths.*, **13**, 183 (1955).
[16] LEE, E. H., *Proceedings of the 1957 Conference on High Rates of Strain* (Institution of Mechanical Engineers, London (1957).
[17] LEE, E. H., *Proceedings of First Naval Structural Mechanics Symposium*, Pergamon Press (1958).
[18] LEE, E. H., RADOK, J. R. M. and WOODWARD, W. B., *Trans. Soc. Rheology*, vol. III, 41 (1959).
[19] LOVE, A. E. H., *Mathematical Theory of Elasticity*, Cambridge University Press, 4th edition (1944).
[20] FERRY, J. D. and WILLIAMS, M. L., *J. Colloid Sci.*, **7**, 347 (1952).

[21] FERRY, J. D. and FITZGERALD, E. R., *Proc. 2nd International Congress in Rheology*, Butterworths, London (1954).
[22] HUNTER, S. C., *J. Mech. Phys. Sol.*, **8**, 219 (1960).
[23] BOUSSINESQ, M. J. (1885). See TODHUNTER and PEARSON—*History of Theory of Elasticity*, vol. II, Part 2, 260, Dover reprint (1960).
[24] FREUDENTHAL, A. M. and SHINOZUKA, M., Columbia University, Dept. of Civil Eng. and Mech. Eng. Report No. 1, CU–1–61–ONR 266(78) CE (1961).
[25] LEE, E. H. and RADOK, J. R. M., *J. Appl. Mech.*, **27**, 438 (1960).
[26] GRAHAM, G. A. C., Unpublished results (1965).
[27] HUNTER, S. C., *J. Appl. Mech.*, **28**, 611 (1961).
[28] CORNELIUSSEN, A. H. *et al.*, Brown University Report NORD 18594/5 (1961).
[29] LEE, E. H. and KANTER, T., *J. Appl. Phys.*, **24**, 1115 (1953).
[30] LEE, E. H. and MORRISON, J. A., *J. Polymer Sci.*, **19**, 93 (1956).
[31] BERRY, D. S. and HUNTER, S. C., *J. Mech. Phys. Sol.*, **4**, 72 (1956).
[32] BERRY, D. S., *Phil. Mag.*, **25**, 100 (1958).
[33] HILLIER, K. W. and KOLSKY, H., *Proc. Phys. Soc. London*, **B.62**, 111 (1949).
[34] HILLIER, K. W., *Proc. Phys. Soc. London*, **B.62**, 701 (1919).
[35] KOLSKY, H., *Phil. Mag.*, **8**, 693 (1956).
[36] RAYLEIGH, J. W. S., *The Theory of Sound*, vol. I, p. 279 (1896); Dover Reprint (1945).
[37] BLAND, D. and LEE, E. H., *J. Appl. Phys.*, **27**, 967 (1955).
[38] BERRY, D. S., *J. Mech. Phys. Sol.*, **3**, 177 (1958).
[39] BLAND, D., *Proc. of the 1957 Conference on High Rates of Strain*, Institution of Mechanical Engineers, London (1957).
[40] CHAO, C. C. and AUCHENBACH, J. D., *Stress Waves in Anelastic Solids*, Editors, H. KOLSKY, W. PRAGER; *Proc. of IUTAM Conf.* held at Brown University, 1963, Springer-Verlag, Berlin (1964).
[41] NAGHDI, P. M. and ORTHWEIN, W. C., *Q. Appl. Maths.*, **18**, 107 (1960).
[42] ZORSKI, H., *Stress Waves in Anelastic Solids*, Editors, H. KOLSKY and W. PRAGER, Springer-Verlag, Berlin (1964).
[43] MIKLOWITZ, J., *Stress Waves in Anelastic Solids*, Editors, H. KOLSKY and W. PRAGER, Springer-Verlag, Berlin (1964).
[44] LOCKETT, F. J., *J. Mech. Phys. Sol.*, **9**, 215 (1961).

THE DYNAMICS OF SOLID PROPELLANT
ROCKET MOTORS

J. H. BALTRUKONIS

Mechanics Division, The Catholic University of America
Washington, D.C.

Abstract—From the point of view of dynamics, a solid propellant rocket motor is a unique structure in that it is composed of a substantial mass of propellant material case-bonded to a relatively massless, thin-walled cylinder. The mechanical properties of the propellant are such that it contributes little to the stiffness of the composite structure but it does contribute to the dynamic characteristics of the structure because of its mass. Furthermore, due to the viscoelastic character of the propellant, it can be expected to provide considerable damping to the system. At this point in the development of the art of design of solid propellant rocket motors there are no clear-cut or well-founded methods to evaluate quantitatively the contributions of the propellant to the dynamic responses of the composite structure. It is clear that unless such methods are devised, it will be difficult to arrive at accurate missile designs.

In this paper a survey of the dynamic problems of solid propellant rocket motors is presented starting from the simplest model thereof and proceeding, step-by-step, to the consideration of more sophisticated and realistic models. The consideration is restricted to infinitesimal deformations of propellant grains with linear mechanical properties. Substantial progress has been achieved towards the solution of many important dynamical problems. We shall attempt to summarize the pertinent developments and indicate along which lines we feel future study should proceed. A few illustrative solutions are included in areas wherein progress has been substantial.

1. INTRODUCTION

Structural dynamics concerns the analysis, by theoretical and/or experimental means, of the interactions of time-dependent loads and/or deformations externally applied to a structure or structural element and the internal stress and displacement response wherein inertial effects must be included in the analysis. It is the objective of this paper to present a survey of the field of structural dynamics of solid propellant rocket motors, to discuss those aspects of the subject which are of particular interest to the author, and to recommend those areas in which further study should prove fruitful and rewarding. It is not our objective to present a bibliographical survey of the field and, consequently, many specific, individual contributions will probably be overlooked. There is no claim of uniqueness for this survey of the field nor do we maintain that it is complete since it is inevitable that a study of this sort will be biased to a large extent by the limitations, interests and viewpoint of the author.

The first logical step in a task of this sort is to delimit the field under consideration. In general, we shall not be interested in the dynamics of complete rockets or missiles which may consist of several stages. Instead, we shall limit our concern to individual solid propellant rocket motors; i.e. casing plus propellant.

We shall not be interested in any attachments to the casing such as rocket nozzles, guidance and control system assemblies, etc. It is not intended to imply that the dynamics of complete rockets is not important but rather the intention is to limit the scope of this presentation.

A solid propellant rocket motor is an unusually complicated structure, at least from the standpoint of its analysis. It consists of a thin, circular cylindrical casing with domed end closure. The energetic propellant grain is bonded to the casing along its outer cylindrical surface. Frequently, a rubber liner is interposed between the grain and casing for purposes of insulation. The flow of the gases developed by surface combustion of the solid propellant occurs through passages of relatively complex geometry within the grain to the one or more nozzles in the aft dome of the motor. The motor casing material is usually an elastic material such as steel though there has been a recent trend to casings wound of fiberglass filaments and impregnated with some sort of hard resin.

The propellant material is a composite, consisting of an elastomeric binder, a crystalline oxidizer and dispersed solid materials such as aluminum particles. This material is very compliant relative to the casing, is time- or frequency-dependent and is highly temperature-sensitive. Finally, the grain is very massive compared to the casing usually constituting from 80 to 95 per cent of the total mass of the motor.

Clearly, analysis of this structure for its responses to various dynamic stimuli is an imposing task indeed. The usual first step in the analysis of a complicated structure is the formulation of a tractable mathematical model. The structure involves several fundamental difficulties but probably the principal ones are (1) the complex geometry of the internal passages in the propellant grain; and (2) the fact that the motor is of finite length thereby introducing possible inter-action of end effects. These two difficulties are of the same nature as the complications that have plagued elasticians from the very beginnings of the field of elasticity. Consequently, at the outset, it seems wise to idealize the structure to the extent that these complications are no longer present. Thus, we consider a mathematical model that is infinitely-long with a circular perforation. We do not include a liner so that the motor consists only of grain and casing. We further restrict the present consideration to linear analysis; i.e. we consider only infinitesimal deformations of linear materials. These restrictions may not be as severe as they seem when it is realized that most of the dynamic environments of interest will result in very small displacements within the linear range of the materials under consideration. Investigations on materials properties have revealed that, for small strains, propellants typically behave as linearly-visco-elastic solids.

2. ELASTIC GRAINS

The mathematical model which we have thus far devised is still too complicated for initial studies. Thus, we introduce the further assumptions that the grain is perfectly elastic with no internal perforation and, since the casing is very

stiff relative to the core, that the casing be perfectly rigid. Therefore, our initial, very crude model of a solid propellant rocket motor consists of an infinitely-long composite cylinder with a rigid outer layer and a very compliant, solid, elastic core. Investigation of such a model, however crude, will begin to yield valuable information concerning natural frequencies and displacement and stress fields corresponding to normal modes. Such information is of immediate utility, for example, in the design of the guidance systems whose reliability depends, to a large extent, on estimates of natural frequencies and mode shapes of the rocket motor.

Other possible applications are dynamic loads analyses, staging studies, transportation and handling studies, etc. Over and above these practical applications, initial analyses of crude mathematical models provide the analyst with the experience required for subsequent refinement of the model. Additionally, a catalog of solutions is rapidly developed which may prove to be very useful as checks on the solutions of more refined models.

The natural coordinate system for the formulation of the problem posed is the polar cylindrical system. There has long been activity within the general area of dynamics of elastic bodies in polar cylindrical coordinates. The earliest formulation of a problem by means of the dynamical equations of elasticity in cylindrical coordinates is due to Pochhammer [1] and Chree [2], who independently investigated longitudinal and transverse wave propagation in infinitely-long circular rods with traction-free surfaces. An excellent survey of the history of this problem was presented by Abramson, Plass and Ripperger [3]; nevertheless, it would be useful and interesting to mention a few of the more important investigations. Following Pochhammer and Chree the next study that should be mentioned is due to Ghosh [4], who derived dispersion equations for longitudinal wave propagation in thick- and thin-walled, infinitely-long, hollow, circular cylinders with both surfaces free of traction and with one surface traction-free and the other rigidly clamped.

Bancroft [5] was among the first to publish numerical solutions of the dispersion equations for longitudinal wave propagation. In addition, he recorded the dispersion equation for transverse wave propagation in infinitely-long, circular rods with traction-free surfaces but no numerical work was indicated. Hudson [6] carried out some numerical work with the dispersion equation for transverse wave propagation but arrived at the erroneous conclusion that there was only one mode of propagation of transverse waves. This error was subsequently propagated by Davies [7] and Kolsky [8], among others, and was finally pointed out by Abramson [9], who calculated several dispersion curves in the first mode of propagation of transverse waves.

McFadden [10] was concerned with radial vibrations in hollow, thick-walled cylinders, while Gazis [11] presented a study of plane strain vibrations in hollow cylinders with traction-free surfaces. The most complete study, to date, by means of the dynamical equations of elasticity, was presented by Gazis [12] on the longitudinal and transverse wave propagation and free vibrations in infinitely-long, thick-walled cylinders with traction-free surfaces. Other pertinent studies

were reported by Herrmann and Mirsky [13], Mirsky and Herrmann [14, 15], Greenspon [16–18], Bird, Hart and McClure [19] and Bird [20].

The field and constitutive equations for dynamic deformations of compressible elastic continua in polar cylindrical coordinates may be reduced to the following three equations of motion:

$$\nabla^2 u_r - \frac{u_r}{r^2} - \frac{2}{r^2}\frac{\partial u_\theta}{\partial \theta} + \frac{1}{1-2\nu}\frac{\partial \Delta}{\partial r} = \frac{\rho}{G}\frac{\partial^2 u_r}{\partial t^2} \tag{1a}$$

$$\nabla^2 u_\theta - \frac{u_\theta}{r^2} + \frac{2}{r^2}\frac{\partial u_r}{\partial \theta} + \frac{1}{1-2\nu}\frac{1}{r}\frac{\partial \Delta}{\partial \theta} = \frac{\rho}{G}\frac{\partial^2 u_\theta}{\partial t^2} \tag{1b}$$

$$\nabla^2 u_z + \frac{1}{1-2\nu}\frac{\partial \Delta}{\partial z} = \frac{\rho}{G}\frac{\partial^2 u_z}{\partial t^2} \tag{1c}$$

Solutions of these equations of motion are readily obtained by means of three displacement potentials as follows:

$$u_r = \frac{\partial \phi}{\partial r} + \frac{\partial^2 \psi}{\partial r \partial z} + \frac{1}{r}\frac{\partial \chi}{\partial \theta} \tag{2a}$$

$$u_\theta = \frac{1}{r}\frac{\partial \phi}{\partial \theta} + \frac{1}{r}\frac{\partial^2 \psi}{\partial \theta \partial z} - \frac{\partial \chi}{\partial r} \tag{2b}$$

$$u_z = \frac{\partial \phi}{\partial z} - \left(\frac{\partial^2}{\partial r^2} + \frac{1}{r}\frac{\partial}{\partial r} + \frac{1}{r^2}\frac{\partial^2}{\partial \theta^2}\right)\psi. \tag{2c}$$

It may be verified by direct substitution that eqns. (1) are identically satisfied by these components of displacement provided we take the displacement potentials as solutions of the following differential equations:

$$\nabla^2 \phi = c_c^{-2}\frac{\partial^2 \phi}{\partial t^2} \tag{3a}$$

$$\nabla^2 (\psi, \chi) = c_s^{-2}\frac{\partial^2}{\partial t^2}(\psi, \chi), \tag{3b}$$

where c_c and c_s denote the dilatational and shear wave velocities, respectively, and are given by

$$c_c^2 = \frac{1}{\kappa^2}\frac{G}{\rho} \tag{4a}$$

$$c_s^2 = \frac{G}{\rho} \tag{4b}$$

$$\kappa = \frac{c_s}{c_c} = \left[\frac{1-2\nu}{2(1-\nu)}\right]^{1/2} \tag{4c}$$

We recognize the differential equations (3) as wave equations, solutions of which are well known. On selection of appropriate solutions of these wave

equations, the displacements follow from eqns. (2), while the components of stress are obtained from the following stress–displacement relations:

$$\sigma_r = 2G \left(\frac{\partial u_r}{\partial r} + \frac{\lambda}{2G} \Delta \right) \tag{5a}$$

$$\sigma_\theta = 2G \left(\frac{1}{r} \frac{\partial u_\theta}{\partial \theta} + \frac{u_r}{r} + \frac{\lambda}{2G} \Delta \right) \tag{5b}$$

$$\sigma_z = 2G \left(\frac{\partial u_z}{\partial z} + \frac{\lambda}{2G} \Delta \right) \tag{5c}$$

$$\tau_{r\theta} = G \left(\frac{1}{r} \frac{\partial u_r}{\partial \theta} - \frac{u_\theta}{r} + \frac{\partial u_\theta}{\partial r} \right) \tag{5d}$$

$$\tau_{rz} = G \left(\frac{\partial u_z}{\partial z} + \frac{\partial u_z}{\partial r} \right) \tag{5e}$$

$$\tau_{\theta z} = G \left(\frac{\partial u_\theta}{\partial z} + \frac{1}{r} \frac{\partial u_z}{\partial \theta} \right) \tag{5f}$$

Let us now illustrate the application of this general theory in the calculation of the natural frequencies and normal modes of the initial crude model for the solid propellant rocket motor. Since the grain is solid, the boundary conditions are given by

$$u_r \bigg|_{r=a} = u_\theta \bigg|_{r=a} = u_z \bigg|_{r=a} = 0 \tag{6}$$

The simplest modes of vibration are the so-called axial-shear modes. These are defined as those modes of free vibration in which the only non-zero component of displacement is that parallel to the axis of the cylinder. Furthermore, this axial displacement component depends only on the coordinates in the plane of a cross-section. These modes are of fundamental importance if for no other reason than that they are among the very few modes for which exact, closed-form solutions of the three-dimensional equations of elasticity are possible. There are, however, other reasons for concern with axial-shear modes. They represent limiting flexural or longitudinal modes; i.e. they are flexural or longitudinal wave modes with infinite wave-length. In accord with their definition we seek solutions of the equations of elasticity in the form

$$u_r = u_\theta = 0 \tag{7a}$$

$$u_z = W(r) e^{i\omega t} \cos n\theta \tag{7b}$$

Substitution into eqns. (1) results in the following single equation:

$$W'' + \frac{1}{r} W' + \left(\frac{\rho \omega^2}{G} - \frac{n^2}{r^2} \right) W = 0 \tag{8}$$

wherein primes denote differentiation with respect to the argument. This is

the well-known nth-order Bessel equation which has the following general solution:

$$W(r) = C_{n1}J_n\left(\frac{\Omega r}{a}\right) + C_{n2}Y_n\left(\frac{\Omega r}{a}\right) \tag{9a}$$

where Ω is a dimensionless frequency coefficient defined by

$$\Omega^2 = \frac{\rho\omega^2 a^2}{G}, \tag{9b}$$

C_{n1} and C_{n2} are arbitrary constants which must be evaluated such that the boundary conditions will be satisfied, and J_n and Y_n are the nth-order Bessel functions of the 1st and 2nd kinds, respectively. In view of eqns. (7) the boundary conditions given by eqns. (6) reduce to the following single condition:

$$W(a) = 0$$

This condition will be identically satisfied provided that we take C_{2n} to vanish and that

$$J_n(\Omega) = 0 \tag{10}$$

This result constitutes the frequency equation in the present problem. It defines a doubly-infinite family of natural frequencies and normal modes; i.e. corresponding to each value of n we find an infinite number of roots of eqn. (10). It is clear from eqn. (9a) that the $n = 0$ modes are axisymmetric whereas the modes for which $n \geq 1$ are antisymmetric. In view of eqns. (9a), and (7) we observe that all the stresses vanish with the exception of the shear stresses τ_{rz} and $\tau_{\theta z}$ and the latter vanishes for the axisymmetric modes. Clearly, this general type of vibration is pure shear in nature accounting, partially, for the name axial-shear. These modes, among others, were thoroughly investigated in Ref. [21].

Another important class of vibrations occurs when the axial component of displacement vanishes identically yielding a transverse mode of vibration. Such a mode of vibration occurs when we take

$$\phi = C_{n1}J_n\left(\kappa\Omega\,\frac{r}{a}\right)e^{i\omega t}\cos n\theta \tag{11a}$$

$$\psi = 0 \tag{11b}$$

$$\chi = C_{n2}J_n\left(\Omega\frac{r}{a}\right)e^{i\omega t}\sin n\theta \tag{11c}$$

It is immediately clear from eqns. (2) that we obtain a plane strain mode of vibration wherein u_z vanishes identically. Substitution into eqns. (2) and, thence, into the boundary conditions given by eqns. (6) results in the following frequency equation:

$$J_{n-1}(\Omega)\,J_{n+1}(\kappa\Omega) + J_{n+1}(\Omega)\,J_{n-1}(\kappa\Omega) = 0 \tag{12}$$

where we have used the recurrence relations for the Bessel functions. These transcendental frequency equations define a doubly infinite set of natural circular frequency coefficients which depend upon Poisson's ratio. In Ref. [22] this

dependency is investigated in detail. The first four branches of the first four modes of vibration are plotted in function of κ which depends only upon Poisson's ratio. Additionally, the displacement fields for several different modes are plotted.

The last problem of interest concerning this initial crude model is that of transverse wave propagation. In Ref. [23] this problem was treated in some detail. The dispersion equations were derived and several branches were plotted. In addition, it was pointed out that the dispersion equations degenerate for infinite wavelengths into two uncoupled frequency equations defining the axial-shear and transverse vibrations modes which we have discussed above.

Before proceeding to the refinement of our initial mathematical model, mention should be made of an interesting problem that arises in connection with eqn. (12), the frequency equation for free, transverse vibrations. It was mentioned that the natural frequency depends upon Poisson's ratio. In Ref. [22] it was demonstrated that finite, real natural frequencies exist when the material of the core is ideally incompressible; i.e., when Poisson's ratio has the value $\frac{1}{2}$. A question immediately arises: "How can natural frequencies exist for an incompressible material when it occupies the entire internal volume of the tank?" In Ref. [24] it was demonstrated that, as the core material tends to become incompressible; i.e. as Poisson's ratio tends to $\frac{1}{2}$, the frequency spectrum tends to a simple line spectrum. Clearly, this kind of a frequency spectrum is physically impossible. That this should be the case is not surprising since the ideally incompressible material is a hypothetical material which cannot exist in nature. Nevertheless, the assumption of such a material is quite regularly used in-practice. The behavior mentioned above is simply one difficulty that can arise from the application of such an assumption. Finally, we draw attention to a few interesting studies due to Magrab [25–27] concerning the displacement and stress fields in the solid grain due to steady-state, forced harmonic oscillation of the rigid case.

On the basis of the studies cited we conclude that our initial crude model has been thoroughly investigated and that its steady-state response is adequately understood. Therefore, we proceed to a slight refinement of our mathematical model by allowing for a circular internal perforation of the grain. Now our model consists of an infinitely-long, two layered cylinder with the outer layer ideally-rigid and the inner layer elastic. The boundary conditions in this case are given by the following:

$$\sigma_r \bigg|_{r=b} = \tau_{r\theta} \bigg|_{r=b} = \tau_{rz} \bigg|_{r=b} = 0 \tag{13a}$$

$$u_r \bigg|_{r=a} = u_\theta \bigg|_{r=a} = u_z \bigg|_{r=a} = 0 \tag{13b}$$

where a and b denote the external and internal radii, respectively, of the grain. Equations (13a) express the conditions that the internal grain perforation be free of surface tractions, while eqns. (13b) result from the assumption of an ideal bond between the grain and rigid casing.

For the axial-shear mode of vibrations we seek solutions in the form given by eqn. (7) so that eqn. (8) is the governing equation of motion while eqn. (9a) gives an admissible solution. In view of eqns. (5), (7) and (9a) we find that all but two of the boundary conditions given by eqns. (13) are trivially satisfied and these two conditions result in the following:

$$C_{n1}J_n(\Omega) + C_{n2}Y_n(\Omega) = 0$$

$$C_{n1}J_n'\left(\Omega\frac{b}{a}\right) + C_{n2}Y_n'\left(\Omega\frac{b}{a}\right) = 0 \qquad (n = 0, 1, 2, \ldots)$$

This is a homogeneous system of linear, algebraic equations in the unknown constants C_{n1} and C_{n2}. Such a system can have non-trivial solutions only if the determinant of the coefficients of the unknowns vanishes identically. Thus, we are led to the following frequency equations:

Axisymmetric modes:

$$J_0(\Omega)\,Y_1\left(\Omega\frac{b}{a}\right) - J_1\left(\Omega\frac{b}{a}\right)Y_0(\Omega) = 0 \tag{14a}$$

Anti-symmetric modes:

$$J_n(\Omega)\,Y_n'\left(\Omega\frac{b}{a}\right) - J_n'\left(\Omega\frac{b}{a}\right)Y_n(\Omega) = 0, \qquad (n = 1, 2, \ldots) \tag{14b}$$

The zeros of these frequency equations were calculated in Ref. [21].

In Ref. [28] the problems of plane strain vibrations and transverse wave propagation in the more refined model are treated. In the case of transverse wave propagation none of the boundary conditions given by eqns. (13) is trivially satisfied so that a dispersion equation is obtained in the form of a 6 × 6 determinant set equal to zero. The elements of the determinant are, in general, linear combinations of nth order Bessel functions of the first and second kind. This dispersion equation is written in Ref. [28] and sample calculations were carried out in Ref. [29] for an incompressible grain. In Ref. [28] it is demonstrated that the dispersion equation governing transverse wave propagation degenerates for infinite wavelength to two uncoupled frequency equations. One of these is that for axial-shear modes of vibration as given by eqn. (14b) and the other is that governing plane strain vibrations. The latter frequency equation is a 4 × 4 determinant involving nth order Bessel functions of the first and second kind set to zero. Four branches for each of the first four modes of vibration were calculated in Ref. [30] for an incompressible grain.

The next refinement we can make in our mathematical model of the rocket motor is to allow for an elastic casing so that our new model consists of a composite cylinder of two concentric elastic layers both of which are infinitely long. In general, the stiffness of the grain will be considered small as compared with that of the casing material in deference to the origins of the problem. The understanding of the behavior of such a model should shed considerable light

upon the rocket motor problem. To be sure, the outer layer which models the motor casing will usually be thin relative to its mean radius and, consequently, shell theory may be used in describing its behavior. However, for the time being, we shall treat both layers by means of elasticity theory as given in eqns. (1)–(5). We shall return, subsequently, to the use of shell theory in treating the behavior of the outer layer. In order to associate a given quantity with one or the other of the two layers, we append a "1" when referring to the outer layer and a "2" when reference to the inner layer is intended. Thus, u_{z_2} denotes the axial component of displacement in the inner layer, while u_{z_1} denotes the same quantity in the outer layer. In accord with this convention, the boundary conditions are given by

$$\sigma_{r_1}\bigg|_{r=r_1} = \tau_{r\theta_1}\bigg|_{r=r_1} = \tau_{rz_1}\bigg|_{r=r_1} = 0 \qquad \text{(15a, b, c)}$$

$$u_{r_1}\bigg|_{r=a} = u_{r_2}\bigg|_{r=a} \qquad \text{(15d)}$$

$$u_{\theta_1}\bigg|_{r=a} = u_{\theta_2}\bigg|_{r=a} \qquad \text{(15e)}$$

$$u_{z_1}\bigg|_{r=a} = u_{z_2}\bigg|_{r=a} \qquad \text{(15f)}$$

$$\sigma_{r_1}\bigg|_{r=a} = \sigma_{r_2}\bigg|_{r=a} \qquad \text{(15g)}$$

$$\tau_{r\theta_1}\bigg|_{r=a} = \tau_{r\theta_2}\bigg|_{r=a} \qquad \text{(15h)}$$

$$\tau_{rz_1}\bigg|_{r=a} = \tau_{rz_2}\bigg|_{r=a} \qquad \text{(15i)}$$

$$\sigma_{r_2}\bigg|_{r=r_2} = \tau_{r\theta_2}\bigg|_{r=r_2} = \tau_{rz_2}\bigg|_{r=r_2} = 0 \qquad \text{(15j, k, l)}$$

For the axial–shear mode of vibration the only non-zero component of displacement is the axial component and we take it in the form

$$u_{zj} = \left[C_{j1}J_n\left(\Omega_j\,\frac{r}{a}\right) + C_{j2}Y_n\left(\Omega_j\,\frac{r}{a}\right)\right] e^{i\omega t} \cos. n\theta, \qquad (j=1, 2) \quad \text{(16a)}$$

where

$$\Omega_j^2 = \frac{\rho_j\omega^2 a^2}{G_j}, \qquad (j=1, 2) \qquad \text{(16b)}$$

Direct substitution reveals that the equations of motion given by eqns. (1) are identically satisfied for this displacement field. Substituting into eqns. (5) we find that the only non-zero components of stress are the following:

$$\tau_{rzj} = \frac{G_j\Omega_j}{a}\left[C_{j1}J_n'\left(\Omega_j\,\frac{r}{a}\right) + C_{j2}Y_n'\left(\Omega_j\,\frac{r}{a}\right)\right] e^{i\omega t}\cos. n\theta \qquad \text{(17a)}$$

$$\tau_{\theta zj} = -\,G_j\,\frac{n}{r}\left[C_{j1}J_n\left(\Omega_j\,\frac{r}{a}\right) + C_{j2}Y_n\left(\Omega_j\,\frac{r}{a}\right)\right] e^{i\omega t}\sin. n\theta \qquad \text{(17b)}$$

$$(j=1, 2)$$

We see immediately that 8 of the twelve boundary conditions given by eqns. (15) are trivially satisfied and only the conditions given by eqns. (15c, f, i, l) remain to be satisfied. Substitution into the latter conditions results in a homogeneous system of four linear, algebraic equations in the unknown constants C_{j1} and C_{j2}. The necessary and sufficient condition that non-trivial solutions of this system exist is that the determinant of the coefficients of the unknowns vanishes identically. Thus, we obtain the following frequency equations:

$$
\begin{vmatrix}
J_n'\left(\Omega_1 \dfrac{r_1}{a}\right) & Y_n'\left(\Omega_1 \dfrac{r_1}{a}\right) & 0 & 0 \\[2ex]
J_n'(\Omega_1) & Y_n'(\Omega_1) & J_n'(\Omega_2) & Y_n'(\Omega_2) \\[2ex]
Ra J_n(\Omega_1) & Ra\, Y_n(\Omega_1) & J_n(\Omega_2) & Y_n(\Omega_2) \\[2ex]
0 & 0 & J_n'\left(\Omega_2 \dfrac{r_2}{a}\right) & Y_n'\left(\Omega_2 \dfrac{r_2}{a}\right)
\end{vmatrix} = 0 \quad (18a)
$$

where $n = 0, 1, 2, \ldots$. On expansion and rearrangement, these frequency equations reduce to the following:

$$f_{1n}h_{2n} - Rah_{1n}f_{2n} = 0, \qquad (n = 0, 1, 2, \ldots) \qquad (18b)$$

where

$$f_{jn} = J_n'(\Omega_j) Y_n'\left(\Omega_j \frac{r_j}{a}\right) - J_n'\left(\Omega_j \frac{r_j}{a}\right) Y_n'(\Omega_j) \qquad (19a)$$

$$\qquad\qquad\qquad\qquad (j = 1, 2)$$

$$h_{jn} = J_n(\Omega_j) Y_n'\left(\Omega_j \frac{r_j}{a}\right) - J_n'\left(\Omega_j \frac{r_j}{a}\right) Y_n(\Omega_j) \qquad (19b)$$

$$R = \frac{\rho_2}{\rho_1} \qquad (19c)$$

$$\alpha^2 = \frac{\Omega_1^2}{\Omega_2^2} = \frac{G_2/G_1}{\rho_2/\rho_1} \qquad (19d)$$

The frequency equation given by eqn. (18) is an implicit function relating the density ratio ρ_2/ρ_1, the ratio of the shear moduli G_2/G_1, the radius ratios r_1/a and r_2/a, and one or the other of the two frequency coefficients Ω_1 or Ω_2. In Ref. [31] it is shown that this frequency equation includes eqns. (10) and (14) as special cases, as it should. Additionally, various branches of the frequency equation are plotted in order to establish the conditions under which the earlier simpler solutions can be used. In general, it would seem that when the casing is reasonably thin, the assumption of a rigid casing is acceptable only for axisymmetric, axial-shear modes.

For transverse (plane strain) vibrations of the composite cylinder we take the axial displacement to vanish identically and all displacements and stresses

to be independent of the z coordinate variable. Under these conditions τ_{rz} and $\tau_{\theta z}$ vanish identically and four of the twelve boundary conditions given by eqns. (15) are trivially satisfied. Substitution into the remaining boundary conditions results in a system of 8 homogeneous, linear, algebraic equations in the 8 unknown constants. The necessary and sufficient condition that non-trivial solutions of this system exist is that the determinant of the coefficients of the unknowns must vanish. Thus, the frequency equation is obtained in the form of an 8×8 determinant set to zero. In general, the elements of the determinant are linear combinations of nth order Bessel functions of the first and second kinds. Calculations of natural frequencies have been carried out in Ref. [32] for a case wherein the outer layer (casing) is very much stiffer than the inner layer (grain). In this particular case the various branches of the frequency equation have been plotted and analysed for modes wherein $n = 1$; i.e. for modes that have only a single nodal diameter. Modes of vibration have been identified that degenerate to pure grain and pure casing modes. A pure grain mode is defined as that mode of vibration existing in the grain when the case is perfectly rigid while a pure casing mode occurs in an empty casing. It was shown that, for typical geometries and material parameter values, the lowest $n = 1$ casing mode is substantially higher than the lowest $n = 1$ grain mode. It is demonstrated that the natural frequency of the lowest casing mode is very sensitive to grain thickness. It may be possible to include this effect in an approximate solution based on shell theory wherein the mass of the grain is lumped with the mass of the thin casing and the stiffness of the grain is neglected. This possibility should be exploited. Additionally, it was shown that the grain modes are relatively insensitive to variations in casing thickness indicating that, at least for the material parameters considered, the coupling of casing and grain rigidities is relatively weak. It follows that reasonable approximations to the natural frequencies of the grain modes can be obtained by assuming that the casing is perfectly rigid. The studies of Ref. [32] were limited to $n = 1$ modes. Work is in progress at The Catholic University of America to obtain similar results for $n = 2, 3, 4$ modes. The frequency equation has been programmed for machine computation, the program has been checked and data produced. It remains to analyze the data presently available and to supplement it as required.

As previously mentioned, it is possible to use thin shell theory in treating the deformation of the casing rather than elasticity theory. However, since thin shell theory is not substantially simpler than elasticity theory in this particular application, there appears to be little profit especially since elasticity theory must be used for the grain. Sann and Shaffer [33] have performed an interesting study wherein shell theory was used for the casing. Although the frequency equations are developed for all modes of transverse vibrations, numerical results and analysis are presented only for axisymmetric modes. Two different solutions are presented: one applicable to a compressible grain and the other to an incompressible grain. It is found that, with a compressible core, the axisymmetric mode has two uncoupled motions; one is a "rigid" rotation of the casing with a twisting of the grain and the other is a purely radial motion. The latter motion

is not present in an incompressible grain. Some simplified frequency equations are also presented for limiting extremes of rigidity and density ratios.

The steady-state, transverse wave propagation problem for the two-layered, elastic cylinder remains for further treatment. None of the boundary conditions given by eqns. (15) is trivially satisfied in this case so that the dispersion equation takes the form of a 12×12 determinant set equal to zero. This dispersion equation is readily written down but it remains to calculate its branches and perform the requisite analyses thereof.

We are once again ready for an additional refinement of our mathematical model. There are two types of refinements that can be made, both of which are fraught with difficulties: (1) complicated internal perforation and (2) finite length. It would appear that each of these possible refinements requires individual treatment.

Let us first consider the problem of the complicated geometry of the internal perforations of the grain. These internal passages are usually three-dimensional in character having shapes that are usually dictated by the considerations of internal ballistics. Little has been accomplished concerning the dynamics of such motors nor is it likely that a great deal will be achieved in the near future other than numerical solutions of specific problems. However, it frequently happens that these internal grain perforations are two-dimensional in nature over substantial portions of the total length of the motor. In these portions the grain cross-section is circular, of course, with a star-shaped perforation. Therefore, it is not unreasonable to consider an infinitely-long grain with such a cross-section. A considerable volume of work has been accomplished with this model of a rocket motor and in the following paragraphs we shall attempt to survey at least a portion of the work with which the author has a familiarity.

For a mathematical model consisting of an infinitely-long, circular grain with a complicated internal perforation, ideally bonded along its outer periphery to a rigid casing, the boundary conditions are that along the outer periphery the displacements must vanish while the periphery of the complicated internal perforation must be traction-free. The latter condition is expressed analytically as follows:

$$\sigma_r n_r + \tau_{r\theta} n_\theta = 0$$
$$\tau_{r\theta} n_r + \sigma_\theta n_\theta = 0 \text{ along } S(r, \theta) = 0 \qquad (20)$$
$$\tau_{rz} n_r + \tau_{\theta z} n_\theta = 0$$

where $S(r, \theta) = 0$ defines the internal perforation and n_r and n_θ denote the components in the radial and circumferential directions of the unit normal drawn outwardly with respect to the domain under consideration. In writing this condition we have taken n_z, the axial component of the unit normal, to vanish since the grain is cylindrical. Our initial considerations concerning this problem should be directed toward developing a method of solution. For this reason we choose to simplify the problem by considering a solid cylindrical bar with its outer periphery having the same shape as the internal perforation of the grain. Thus, the boundary condition applicable to this bar problem is given exactly by

eqn. [20]. Basically, the only difference between the bar problem and the grain problem is that the displacement boundary conditions are absent in the former. Consequently, techniques successfully applied in the bar problem should also be successful for the grain problem.

Additionally, for the sake of simplicity, we concern ourselves only with the axial-shear mode of free vibrations. Thus, we seek solutions in the form

$$\phi = \chi = 0 \tag{21a}$$

$$\psi = \Psi(r, \theta)\, e^{i\omega t} \tag{21b}$$

Accordingly, eqns. [2] reduce to

$$u_r = u_\theta = 0 \tag{22a}$$

$$u_z = -\, e^{i\omega t}\, \nabla_1^2\, \Psi\, (r, \theta) \tag{23b}$$

and eqns. (3) degenerate to the following single Helmholtz equation:

$$\nabla_1^2\, \Psi = -\, \frac{\rho\omega^2}{G}\, \Psi \tag{23}$$

Finally, as a consequence of eqns. (22), the stress-displacement equations given by eqns. (5) become

$$\sigma_r = \sigma_\theta = \sigma_z = \tau_{r\theta} = 0 \tag{24a}$$

$$\tau_{rz} = \rho\omega^2\, \frac{\partial \Psi}{\partial r}\, e^{i\omega t} \tag{24b}$$

$$\tau_{\theta z} = \rho\omega^2\, \frac{1}{r}\, \frac{\partial \Psi}{\partial \theta}\, e^{i\omega t} \tag{24c}$$

Now, it can be shown* that the outward unit normal to S in the plane of S is given by

$$\mathbf{n} = \mathbf{i} n_r + \mathbf{j} n_\theta = \frac{\nabla S}{|\nabla S|}$$

where

$$\nabla S = \mathbf{i}\, \frac{\partial S}{\partial r} + \mathbf{j}\, \frac{1}{r}\, \frac{\partial S}{\partial \theta}$$

It follows that

$$n_r = \frac{\partial S}{\partial r}\, |\nabla S|^{-1} \tag{25a}$$

$$n_\theta = \frac{1}{r}\, \frac{\partial S}{\partial \theta}\, |\nabla S|^{-1} \tag{25b}$$

$$|\nabla S| = \left[\left(\frac{\partial S}{\partial r} \right)^2 + \left(\frac{1}{r}\, \frac{\partial S}{\partial \theta} \right)^2 \right]^{1/2} \tag{25c}$$

---

* See, for example, Wylie [34].

In view of eqns. (24) and (25) the boundary conditions given by eqns. (20) reduce to the following single condition:

$$\left[\frac{\partial \Psi}{\partial r}\frac{\partial S}{\partial r} + \left(\frac{1}{r}\frac{\partial \Psi}{\partial \theta}\right)\left(\frac{1}{r}\frac{\partial S}{\partial \theta}\right)\right]\Bigg|_S = 0 \tag{26}$$

Thus, the problem has been reduced to one of finding a solution of eqn. (23) such that the boundary condition given by eqn. (26) will be identically satisfied.

Closed-form solution of the problem posed above is not feasible so we shall be content with approximate solutions.

In Ref. [35] the collocation method is applied to solve the problem for a star-shaped boundary (with four star tips) given by

$$S(r, \theta) = r - a - b\cos 4\theta = 0 \tag{27}$$

We readily recognize the similarity of this family of plane curves to the boundary curve of the internal perforation of many common solid propellant rocket motors. Another advantage of this family is the fact that the circle is one curve of the family. Consequently, solutions can be degenerated to those for circular boundaries. Since the latter are available, we have a ready means for checking the results. The collocation method used consisted in taking a solution in the form of a finite sequence of solutions of eqn. (23) and satisfying the boundary condition given by eqn. (26) at a finite number of points on the boundary. Little is known concerning convergence of the collocation method applied to eigenvalue problems such as the present case. It is generally presumed that, provided a sufficient number of collocation points are used, the resulting eigenvalues will be reasonably accurate. Even less is known concerning the manner of distributing the collocation points along the boundary although it is generally presumed that the distribution becomes less important as the number of collocation points increases. In this study the first four natural frequency coefficients were calculated and plotted in function of the parameter b/a which governs the length of the star tips. When $b/a = 0$, the bar is circular and as b/a increases the star tip grows longer. The study concludes that, for the problem under consideration, the collocation method is very sensitive to the distribution of collocation points. Furthermore, little convergence is demonstrated for as many as seven collocation points taken within an octant of the boundary. In view of the fact that it is not possible to obtain exact, closed-form solutions in problems of this type, procedures for obtaining upper and lower bounds on the branches of the frequency equation are sorely needed. Only then can we be expected to make definitive statements concerning error in approximate procedures. Such bounding techniques frequently begin with estimates of the eigenvalues. Perhaps the value of collocation method lies in its ability to provide these estimates fairly easily and quickly.

Jain [36] has introduced a new kind of collocation procedure which eliminates some of the difficulties of the boundary collocation method referred to above. He refers to the method as *extremal point collocation*. He has applied the new

method with striking success to the solution of several boundary value problems. The method requires the initial selection of a finite number of collocation points. This selection is arbitrary as in boundary collocation. Instead of requiring that the error in satisfaction of the boundary conditions vanish at the collocation points, as in boundary collocation, in extremal point collocation it is required that the error at adjacent collocation points be equal in magnitude but opposite in sign. Furthermore, the error at the collocation points must be larger than that at any other boundary point. It is from the latter condition that the method derives its name. In order to satisfy these collocation conditions, an iterative procedure is required by means of which the distribution of collocation points is determined. Extremal point collocation has two distinct advantages. Selection of the collocation points is not arbitrary, instead it is determined by the method. In ordinary collocation there is no control over the maximum error or the distribution of error. In extremal point collocation the error can nowhere exceed that at the collocation points and the error is uniformly distributed over the entire boundary.

In Ref. [37] the problem defined by eqns. (23), (26) and (27) was solved using extremal point collocation. In this study it is shown that the method is an effective technique for the calculation of eigenvalues. It is relatively simple to use provided that a large-scale computer is available. The method converges rapidly and yields reasonably accurate results even for a small number of collocation points. The question of accuracy requires further study by means of a method wherein the eigenvalues can be bounded.

Let us return to the boundary conditions given by eqns. (20) for further consideration. If we substitute into eqns. (20) from eqns. (24), we obtain

$$\left(\frac{\partial \Psi}{\partial r} n_r + \frac{1}{r} \frac{\partial \Psi}{\partial \theta} n_\theta \right) \Bigg|_S = 0$$

The quantity on the left is the normal derivative which defines the rate of change of ψ in the direction of the normal to S. Thus, the boundary condition that requires that the lateral surface of the bar be traction-free can also be written in the following form:

$$\frac{\partial \Psi}{\partial n} \Bigg|_S = 0 \tag{28}$$

This form suggests that there may be some advantage in conformally mapping the bar cross-section onto a unit circle. If the conformal transformation is defined by

$$w = w(\xi)$$

where $w = re^{i\theta}$ defines the real plane while $\xi = Re^{i\mu}$ defines the complex plane, the boundary condition given by eqn. (28) becomes

$$\frac{\partial \Psi}{\partial R} \Bigg|_{R=1} = 0 \tag{29}$$

To be sure, satisfaction of this boundary condition is a trivial task compared to satisfaction of the boundary condition given by eqn. (28). However, we should hasten to point out that, by conformal transformation, we have simplified the task of satisfying the boundary conditions but we have complicated the task of finding solutions of the differential equation of motion since it, too, must be transformed. It can be shown* that the plane, Laplacian operator transforms according to

$$\frac{\partial^2 \Psi}{\partial r^2} + \frac{1}{r}\frac{\partial \Psi}{\partial r} + \frac{1}{r^2}\frac{\partial^2 \Psi}{\partial \theta^2} = \left|\frac{d\xi}{dw}\right|^{-2} \left(\frac{\partial^2 \Psi}{\partial R^2} + \frac{1}{R}\frac{\partial \Psi}{\partial R} + \frac{1}{R^2}\frac{\partial^2 \Psi}{\partial \mu^2}\right) \qquad (30)$$

and it follows, therefore, that, under the conformal transformation, eqn. (23) becomes

$$\frac{\partial^2 \Psi}{\partial R^2} + \frac{1}{R}\frac{\partial \Psi}{\partial R} + \frac{1}{R^2}\frac{\partial^2 \Psi}{\partial \mu^2} = -\frac{\rho\omega^2}{G}\left|\frac{d\xi}{dw}\right|^2 \Psi \qquad (31)$$

It is immediately clear that we will probably have difficulties finding solutions of this differential equation. Nevertheless, this formulation of the problem proves advantageous in certain circumstances. For example, common approximate methods of solution of problems of this type such as Rayleigh's principle or the Ritz method require trial functions that satisfy the boundary conditions. In the transform plane such trial functions can be formulated with little difficulty.

In Ref. [38] conformal transformation is used as outlined above in the solution of the problem of axial-shear vibrations of a star-shaped bar with a cross-section in the form of a four-lobed epitrochoid. The epitrochoidal boundary was chosen since its conformal mapping onto the unit circle is relatively simple and since it possesses the general characteristics of the solid propellant rocket grain perforation. To solve the problem in the complex plane the collocation method is applied wherein the boundary condition is identically satisfied and the error in satisfaction of the differential equation is collocated at a finite number of points in the interior of the unit circle. The results were considered favorable though some difficulty was encountered with regard to the spatial distribution of collocation points.

Among the many methods available for the solution of eigenvalue problems the methods of Rayleigh and Ritz are probably the most familiar. These methods yield upper bounds on the eigenvalues but, in the absence of exact values, it is difficult to estimate the error in the approximate solution. Temple [39] suggested a method for estimating the error in each stage of an iteration procedure directed toward the precise determination of the lowest eigenvalue. Temple's method can be interpreted as one which establishes the lower bound. A very powerful method for the determination of upper and lower bounds on all eigenvalues has been developed independently by Kohn [40] and Kato [41], as a generalization of Temple's method. This method was applied in Ref. [42] for

---

* See, for example p. 629 of Wylie [34].

the calculation of the natural frequencies in axial-shear vibrations of circular and epitrochoidal bars. The resulting bounds were extremely accurate for the fundamental natural frequency but the accuracy deteriorated somewhat for the high natural frequencies. However, it should be pointed out that the bounds can be improved at will if one is willing to expend the requisite additional effort.

In an eigenvalue problem it is required to find one or more constants λ, called eigenvalues, and corresponding functions β, called eigenfunctions, such that a differential equation

$$M[\beta] = \lambda N[\beta]$$

is satisfied throughout a domain D subject to certain boundary conditions on the boundary of D. In general, the domain D may be either a one- or a two-dimensional continuum. For many eigenvalue problems $M[\ldots]$ and $N[\ldots]$ are both linear, self-adjoint, positive-definite, differential operators with the order of M greater than N. Under these conditions the eigenvalues are real and positive and the eigenfunctions form an orthogonal set. When the eigenvalue does not appear in the boundary conditions, the eigenvalue problem is called *special* provided that the operator N has the form

$$N[\beta] = g\beta$$

where g is a prescribed continuous function which is positive throughout the domain D. Thus, the governing differential equation for special eigenvalue problems becomes

$$M[\beta] = \lambda g\beta$$

We see immediately that eqns. (23) and (31) have this form and, since the eigenvalue does not appear in the boundary condition, it is clear that the axial shear vibrations problem is a special eigenvalue problem in both the real and complex planes. Therefore, we can make use of the methods that have been developed for special eigenvalue problems. Collatz [43] has developed a procedure for obtaining upper and lower bounds in special eigenvalue problems. Using a trial function which satisfies the boundary conditions, but not necessarily the differential equation, a few simple operations are performed and the upper and lower bounds result. However, these bounds may not be very good unless the trial function is close to the exact solution of the problem. The fact that the method is relatively simple to apply for any given function indicates that it might become much more useful if a systematic procedure were added for "choosing" these trial functions. Such a procedure was developed by Appl and Zorowski [44]. Another such method was developed in Ref. [45] and applied in the solution of the axial-shear vibrations problem for an epitrochoidal bar. The bounds obtained were adequate and subject to additional refinement but the effort involved is probably less than that required to obtain Kohn–Kato bounds.

We have discussed a number of techniques that should prove useful in the solution of the vibrations problem for the rocket motor model consisting of an infinitely-long, circular grain with a complicated internal perforation, ideally

bonded along its outer periphery to a rigid casing. The more effective of these techniques require trial functions that satisfy the boundary conditions. It is clear, therefore, that a key requirement is a technique for conformally transforming the circular domain with a complicated perforation onto a circular annulus. Wilson [46] has developed such a technique but it is limited to the case that the web fraction* is relatively small. For example, Arango [47] has shown that, when the perforation has four axes of symmetry, the error in mapping the external boundary increases rapidly when the web fraction increases beyond 0.5. When the web fraction reaches the value 0.9, the outer boundary has lost all semblance of a circle. This error arises due to the fact that Wilson treated the conformal transformation of an infinite domain with a hole into another such domain. Consequently, while the mapping function accurately transforms the internal boundary into the unit circle, the external boundary transforms only approximately into a circle. Rim and Stafford [48] have very recently presented a simple method of deriving approximate mapping functions in the form of low order polynomials which conformally transforms an annular region into one whose inner and outer boundaries are star-shaped and circular, resp. The derivation is based on the Schwarz–Christoffel transformation. This method has the same accuracy problems in transforming the outer boundary as Wilson's method. This concern with the accuracy of the transformation of the external boundary is of substantial importance since, while the web fraction may be relatively small in the unburned solid propellant grain, it will increase toward unity as a consequence of the burning process. It should be clear, therefore, that it is essential to develop techniques for the conformal transformation of finite, doubly-connected domains.

Laura [49] has developed such a technique based on numerical integration of a pair of dual integral equations derived by Kantorovich and Muratov [50] for the purpose of conformal transformation of an arbitrary, finite, doubly-connected region onto a circular annulus. Laura demonstrates that, if the domain under consideration has one or more axes of symmetry and one of the boundaries is a circle, the system of two integral equations simplifies considerably. Several illustrative transformations are presented including the transformation of a domain which is typical of a solid propellant rocket motor. The accuracy of the technique is exceptional.

For purposes of illustration, let us consider a grain cross-section with 4 axes of symmetry. An octant of this cross-section is shown in Fig. 1 between the heavily-accented inner and outer boundaries. The outer boundary is a circle with a radius of 18 in. while the inner boundary has a maximum radius of 9 in. and a minimum radius of 3 in. The inner and outer boundaries are further identified with the captions $R = 1.0$ and $R = b = 2.61$, resp. A mapping function of the following form was used to conformally transform (approximately but with

---

* Web fraction is defined as the ratio of the diameter of the circle circumscribing the inner boundary of a doubly connected region to the diameter of the circle circumscribing the outer boundary.

more than adequate accuracy) the domain between the inner and outer boundaries in Fig. 1 onto a circular annulus with unit inner radius:

$$w = \sum_{j=0}^{N} A_{1-jp}\,\xi^{1-j}{}_p + \sum_{j=1}^{M} A_{1+jp}\,\xi^{1+j}{}_p \tag{32}$$

wherein p denotes the number of axes of symmetry. In this case we had 4 axes of symmetry and, therefore, we took $p = 4$. A twelve term mapping function was used; i.e. we took $M = 1$ and $N = 10$. A larger number of terms would have
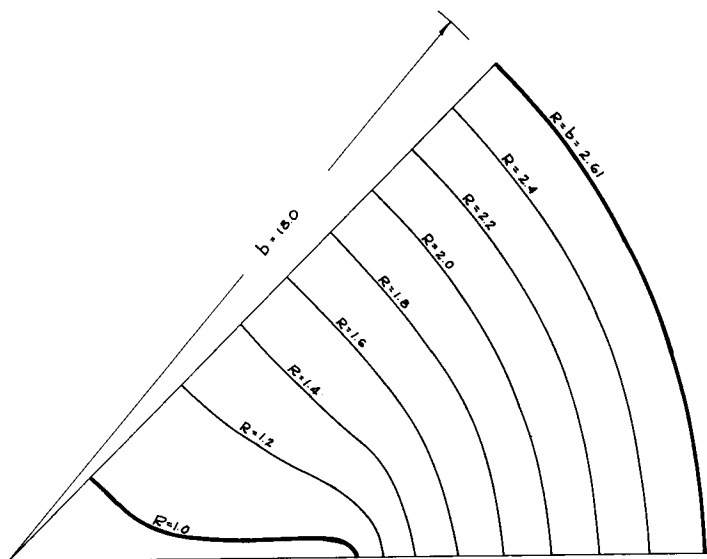
FIG. 1. First approximation to a set of burning curves for a typical solid propellant rocket motor.

resulted in a more accurate mapping. The unknown coefficients, A_{1+jp}, in eqn. (32) were evaluated by Laura's method. Using this mapping function seven additional circles in the complex plane, intermediate between the inner and outer boundaries, were transformed onto the curves shown in Fig. 1. Each of the contours shown is identified by the radius of the circle in the complex plane upon which it maps. Thus, the curve $R = 1.6$ transforms into the circle with radius 1.6, the curve $R = 2.0$ transforms into the circle with radius 2.0, etc. If one were able to stop the burning process in a solid propellant rocket motor at seven instants of time between ignition and burnout and to plot the shape of the inner boundary at each time, the so-called "burning curves" would be obtained. The resulting contours would look much like the curves of Fig. 1. Thus, at a first approximation, we regard the contours of Fig. 1 as a set of burning curves for a typical solid propellant rocket motor. Incidentally, it should be pointed out that, if actual burning curves were given, they could be conformally transformed onto circles in the complex plane with exceptional accuracy using Laura's method.

With the mapping function known it is not a difficult task to calculate the natural frequencies in the axial-shear mode for each of the regions of Fig. 1. The results would provide estimates of how the natural frequencies change during the burning process. There are any number of approximate procedures available for this calculation. We choose to use Galerkin's method. The applicable equation of motion is given by eqn. (31) which we choose to rewrite as follows:

$$\frac{\partial^2 \Psi}{\partial R^2} + \frac{1}{R} \frac{\partial \Psi}{\partial R} + \frac{1}{R^2} \frac{\partial^2 \Psi}{\partial \mu^2} + \lambda^2 g(R, \mu) \Psi = 0 \tag{33a}$$

wherein

$$\lambda^2 = \frac{\rho \omega^2 b^2}{G} \tag{33b}$$

$$g(R, \mu) = \frac{1}{b^2} \left| \frac{d\xi}{dw} \right| \tag{33c}$$

The quantity $g(R, \mu)$ was calculated using eqn. (32). The appropriate boundary conditions are

$$\Psi \bigg|_{R = b} = 0 \tag{34a}$$

$$\frac{\partial \Psi}{\partial R} \bigg|_{R = a} = 0 \tag{34b}$$

The first of these conditions expresses the fact that the displacement at the outer periphery of the grain must vanish since the grain is ideally bonded to a rigid case. The second condition expresses the fact that the inner contour is free of tractions. The quantity a will take on 7 different values corresponding to the 7 different burning curves in Fig. 1. The following trial function, satisfying the boundary conditions, was used:

$$\Psi(R, \mu) \approx \sum_{n=1}^{S} B_n W_n(R) = \sum_{n=1}^{S} B_n \left[\left(\frac{R}{b} \right)^2 - 2 \left(\frac{a}{b} \right) \left(\frac{R}{b} \right) + \left(2\frac{a}{b} - 1 \right) \right]^n \tag{35}$$

We have chosen to ignore the μ-dependency, which we are at liberty to do since we are attempting an approximation. If the μ-dependency had been included, the resulting approximation would have been better than that obtained using eqn. (35). For these calculations we used a one-term trial function; i.e. $S = 1$. Substitution from eqn. (35) into eqn. (33a) results in

$$\epsilon(R, \mu) = \sum_{n=1}^{S} B_n \left[W_n''(R) + \frac{1}{R} W_n'(R) + \lambda^2 g(R, \mu) W_n(R) \right] \tag{36}$$

where $\epsilon(R, \mu)$ is an error function which does not, in general, vanish since, in general, W_n is not an eigenfunction. Galerkin's method requires that the error

function $\epsilon(R, \mu)$ be orthogonal to the trial functions $W_n(R)$ throughout the domain of interest; i.e.

$$\int_D \epsilon(R, \mu) W_n(R) \, dD = 0, \qquad (n = 1, 2, \ldots, S) \qquad (37)$$

Performing the indicated itegration results in S homogeneous, linear, algebraic equations in the S unknown constants B_n. We obtain a frequency equation by requiring that the determinant of the coefficients of the unknowns vanish identically. This frequency equation was solved 7 times for the lowest natural circular frequency coefficient corresponding to the 7 different values of a. The results have been plotted in Fig. 2. The horizontal coordinate in Fig. 2 is the
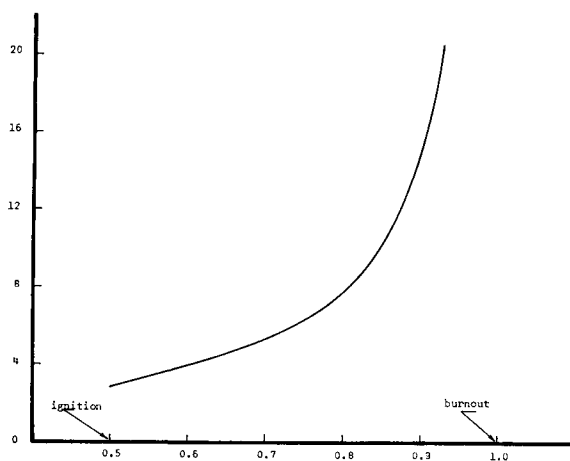
FIG. 2. Variation of the fundamental natural circular frequency coefficient in the axial-shear mode with web fraction for a typical solid propellant rocket motor.

web fraction but, since the web fraction will be a function of time as the burning process proceeds, the plot in Fig. 2 shows the variation of the lowest natural circular frequency coefficient with time throughout the burning process from ignition to burnout. We see that the natural frequency increases rapidly as the motor burns out which is not an unexpected result. Such information is of extreme importance in the design of a guidance loop for the vehicle in which the motor is to be used.

It has been demonstrated that substantial progress has been made concerning the treatment of complicated grain perforations when these passages are substantially two-dimensional. Conformal transformation of the perforation by Laura's method should open the door to the use of a variety of acceptable methods for calculating natural frequencies in various modes of vibration and to the study of various steady-state and forced vibrations problems. Incidentally, it is worth pointing out that Laura's method is equally applicable to the study of problems wherein inertia effects are unimportant such as quasi-static internal

pressurization. Thus far only axial-shear modes of vibration have been considered for grains with complicated perforations. Additional effort is required on transverse modes and in wave propagation studies. When the geometry of the perforation varies rapidly with distance parallel to the motor axis, application of these two-dimensional methods becomes questionable. Little, if any, work is being accomplished on these three-dimensional problems. It would seem that future work in this area will be confined to the application of finite difference techniques.

We come now to the consideration of the ultimate refinement of our model of a solid propellant rocket motor: consideration of a model of finite length. Most of the modern solid propellant rocket motors are short with length-to-diameter ratios of the order of unity not uncommon. Little has been accomplished with the study of such dynamic problems. However, much is being done with quasi-static problems of this nature, particularly using finite difference schemes of various types. The development of understanding of finite length effects and the study of the validity of our two-dimensional results when applied to relatively short motors are probably the most important unsolved problems in solid propellant motor dynamics today. Some little work is being accomplished but there is a noticeable lack of literature on the subject. We should call attention to the experimental study of the vibrations of short, solid elastic cylinders due to McMahon [51]. Extensive experiments were performed and comparisons with available theory presented. However, the available theories were limited to thick disk and Timoshenko beam theories. It should be clear that much future effort should be expended in the area of finite length cylinders.

3. VISCOELASTIC GRAINS

The study of elastic grains has been reasonably active as can be judged from the detail of our discussion thereof. This is as it should be since, because of the elastic-viscoelastic correspondence principle,* solutions of elastic grain problems are intimately related to the solutions of viscoelastic grain problems. This principle states that the Laplace- or Fourier-transformed solution of a viscoelastic problem can be obtained from the Laplace- or Fourier-transformed solution of the associated elastic problem by replacing the elastic constants therein with appropriate functions of the Laplace or Fourier transform parameter. Therefore, in principle, it would seem that one can always obtain the viscoelastic solution associated with a given elastic solution. In practice, the situation is not quite so straightforward since inversion of the viscoelastic solution remains to be accomplished. To be sure, exact inversion is always preferable when possible. In the practical situation this is rarely possible since the quantities replacing the elastic constants are usually measured material property functions of the Laplace or Fourier transform parameter available only in curve or tabular form. It should be clear, therefore, that a considerable

---

* See Alfrey [52], Lee [53] and Sips [54, 55].

effort should be mounted concerning approximate techniques for performing Laplace and Fourier transformations and inversions. In this regard we should mention the methods discussed by Schapery [56] and Cost [57] for the Laplace transform and by Solodovnikov [58] and Papoulis [59] for the Fourier transform. Assuming that approximate inversion methods will be available, our principal concern should be with elastic problems since these could be readily converted to viscoelastic solutions. Clearly, therefore, those difficulties that arise in elastic problems will remain with us in viscoelastic problems; for example, the finite length difficulty is still troublesome. Summarizing, it seems evident that visco-elastic problems present no fundamental difficulties that are not inherent in the associated elastic problems; the computational problem is more complicated and tedious but the basic qualities of the two types of problems remain the same.

Because of the intimate relationship of elastic and viscoelastic problems and because of our rather lengthy discussion of elastic grain problems, we shall not belabor the viscoelastic problem area. However, we will mention a few pertinent investigations and present an illustrative solution, just enough to impart the flavor of the problem.

Gottenberg [60] has reported the results of an experimental investigation of steady-state, transverse vibrations of a long, steel cylindrical tube containing an inert propellant with a circular perforation. Many bending modes were detected and the resonant frequencies and mode shapes compared with the predictions of a Timoshenko beam theory in which the bending stiffness of the propellant was neglected relative to the casing stiffness but the additional mass of the inert propellant was included. The comparisons were quite adequate for engineering purposes. Substantial difficulties were encountered in detecting modes other than bending modes. However, one axisymmetric, longitudinal mode and a few breathing modes were identified. No theory was available for comparison with these modes.

Henry and Freudenthal [61] reported the results of an extensive analytical investigation of the steady–state, forced vibrations of a thick-walled visco-elastic cylinder contained by and bonded to a thin, cylindrical shell. Only axisymmetric solutions were considered. Complex frequency response functions were determined which may be easily used for arbitrary and random inputs by means of the well-established methods of generalized harmonic analysis. The study is broken down into three steps: (1) the thick-walled cylinder, (2) the thin shell, and (3) the composite cylinder. For a thick-walled, elastic cylinder the solutions of eqns. (1)–(5) are developed in the usual manner expanding the normal tractions on the inner boundary and the normal and tangential tractions on the outer boundary in Fourier trigonometric series in the axial coordinate. The boundary conditions on the lateral surfaces are identically satisfied but, rather than requiring the axial normal and shear stresses to vanish over the ends, the axial normal stress and the radial displacement are required to vanish. As a consequence of this relaxation of the boundary conditions, the physical significance of the results has been obscured to a certain extent. The difference between this "finite-length" solution and the infinite-length solution is not clear. In order to obtain the

viscoelastic solution, the elastic-viscoelastic correspondence principle is invoked wherein, for a forced vibrations problem, the elastic constants are replaced by complex material property functions of frequency. Membrane theory is used for the thin elastic casing and a higher-order shell theory is included in an appendix. The latter should be used when the membrane theory is inadequate; for example, for external loads of acoustic nature. The assumption that the propellant and case form a continuous structure at their interface requires continuity of displacements and, therefore, produces strong coupling of the motions of grain and casing. This coupling is considered of primary importance and, therefore, the interaction is treated rigorously. The internal pressure is taken as harmonic and a large volume of numerical results is presented for the fundamental radial mode. It is concluded "that any analysis of a solid fuel rocket motor which does not take into consideration the viscoelastic effects of the propellant would not give a true overall picture". Another important observation is arrived at by varying the grain geometry in simulation of the state of the composite structure at various stages of the burning process. The results indicate that, for certain ranges of frequency, there occurs a considerable increase in the amplitudes of stress and displacements. The implication is that the critical period in rocket operation would occur in the later stages of the burning process when the propellant is almost completely burned out. Thus, the important frequencies might be close to the fundamental radial mode of the casing.

In Ref. [62] the stress response to pressure transients has been investigated in an infinitely-long, two-layered cylinder having a thin, incompressible, elastic outer layer and an inner layer of an incompressible, two-parameter Voigt material. This composite structure was taken as a crude mathematical model of a solid propellant rocket motor. The particular problem of interest concerned the circumferential stress response of the case to the pressure transients induced at ignition in the grain perforation. Two different pressure programs were studied in some detail: a square ignition pulse and a triangular ignition pulse followed by a pressure, constant in time. By solving the elastic problem first and then invoking the correspondence principle to obtain the viscoelastic solution, it was shown that the stress response is rather insensitive to the shape of the pulse. However, it was also demonstrated that the duration of the transient is important. When the duration of the transient is an order of magnitude smaller than the natural period of the cylinder in the radial mode, the stress response barely reflects the presence of the ignition pulse. However, as the duration of the transient approaches the natural period, the circumferential stress approaches the stress level corresponding to the pressure magnitude of the transient. The implication as far as casing and igniter design should be evident. If one is to economize on casing weight but nonetheless maintain rapid and positive ignition, the igniter must be designed such that the pressure transient will persist for a time no larger than one order of magnitude smaller than the natural period of the motor in the radial mode.

Lockett [63] presented the results of a study of significant importance with regard to the analysis of transient responses in viscoelastic materials. He dis-

cussed the effect produced by a rapid, but not discontinuous, change in pressure at the surface of a spherical cavity in an infinite, viscoelastic medium. Invoking the correspondence principle, Lockett obtains the solution to the viscoelastic problem from the Fourier transform of the associated elastic problem by replacing therein the elastic shear and bulk moduli with the viscoelastic complex shear and bulk modulus functions of circular frequency. Thus, he is subsequently concerned with performing inverse transformations. It is the manner of performing these inversions that is significant. Before proceeding to the actual inversion procedure, Lockett discusses the nature of modulus functions that should be used and the character of the pressure-time history. Most solutions to viscoelastic problems appearing in the literature are either left in the integral form or are specialized to some simple spring-dashpot representation for the complex moduli. However, it has been shown by Kolsky and Shi [64] that, in general, these simple models do not adequately represent the behavior of real, viscoelastic materials. Thus, if only the solution to a particular problem is required, it would seem advisable to use the experimental data directly in the numerical inversion of the Fourier-transformed solutions. If it is desired to keep a number of parameters in the solution, then mathematical models should be chosen which fit the experimental data well, even though they may not correspond to a simple spring-dashpot configuration. The simple forms of modulus functions corresponding to spring-dashpot models only have an advantage in the solution of simple problems when it may be possible to evaluate the integrals explicitly. In his subsequent numerical work Lockett takes a constant bulk modulus; i.e. he assumes that the material is elastic in dilatation, and for the complex shear modulus he uses an analytical expression that has been derived from curve fitting to experimental measurements performed on real, viscoelastic materials. For a pressure-time history Lockett selects a time function which has the following complex Fourier transform:

$$\bar{p}(\omega) = \begin{cases} 0, & 0 \le \omega \le \omega_1 \\ \dfrac{p_0}{i\omega}, & \omega_1 \le \omega \le \omega_2 \\ 0, & \omega_2 \le \omega \le \infty \end{cases} \tag{38}$$

wherein the range (ω_1, ω_2) defines the range in which accurate measurements are available of the complex shear modulus. It follows that, since the Fourier transform of the pressure-time history is a factor in the transformed solution, the exact solution in both the elastic and viscoelastic problems is a finite integral over the range (ω_1, ω_2) within which the shear modulus is accurately known. The following pressure-time history is obtained by inversion of the Fourier transform given by eqn. (38):

$$p(t) = \frac{p_0}{\pi} \int_{\omega_1}^{\omega_2} \frac{\sin \omega t}{\omega} \, d\omega = \frac{p_0}{\pi} [\text{Si}(\omega_2 t) - \text{Si}(\omega_1 t)] \tag{39}$$

where $\text{Si}(x)$ denotes the sine integral which has been tabulated by Jahnke and Emde [65] and Abramowitz and Stegun [66], among others. For ω_2 very much

21

larger than ω_1 this pressure program has the shape shown in Fig. 3. Lockett considers this loading in its own right and not as an approximation to an exactly square loading. The latter is not obtainable in practice, so the loading shown in Fig. 3 is more realistic. Obviously, the rise-time of the pressure program can be made shorter by increasing ω_2 up to the upper limit of the frequency range in which the shear modulus is well-defined. The Fourier inversions of the transformed solutions are now performed numerically since integration is over a finite frequency range only. Locket completes the solution and arrives at some interesting conclusions concerning the differences between elastic and visco-elastic solutions.
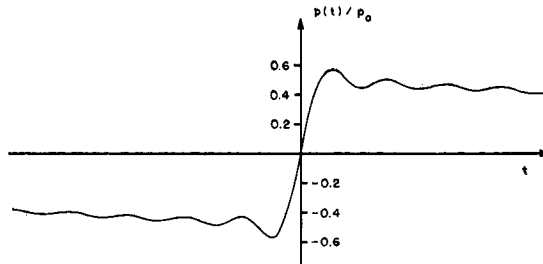
Fig. 3. First version of the alternate pressure program.

Making use of Lockett's suggestions the problem of dynamic internal pressurization was solved in Ref. [67] for an infinitely-long, incompressible, viscoelastic cylinder case-bonded to a thin elastic tank. The pressure–time history of Fig. 3 has some of the character of a pressure–time program of a solid propellant rocket motor but it has two important deficiencies: the applied pressure is negative for time less than zero and the pressure rise starts at negative time. Both of these deficiencies were corrected by appropriate shifting of axes so that eqn. (39) becomes

$$\frac{p(t)}{p_0} = \frac{1}{2} + \frac{1}{\pi}\left[\mathrm{Si}(\omega_2 t - \pi) - \mathrm{Si}\left(\omega_1 t - \pi\frac{\omega_1}{\omega_2}\right)\right] \qquad (40)$$

This expression defines the one-parameter, ω_2/ω_1, family of curves shown in Fig. 4. We see that these curves possess most of the characteristics of actual pressure–time programs for solid propellant rocket motors. We see a finite rise time which is controlled principally by the value of ω_2 and given very closely by

$$t_R = \frac{2\pi}{\omega_2} \qquad (41)$$

The family of curves rises to a maximum and then oscillates about a quasi-static curve whose shape depends upon the value of the ratio ω_2/ω_1. In Ref. [67] a value of 1000 was used for this ratio. For this value the oscillation is about a curve that is approximately parallel to the dimensionless time axis at least for a substantial period of time. Since attention was focused on the immediate dynamic effects of the pressurization, it mattered little that the pressure program decreases

gradually for long times. The Fourier transform of the pressure program is given
by

$$\frac{\bar{p}(\omega)}{p_0} = \pi\delta(\omega) + \frac{e^{-i\pi\omega/\omega_2}}{i\omega} [H(\omega - \omega_1) - H(\omega - \omega_2)] \tag{42}$$

This transform is non-zero over a limited frequency range only so that, ulti-
mately, the inversion integrals can also be evaluated by numerical methods.
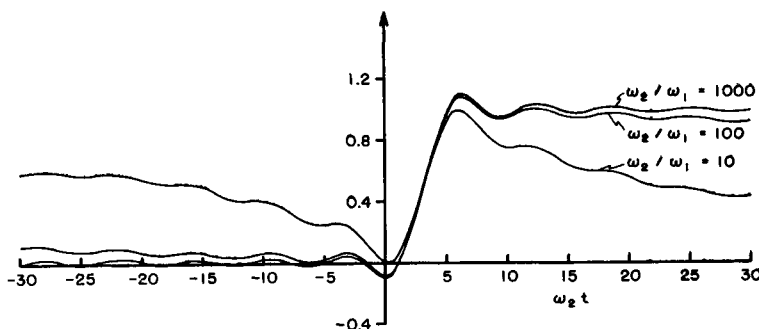
Fig. 4. Pressure-time program applied to the inner cylindrical surface of the core.

The shear storage and loss moduli used in the investigation were the actually
measured data shown in Fig. 5. These material properties were introduced
into the transformed solution by expressing the shear storage modulus in the
following form:

$$G'(\omega) = G_0 + \sum_{n=1}^{N} G_n \frac{\omega^2\tau_n^2}{1 + \omega^2\tau_n^2} \tag{43a}$$

wherein $G_0, G_1, G_2, \ldots, G_N, \tau_1, \tau_2, \ldots, \tau_N$ and N are arbitrary constants which
must be evaluated such that eqn. (43a) will yield a good approximation to the
shear storage modulus shown in Fig. 5(a) in the frequency range of interest.
Equation (43a) is the analytical representation for the shear storage modulus for
the $(2N + 1)$-parameter Maxwell material. Thus, use of this expression implies
that we have idealized the solid propellant as a linearly-viscoelastic, $(2N + 1)$-
parameter Maxwell material. It is clear in eqn. (43a) that G_0 constitutes the
shear storage modulus at zero frequency and, on the basis of extrapolation of the
data of Fig. 3(a), the value selected was

$$G_0 = 400 \text{ psi}$$

The remaining parameters in eqn. (43a) were evaluated by means of a method
introduced by Schapery [68] wherein the τ_n's were arbitrarily assigned and the
G_n's evaluated by solving a system of N linear algebraic equations obtained by
the collocation method. Five collocation points were used and the resulting
analytical expression agreed with the curve of Fig. 5(a) to within the width of a
pencil line. The analytical expression for the shear loss modulus for the

$(2N + 1)$-parameter Maxwell material, which is also required, is given by

$$G''(\omega) = \sum_{n=1}^{N} G_n \frac{\omega \tau_n}{1 + \omega^2 \tau_n^2} \tag{43b}$$

It is clear, therefore, that the shear storage and loss moduli are not independent since the unknown parameters were evaluated from shear storage modulus data
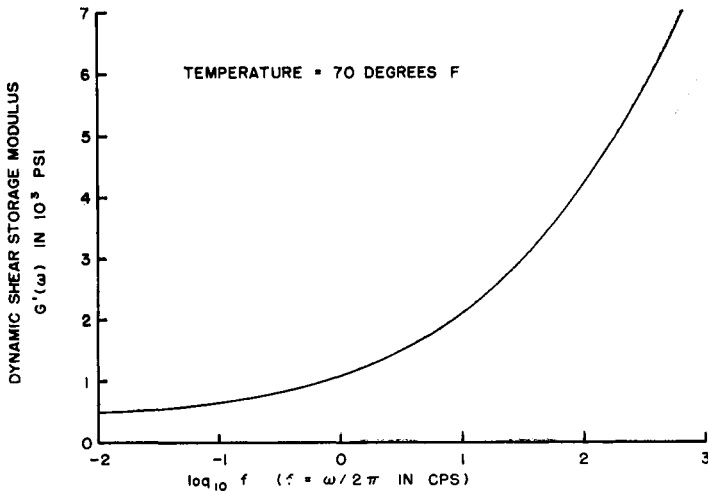
FIG. 5a. Dynamic shear storage modulus as a function of frequency for Hercules Powder Co. CYH solid propellant.
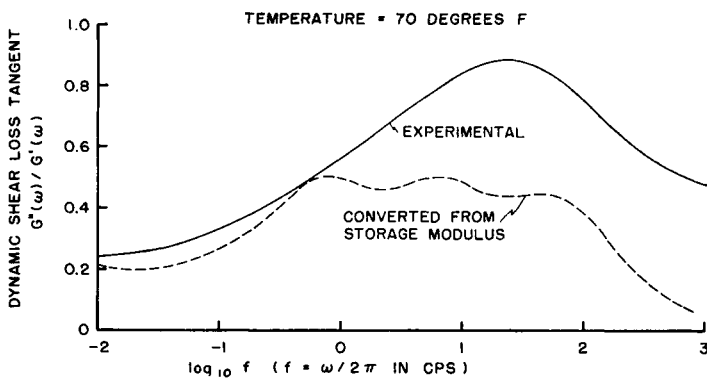
FIG. 5b. Dynamic shear loss tangent as a function of frequency for Hercules Powder Co. CYH solid propellant.

and these same parameters allow immediate calculation of the shear loss modulus by means of eqn. (43b). This result is not surprising and was recognized by Gross [69] when he calculated the following exact interrelation between these two material property functions:

$$G''(\omega) = \frac{2}{\pi} \int_0^\infty G'(a) \frac{\omega}{a^2 - \omega^2} \, da \tag{44}$$

As an interesting experiment, the parameters calculated by means of Schapery's method using eqn. (43a) and the shear storage modulus data of Fig. 5(a) were used in eqn. (43b) to calculate the shear loss modulus. The results are plotted as a dotted curve in Fig. 5(b). We observe a very substantial disagreement between this result and the measured experimental data. This discrepancy has not been explained. Rather than using the experimental data of Fig. 5(b), eqn. (43b) was used for the shear loss modulus.

Making use of the transformed pressure program given by eqn. (42) and the material property functions shown in eqns. (43) the transformed stresses and displacements in the two-layered cylinder were calculated. The inversion integrals were evaluated numerically with relative ease since they were integrals over a finite frequency range only. The results for the circumferential stress at the internal perforation are shown in Fig. 6. These results display some interesting features to which we should draw attention. First, we draw attention to the small perturbations displayed by all solutions for time less than zero and for time greater than zero although, in the latter time regime, they may be obscured by larger oscillations. These perturbations of the calculated responses are clearly due to the small perturbations present in the pressurization program. These small oscillations can be ignored since our interest concerns the gross responses due to the gross pressure increase. Next, quasi-static solutions corresponding to all transient solutions were obtained (and plotted in Fig. 6) by taking the specific weights of both case and grain equal to zero. Now, we observe that, for the larger perforation (7.0 in.) the circumferential stress at the internal perforation is compressive despite the fact that the accompanying circumferential strains are tensile. (See Fig. 6(a).) This same effect was noted in Ref. [70] and was explained therein. We summarize the explanation here for purposes of completeness. The circumferential stress may be thought of as consisting of two components: a hydrostatic compressive component due to the compression of the core against the restraint offered by the case and a tensile component due to radial growth of the core under pressurization. If the core is sufficiently thin, such that the case restraint is important, then the compressive component is larger than the tensile component and the resulting circumferential stress is compressive even though the circumferential strain is tensile. This is undoubtedly the situation when $a = 7.0$ in. It is clear that, with the appropriate combination of material properties and geometry, the opposite could also be true. As a matter of fact, we see from Fig. 6(b) that, for $a = 1.3$ in. and for both rise times, the circumferential stress at the internal perforation and the accompanying circumferential strain are both tensile. It seems obvious in this situation that case restraint plays the subordinate role.

Now, we observe that for the 40 msec rise time the transient and quasi-static solutions coincided, for all practical purposes, for all times and in all cases considered. It seems clear that the 40 msec rise time is long compared to the fundamental natural period of the cylinder and, under these conditions, the transient and quasi-static formulations of the problem are equally valid thus accounting for the good agreement. However, for the shorter rise time we
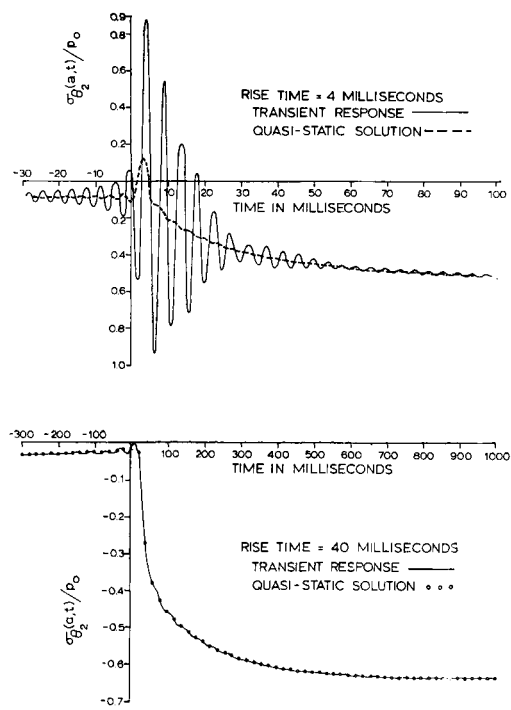
FIG. 6a. Dimensionless circumferential stress response at internal perforation $(r = a)$:
$a = 7.0$ in.
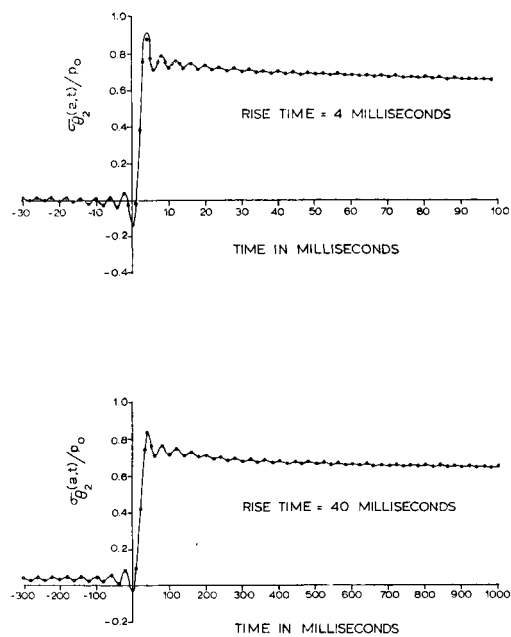
FIG. 6b. Dimensionless circumferential stress response at internal perforation $(r = a)$:
$a = 1.3$ in.

observe a substantial transient at small times and for the larger perforation. (See Fig. 6(a).) We also observe that the transient does not occur for the shorter rise time and for the smaller perforation. There appear to be two possible explanations of this behavior. For the larger perforation we have shown that the elastic casing plays a major role. The presence of this elastic storage element could account for initiation of the transient oscillation and for sustaining it thereafter. For the smaller perforation we have already demonstrated that the case plays a subordinate role and since there is a lack of the elastic storage element, the transient oscillation, if initiated at all, would attenuate very rapidly as a consequence of the dissipative quality of the core material which plays the major role. There is another possible explanation. In Fig. 6(a) for the smaller rise time we see that the period of the transient oscillation, which is, of course, the fundamental natural period of the composite cylinder, has a value of about 4 or 5 msec. Thus, since the rise time very nearly coincides with the natural period of the cylinder, we expect to excite a substantial oscillation which will rapidly attenuate. For the smaller perforation, the natural period changes and the rise time no longer coincides and we do not expect to see a large transient oscillation. It is difficult, without extensive study, to choose between these explanations although we do favor the latter. There are, undoubtedly other features of these results that bear further discussion but we feel that we have drawn attention to the salient features.

Achenbach [71,72] has recently completed two investigations of general import. The first of these concerns the transient, dynamic response of an incompressible, elastic grain with an ablating circular port case-bonded to a thin, elastic case. Despite the fact that this study concerns an elastic grain, it is discussed here because of its close relationship with the second study. An internal pressure program in the form of a step function in time is applied and an approximate solution obtained by asymptotic integration of the equation of motion. It is demonstrated that burning time affects the period of the vibratory response but not the amplitude thereof. In the second investigation, Ref. [72], the dynamic response is calculated in an infinitely -long, composite cylinder consisting of a thick-walled cylinder of an incompressible, viscoelastic material case-bonded to a thin elastic shell. Two dynamic loadings are treated: a time step in internal pressure and a time step in external pressure. The latter loading condition is applied to an inoperative motor in a missile launching silo. The problem is solved, numerical results plotted and discussed for a grain of a standard, linear solid (three-parameter Maxwell material). The manner of solution is discussed when measured data are used for the grain shear modulus.

We can judge by the character of these last few references that a great deal has been accomplished concerning transient, dynamic responses in viscoelastic grains. However, additional effort is required to perfect and simplify the application of the approximate methods for performing Fourier transforms and inversions. Then we can look forward to solving many transient dynamic problems using as input measured pressure programs and material property functions.

A great deal has been achieved in the solution of general wave propagation problems in linear viscoelasticity. See, for example, Ref. [8], [73]–[91]. This list of references is by no means complete nor is it a listing of the more important papers. Despite the fact that so much effort has been expended in investigating this general problem, thereby testifying to its importance, I was unable to locate a single reference involving a solution of direct applicability to solid propellant rocket motors. It seems evident therefore, that a considerable effort is required to elucidate those environments that give rise to wave propagation problems and in solving the problems posed.

4. CONCLUSION

We have completed a survey of dynamic problems in solid propellant rocket motors. Attention was restricted to linear analysis of elastic and viscoelastic grains. It was not intended that this survey should be a bibliographical study but rather a presentation of progress in the field in an attempt to establish the current state-of-the-art. Many important related areas have been omitted in the interests of conservation of time and space. Consider, for example, nonlinear dynamic problems, shock problems, coupled thermo-mechanical problems, acoustic instability problems, and experimental measurement of propellant properties. Effort should be continued and expanded in these important areas among others. We have accomplished a great deal with regard to the dynamic problems of solid propellant rocket motors; however, additional effort is absolutely essential to extend the goals that we have already reached.

REFERENCES

[1] POCHAMMER, L., "Ueber Fortpflanzunggeschwindigkeiten kleiner Schwingungen in einem unbegrenzten isotropen Kreiszylinder", *J. f. reine u. angew. Math. Crelle*, **81**, 324–336 (1876).
[2] CHREE, C., "The equations of an isotropic elastic solid in polar and cylindrical coordinates, their solution and application", *Trans. Cambridge Phil. Soc.* **14**, 250 (1889).
[3] ABRAMSON, H. N., PLASS, H. J. and RIPPERGER, E. A., "Stress wave propagation in rods and beams", *Advances in Applied Mechanics*, Edited by H. L. Dryden and Th. von Karman, Academic Press, New York City (1958), **5**, 111–194.

[4] GHOSH, J., "Longitudinal vibrations of a hollow cylinder", *Bull. Calcutta Math. Soc.*, **14**, 31 (1923).

[5] BANCROFT, D., "The velocity of longitudinal waves in cylindrical bars", *Phys. Rev.* **59**, 588 (1941).

[6] HUDSON, G. E., "Dispersion of elastic waves in solid circular cylinders", *Phys. Rev.*, **63**, 46 (1943).

[7] DAVIES, R. M., "A critical study of the Hopkinson pressure bar", *Phil. Trans. Roy. Soc.* (*London*), Series A, **240**, 375 (1948).

[8] KOLSKY, H., *Stress Waves in Solids*, Oxford University Press, London (1953).

[9] ABRAMSON, H. N., "Flexural waves in elastic beams of circular cross section", *J. Acoust. Soc. Amer.*, **29**, 42 (1957).

[10] MCFADDEN, J. A., "Radial vibrations of thick-walled hollow cylinders", *J. Acoust. Soc. Amer.*, **26**, 714 (1954).

[11] GAZIS, D. C., "Exact analysis of the plane strain vibrations of thick-walled hollow cylinders", *J. Acoust. Soc. Amer.*, **30**, 786 (1958).

[12] GAZIS, D. C., "Three-dimensional investigation of the propagation of waves in hollow circular cylinders", *J. Acoust. Soc. Amer.*, **31**, 568 (1959).

[13] HERRMANN, G. and MIRSKY, I., "Three-dimensional and shell theory analysis of axially symmetric motions of cylinders", *J. Appl. Mech.*, **23**, 563 (1956).

[14] MIRSKY, I. and HERRMANN, G., "Nonaxially symmetric motions of cylindrical shells", *J. Acoust. Soc. Amer.*, **29**, 1116 (1957).

[15] MIRSKY, I. and HERRMANN, G., "Axially symmetric motions of thick cylindrical shells", *J. Appl. Mech.*, **25**, 97 (1958).

[16] GREENSPON, J. E., "Flexural vibrations of a thick-walled circular cylinder", *Proc. Third U.S. Nat'l. Cong. Appl. Mech.* Amer. Soc. Mech. Engrs., New York City (1958) p. 163.

[17] GREENSPON, J. E., "Vibrations of thick cylindrical shells", *J. Acoust. Soc. Amer.*, **31**, 1682 (1959).

[18] GREENSPON, J. E., "Flexural vibrations of a thick-walled circular cylinder according to the exact theory of elasticity", *J. Aero-Space Sci.*, **27**, 37 (1960).

[19] BIRD, J. F., HART, R. W. and MCCLURE, F. T., "Vibrations of thick-walled hollow cylinders: exact numerical solutions", *J. Acoust. Soc. Amer.*, **32**, 1404 (1960).

[20] BIRD, J. F., "Vibrations of thick-walled hollow cylinders: approximate theory", *J. Acoust. Soc. Amer.*, **32**, 1413 (1960).

[21] BALTRUKONIS, J. H. and GOTTENBERG, W. G., "Thickness-shear vibrations of circular bars", *J. Acoust. Soc. Amer.*, **31**, 734 (1959).

[22] BALTRUKONIS, J. H., "Free transverse vibrations of a solid elastic mass in an infinitely-long, rigid, circular-cylindrical tank", *J. Appl. Mech.*, **27**, 663 (1960).

[23] BALTRUKONIS, J. H. and GOTTENBERG, W. G., "Transverse wave propagation in a solid, elastic mass contained by an infinitely-long, rigid circular-cylindrical tank", *Proc. Fourth Midwestern Conf. on Solid Mechanics*, Univ. of Texas, Austin, Texas (1959) p. 396.

[24] BALTRUKONIS, J. H., "Forced transverse vibrations of a solid elastic core case-bonded to an infinitely-long, rigid, cylinder", The Catholic University of America, Tech. Rep. No. 1 to NASA under Research Grant No. NsG–125–61 (August 1961).

[25] MAGRAB, E. B., "A number of observations from the forced vibrations of a solid elastic cylinder case-bonded to a rigid tank", Hercules Powder Co., Magna, Utah, Tech. Rep. No. MTO–269–38 to Headquarters, Air Force Systems Command, USAF, Los Angeles, Calif., under Cont. No. AF 04(647)–243 (19 April 1963).

[26] MAGRAB, E. B., "Effect of Poisson's ratio on the displacement fields of a vibrating solid elastic cylinder", Hercules Powder Co., Magna, Utah, Tech. Rep. No. MTO–269–45 to Headquarters, Air Forces Systems Command, USAF, Los Angeles, Calif. under Cont. No. AF 04(647)–243 (8 July 1963).

[27] MAGRAB, E. B., "Stress distributions in a vibrating solid elastic cylinder case-bonded to a rigid tank", Hercules Powder Co., Magna, Utah, Tech. Rep. No. MTO–269–46 to Headquarters, Air Force Systems Command, USAF, Los Angeles, Calif. under Cont. No. AF 04(647)–243 (19 July 1963).

[28] BALTRUKONIS, J. H., GOTTENBERG, W. G. and SCHREINER, R. N., "Dynamics of a hollow, elastic cylinder contained by an infinitely-long, rigid, circular-cylindrical tank", *J. Acoust. Soc. Amer.*, **32**, 1539 (1960).

[29] BALTRUKONIS, J. H., GOTTENBERG, W. G. and SCHREINER, R. N., "Transverse wave propagation in a hollow, incompressible, elastic mass contained by an infinitely-long, rigid, circular-cylindrical tank", Space Technology Laboratories, Inc., Los Angeles, Calif., Tech. Rep. No. EM–9–23/TR–59–0000–00865 (28 October 1959).

[30] BALTRUKONIS, J. H., "Free transverse vibrations of an incompressible elastic mass contained by an infinitely-long rigid, circular-cylindrical tank", Space Technology Laboratories, Inc., Los Angeles, Calif., Tech. Rep. No. EM 9–24/TN–59–0000–00329 (29 October 1959).

[31] BALTRUKONIS, J. H., GOTTENBERG, W. G. and SCHREINER, R. N., "Axial-shear vibrations of an infinitely-long composite circular cylinder", *J. Acoust. Soc. Amer.* **33**, 1447 (1961).

[32] BALTRUKONIS, J. H., CHI, M. and GOTTENBERG, W. G., "Free transverse vibrations in an infinitely-long, layered elastic cylinder", The Catholic University of America, Washington, D.C., Tech. Rep. No. 3 to NASA under Res. Grant No. NsG–125–61 (August 1962).

[33] SANN, R. I. and SHAFFER, B. W., "Free transverse elastic vibrations of a solid cylinder bonded to a thin casing", New York University.

[34] WYLIE, C. R., Jr., *Advanced Engineering Mathematics*, McGraw-Hill, New York (1960), 2nd Ed., pp. 480 ff.

[35] BALTRUKONIS, J. H., "Axial shear vibrations of star-shaped bars by the collocation method" The Catholic University of America, Washington, D.C., Tech. Rep. No. 4 to the Hercules Powder Co., Magna, Utah under Research Sub-cont. No. 69, AF 04(647)–243 (May 1963).

[36] JAIN, M. K., "On collocation method for physical problems", *Proc. 6th Congr. Theor. and Appl. Mech. and Symposium on High Speed Computation Methods and Machines*, Delhi, India, Dec. 23–26, 1960.

[37] BALTRUKONIS, J. H., "Axial shear vibrations of star-shaped bars by extremal-point collocation", The Catholic University of America, Washington, D.C., Tech. Rep. No. 3 to the Hercules Powder Co., Magna, Utah under Res. Sub-cont. No. 177, AF04 (647)–243 (March 1964).

[38] BALTRUKONIS, J. H., CASEY, K. B., CHI, M. and LAURA, P. A., "Axial-shear vibrations of star-shaped bars—an application of conformal transformation", The Catholic University of America, Washington, D.C., Tech. Rep. No. 4 to NASA under Res. Grant No. NsG–125–61 (October 1962).

[39] TEMPLE, G., "The computation of characteristic numbers and characteristic functions", *Proc. London Math. Soc.*, **29**, 257 (1928); "The theory of Rayleigh's principle as applied to continuous systems", *Proc. Roy. Soc.*, **69**, 276 (1928).

[40] KOHN, W., "A note on Weinstein's variational method", *Phys. Rev.*, **71**, 902 (1947).

[41] KATO, T., "On upper and lower bounds of eigenvalues", *J. Phys. Soc.*, (*Japan*), **4**, 334 (1949).

[42] BALTRUKONIS, J. H., CHI, M. and LAURA, P., "Axial shear vibrations of star-shaped bars—Kohn-Kato bounds", The Catholic University of America, Washington, D.C., Tech. Rep. No. 1 to the Hercules Powder Co., Magna, Utah under Res. Sub-cont. No. 69, AF 04(647)–243 (October 1962).

[43] COLLATZ, L., *Eigenwertaufgaben mit technischen Anwendung*, Akademische Verlagsgesellschaft M. G. H., Leipzig (1949) p. 126.

[44] APPL, F. C. and ZOROWSKI, C. F., "Upper and lower bounds for special eigenvalues", *J. Appl. Mech.*, **26**, 246 (1959).

[45] BALTRUKONIS, J. H. and CHI, M., "Collatz bounds and the collocation method", The Catholic University of America, Washington, D.C., Tech. Rep. No. 6 to NASA under Res. Grant No. NsG–125–61 (July 1964).

[46] WILSON, H. B., Jr., "Conformal transformation of a solid propellant grain with a star-shaped internal perforation onto an annulus", *ARS J.*, **30**, 780 (1960).

[47] ARANGO, R., "A simple method of conformal transformation of a solid propellant rocket motor cross-section", M.S.E. Dissertation, Mechanics Div., The Catholic University of America, Washington, D.C. (1964).

[48] RIM, K. and STAFFORD, R. O., "Derivation of mapping functions for star-shaped regions", NASA Contractor Rep. No. NASA CR–192 (March 1965).

[49] LAURA, P. A., "Conformal mapping of a class of doubly connected regions", The Catholic University of America, Washington, D.C., Tech. Rep. No. 8 to NASA under Res. Grant. No. NsG–125–61 (March 1965).

[50] KANTOROVITCH, L. V. and MURATOV, V., "Conformal mapping of simply and multiply connected regions", (In Russian), *Works of the Scientific Research Institute of Mathematics and Mechanics*, Leningrad State University, Leningrad (1937).

[51] McMahon, G. W., "An experimental study of the vibrations of solid, isotropic elastic cylinders", Naval Research Establishment, Dartmouth, N.S., Canada, Rep. No. 63/4 (March 1963).

[52] Alfrey, T., Jr., "Non-homogeneous stresses in viscoelastic media", *Q. Appl. Math.*, **2**, 113 (1944).

[53] Lee, E. H., "Stress analysis in viscoelastic bodies", *Q. Appl. Math.*, **13**, 183 (1955).

[54] Sips, R., "Propagation phenomena in elastic-viscous media", *J. Polymer Sci.*, **6**, 285 (1951).

[55] Sips, R., "General theory of deformation of viscoelastic substances", *J. Polymer Sci.*, **7**, 191 (1952).

[56] Schapery, R. A., "Approximate methods of transform inversion for viscoelastic stress analysis", *Proc. Fourth U.S. Nat'l. Congr. Appl. Mech.*, Amer. Soc. Mech. Engrs., New York City (1962), 1075.

[57] Cost, T. L., "Approximate Laplace transform inversions in viscoelastic stress analysis", *AIAA Solid Propellant Rocket Conference*, Palo Alto, Calif., January 29–31, 1964, Preprint No. 64–132.

[58] Solodovnikov, V. V., *Introduction to the statistical dynamics of automatic control systems*, Dover Publications, New York (1960) (Original Russian edition was published in 1952) p. 31 ff.

[59] Papoulis, A., *The Fourier Integral and Its Applications*, McGraw-Hill, New York (1962) pp. 53 ff.

[60] Gottenberg, W. G., "Semiannual Report on Vibration Characteristics of Solid Propellant Rocket Engines—1 January 1959 to 30 June 1959" Space Technology Laboratories, Inc., Los Angeles, Calif., Tech. Rep. No. TR–59–0000–00716, Prepared for the Air Force Ballistic Missile Division under Cont. No. 04(647)–309.

"Semiannual Report on Vibration Characteristics of Solid Propellant Rocket Motors—1 July through 31 December 1959", Space Technology Laboratories, Inc., Los Angeles, Calif., Tech. Rep. No. TR–59–0000–09951 Prepared for the Air Force Ballistic Missile Division under Cont. No. AF 04(647)–309.

"Experimental study of the vibrations of a circular cylindrical shell", *J. Acoust. Soc. Amer.*, **32**, 1002 (1960).

[61] Henry, L. A. and Freudenthal, A. M., "Forced vibrations of a viscoelastic cylinder case-bonded to a thin elastic shell", Columbia University, New York City, Tech. Rep. No. 22 to the Office of Naval Research under Cont. No. Nonr 266(78) (January 1964).

[62] Baltrukonis, J. H., "Stress response at ignition of a long, case-bonded, solid propellant rocket motor", The Catholic University of America, Washington, D.C., Tech. Rep. No. 2 to the Hercules Powder Co., Magna, Utah under Res. Sub-cont. No. 69, AF 04(647)–243 (October 1962).

[63] Lockett, F. J., "Interpretation of mathematical solutions in viscoelasticity theory illustrated by a dynamic spherical cavity problem", *J. Mech. Phys. Solids*, **9**, 215 (1961).

[64] Kolsky, H. and Shi, Y. Y., "The validity of model representation for linear viscoelastic behavior", Brown Univ., Providence, R.I., Tech. Rep. No. 5 to the Office of Naval Research under Cont. No. Nonr 562(14) (January 1958).

[65] Jahnke, E. and Emde, F., *Tables of Functions with Formulae and Curves*, Dover Publications, New York (1945) pp. 1 ff.

[66] Abramowitz, M. and Stegun, I. A. (Editors) *Handbook of Mathematical Functions with Formulas, Graphs and Mathematical Tables* U.S. Government Printing Office, Washington, D.C. 20402 (1964) p. 228 ff.

[67] Baltrukonis, J. H. and Magrab, E. B., "Dynamic internal pressurization of an infinitely-long, thick-walled, linearly-viscoelastic cylinder case-bonded to a thin elastic tank", The Catholic University of America, Washington, D.C., Tech. Rep. No. 2 to the Hercules Powder Co., Magna, Utah under Res. Sub-cont. No. 177, AF 04(647)–243 (February 1964).

[68] Schapery, R. A., "A simple collocation method for fitting viscoelastic models to experimental data", California Institute of Technology, Pasadena, Calif., Tech. Rep. No. GALCIT SM 61–23A (November 1961).

[69] Gross, B., *Mathematical Structure of the Theories of Viscoelasticity*, Hermann et Cie., Paris (1953) p. 26.

[70] Baltrukonis, J. H. and Magrab, E. B., "Linear transient analysis of the stage III Minuteman motor considering the propellant as an incompressible two-parameter Voigt material", Hercules Powder Co., Magna, Utah, Tech. Rep. to the Air Force Ballistic Missile Division under Cont. No. AF 04(647)–243, Task 9 Minuteman Support Program.

[71] ACHENBACH, J. D., "The dynamic response of an encased elastic cylinder with ablating inner surface", to be published as a Technical Note in *AIAA Journal*.

[72] ACHENBACH, J. D., "The dynamic response of a long case-bonded viscoelastic cylinder", accepted for publication as a paper in *AIAA Journal*.

[73] O'NEIL. H. T., "Reflection and refraction of plane shear waves in viscoelastic media", *Phys. Rev.*, **75**, 928 (1949).

[74] ADLER, F. T., SAWYER, W. M. and FERRY, J. D., "Propagation of transverse waves in viscoelastic media", *J. Appl. Phys.*, **20**, 1036 (1949).

[75] LEE, E. H. and KANTER, I., "Wave propagation in finite rods of viscoelastic material", *J. Appl. Phys.*, **24**, 115 (1953).

[76] GLAUZ, R. D. and LEE, E. H., "Transient wave analysis in a linear time-dependent material", *J. Appl. Phys.*, **25**, 947 (1954).

[77] LEE, E. H. and MORRISON, J. A., "A comparison of the propagation of longitudinal waves in rods of viscoelastic materials", *J. Polymer Sci.*, **19**, 93 (1956).

[78] LEE, E. H., "Wave propagation in anelastic materials", *Deformation and Flow of Solids*, Springer-Verlag, Berlin (1956).

[79] MORRISON, J. A., "Wave propagation in rods of Voigt material and viscoelastic materials with three-parameter models", *Q. Appl. Math.*, **14**, 153 (1956-7).

[80] HANIN, M., "Propagation of an aperiodic wave in a compressible viscous medium", *J. Math. Phys.*, **36**, 234 (1957-8).

[81] NAAKE, H. J. and TAMM, K., "Sound propagation in plates and rods of rubber-elastic materials", *Acustica*, **8**, 65 (1958).

[82] BERRY, D. S., "Stress propagation in viscoelastic bodies", *J. Mech. Physics of Solids*, **6**, 177 (1958).

[83] BLEICH, H. H. and SACKMAN, J. L., "An approximation in problems of viscoelastic wave propagation", Columbia University, New York City, Tech. Rep. No. 10 to ONR under Cont. No. Nonr–266(34) (September 1960).

[84] THACHER, J. H. and BALTRUKONIS, J. H., "Inertia effects in the tensile stress relaxation test", The Catholic University of America, Washington, D.C., Tech. Rep. No. 1 to the Allegany Ballistics Laboratory, Rocket Center W. Va. under Res. Sub-cont. No. 72/NOrd 16640 (December 1962).

[85] KOLSKY, H. and LEE, S. S., "The propagation and reflection of stress pulses in linear viscoelastic media", Brown University, Providence, R.I., Tech. Rep. No. 5 to ONR under Cont. Nonr 562(30) (May 1962).

[86] ACHENBACH, J. D., "Wave propagation in a three-parameter viscoelastic material", Ph.D. dissertation, Stanford University, Palo Alto, Calif. (1962).

[87] CHU, BOA-TEH, "Stress waves in isotropic linear viscoelastic materials", *J. de Mecanique*, **1**, 439 (1962).

[88] VALANIS, K. C., "Wave propagation in viscoelastic solids with measured relaxation or creep functions". Purdue University, Lafayette, Indiana, Report No. A & ES 63–1 to Lockheed Propulsion Co. under Cont. No. AF94 (611)–8539 (June 1963).

[89] GUESS, J. F. and THURSTON, G. B., "Measurement of the dynamic flexural response of beams and plates", Oklahoma State University, Stillwater, Okla., Tech. Rep. to ONR under Cont. No. Nonr–2595(03) (October 1963).

[90] LIFSHITZ, J. M., "A stress wave study of the dilatational response of some viscoelastic solids", Brown University, Providence, R.I., Tech. Rep. No. 8 to ONR under Cont. No. Nonr 562(30) (August 1964).

[91] FISHER, G. M. C. and GURTIN, M. E., "Wave propagation in the linear theory of viscoelasticity", Brown University, Providence, R.I., Tech. Rep. No. 28 to ONR under Cont. No. Nonr 562(25) (August 1964).

EXPERIMENTAL CHARACTERIZATION OF NONLINEAR VISCOELASTIC MATERIALS

F. J. LOCKETT

National Physical Laboratory
Teddington, Middlesex, England

Abstract—Increasing use is being made of materials under conditions for which nonlinear time-dependent mechanical behaviour is important. This has led to the formulation of theories to describe this type of behaviour, and to the problem of determining experimental methods by which constitutive parameters may be evaluated. Work in this field has followed two approaches: empirical, in which a mathematical description is constructed around available experimental results; and rational, in which a mathematical theory is developed upon firm physical foundations, and experiments are then designed to determine the constitutive constants or functions.

The main part of the present paper is concerned with the rational approach to the problem for nonlinear viscoelastic behaviour, with particular emphasis on recent results. Theories are considered for solid and fluid types of behaviour, and the experimental methods which result from the analyses include three-dimensional creep and stress-relaxation studies, dynamic tests, and various forms of viscometric measurement. Reference is made to the results of experimental investigations where these are available. In addition, a section is devoted to the rational approach for finite elastic behaviour.

1. INTRODUCTION

In recent years increasing use has been made of materials under conditions for which their behaviour is both nonlinear and time-dependent. At first, most of the problems were concerned with the creep behaviour of metals, and theories were therefore designed to describe such behaviour of these materials. These theories were not developed from first principles, even on a phenomenological basis, but were empirical representations of the type of behaviour that was observed in conventional experiments. Empirical theories have both strength and weakness. To their credit, they are usually simple and can be applied to practical stress analysis problems. In fact they are the obvious and only choice that one can make if results are required in a short time. However, this does not imply that they are to be preferred in the long run. On the debit side, empirical formulae may give only crude descriptions of the actual behaviour, and in the absence of experimental proof, there is no justification for assuming that an empirical formula which is chosen to satisfy one set of experimental results will be adequate to model an entirely different situation.

During the last decade attention has turned more to the nonlinear viscoelastic behaviour of materials such as high polymers and non-Newtonian fluids. Many of these materials do not exhibit a sharp yield. It is, therefore, natural to describe them using extensions of the theories of elasticity and viscosity rather than that of plasticity. The subject may then be set upon a rational foundation, and the last few years have seen a blossoming of the theory to very general and

elegant forms. However, there is a tendency for work in this field to be somewhat divorced from practical application, and there arises the need to bridge this gap. One problem is that of specifying the experimental programs which are necessary to measure the material functions and constants which appear in the theories. The main purpose of the present paper is to survey the published work in this field. In general, no reference will be made to experimental techniques which have not been analysed in the context of one of the rational theories.

Since the mechanical behaviour of a material depends on a number of factors, some of which will be ignored here, it is necessary to state the assumptions and restrictions upon which the discussion is based. We shall restrict ourselves to mechanical effects; it will be assumed that any temperature fields which are produced in the material are insufficient to cause significant thermal expansion or to affect the mechanical properties. Theories of nonlinear thermovisco-elasticity do exist, but their use would make the present task prohibitive. We shall also assume that there is an initial undeformed state in which the material is both isotropic and homogeneous, and we shall confine ourselves to a description of the material under conditions before the onset of failure. Further, no explicit account will be taken of chemical or physical changes which may occur due to crystallization, dewetting, polymerization, etc. It is possible that the phenomenological theory may describe these changes in certain situations, but this should be regarded as fortuitous. The much broader question of deciding under what conditions a particular theory is applicable to a given material will not be discussed. In general some over-experimentation will give an indication of the answer to this question.

Despite all of the restrictions imposed above the problem is not trivial, and we may consider the whole range of material behaviour from that of elastic solids to that of viscous fluids. However, since this conference is concerned with solid propellants, we shall place the main emphasis on solid behaviour.

After a very brief comment on empirical methods in Section 2, the foundations of some of the rational theories are summarized in Section 3. The next two sections are particularly relevant to the solid propellant field. Section 4 gives a survey of methods of characterizing finite elastic behaviour, and Section 5 deals with stress-relaxation and creep studies for nonlinear viscoelastic materials. The final section discusses methods which are primarily suitable for non-Newtonian fluids, but which are applicable to solids in some cases. Where possible, reference is made to the results of experimental investigations.

Many of the methods that will be discussed here have not yet been applied to solid propellant materials. Thus, this paper provides a review of techniques which may be employed to obtain a better characterization of solid propellant behaviour.

2. EMPIRICAL CHARACTERIZATION

The creep behaviour of metals has been of practical importance for some years, and a considerable amount of work has appeared in the literature which is aimed at an adequate characterization of these materials. Almost all of this

work is of an empirical nature, the particular forms of theory being suggested by available experimental results and chosen because of their relative simplicity. A survey paper dealing with stress analysis in the presence of creep is given by Finnie [1]. We shall make only a few general remarks here.

A great deal of the literature is concerned with creep under constant load, and the theories are particularly important for situations which are statically determinate. Under this restriction the theories fall into one of two classes: steady creep and non-steady creep.

When a material is subjected to a constant load, it responds with an instantaneous elastic strain, followed by a transient response in which the strain-rate decreases with time, and eventually the strain rate may tend to a constant value. In this final stage the material exhibits steady-state creep. In many analyses only this component of the strain is retained; the elastic and transient components are often neglected.

Thus, for steady-state creep under constant load, the one-dimensional constitutive relation may be expressed in the form

$$\epsilon = f(\sigma)t, \qquad \dot{\epsilon} = f(\sigma) \tag{2.1}$$

where $\epsilon, \dot{\epsilon}, \sigma$ and t denote strain, strain rate, stress and time respectively, and the function f may be nonlinear. The following forms have found particular use in practice:

$$\dot{\epsilon} = B\sigma^n, \qquad \dot{\epsilon} = C \sinh\left(\frac{\sigma}{d}\right), \qquad \dot{\epsilon} = D \exp\left(\frac{\sigma}{s}\right) \tag{2.2}$$

where B, n, C, d, D and s are constants whose values are chosen to model the results of uniaxial tests performed under constant load.

If the creep curve under constant load does not tend to a linear form, then the material is said to exhibit non-steady creep. In this case it is usual to assume the empirical form

$$\dot{\epsilon} = F(\sigma)\, G(t) \tag{2.3}$$

which implies that the creep curves at different stress levels have the same geometric form. This may or may not be justifiable for a particular material. A form of (2.3) which has been used many times is

$$\dot{\epsilon} = B\sigma^n t^m \tag{2.4}$$

where B, n and m are constants which are determined from creep curves obtained in uniaxial tests at various constant loads.

In order to describe three-dimensional behaviour various generalizations of the form (2.3) are used, e.g.

$$\dot{\epsilon}_{ij} = F_{ij}(\sigma_{rs})\, G(t) \tag{2.5}$$

where the empirical forms which are assumed for F_{ij} are suggested by the theories of plasticity or finite elasticity. Numerous papers on this subject can be found in the engineering literature and we shall not attempt to summarize

them here. Nor shall we discuss the empirical theories which have been proposed to describe creep under varying load. Instead we shall turn our attention to attempts which have been made to give practical utility to the continuum mechanical theories of nonlinear viscoelasticity.

3. THE CONTINUUM THEORIES

In the last decade attention has been given to the formulation of mathematical theories of great generality for the description of nonlinear time-dependent material behaviour. In this section we shall give a brief introduction to some of these theories. Almost all of the experimental investigations which will be discussed use as their starting point a particular form of one of two theories : the integral formulation of Green and Rivlin [2–4] and the differential form of Rivlin and Ericksen [5].

3.1. *Integral Formulation*

The theory for so-called simple materials was due to Green and Rivlin [2–4] and has been discussed further by Noll [6] and others.

Consider a body which is initially in an undeformed isotropic state and let the rectangular Cartesian coordinates of a typical material element be denoted by $X_i (i = 1,2,3)$. At a later time τ, after the material has been deformed, this element will occupy some new position $x_i(X_j, \tau)$. The deformation of the material can be characterized by the matrix of deformation gradients $\mathbf{F}(\tau) = || \partial x_i / \partial X_j ||$, and it can be shown that $\mathbf{F}$ is expressible in the forms

$$\mathbf{F} = \mathbf{RM} = \mathbf{NR} \tag{3.1}$$

where $\mathbf{R}$ is orthogonal and $\mathbf{M}$ and $\mathbf{N}$ are positive definite and symmetric. This unique decomposition of $\mathbf{F}$ expresses the fact that the deformation of each material element may be considered as composed of two parts : a rigid rotation $\mathbf{R}$, followed by a pure stretch $\mathbf{N}$, or preceded by a pure stretch $\mathbf{M}$.

A simple material is defined as one for which the value of the stress matrix $\boldsymbol{\sigma}$ in a material element at time t depends only upon the values of $\mathbf{F}(\tau)$ in that same element at all times up to and including the time t. It has been shown [2–4, 6] that the constitutive relation may be written in the form

$$\boldsymbol{\sigma}(t) = \mathbf{R}(t) \, \mathbf{S} \left\{ \begin{matrix} t \\ \mathbf{E}(\tau) \\ -\infty \end{matrix} \right\} \mathbf{R}^T(t) \tag{3.2}$$

where $\mathbf{R}^T$ is the transpose of $\mathbf{R}$, and $\mathbf{E}$ is defined by

$$2\mathbf{E} = \mathbf{F}^T\mathbf{F} - \mathbf{I} \tag{3.3}$$

where $\mathbf{I}$ is the unit matrix. $\mathbf{E}$ is a finite strain matrix which reduces to the classical strain matrix if displacement gradients are assumed to be small.

In (3.2) **S** represents a nonlinear matrix functional which can be expressed in the form*

$$\mathbf{S(E)} = \theta_0\mathbf{I} + \sum_{n=1}^{5} \int_{-\infty}^{t} \dots \int_{-\infty}^{t} \theta_n(t - \tau_1, \dots, t - \tau_n)\,\dot{\mathbf{E}}(\tau_1) \dots \dot{\mathbf{E}}(\tau_n)\,\mathrm{d}\tau_1 \dots \mathrm{d}\tau_n \tag{3.4}$$

where the relation has been written in terms of the strain-rate matrix $\dot{\mathbf{E}}$. The quantities θ_α are functions of their indicated arguments and polynomials in expressions of the form

$$\int_{-\infty}^{t} \dots \int_{-\infty}^{t} \xi_m(t - \tau_1, \dots, t - \tau_m)\,\mathrm{tr}\,[\dot{\mathbf{E}}(\tau_1) \dots \dot{\mathbf{E}}(\tau_m)]\,\mathrm{d}\tau_1 \dots \mathrm{d}\tau_m, (m = 1, \dots, 6) \tag{3.5}$$

The functions (3.5) are invariants of the strain history, in which the ξ_m are functions of their indicated arguments only, and tr **a** denotes the trace of the matrix **a** (i.e. tr $\mathbf{a} = a_{11} + a_{22} + a_{33}$).

Equation (3.2) may be written as

$$\mathbf{\Sigma}(t) = \mathbf{R}^T\,\sigma\mathbf{R} = \mathbf{S(E)} \tag{3.6}$$

where $\mathbf{\Sigma}(t)$ represents the stress matrix evaluated in a coordinate system which has been rotated with the rigid body part of the deformation. The constitutive relation (3.2) may also be expressed† in a similar form in which **R** is replaced by **F**, and **S** is replaced by a new matrix functional of **E**. However, the form (3.2) is the most convenient for our present purposes.

If the functions θ_α are expressed as polynomials in the invariants (3.5), then (3.4) yields (see [7])

$$\mathbf{\Sigma}(t) = \int_{-\infty}^{t} \{\mathbf{I}\psi_1 T_1 + \psi_2 \mathbf{M}_1\}\mathrm{d}\tau_1$$

$$+ \int\int_{-\infty}^{t} \{\mathbf{I}\psi_3 T_1 T_2 + \mathbf{I}\psi_4 T_{12} + \psi_5 T_1 \mathbf{M}_2 + \psi_6 \mathbf{M}_1 \mathbf{M}_2\}\mathrm{d}\tau_1\mathrm{d}\tau_2$$

$$+ \int\int\int_{-\infty}^{t} \{\mathbf{I}\psi_7 T_{123} + \mathbf{I}\psi_8 T_1 T_{23} + \psi_9 T_1 T_2 \mathbf{M}_3 + \psi_{10} T_{12}\mathbf{M}_3$$

$$+ \psi_{11} T_1 \mathbf{M}_2 \mathbf{M}_3 + \psi_{12}\mathbf{M}_1\mathbf{M}_2\mathbf{M}_3\}\mathrm{d}\tau_1\mathrm{d}\tau_2\mathrm{d}\tau_3 + \dots \tag{3.7}$$

In this expression ψ_1 and ψ_2 are functions of $t - \tau_1$; ψ_3, $\dots$, ψ_6 are functions of $t - \tau_1$ and $t - \tau_2$; etc., and these are the functions which characterize the mechanical behaviour of a particular material. In addition

$$\mathbf{M}_\alpha = \dot{\mathbf{E}}(\tau_\alpha),\ T_\alpha = \mathrm{tr}\,\mathbf{M}_\alpha,\ T_{\alpha\beta} = \mathrm{tr}[\mathbf{M}_\alpha\mathbf{M}_\beta],\ \text{etc.} \tag{3.8}$$

---

* It is assumed that the material is of the hereditary type and **S** satisfies certain continuity conditions which have been discussed elsewhere. Equations (3.4) and (3.5) are written in a different form from that given originally in [2–4], but they represent a statement of the same results.

† This is the form given in [2–4]. It can be obtained from (3.2) by setting $\mathbf{R} = \mathbf{FM}^{-1}$ and including the dependence on **M** in the functional using the relation $\mathbf{M}^2 = 2\mathbf{E} + \mathbf{I}$.

Provided that the inverse functional exists, (3.6) yields

$$E(t) = S^{-1}(\Sigma(\tau))\tag{3.9}$$

which leads to an expression similar to (3.7) where the roles of E and Σ are interchanged.

The most general experimental method that will be referred to in this paper retains all of the terms which are written explicitly in (3.7) and neglects fourth and higher order terms. A method is given for determining the functions $\psi_1, \ldots, \psi_{12}$. The reason for truncating the series after the third order terms is a practical one: the experimental program for higher order theories would be prohibitive at the present time. The analysis is likely to be best suited to materials which do not exhibit a sharp yield, so that stress-strain curves may be represented by smooth curves. It has been shown that the theory is applicable to a number of real materials (see Section 5).

If it is assumed that the deformation in the material is unaffected by an additional hydrostatic pressure, then (3.7) reduces to the form [8]

$$\Sigma^D(t) = \int\limits_{-\infty}^{t} \phi_1 M_1 d\tau_1 + \int\limits_{-\infty}^{t}\!\!\int \phi_2 M_1 M_2 d\tau_1 d\tau_2 + \int\limits_{-\infty}^{t}\!\!\int\!\int \{\phi_3 T_{12} M_3$$
$$+ \phi_4 M_1 M_2 M_3\} d\tau_1 d\tau_2 d\tau_3 + \ldots\tag{3.10}$$

where Σ^D denotes the deviatoric stress matrix in the rotated coordinate system. It is noted that this restriction implies that the material is incompressible, but it also requires that the other mechanical properties are independent of hydrostatic pressure. The relation (3.10) is also discussed in Section 5.

A number of experimental investigations have been analysed using a one-dimensional form of eqn. (3.7). In particular, if we consider the extension of a fibre or rod, then no rotation of the material elements is produced. Thus $R = I$ and $\Sigma = \sigma$, and the one-dimensional form of (3.7) is

$$\sigma(t) = \int\limits_{-\infty}^{t} J(t - \tau)\dot{E}(\tau)\,d\tau + \int\limits_{-\infty}^{t}\!\!\int K(t - \tau_1, t - \tau_2)\dot{E}(\tau_1)\dot{E}(\tau_2)\,d\tau_1 d\tau_2$$
$$+ \int\limits_{-\infty}^{t}\!\!\int\!\int L(t - \tau_1, t - \tau_2, t - \tau_3)\dot{E}(\tau_1)\dot{E}(\tau_2)\dot{E}(\tau_3)\,d\tau_1 d\tau_2 d\tau_3$$
$$+ \ldots\tag{3.11}$$

or a similar expression in which the roles of σ and E are interchanged. Also, since $E = \epsilon + \frac{1}{2}\epsilon^2$, where ϵ is the classical strain measure, (3.11) can be expressed in a similar form in which E is replaced by ϵ.

3.2. Differential Formulation

In the differential formulation of Rivlin and Ericksen [5] it is assumed that the stress in a material element at time t can be expressed as a polynomial in the values of the gradients of displacement, velocity, acceleration, second acceleration, etc., in that element at time t. It has been shown [5, 9–13] that

$\sigma(t)$ may then be expressed as a polynomial, whose form is known, in the matrices C, A_1, A_2, ... which are defined by

$$C = FF^T, \qquad A_\alpha = \left|\left| A_{ij}^{(\alpha)} \right|\right|, \tag{3.12}$$

$$\left. \begin{aligned} A_{ij}^{(1)} &= \frac{\partial v_i^{(1)}}{\partial x_j} + \frac{\partial v_j^{(1)}}{\partial x_i}, \\ A_{ij}^{(\alpha+1)} &= \frac{\partial A_{ij}^{(\alpha)}}{\partial t} + v_m^{(1)} \frac{\partial A_{ij}^{(\alpha)}}{\partial x_m} + A_{mj}^{(\alpha)} \frac{\partial v_m^{(1)}}{\partial x_i} + A_{im}^{(\alpha)} \frac{\partial v_m^{(1)}}{\partial x_j} \end{aligned} \right\} \tag{3.13}$$

where summation is implied over repeated suffices. In these definitions $v_i^{(1)}$ represents the velocity, i.e. $v_i^{(1)} = Dx_i/Dt$, where D/Dt denotes the material derivative. Thus

$$\sigma(t) = \text{poly}\,(C, A_1, A_2, \ldots) \tag{3.14}$$

The precise form of the polynomial has been determined by Spencer and Rivlin [10–13] for an arbitrary number of kinematic matrices A_α.

A Rivlin–Ericksen fluid is defined as a Rivlin–Ericksen material for which the stress is independent of the deformation C, but depends on the deformation rate and higher rates. The matrix C can then be omitted from the polynomial (3.14), i.e.

$$\sigma(t) = \text{poly}\,(A_1, A_2, \ldots) \tag{3.15}$$

In the case of a purely elastic material $\sigma(t)$ depends only on the matrix C. The constitutive relation (3.14) can then be expressed in the form (see, for example, [9])

$$\sigma = \alpha_0 I + \alpha_1 C + \alpha_2 C^2 \tag{3.16}$$

where α_0, α_1 and α_2 are polynomials in the invariants $\text{tr}C$, $\text{tr}C^2$ and $\text{tr}C^3$. Alternatively the functions α_i, which characterize the mechanical properties of the material, may be expressed in terms of the three strain invariants

$$I_1 = \text{tr}C, \qquad I_2 = \tfrac{1}{2}[(\text{tr}C)^2 - \text{tr}C^2], \qquad I_3 = \det C \tag{3.17}$$

For a perfectly elastic material [14] α_0, α_1 and α_2 may be derived from a strain-energy function $W(I_1, I_2, I_3)$ via the relations

$$\alpha_0 = 2I_3^{1/2} \frac{\partial W}{\partial I_3}, \; \alpha_1 = \frac{2}{I_3^{1/2}} \left(\frac{\partial W}{\partial I_1} + I_1 \frac{\partial W}{\partial I_2} \right), \; \alpha_2 = -\frac{2}{I_3^{1/2}} \frac{\partial W}{\partial I_2} \tag{3.18}$$

Thus, for a perfectly elastic material, determination of the material functions α_0, α_1, and α_2 is equivalent to the determination of the strain-energy function W.

4. CHARACTERIZATION OF FINITE ELASTIC BEHAVIOUR

The mechanical properties of solid propellants are both nonlinear and time-dependent under a number of loading conditions which are of practical interest. However, a theory has not yet been evolved which both describes these properties adequately in all cases and is sufficiently simple to permit the necessary analysis and experimentation to be performed in a reasonable time. Consequently, the

stress analyst is content at first to use solutions obtained under the assumption of linear elastic behaviour (see, for example, [15]). As a next approximation to the true behaviour there are two possible choices: linear viscoelasticity for problems in which time effects make linear elastic theory inadequate, and finite elasticity for situations in which nonlinearity is particularly relevant. The first of these choices will be discussed at this conference by Professor Kolsky. A review of solutions to problems of practical interest to the rocket engineer has been given by Williams [16].

Before proceeding to a discussion of nonlinear viscoelastic characterization, we shall present a brief summary of the characterization of finite elastic behaviour. In a sense this forms an introduction to the general problem, and it is of practical importance because the methods are more tractable than those for viscoelastic behaviour. Use of finite elasticity theory in the solution of solid propellant problems has been attempted, for example, by Dong et al. [17] and Wiegand [18].

A great deal of the fundamental work in the field of experimental characterization of finite elastic materials is due to Rivlin and Saunders [19, 20], Rivlin [21], Gent and Rivlin [22], and Treloar [23]. This work has been very adequately summarized by Green and Adkins [24] and by Eringen [25], and will be only briefly summarized here.

If the material is incompressible, which is assumed in all of the papers mentioned above, $I_3 = 1$ and α_0 is replaced by an arbitrary hydrostatic pressure p. Thus (3.16) and (3.18) yield

$$\boldsymbol{\sigma} = -p\mathbf{I} + 2\left(\frac{\partial W}{\partial I_1} + I_1 \frac{\partial W}{\partial I_2}\right)\mathbf{C} - 2\frac{\partial W}{\partial I_2}\mathbf{C}^2 \qquad (4.1)$$

where $W = W(I_1, I_2)$, and the experimental problem is to determine the form of W.

In their experimental work, Rivlin and Saunders [19, 20] applied biaxial loads f_1 and f_2 to the edges of a thin rubber sheet so as to produce a pure homogeneous strain with extension ratios λ_i in the directions of the x_i-axes. By varying the λ_i in such a way that either I_1 or I_2 remained constant, they were able to use (4.1), and the measured values of f_1 and f_2 required to produce the extensions, to determine $\partial W/\partial I_1$ and $\partial W/\partial I_2$ for various values of I_1 at constant I_2, and vice versa.

The experimental results obtained by this method suggested that, for the vulcanized rubber used in the experiments, the strain-energy function was of the form

$$W = C_1(I_1 - 3) + f(I_2 - 3) \qquad (4.2)$$

where C_1 is a constant and f is a function of I_2 alone. Special cases of (4.2) are the form derived from the simple molecular theory of elasticity (in which $f \equiv 0$), and the expression for a Mooney material

$$W = C_1(I_1 - 3) + C_2(I_2 - 3) \qquad (4.3)$$

in which C_1 and C_2 are constants.

In further experiments [19, 20] the validity of the strain-energy function (4.2) was checked in other experimental situations. These involved pure shear of a strip of rubber, pure shear superposed on simple extension, simple elongation, uniform two-dimensional extension of a sheet, torsion of a rod, and extension and torsion of a tube. It was found that the function (4.2) was adequate to describe the given material over a wide range of values of the invariants I_1 and I_2, whereas the Mooney expression (4.3) was adequate in some cases but not in all.

A number of solutions to problems in finite elasticity theory have been obtained using particular forms for the strain-energy function W. Many of these are empirical expressions which were chosen because of their simple form. A rational approach to the problem of giving explicit approximations for W has been discussed by Rivlin [14], but actual experimental results are limited.

A special form of strain-energy function, for an incompressible isotropic material of a type proposed by Mooney [26], has been investigated by Carmichael and Holdaway [27]. For this material W may be expressed in terms of a (stress-) function of one variable. Using a semi-empirical approach the predictions of this theory were compared [27] with the experimental results of Treloar [28] for simple extension, shear, and two-dimensional extension of rubber. It was found that excellent agreement could be obtained in all cases using a three parameter model for the stress function.

The more general problem of determining the strain-energy function for a compressible material has been considered by Blatz and Ko [29]. W is now a function of all three invariants, and eqns. (3.16) and (3.18) can be used together with suitable experimental data to determine the derivatives of the strain-energy function with respect to the invariants. This experimental investigation used a highly compressible polyurethane foam rubber, and data were obtained in simple extension, strip-biaxial extension, and uniform biaxial tension. Photographs of the experimental setups are given in [29]. In the analysis compressibility effects were not taken into account in a rational manner, but rather by assuming an empirical power relation connecting the third invariant and the extension ratio in simple extension. This assumption, which in effect introduces a Poisson's ratio, was justified by its ability to model the experimental data.

In addition, the strain-energy function W was expanded as a power series in the invariants and only the leading terms were retained. In effect the constitutive relation used was a generalization for a compressible material of the Mooney expression (4.3). It was found that, for a continuum (virtually incompressible) version of the material, the first Mooney term was the most significant, whereas, for the compressible foam material, the second Mooney term was dominant. For the foam material it was found that an adequate form of W was

$$W = C \left\{ \left(\frac{I_2}{I_3} - 3 \right) + 2(I_3^{1/2} - 1) \right\} \tag{4.4}$$

where the first term represents the modified Mooney term and the second term appears only in the theory for compressible materials.

Spencer [30] has proposed a theory to describe finite deformations of an almost incompressible elastic solid, in which the strain-energy function is represented by three functions of I_1 and I_2: the dependence on I_3 is explicit. This theory may be useful for describing real materials, but the method of determining the strain-energy function has not yet been given, though it should be similar to that for incompressible materials.

5. CREEP AND STRESS-RELAXATION

We now turn our attention to the principal topic of the present paper—the experimental characterization of nonlinear time-dependent materials. In the present section attention will be confined to creep and stress-relaxation studies: these are most suitable for solid-like materials such as high polymers and solid propellants. In Section 6 we shall consider methods which are particularly suitable for application to viscoelastic liquids, but which may also be applicable to those solid-like materials which exhibit the type of mechanical behaviour normally associated with fluids.

5.1. *Stress-relaxation in a Material with a Restricted Memory*

We begin the discussion of this section by considering an analysis which is similar to those of the previous section, and so forms a bridge between the two types of behaviour.

Suppose that, during the short interval of time $(0, \tau_0)$, a body is deformed from its initial undeformed isotropic state into some other state, and suppose that the deformation in existence at time τ_0 is maintained constant thereafter. We enquire into the stresses required to maintain this deformation. Further, we consider materials for which, for sufficiently large times, the stress is in-dependent of the deformation path followed during the time interval $(0, \tau_0)$. For this type of material the stress at time t is a function only of the deformation and of t.

Bergen, Messersmith and Rivlin [31] considered an incompressible material of this type and deduced a constitutive relation of the form (3.16) in which $\alpha_i = \alpha_i(I_1, I_2, t)$. Provided that the displacement gradients are small compared with unity, σ may be written in terms of the classical strain matrix ϵ:

$$\sigma = -p\mathbf{I} + \beta_1\epsilon + \beta_2\epsilon^2 \qquad (5.1)$$

where the β_i may be expressed as functions of t and of the invariants $J_1 = I_1 - 3$ and $J_2 = I_1 - I_2$ (which may also be written in terms of ϵ).

Bergen *et al.* [31] performed experiments with samples of a vulcanized, heavy-filled, synthetic rubber and four polyvinylchloride compositions to determine the function β_1 in situations where the last term in (5.1) is negligible. These experiments took the form of small extension and combined small extension and small torsion tests on a cylindrical tube. The tensile forces and torsional couples

required to maintain certain deformations at constant values were measured at times large compared with those in which the deformations were applied.

By making the assumption that, in the extension tests, the value of β_1 does not vary significantly throughout the specimen, the dependence of β_1 on J_1 and J_2 was determined for a given value of t. The results suggested that β_1 was substantially independent of J_2 for the chosen values of t, and satisfactory agreement was obtained between results determined from extensional and combined extension/torsion experiments. In the analysis of the latter experiments allowance was made for a variation in the radial direction of the value of β_1 in the specimen. It was also shown that the experimental results were consistent with the assumption that the dependence of β_1 on time and on the invariants was separable.

5.2. *Creep and Stress-relaxation in One Dimension*

We shall now discuss creep in one-dimensional extension at extension ratios for which the linear classical theory of viscoelasticity is inadequate. Of course, a one-dimensional analysis is not sufficient for use in the solution of three-dimensional problems such as those encountered in rocket applications. However, a theory of one-dimensional behaviour is valuable in other fields (e.g. synthetic fibres), and a number of experimental investigations have been carried out using a rational approach to the determination of constitutive parameters.

For small extensional creep deformation the strain $\epsilon(t)$ and extension ratio $\lambda(t)$ may be expressed

$$\epsilon(t) = \lambda(t) - 1 = \int_{-\infty}^{t} \phi(t - \tau)\,\dot{\sigma}(\tau)\,\mathrm{d}\tau \tag{5.2}$$

where $\phi(t)$ is a creep function and $\sigma(t)$ may be interpreted as either the nominal or true stress. For a given class of materials this relation may be adequate up to strains of a certain order. At higher values (5.2) becomes inadequate. Then a possible representation is an expression of the form (3.11). We shall return to this later.

Alternatively it may be possible to choose some other response function for use on the left-hand side of (5.2) which will allow that equation to be applicable up to a higher strain limit. This approach has been used by a number of authors. In particular Leaderman [32] discovered response functions which allow a linear relation to be used to describe the longitudinal creep and recovery of a specimen of plasticized polyvinylchloride for strains up to 27 per cent. An expression of the form

$$\rho(t) = \int_{-\infty}^{t} \phi(t - \tau)\,\dot{\sigma}(\tau)\mathrm{d}\tau \tag{5.3}$$

gave good agreement with experimental results provided that $\rho(t)$ is interpreted as

$$\rho(t) = \frac{(\lambda - \lambda^{-2})\,(1 + k_1\lambda^{-1})}{3(1 + k_1)} \tag{5.4}$$

or

$$\rho(t) = \frac{(\lambda^2 - \lambda^{-1})(1 + k_2\lambda^{-1})}{3(1 + k_2)} \qquad (5.5)$$

depending respectively on whether $\sigma(t)$ is considered the nominal or true stress.

The expressions (5.4) and (5.5) are quasi-empirical measures of strain response, which do however have a rational basis in the theory of Mooney elastic materials. For a finite elastic deformation the stress required to produce a simple elongation λ is [24]

$$\sigma = 2(\lambda^2 - \lambda^{-1})\left(\frac{\partial W}{\partial I_1} + \frac{1}{\lambda}\frac{\partial W}{\partial I_2}\right) \qquad (5.6)$$

and the two derivatives of W are constant for an incompressible Mooney material. Thus, the stress is proportional to a response function of the form (5.5) for this elastic material, and it is not unreasonable to use a similar measure in viscoelastic analyses. Its success in the analysis of Leaderman's experiments [32] supports this assumption.

Of course a linear relation of the form (5.3) does not remove the nonlinearity from a stress analysis problem. The form (5.3) merely transfers the nonlinearity (in the displacements) onto the left-hand side of the equation. There is as yet no theoretical indication of the conditions under which such a representation is possible.

We now return to the representation of creep and recovery data by an integral relation of the form (3.11), i.e.

$$\epsilon(t) = \int_{-\infty}^{t} J(t - \tau)\,\dot\sigma(\tau)\,\mathrm{d}\tau + \int\int_{-\infty}^{t} K(t - \tau_1, t - \tau_2)\,\dot\sigma(\tau_1)\,\dot\sigma(\tau_2)\,\mathrm{d}\tau_1\mathrm{d}\tau_2$$

$$+ \int\int\int_{-\infty}^{t} L(t - \tau_1, t - \tau_2, t - \tau_3)\,\dot\sigma(\tau_1)\,\dot\sigma(\tau_2)\,\dot\sigma(\tau_3)\,\mathrm{d}\tau_1\mathrm{d}\tau_2\mathrm{d}\tau_3 + \ldots \quad (5.7)$$

We shall confine our discussion to the relation which is terminated after the term of the third order.

Leaderman, McCrackin and Nakada [33] used an expression of this form to interpret Leaderman's [32] experimental results. They did not start out with the relation (5.7) and then ask what experiments would be necessary to determine the functions J, K and L (this question has been answered in [7] and will be discussed later). In fact the experiments performed in [32] are not sufficient to determine the functions K and L completely. However, it is shown in [33] that provided a strain measure $\rho(t)$ does exist for which a linear relation (5.3) is valid, then a relation of the form (5.7) is implied, and the functions J, K and L can be written simply in terms of the function ϕ appearing in (5.3). The experimental results of [32] were shown to be consistent with this reformulation of the theory. It was found that for strains up to 20 per cent the first two terms on the right-hand side of (5.7) were dominant, the third term giving a significant

contribution only over the further 7 per cent of strain covered in the experiments.

A somewhat similar experimental investigation has been conducted by Ward and Onat [34] using fibres of oriented polypropylene, but they presented a more rational analysis of their results. Extensional creep experiments were performed in which the load was either increased or removed at some later time. These experiments are sufficient to determine the functions J and K completely and the function L partially. Ward and Onat found that their material exhibited significant nonlinearity for strains of only one or two per cent. In this range the contribution of the second term on the right-hand side of (5.7) was found negligible, the nonlinearity being represented by the third term.

5.3. Creep and Stress-relaxation in Three Dimensions

Bernstein, Kearsley and Zapas [35] have considered simple finite theories for an incompressible solid and an incompressible fluid, and have compared the predictions of these theories with the experimental results of a stress-relaxation test in simple extension.

The theory which they used for the solid material is essentially equivalent to (3.7) in which only the first order terms are retained. Since the material is incompressible, this relation gives an expression for the deviatoric stress matrix, which can be written

$$\mathbf{\Sigma}^D(t) = \int_{-\infty}^{t} [\mathbf{I} \, \psi_1 \, \text{tr} \, \dot{\mathbf{E}}(\tau) + \psi_2 \, \dot{\mathbf{E}}(\tau)]d\tau \tag{5.8}$$

This form is different from that obtained by retaining only the first order term in (3.10). Pipkin [8] showed that the terms in $\text{tr}\dot{\mathbf{E}}$ could be expressed in terms of higher order expressions, thus (5.8) represents a different approximation from the first-order version of (3.10).

The fluid theory is of a type proposed by Coleman and Noll [36] in which the dependence of the stress at time t upon the deformation at each previous instant is expressed in terms of an elastic potential. Thus the effect of the configuration at time $\tau < t$ on the stress at time t is equivalent to the effect of stored elastic energy with the configuration at time τ as the preferred configuration.

Bernstein *et al.* [35] have shown that the constitutive relation for a stress-relaxation test can be expressed as

$$\boldsymbol{\sigma} = -p\mathbf{I} + (a_0 + a_1 \, \text{tr}\mathbf{c}) \, \mathbf{c} + a_2 \mathbf{c}^2, \tag{5.9}$$

where a_0, a_1 and a_2 are functions of time only, and

$$\mathbf{c} = \mathbf{f}\mathbf{f}^T, \tag{5.10}$$

where $\mathbf{f}$ is the (constant) gradient of the deformation during the stress-relaxation test with respect to the undisturbed state. They compared the predictions of these theories with experimental results obtained with plasticized polyvinyl-chloride, polyisobutylene, and sulfur vulcanizates of butyl rubber. For the

extensional situation investigated the results were in agreement with the fluid type of theory.

The most general rational analysis which has so far been given for the determination of constitutive functions using creep or stress-relaxation techniques is that due to Lockett [7]. This analysis shows how the functions $\psi_1, \ldots, \psi_{12}$ appearing in the constitutive relation (3.7) may be determined in principle. It should be noted that the experiments seek to determine two functions of one variable, four functions of two variables, and six functions of three variables, and it might therefore be expected that the experiments may be both numerous and difficult to perform. However, the experimental program is not as complex as might be expected, and it is not necessary to perform all of the experimental program in order to find *some* of the material functions. In addition it is never necessary to solve a system of more than three simultaneous equations when analysing the results.

The experimental program will be given here in the form of stress-relaxation tests, but it is noted that a corresponding set of creep tests is defined by interchanging the roles of stress and strain. The stress-relaxation experiments are of the following four types, in which the specified finite strain components have to be applied, while the other strain components are restrained at zero values:

$$
\begin{aligned}
&\text{(I) } E_{11} = AH(t) + BH(t-k) + CH(t-l) \\
&\text{(II) } E_{11} = AH(t), \ E_{22} = BH(t-k) + CH(t-l) \\
&\text{(III) } E_{11} = AH(t), \ E_{22} = BH(t-k), \ E_{33} = CH(t-l) \\
&\text{(IV) } E_{11} = AH(t), \ E_{12} = E_{21} = BH(t-k) + CH(t-l)
\end{aligned}
\right\} \quad (5.11)
$$

These experiments correspond respectively to uniaxial, biaxial, triaxial, and combined extension and shear tests. The quantities A, B, C, k and l are constants and H denotes the Heaviside step-function ($H(x) = 0, x < 0$: $H(x) = 1$, $x > 0$). Thus we have to consider stress-relaxation tests in which a number of strain increments are imposed at different times and in different strain components. The one-dimensional creep and recovery tests referred to in Section 5.2 are equivalent to *creep* tests of class I, in which $C = 0$ and $B = -A$.

In each of the experiments certain stress components must be measured. However, since no rotation of the material elements is produced in experiments I–III, $\Sigma = \sigma$ in these tests. The interpretation $\Sigma = R^T \sigma R$ is necessary only in the experiments of type IV. It is shown in [7] that ψ_1 and ψ_2 are determined from the results of the experiments of type I; $\psi_3, \ldots, \psi_8$ from type II; $\psi_9, \ldots, \psi_{11}$ from type III; and finally ψ_{12} from type IV.

Experiments of each type have to be performed for a number of values of the parameters A, B, C, k and l. The analysis then leads to the values of the functions ψ_i in the form $\psi_i(t, t-k, t-l)$, in which continuous values of t are recorded, but only discrete values of k and l. If n is the number of values of k or l which is sufficient to map adequately the function ψ_i, then the total number of experiments required to determine the twelve functions ψ_i is a function of n,

and some typical values are shown in the following table.

	Linear	Nonlinear (Third order)	
		$n=5$	$n=10$
One-dimensional	1	26	73
Three-dimensional	2	143	483
Three-dimensional (incompressible)	1	100	322

In addition to the three-dimensional nonlinear values, we have also shown the values for the linear material and for the nonlinear relations (3.10) and (3.11). Both of these special cases are discussed in detail in [7].

The number of experiments required for the characterization of a nonlinear material via this method would be prohibitively large if they had to be performed for each and every material. The analysis [7] was presented in the hope that its application (partial or complete) to a few chosen materials will indicate which are the significant terms in the constitutive relation (3.7).

The experimental program outlined above is not unique, but it makes the maximum use of situations in which $R = I$ and $\Sigma = \sigma$. These situations are most easily analysed. An experimental investigation of the mechanical properties of polyethylene using equation (3.7) and some of the results of [7] has been made by Lifshitz [37]. Here creep tests in tension and in torsion were performed at different stress levels on tubular specimens. It was found that a third-order equation of the form (5.7) was necessary to describe the tension results, whereas the torsion experiments could be described by first and third order terms. Reference [37] is the only known experimental work so far conducted using the rational approach of [7]. Combined tension and torsion experiments on polyvinylchloride specimens have been made by Onaran and Findley [38] but their analysis is purely empirical.

We have seen above that an entirely rational approach can result in a large number of experiments to determine a large number of material functions. An obvious course to follow is to simplify the constitutive relation by some plausible physical argument in order to reduce the number of material functions, though some experimental verification of the simplified constitutive relation must then be made. Such an analysis has been given by Lianis [39] using a constitutive relation due to Coleman and Noll [36] for materials with fading memories. For these materials deformations which occurred in the distant past have smaller effects on the present stresses than more recent deformations. The theory is a low order form which is applicable to motions which were " slow" in the recent past. The mechanical properties of the material are characterized by three elastic-response functions which depend on the three strain invariants and eight stress-relaxation functions which depend on time as well as on the strain invariants.

On the basis of some experimental evidence, Lianis chose a simple form for the

invariant-dependence of the long-time equilibrium behaviour for stress-relaxa-
tion (that for a Mooney material), and assumed that the instantaneous elastic
response had the same form of dependence on the invariants. The stress-
relaxation functions were assumed to be independent of the invariants. Under
these assumptions the constitutive relation for an incompressible material has
the following form in rectangular Cartesian coordinates:

$$\sigma(t) = -p(t)\mathbf{I} + (\phi + I_1\xi)\,\mathbf{B} - \psi\mathbf{B}^2 + 2\int_{-\infty}^{t} \phi_0(t-\tau)\,\dot{\mathbf{C}}_t(\tau)\,\mathrm{d}\tau$$

$$+ \mathbf{B}\int_{-\infty}^{t} \phi_1(t-\tau)\,\mathbf{C}_t(\tau)\,\mathrm{d}\tau$$

$$+ \int_{-\infty}^{t} \phi_1(t-\tau)\,\dot{\mathbf{C}}_t(\tau)\,\mathrm{d}\tau\,\mathbf{B} + \mathbf{B}^2\int_{-\infty}^{t} \phi_2(t-\tau)\,\dot{\mathbf{C}}_t(\tau)\,\mathrm{d}\tau$$

$$+ \int_{-\infty}^{t} \phi_2(t-\tau)\,\dot{\mathbf{C}}_t(\tau)\,\mathrm{d}\tau\,\mathbf{B}^2 + \mathbf{B}\int_{-\infty}^{t} \phi_3(t-\tau)\,\dot{I}_1(\tau)\,\mathrm{d}\tau \quad (5.12)$$

In this relation

$$\mathbf{B} = \mathbf{F}(t)\,\mathbf{F}^T(t),$$
$$\mathbf{C}_t(\tau) = \mathbf{F}_t^T(\tau)\,\mathbf{F}_t(\tau), \qquad \mathbf{F}_t(\tau) = \left|\left|\,\partial x_i(\tau)/\partial x_j\,\right|\right| \quad (5.13)$$

and the dot denotes the material derivative. $\mathbf{F}$ and I_1 have been defined previously.
Since the material was assumed to have a fading memory, it was appropriate
to define the strain history $\mathbf{C}_t$ in terms of the gradients of the deformation with
respect to the present configuration.

In (5.12) the material properties are represented by the constants ϕ, ξ and ψ
and the relaxation functions ϕ_i. The constants may be determined from the long-
time equilibrium behaviour of the material in a uniaxial stress-relaxation test,
and Lianis showed that the ϕ_i could be determined in simple extension, strip-
biaxial tension, homogeneous biaxial tension, and simple torsion tests of the
stress-relaxation type. In principle only two of these types of experiments are
necessary to determine the ϕ_i. It has been shown [39] that the experimental
results of Mullins [40], for peroxide vulcanizates of natural rubber, and of [35]
compare favourably with the predictions of the simplified constitutive relation
(5.12).

Lianis [39] has also used (5.12) to discuss the superposition of small dynamic
strains onto large static deformations. He has shown that measurement of the
real and imaginary parts of the complex modulus for axial vibrations of a pre-
strained bar yield information about the functions ϕ_i. Again comparison of
actual experimental results (obtained by Mason [41] using natural rubber)
confirm the adequacy of (5.12) for the situations investigated.

5.4. Vibrational Response of Nonlinear Materials

Finally we mention an experimental method which is not of the creep or
stress-relaxation type, but which employs a constitutive relation of the type (3.11).

For linear viscoelastic behaviour the mechanical properties of a material can be determined by subjecting it to sinusoidally time-dependent stresses or strains, and measuring the corresponding strain or stress response. The magnitude and phase of the response, measured as functions of frequency, are sufficient to determine the material properties.

An analogous analysis has been given by Lockett and Gurtin [42] for one-dimensional nonlinear behaviour described by (3.11). Complex compliances or complex moduli of orders higher than the first are introduced, and it is shown that these functions can be determined in vibration experiments in which the inputs have a number of frequency components, e.g.

$$\epsilon(t) = \sum_{n=1}^{N} A_n \sin(\omega_n t) \qquad (5.14)$$

We are not aware of any experimental investigation using this analysis. In fact it is possible that this form of vibration testing will not be suitable for testing nonlinear materials since the stress levels required to exhibit nonlinearity may result in sufficient energy dissipation to violate the assumption of isothermal behaviour.

6. VISCOMETRIC METHODS OF MEASUREMENT

6.1. Introduction

The most common types of apparatus used by the rheologist are various forms of viscometer: concentric cylinder (Couette), cone-and-plate, parallel plate, capillary, etc. These instruments are used to measure the viscosity of Newtonian fluids or the rate-dependent viscosity of non-Newtonian fluids, and in some cases provision has been made for measuring normal stress effects.

Methods of this type are particularly suitable for investigating the mechanical behaviour of liquids, and as a result of this fact most of the rational analyses of these instruments have used a fluid type of constitutive relation, for example (3.15). Some of the instruments mentioned above can be used to measure elastic effects (for example, recoil after removal of the load [43]), but no rational analyses of these effects appear to have been given.

However, the assumption of a fluid theory does not restrict application of the methods to liquids alone, since many solid-like materials exhibit the type of mechanical behaviour normally associated with fluids. This has been found to be the case for a number of solid propellant materials (see, for example [44]).

In addition to the restriction placed on the material by the adoption of a fluid theory, the type of material for which a given method is applicable also depends on the instrument which is used. In many cases an instrument which is designed for use with liquids can be adapted to handle solid types of material. Thus the Couette viscometer, which is used to investigate liquids, is equivalent to the rubber rheometer [45] and the Ward plastometer [46] which have been used to study solid-like materials including solid propellants [44, 46]. In what follows we shall

discuss methods in rather general terms, without dwelling upon their relative merits for use with liquids and solids.

Before proceeding to a discussion of more complete rational analyses, we shall mention a number of investigations which have been conducted on a partially rational basis, or for which no rational analysis has been given. We shall not attempt to cover all of the literature in this field, but shall mention only those papers which have some relevance to the main aims of the present paper. Descriptions of various forms of viscometer have appeared many times in the literature (see, for example, [43, 45, 47]) and a discussion of the formulation of constitutive relations, and of some experimental methods, has been given in [25, 48, 49].

Philippoff and Gaskins [50] have reported the results of experiments conducted with a conicylindrical viscometer using molten samples of polyethylene and plasticized polyvinylbutyral. Their experiments were conducted at temperatures in the range 108–230°C and at shear rates of $5 \times 10^{-5} - 10^3$ sec^{-1}. Non-Newtonian behaviour at the higher shear rates was demonstrated by plots of shear stress versus rate of shear. The same authors [51] have also discussed a number of approximate theories for the capillary viscometer, and have compared them with some of the available experimental data.

Results obtained using a number of different types of viscometer with various solutions of Cellulose derivatives have been compared by Brodnyan et al. [52], and they have shown that the results are consistent if the data are treated properly. An instrument has been described by Hoppmann and Miller [53] which consists of a container into which one of a number of rotating "flow generators" can be immersed (the Couette and cone-and-plate viscometers are special cases). Provision is made for visualization of the streamlines of the motion, and it is suggested that measurements of the secondary flow can be used to deduce material properties. No analysis of this worthwhile suggestion is yet available.

An investigation into the flow characteristics of a number of asphalts using a rotational viscometer was made by Gaskins et al. [54]. They measured creep under constant load and recovery upon removal of the load, and deduced the viscosity of the material using a linear theory. This experimental technique may be used to investigate nonlinear material behaviour if a suitable analysis is made available.

Finally we mention three types of viscometer which are in use, but which require more exact analyses if they are to be of significant value in the study of nonlinear behaviour. McCabe [55] and McCabe and Mueller [56] describe a rotational plastograph and a capillary rheometer for use with elastomers under conditions which approximate those of manufacturing processes.

It has been suggested by West [57] that the (low shear rate) viscosity of highly viscous materials may be deduced from the slump under gravity of a cylindrical specimen which is supported only on its vertical curved surface. If a more precise analysis is produced, this method may be of interest in the solid pro-pellant field, due to the analogy with the problem of vertical storage of rocket motors under gravitational loading. An indication of this possibility has been

given by Vernon *et al.* [58] who have subjected model rocket-motors to simulated vertical loadings of several-*g* in centrifuge tests.

6.2. *Characterization of Bingham Materials*

We shall now consider a fluid for which the stress depends on only the first kinematic matrix A_1. In theories of this kind A_1, is often denoted by d or D. The stress may then be expressed in terms of D and its invariants, or, alternatively D may be expressed as a function of σ and its invariants. We consider a particular empirical form which is based on a plastic yield condition, and which has been found to be useful in characterizing some real materials. For an incompressible Bingham material

$$
\left.
\begin{aligned}
2\mu D &= \left(1 - \frac{\tau_c}{\theta}\right)s, \qquad \theta \geqslant \tau_c \\
D &= 0, \qquad\qquad\quad \theta \leqslant \tau_c
\end{aligned}
\right\}
\tag{6.1}
$$

where τ_c and μ are constants, $\theta = (\frac{1}{2}\,\mathrm{tr}\,s^2)^{1/2}$, and s is the deviatoric stress matrix. Consequently, for this material, no flow occurs until the invariant reaches a critical value, and flow takes place with constant viscosity thereafter.

The material constants can be determined by Couette or capillary viscometry [59] or by using a cone-and-plate instrument [60]. In the second paper Boardman and Whitmore [60] included a Newtonian boundary layer and showed that the Bingham properties can be determined from viscometric measurements. The boundary layer is claimed to model inhomogeneities which are found in practice to occur next to the boundaries. The theory was shown to be qualitatively correct for china clay suspensions, but no quantitative verification is yet available.

Slibar and Paslay [61] considered a Bingham material for which the constant τ_c is replaced by the function

$$
\tau_c = \tau_1 - \frac{L(\tau_1 - \tau_0)}{\beta + L}
\tag{6.2}
$$

where

$$
L = \int_{-\infty}^{t} \mathrm{tr} D^2(\xi)\, e^{-\alpha(t-\xi)} d\xi
\tag{6.3}
$$

Thus the critical stress τ_c is assumed to have a particular form of dependence on the past history of deformation. The authors claim that the material constants μ, β, τ_0, τ_1 and α can be determined from the analysis of Couette [61] and capillary [62] viscometers, but they do not indicate explicitly how this would be done.

Vernon [44] has investigated the mechanical properties of a number of plastic solid propellants using a Ward plastometer. He found that the shear stress and shear strain rate were connected by a relation of the Bingham type, but the behaviour was not adequately represented by (6.1) or (6.2). The results show that both the viscosity and the yield stress are rate-dependent.

6.3. *Measurement of Normal Stress Effects*

Finally we shall look at a number of analyses which have been based on the constitutive relation for simple fluids. An approximation which yields a more tractable theory, and which might be of some practical importance, is the specialization of the theory to slow steady flows. In this theory (see Langlois and Rivlin [63]) the velocity field is assumed to be small and only terms up to a certain order in the velocity are retained in the theory. Thus, in the second order theory for steady flow of an incompressible fluid, the constitutive relation has the simple form

$$\sigma + p\mathbf{I} = \eta\mathbf{A}_1 + \beta\mathbf{A}_1^2 + \gamma\mathbf{A}_2, \qquad (6.4)$$

where p is a hydrostatic pressure and η, β and γ are material constants. Coleman and Markovitz [64, 65] have shown that combinations of these material constants can be determined in experiments conducted with Couette, capillary, parallel plate and cone-and-plate viscometers—provided that certain normal stresses can be measured. Thus the difference in the values of the radial stresses at the two cylinders must be measured in the Couette viscometer experiment and in the case of axial flow between concentric cylinders. Similarly the experimenter must measure the difference of the normal pressures on the discs in the parallel disc experiment, and the variation of the normal stress over the plate in the cone-and-plate experiment. If experiments are conducted with all of the viscometers mentioned above, then the constants η, β and γ are overdetermined, and some cross checking may be made. In [65] the values of β and γ were deduced from the parallel disc and Couette measurements of Markovitz and Brown [66] for polyisobutylene–cetane solutions, and the calculated values compared favourably with the value of $\beta + \gamma$ obtained from cone-and-plate data. Markovitz and Coleman [65] have also shown that γ may be determined by measuring normal stress effects for a second-order non-steady flow in simple shear.

Infinitesimal dynamic perturbations of slow steady flows of arbitrary order have been investigated by Lockett [67] with the third order theory for perturbation of viscometric flows considered in detail. The relevant mechanical properties of the material are characterized by two infinite sets of constants, and it is shown that, in principle, a finite number (which depends on experimental accuracy) of these constants may be determined using a modified form of Couette viscometer or Ward plastometer. In the experiments the material is constrained in the axial direction by a set of annular rings, and a perturbation of the Couette flow is imposed by a small time-dependent component of the applied torque. It is necessary to measure the velocity profile of the basic undisturbed Couette flow, and the radial and axial stresses at the stationary cylinder. No experiments have yet been conducted along these lines, but the theory offers a rational extension to the experiments which have been performed.

Markovitz and Williamson [68] have made normal stress measurements with polyisobutylene solutions in a cone-and-plate instrument. Using manometers at various radial distances across the plate they were able to plot the normal stress as a function of radial distance. Their results were shown to be in agree-

ment with the second order theory (6.4), and comparisons with the implications of other theories were made. Experimental results obtained by Greensmith and Rivlin [69] with high polymer solutions in a parallel plate instrument also support the theory (6.4). A detailed description of their careful experimentation is given in [69].

It has been shown (for example, [70, 71]) that for a number of very general types of incompressible fluid, including Rivlin–Ericksen fluids, the material properties which are relevant to the class of steady laminar viscometric flows can be represented by three functions of the rate of shear. One of these functions is the rate-dependent viscosity commonly measured by rheologists, and the other two are measures of normal stress effects. In fact, with suitable choices of coordinates, the deviatoric stress matrix s may be expressed, for these viscometric flows, in the form [66]

$$s_{12} = \dot{\gamma}\eta(\dot{\gamma}), \qquad s_{23} = s_{13} = 0, \qquad s_{ii} = -\nu_i(\dot{\gamma}) \tag{6.5}$$
$$(i = 1, 2, 3, \text{ indices not summed})$$

where $\dot{\gamma}$ is the rate of shear for the appropriate geometry, η is the rate-dependent viscosity, and only two of the functions ν_i are independent since $\nu_1 + \nu_2 + \nu_3 = 0$.

Since the functions ν_i are even functions which vanish at zero rate of shear, they may be approximated at low shear rates by

$$\nu_i = k_i \dot{\gamma}^2 \tag{6.6}$$

where k_i are constants. Markovitz and Brown [66] have shown that k_i can be determined from normal stress measurements obtained with parallel disc and cone-and-plate instruments, using polyisobutylene-cetane solutions in their experiments. The constants k_i may also be evaluated in terms of the material constants of the second order fluid (6.4).

Markovitz and Brown also note that the function ν_3 (corresponding to the normal stress in the neutral direction) can be determined as a function of rate of shear from normal stress measurements in the cone-and-plate experiment, provided that inertia effects are negligible and that the angle between cone and plate is small. It has been suggested that the other independent function ν_i may be simply proportional to ν_3, but the experimental results of [66] contradict this hypothesis for the fluids investigated. In general the second normal stress function must be measured by some other rational means. The rate-dependent viscosity η may of course be determined from torque/angular velocity measurements with any of the rotational viscometers.

Finally we note that a number of authors have used constitutive relations which are generalizations of the differential form of the linear viscoelastic relation:

$$\left(a_0 + a_1 \frac{\partial}{\partial t} + a_2 \frac{\partial^2}{\partial t^2} + \ldots\right) \sigma = \left(b_0 + b_1 \frac{\partial}{\partial t} + b_2 \frac{\partial^2}{\partial t^2} + \ldots\right) \epsilon, \ldots \tag{6.7}$$

in which a_i and b_i are constants. Generalizations to nonlinearity have been obtained by replacing the partial time-derivatives by material or convected

23

derivatives (see Oldroyd [72–74] and Markovitz [75]). Analyses of viscometric flows based on this type of model have been given by Williams and Bird [76] and others.

7. CONCLUSIONS

The mechanical properties of incompressible elastic materials can be represented by a single function $W(I_1, I_2)$, and a rational approach to the determination of this function leads to a feasible set of experiments. For some materials the experimental results may indicate a form of strain energy function which is just as simple as empirical relations chosen on a less rigorous basis.

In contrast, representation of nonlinear viscoelastic behaviour by one of the general theories necessitates an experimental program which may be prohibitively large. Attention should therefore be directed towards the representation of behaviour under certain special conditions, such as "slow" motion, stress-relaxation for constant deformation, creep under constant load, etc. However, it is valuable to view such results in the context of the general theory so that, as more situations are investigated, a better understanding of the general behaviour is developed.

REFERENCES

[1] FINNIE, I., *Applied Mechanics Reviews*, **13**, 705 (1960).
[2] GREEN, A. E. and RIVLIN, R. S., *Arch. Rat. Mech. Anal.*, **1**, 1 (1957).
[3] GREEN, A. E., RIVLIN, R. S. and SPENCER, A. J. M., *Arch. Rat. Mech. Anal.*, **3**, 82 (1959).
[4] GREEN, A. E. and RIVLIN, R. S., *Arch. Rat. Mech. Anal.*, **4**, 387 (1960).
[5] RIVLIN, R. S. and ERICKSEN, J. L., *J. Rat. Mech. Anal.*, **4**, 323 (1955).
[6] NOLL, W., *Arch. Rat. Mech. Anal.*, **2**, 197 (1958).
[7] LOCKETT, F. J., *Int. J. Eng. Sci.*, **3**, 57 (1965).
[8] PIPKIN, A. C., *Proc. Princeton Univ. Conf. on Solid Mechanics* (1963).
[9] RIVLIN, R. S., *J. Rat. Mech. Anal.*, **4**, 681 (1955).
[10] SPENCER, A. J. M. and RIVLIN, R. S., *Arch. Rat. Mech. Anal.*, **2**, 309 (1959).
[11] SPENCER, A. J. M. and RIVLIN, R. S., *Arch. Rat. Mech. Anal.*, **2**, 435 (1959).
[12] SPENCER, A. J. M. and RIVLIN, R. S., *Arch. Rat. Mech. Anal.*, **4**, 214 (1960).
[13] RIVLIN, R. S., *J. Appl. Math. Phys. (ZAMP)*, **13**, 589 (1962).
[14] RIVLIN, R. S., *Proc. First Symp. Naval Struct. Mech.*, Pergamon, p. 169 (1960).
[15] WILLIAMS, M. L., BLATZ, P. J. and SCHAPERY, R. A., *GALCIT–SM–61–5* (1961).
[16] WILLIAMS, M. L., *Amer. Inst. Aero. Astro. Journal*, **2**, 785 (1964).
[17] DONG, S. B., HERRMANN, L. R., PISTER, K. S. and TAYLOR, R. L., *Inst. Eng. Res.*, Univ. Calif., Berkeley, Series 100, Issue 18, (1962).
[18] WIEGAND, J. H., Aerojet-General Corp., Rept. 0411–10Q–2 (1961).
[19] RIVLIN, R. S. and SAUNDERS, D. W., *Phil. Trans. A*, **243**, 251 (1951).
[20] RIVLIN, R. S. and SAUNDERS, D. W., *Trans. Faraday Soc.*, **48**, 200 (1952).
[21] RIVLIN, R. S., *J. Appl. Phys.*, **18**, 444 (1947).
[22] GENT, A. N. and RIVLIN, R. S., *J. Polymer Sci.*, **28**, 625 (1958).
[23] TRELOAR, L. R. G., *The Physics of Rubber Elasticity*, Clarendon Press, Oxford (1958).
[24] GREEN, A. E. and ADKINS, J. E., *Large Elastic Deformations*, Clarendon Press, Oxford (1960).
[25] ERINGEN, A. C., *Nonlinear Theory of Continuous Media*, McGraw Hill, New York (1962).

[26] MOONEY, M., *J. Appl. Phys.*, **11**, 582 (1940).
[27] CARMICHAEL, A. J. and HOLDAWAY, H. W., *J. Appl. Phys.*, **32**, 159 (1961).
[28] TRELOAR, L. R. G., *Rubber Chem. and Technol.*, **17**, 813 (1944).
[29] BLATZ, P. J. and KO, W. L., *Trans. Soc. Rheol.*, **6**, 223 (1962).
[30] SPENCER, A. J. M., *Proc. IUTAM Conf. Second Order Effects in Elasticity, Plasticity and Fluid Dynamics*, Haifa 1962, Pergamon, p. 200 (1964).
[31] BERGEN, J. T., MESSERSMITH, D. C. and RIVLIN, R. S., *J. Appl. Poly. Sci.*, **3**, 153 (1960).
[32] LEADERMAN, H., *Trans. Soc. Rheol.*, **6**, 361 (1962).
[33] LEADERMAN, H., MCCRACKIN, F. and NAKADA, O. *Trans. Soc. Rheol.*, **7**, 111 (1963).
[34] WARD, I. M. and ONAT, E. T., *J. Mech. Phys. Solids*, **11**, 217 (1963).
[35] BERNSTEIN, B., KEARSLEY, E. A. and ZAPAS, L. J., *Trans. Soc. Rheol.*, **7**, 391 (1963).
[36] COLEMAN, B. D. and NOLL, W., *Rev. Mod. Phys.*, **33**, 239 (1961).
[37] LIFSHITZ, J. M., Brown Univ., Div. of Appl. Math., Report Nonr 562 (30)/10 (1964).
[38] ONARAN, K. and FINDLEY, W. N., *Proc. Joint. Internat. Conf. on Creep* (1963).
[39] LIANIS, G., Purdue Univ., Report A & ES 63-11 (1963).
[40] MULLINS, L., *J. Appl. Polymer Sci.*, **2**, 257 (1959).
[41] MASON, P., *J. Appl. Polymer Sci.*, **1**, 63 (1959).
[42] LOCKETT, F. J. and GURTIN, M. E., Brown Univ., Div. of Appl. Math., Report Nonr 562 (30)/7 (1964).
[43] GASKINS, F. H. and PHILIPPOFF, W., *J. Appl. Poly. Sci.*, **2**, 143 (1959).
[44] VERNON, J. H. C., *Bull. Third Meeting ICRPG Working Group on Mech. Behav.*, **1**, 153 (1964).
[45] MOONEY, M., *Rheology* (Ed: F. R. Eirich), Academic Press, New York, Vol. II, pp. 181–232 (1958).
[46] FREEMAN, P. R., THOMAS, A. J. B. and VERNON, J. H. C., Ministry of Aviation, E.R.D.E. Tech. Memo. 12/M/60 (1960).
[47] OKA, S., *Rheology* (Ed: F. R. Eirich), Academic Press, New York, Vol. III, pp. 17–82 (1960).
[48] TRUESDELL, C. *Trans. Soc. Rheol.*, **4**, 9 (1960).
[49] TRUESDELL, C. *Proc. IUTAM Conf. Second Order Effects in Elasticity, Plasticity and Fluid Dynamics*, Haifa 1962, Pergamon, p. 1 (1964).
[50] PHILIPPOFF W. and GASKINS, F. H., *J. Poly. Sci.*, **21**, 205 (1956).
[51] PHILIPPOFF, W. and GASKINS, F. H., *Trans. Soc. Rheol.*, **2**, 263 (1958).
[52] BRODNYAN, J. G., GASKINS, F. H., PHILIPPOFF, W. and LENDRAT, E. G., *Trans. Soc. Rheol.*, **2**, 285 (1958).
[53] HOPPMANN II, W. H. and MILLER, C. E., *Trans. Soc. Rheol.*, **7**, 181 (1963).
[54] GASKINS, F. H., BRODNYAN, J. G., PHILIPPOFF, W. and THELEN, E., *Trans. Soc. Rheol.*, **4**, 265 (1960).
[55] MCCABE, C. C., *Trans. Soc. Rheol.*, **4**, 335 (1960).
[56] MCCABE, C. C. and MUELLER, N. N., *Trans. Soc. Rheol.*, **5**, 329 (1961).
[57] WEST, D. C., *Trans. Soc. Rheol.*, **6**, 81 (1962).
[58] COOKE, S., SPICKERNELL, G. J., TREADGOLD, A. R. and VERNON, J. H. C., Ministry of Aviation, E.R.D.E. Report 3/R/65 (1965).
[59] PASLAY, P. R. and SLIBAR, A., *Trans. Soc. Rheol.*, **2**, 255 (1958).
[60] BOARDMAN, G. and WHITMORE, R. L., *Brit. J. Appl. Phys.*, **14**, 391 (1963).
[61] SLIBAR, A. and PASLAY, P. R., *J. Appl. Mech.*, **30**, 453 (1963).
[62] PASLAY, P. R. and SLIBAR, A., *Ingenieur-Archiv.*, **32**, 66 (1963).
[63] LANGLOIS, W. E. and RIVLIN, R. S., *Rend. di Matematica*, **22**, 169 (1963).
[64] COLEMAN, B. D. and MARKOVITZ, H., *J. Appl. Phys.*, **35**, 1 (1964).
[65] MARKOVITZ, H. and COLEMAN, B. D., *Advances in Solid Mechanics*, Academic Press, New York, pp. 69–101 (1964).
[66] MARKOVITZ, H. and BROWN, D. R., *Trans. Soc. Rheol.*, **7**, 137 (1963).
[67] LOCKETT, F. J., *Int. J. Eng. Sci.* (to appear).
[68] MARKOVITZ, H. and WILLIAMSON, R. B. *Trans. Soc. Rheol.*, **1**, 25 (1957).
[69] GREENSMITH, H. W. and RIVLIN, R. S., *Trans. Roy. Soc.*, A245, 399 (1953).
[70] COLEMAN, B. D. and NOLL, W. *Arch. Rat. Mech. Anal.*, **3**, 289 (1959).
[71] MARKOVITZ, H., *Trans. Soc. Rheol.*, **1**, 37 (1957).
[72] OLDROYD, J. G., *Rheology* (Ed: F. R. Eirich), Academic Press, New York, Vol. I, pp. 653–682 (1956).

[73] OLDROYD, J. G., *Proc. Roy. Soc.*, **A245**, 278 (1958).
[74] OLDROYD, J. G., *Proc. IUTAM Conf. Second Order Effects in Elasticity, Plasticity and Fluid Dynamics*, Haifa 1962, Pergamon, p. 699 (1964).
[75] MARKOVITZ, H., *Trans. Soc. Rheol.*, **6**, 349 (1962).
[76] WILLIAMS, M. C. and BIRD, R. B., *Ind. Eng. Chem., Fund.*, **3**, 42 (1964).

EXPERIMENTAL STUDIES OF THE MECHANICAL BEHAVIOR OF LINEAR VISCOELASTIC SOLIDS

H. KOLSKY

Brown University, Providence, R.I.

Abstract—In order to characterize the linear viscoelastic behavior of a material, measurements must be made over a wide range of time scales. In considering the response to stresses varying sinusoidally with time, frequencies from one cycle per hour to tens of megacycles per second should be covered; and in creep and stress relaxation measurements, the time scale is further extended to months or even years. Thus an extremely large number of different experimental techniques have to be used; these are reviewed and discussed in this paper. In addition the representation of these experimental results by various mathematical and mechanical models is considered, and the relation between chemical composition and viscoelastic properties is briefly discussed. Finally, recent experimental work on the propagation of stress waves in viscoelastic solids is described particularly from the point of view of the results obtained on the dilatational viscosity of some high polymers.

1. INTRODUCTION

During the last two decades a considerable amount of work has been done on measuring the mechanical properties of linear viscoelastic solids, and there is now an extensive literature [1–4] which describes the results of these measurements and the experimental techniques which have been used to make them. This paper is not intended to review the entire field of experimental work on viscoelastic solids but rather to discuss the relative usefulness of the various types of measurement and the experimental problems associated with the different techniques.

The subjects discussed in an article of this sort are necessarily influenced by the particular interests of the writer, and in this paper the propagation of stress waves in viscoelastic solids is given some prominence as this is a subject in which there have been some interesting experimental developments and one with which the present author is especially familiar.

The purpose of carrying out experimental investigations on viscoelastic solids has been twofold. The first aim has been to define the mechanical properties of plastics and other high polymers in order either to be able to predict the deformations produced in mechanical structures which contain such viscoelastic elements when forces are applied to them, or alternatively to determine the stresses which are set up when the structure is deformed in a prescribed manner. The second aim has been to study the relation between the mechanical properties and the chemical and molecular structure of high polymers in order to achieve a better understanding of viscoelastic behavior on a microscopic level and

ultimately to predict the type of mechanical behavior which corresponds to particular molecular configurations. Up to the present the first aim has met with very much more success than the second. Most of the present paper will be devoted to measurements concerned with the stress analysis applications of the subject, but some discussion of the molecular aspects of viscoelastic behavior will also be included.

In one-dimensional problems in viscoelastic stress analysis there is only one relevant stress component σ and one strain component ϵ. The problem is then to find the stress history $\sigma(t)$ when the strain history $\epsilon(t)$ is given or vice versa. Now since for a linear viscoelastic solid the principle of superposition holds, we have that if $\epsilon(t)$ is expressed as the sum of a set of 'component' functions

$$\epsilon(t) = \epsilon_1(t) + \epsilon_2(t) + \ldots + \epsilon_n(t)$$

then

$$\sigma(t) = \sigma_1(t) + \sigma_2(t) + \ldots + \sigma_n(t) + \ldots$$

where $\sigma_1(t)$ is the stress history corresponding to $\epsilon_1(t)$, $\sigma_2(t)$ corresponds to $\epsilon_2(t)$ and $\sigma_n(t)$ corresponds to $\epsilon_n(t)$.

Thus, if we know the relation between $\sigma_n(t)$ and $\epsilon_n(t)$ for each of these functions, we can find $\sigma(t)$ for any given $\epsilon(t)$ or vice versa. There are of course a number of such standard component functions which could be conveniently chosen and much of the present article is concerned with how the mechanical response to such standard loadings or deformations can be measured experimentally over sufficiently wide ranges of time to enable the problems of static and dynamic viscoelastic stress analysis to be solved.

When we come to three-dimensional problems in isotropic viscoelastic solids, the situation is complicated by the fact that, in general, two distinct viscoelastic types of behavior have to be taken into account. These are the viscoelastic response of the material for shear deformation, and the dilatational response associated with volume changes.

In classical elasticity the relation between the stress tensor, σ_{ij}, and the strain tensor, ϵ_{ij}, for an isotropic solid is

$$\sigma_{ij} = 2\mu\epsilon_{ij} + (K - \tfrac{2}{3}\mu)\,\epsilon_{kk}\delta_{ij} \tag{1}$$

where μ is the shear modulus, K is the bulk modulus and δ_{ij} is the Kronecker delta ($\delta_{ij} = 1$, $i = j$; $\delta_{ij} = 0$, $i \neq j$). We may rewrite (1) in terms of the stress and strain deviators thus

$$s_{ij} = \sigma_{ij} - \tfrac{1}{3}\sigma_{kk}\delta_{ij}$$

and

$$e_{ij} = \epsilon_{ij} - \tfrac{1}{3}\epsilon_{kk}\delta_{ij}.$$

Then we have

$$s_{ij} = 2\mu e_{ij} \tag{2}$$

and

$$\sigma_{ii} = Ke_{ii}. \tag{3}$$

In linear viscoelasticity we may consider the three dimensional deformation of an element in terms of its deviatoric and dilatational strains and then express

s_{ij} and σ_{ii} as a sum of separate standard functions of time as we have done in the one-dimensional case. If we know the response to such standard loadings, we can then use the principle of superposition to determine the stress history from the strain history or vice versa.

Perhaps the simplest standard function $\epsilon(t)$ is a deformation which varies sinusoidally with time at a constant angular frequency p. Then if $\epsilon(t) = A \cos pt$, $\sigma = E^*A \cos(pt - \delta)$; or in complex notation if

$$\epsilon(t) = A \exp(ipt), \qquad \sigma(t) = (E_1 + iE_2) A \exp(ipt)$$

where $E^{*2} = E_1^2 + E_2^2$ and $\tan \delta = E_2/E_1$; $E_1 + iE_2$ is called the complex elastic modulus.

Thus if the strain history is expressed as a Fourier sum

$$\epsilon(t) = \Sigma A_n \exp(inp_0 t)$$

then

$$\sigma(t) = \Sigma A_n (E_1 + iE_2)_n \exp(inp_0 t)$$

where $(E_1 + iE_2)_n$ in each term of the series has the value measured at an angular frequency np_0; or if we express $\epsilon(t)$ as a complex Fourier integral

$$\epsilon(t) = \int_0^\infty A_p \exp(ipt)\, dp$$

(where A_p is in general complex) then

$$\sigma(t) = \int_0^\infty A_p(E_1 + iE_2) \exp(ipt)\, dp$$

E_1 and E_2 being functions of p which have to be determined experimentally. [We can of course equally well determine the strain history from the stress history; thus,
if

$$\sigma(t) = \int_0^\infty B_p \exp(ipt)\, dp$$

then

$$\epsilon(t) = \int_0^\infty B_p\, (J_1 + iJ_2) \exp(ipt)\, dp$$

where $J_1 + iJ_2$ is the complex compliance: $J_1 + iJ_2 = 1/(E_1 + iE_2)$.]

Another method of describing the response of a linear viscoelastic solid to an arbitrary stress history is in terms of the stress relaxation functions $\bar{\psi}(t)$. $\sigma(t)$ is here decomposed in terms of a set of step functions. Thus if the material is suddenly strained by an amount ϵ_τ at time $t = \tau$, the stress σ_t at time t is given by

$$\sigma_t = \epsilon_\tau \bar{\psi}(t - \tau).$$

If the strain history is $\epsilon(t)$, the stress history can, by the principle of superposition, be expressed as

$$\sigma(t) = \int_{-\infty}^{t} \bar{\psi}(t - \tau) \frac{d\epsilon(\tau)}{d\tau} \, d\tau.$$

Alternatively this can be expressed as

$$\epsilon(t) = \int_{-\infty}^{t} \psi(t - \tau) \frac{d\sigma(\tau)}{d\tau} \, d\tau$$

where $\psi(t)$ is the creep function and gives the value of the strain produced by a unit step function in stress at time t where constant unit stress is suddenly applied to the material at time $t = 0$ and maintained.

Another form of Boltzmann's superposition principle is in terms of the response of the material to a unit Dirac delta function in stress or strain. Thus if $F(t - \tau)$ is the strain produced by unit delta function loading at time $t = \tau$, we have

$$\epsilon(t) = \int_{-\infty}^{t} F(t - \tau) \, \sigma(\tau) \, d\tau$$

A similar expression for stress in terms of strain can be written in terms of the response to a delta function deformation strain. From a practical point of view the response to such delta function loading is in general of less interest than the response to step loading, although it will be shown later that this concept is of value in some wave propagation problems.

It should be emphasized that all the foregoing discussion of one dimensional response can be extended to three-dimensional problems if the viscoelastic behavior of the material in both shear and dilatation is known.

2. EXPERIMENTAL

In engineering problems the range of total loading times which are of interest can extend from a few microseconds (the duration of a sharp impact), to many years or decades (the periods for which civil engineering structures must withstand stresses). In order to predict the response of structures to arbitrary loadings of these total durations, the response to standard loadings (of the type described earlier) must be known over even wider ranges of times. Thus, for example, the impact of a small steel ball on a viscoelastic block may have a total duration of 50 μsec, but in order to calculate the stresses set up in the block as a result of the impact with any degree of accuracy in terms of complex moduli, the response of the material at frequencies as high as 1 Mc/s must be known. Therefore, in order to specify the mechanical properties of a viscoelastic material for use in stress analysis problems, measurements may have to be made over a range of times where the longest time is 10^{14} times as great

as the shortest time; and if the purpose of the measurements is to study the relation between mechanical properties and molecular structure, the response of the material for very much shorter loading times (fractions of a microsecond) may be of interest, so that in this case an even wider range of frequencies have to be investigated.

This enormous range of time-scales which have to be investigated experimentally means that a whole range of different experimental techniques have to be employed to study the mechanical response of these materials. The principles underlying these methods are outlined below.

As mentioned in the Introduction, the most usual standard loadings are step functions in stress and strain and sinusoidal oscillations. By applying a step function deformation and observing how the stress changes with time, the relaxation function $\bar{\psi}(t)$ is found. Alternatively the deformation produced by a constant stress measured as a function of time gives the creep function $\psi(t)$. When the specimen is introduced into a mechanical system which is oscillating at a constant frequency, the complex modulus can be measured. This can be done in a number of ways as described below.

3. CREEP MEASUREMENTS

The experimental requirement here is to apply a constant stress to the specimen and measure the strain. When the strains are sufficiently small and the times of interest are reasonably long ($>$ 10 sec), the measurements involve no particular difficulties and can be carried out with comparatively simple test apparatus. In uniaxial creep tests when the strain is no longer sufficiently small for the cross-sectional area to be considered constant throughout the test, the load must be lowered in order to keep the stress constant.   This can be done in a number of ways, among the simplest of which is that employed by Andrade [5]. The principle of this method is to use a suitably shaped loading weight which is lowered into water as the deformation increases.

In order to carry out creep measurements for times less than one second, two problems arise: the first is to find a method of applying a constant load sufficiently rapidly and to do so without setting the system into oscillation; the other difficulty is the recording of the strains in very short times.

When creep measurements are carried out in shear, the problem of changing cross section does not arise. Figure 1 shows schematically the experimental arrangements used by Benbow [6] for measuring the torsional creep in rods of viscoelastic solids. In order to apply the load rapidly an electromagnetic method is used. A light coil of wire is fitted to the end of the specimen and a direct current is suddenly passed through it. The coil is in the field of a strong permanent magnet and the time of application of the torque is limited only by the electrical inductance of the coil. In the experiments, the shortest time over which creep measurements could be made was limited by the mechanical inertia of the specimen and the coil attached to it. When the direct current was first applied, the specimen performed a few heavily damped torsional oscillations. During

the time that these oscillations were of finite amplitude, the value of the strain had to be inferred from the mean value of the displacement. The torsional strain was measured by recording the rotation of a small mirror which was attached to the specimen and which reflected a collimated light beam. For times less than 10 sec the rotation was recorded photographically, whereas for times greater than this the rotations were measured visually on a graduated scale about 1 m from the mirror. Benbow was able to use this apparatus to determine creep curves for a single specimen for times between 0.04 sec to 12 hr.
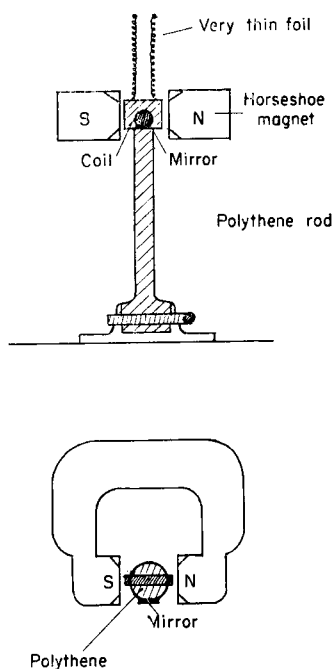
FIG. 1. Apparatus for measurements of torsional creep (after Benbow [6]).

4. STRESS RELAXATION MEASUREMENTS

The principal difficulty in determining the stress relaxation function for a viscoelastic solid is that this involves keeping the specimens at constant length and at the same time measuring the strain. Thus if the stress is produced by the extension of a spring connected in series with the specimen, the relaxation of stress in the specimen results in a shortening of the spring and a lengthening of the specimen. One method of overcoming the difficulty is to use a stress measuring device which is very much stiffer than the specimen so that the change in length can be neglected. Another method is to employ a servomechanism which will restore the specimen to its original length as the stress relaxes. A simpler method is to load the specimen with weights and maintain the length of the specimen constant by removing weights as the stress in the specimen

relaxes. Electrical contacts can be used to indicate that the length of the specimen has been restored to a length which does not differ from its proper value by more than some small pre-determined amount. Stein and Tobolsky [7] describe the use of such an apparatus.

5. SINUSOIDAL OSCILLATIONS

The lower limit of time over which creep and stress-relaxation measurements can be made is determined by the inertia of the specimen and its associated loading system. The extent to which the size of the specimen and the inertia of the system can be reduced is limited. Benbow's measurements of creep 40 milliseconds after the load had been applied are probably close to the lower limit of time for which creep measurements can be made with simple loading apparatus. In order to investigate the mechanical properties of a viscoelastic solid for times substantially shorter than this, it is most convenient to employ sinusoidal deformation of the specimen and to measure the complex modulus as a function of frequency, rather than the creep function or the stress-relaxation function as functions of time. Although in any one experiment the properties at only one frequency are determined, the methods of measurement are in general much simpler and do not involve the high speed recording equipment which is required for short time creep or stress relaxation measurements.

There are three separate experimental methods for determining the complex modulus of a specimen in sinusoidal oscillation. These methods are termed forced oscillations, free oscillations and resonance respectively. In the method of forced oscillations a mechanical system drives the specimen in sinusoidal oscillation and the measurements that have to be made are the stress amplitude σ_0, the strain amplitude ϵ_0, and the phase angle δ between stress and strain. As shown in the introduction, the complex modulus can be determined from these quantities since σ_0/ϵ_0 is equal to $(E_1^2 + E_2^2)^{1/2}$ and $\tan \delta = E_2/E_1$.

This method can be used at frequencies where the inertia of the specimen and the associated apparatus can be ignored. Experimental arrangements which employ this method have been used by Lethersich [8], Markovitz et al. [9], and Benbow [10]. Figure 2 shows the apparatus used by Benbow, who employed it to measure the shear properties of rods of polymers and organic glasses at frequencies between one or two cycles per second and one cycle in several hours. As will be discussed later, since these measurements cover part of the same time range as that measured by the creep apparatus shown in Fig. 1 a direct comparison between the results can be made.

In the apparatus shown in Fig. 2 one end of the rod specimen was fixed at its lower end. At the upper end a sinusoidal force was applied by an oscillating torsion head through a metal wire of known torsional stiffness. The head was driven by a synchronous motor through a twelve-speed gear box and a harmonic transformer which converted the rotation into an oscillatory motion. The measurements were made by reflecting collimated light beams from two mirrors using conventional galvanometer lamp and scale systems. One of the mirrors

was attached to the torsion head and the other to the top of the specimen. The rotation of the latter gave the torsional strain of the specimen directly. The stress could be inferred from the difference between the angles of rotation of the two mirrors since this difference gave the torsional strain in the wire, the stiffness of which was known.
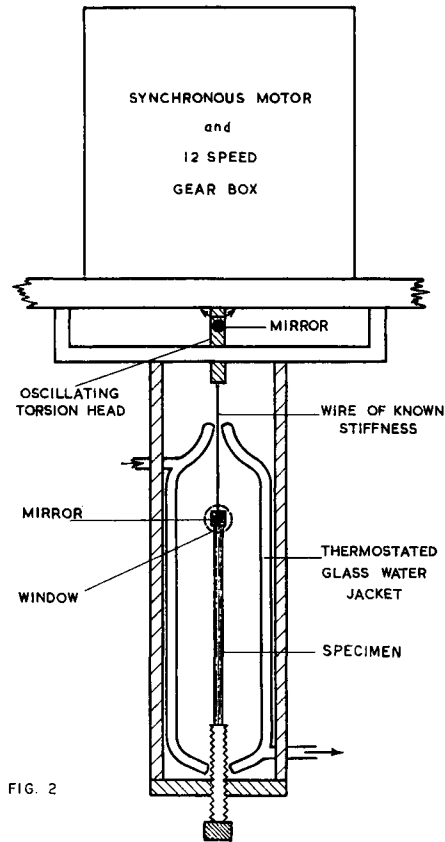
FIG. 2. Apparatus for low frequency forced torsional oscillations (after Benbow[10]).

The method of forced oscillation described above is convenient at frequencies which are very low compared with the natural frequencies of oscillation of the system. At frequencies which are comparable with these natural frequencies, i.e. at frequencies where the inertia of the loading system and of the specimen itself can no longer be neglected, methods which depend on free vibrations or on forced resonance must be employed. In the free vibration method either the specimen itself or the specimen loaded with suitable additional inertia is set into free vibration and the period of the vibrations and their rate of decay are measured. The rate of decay of the vibration is generally characterized by the logarithmic decrement Δ' which is defined as the natural logarithm of the

ratio of the amplitudes of two successive oscillations on the same side of the equilibrium position. When $E_2/E_1 < 0.1$, which is true for most hard polymers, the value of E_1 can be calculated from the period of the oscillation and the inertia of the vibrating system, and $\Delta' \simeq \pi E_2/E_1$ so that E_2 can then be found. Lethersich [8] and Benbow [10] describe a number of experimental methods for studying the free torsional oscillation of polymer specimens. Figure 3 shows diagrammatically a method used by Bodner and Kolsky [11] for measuring extensional and flexural vibrations of rod shaped specimens. The specimen which was freely suspended was set into vibration by passing an alternating current through the driving coil. The frequency of this alternating current was set as close as possible to the natural frequency of the rod and coils. The current was then switched off, and the amplitude and frequency of the free oscillation were measured by recording photographically the electrical output of the pick-up coil on a cathode ray oscillograph. Either extensional or flexural vibrations
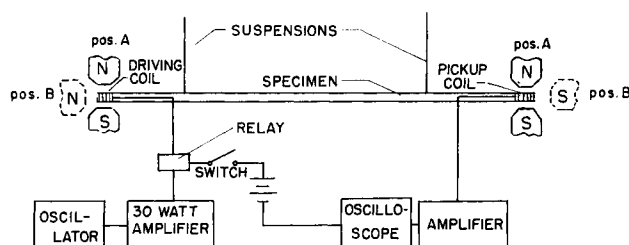
FIG. 3. Experimental arrangement for free vibration and resonance measurements.

may be set up depending on the direction of the magnetic field (in the diagram, positions A and B of the magnets correspond to flexural and extensional vibrations respectively) and the specimen may be excited in its fundamental mode or one of its higher harmonics. The deformations for both the flexural and extensional measurements correspond to simple extension so that the method enables the complex values of Young's modulus to be measured. By choosing the length and cross section of the specimen suitably the frequency ranges in the longitudinal and extensional measurements can be made to overlap, and a large range of frequency can be covered for a single specimen. In the work referred to above [11] a frequency range of 17–4500 c/s was covered in investigations on the viscoelastic properties of a lead bar. The lower frequency limit could be further decreased by attaching additional inertia to the ends of the bar.

The apparatus used for resonance measurements is similar to that employed for studying free vibration except that a carefully calibrated oscillator of variable frequency and constant amplitude is required. The driving frequency is varied. From the value of the frequency, N, which produces the maximum amplitude of vibration, the value of E_1 can be calculated as in the free vibration measurements. To find E_2 the two frequencies on either side of resonance at

which the amplitude of the vibrations has half the maximum value are determined. If these are N_1 and N_2, and if $E_2/E_1 \ll 1$ (in practice $E_2/E_1 < 0.1$), we may use the approximate relation

$$\sqrt{3}\,\frac{E_2}{E_1} \simeq \frac{N_2 - N_1}{N}.$$

The resonance method is generally simpler to use experimentally than the free vibration method and can be employed when the damping of the system is too high for free oscillations to occur. However, it has the disadvantage that the magneto-mechanical coupling between the driving coil and the magnetic field can cause large errors (cf. Davies and James [12] and Hillier [13]).

From a theoretical point of view there is a certain difficulty about the interpretation of the measurements both in the resonance and the free vibration methods. What is required are the values of E_2 and E_1 at a given frequency; in the resonance method, a range of frequencies is used to determine E_2. Fortunately the change in E_2 is very small over the comparatively narrow frequency range used in determining the resonance peak, and in most polymers the errors involved are negligible. With free oscillation a similar difficulty arises since the Fourier spectrum of a damped oscillation is not confined to a single frequency but contains components over a range of frequencies. Here again the error involved with real viscoelastic solids by neglecting this frequency spread is very small.

The lower limit of frequency for which free vibration methods can be used to study viscoelastic properties is of the order of one cycle in ten seconds. This involves using a small viscoelastic sample as the restoring element in a vibrating system containing large masses. The resonance method is not easily applicable at such low frequencies.

The upper limit of frequency for both the free vibration and resonance methods is set by the highest harmonic which can be excited in a specimen which has been as lightly loaded as possible. For viscoelastic solids frequencies of 10 or 20 kc/s are probably the highest that can be measured in this way.

6. WAVE PROPAGATION

Where the wavelength of mechanical waves becomes comparable with the dimensions of the specimen, the problem is one of wave propagation rather than of vibration. Since the velocity of stress waves in hard viscoelastic solids is of the order of 1000 m/sec, the frequencies at which the wavelength is of the order of 10 cm is 10 kc/s. In the free oscillation and resonance experiments described above, the highest frequencies used correspond to standing wave patterns in the specimens, but at even higher frequencies, standing wave techniques become difficult and methods employing travelling waves have to be used.

The values of E_1 and E_2 can be found from the phase velocity and the attenuation of a train of plane sinusoidal waves travelling through a linear viscoelastic medium. Thus if a plane wave of angular frequency p is travelling through a

viscoelastic solid and the stress σ_0 at the origin, $x = 0$, is given by

$$\sigma_0 = A \cos pt \tag{4}$$

then the stress σ_x, after the wave has travelled a distance x, will be

$$\sigma_x = A \exp(-\alpha x) \cos p \left[t - \frac{x}{c} \right] \tag{5}$$

where α and c are called respectively the attenuation coefficient and the phase velocity of the wave, and are functions of p. From the values of α and c the relevant complex elastic modulus can be found. Thus if the waves considered are extensional waves travelling along a thin viscoelastic rod, the relevant modulus is the complex Young's modulus. The relations for c and α are

$$c = \left[\frac{E^*}{\rho} \right]^{\frac{1}{2}} \sec \left(\frac{\delta}{2} \right) \tag{6}$$

and

$$\alpha = \frac{p \tan(\delta/2)}{c} \tag{7}$$

where $E^{*2} = E_1^2 + E_2^2$ and $\tan \delta = E_2/E_1$.

Relations (6) and (7) hold for any type of plane viscoelastic wave if $E_1 + iE_2$ is taken to be the appropriate modulus. Thus for torsional waves in a circular rod E_1 and E_2 are the real and imaginary parts of the shear modulus, G, whereas for longitudinal waves of plane strain travelling through a large block of viscoelastic solid they correspond to the real and imaginary parts of the modulus $K + \frac{4}{3} G$, where K is the bulk modulus.
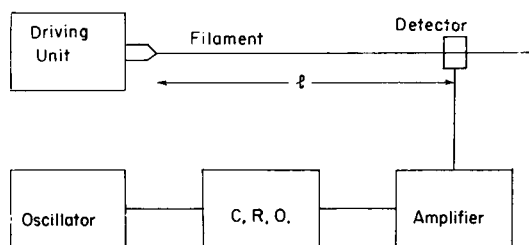
FIG. 4. Apparatus for wave propagation experiments in filaments.

Figure 4 shows schematically an apparatus used for measuring the velocity and attenuation of extensional waves along viscoelastic filaments. Such experimental arrangements have been described by a number of workers [14–18] to study the viscoelastic properties of polymeric fibers. As may be seen from Fig. 4 the waves are excited in the filament by a transducer. This may be electromagnetic, for example a moving coil loudspeaker, a piezoelectric or ferroelectric crystal, or a magnetostrictive rod; which of these is chosen will depend on the frequency range and the mechanical power required. The transducer is con-

nected to one end of the filament in such a way that longitudinal stress waves are propagated down the filament. The filament may be kept just taut or alternatively may be stretched to any desired pre-strain by a suitable loading mechanism. The detector is a probe of small mass, one end of which is in contact with the specimen and the other end is attached to a piezoelectric crystal. The detector can be moved along the filament so that the phase and the amplitude of the vibration can be found as a function of the distance x between the transducer and the detector. As may be seen from (4) and (5) the phase angle between the vibrations is equal to px/c and the ratio of the amplitude is $\exp(-\alpha x)$. Thus α and c, and hence E_1 and E_2, can be found. In the above discussion the reflection of the waves by the detector has been ignored. Such reflections, however, can be allowed for [16, 17].

Continuous wave methods can be used for frequencies from about 500 c/s up to about 50 kc/s. At frequencies much in excess of this, the wavelengths become too small for accurate phase measurements, and ultrasonic pulse techniques are employed. This method has been used for high polymers by a number of workers including Ivey, Mrowca and Guth [19], and Nolle and Sieck [20] at frequencies up to several megacycles per second. This pulse method is the only one that is feasible at such high frequencies, but suffers from two limitations.

First, since longitudinal pulses are usually the only ones that can be propagated through polymers, the relevant modulus corresponds neither to Young's modulus E nor to the shear modulus G, but to $K + \frac{4}{3}G$. It is consequently difficult to correlate the results with those at lower frequencies obtained by other methods. If experiments could also be carried out with ultrasonic shear pulses at the same frequencies as those used with the longitudinal pulses, the complex bulk modulus $K_1 + iK_2$ as well as the complex shear modulus $G_1 + iG_2$ could be determined. The attenuation of shear waves of such high frequencies in most real viscoelastic solids is too great, however, for such measurements to be made.

The second limitation to the method is the fact that a pulse of finite duration does not consist of a single frequency but is composed of a narrow band of frequencies. The velocity of such a pulse in a medium which is dispersive (i.e. where c depends on the frequency p) but which does not attenuate the waves (i.e. $\alpha = 0$) differs from c by the quantity $\Lambda(dc/d\Lambda)$, where Λ is the wavelength. Where there is attenuation as well as dispersion, the significance of group velocity is not easy to formulate, and the interpretation of the 'time of transit' of an ultrasonic pulse in terms of the phase velocity involves some theoretical difficulties.

The propagation of stress waves of arbitrary shape is of interest both as a method of studying the dynamic viscoelastic properties of materials and in connection with the use of such materials as shock insulators in engineering applications. For linear viscoelastic solids the principle of superposition applies; if the values of c and α (or E_1 and E_2) are known for sinusoidal waves over a sufficiently wide range of frequencies, a Fourier analysis of the initial pulse enables the shape of the pulse after any distance of travel to be synthesized.

Thus for a plane stress pulse at the origin $x = 0$ the stress $\sigma(0, t)$ may be expressed as a Fourier integral

$$\sigma(0, t) = \int_0^\infty A_p \exp(ipt) \, dp \qquad (8)$$

where A_p is in general complex. The stress $\sigma(x, t)$ produced by the pulse a distance x from the origin is then given by

$$\sigma(x, t) = \int_0^\infty A_p \exp\left[ipt - \left(\alpha + \frac{ip}{c}\right) x\right] dp \qquad (9)$$
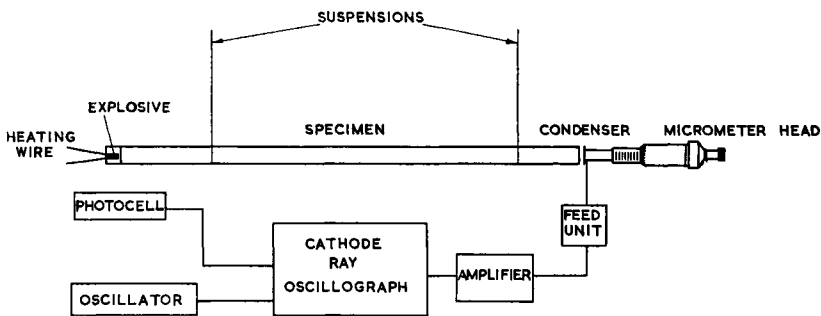
FIG. 5. Apparatus for pulse propagation experiments in rods.

Figure 5 shows an experimental arrangement used by the present author [21] for studying pulse propagation in viscoelastic rods. The pulse is here produced by a small explosive charge of lead azide which is detonated at one end of the rod. The pulse arriving at the opposite end is detected by means of a capacitor gauge the output of which is amplified and fed to a cathode-ray oscillograph where it is recorded photographically. The oscillograph is triggered by a photocell relay which in turn is actuated by the light from the explosion. It is found that an initially symmetrical pulse assumes an asymmetrical shape as a result of the higher phase velocity of its high frequency Fourier components. It also gradually increases in breadth as a result of the finite attenuation of the solid. Figure 6 shows the shape of a pulse, originally about 2 μsec in duration after it has travelled through 60 cm of polyethylene. The observed shape is compared in the figure with that calculated by numerical Fourier synthesis using the experimental results of Hillier [13] for c and α for sinusoidal waves travelling through this plastic in the relevant range of frequencies. The synthesis involved approximating to the Fourier integral given in (9) by a Fourier sum of 64 terms. It may be seen that the agreement between the calculated and the observed values is quite close. In this investigation [21] it was also shown that if it is assumed that tan δ is independent of frequency any sharp pulse will assume a 'universal shape' and this shape can be predicted theoretically. As will be shown later in this paper, for many high polymers tan δ is relatively constant over

24

wide ranges of frequency, and experimental observations [21] show that stress pulses do in fact approximate to this universal shape.

The propagation of plane stress pulses of arbitrary shape through blocks of viscoelastic solids could be treated in the same way as pulses travelling along viscoelastic rods except that $K + \frac{4}{3}G$ is now the relevant modulus. There are numerous experimental studies of the determination of the viscoelastic properties of polymers in shear and in simple extension, but there is very little information about the response of these materials to purely hydrostatic stresses. The reasons for this are that there are inherent experimental difficulties in applying oscillating hydrostatic pressures to a viscoelastic sample, and creep or stress relaxation measurements are often invalidated by macroscopic cavities in the specimen or bubbles in the fluid used for communicating the pressure.
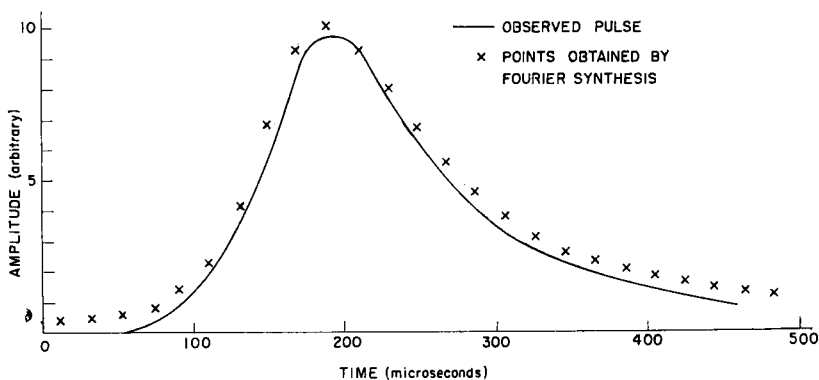
Fig. 6. Comparison between observed pulse shape in polyethylene rod and values calculated by Fourier synthesis.

McKinney, Edelman, and Marvin [22] have, however, carried out bulk measurements in the frequency range of 50–5000 c/s by confining a sample in a cavity under oil and applying a sinusoidally varying pressure, whilst Matsuoka and Maxwell [23] have studied the creep behavior of viscoelastic solids under hydrostatic pressure. A discussion of this and other work on bulk properties will be found in the book by Ferry [4].

In theory, the viscoelastic behavior for volume changes could be deduced from a knowledge of the behavior of a specimen in simple extension, where the relevant modulus is Young's modulus, E, and in shear where the rigidity modulus G is operative. Unfortunately for most viscoelastic solids the bulk modulus K is much greater than G (i.e. Poisson's ratio approaches 0.5). Under these conditions the value obtained for the bulk modulus becomes extremely sensitive to small errors in the determination of E and G. Thus for an elastic material which has a Poisson's ratio of 0.45, errors of 1 per cent in both E and G can lead to an apparent value of K which is 2.5 times its true value.

In the absence of reliable data of the bulk behavior of polymers under dynamic loading, the change in shape of a dilatational stress pulse cannot be predicted

theoretically; in contrast, measurements of change in pulse shape can be used to study the bulk viscoelastic properties of solids. This has been done by Lifshitz and Kolsky [24] who investigated the propagation of spherically diverging stress pulses in blocks of polyethylene, polymethylmethacrylate ("plexiglas") and polystyrene. The observed pulse shapes were compared with those predicted on the basis of a number of different *a priori* assumptions about bulk visco-elastic behavior of polymers. Thus it has often been assumed that bulk losses could be neglected compared with shear losses so that K_2 could be taken to be zero and K_1 taken to be a constant independent of frequency. At the other extreme it has sometimes been assumed [25] that $K_2/K_1 = G_2/G_1$, in other words, the loss angle δ is the same for dilatation as it is for shear. This latter assumption is equivalent to assuming that Poisson's ratio is a constant independent of frequency. This assumption has been justified partly on the grounds that it greatly simplifies the solution of stress analysis problems for viscoelastic structures, and partly by the somewhat implausible physical argument that the same long-chain molecules are involved in shear as in dilatation.

CALCULATED; {A ... TAN δ_K = 0.000
B ... TAN δ_K = 0.023
C ... TAN δ_K = 0.110 = TAN δ_G}

o o o EXPERIMENTAL

u(t)

ARBITRARY UNITS

μ sec
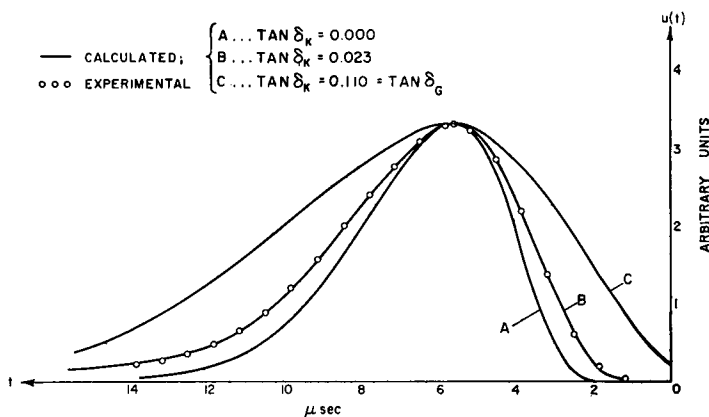
FIG. 7. Comparison between the experimental results and the predicted shapes of spherical pulses in polyethylene.

Figure 7 shows the shape of the displacement–time curve observed for a spherical stress pulse in a polyethylene block. The experimental results are compared with the pulse shapes predicted on the basis of two extreme assumptions discussed above, i.e. $K_2 = 0$ and $K_2/K_1 = G_2/G_1$ where K_2/K_1 is equal to tan δ_K (δ_K is the loss angle for bulk deformation) and $G_2/G_1 = \tan \delta_K$. It may be seen that the observed pulse shape agrees with the results of neither of the two extreme assumptions but fits remarkably well to the curve obtained on the assumption that tan $\delta_K = 0.2$ tan δ_G. The results for spherical pulses in poly-methyl methacrylate again showed that the assumption that the loss in bulk was about one-fifth of the loss in shear gave excellent agreement with the observed pulse shapes. The losses in polystyrene were too small for very definite conclusions to be reached from the experimental results, but it was, however,

shown that the same assumption about the ratio between bulk and shear losses led to satisfactory agreement with the observed propagation of pulses in this material.

7. CONCLUSION

We now return to the two reasons for measuring the viscoelastic properties of polymers discussed in the introduction, namely (a) to provide the necessary data for the solution of stress analysis problems and (b) to study the relation between mechanical properties and chemical structure. We will first discuss the stress analysis aspects of the subject.

In order to solve a stress analysis problem we need to find the stresses or strains in a structure as a function of time. This involves a knowledge of the viscoelastic properties for which the problem needs to be solved. Now as discussed in the introduction, the data may be in the form of the creep function, the stress relaxation function or the complex moduli. From an experimental point of view it is often more convenient to measure one rather than another of these quantities. For example for very short times creep measurements are difficult to carry out whereas for very low frequencies vibration measurements become impractical. Now from the theory of linear viscoelasticity it may be shown (e.g. Gross [26] and Ferry [4]), that integral relations exist between the various viscoelastic functions. For example, the stress relaxation function $\psi(t)$ may be expressed in terms of either the real or the imaginary component of the complex modulus. Thus

$$
\begin{aligned}
\psi(t) - E_0 &= \frac{2}{\pi} \int_0^\infty \frac{E_1 - E_0}{p} \sin pt \, \mathrm{d}p \\
&= \frac{2}{\pi} \int_0^\infty \frac{E_2}{p} \cos pt \, \mathrm{d}p
\end{aligned}
\tag{10}
$$

where E_0 is the limiting value of E_1 at "zero" frequency. Similarly the components of the complex compliance, J_1 and J_2 at any one angular frequency p can be expressed in terms of the creep function $\psi(t)$, thus

$$
J_0 - J_1 = p \int_0^\infty [J_0 - \psi(t)] \sin pt \, \mathrm{d}t
$$

and
$$
\tag{11}
$$
$$
J_2 = p \int_0^\infty [J_0 - \psi(t)] \cos pt \, \mathrm{d}t
$$

where J_0 is the limiting value of J_1 at zero frequency.

Now $J_1 + iJ_2 = 1/(E_1 + iE_2)$ so that the relation between the components of the compliance and those of the modulus are simple algebraic ones.

As mentioned earlier, Benbow [6] made measurements of the creep function and dynamic modulus of polyethylene over wide ranges of time and frequency which correspond to each other. He was consequently able to compare the

results using (11). Figure 8 shows such a comparison between the values of tan δ for polyethylene in shear measured directly with the apparatus shown in Fig. 2 and the values obtained by numerical Fourier analysis from creep measurements made with the apparatus shown in Fig. 1. It may be seen that the calculated curve agrees with the direct measurements within the experimental error. This type of conversion can, however, only be carried out if values of the creep function are known over a sufficiently wide range of t for integrals of the type used in (11) to be evaluated with some pretense of accuracy.
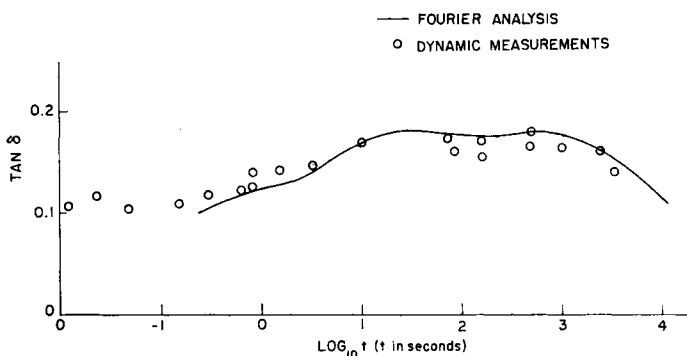
FIG. 8. Comparison of the values of tan δ in polyethylene obtained from vibration and creep measurements.

It may be seen from Fig. 8 that the value of tan δ changes very little with frequency over a frequency range of a million to one. This is characteristic of the viscoelastic behavior of most high polymers over large frequency ranges but does not apply when they are near their transition temperatures. The transition temperature corresponds to a second order phase change when the material changes from a glass-like to a rubber-like state, and this region is characterized by large changes both in the real part of the modulus and in large values of tan δ.

The dependence of tan δ on frequency for another high polymer polymethyl methacrylate can be seen in Fig. 9. (In this figure the ordinates are $\log_{10}\varDelta'$ where $\varDelta'$ is the logarithmic decrement and is equal to π tan δ.) It may be seen that for this polymer too, the value of tan δ does not change much with frequency.

Now the stress relaxation function can be expressed in terms of integrals involving either E_1 or E_2, see (10), so that these quantities are clearly not independent. In fact, if E_1 is known over a sufficiently wide range of frequency, E_2 can be calculated; and similarly if E_2 is known over a sufficiently wide range of frequencies, the changes of E_1 with frequency can be determined. In the particular case where tan δ is small (<0.1) and independent of frequency over a sufficiently wide range of frequencies, the following approximate relation may be used for expressing E_1 as a function of frequency:

$$E_1 \simeq E_1(p_0) \left[1 + \frac{2 \tan \delta}{\pi} \ln \frac{p}{p_0} \right] \tag{12}$$

where $E_1(p_0)$ is the value of E_1 at some reference frequency p_0 in the frequency range considered. (See [21] and [27].) This assumption, namely that tan δ is independent of frequency, was referred to earlier in this paper in connection with the "universal pulse shape" predicted for extensional stress pulses in rods. For such pulses it was found that (12) leads to pulse shapes which agree very well with those observed experimentally.
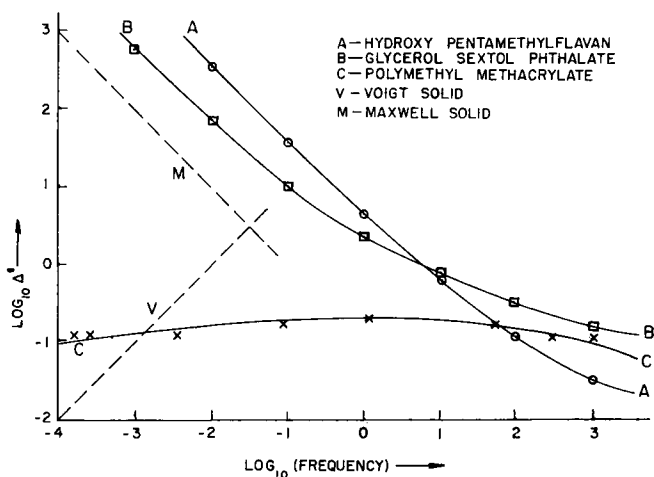
FIG. 9. Comparison between the experimental values of Δ' ($= \pi \tan \delta$) for two organic glasses and for a glass-like high polymer.

In the mathematical treatment of linear viscoelasticity, problems have often been treated in terms of a relation between stress and strain which is in the form of a linear differential equation. Thus for a single stress component σ and a single strain component ϵ, the stress-strain relation may be written as

$$P\sigma = Q\epsilon \tag{13}$$

where P and Q are linear differential operators, i.e.

$$P = a_0 + a_1 D + a_2 D^2 + \ldots$$

and

$$Q = b_0 + b_1 D + b_2 D^2 + \ldots$$

where D is the operator d/dt. It may be shown that if a sufficiently large number of terms are taken in the polynomials for P and Q the viscoelastic behavior of a linear solid can be approximated to, over as wide a range of time or frequency as desired. If, however, more than two or three terms are taken in the polynomials, the formulation of even simple stress analysis problems leads to differential equations of high order which are difficult to handle. Consequently much of the theoretical work has been carried out using stress–strain relations which

involve only one or two terms in the operators. Thus, if only the constant term is taken in P and the first two terms are taken in Q, we have

$$a_0\sigma = b_0\epsilon + b_1 \frac{d\epsilon}{dt} \qquad (14)$$

This is the stress–strain relation for a Voigt solid. The mechanical behavior of such a solid can be represented by a model consisting of a spring which obeys Hooke's Law, and a viscous element, often called a dashpot, which obeys Newton's Law of viscosity. The spring is assumed to be connected *in parallel* with the dashpot.

If, instead, the first two terms of the polynomial are taken for P and only the second term for Q, we have

$$a_0\sigma + a_1 \frac{d\sigma}{dt} = b_1 \frac{d\epsilon}{dt}. \qquad (15)$$

This is the stress–strain relation for a Maxwell solid and the mechanical behavior which it describes can be represented by a spring connected *in series* with a dashpot.

The use of such simplified constitutive relations enables a few stress analysis problems to be solved in closed form, but as may be seen from Fig. 9 the values of tan δ which these equations predict, the broken lines V and M in the figure, bear little relation to those observed experimentally in high polymers such as polymethyl methacrylate. For a Voigt solid (also often termed a Kelvin solid) tan δ is proportional to the frequency, whereas for the Maxwell solid it is inversely proportional to frequency. Thus in covering a frequency range of 10^6, tan δ for both of these solids will change by a factor of a million; instead for most high polymers, in the glassy state, it remains sensibly constant.

Now it may be shown that the mechanical behavior of any linear viscoelastic solid which is described by (13) can be represented by a model consisting of a series of Maxwell elements connected in parallel or of Voigt elements connected in series. If a unit step function in strain is applied to a Maxwell solid at time $t = 0$, the stress at time t is $A \exp(-t/\tau)$ where: τ is a_1/a_0 in (15) and is called the *relaxation time* of the solid; A is the value of σ immediately after the unit strain has been applied; and $A \exp(-t/\tau)$ is equal to $\bar\psi(t)$, the stress relaxation function of the solid. For a material that behaves like a series of n Maxwell models joined in parallel the stresses are additive so that the stress relaxation function is now

$$\bar\psi(t) = \sum_1^n A_r \exp(-t/\tau_r) \qquad (16)$$

where A_r and τ_r are the values of the initial stress and of the relaxation time for the rth Maxwell element.

In the limit, a continuous distribution of Maxwell elements with values of τ between zero and infinity may be considered and (16) may be written as

$$\bar\psi(t) = \int_0^\infty f(\tau) \exp\left(-\frac{t}{\tau}\right) d(\ln \tau) \qquad (17)$$

where $f(\tau)$ is called the *relaxation time spectrum* of the solid, such spectra playing a central role in the interpretation of linear viscoelastic behavior in terms of microscopic or molecular mechanisms. (The use of a logarithmic time scale in (17) is found to be more convenient than using a linear one.) If instead of considering a model of Maxwell elements connected in parallel we take a set of Voigt elements connected in series, we obtain an expression similar to (17) for the creep function $\psi(t)$, thus

$$\psi(t) = \int\limits_{0}^{\infty} g(\tau') \left(1 - \exp\left(-\frac{t}{\tau'}\right)\right) \mathrm{d}(\ln \tau')$$

where τ' is called the *retardation time* and is equal to b_1/b_0 in (14). The function $g(\tau')$ is called the retardation time spectrum.

The reason that these spectra have assumed importance is the fact that if a single well-defined microscopic or molecular process is responsible for the visco-elastic effects of a solid, the behavior may often be described by a single Maxwell element or a simple Voigt element. The relaxation time of the Maxwell element or the retardation time of the Voigt element then corresponds to the character-istic time of the microscopic process. The relaxation time spectrum (or the retardation time spectrum if it is a Voigt element) then consists of a single line and if there are a discrete number of different processes, the spectrum will consist of a series of "lines" and the "strength" of these lines will correspond to the values of A_r in (16). In the limit, the spectrum $f(\tau)$ should give an indication of the relative importance of various microscopic processes which have character-istic relaxation times. For metals, Zener [28] described a series of such micro-scopic processes, e.g. thermal flow across intercrystalline boundaries, and showed that the relaxation-time spectrum will have a series of peaks which correspond to these separate processes. With high polymers the situation is much more complex. The relaxation-time spectra are generally very flat and it is difficult to associate the peaks which are often present with individual molecular mechanisms. One exception is the transition from the glassy to the rubber-like state in amorphous polymers. This transition shows a large peak in the re-laxation time spectrum which corresponds to the large peak in tan δ.

When we come to solids which are not high polymers but consist of much smaller molecules, the viscoelastic behavior does not lead to flat relaxation time spectra but can show very sharp peaks. Benbow [10] and Benbow and Wood [29] have studied such materials which they term "organic glasses"; these are liquids which do not crystallize on cooling but assume a glass-like structure. They were able to show that where there was very little chemical association between the molecules as with 2'-hydroxy 2:4:4:6:5' pentamethylflavan (PMF) the solid behaved like a single Maxwell element over several decades of frequency. This can be seen in Fig. 9 where the values of tan δ = Δ'/π for this material decreases approximately inversely with frequency in the ranges from 1 c/s in 100 sec to 100 c/s. The relaxation spectrum of this material is thus very sharp and appoximates to a single line. Another organic glass is glycerol sextol

pthalate (GSP). This shows a region of about two decades of frequency where tan δ is inversely proportional to frequency, although the departure here from Maxwellian behavior takes place at a much lower frequency than with PMF, and tan δ for frequencies higher than this tends to approach a constant value as it does in high polymers. The relaxation time spectrum is also much broader than for PMF.

Now GSP has larger molecules than PMF and also associates more strongly forming molecular complexes which are flexible and may behave more like long chain polymers. Benbow and Wood [29] have concluded that at sufficiently high frequencies all the organic glasses they investigated have flat relaxation time spectra as polymers do, with tan δ independent of frequency. The frequency at which this transition occurs is, however, higher the smaller the molecular size whereas the "terminal" value of tan δ is greater the more flexible the molecule. It would thus appear that a study of the viscoelastic properties of such simpler materials may be one of the more helpful approaches to the correlation of the viscoelastic properties of glass-like polymers and their chemical structures.

The foregoing discussion on polymers and glasses has been concerned with their mechanical behavior under shear deformations. It is difficult to discuss the significance of volume viscoelastic properties since there are so very few reliable experimental data. The results of Lifshitz and the author [24] on spherical waves in polymers seem to show that the observed dilatational viscoelastic behavior follows that in shear. It may be speculated that the true volume losses in a polymer are very small indeed and of the same order as that observed in nonpolymeric solids. The observed losses may then be due to microscopic or submicroscopic voids in the material where dilatational strains result in appreciable shear deformations. In other words, what is observed as pure dilatation in the large may well be a combination of dilatation and shear in the small. Further investigation of this apparent correlation between volume and shear losses would clearly be helpful in settling this point.

In this paper no mention has so far been made of the role of temperature on viscoelastic properties of high polymers. The properties of these materials are extremely sensitive to temperature changes and any treatment of the subject of viscoelasticity would be incomplete without some discussion of temperature effects.

Alexandrov and Lazurkin [30] were amongst the first to carry out experiments on the relation between the effect of temperature and effect of time of loading on the mechanical behavior of rubber-like materials. A summary of their work and that of others is given in the monograph by Treloar [31]. Alexandrov and Lazurkin suggested that since the deformation of a rubber-like material is a thermally activated process, a direct relation should exist between the temperature dependence and the time dependence of rubber-like elasticity. They made measurements at frequencies between one cycle in 10 sec and 1000 c/s and at temperatures between −180°C and 200°C. The results showed that the curves of stiffness against frequency taken at different temperatures are similar in shape but move along the frequency axes as the temperature is increased.

Ferry [32, 4] has extended these ideas and has shown how values of the complex modulus over a very large frequency range at one temperature may be derived from measurements over a restricted frequency range made at several temperatures. The underlying hypothesis implies that the relaxation-time spectrum of a polymer moves as a whole when the temperature is changed; the theory also considers the effect of thermal expansion which results in changes in the average intermolecular distances. Thus if at temperatures T_0 and T the material has densities ρ_0 and ρ respectively and the real part of the shear modulus is given by functions $G_1(p_0)$ and $G_1(p)$ respectively, then

$$\frac{G_0(p)}{G_1(p_0)} = \frac{\rho T}{\rho_0 T_0}$$

where p_0 and p are "corresponding" frequencies at T_0 and T and represent the shift of the relaxation-time spectrum with temperature. Also, p/p_0 is a factor a_T which depends on T and T_0 and is found empirically by matching results at adjacent temperatures.

The Ferry transformation when it applies can reduce the experimental labor enormously as has been shown by Marvin [33] in correlating experimental data on the viscoelastic properties of polyisobutylene. It would, however, be hazardous to use it for extrapolation over wide frequency ranges and its general range of validity is still somewhat uncertain.

REFERENCES

[1] ALFREY, T., *Mechanical Behavior of High Polymers*, Interscience, New York (1948).
[2] *Die Physik der Hochpolymeren*, ed. H. A. STUART, Springer-Verlag, Berlin (1956).
[3] *Rheology, Theory and Applications*, ed. F. EIRICH, Academic Press, New York (1958).
[4] FERRY, J. D., *Viscoelastic Properties of Polymers*, John Wiley, New York (1961).
[5] ANDRADE, E. N. de C., *Proc. Roy. Soc.*, A84, 1 (1910); 90, 339 (1914).
[6] BENBOW, J. J., *Proc. Phys. Soc.*, 69, 885 (1956).
[7] STEIN, R. S. and TOBOLSKY, A. V., *Text. Res. J.*, 18, 302 (1948).
[8] LETHERSICH, W., *Brit. J. Appl. Phys.*, 1, 294 (1950).
[9] MARKOVITZ, H., YAVORSKY, P., HARPER, R. C., ZAPAS, L. J. and DeWITT, T. W., *Rev. Sci. Instrum.*, 23, 430 (1952).
[10] BENBOW, J. J., *Proc. Phys. Soc.*, B67, 120 (1954).
[11] BODNER, S. R. and KOLSKY, H., *Proc. 3rd U.S. Nat. Congress of Appl. Mech.*, p.495, ASME, New York (1958).
[12] DAVIES, R. M., and JAMES, E. G., *Phil Mag.*, 18, 1023 (1934).
[13] HILLIER, K. W., *Proc. Phys. Soc.*, B64, 998 (1951).
[14] BALLOU, J. W. and SILVERMAN, S., *J. Acous. Soc. Amer.*, 16, 113 (1944).
[15] NOLLE, A. W., *J. Appl. Phys.*, 19, 753 (1948).
[16] HILLIER, K. W. and KOLSKY, H., *Proc. Phys. Soc.*, B62, 111 (1949).
[17] BALLOU, J. W. and SMITH, J. C., *J. Appl. Phys.*, 20, 493 (1949).
[18] HILLIER, K. W., *Proc. Phys. Soc.*, B62, 701 (1949).
[19] IVEY, D. G., MROWCA, B. A. and GUTH, E., *J. Appl. Phys.*, 20, 1481 (1949).
[20] NOLLE, A. W. and SIECK, P. W., *J. Appl. Phys.*, 23, 888 (1952).

[21] KOLSKY, H., *Phil. Mag.*, **1,** 693 (1956).

[22] McKINNEY, J. E., EDELMAN, S. and MARVIN, R. S., *J. Appl. Phys.*, **27,** 425 (1956).

[23] MATSUOKA, S. and MAXWELL, B., *J. Polymer Sci.*, **32,** 131 (1958).

[24] LIFSHITZ, J. M. and KOLSKY, H., Tech. Rep. ARPA/AM–14, Brown University, January 1965. *J Math. Phys. Solids* (in press).

[25] QUIMBY, S. L., *Phys. Rev.*, **25,** 558 (1925).

[26] GROSS, B., *Mathematical Structure of the Theories of Viscoelasticity*, Hermann, Paris (1953).

[27] HUNTER, S. C., *Progress in Solid Mechanics* (ed. I. N. Sneddon and R. Hill), Vol. I, p. 1 (1959).

[28] ZENER, C., *Elasticity and Anelasticity of Metals*, University Press, Chicago, 1948.

[29] BENBOW, J. J. and WOOD, D. J. C., *Trans. Farad. Soc.*, **54,** 1581 (1958).

[30] ALEXANDROV, A. P. and LAZURKIN, J. S., *Acta Phys. URSS*, **12,** 647 (1940).

[31] TRELOAR, L. R. G., *The Physics of Rubber Elasticity*, Clarendon Press, Oxford (1958).

[32] FERRY, J. D., *J. Amer. Chem. Soc.*, **72,** 374 (1950).

[33] MARVIN, R. S., *Proc. 2nd Int. Congr. on Rheology*, p. 156, Butterworths, London (1954).

EXPERIMENTAL STRAIN AND STRESS
ANALYSIS OF SOLID PROPELLANT
ROCKET MOTORS

A. J. DURELLI

The Catholic University of America
Washington, D.C.

Abstract—A review is made of the methods used to strain-analyze solid propellant rocket motor shells and grains when subjected to different loading conditions. The review includes methods directed at the determination of strains in actual rockets and also at the determination of strains in rocket models. The surveyed methods include two- and three-dimensional photo-elasticity, brittle coatings, electrical strain gages, moiré, grids, etc.

Preface—Few engineering problems have presented in shorter time a greater amount of interest and more difficulties in their solution than the strain and stress analysis of solid rocket propellants when subjected to the numerous loading conditions to which they may be subjected either in flight, in storage, or in transportation. The difficulties in the analysis are, to a large extent, a consequence of the fact that the motor is a composite structure, and that the materials used in this composite structure are relatively new, exhibiting properties appreciably different from the properties of the more commonly used engineering materials such as steel, aluminum, and concrete. Difficulties also arise because few structures are designed to work under a state of strain and stress so near to the one associated with failure.

As difficulties have developed in the functioning of solid rocket propellants, great emphasis has been given to studies directed at improving the quality of the propellant material, and even greater emphasis has been placed on the so-called characterization of these materials, or, in other words, on the study of their viscoelastic properties.

There has been a strong belief for many years that stress analysis methods were sufficiently advanced to be used in the solution of rocket problems, but that they could not actually be applied because of the lack of knowledge of the required physical constants of the materials. This belief was not universally shared,* but was predominant in several leading circles and was responsible for an extraordinary concentration of interest in mechanical properties of solid propellants and a correspondingly extraordinary development of viscoelasticity theory and testing. As a consequence of this concentration, studies in both theoretical and experimental stress analyses of grains and motors have been underemphasized for a long time. In recent years some important developments in theoretical stress analysis have taken place,† but the number of experimental stress analysis contributions is still extremely small. It is estimated that of the approximately 700 papers dealing with solid rocket structural integrity that have been abstracted and classified recently, no more than 2 per cent deal with experimental strain and stress analysis methods applied to rocket grains and cases. As an example of the emphasis on material testing, consider the large program of experimental stress analysis which was published under the title "Study of Mechanical Properties of Solid Rocket Propellants". It seems that the underemphasis on strain analysis, in general, and in particular on the application of experimental strain analysis techniques to grain and case research and design should be carefully re-evaluated.

This review should not be considered exhaustive, but rather informative. It covers a broad part of the field in a systematic manner and attempts to give the reader a critical picture of the

---

* See, for instance, comments by A. V. Tobolsky in *Proc. 10th Meeting of the JANAF*, SPIA-PP3, Dec. 1954, pp. 37–54.

† See in particular, among others, papers by C. H. Parr, A. M. Messner, and H. B. Wilson

state of the art. A large amount of the information related to the field, however, has been published in reports, many of which are not easily available. Some parts of the review have been deliberately emphasized, either because they have been considered more important or because they refer to new methods not yet adequately covered in the literature.

1. INTRODUCTION

Solid propellant motors are composite structures of two very dissimilar materials. The geometry of one part of the structure—the case or shell—is relatively simple and can be considered essentially as a thin-walled pressure vessel. The geometry of the grain, on the other hand, is extremely complicated.

Material properties and the development of materials are studied, in general, apart from strain and stress analysis, and will not be mentioned here except to remark on the relative rigidities of case and grain, and to note the possibility of heterogeneous, anisotropic, viscoelastic and non-linear behavior. The paper will be limited to a discussion of strain and stress either in the actual rocket or in models simulating rocket components. As is the case in other structures, the approach to solve the strain and stress analysis problem can be either theoretical or experimental, or both. In this review, only experimental methods will be discussed at length, although some alternative theoretical methods will be noted.

For purpose of completeness and to familiarize the reader who is not acquainted with the over-all problem, the definition of the geometry of the structure of the materials used and the loading conditions to which the structure is subjected are given below.

1.1. *Geometry of the Grains*

A typical geometry of a solid rocket motor is illustrated in Figs. 1.1 and 1.2, which show respectively a meridian cross section and a transverse cross section of one of these motors. The particular design shown in these figures does not reproduce exactly any rocket motor, but it is realistic in the sense that the geometry contains many of the essential features found in rocket motors. The grain may be more or less long, it may have a liner at the interface with the case, and it may have lateral ports, as shown in Fig. 1.1. The case may be very rigid, as when made of steel, or it may be relatively flexible, as when made of glass-fiber reinforced epoxy. The star configurations shown in Fig. 1.2 may correspond to different transverse cross sections of the grain, as-cast, or may correspond to successive stages of burning of the original design.

It is obvious from Figs. 1.1 and 1.2 that the body to be stress-analyzed is made of two different materials bonded totally or partially to each other at their
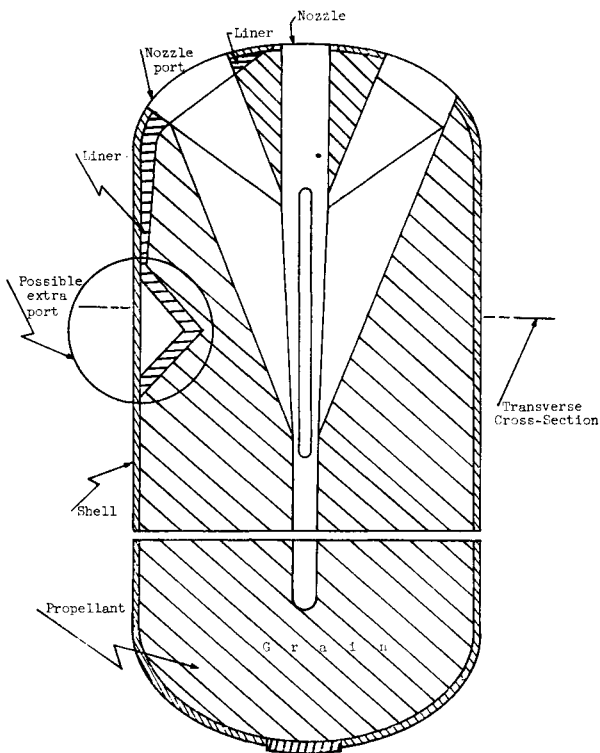
FIG. 1.1. Example of meridian cross section of a solid propellant rocket motor.
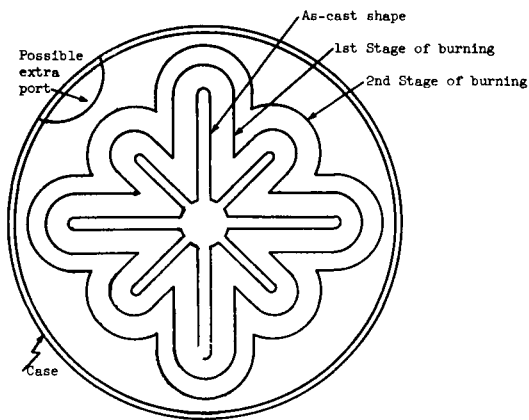
FIG. 1.2. Example of transverse cross section of a solid propellant rocket motor at several stages of burning.

interface. The problem is therefore a problem of stress distribution in a composite body. It is also obvious that in the process of burning the internal boundary changes as function of time.

In this paper, consideration will be given to the analysis of strains and stresses in both the case or shell and the grain.

1.2. *Material Properties of the Propellant and Case*

The modulus of elasticity of the case material is much higher than the modulus of elasticity of the grain, although it may vary from 30×10^6 psi (steel) to about 2×10^6 psi (fiber-glass reinforced epoxy). The modulus of elasticity of the grain (propellant) is of the order of 1000 psi.

In general, the case material is elastic. The propellant is usually linearly viscoelastic, although some propellants exhibit nonlinear viscoelastic behavior. The case may be heterogeneous and anisotropic (glass-fiber wound on epoxy), or homogeneous at the engineering scale (steel). The propellant may be anisotropic, is usually heterogeneous, and frequently exhibits different behavior under tension and compression.

The coefficient of thermal expansion of the propellant is several times larger than the coefficient of thermal expansion of the case.

1.3. *Loading Conditions of the Grain*

Several loadings may act successively or simultaneously on a rocket propellant grain. Among the most important, the following should be mentioned: (1) uniform internal pressure, (2) local difference of pressure inside the grain, (3) thermal loading of the shrinkage type, (4) thermal gradient loading, (5) thermal transient loading, (6) acceleration loads, (7) body forces (in storage), (8) vibrations, and (9) residual stresses. In some cases stresses produced in the process of curing and stresses resulting from core pulling may also have to be considered.

Most of the analyses conducted so far have dealt with pressure and restrained shrinkage type of loadings. Recently, the study of axial acceleration loads has developed great interest.

2. DETERMINATION OF STRAINS AND STRESSES
IN THE ACTUAL PROPELLANT GRAIN

2.1. *Introduction*

This chapter deals with experimental methods used to determine strains on (1) the inside, or core, surface of solid rocket propellants, (2) at the interface between case and propellant, and (3) inside the propellant. Of particular interest are the strains in fillets and at the bonded interface where failure is likely to occur. A desirable feature would be the remote recording of strains.

There exists today an imposing array of experimental methods designed to measure displacements and determine strains. Most of the methods were originally designed to determine strains in the commonly used engineering materials (metals, concrete, wood, etc.). These materials exhibit a modulus of

elasticity of the order of 10^6 psi. Solid rocket propellants have a modulus of elasticity of the order of 10^3 psi. This great difference presents problems in the use of most gages commonly designed for engineering materials. One approach to the solution of the problem is the adaptation of one of those methods to the measurement of strains on the soft rubber-like surface of the rocket propellant. Another approach is to choose a method that has already been used to measure strains on soft materials, and extend its application to the present problem. In the first approach noted above, the difficulty lies usually in the reinforcement effect produced by the presence of the gage, an effect which will be discussed below. In the second approach, difficulties arise in the application of simple optical devices to complicated geometries and to field conditions. A third approach that suggests itself is the development of entirely new principles for the measurement of strain. Several rather novel methods will be noted in this chapter. An evaluation of several of the methods reviewed can be found in [1].

2.2. The Reinforcement Effect

If any relatively rigid device is mounted on or in a lower modulus-of-elasticity medium such as the propellant material to record change in length, these changes in length will generally be influenced by the presence of the device.

This can be illustrated by consideration of a simple, tensile specimen of propellant material with a long, thin wire embedded at the center of the specimen in the direction of loading, and assuming a bond between wire and medium. Neglecting end effects, the relationship of the strain in the direction of loading without the wire (ϵ_n) to the corresponding strain with the wire (ϵ_r), which is common to both wire and propellant, can be shown to be

$$\epsilon_r = \epsilon_n \frac{A_p E_p}{A_p E_p + A_w E_w} \tag{2.1}$$

where A and E represent cross-section area and Young's modulus, respectively, and the subscripts p and w refer to the propellant and wire, respectively. Since the area of the wire is small, the serious reinforcement effect is produced when the Young's modulus of the wire is many times that of the propellant (e.g. $E_w = 30,000,000$ psi, $E_p = 1000$ psi). The same reasoning can be applied to cases where the gradients of stresses are present, such as the edge of a beam under bending. In these cases, the reinforcement effect is even more pronounced.

The disturbance effect, in practice, is usually greater than the one suggested by the above relationship, because of the influence at the ends of the rigid device (Fig. 2.1). Considerations of this problem and suggestions on the use of rigid gages on viscoelastic materials can be found in [2].

2.3. Electrical Strain Gages

2.3.1. Resistance-type gage on the surface.

The electrical resistance strain gage is by far the most popular device for measuring strain today. Both the wire and foil type have been developed extensively, applied to different types of problems, and associated to different kinds

25

of equipment. It is also common practice to record remotely the response of these gages. With this background of development, it seems that it would be desirable to extend the usefulness of this type of gage to the case of solid propellant materials.

As shown in the previous section, the foil or wire gage on propellants will reinforce the vicinity of the gage so that the gage will not record the strain that would have been produced had the gage not been there. If this relationship between the recorded (or experimentally determined) strain and the true strain (the strain that would have been at the point had the gage not been there) can

The pattern without the gage would be
a series of equally spaced lines
parallel to the top aud bottom sides.
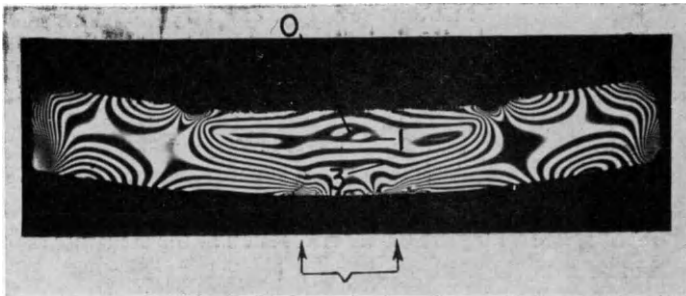
C–1 Wire Strain Gage
in this Area on Edge

Note Higher Order
Fringes at Ends of Gage

FIG. 2.1. Isochromatic pattern of a urethane rubber beam with an electric wire gage cemented to its bottom side, when subjected to bending.

be determined, then the gage can still give a meaningful record. The relationship, to be most useful, should be the same, regardless of strain biaxiality, and should be the same from gage to gage.

Several tests were conducted to explore this approach. Gages were mounted on a series of specimens of urethane rubber (Hysol 4485), a transparent material which has approximately the elastic properties of the propellant ($E = 490$ psi, $\nu = 0.47$). Different model geometries allowed the study of the reinforcement relationship in strain fields which have different ratios of principal strains. It also allowed the study of the reinforcement when the model was subjected only to forces or displacements as opposed to the more complex loading by thermal effects where the elastic constant of the material may vary.

In particular, two types of gages were tested: a foil type (Budd C6–121) $\frac{1}{8}$ in. $\times$ $\frac{1}{8}$ in. $\times$ 0.00015 in. thick on plastic backing (total thickness = 0.001 in.) and a wire type (Baldwin A–7) $\frac{1}{4}$ in. $\times$ $\frac{3}{32}$ in. $\times$ 0.0015 in. diameter wire cemented

between two layers of paper (total thickness = 0.004 in.). Three types of cement were used: an epoxy (Budd B-3), ordinary rubber cement, and the model material itself (Hysol 4485). Figure 2.2 illustrates photoelastically the reinforcement effect in a disk. Since the gage is cemented on the surface of the disk and the fringes are an integral effect across the thickness of the disk, the local disturbance produced by the gage is appreciably larger than the one shown in the photographs.

In all of the tests conducted on the various combinations of specimens, cement, and gage, the relationship of the load to the recorded strain was, except for one case, linear. Thus, for any load, or more directly for any stress, there was a given amount of recorded electrical output directly proportional to strain. The results of the tests can then be characterized by a number giving the numerical relationship between the strain that would have been there if the gage had not been there
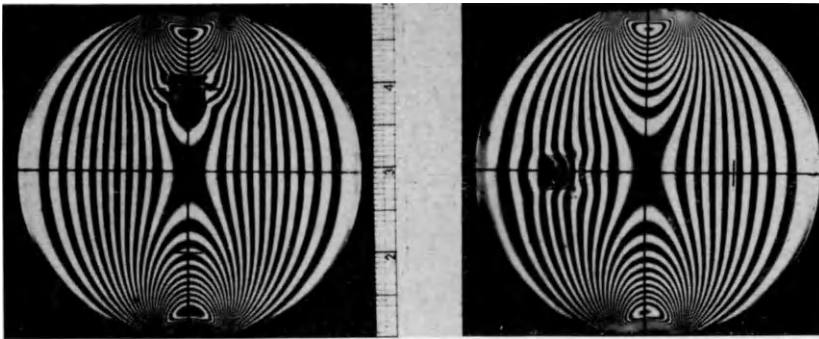
FIG. 2.2. Isochromatics in urethane rubber disk subjected to diametral compression, showing the extent of reinforcement produced by a strain gage.

(true strain), and the recorded value of strain (measured strain). Unfortunately, these ratios were not reproducible, due probably to the fact that the amount of cement used to attach each gage cannot be kept constant. It is also noticeable that ratios were not independent of biaxiality.

Similar tests with semiconductor gages have been reported [18]. These gages show an output 50 to 60 times greater than that of the wire and foil, but were found very difficult to handle (brittle) and exhibited nonreproducible behavior.

It is concluded that with the present state of the art, the wire or foil resistance strain gage cannot be expected to give an accurate indication of strain when mounted directly on the propellant unless some means is available to calibrate each gage individually after it has been cemented.

2.3.2. *Embedded strain gage capsules.*

One or several standard electrical resistance gages can be embedded in a material of essentially the same elastic properties as the material to be studied, and in a sufficiently large volume of the material so that the over-all response is not appreciably affected by the local reinforcement of the gage (Fig. 2.3). The

unit or capsule is then calibrated by applying known strains and recording the responses of the gage. Finally, the capsule is mounted in the material to be analyzed at the point of interest.
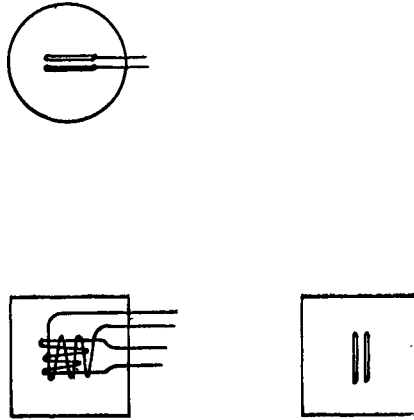
FIG. 2.3. Sketch showing location of standard wire or foil strain gages embedded in capsules.

Two such capsules are shown in Fig. 2.4. These capsules were calibrated. The calibration shows that the true-strain-over-measured-strain ratio is a reproducible quantity that can be measured in the laboratory before the capsule is inserted in the propellant [3].
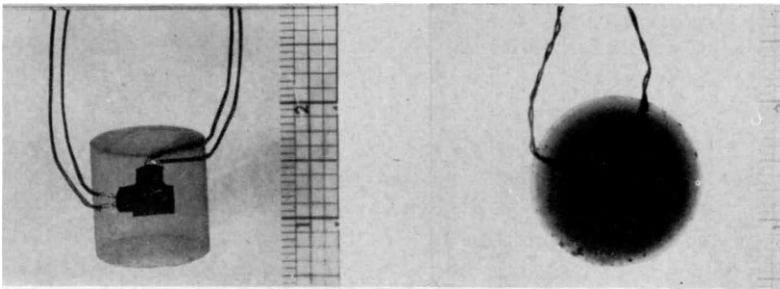
FIG. 2.4. Two urethane rubber capsules with embedded strain gages.

To completely validate the method, it is necessary that either (1) the strain gage be embedded in a capsule of the actual propellant, (2) the gage be embedded in a capsule of a material with the same mechanical and thermal properties as those of the propellant, or (3) the capsule be stiffer or more compliant than the propellant. However, the influence of a change in the mechanical properties of the material of the capsule on the calibration of the capsule must be determined.

Although it seems possible to extend this method to record the strain in a small fillet, it will obviously be better suited to measure interior strains.

2.3.3. *Helical strain gages.*

A variation of the method described above consists in the use of a specially designed helical strain gage wire. The helical configuration will reduce the reinforcement effect and may not require previous embedding in a capsule. The helix could be left floating in the propellant, although the technique to do this properly may be quite difficult. It was reported that when embedded in a propellant or polyurethane rubber, a gage of this type showed a strain of about 6000×10^{-6} for a deflection of 25 per cent [4].

2.3.4. *Capacitance-type gage.*

A capacitor gage has the advantage that only the material in which it is embedded need span the base length and, therefore, the reinforcement effect is reduced. Capacitor gages have been used primarily as transducers to measure various types of displacement phenomena at high speeds and high frequency. In general, the resistance-type gage has proved simpler for static strain measurement. However, in the propellant grain, where the resistance-type gage produces considerable reinforcement, and the advantage of an electrical signal for remote recording is desirable, the capacitor gage may be the more useful method.

A number of thin metal plates (about $\frac{3}{16}$ in. $\times \frac{3}{16}$ in.) with attached coaxial cable were embedded in urethane rubber at from $\frac{1}{8}$ in. to $\frac{1}{2}$ in. apart. In two of these specimens, actual propellant material was placed between the plates. In another, just two wires were embedded. Measurable values were obtained from all the samples with a capacitance bridge. An increase in capacitance was noted with compressive strains [1].

The preliminary models and measurements indicate some promise for thi, method, although it is obvious that additional thought must be given to design, manufacture, and measurement circuits.

2.3.5. *Conducting rubber method.*

Another possible method of obtaining a remote electrical signal from strain in the propellant, without reinforcing the area where strain is measured, is the use of conducting rubber threads either mounted on the propellant surface or embedded in the propellant. If resistance could be measured, as with the metal resistance gages, then strain could be recorded in this manner. No record has been found of tests conducted using this method.

2.3.6. *Piezoresistance gage.*

The piezoresistance property of silicon splinters has been used in gages to determine the force acting on the gage. The gage is very small (of the order of 0.1 in.), and it is claimed that a good estimate can be made of the stress at a point by means of this unidirectional gage. The lack of linearity of the response has been studied and minimized. Successfully reproducible calibrations have been

reported [5]. It seems that the considerations made in Section 2.3.2 should also be applied to this kind of gage. The design characteristics of this gage are shown in Fig. 2.5.

Another application of piezoelectric elements is reported in [18]. The gage uses standard crystal accelerometer procedures and is available commercially [19]. Three elements are embedded in a capsule of RTV 501 silicone rubber (modulus smaller than 900 psi). It is claimed that the instrument behaves linearly and reproduces the output well. The gage can detect only strains of frequency higher than 10 cps.
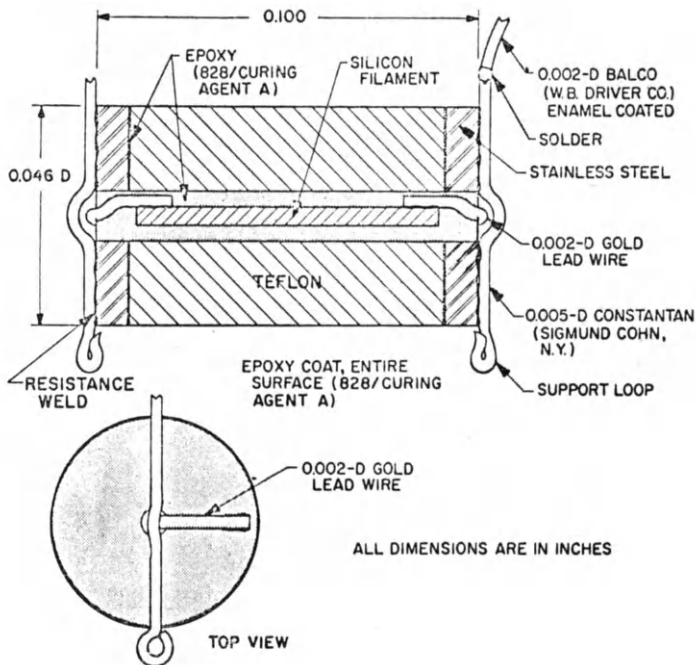
FIG. 2.5. Piezoresistance gage.

2.4. *Hydraulic Strain Gage*

This gage is made of a small, hollow, metal, cylindrically-shaped bellows which is embedded in the propellant. The curved surface is corrugated to allow appreciable axial motion. The inside of the bellows consisted of a chamber which is filled with fluid. A small tube leading from the bellows allows the recording of variations in the fluid due to changes in the axial length of the bellows, which, in turn, allows determination of the strains [4].

2.5. *Boroscope*

The principles of determining strains using optical means are well known. Several instruments have been designed to record strains on low modulus specimens under load.

The application of those principles to the determination of strains on the internal surface of a grain requires several steps:

1. A method of making observable marks on the propellant and development of a method to locate and focus on the marks with an optical system.
2. Design of the optical system to transmit the mark to an observer outside the rocket.
3. A measuring device to record the true length between marks.

The porous nature of the propellant makes marking the material difficult. It was found that after sanding the propellant surface with 180 grit emery cloth, India ink could be used to produce a clear, if still somewhat ragged, line. Better results could be obtained if previous to the marking of the surface, it is smoothed by a very thin layer (about 0.002 in.) of latex or of urethane rubber. The India ink lines or the scribed lines could then be placed more precisely on the surface of the rubber. The thickness of this layer is so small or the properties of the layer of rubber and those of the propellant are so very close that no change in strain condition would be expected.

Another approach would be to use some of the natural marks present in the propellant, such as oxidizer spots. This method has the advantage of being simpler as far as the preparation of the surface is concerned. It requires more precise and elaborate analysis of the records.

In order to see marks on the inner core of a rocket grain, an instrument such as the boroscope shown in Fig. 2.6 is needed. In order to read the distance

GAERTNER M 202T
FILAR EYEPIECE MICROMETER
WITH REVOLUTION COUNTER

45° MIRROR

MICROSCOPE WITH RELAY LENSES   LIGHT

ROCKET PROPELLANT
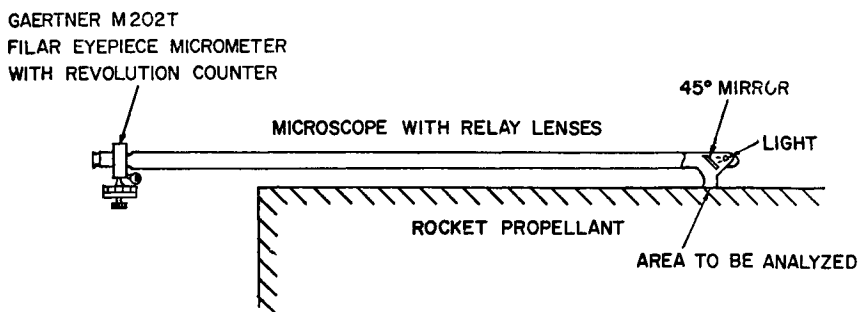
AREA TO BE ANALYZED

FIG. 2.6. Sketch of a boroscope to determine strains on the inside of a propellant grain in storage.

between marks, this instrument has a mounting ring to set down over the point to be analyzed and to fix the local distance. A bulb in the head provides light. A 45° mirror transmits the image through the tube. A system of lenses brings the image to the eyepiece which has a micrometer with a revolution counter. This unit has a hairline mounted on a calibrated screw that can traverse the field and note the distance between any two points. The eyepiece micrometer has 4000 divisions which allow a sensitivity of approximately $\pm$ 0.00025 in./in. (assuming an accuracy of $\pm$ 1 division). Rotating the eyepiece would allow measurement of length in any direction in the field [1].

2.6. Embedded Pellets

A variation of the previous method uses X-rays as the "optical" device [6, 7]. Small steel spheres are embedded in the solid propellant and the distance between spheres recorded before and after loading with an X-ray scanner. The method has been proved to be very accurate in laboratory models.

It has also been suggested that the pellets be magnetic and that the determination of their position be made by means of three small light-weight magnetometers with three sensing heads which would locate the pellets by triangulation. In principle, the system could work in flight, and in some of the results published, an accuracy of one per cent is claimed when the order of the strains is 15 per cent [8].

2.7. Replica Techniques

A recognized method of strain measurement which has several advantages but does not present the possibility of remote reading is the replica technique Here, a plaster, plastic, or low-fusion temperature metal impression is made of the area to be analyzed before and after loading, and the two impressions compared under a microscope to note variations in length between random marks (or, if necessary, scratches made before loading). The replica technique is essentially a laboratory method.
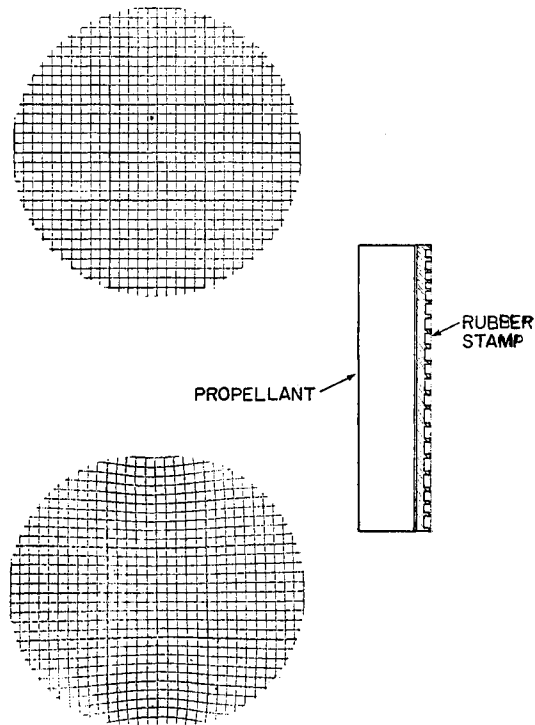
FIG. 2.7. Imprints of rubber stamp cemented to a propellant disk before and after loading.

A modification of this technique has been suggested. The surface of the propellant might be coated with ink, and an impression of the surface taken before and after loading that could be observed with a measuring microscope. Another variation of this method would be for soft rubber lines to be cemented to the model and inked so that an impression of the lines could be obtained. Essentially, the rubber lines would act like an ordinary office rubber stamp.

To illustrate the method, a rubber stamp with a rectangular gridwork was cemented to the face of a 1 in. thick × 3 in. diameter disk of propellant material. The grid network was inked with stamp pad ink and an impression made on paper. The disk was then loaded along the vertical diameter and another impression of the network was made. The impressions are shown in Fig. 2.7.

2.8. Surface Coatings

There are at least three methods of whole-field strain determinations of a surface that warrant consideration. None of them, unfortunately, is well suited for determining strains in sharp fillets. However, the methods would find application when the propellant has a flat end of the same geometry as the general cross-section of the grain, and is accessible to view. Here the strains at the cross-section of the fillet would give a good approximation of the strains in the fillets in the central portion of the rocket.

The grid method.—A sharp set of lines is marked on, or cemented to, the flat surface and photographed before and after loading. Measurements on the photographs, using a comparator, can give the strain at any desired point. Use of the technique to measure changes in bore diameters has been reported in [4].

The moiré method.—A very dense grating of uniformly spaced parallel lines must be printed on or bonded to the flat surface, and a master pattern of the same sort on glass or film laid over it. Any displacement of one grating with respect to the other produces interference fringes that can be interpreted as loci of points with the same displacements in the direction perpendicular to the grating line direction. From the displacements, the strains can be obtained by differentiation. The method has the advantage of not introducing reinforcement on the surface to be investigated. The thickness of the photographically deposited coating is also negligible. Strains are recorded faithfully. An application of moiré to the surface of some specimens made with propellant material has been published in [9]. Figures 2.8 and 2.9 show the fields of displacement components u and v in a ring of propellant subjected to large deformation. The influence of nonlinearity or heterogeneity can be studied precisely with this method.

Birefringent coatings.—Birefringent coatings have also been considered. By cementing the coatings to the propellant surface and recording the fringe pattern or color pattern photographically, the shear strains can be determined. More elaborate analysis should be used to obtain the complete strain field. For sufficient sensitivity, the birefringent coating thickness should be of the order of 0.100 in. Urethane rubber, rather than the more common epoxy coatings, is
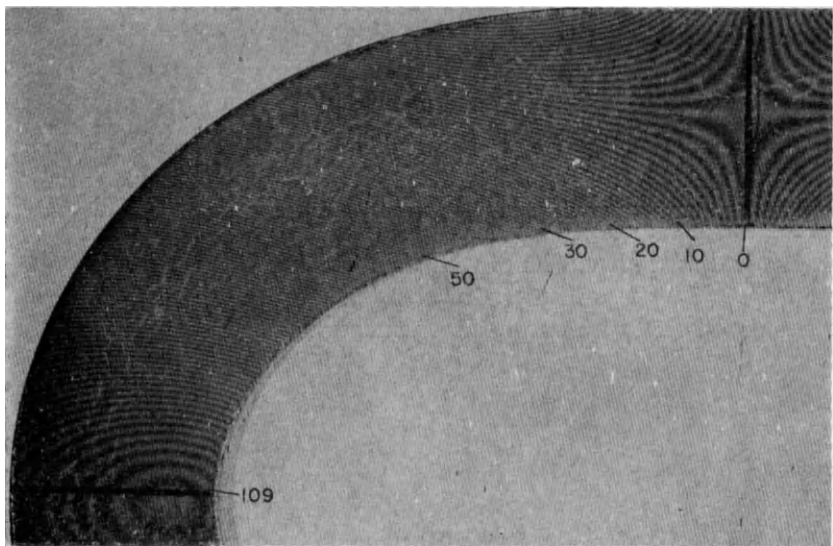
FIG. 2.8. Moiré fringes on the surface of a solid propellant circular ring subjected to large deformation (*u* field).
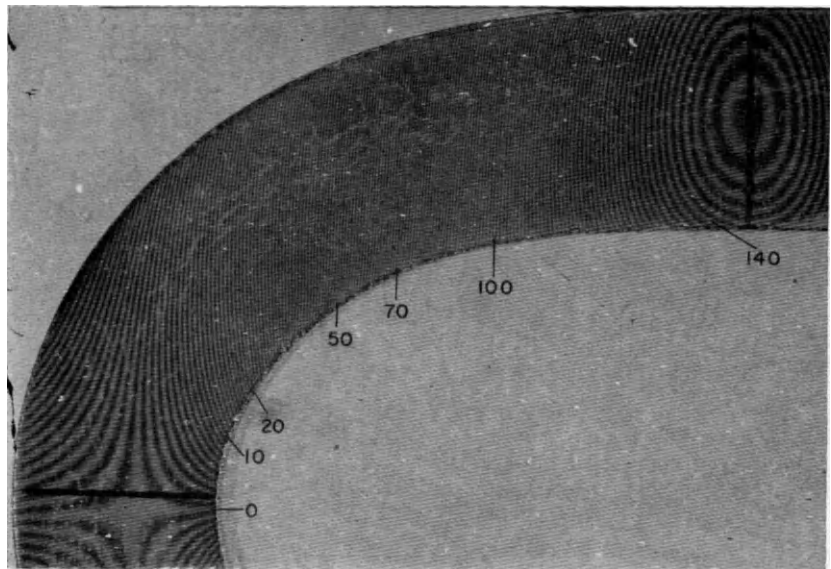
FIG. 2.9. Moiré fringes on the surface of a solid propellant circular ring subjected to large deformation (*v* field).

(The extraneous moiré effect, which is visible by itself in the background, is produced by the half-tone screen used in printing. Only the boldest pattern, which gives the star and the loop, is meaningful.)

recommended because of its low modulus of elasticity. Contributions to the development of this technique can be found in [10] and [11]. An example of application of photoelastic coating to a propellant disk diametrically loaded is shown in Fig. 2.10. The large irregularities in the isochromatic pattern associated with the heterogeneity and anisotropy of the propellant material are noticeable in the figure. Application to a star-shaped geometry is shown in [12] and also described in [13].
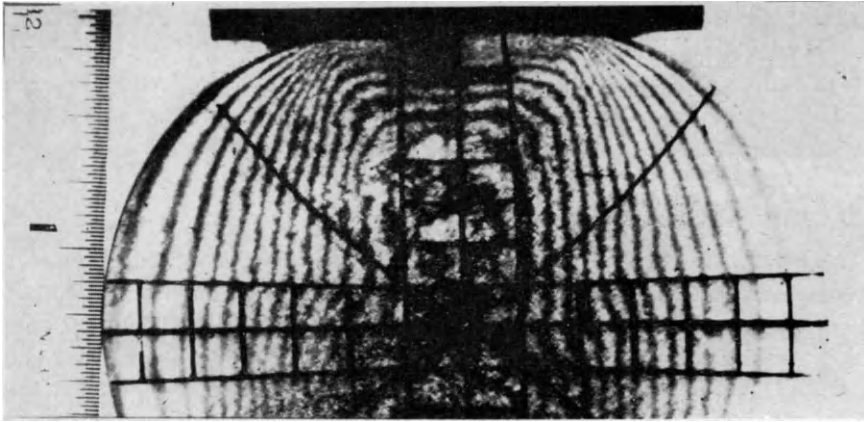
FIG. 2.10. Isochromatics in a rubber coating bonded to a propellant disk subjected to diametral compression.

2.9. Shear Strain Transducer

The determination of strains at the interface between propellant and case is of particular interest and has been the object of a special study [8].

The transducer is a low-modulus semiconductor, consisting of two piezo-resistive silicon elements, each mounted at 45° with respect to the sensitive axis, and perpendicular to each other. These elements form arms of a Wheatstone bridge. Under the effect of normal strain, both elements undergo the same resistance change. Under shear strain, one element deforms under compression and the other under tension. The gage can be encapsulated with the advantages indicated in Section 2.3.2.

The gage could also determine normal strains independently of the shear strains by determining the output of each element individually. As reported, the gage is used at present in such a way that under normal strain input, the elements are subjected to the same resistance changes and the bridge remains in balance.

2.10. Bore Displacement Measurements

When the internal perforation is circular and concentric with the outside boundary, strains at the bore surface can be determined easily from measurements of the change in diameter of the core. These measurements can be obtained from linear differential transformers or from a thin, prestressed cantilever beam,

resting against the bore surface and recording the change in diameter through the response of an electrical strain gage cemented to the beam [4]. The description of the design of a probe using a linear differential transformer has been made in [14]. An application to the determination of core deformations in a grain subjected to axial acceleration can be found in [15]. It may be worth noting that parallel developments are taking place in the mining industry. For example, a probe to determine core-hole deformations is described in [16]. It has also been noted that three-dimensional photoelastic studies of the bottom of oil wells can be applied to the problem of the stress distribution at the circular end of the bore in rocket grains.

When the inside perforation is star-shaped, the technique of measurement is somewhat more difficult but still feasible. A suggestion about the use of these displacement measurements to determine strains will be presented in Section 5.

2.11. *Pressure Transducers*

There are instruments embedded in grains which are designed to measure pressures. Some of them take advantage of the piezoelectric property of crystals; others measure the deflection of a diaphragm (or thin circular plate) supported along its edge. Very reliable results are reported from some of these instruments. Careful calibration in a medium having the same mechanical properties as the propellant is necessary. It should be remembered that the deflection of a diaphragm against which a medium rests, will have an influence on the pressure distribution in that medium; and that, although the gage may be precise and sensitive, it may not measure the desired pressure in the medium. A design that has found several applications is commercially available [17]. It should also be pointed out that, to be complete, the calibration of these gages should include their response to laterally applied loads.

2.12. *Accelerometers*

All the instruments described previously have been designed to measure displacements or forces, or to determine strains. Frequently, useful information can be obtained from the determination of accelerations at selected points of the shell or of the grain. Many instruments are available commercially for this purpose. Their use in the mass of the propellant presents difficulties because of the difference in density between the accelerometer and the propellant, and, in general, the lack of sufficient sensitivity of the accelerometer.

Some accelerometers use strain gages. They are basically a single-degree-of-freedom spring system with a Wheatstone bridge, composed of four strain gages, attached to the spring system. An acceleration produces a strain which can be recorded.

Accelerometers can also be designed using piezoelectric crystals. The voltage produced by the crystals is proportional to the acceleration of the mass of the system. The design of a successful three-directional piezoelectric accelerometer is reported in [18].

3. DETERMINATION OF STRAINS AND STRESSES
IN THREE-DIMENSIONAL MODELS OF GRAIN

3.1. *Introduction*

In Section 2 a description was given of several methods that can be used to determine strains in actual propellant grains. It is obvious from that chapter that the determination of strains in actual grains is very difficult. (The translation of the so-determined strains into stresses would usually be an unreasonable ambition.)

Another approach which offers better chances of success and may provide useful information to the grain designers consists in the manufacturing of scaled-down models of the grain and their study under controlled conditions. The loads applied to the model simulate the ones acting on the grain. Also, some assumptions have to be accepted.

3.2. *Simplifying Assumptions for Model Analysis*

Grain and case materials will be assumed to be elastic and to behave linearly. Both will be assumed to be isotropic and homogeneous. Several of the consequences of these assumptions on designers' work have been mentioned elsewhere [20]. The assumption concerning the uniformity of pressure distribution at the interface between grain and case is discussed in Section 3.3.

3.3. *Pressure Loading on Three-Dimensional Models of Grains*

In the present state of development of experimental stress analysis techniques, photoelasticity is the method best suited to determine the distributions in models subjected to three-dimensional states of stress.

In most of the tests conducted at present using the conventional or "freezing" technique of three-dimensional photoelasticity, epoxy resins are used for the model material. The technique consists of machining the desired shape from a block of epoxy such as Hysol 4290, loading it in an oven, and allowing it to cool slowly under load. Slices are removed from the "frozen" specimen after it is back to room temperature and the load has been removed. This machining technique, however, becomes difficult and expensive when the shapes are as complicated as the one shown in Fig. 1.1. Two alternative methods have been proposed to avoid this difficulty. The first consists in machining the model by sections, as two-dimensional models, and cementing the sections one to the other. This method is still in process of development. The second consists in casting the epoxy resin to final shape. This method requires the use of the proper cores to avoid seizing, and presents the danger of contaminated edges. Although this technique is not completely under control either, it has already given some meaningful results. Figure 3.1 shows a model manufactured by casting, then sliced, and its slices replaced in their original position. Three sorts of slices were taken: meridian, hoop (or transverse), and radial (near the head of the model). The white core shown in the figure is plaster, and has been used only to hold the slices in place. Typical hoop and meridian slices are shown in Figs. 3.2

and 3.3. In this particular case, stress concentrations on the meridian planes are much lower than stress concentrations on the transverse planes.

A model such as the one shown in Fig. 3.1 could be cemented to a case and the composite structure subjected to pressure. This method is the most direct and the one that reproduces the prototype better, provided that the relative values of the modulus of elasticity of case and propellant are approximately the same
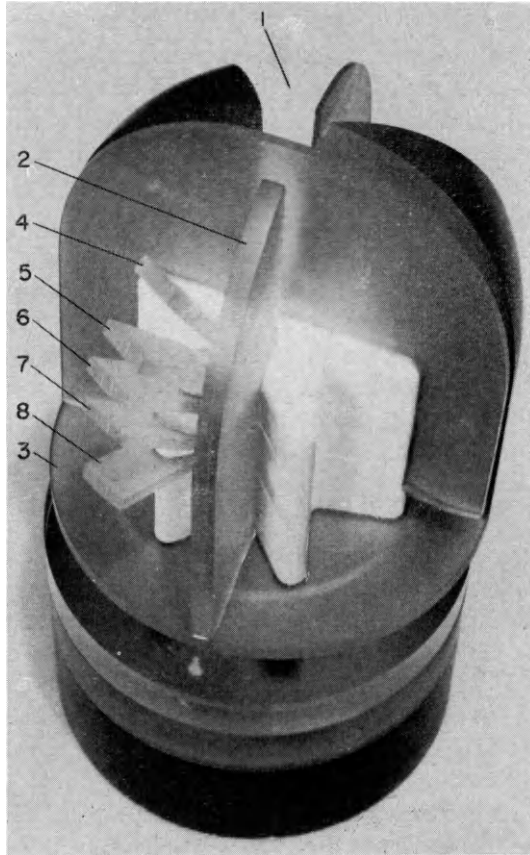
FIG. 3.1. Photograph of a reconstructed model of a thick walled pressure vessel with star shaped internal configuration and semi-spherical outside end.

in the model at the testing temperature and in the prototype. It can be used with several experimental stress analysis methods (brittle coatings, photoelasticity coatings, gages, etc.), but presents inherent difficulties when used with the "freezing" technique of three-dimensional photoelasticity. As the plastic is cooled from the critical temperature, two simultaneous phenomena take place: the "freezing" of the birefringence associated with the stresses produced by the pressure, and the "freezing" of the birefringence associated with the stresses produced by the restrained shrinkage of the plastic bonded to the case. Two

tests would be necessary to separate the effects of the two loading conditions.

The use of unbonded models subjected to internal pressure to determine the stresses present in bonded grains is based on the assumption that part of the pressure is taken by the case and part of the pressure is taken by the grain. It is also assumed that the grain web is sufficiently thick for this pressure to be transmitted uniformly at the interface between grain and case. When the case is
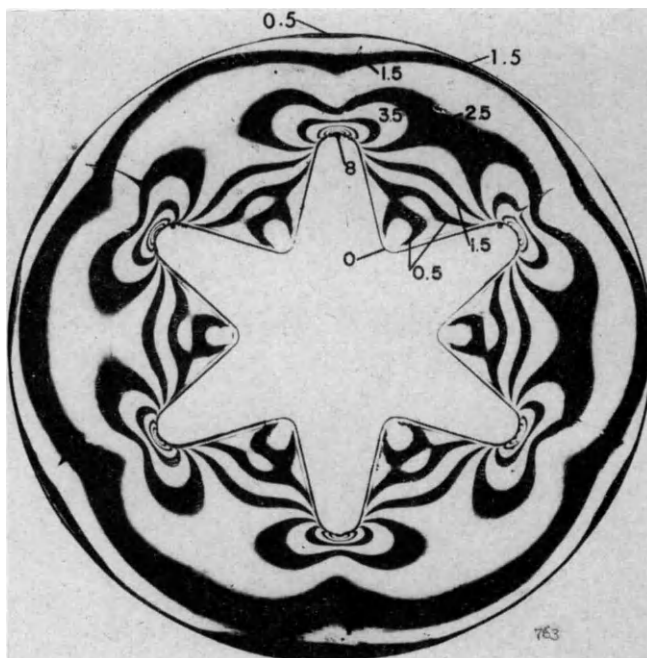
FIG. 3.2. Frozen isochromatics in the transverse slice of an epoxy model of a propellant grain, subjected to internal pressure.

thin and the grain is circular, this interface pressure (p') for the case of plane strain is given by:

$$p' = \frac{2(1-\nu)a^2p}{[a^2+(1-2\nu)b^2]+\dfrac{(b^2-a^2)(1-\nu_c^2)bE}{(1+\nu)hE_c}} \tag{3.1}$$

where p is the internal pressure, ν_c and E_c are the elastic constants of the case, ν and E are the elastic constants of the propellant, b and a are the outside and inside diameters of the grain, respectively, and h is the case thickness. If the grain is not circular but is star-shaped, the inside diameter is assumed to lie between the bottom of the fillets of the star and the tip of the star, probably much closer to the bottom of the fillets. A study of the radial rigidity of star-shaped grains is reported in [21].

Important contributions to the solution of the stress distribution in three-dimensional circular cylinders have been made lately by investigators, using numerical methods [22, 23].

3.4. *Restrained Shrinkage in Three-Dimensional Models of Grains*

To determine restrained shrinkage stresses, it is also possible to use a method that follows the conventional techniques of three-dimensional photo-elasticity.
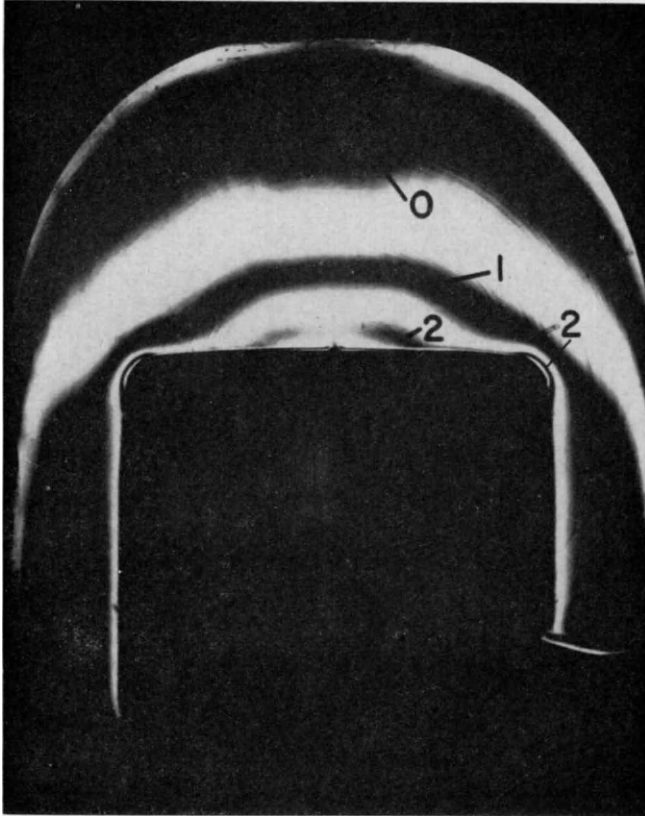
FIG. 3.3. Frozen isochromatics in a meridian slice of an epoxy model of a propellant grain model, subjected to internal pressure.

An epoxy model of the grain, either cast or machined, is cemented to the case along the bonded interface. The composite model is then subjected to the conventional heating cycle. This method has not been tried as yet. It has the disadvantage of requiring the previous machining or casting of the model and a careful cementing to the case.

Alternatively, it is also possible to cast epoxies inside the case and let them adhere to the wall of the case. In the process of curing and cooling, the plastic will shrink and develop the same state of stress as produced by a uniform and

steady drop in temperature. In general, however, the conventional three-dimensional techniques used without adaptation are not applicable because the epoxy resin would not have enough strength to stand the large shrinkage produced during the curing and cooling process. Effort has been directed, therefore, to either decrease the shrinkage or to increase the strength of the model materials, or both. The results of two formulations independently developed have been published [24].

One method of casting is illustrated in Fig. 3.4. A plexiglas core is used to cast urethane rubber around it. After removing the plexiglas core from the rubber
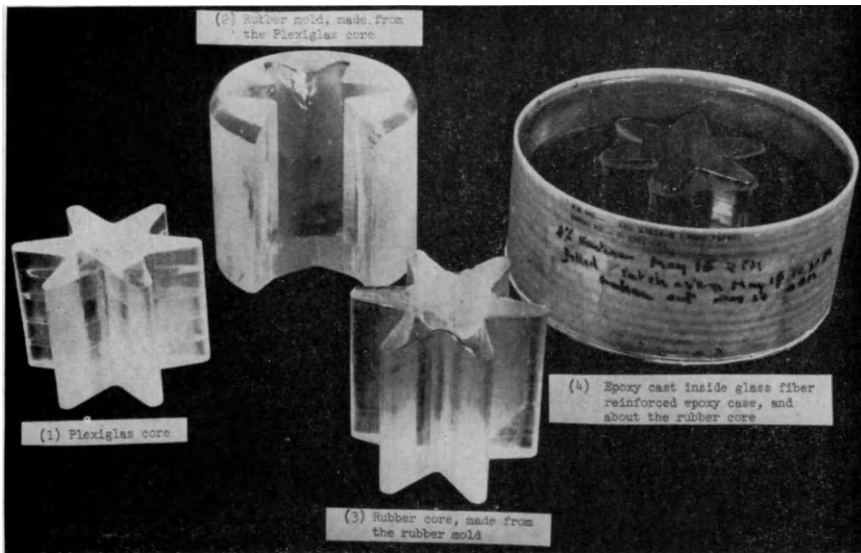
FIG. 3.4. Method used to prepare models to determine stress distributions in three-dimensional shrinkage problems.

casting, the casting is used as a mold to cast in it a urethane rubber core. This core is removed from the mold, and after being coated with a parting compound it is used for the epoxy casting. The outside mold of the epoxy casting is a glass-fiber reinforced epoxy shell. (In other cases, steel has also been used successfully.) The epoxy resin bonds to the outside shell but separates from the non-adhering core. After the epoxy has been cured and brought back to room temperature, the model is sliced, as in the conventional three-dimensional photoelasticity techniques. A section of a cast model showing bonded and unbonded portions of the case and grain is shown in Fig. 3.5. Typical meridian slices from other models are shown in Fig. 3.6. This method requires special calibration procedures and the knowledge of the amount of shrinkage that the model undergoes.

It is also possible to obtain displacements from the three-dimensional photoelasticity models. The displacements along the free boundaries of a short

cylinder subjected to shrinkage while bonded to an outer shell are shown in Fig. 3.7.

The solution of restrained shrinkage problems has also been approached using numerical methods [22, 23].
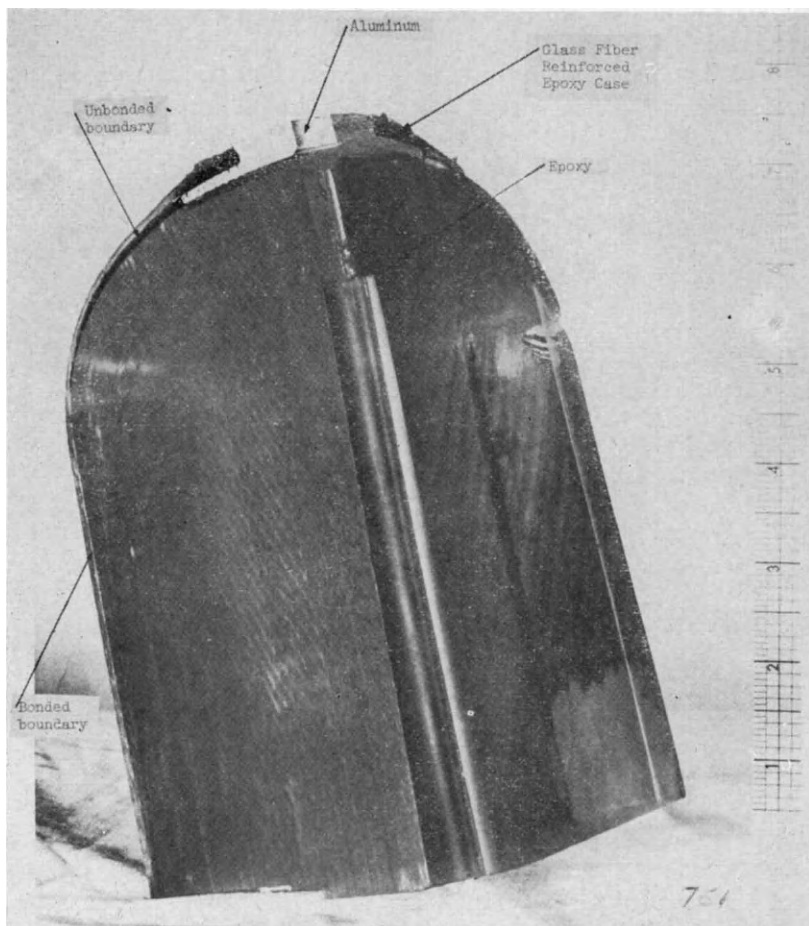
FIG. 3.5. Model of a partially bonded propellant grain.

3.5. *Gradient Thermal Loading in Three-Dimensional Models of Grains*

The solution of this problem can be approached by embedding some sensing elements in a model of the grain made of a transparent material. When epoxies are used, a sandwich can be prepared consisting of polarizing and analyzing films with an epoxy sheet in between. This sandwich can be embedded in the model, usually also made of epoxy [25]. When soft materials such as urethane rubber are used for the model, the embedded sensor can be a grid network of rubber threads [26] or one of the gratings used to produce moiré [27].

3.6. *Axial Acceleration (or Body Forces) on Three-Dimensional Models of Grains*

The strain–stress distributions under a steady state of acceleration correspond to the distributions due to deadweight.

There are several ways of approaching the solution of this problem, which is not simple.

The conventional "freezing" technique of three-dimensional photoelasticity could be used, loading an epoxy model in a centrifuge. The interpretation of the
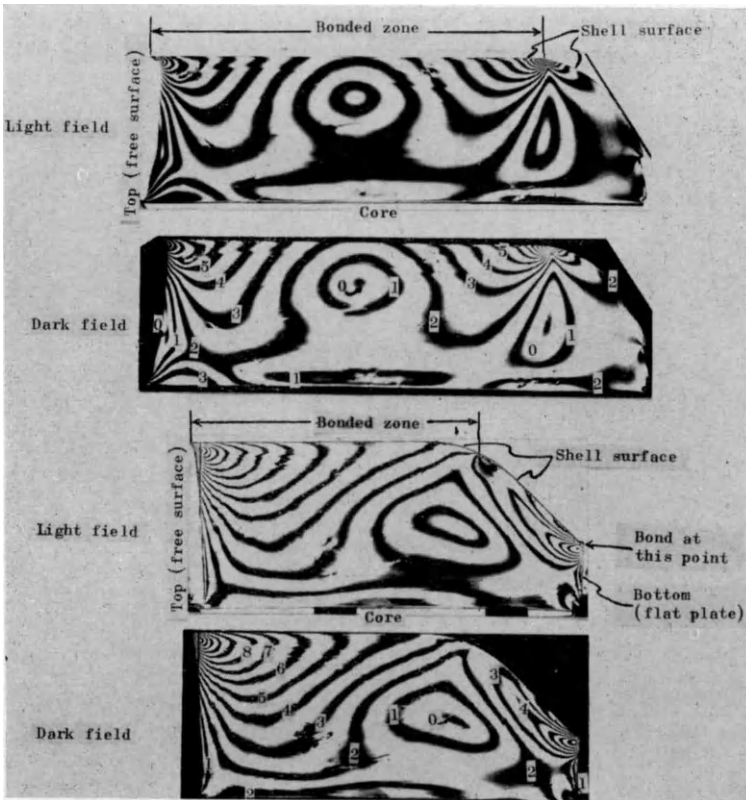
FIG. 3.6. Isochromatic patterns from the meridian slices of two cylindrical three-dimensional epoxy models bonded on the outer surface to a fiberglass shell.

results is complicated, however, by the fact that, as with the pressure loading, two states of stress will be simultaneously imposed on the model: one state of stress is that associated with the required acceleration, and the second state of stress is that associated with the differential shrinkage of case and grain (Section 3.4). The results of both loadings should be analyzed independently.

An alternative method would consist of the use of the "creeping" or "curing" methods of three-dimensional photoelasticity, which does not require heat to "lock in" the birefringent effect.

Attempts at qualitative determinations of the deformed shape of the core surface and of the bottom face of circular grains, using gelatin models, have been mentioned in [28] and [29]. An application to an actual grain subjected to acceleration has been mentioned in [15].
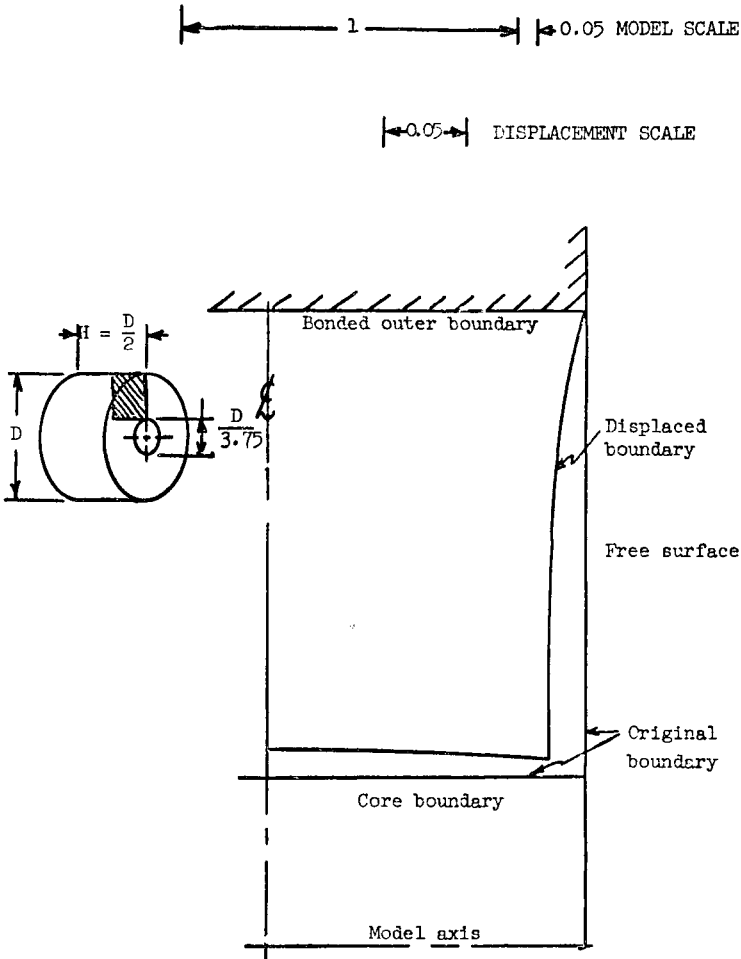
FIG. 3.7. Displacement field on boundary of circular cylinder subjected to 0.0066 shrinkage while bonded to a rigid outer shell.

4. DETERMINATION OF STRAINS AND STRESSES USING TWO-DIMENSIONAL MODELS

4.1. *Introduction*

Three-dimensional photoelasticity techniques are much more costly and time-consuming than two-dimensional photoelasticity techniques. It is natural, therefore, that an effort should be made to simulate at least part of the conditions of the three-dimensional problem in a two-dimensional test. Only in a few cases

will this simulation be rigorous, but it may frequently be useful. Two-dimensional stress analysis of plates with a geometry similar to the geometry of the transverse cross section of the grain, loaded by pressure or by restrained shrinkage, has been described in [20] and [21].

It is understood that the cylinder is long, and that the transverse cross section is the same along the axis of the cylinder. In some cases, however, designers may obtain some approximate conclusions from two-dimensional tests, even when the transverse cross section of the grain is not rigorously the same at all stations along the axis of the grain. Although somewhat less efficiently, two-dimensional stress analysis of plates with geometry similar to geometry of the meridian cross section of the grain, can also be conducted, as will be shown in Section 4.7.

4.2. Transverse Cross Section (Pressure Loading)

4.2.1. Description of the simulation.

An illustration of these approximations is shown in Fig. 4.1. It is assumed that for transverse cross sections far from the ends, the propellant is in a state of plane strain with a zero, or sometimes a non-zero but constant, axial strain. This assumption applies to both the pressure-loading and the restrained shrinkage-loading conditions. It is shown in the theory of elasticity that for the case of applied pressure, the in-plane state of stress in these cross sections is the same as the one present in thin disks of the same geometry, free on their top and bottom faces, loaded by pressure in the plane, and therefore subjected to plane stress. This justifies the use in experimental analysis of thin plates subjected to pressure to determine the state of stress in the central portions of the grain.

It is also shown in the top right box of Fig. 4.1 that the maximum shear stress distribution in the perforated disk is the same, whether the pressure is applied to the inside or to the outside boundary. This follows directly from the fact that the addition of an isotropic state of stress does not change the shears. If an isotropic state of tensile stress of magnitude equal to the pressure is added to the disk subjected to internal pressure, the internal boundary will become free, and the outside boundary will be subjected to a uniform applied radial tensile stress. The change in sign of the tensile stress into compressive stress or applied pressure does not change the shear stress. This reasoning substantiates the soundness of the experimental practice which consists of applying pressure to the outside boundary of perforated photoelastic models rather than to the inside boundary. Here again as in some phases of three-dimensional analysis, the solution of the problem could be approached using numerical methods [30].

4.2.2. Techniques.

The description of the techniques used for these two-dimensional simulations and the description of the evaluation of the results obtained from them can be found in [20] and [31]. The method takes advantage of a device described in [32] which is basically a rubber tube that follows the contour of the boundary (Fig. 4.2) as pressure is applied to the tube, and the reactions are taken on three sides
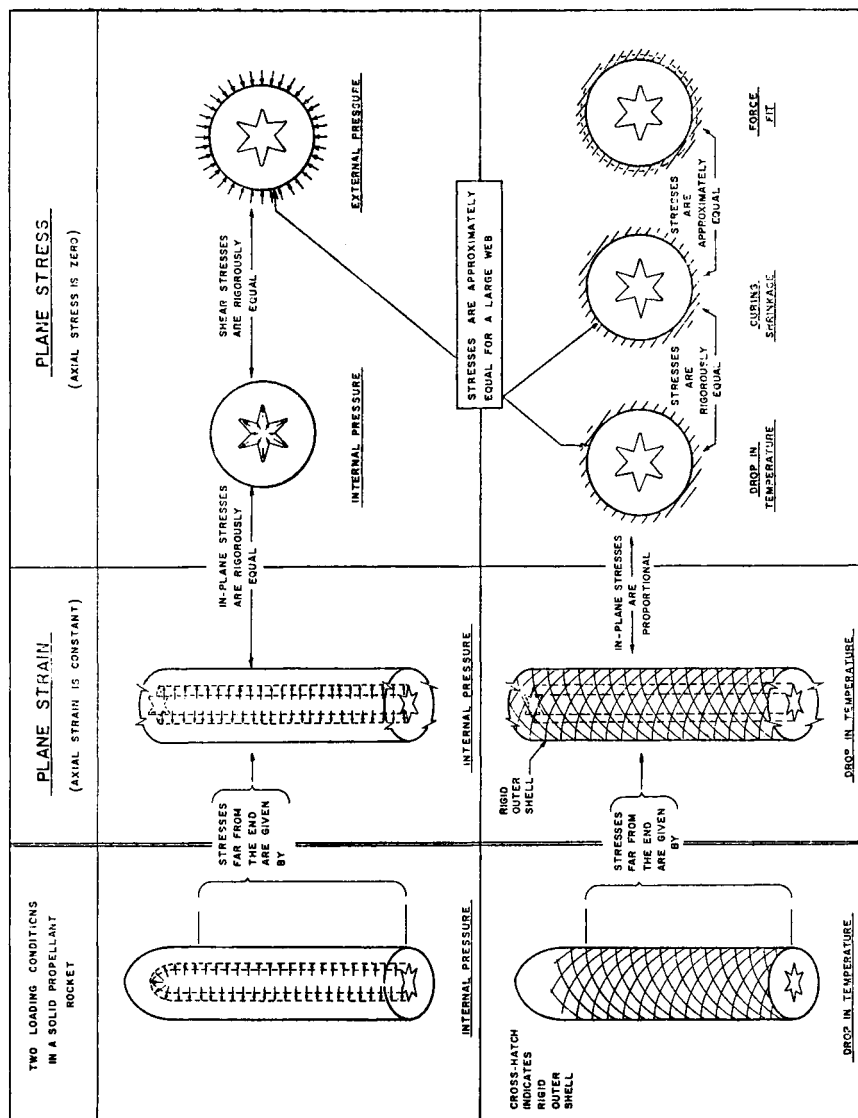
Fig. 4.1. Two-dimensional simulation of the hoop stresses in a rocket grain.

by the device and on the fourth side by the model. Results obtained with this device have been published in many reports and papers, among which is [33]. Since the publication of these papers, the techniques have been further developed to include applications to very complicated boundaries. The isochromatics
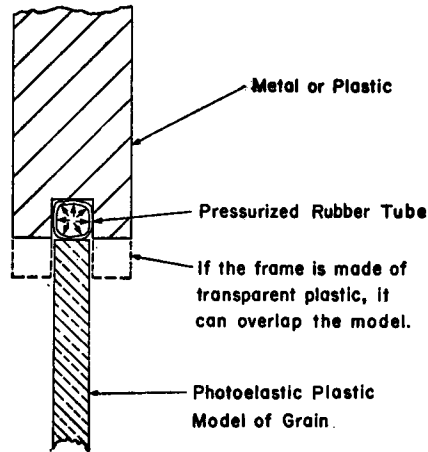
FIG. 4.2. Detail of the device to apply uniform pressure to a model of complicated shape.

obtained when the uniform pressure is applied to the outside boundary of a scalloped transverse cross section of a grain, are illustrated in Fig. 4.3. Figure 4.4 shows the device used to apply uniform pressure to parts of a boundary.

4.3. Transverse Cross-Section (Restrained Shrinkage)

4.3.1. Description of simulation.

If two different materials are bonded together, the same state of strain will be obtained, whether shrinkage results from the curing process of one of the materials, or as a consequence of a change in temperature when the two materials have different coefficients of expansion. The same contraction should produce the same state of strain. The bottom half of Fig. 4.1 applies to the case of restrained shrinkage, a reasoning similar to the one applied in Section 4.2.1 to pressure loading.

It is pointed out in Fig. 4.1 that when the web is relatively thick with respect to the radius of the grain, the solution obtained from applied pressure is also approximately the same as the one obtained from shrinkage.

Two-dimensional models subjected to curing shrinkage or to a drop in temperature, however, will not be in a state of plane stress at the bonded boundaries due to the out-of-plane restraint. This problem is sometimes called "pinching" [31].

Another alternative way of determining shrinkage stresses is also sketched in Fig. 4.1. It consists of force-fitting a rubber model into an undersized ring. The solution so obtained is the same as the one obtained from the other two methods, provided the web is relatively thick.
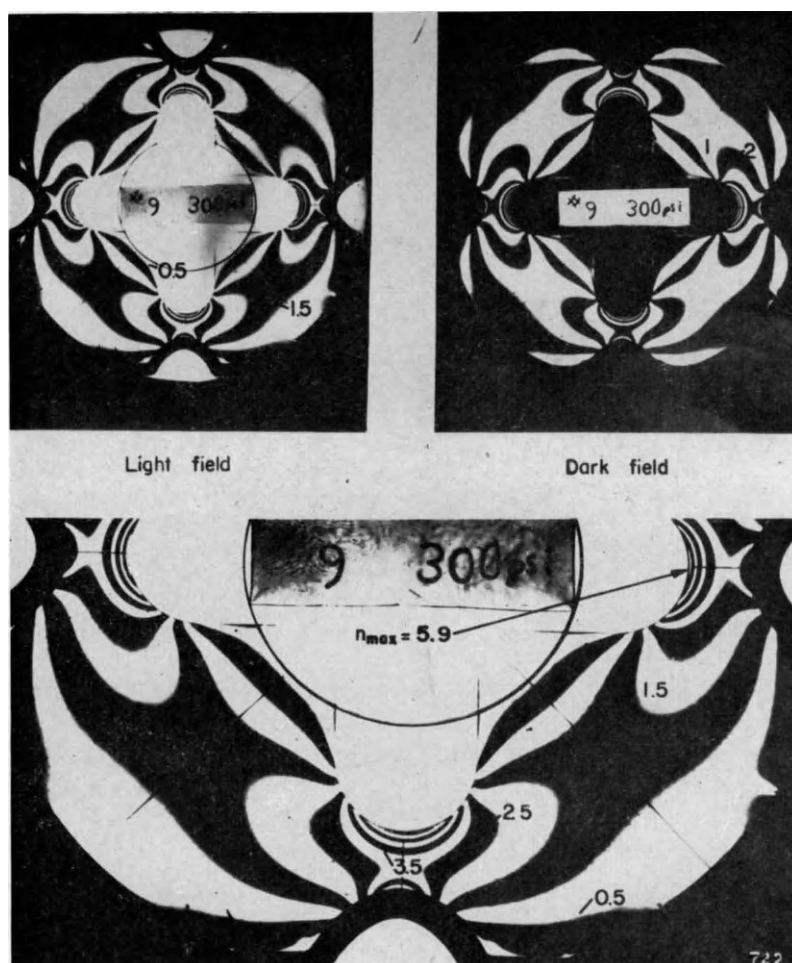
FIG. 4.3. Isochromatics in a perforated disk, subjected to uniform pressure on its scalloped outside contour.

4.3.2. *Technique for thermal loading*

A scaled two-dimensional model of the cross section (the same as the one used in the previous test for internal pressure or, preferably, one made of soft urethane rubber) is cemented at the outside boundary to a steel ring. The temperature of both steel ring and plastic model is lowered by the same amount. The fringes corresponding to the resulting shear stress are observed in a polariscope and interpreted by calibration. Details of the test setup can be found in [35].

4.3.3. *Technique using mechanically applied displacements.*

The photoelastic stress and strain pattern produced by a thermally loaded two-dimensional model (Section 4.3.2) can be simulated by a mechanical deformation on the outer boundary of the type $u_r = Kr$ where u_r is the radial

displacement, K is a constant, and r is the distance of the point at the boundary from the center [35]. The approach is justified if the thermal loading is thought of as a displacement on the outer boundary of the type $u_r = a\Delta Tr$.
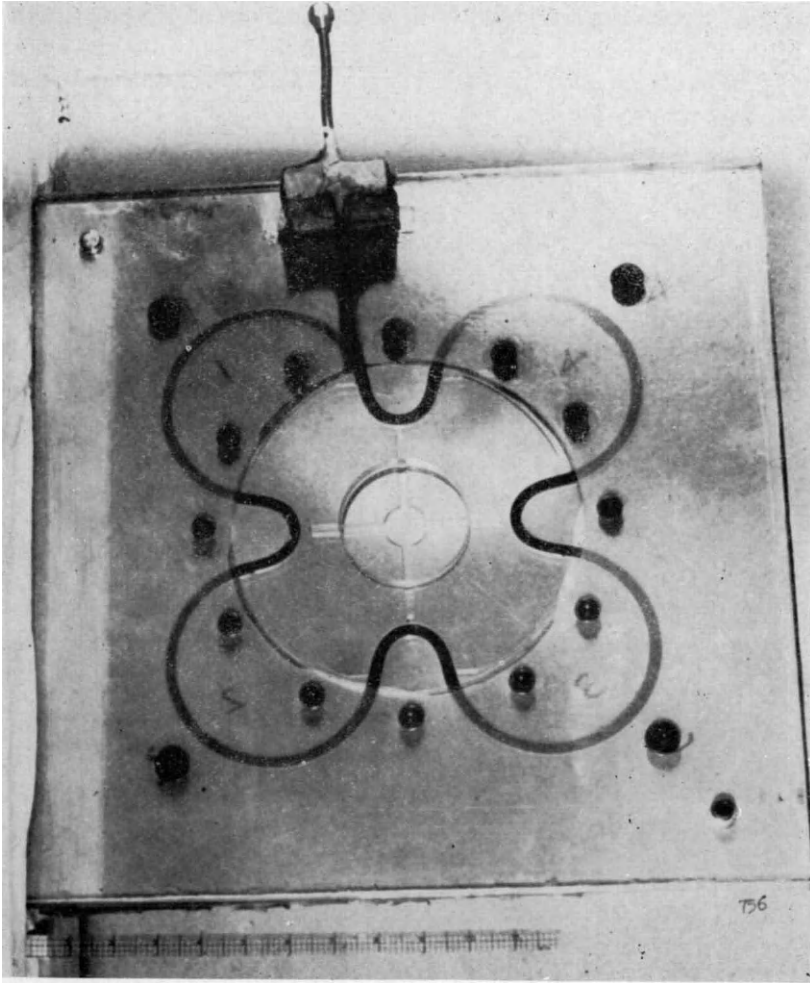
FIG. 4.4. Device used to apply uniform pressure to parts of the outside boundary of a two-dimensional propellant-grain model.

A perforation in the shape of the outer contour of the grain is made in a sheet of metal or rigid plastic. A grain model, oversized by about one per cent relative to the rigid perforation, is made of a soft plastic such as urethane rubber. The slightly oversized model is then forced into the rigid perforation. The resulting photoelastic patterns show some irregularities along the outer boundary due to small imperfections in the contact surfaces; however, these irregularities do not

extend to the fillets of the inner boundary, which are the main region of interest, and can be ignored in the determination of the stress concentrations.

4.3.4. *Curing shrinkage technique.*

A plate of urethane rubber is cast inside a ring of the same configuration as the case, and the rubber is allowed to bond to the ring during curing. A male mold of the shape of the core is used in the central part of the plate with a parting agent on its boundary to let the rubber, bonded to the outside boundary
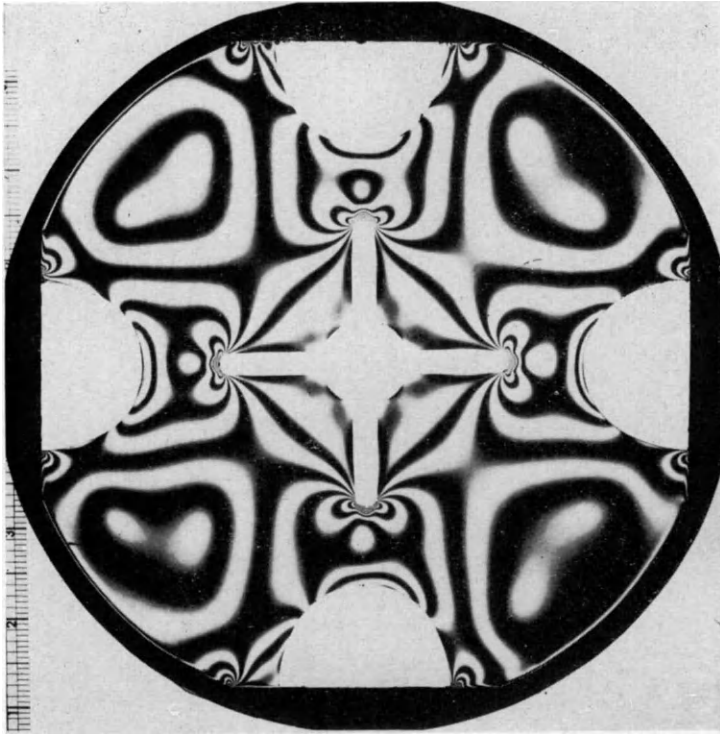
FIG. 4.5. Isochromatics in a perforated disk subjected to shrinkage restrained at some parts of its scalloped outside contour.

move away from the inside boundary. The pattern obtained following this procedure will be the same as the ones described above, and the method can be used as an alternative method for the determination of the two-dimensional stress distribution produced by uniform and steady thermal loading in bonded grains. The application of the curing shrinkage technique to the transverse cross-section of grain exhibiting a scalloped boundary is shown in Fig. 4.5. Here the shrinkage is restrained only at some parts of the boundary. The boundary of the scallops is free. A similar method using an epoxy resin is described in [21].

4.4. *Transverse Cross Section (Steady Thermal Gradient Loading)*

4.4.1. *Assumptions.*

It is assumed that the temperature is the same along lines parallel to the longitudinal axis of the cylinder. It is further assumed that the temperature is the same at all points of the inside boundary and also the same at all points of the outside boundary, but that this value is different from the value at the inside boundary. There may be other perforations in between the inside and outside boundaries. Finally, it is also assumed that the plane stress solution of the problem is significant in the evaluation of the three-dimensional grain.

4.4.2. *Technique of mechanical analogy.*

An important simplification of the analysis was introduced independently by Muskhelishvili and Biot, who presented a rigorous mechanical analogy of the thermal phenomenon. The correct stress distribution can be obtained if the multiply-connected cylinder is made simply-connected by the necessary number of cuts and if certain distortions are applied to the lips of each of those cuts. The magnitude of these distortions can be determined by solving Laplace's equation for that particular configuration. This can be done relatively easily by using one of Laplace's analogies such as the electrolytic tank. The problem therefore is simplified into one of determining by photoelasticity in a transparent model the stresses produced by mechanically applied distortions to certain boundaries of the model. An example of this method of working [36] is shown in Figs. 4.6 and 4.7. The method has also been applied for parametric studies of grain geometry [37].

4.4.3. *Technique by thermal loading.*

The steady state thermal gradient problem described above lends itself to direct photoelastic analysis. A transparent model of a photoelastic material (CR–39, epoxy, or urethane rubber) is subjected, for instance, to one temperature around the outside boundary and another temperature at the inside boundary. A low temperature can be produced by using dry ice or cold air which is sent through a box containing dry ice. The faces of the model are insulated with plastic plates to insure that the heat transfer is produced in the plane of the model. Photographs can be taken in the usual way.

4.5. *Transverse Cross Section (Transient Thermal Gradient Loading)*

4.5.1. *Assumptions.*

Changes in temperature in the propellant are relatively slow. Frequently, it is considered that inertial effects have no importance. Within this assumption, thermal stresses can be determined, as for the case of steady gradient, by actual thermal loading of a model. Successive photographs can be taken at different intervals corresponding to the development of the thermal transient phenomenon.

4.5.2. *Techniques.*

An illustration of the procedure that can be followed is shown in Figs. 4.8 and 4.9. A sudden change in temperature is applied either to the inside perforation of the grain model (Fig. 4.8) or to its outside periphery (Fig. 4.9). The drop in temperature can be produced by means of dry ice or by a current of cold
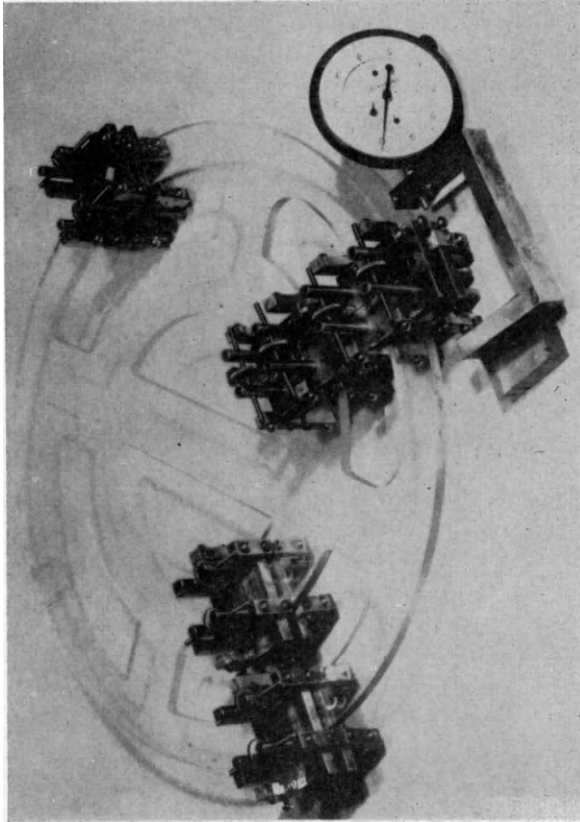
FIG. 4.6. Photoelastic model of a multiply-connected cylinder.

air. If necessary, temperatures can be recorded, using thermocouples (Fig. 4.9). Epoxy has been found to be the best material for this kind of investigation because of its high optical sensitivity to the thermal loading and also because the fringe value is little influenced by the change in temperature within the practical range of temperatures used in the test.

4.6. *Transverse Cross Section (Gravitational Loading)*

It is possible to obtain useful information from large models of the grain transverse cross section, manufactured using urethane rubber. This material is transparent and is very sensitive to stress photoelastically. If the model is

sufficiently thick, enough response can be obtained for a quantitative analysis using photoelasticity and grids, or photoelasticity and moiré. An illustrative example of isochromatics and grid distortions in a urethane rubber ring subjected to gravitational force is shown in Fig. 4.10.
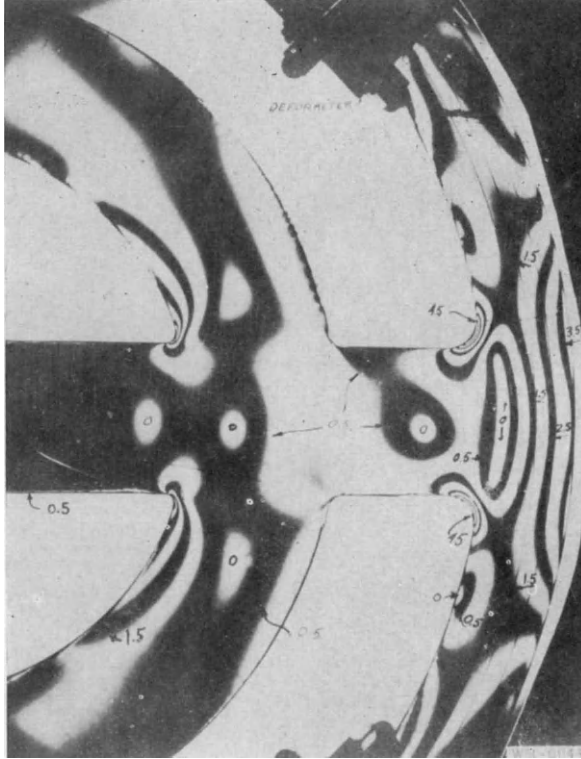
FIG. 4.7. Light-field photograph of a portion of a photoelastic model which has been loaded by using deformeters to simulate a thermal gradient loading.

4.7. *Meridian Cross Section (Restrained Shrinkage)*

Various studies [38, 39] show the relationship of stress and strain concentration factors in two-dimensional bodies with the three-dimensional counterpart generated by rotating the two-dimensional body about an axis (either its own axis of symmetry or an axis outside the body). These studies, in general, show (1) a decrease of the stress concentration factor in the three-dimensional bodies with respect to stress concentration factors in the two-dimensional model, and (2) for those cases in which the point of concentration is far from the axis of rotation (in terms of the dimensions defining the point—radius of fillet, depth of notch, or the like)—the concentration factors are about the same for both cases.

4.7.1. *Small axial perforation.*

The "engineering" reasoning supporting the use of two-dimensional models of the meridian cross section of the rocket grain to obtain an approximation of the stresses due to restrained shrinkage in certain regions of the three-dimensional counterpart is given elsewhere [31]. It is suggested that a two-dimensional model with the outline of the meridian cross section of a rocket grain with a small core
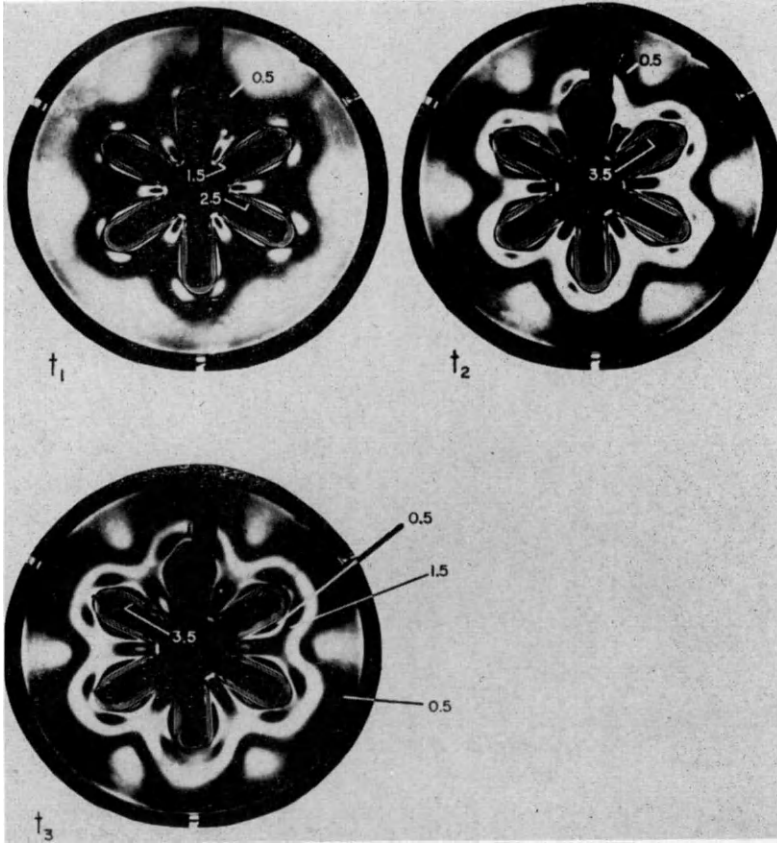
FIG. 4.8. Transient isochromatics in a star-shaped epoxy model subjected to a sudden change in temperature at the inside boundary.

bonded along corresponding boundaries and subjected to shrinkage will give an approximation of the stresses in the neighbourhood of the boundary of the three-dimensional counterpart.

Figure 4.11 shows a two-dimensional model bonded on two sides. This model was used to study the stresses at the fillets of different geometries near the interface. The purpose of the model analysis was only to determine the relative value of the stresses in the fillets. An approximate solution was therefore acceptable.

Figure 4.11 shows also a meridian plane slide taken from a three-dimensional of a cylinder bonded on its outer diameter and with a core diameter equal to $\frac{1}{4}$ of the outer diameter. The pattern has a marked similarity to the two-dimensional model shown in Fig. 4.11. This seems to substantiate the approximations inherent in the reasoning mentioned above.
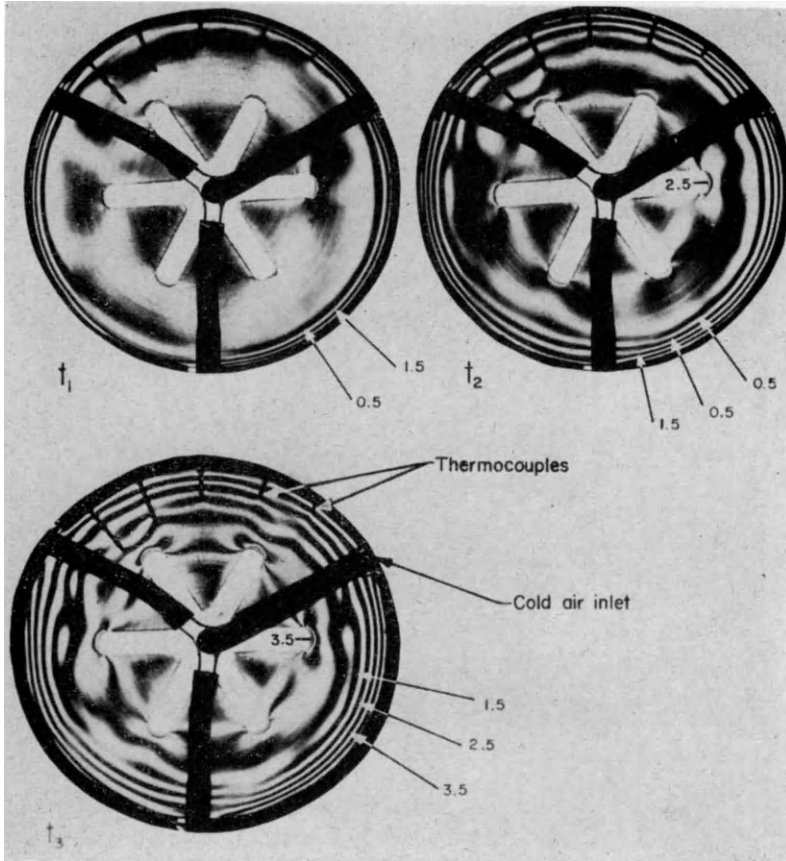
FIG. 4.9. Transient isochromatics in a star-shaped epoxy model subjected to a change in temperature at the outside boundary.

The out-of-plane restraint that takes place on the bonded boundaries of the two-dimensional models when subjected to shrinkage ("pinching") is noticeable on the top photograph of Fig. 4.11.

4.7.2. Large axial perforation.

If a two-dimensional model is bonded on one edge only, it can be shown that the solution of the plane-stress case corresponds to the plane-strain solution of a long bar bonded on one surface which, in turn, could be compared approximately to the stresses in the meridian cross section of a thin-walled, circular cylinder with a meridian cross-section between its inner and outer diameters

of the same shape as the shape of the two-dimensional model and bonded on the outer diameter to a rigid shell. Figure 4.12 shows the isochromatics in a meridian slice of a circular cylinder with an outer diameter $1\frac{2}{3}$ times the inner diameter. Figure 4.13 shows the isochromatics in a two-dimensional model bonded on one
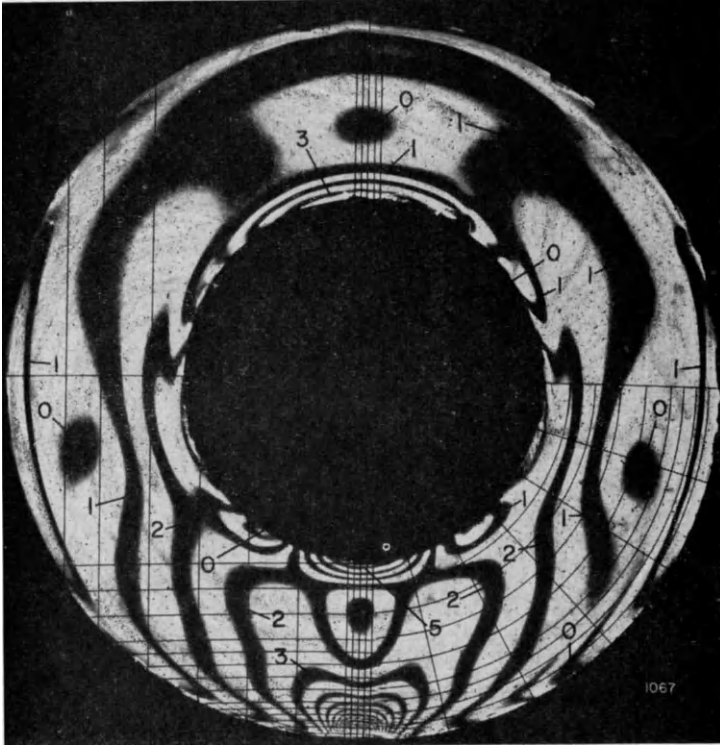
FIG. 4.10. Isochromatic pattern in a urethane rubber ring subjected to gravitational loading.

boundary. Figure 4.14 is a comparison of the two models in terms of maximum shear stress along the interface, normalized in terms of the maximum shear stress on the interface far from the corner. This comparison also seems to substantiate the approximations inherent in the reasoning presented above.

5. DETERMINATION OF STRAINS AND STRESSES IN THE GRAIN FROM CORE DISPLACEMENT

Measurements in Grain Models

Under the conditions of linear behavior of the material and constant boundaries, the strain (and stress) at one point in a body will be some multiple of the strain (and stress) at any other part of the body, despite variations in the magnitude of load. Where this is so, a displacement between any two points on the body will have a fixed linear relationship with any strain or stress in the body, irrespective of variations in the magnitude of the load.
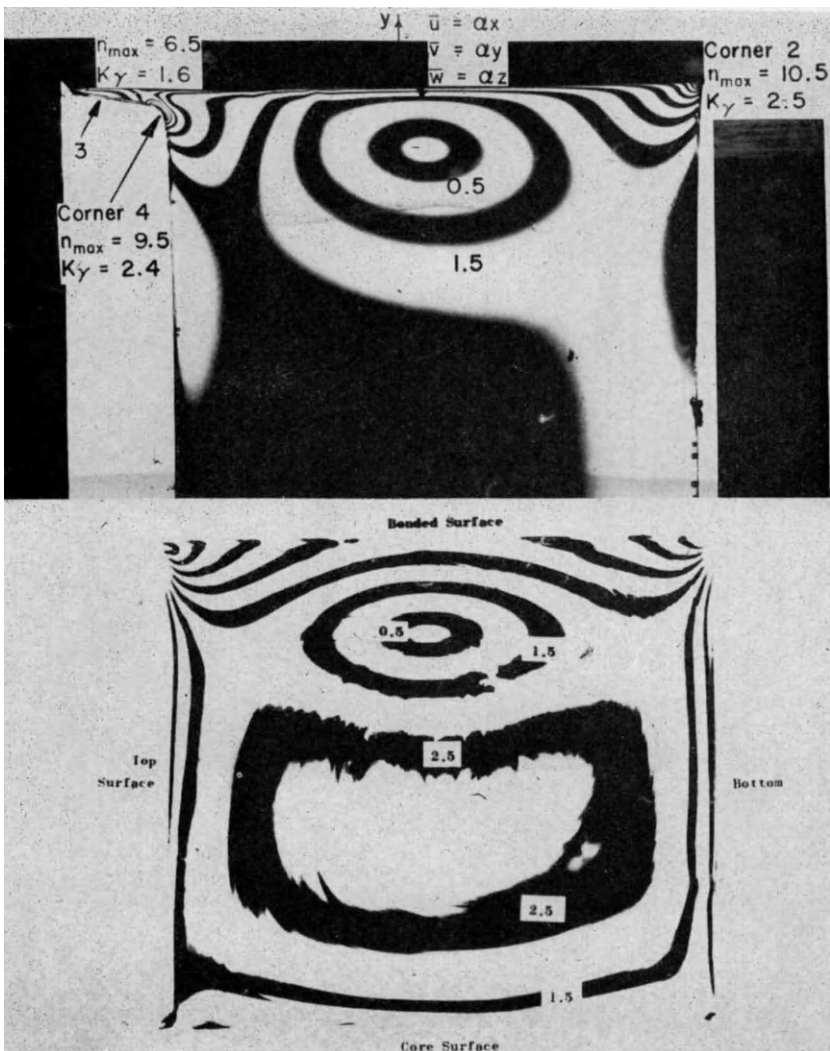
Fig. 4.11. (top) Isochromatic patterns on a two-dimensional shrinkage model bonded on two short sides.

(bottom) Isochromatic pattern in a meridian slice taken from a thick-walled hollow cylinder.

Thus, if it were possible to measure accurately the distance across the core surface of a rocket motor, and if the relationship between the change in this distance and the strains or stresses in a fillet could be determined, then, under the above-mentioned conditions, it would be possible to determine the strains or stresses in a fillet from a measurement of the change in length of the core diameter.

Methods of displacement measurement exist, which are relatively easy to use and of sufficient accuracy to determine the change in diameter of the grain core

27
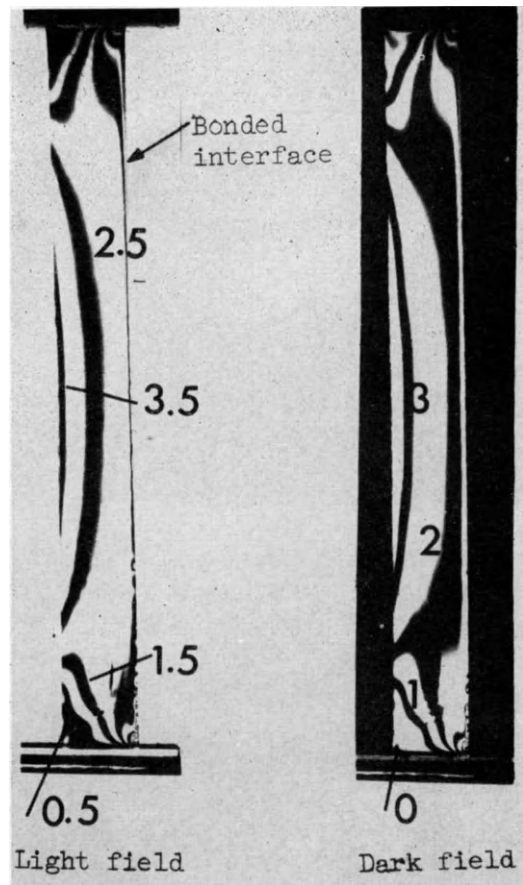
FIG. 4.12. Isochromatic pattern in a meridian slice taken from a thin-walled hollow circular cylinder (outer to inner diameter ratio of 1.67.)
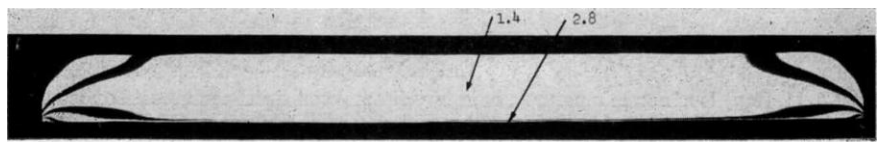
FIG. 4.13. Isochromatics in a strip subjected to restrained shrinkage on one of its long sides.

when the rocket is subjected to thermal loads in storage. It is possible to relate these displacement measurements to the strains by a calibration procedure which could be conducted in actual grains, or scaled-down grains, or, as it will be shown below, in small-sized photoelastic models.

If the calibration is made on scaled-down models of any sort, then the relationship becomes one of model analysis. Consider, then, four cases where the model
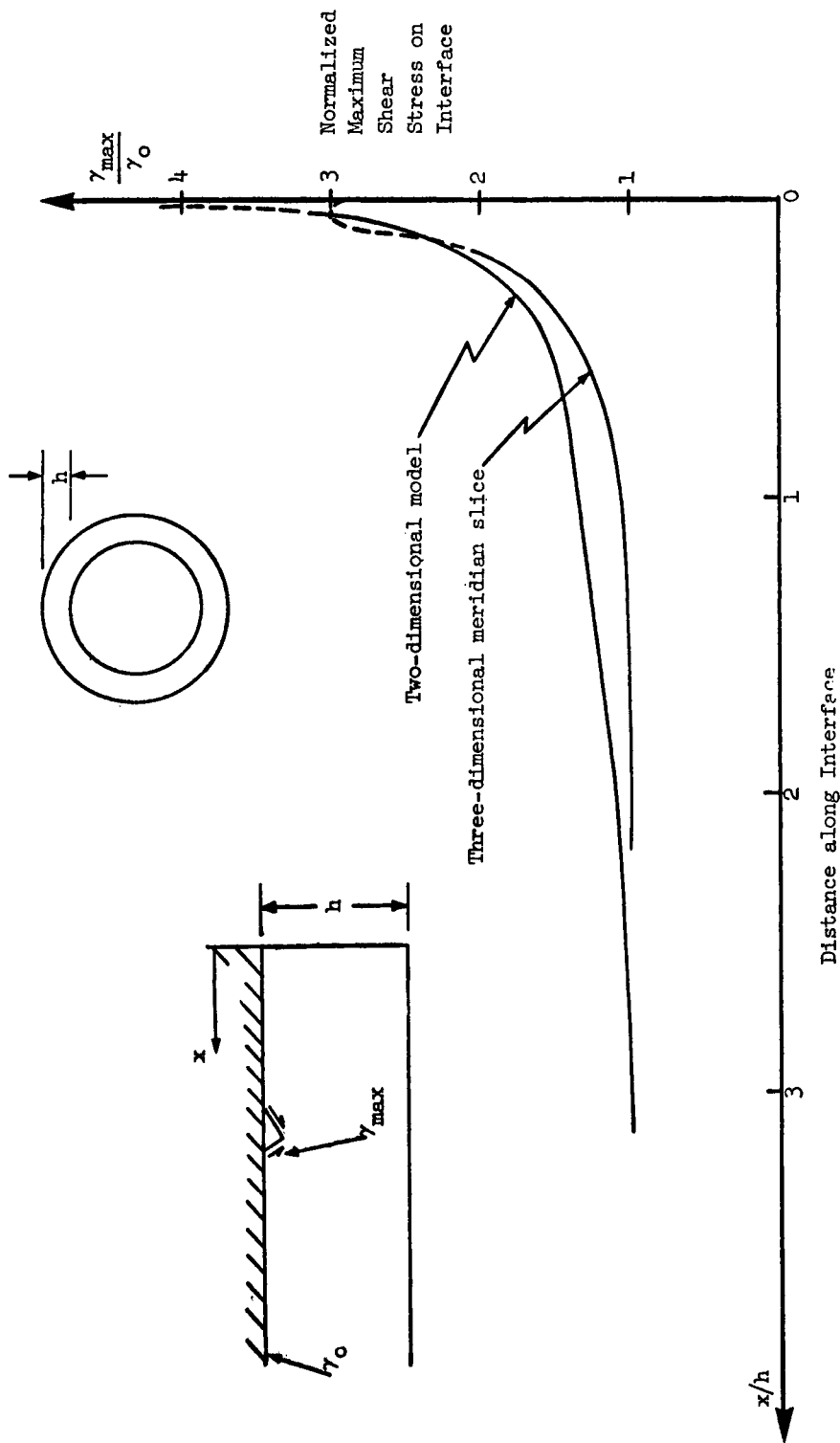
FIG. 4.14. Comparison of normalized shear stresses at a bonded interface in two- and three-dimensional models.

is a geometrically scaled-down version of a part of the rocket grain and made of a material which may be different from that of the propellant.

Cases 1 *and* 2.—For the part of a rocket grain which is subjected to internal pressure and is in a state of plane stress (case 1) or a state of plane strain (case 2), the relationships between core displacements, strains and stresses on propellant and model are given by:

$$\epsilon_p = \frac{\delta_p}{D_p} \frac{D_m}{\delta_m} \epsilon_m = \frac{1}{\lambda} \frac{\delta_p}{\delta_m} \epsilon_m$$

$$\sigma_p = \frac{\delta_p}{D_p} \frac{D_m}{\delta_m} \frac{E_p}{E_m} \sigma_m = \frac{1}{\lambda} \frac{\delta_p}{\delta_m} \frac{E_p}{E_m} \sigma_m$$

(5.1)

where p and m refer to the propellant and model, respectively

$\epsilon =$ the strain at corresponding points on the propellant and model

$\delta =$ the actual change in length of the core diameter

$D =$ the core diameter

$\lambda = \dfrac{D_p}{D_m}$, the scale factor

$\sigma =$ the stress at corresponding points on the propellant and model

$E =$ Young's modulus

It is assumed that the Poisson's ratios for the propellant and the model are approximately the same, which is not unreasonable for the usual range of propellants and model materials.

Case 3.—For the part of a rocket grain which is subjected to a uniform steady thermal loading, restricted on the outer boundary, and in a state of plane stress, the comparable relationships will be:

$$\epsilon_p - a_p \Delta T_p = \left[\left(\frac{\delta_p}{D_p} - a_p \Delta T_p \right) \Big/ \left(\frac{\delta_m}{D_m} - a_m \Delta T_m \right) \right] \left(\epsilon_m - a_m \Delta T_m \right)$$

$$\sigma_p = \left[\left(\frac{\delta_p}{D_p} - a_p \Delta T_p \right) \Big/ \left(\frac{\delta_m}{D_m} - a_m \Delta T_m \right) \right] \frac{E_p}{E_m} \sigma_m$$

(5.2)

where the terms and assumptions are as shown above and in addition:

$a =$ the coefficient of thermal expansion (if a is not a constant over the temperature range, the thermal strain terms must take the form

$$\int_{T_1}^{T_2} a\Delta T)$$

$\Delta T =$ the change in temperature over which δ, ϵ and σ are measured (for a drop in temperature, the value is negative)

Note here that ϵ and δ are the actual measured quantities on grain and model. In the case of the strains, the significant quantity is the $(\epsilon - a\Delta T)$ term, since it represents the stress-producing strain.

Case 4.—For the part of the grain which is subjected to a uniform steady thermal loading, restricted on the outer boundary, and in a state of plane strain, the comparable relationships will be:

$$\epsilon_p - (1+\nu)\,a_p \varDelta T_p = \left[\left(\frac{\delta_p}{D_p} - (1+\nu)\,a_p \varDelta T_p\right) \middle/ \left(\frac{\delta_m}{D_m} - (1+\nu)\,a_m \varDelta T_m\right)\right]$$

$$[\epsilon_m - (1+\nu)\,a_m \varDelta T_m]$$

$$\sigma_p = \left[\left(\frac{\delta_p}{D_p} - (1+\nu)\,a_p \varDelta T_p\right) \middle/ \left(\frac{\delta_m}{D_m} - (1+\nu)\,a_m \varDelta T_m\right)\right]\frac{E_p}{E_m}\,\sigma_m$$

(5.3)

where the terms and assumptions are as above and in addition:

   ν = Poisson's ratio of both propellant and model material

In all four cases it has been assumed that each model, corresponding to the grain being analyzed, is in the same condition as the grain with respect to the type of loading and with respect to the state of stress, either plane stress or plane strain. However, for large web grain analysis, it is possible to use one of the four model analyses mentioned above in association with the other three cases, as illustrated in Fig. 4.1.

Further, if the analysis is restricted to transverse stresses, strains, and displacements, use can be made of the fact that the stress distribution for a plane stress problem is the same as the stress distribution for the corresponding plane strain problem. This allows the application of any stress ratio computed from either of the two-dimensional plane stress models (cases 1 and 3) to the plane strain counterpart (cases 2 and 4, respectively). If the web of the grain is sufficiently large, a stress ratio computed from a model of any of the four cases can be applied to all four cases.

This application, however, holds only for stress ratios. The strain ratios are not, in general, equal in the plane stress and corresponding plane strain field. However, they are equal if the ratios are between free boundary strains. It should also be pointed out that a core displacement can be considered as a free boundary strain, since it is completely determined by the strains about the core, which are all free boundary strains.

In summary, a two-dimensional plane stress photoelastic analysis of the pressure or thermal type can be applied to either thermal or pressure loading of a rocket grain part under plane-stress or plane-strain—assuming Poisson's ratio is approximately the same in the photoelastic model and in the propellant, and the web thickness is large—to determine the free boundary fillet strains from a displacement measurement of the core.

Three tests illustrating the application of this method are described in [1].

The first model is shown in Fig. 5.1. The model loaded with a uniform pressure on the outer periphery is CR–39. The required properties are $F_e = 0.00073$ in./fringe and $\nu = 0.42$. The model core diameter is 4.04 in. If the bottom of the fillet where the strain is the highest is chosen as the point of analysis, then for the load shown in the figure, $n = 6.1$ fringes, and the tangential
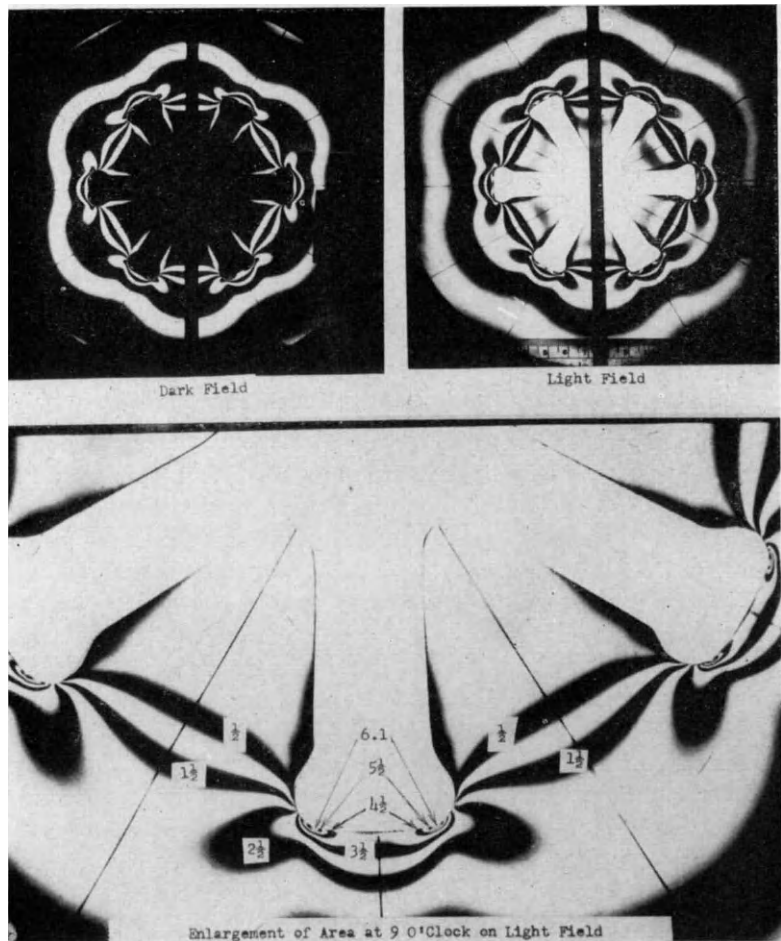
FIG. 5.1. Isochromatic fringe patterns of a rocket-grain model subjected to pressure.

strain is

$$\epsilon_m = \frac{2nF_\epsilon}{1 + \nu} = 0.00627 \text{ in./in.}$$

One ten-thousandths of an inch dial gages were used to measure the displacement of the core surface. This displacement for the pressure which gave 6.1 fringes was 0.0105 in. which gives $\epsilon_m/(\delta_m/D_m) = 2.41$. Using this photoelastic value and measurement of the model core (case 1), the strain in the prototype as a function of the measurement of the core displacement in the prototype (case 4) is given by

$$\epsilon_p - (1 + \nu) a_p \Delta T_p = 2.41 \left(\frac{\delta_p}{D_p} - (1 + \nu) a_p \Delta T_p \right) \tag{5.4}$$

The second test setup is shown in Fig. 5.2. The model was subjected to a uni-
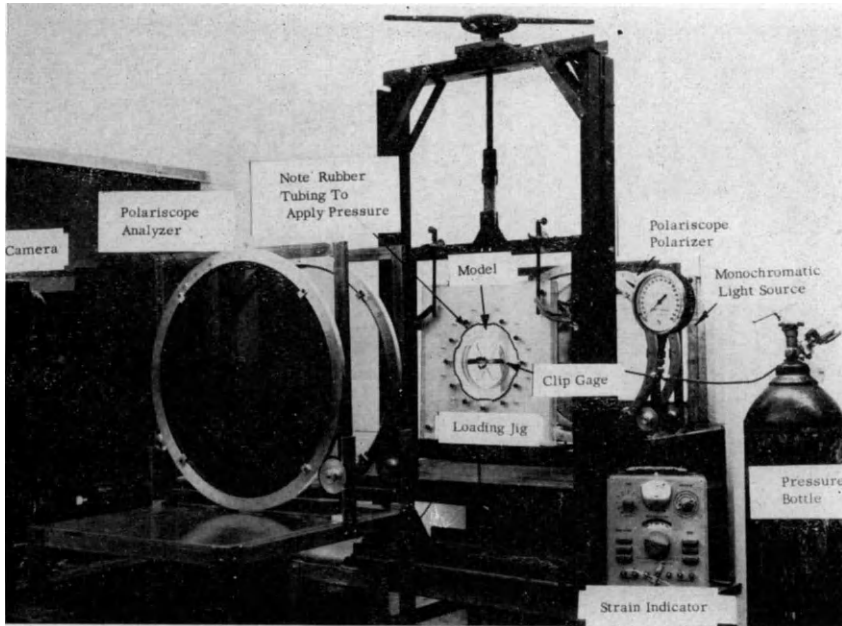
FIG. 5.2. Test set-up to apply a uniform pressure to the outer periphery of a rocket-grain model.

form pressure on the outer periphery. The measured quantities are $n = 10.0$ at the fillet, $\delta_m = 0.0145$ in. (a clip-type strain gage was used here to measure deflections), and $D_m = 4.40$ in. The model material constants are the same as before, and the equation for the peak strain in this design therefore is:

$$\epsilon_p - (1 + \nu)\, a_p \Delta T_p = 3.12 \left(\frac{\delta_p}{D_p} - (1 + \nu)\, a_p \Delta T_p \right) \qquad (5.5)$$

The loading of the third model is shown in Fig. 5.3. The model was bonded to an outer steel ring and the assembly placed in a cold chamber. The temperature was lowered, and the fringe pattern shown in Fig. 5.4 was obtained.

$n = 9.0$
$\delta_m = 0.045$ in.
$F = 1.40$ psi/fringe
$E = 330$ psi
$a_m = 104 \times 10$ in./in./°F
$\Delta T_m = -119$°F

As before, $D_m = 4.40$ in. and the resulting expression is

$$\epsilon_p - (1 + \nu)\, a_p \Delta T_p = 3.36 \left(\frac{\delta_p}{D_p} - (1 + \nu)\, a_p \Delta T_p \right) \qquad (5.6)$$

The variation between the expressions obtained from thermal loading (5.6) and pressure loading (5.5) can be ascribed primarily to experimental errors and, to some extent, to the variation in the boundary conditions used in the two methods.
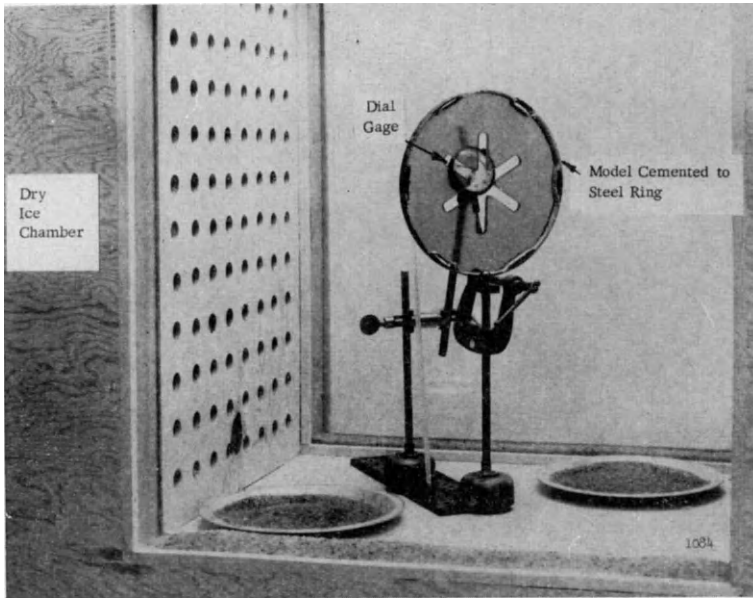
FIG. 5.3. Test set-up for applying a uniform drop in temperature to a rocket-grain model bonded on the outer periphery to a steel ring. The dial gage measures the change in core diameter.

It has been pointed out that the assumption of linear viscoelastic behaviour of the propellant does not hold for some propellant materials at high strains when the so-called "dewetting" occurs. For this case it is suggested that a more elaborate model analysis be conducted with the propellant material itself as the model material, and a thermal loading similar to the one outlined above. The loading would have to be continued to failure, and the simple strain displacement relationship shown above would be replaced with an experimentally obtained curve for any point of interest. The curve will be a strain-displacement curve with the temperature as a parameter. The use of the actual propellant would require a different method of measuring strains on the model, possibly one of the techniques discussed in Section 2.8. If the experimental method used gave a whole-field analysis, then any point of interest could be chosen to draw a curve, and the complete analysis could be a family of curves for various points. This analysis could then be applied to a grain of any size and of similar geometry.

6. OPTIMIZATION OF FILLET SHAPE

The photoelastic analyses described in Section 4 permit a relatively easy determination of the fillet shape that would produce the minimum stress. This is done empirically by observing the position of the zones of the contour of the fillet at which the photoelastic fringes are concentrated. The fillet shape is changed by building up the material at those zones or by slightly removing some
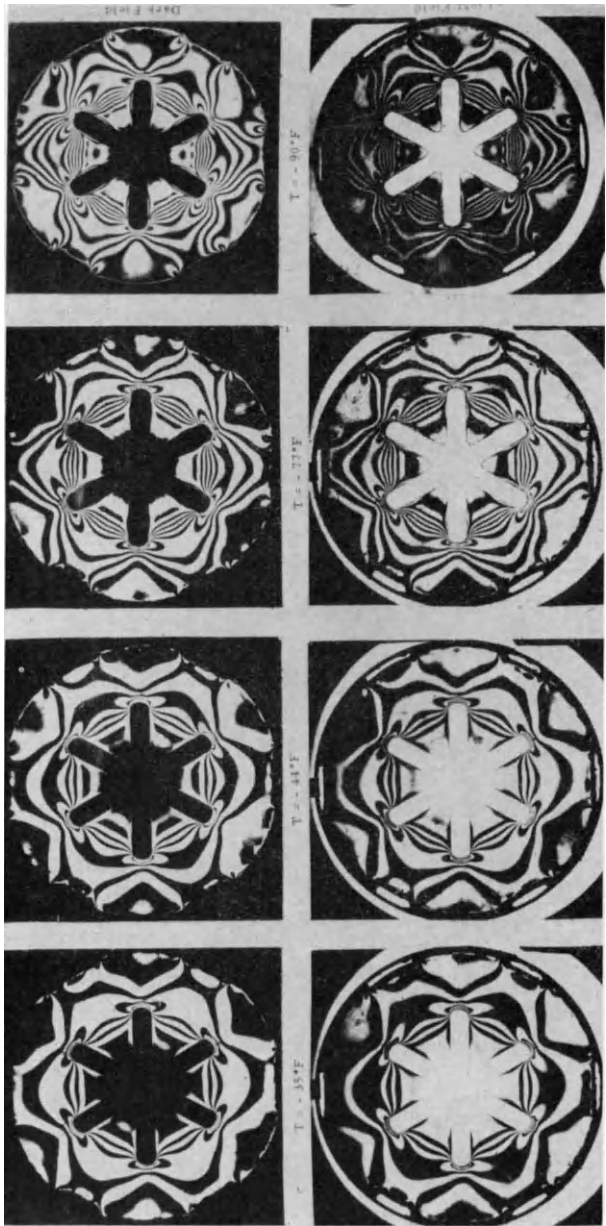
FIG. 5. 4. Isochromatic fringe patterns of a urethane rubber grain bonded to a steel ring on its outer periphery and subjected to four levels of decreasing temperature.

material at another zone of the fillet. Usually, shapes as they are designed by the grain designer show concentrations at the two extremes of the fillet. Some removal of material at the zone between those two extremes will decrease the stress concentration. The optimum design in this way of working is obtained when one fringe lies along the length of the fillet (Fig. 6.1).
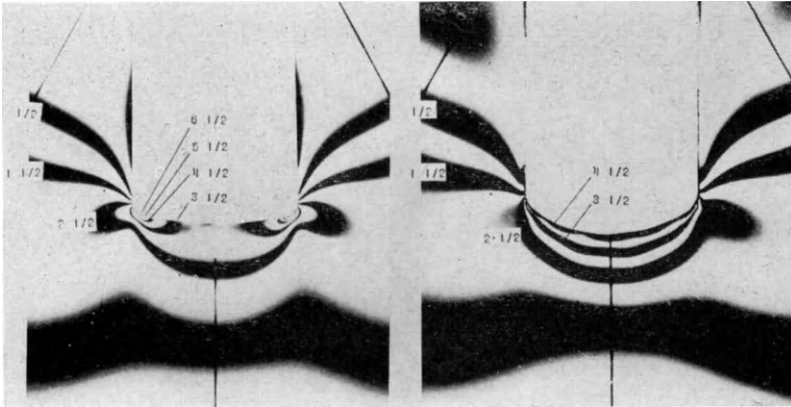
FIG. 6.1. Fringe patterns obtained for the original and optimized designs of a fillet contour.

A systematic series of tests was conducted to determine the optimum tip form of a particular grain geometry known as H-R grain. It was found that for that particular geometry, the optimum tip form is approximately elliptical. The ellipse had to be "bent" to conform to the circular shape of the grain, as shown in Fig. 6.2. A summary of the series of tests conducted is shown in Fig. 6.3. The ratio of the two semiaxes was given as a function of the geometric parameters by means of a formula [40].

A fillet can be "optimized" only for one particular loading condition. In general, optimum shapes are different for each loading condition. Following some of the considerations presented in Fig. 4.1, it can be expected, however, that the optimum fillet shape for a disk with a star perforation will be approximately the same when the disk is subjected to uniform pressure and when it is subjected to restrained shrinkage.

7. DETERMINATION OF STRAINS AND STRESSES IN TESTING SPECIMENS

7.1. *Introduction*

The mechanical properties of solid propellants are quite different from the mechanical properties of most commonly used engineering materials. Several of the standard methods of testing have been applied to solid propellants, but thought has also been given to other methods that may be better adapted to the particular properties of propellants. Experimental strain analysis techniques have been used in the development of the new specimens.
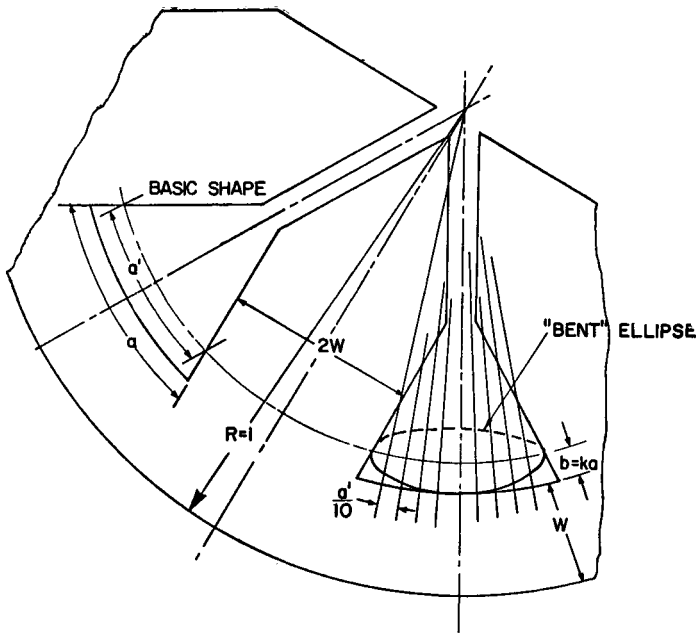
FIG. 6.2. Geometry of H-R grain (the method of laying out the tip form is also shown.)

THE VALUES GIVEN CORRESPOND TO OPTIMUM b/a FOR THE PARTICULAR GEOMETRY
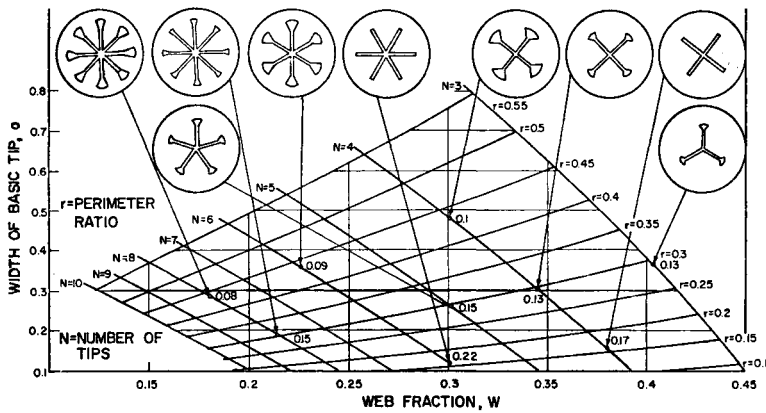
FIG. 6.3. Relationship between the geometric parameters in H-R grains.

7.2. *Strains and Stresses in Disks Subjected to Large Diametral Compression*

The tensile strength of some materials such as ceramics and concrete has been obtained for many years using cylinders and disks subjected to diametral compression. In some European and South American countries, the method is one of the standard methods for the determination of the tensile strength of concrete. The advantages are obvious, since disks are much easier to load than the tensile

A. J. DURELLI

specimens of the dog-bone type. In this kind of specimens, failure usually starts at the center. It is to be noted, however, that at the center of a disk subjected to diametral compression, the state of stress is biaxial and the two principal stresses are of opposite sign. Advantage has been taken of this fact to study the failure of propellants when subjected to biaxial conditions. To vary the degree of biaxiality, the disk can be made elliptical and loaded along the major or minor axis, depending on the desired ratio of principal stresses. Theoretical and experimental studies on circular and elliptical disks have been reported in [41].

An associated problem of great interest is the study of the change in strain and stress distribution taking place as the disk is loaded, flattens at the zone of contact, and is subjected to deformations of the order of 25 per cent. Figure 7.1
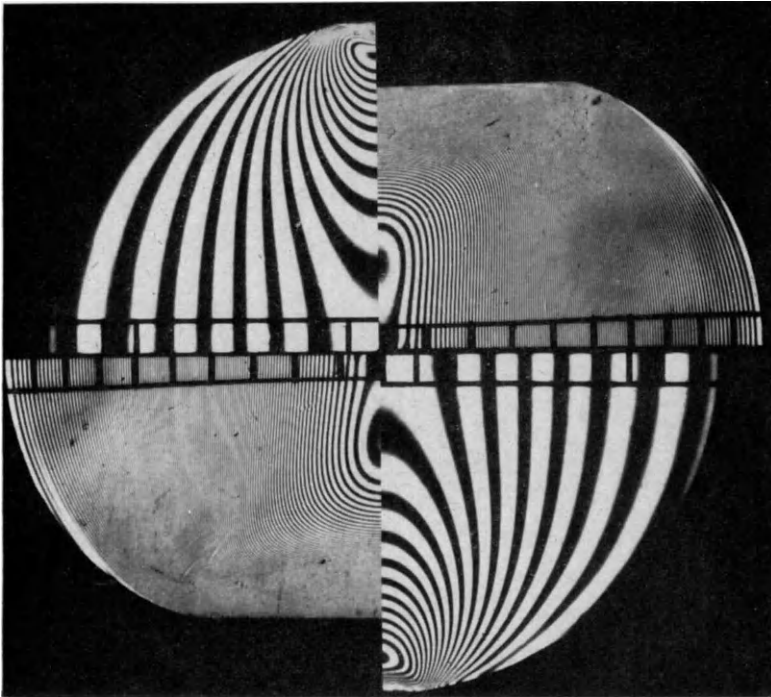
FIG. 7.1. Isochromatics and grids in a polyurethane rubber disk (solithane 113) subjected to diametral loading at two levels of load.

illustrates the isochromatics corresponding to small and large deformations in a polyurethane rubber circular disk. Figure 7.2 summarizes the results obtained for the center of the disk [42].

7.3. *Strains and Stresses in "Biaxial Strips"*

The specimen consists of a narrow strip, bonded or clamped along its long edges, between rigid metal plates. When the specimen is extended, the rigid plates inhibit lateral contraction; and if the specimen is sufficiently long, the

state of stress $\sigma_2 = \nu\sigma_1$ can be expected. To avoid failure at the corners, the specimen had to be redesigned using three-dimensional photoelasticity. A specimen with an I-shaped cross section was developed [21].

Another contribution to the development of a biaxial tester can be found in [43]. A sheet of propellant is pulled simultaneously in two perpendicular directions by means of whippletree arrangements. The two loads are independent and may have any ratio. The biaxiality has been verified using grids.
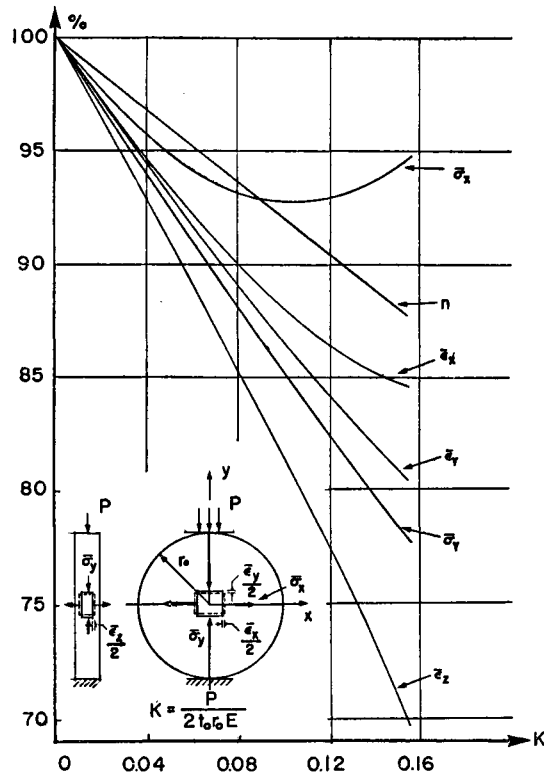
FIG. 7.2. Stresses and strains, as function of load, at the center of a disk diametrically loaded, given as percent of the values obtained from the small strain theory.

7.4. Strains and Stresses in "Poker-Chip" Specimens

The "poker chip" is a thin specimen in the shape of a circular disk bonded on each of its faces to a rigid grip or anvil. The two grips are pulled apart, resulting in a state of triaxial tension in the center of the disk.

An experimental stress analysis of this specimen, conducted using the "creeping" method of three-dimensional photoelasticity, was reported in 1954 in [44]. It was also mentioned in [45]. Important theoretical contributions to the study of the problem have been reported in [46] and [47].

7.5. Strains and Stresses in an Expanded Diaphragm

Another method used to study the properties of propellants when subjected to biaxial tensile stresses consists in pressurizing a thin disk-shaped membrane of the propellant and following the dome shape it develops as the pressurization is increased. To interpret correctly the results obtained, it is necessary to know with precision the distribution of strains in such a membrane. A simple and ingenuous method to determine this distribution is reported in [48]. Small bright ball bearings glued to the surface of the membrane, reflected light from a source
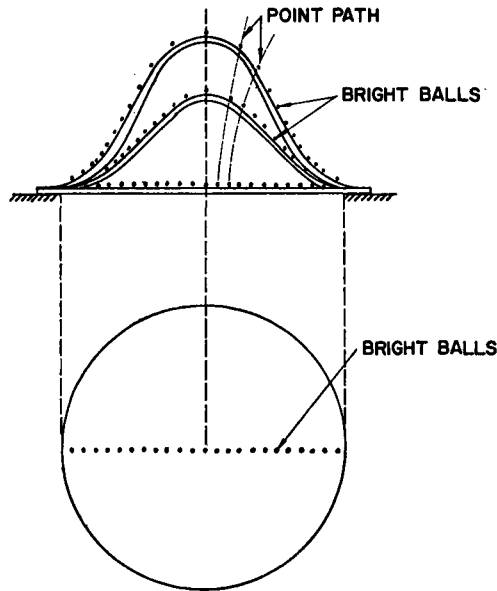
FIG. 7.3. Study of the deformation of a pressurized circular membrane used for biaxial tests.

after each increment of load. Only the specular reflection from the ball bearing registered on the photographic plate. The result was a multiple-exposure plate showing a series of true profiles of the membrane and the paths of each individual point.

7.6. Strains and Stresses in "Scarf" Joint Specimens

The development of the "scarf" joint specimen is directed to the testing of propellant-liner bond strength. It is desirable that the testing specimen exhibit a uniform distribution of stress in the rupture zone free of stress concentrations. Three-dimensional photoelasticity has been used to develop a design of this kind of specimen. The proposed geometry and the associated stress distribution are reported in [49].

8. DETERMINATION OF STRAINS AND STRESSES
IN ROCKET CASES

8.1. *Introduction*

Studies have been conducted to determine experimentally the strain and stress distributions in rocket cases. Usually the prototypes of the cases, or their models, are loaded by internal pressure and can be considered essentially as thin-walled pressure vessels. In some instances, it is important to determine the failure characteristics of these cases also.

8.2. *Steel Cases*

The results of the analysis of three steel cases are reported in [50]. Micrometer measurements of the outside diameter indicated whether the vessel was cylindrical. Two types of imperfections may occur: "out-of-roundness", indicating that the vessel is somewhat elliptical, and "corrugation", indicating local irregularities. Measurements of wall thickness were also taken employing ultrasonic methods.

The actual stress analysis consisted of three phases: First, brittle coatings were applied to determine the stress distributions over the entire outer surfaces. Second, certain regions of interest indicated by the brittle-coating analysis were instrumented with electrical-resistance strain gages, and the response of these gages was followed as the load was increased. Third, the vessels were pressurized until failure occurred, and the location and type of failure were recorded.

Figure 8.1 shows the location and equipment of the electrical strain gages. Figure 8.2 shows a brittle-coating pattern. Figures 8.3 and 8.4 illustrate typical failures.

Determination of strains and stresses in models made of aluminum cases and an inert polyurethane grain, using electrical resistance strain gages, is reported in [51]. The application of photoelastic coatings has been reported in [52].

8.3. *Glass-Reinforced Epoxy Cases*

Similar analysis can be conducted with anisotropic cases similar to the ones manufactured by winding glass-fiber around the motor. An example is shown in Fig. 8.5.

8.4. *Case Joints*

Photoelasticity has been used to help in the design of joints between case and closure at the back end of the motor. These joints often have the same cross-section for all meridian planes, and a first approximation of stress concentration can be obtained from a two-dimensional cross-sectional model of the joint. A pattern obtained using two-dimensional photoelasticity is shown in Fig. 8.6.
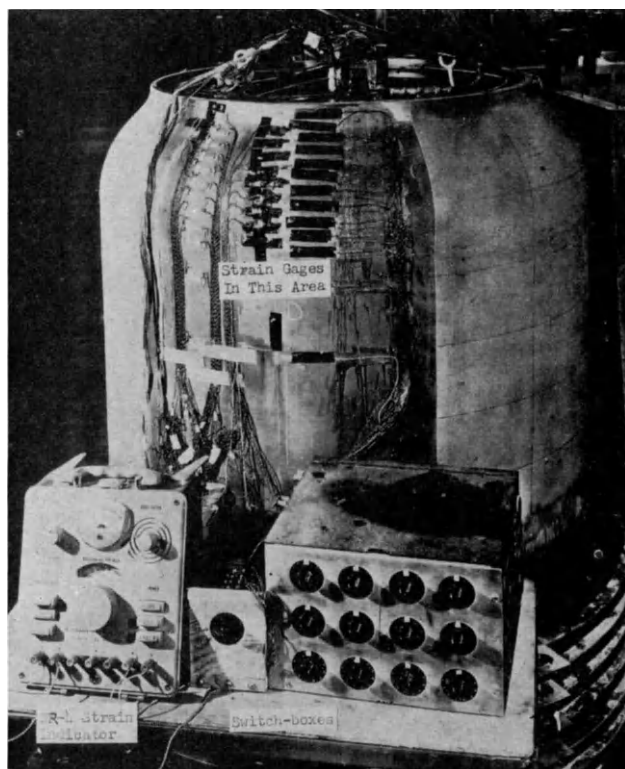
FIG. 8.1. Strain-gage installation and recording equipment employed with a rocket case.

FIG. 8.2. Brittle coating crack pattern over the forward section of the cylindrical shell near the longitudinal weld.

FIG. 8.3. Transition from shear to a tensile type failure as the crack propagated from the circular cylinder into the aft end knuckle.
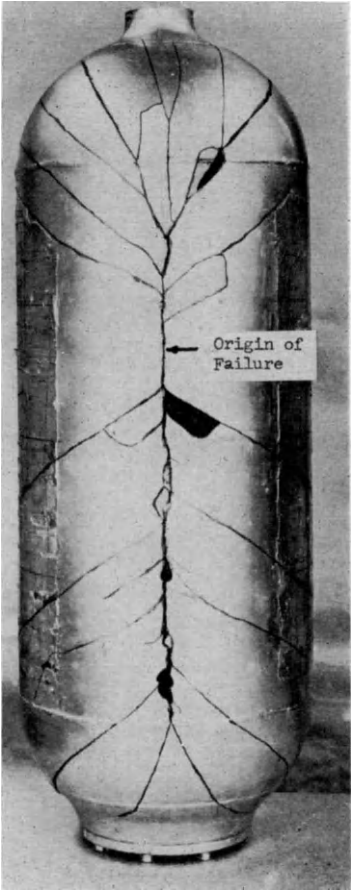
FIG. 8.4. Appearance of cracks produced by bursting a vessel.
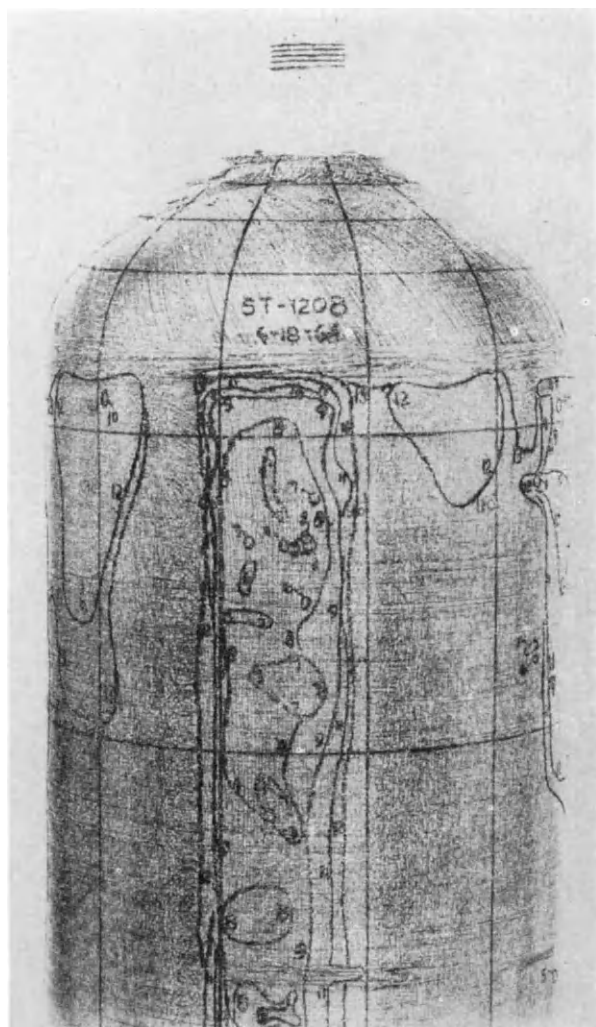
FIG. 8.5. Brittle-coating pattern on a fiber-glass reinforced epoxy case subjected to internal pressure.
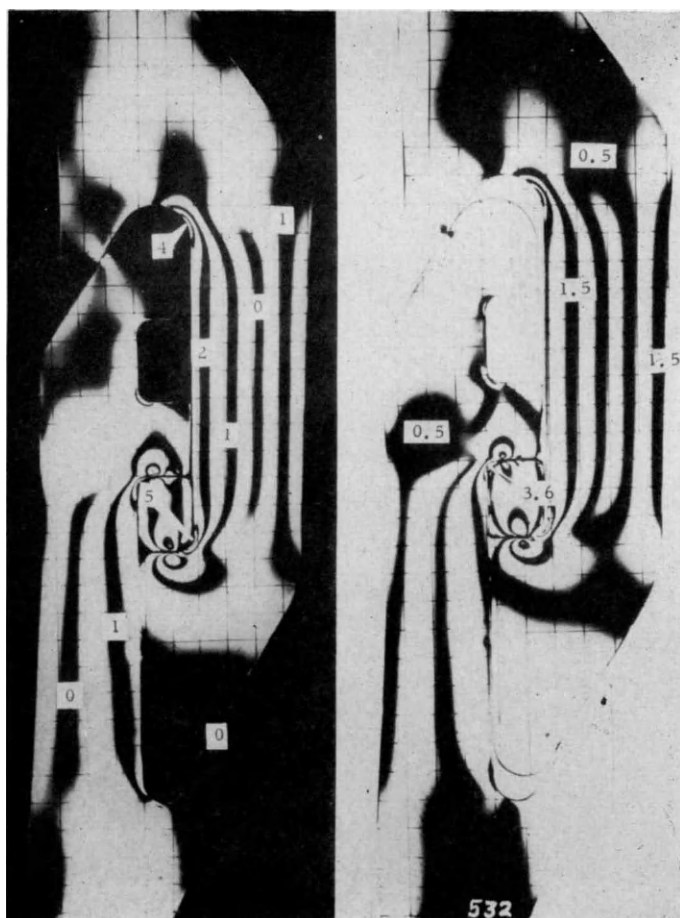
FIG. 8.6. Isochromatic pattern of a two-dimensional model of a closure joint subjected to tension loading.

9. AUXILIARY INVESTIGATIONS

The contributions of stress analysis techniques to the development of new material testing specimens in the solid propellant field have been discussed in Section 7. Another auxiliary field of investigation in which stress analysis techniques have been used is the determination of stresses in matrices with rigid inclusions. These studies find application in the development of a better understanding of the mechanism of reinforcement in glass-fiber reinforced epoxy cases and also in the study of reinforced solid propellants. Two- and three-dimensional photoelasticity techniques have been used. Description of the methods and of some of the results obtained can be found in [53], [54] and [55]. The maximum shear stress distribution associated with seven rigid inclusions embedded in a matrix subjected to shrinkage is illustrated in Fig. 9.1. The restrained shrinkage or "pinching" at the edges of the boundaries presents some problems of interpretation which have been mentioned in [34].

A very useful application of photoelasticity to the testing of actual propellant grains of large size has been reported in [56]. It can be shown, photoelastically, that the stress distribution in the neighbourhood of a star fillet is very closely the same when (1) the fillet is part of a complete pressurized disk with a per-
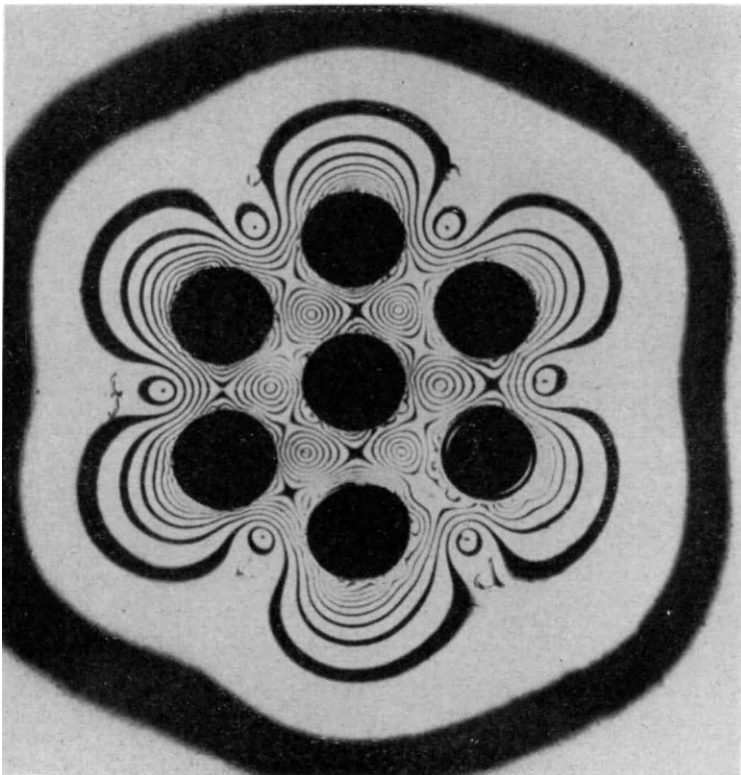
FIG. 9.1. Isochromatic fringe pattern in Hysol 4485 with seven circular inclusions.

forated star and (2) when the fillet is part of only a sector of the disk and the sector is loaded by displacements applied along its two radial faces (Figs. 9.2 and 9.3). It is possible, therefore, to study the strain distribution around the fillet on a sector of the actual grain, instead of using the full-sized grain.
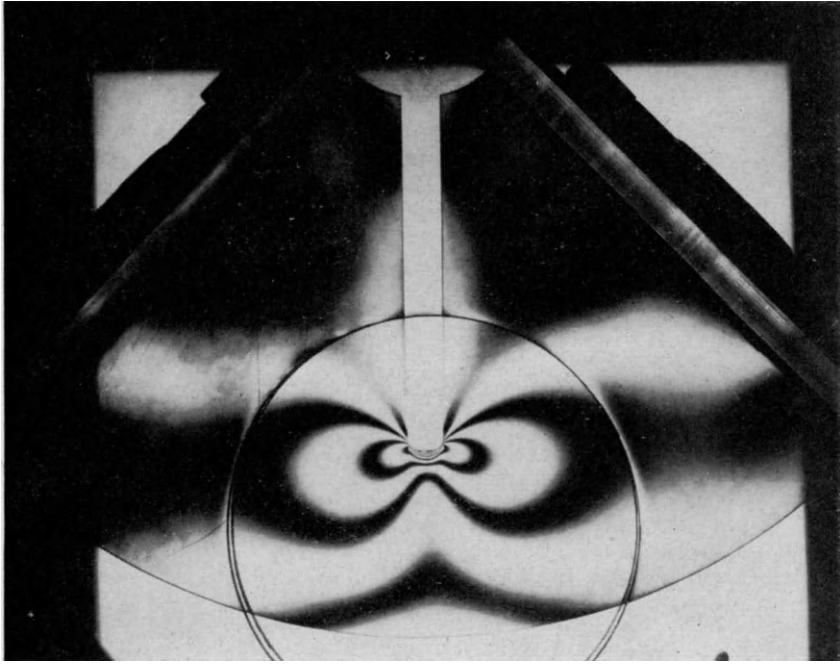
FIG. 9.2. Sector of a model of a grain loaded by displacements applied to its radial edges.
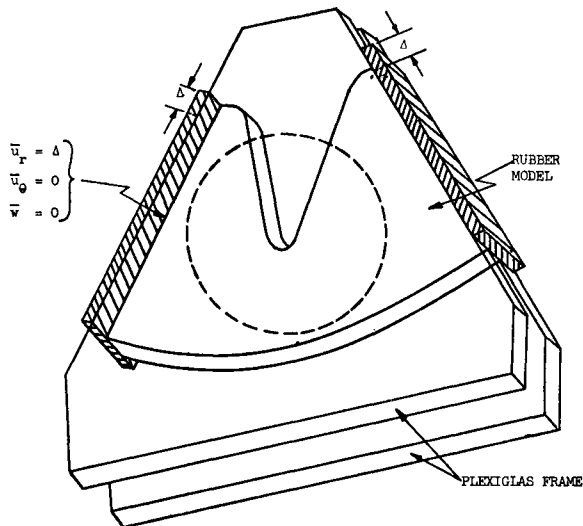
FIG. 9.3. Device used to apply constant radial displacement to a sector.

REFERENCES

[1] DURELLI, A. J. and PARKS, V. J., "Survey and development of methods for the determination of strains in solid propellants", Appendix B, Aerojet-General Corp. Rep. 0411–10F Contract AF 33(600)—40314 S.A. No. 1, 1962.

[2] HULT, JAN, "On the measurement of stresses in solids", *Trans. Chalmers Univ. of Techn.*, *Gothenburg, Sweden*, No. 280, 1963.

[3] DURELLI, A. J. and RILEY, W. F., "Performance of embedded pressure gages under static and dynamic loadings", *Symp. on Soil Mech., Spec. Pub.* 305, ASTM, 1961, pp. 20–37.

[4] WIEGAND, J., "Study of mechanical properties of solid rocket propellants", Aerojet-General Corp. Rep. 0411–10F, March 1962.

[5] SAN MIGUEL, A. and SILVER, R. ,"Radial stress measurements in propellant grains", *Bull. 3rd Meeting, Working Group, Chem. Prop. Ag. Rep.* Vol. 1, Oct. 1964, pp. 607–623.

[6] RASTRELLI, L. U. and DeHART, R. C., "Measurements of strains in solid propellant grains", *20th Meeting Bull. JANAF*, Vol. II, Nov. 1961, pp. 31–41.

[7] RASTRELLI, L. U. and DeHART, R. C., "Studies of internal displacements in solid propellant grains (embedded particle, X-ray detection system)", Contract Nonr–3363(00) (FBM).

[8] DICKEN, G. M. and THACHER, J. H., "Shear strain measurement in solid propellant rocket motors", Am. Inst. of Aero. and Astron. Paper 64–506.

[9] HART, W. D., "Moiré method for the measurement of strains in solid propellants", *Bull. 3rd Meeting, Working Group, Chem. Prop. Inform. Ag. Rep.*, Oct. 1964, pp. 545–560.

[10] SAN MIGUEL, A. and DURAN, E. N., "The formulation and casting techniques of low-modulus photoelastic coatings", Tech. Rep. 32–309, Jet Prop. Lab., Calif. Inst. of Techn., July 19, 1962.

[11] SAN MIGUEL, A., "Propellant strain analysis by the photoelastic coating technique", *20th Meeting Bull.*, Vol. I, Nov. 1961, pp. 163–174 (JANAF).

[12] ZANDMAN, F., REDNER, A. and POST, D., "Photoelastic coating analysis in thermal fields", *Exp. Mech.*, Vol. 3, No. 9, Sept. 1963.

[13] SAN MIGUEL, A., "Propellant strain analysis by the photoelastic coating technique", *20th Meeting JANAF*, Vol. 1, Nov. 1961, pp. 167–173.

[14] LEWIS, CLARKE H., "Motor strain testing", *20th Meeting JANAF*, Vol. 1, Nov. 1961, pp. 91–97.

[15] THACHER, J. H., "Deformation of case-bonded propellants under axial acceleration", *20th Meeting JANAF*, Vol. 1, Nov. 1961, pp. 81–90.

[16] OBERT, L., MERRILL R. H. and MORGAN, T. A., "Deformation gage for determining the stress in mine rock", *Bur. of Mines Rep. of Investigation* 5978, 1962.

[17] Type 4–325 Pressure Transducer, by Consolidated Electrodynamics, Transducer Div., Monrovia, Calif. See also: Allegany Ballistics Lab. (Hercules Powder Co.): Status of the Polaris Selective Experiment Program, Feb. 4, 1965, Appendix A, by G. Dicken.

[18] PERDUE, D. G. and BROWNING, S. C., "Embedment of internal instrumentation in propellant grains", Weapons System 133A; MTO–270–4, August 16, 1963, Hercules Powder Co., Bacchus, Utah (Contract AF–04(647)–243.

[19] Gulton Industries, Inc., "Three-dimensional propellant strain measuring transducer", April 1963.

[20] DURELLI, A. J., "Experimental means of analyzing stresses and strains in rocket propellant grains", *Exp. Mech.*, Vol. 2, No. 4, April 1962, pp. 102–110.

[21] SAMPSON, R. C. and CAMPBELL, D. M., "Contributions of photoelasticity to evaluation of solid propellant motor integrity", Aerojet-General Corp. Paper No. 2, SRO, Nov. 1964.

[22] MESSNER, A., "Propellant grain stress analysis", *Proc. 17th Meeting JANAF-ARPA-NASA Solid Propellant Group*, Vol. 1, May 1961 (Confidential).

[23] PAAR, C. H., "Deformations and stresses in core-bonded solid propellant grains at finite length by numerical methods", *Rohm and Haas Quarterly Progress Rep.* No. P–61–17, Oct. 1961.

[24] SAMPSON, R. C., "A three-dimensional photoelastic method for analysis of differential-contraction stresses", *Exp. Mech.*, Vol. 3, No. 10 (Oct. 1963), pp. 225–234. Discussion by Durelli, A. J., pp. 235–237.

[25] TRAMPOSH, H. and GERARD, G., "An exploratory study of three-dimensional photo-thermoelasticity", *J. App. Mech.*, March 1961, Vol. 28, E, No. 1, pp. 35–40.

[26] DURELLI, A. J. and DANIEL, I. M., "A nondestructive three-dimensional strain-analysis method", *J. App. Mech.*, March 1961, Vol. 28, E, No. 1, pp. 83–86.

[27] SCIAMMARELLA, C. and CHIANG, FU-PEN, "The moiré method applied to three-dimensional elastic problems", *Exp. Mech.*, Nov. 1964, Vol. 4, No. 11, pp. 313–319.

[28] FITZGERALD, E., HARRISON, T. and FRANCIS, E., "Axial slump of a circular port grain", *20th Meeting JANAF*, Nov. 1961, Vol. 1, pp. 157–162.

[29] KNAUSS, W., "Displacements in an axially accelerated solid propellant rocket grain", *20th Meeting JANAF*, Nov. 1961, Vol. 1, pp. 175–191.

[30] WILSON, H. B., Jr., "Stresses owing to internal pressure in solid propellant rocket grains", *ARS Journal*, Vol. 31, No. 3, March 1961, pp. 309–317.

[31] DURELLI, A. J. and PARKS, V. J., "Photoelasticity methods to determine pressure, restrained shrinkage, and transient thermal stress distributions in propellant grain models", *Exp. Mech.*, Vol. 5, No. 2, Feb. 1965, pp. 33–45.

[32] DURELLI, A. J., LAKE, R. L. and TSAO, C. H., "Device for applying loading to boundaries of complicated shape", *Proc. SESA*, Vol. 11, No. 1, 1953, pp. 55–61.

[33] FOURNEY, M. E. and PARMERTER, R. R., "Stress concentration data for internally perforated star grains", U.S. Nav. Ordnance Test Station, China Lake, Calif., Technical Pub. 2728, Dec. 1961.

[34] DURELLI, A. J. and PARKS, V. J., "New method to determine restrained-shrinkage stresses in propellant-grain models", *Exp. Mech.*, Vol. 3, No. 11, November 1963, pp. 263–268.

[35] DANIEL, I. M. and DURELLI, A. J., "Photothermoelastic analysis of bonded propellant grains", *Exp. Mech.*, Vol. 1, No. 3, March 1961, pp. 97–104.

[36] BARRIAGE, J. B. and DURELLI, A. J., "Application of a new deformeter to two-dimensional thermal stress problems", *Proc. SESA*, Vol. 13, No. 2, 1956, pp. 97–106.

[37] ORDAHL, D. D. and WILLIAMS, M. L., "Preliminary photoelastic design data for stresses in rocket grains", *Jet Propulsion (J. of ARS)*, Vol. 27, No. 6, June 1957, pp. 657–662.

[38] ISIBASI, TADASI, "Form-factors of solid of revolutions in relation to those of plane plates", *Res. Inst. for Elasticity Engineering, Kyushu Imperial Univ., Fukuoka, Japan*, Vol. IV, No. 1, June 1947.

[39] MEYER, M. L. and OAK, A. N., "Two-dimensional photoelasticity as a method of approximation to the stresses in three-dimensional problems with a plane or axis of symmetry", *J. Royal Aeronautical Society*, Vol. 66, March 1962, 193–196.

[40] DURELLI, A. J. and LAKE, R. L., "Determination of optimum geometry for star-perforated propellant grains", Final Report, Feb. 1953, to Thiokol Chemical Corp, Huntsville, Alabama.

[41] BRISBANE, J. J., "Further development of a biaxial stress test for viscoelastic materials", Rohm and Haas Rep., pp. 62–66, 1962, and *20th Meeting Bull. JANAF-ARPA-NASA, SPIA-PP14U*, November 1961, Vol. 1, pp. 257–269.

[42] DURELLI, A. J. and MULZET, A., "An experimental analysis of large strains and associated stresses in a linear material". (Thesis for the Master's degree, The Catholic University of America, 1964) to be published in the *J. Eng. Mech. Div. of ASCE.*

[43] SAN MIGUEL, A., "A biaxial tester", *Bull. 3rd Meeting Interagency Chem. Rocket Propulsion Working Group on Mechanical Behavior*, Vol. 1, Oct. 1964, pp. 561–572.

[44] DURELLI, A. J. and DALLY, J. W., "Feasibility study of a method to determine the stress distribution in a disk bonded to two halves of a tensile specimen", Appendix in Report to Frankfort Arsenal Contract DA–11–022–ORD–957: *Fundamentals of Brazing*, Dec. 1, 1954.

[45] DALLY, J. W. and DURELLI, A. J., "New method to 'lock-in' elastic effects for experimental stress analyses", *J. App. Mech.*, Vol. 25, No. 2, pp. 189–195, June 1958.

[46] MESSNER, A. M., "Stress distributions in poker-chip tensile specimens", *Bull. 2nd Meeting Interagency Chem. Rocket Propulsion Working Group on Mechanical Behavior*, Publication No. 28, Oct. 1963, pp. 109–129.

[47] BRISBANE, J. J., "Stresses, strains and displacements in the poker-chip test specimen", *Bull. 2nd Meeting Interagency Chem. Rocket Propulsion Working Group on Mechanical Behavior*, Publication No. 28, Oct. 1963, pp. 337–348.

[48] LONG, R. F., RAINBIRD, R. W. and VERNON, J. H. C., "The biaxial tensile behavior of United Kingdom colloidal and composite propellants", *Bull. 1st Meeting Interagency Chem. Rocket Propulsion Working Group on Mechanical Behavior*, Dec. 1962, pp. 307–336.

[49] DIXON, J. D., "Three dimensional photoelastic analysis of a scarf joint for propellant liner bond strength testing", Rep. PEL–44, Aerojet General Corp., Jan. 1964.

[50] DURELLI, A. J., DALLY, J. W. and MORSE, S., "Experimental study of large diameter thin-wall pressure vessels", *Exp. Mech.*, Vol. 1, No. 2, February 1961, pp. 33–42.

[51] BYNUM, D. and RASTRELLI, L., "Studies of internal displacements in solid propellant grains", Interim Rep. Nonr–3363(00) (FBM), Oct. 1962.

[52] ZANDMAN, F., WALTER, M. and REDNER, S. S., "Stress analysis of rocket motor case by birefringent coating method", *Proc. SESA*, Vol. 19, No. 2, 1962.

[53] DURELLI, A. J. and DANIEL, I. M., "Photoelastic investigation of residual stresses in glass-plastic composites", Sec. 19A, 16th Annual Conf. of Reinforced Plastics Div., Soc. Plastics Industry, Chicago, Ill., 1961.

[54] DANIEL, I. M. and DURELLI, A. J., "Shrinkage stresses around rigid inclusions", *Exp. Mech.*, Vol. 2, No. 8, Aug. 1962, pp. 240–244.

[55] SAMPSON, R. C., "Photoelastic studies of solid propellant grain stress distribution", in J. H. Wiegand's Report 0.411–10F: Study of Mechanical Properties of Solid Rocket Propellants—Aerojet Gen. Corp., Contract AF33(600)–40314, S.A. No. 1, 1962, pp. 159–218.

[56] BILLS, K. and WIEGAND, J. H., "Relation of mechanical properties to solid propellant motor failure", *Am. Inst. Aero. and Astr.*, Vol. 1, No. 9, Sept, 1963, pp. 21116–2124.

PHOTOVISCOELASTICITY

Ellis Harold Dill

Department of Aeronatucs and Astronautics, University of Washington
Seattle, Washington

Abstract—This paper deals with the extension of photoelastic techniques of experimental stress analysis to problems in linear viscoelasticity.

1. INTRODUCTION

Since the experiments of Sir David Brewster, reported before the Royal Society in 1816, the interdependence of electrical polarization and mechanical state which results in artificial birefringence has been recognized. By 1930, laboratories in many countries were making use of birefringent materials to explore the state of stress in a linearly elastic model. Today, photoelasticity is recognized as a standard tool of experimental stress analysis for both two- and three-dimensional problems.

The model materials used in photoelastic studies are usually high polymers for which the dielectric tensor, the stress tensor, and the strain tensor are nearly proportional to each other. In reality, both optical and mechanical creep occur at constant load, but experimental techniques that correctly account for this effect have been developed.

Since the model material is mechanically viscoelastic, the stress field in it is actually determined by the relations of the theory of viscoelasticity. Thus, if an experimental technique can be developed that will yield the actual stress state in the model at all times, a problem in viscoelasticity will have been solved. It is possible to extend the methods of photoelasticity to do this.

The basic idea is to manufacture a transparent birefringent material having mechanical properties similar to those of the prototype material. Then the stress field in a geometrically similar model is proportional to the stress field of the prototype. The stress field in the model is determined by observation of the fringe pattern that occurs when the model is placed between polaroids.

The basic theory required to interpret the experiments was presented by Mindlin [1] and Read [2]. A more complete treatment was given in ref. [4].

2. ANALYTICAL BASIS

2.1. Birefringence

The birefringence exhibited by high polymers can be explained by considering light as an electromagnetic wave propagating through an ideal anisotropic dielectric. During the time of passage of the wave, the displacements of the

443

material are negligible. Therefore, the equations of a dielectric at rest can be used. Furthermore, since we intend to observe only relative intensity of light transmitted, from a nearly monochromatic source, absorption and dispersion will be neglected. The deformation gradients are also restricted to be small. The nature of the wave is then determined by the relation between the free charge potential $\mathfrak{D}$ and the electric field $\mathbf{E}$: In a rectangular Cartesian system x_i,

$$\mathfrak{D}_i = \epsilon_0 K_{ij} E_j. \tag{1}$$

Here ϵ_0 is the dielectric coefficient in free space and K_{ij} will be called the dielectric tensor.

The electromagnetic field equations imply that a plane wave propagated along one principal axis of the dielectric tensor is divided into two linearly polarized waves. The direction of vibration of each wave coincides with one of the remaining principal axes of the dielectric tensor and has a refractive index equal to the square root of the corresponding principal value of the dielectric tensor.

This suggests the introduction of a new tensor N_{ij} which has the same principal axes as the dielectric tensor, but which has principal values N_i equal to the square root of the principal values of the dielectric tensor:

$$N_{ij} = K_{ij}^{1/2} \tag{2}$$

The principal values of N_{ij} are the principal indices of refraction. It will therefore be called the refraction tensor.

The birefringence of a wave propagated along the third principal axis of the refraction tensor is

$$\Delta = N_1 - N_2. \tag{3}$$

Now consider a slice of the material with faces normal to the third principal axis and of thickness h. A plane polarized electromagnetic wave is obtained by passing monochromatic light through a polaroid. When this wave is incident on the dielectric, it is partly reflected and partly transmitted. Another reflection and transmission occurs at the exit surface. By applying the jump conditions of the electromagnetic field equations at each surface and using the solution, cited above, for propagation within the dielectric, the amplitude of the excited wave can be related to the amplitude of the incident wave.

The excited wave is then passed through a second polaroid. If the second polaroid has the axis of polarization at right angles, for example, to that of the first polaroid, the amplitude of transmitted electric field is nearly proportional to the factor

$$I = \sin 2\alpha \sin n\pi \tag{4}$$

where α is the angle between the axis of the polaroid and the principal axes of the refraction tensor N_{ij}, and

$$n = \frac{h\omega}{2\pi c} \Delta. \tag{5}$$

Here n is the fringe order, h is the thickness, ω is the frequency of the light, and c is the velocity of light in free space.

Thus, if the model has nonhomogeneous dielectric properties, there will appear lines of zero light intensity (isoclinics) connecting the points where $a = 0$, $\pi/2$. There will appear lines of relative minimum intensity where the fringe order is an integer (isochromatics). By rotating the polaroids the isoclinic angle at any point can be found. By interpolating between the isochromatic lines, the fringe order at any point can be found. In general, the isoclinic and isochromatic patterns will vary and therefore $a(t)$ and $\Delta(t)$ are functions of time t.

A more complete discussion is found in ref. [4].

2.2. High Polymers

High polymers are made up of large molecules formed by repetition of simple chemical units called monomers. The stress required to stretch a high polymer is due to the change in orientation of the polymer chains, and the change in attraction or repulsion between molecules resulting from changes in distance between them. The birefringence is related to the orientation of the polymer chains. When the polymer is stretched, the stress required to hold it at constant length will gradually diminish. This mechanical relaxation is the result of the rearrangement of the chains. The change in orientation will simultaneously result in a change in birefringence. Thus, a simple relation cannot be expected to exist in general either between birefringence and stress, or between birefringence and strain. Of course, for some materials one relation or the other may be preferred.

Phenomenologically, the relation between stress and strain can be described by the theory of simple materials with fading memory. For small displacement gradients of an isotropic material, the deviatoric stress s_{ij} and deviatoric strain are related by a linear functional. The relation can be put in the form

$$s_{km} = \int_0^t 2G(t - \tau)\, \dot{e}_{km}(\tau)\, \mathrm{d}\tau \tag{6}$$

where $G(t)$ is the shear relaxation modulus. The mean stress $p = \frac{1}{3}\sigma_{rr}$ is related to the volume change $e = \epsilon_{kk}$:

$$p = \int_0^t K(t - \tau)\, \dot{e}(\tau)\, \mathrm{d}\tau, \tag{7}$$

where $K(t)$ is the bulk relaxation modulus.

The inverses of (6) and (7) are

$$2e_{km} = \int_0^t J(t - \tau)\, \dot{s}_{km}(\tau)\, \mathrm{d}\tau \tag{8}$$

$$e = \int_0^t B(t - \tau)\, \dot{p}(\tau)\, \mathrm{d}\tau. \tag{9}$$

The shear creep compliance $J(t)$ and bulk creep compliance $B(t)$ can be

calculated from $G(t)$ and $K(t)$:

$$\int_0^t G(t - \tau)\, J(\tau)\, d\tau = t. \tag{10}$$

For an elastic material $G(t) = G_0 h(t)$ and $J(t) = \dfrac{1}{G} h(t)$ where $h(t)$ is the unit step function.

Since stress and birefringence have, at least in part, similar origins in the orientation of the polymer chains, a relation between the deviatric components n_{km} of the refraction tensor and strain similar to (6) and (7) can be expected to exist:

$$n_{km} = \int_0^t 2\mathfrak{G}(t - \tau)\, \dot{e}_{km}(\tau)\, d\tau, \tag{11}$$

$$N_{kk} = \int_0^t \mathfrak{R}t(t - \tau)\, \dot{e}_{kk}(\tau)\, d\tau. \tag{12}$$

Experience indicates that this is the case. $\mathfrak{G}(t)$ will be called the optical relaxation function.

For certain materials $\mathfrak{G}(t) = \mathfrak{G}_0 h(t)$. Then

$$n_{km} = \mathfrak{G}_0 e_{km}. \tag{13}$$

Such materials are termed "strain-birefringent" and $\mathfrak{G}_0$ is termed the "strain-optic coefficient".

The inverse of (11) is

$$2e_{km} = \int_0^t \mathfrak{F}(t - \tau)\, \dot{n}_{km}(\tau)\, d\tau. \tag{14}$$

The functions $\mathfrak{F}(t)$ and $\mathfrak{G}(t)$ are related by a Volterra integral equation of the type (10).

Combining (8) and (11), the relation between birefringence and stress is obtained:

$$n_{km} = \int_0^t \Psi(t - \tau)\, \dot{s}_{km}(\tau)\, d\tau. \tag{15}$$

The inverse relation is

$$s_{km} = \int_0^t \Phi(t - \tau)\, \dot{n}_{km}(\tau)\, d\tau. \tag{16}$$

The function $\Psi(t)$ will be called the optical creep-function and $\Phi(t)$ the inverse creep-function.

For certain materials it may happen that $\Psi(t) = \Psi_0 h(t)$. Then

$$n_{km} = \Psi_0 s_{km}. \tag{17}$$

Such materials are termed "stress-birefringent" and Ψ_0 the "stress-optic coefficient". This can be expected to happen for cross-linked ideal rubbers.

It should be obvious that there is in general no experiment that can determine whether birefringence is due to stress or strain. A relation between birefringence and strain *implies* a relation between birefringence and stress, and vice versa. Of course, it may happen that the optical relaxation function or the optical creep function may be a more simple curve. This is the case for the "strain-birefringent" material and for the "stress-birefringent" material. In particular, an elastic material which is "strain-birefringent" is also "stress-birefringent ".

It may also be possible to represent the optical creep function or the optical relaxation function as some elementary functions leading to other forms of the relations (11) and (15). Such representations are familiar from the theory of viscoelasticity and may be worthwhile for certain purposes.

Furthermore, it may happen that

$$\Psi(t) = c_1 h(t) + \tfrac{1}{2} c_2 J(t). \tag{18}$$

Then

$$n_{km} = c_1 \sigma_{km} + c_2 e_{km}. \tag{19}$$

Such relations as (13), (17), and (19) are some special cases of the general relations which may hold for some materials, but do not hold in general.

All of the functions characterizing the mechanical and optical properties can be expected to depend on temperature. This is considered in ref. [4].

2.3. *Tension Test*

Consider a long rod subjected to an axial force (Fig. 1). A uniaxial stress field is produced near the center. Choose the x_1-axis along the rod. Then (8) and (9) lead to

$$\epsilon_{11} = \int_0^t D(t - \tau)\, \dot{\sigma}_{11}(\tau)\, d\tau, \tag{20}$$

$$\epsilon_{22} = -\int_0^t \nu(t - \tau)\, D(t - \tau)\, \dot{\sigma}_{11}(\tau)\, d\tau; \tag{21}$$

where

$$J = 2(1 + \nu)\, D, \tag{22}$$

$$\nu(t) = \frac{3J(t) - 2B(t)}{6J(t) + 2B(t)} \tag{23}$$

The function $D(t)$ is called the tensile creep compliance. The function $\nu(t)$ is the transverse contraction ratio in tension and is one generalization of the Poisson ratio. The ϵ_{ij} and σ_{ij} are the strain and stress tensors.

From (3), (5), and (15),

$$n = \frac{h\omega}{2\pi c} \int_0^t \Psi(t - \tau)\, \dot{\sigma}_{11}(\tau)\, d\tau. \tag{24}$$

This agrees with the observations of ref. [3].
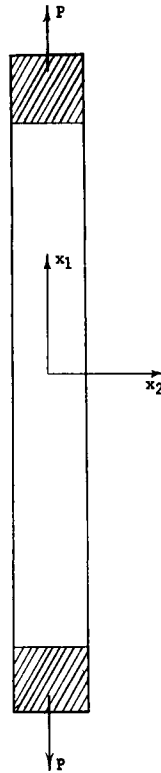
FIG. 1. Tension test.

From (20), (21), and (24), it is evident that the functions $\nu(t)$, $D(t)$, $\Psi(t)$ can be found from the values of σ_{11}, ϵ_{11}, ϵ_{22}, and n in the tension test. By solving the preceding integral equations any other of the functions characterizing the material can be found.

In particular, for a step change in the axial stress σ_{11}, i.e. a creep test,

$$\epsilon_{11} = D(t)\,\sigma_{11}, \tag{25}$$

$$\epsilon_{22} = -\,\nu(t)\,\epsilon_{11}, \tag{26}$$

$$n = \frac{h\omega}{2\pi c}\,\Psi(t)\,\sigma_{11}. \tag{27}$$

2.4. Shear Test

Consider a rectangular sheet of viscoelastic material bonded to a rigid frame as shown in Figs. 2 and 3. By loading the frame in the plane of the sheet, a condition of nearly plane stress is produced. The stress is not uniform over the specimen.

If constant loads are applied to the frame, then the stress and strain at any point of the material will in general vary with time, even though the loads do
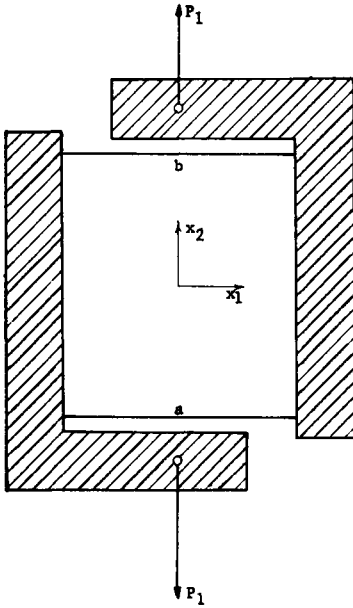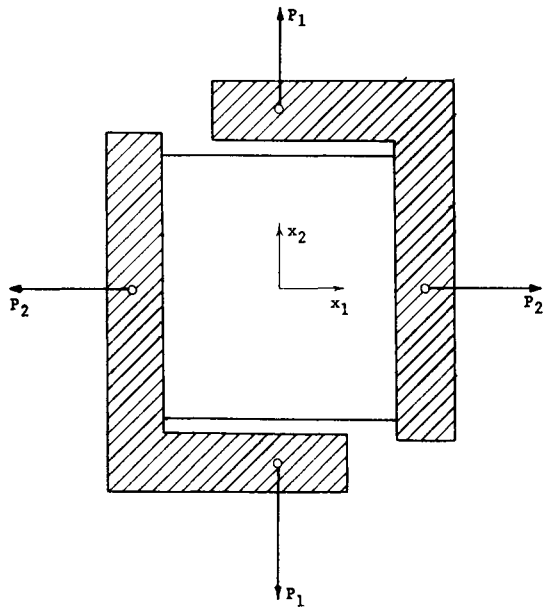
FIG. 2. Shear test.   FIG. 3. Combined shear and tension.

not vary. However, if the transverse contraction ratio ν is constant, then suddenly applied constant loads produce a stress field which is constant and identical to that of a linear elastic material. In this instance, by (15),

$$n_{ij}(t) = \Psi(t)\, s_{ij} \tag{28}$$

Thus,

$$n(t) = \frac{h\omega}{2\pi c}\, \Psi(t)(\sigma_1 - \sigma_2), \tag{29}$$

and the principal axes of stress coincide with the principal axes of the dielectric tensor.

Suppose loads P_1 are applied as shown in Fig. 2. The linear elasticity problem can be solved by photoelasticity. It is found that the shear stress distribution along the x_2-axis is as shown in Fig. 4, while σ_{11} and σ_{22} are zero. Thus, each particle along the x_2-axis experiences a state of pure shear stress:

$$\sigma_1 = -\,\sigma_2 = \sigma_{12}. \tag{30}$$

Then

$$n(t) = \frac{h\omega}{2\pi c}\, \Psi(t)\, 2\sigma_{12}. \tag{31}$$

The principal axes of stress and dielectric tensors are at $45°$ to the x_1-axis.

The sheet may also be subjected to combined tension and shear: If loads P_2 are applied as in Fig. 3, normal stresses are introduced while the shear stress is zero. Consider the point in the center of the specimen. Apply P_2 suddenly at time zero. Apply P_1 suddenly at time t_0. Since the problem is linear, (28) applies
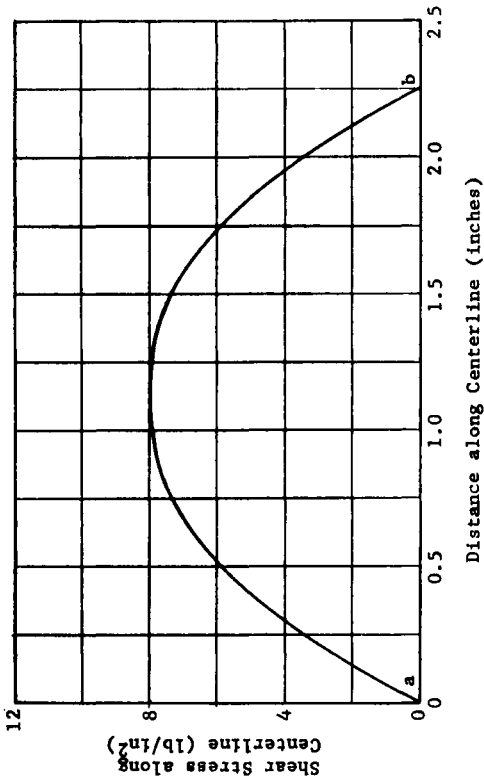
Fig. 4. Shear stress.
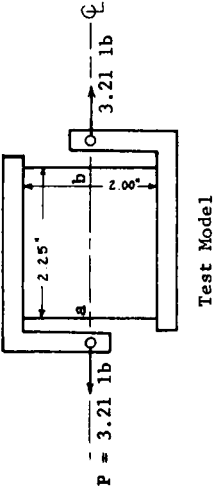
to each loading if time is measured from the instant of application of the load.

The principal axes of stress are initially along the coordinate axes for the load P_1. Upon application of the load P_2, the principal axes of stress suddenly change to an angle given by

$$\tan 2\beta = \frac{2\sigma_{12}}{\sigma_1 - \sigma_2}. \tag{32}$$

The principal axes of the dielectric tensor can be computed from (28):

$$\tan 2\alpha = \frac{\Psi(t - t_0)}{\Psi(t)} \tan 2\beta. \tag{33}$$

The principal axes of the dielectric tensor and stress tensor coincide only at $t < \tau_0$, and $t = \infty$.

2.5. Circular Disk

It is a consequence of linear viscoelasticity that the stress field in a visco-elastic material experiencing plane stress and stress boundary conditions is the same in an elastic material and is independent of the material constants.

Consider a disk of viscoelastic material with circular outer boundary and an irregular hole. If the material is at uniform temperature so that the material properties are homogeneous, then a uniform constant normal pressure suddenly applied to the outer boundary produces a constant stress field. The fringe order at any point is then given by (29).

Suppose that the temperature is not uniform. Suppose that the disk is heated and maintained at a steady-state condition with the inner boundary hotter than the outer boundary. Suppose that the effect of temperature on the initial and long time values of the material functions $\nu(t)$ and $D(t)$ is negligible. Then if a step change in normal pressure on the outer boundary is maintained, the stress field will vary with time. Linear viscoelasticity theory implies that the stress at the initial instant will be the same as for the uniform temperature problem. Subsequently, the hotter portion relaxes to a lower modulus and cannot support its share of the load; one would expect the stress to decrease. Finally, all particles have relaxed and so the material properties again become homogeneous. Visco-elasticity theory implies that the stress will approach the same value as that in the uniform temperature problem.

3. EXPERIMENTAL RESULTS

Experimental work has been conducted by C. Fowlkes at the University of Washington. Some results were given in ref. [5] and a more detailed report will be published elsewhere. This work will now be briefly described.

3.1. Material

After some trials, it was found that a mixture of Araldite brand epoxy resins could be made to reasonably match the creep compliance of a typical solid propellant over a few decades of time. A mixture resulting in a material some-

what more stiff than the normal propellant was used in the actual experiments because it was more convenient to handle. This consists of 45 per cent Araldite 502, 45 per cent Araldite 508, and 10 per cent Araldite 963.

3.2. *Tension Test*

The mechanical and optical properties were determined by a tensile creep test at several temperatures. The specimen is shown in Fig. 5. A weight was suddenly applied by hand, and the change in length, width, and amplitude of light transmitted were recorded automatically by the apparatus shown in Fig. 6.
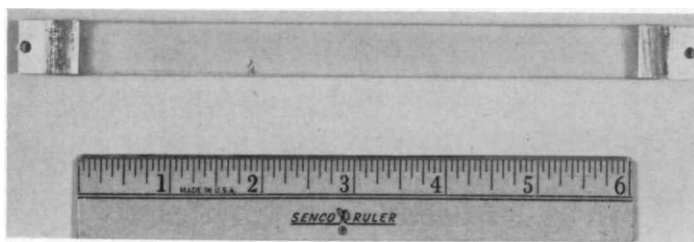
FIG. 5. Tensile specimens.

FIG. 6. Tensile calibration apparatus.   *a*, Light source, 5460°A. *b*, Polarizer.
c, Specimen. *d*, Analyzer. *e*, Photomultiplier. *f*, Recorder.

The longitudinal strain was taken to be the change in length of the specimen divided by the original length. The lateral strain was taken to be the change in width divided by the initial width. The stress was taken to be the load divided by the original area.

The tensile creep compliance calculated from (25) is shown in Fig. 7 for several temperatures. The lateral contraction ratio computed from (26) is shown in Fig. 8 for room temperature.

The amplitude of light transmitted was measured by a photomultiplier tube.
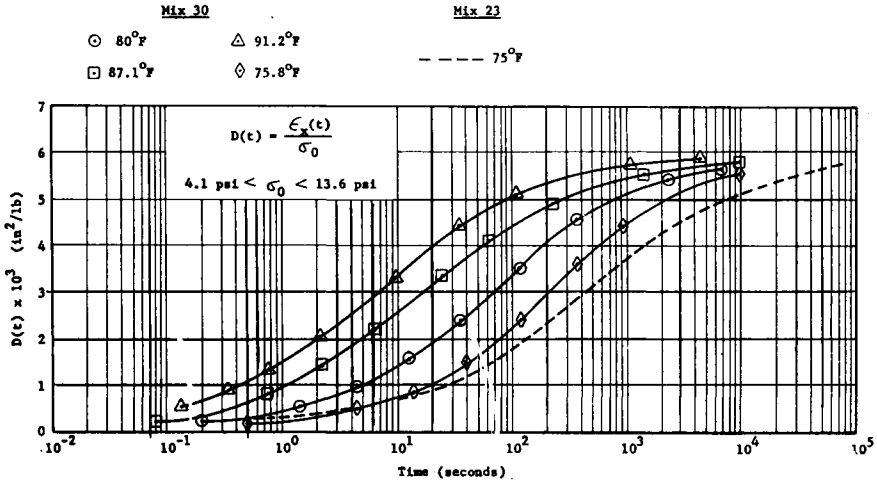
FIG. 7. Tensile creep compliance.
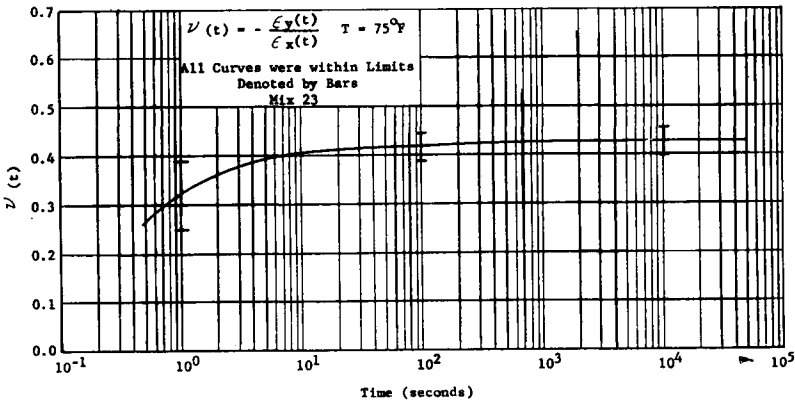
FIG. 8. Transverse contraction ratio.

Using crossed polaroids, minimum light intensity occurs at integer values of n and maximum light intensity at odd multiples of one-half (according to (4)). By noting the times of maximum and minimum intensity, a plot of $\Psi(t)$ according to (27) can be made. The result is shown in Fig. 9 for several temperatures.

The inverse function $\Phi(t)$ was found by numerical solution of the Volterra integral equation. The result is shown in Fig. 10.

Mix 30

Mix 23

⊙ 80°F   △ 91.2°F   ◊ 75.8°F   - - - - 75°F

⊡ 87.1°F   ▽ 84.5°F   ✕ 72°F

$\psi(t) = 8.46 \times 10^{-5} \dfrac{n}{\sigma_0}$ $\psi(t) = 8.15 \times 10^{-5} \dfrac{n}{\sigma_0}$

$$\psi(t) = \frac{2\pi c}{\omega} \frac{n(t)}{\sigma_0 h} \qquad \frac{2\pi c}{\omega} = 5460 \text{ Å}$$

FIG. 9. Optical creep function.

$\bar{\Phi}(t)$ Stress at Constant Fringe Order

——— $\psi(0) \cdot \bar{\Phi}(t)$

— · — $\psi(0)/\bar{\psi}(t)$

$\psi(0) = 0.25 \times 10^{-5}$ in²/lb

Mix 23
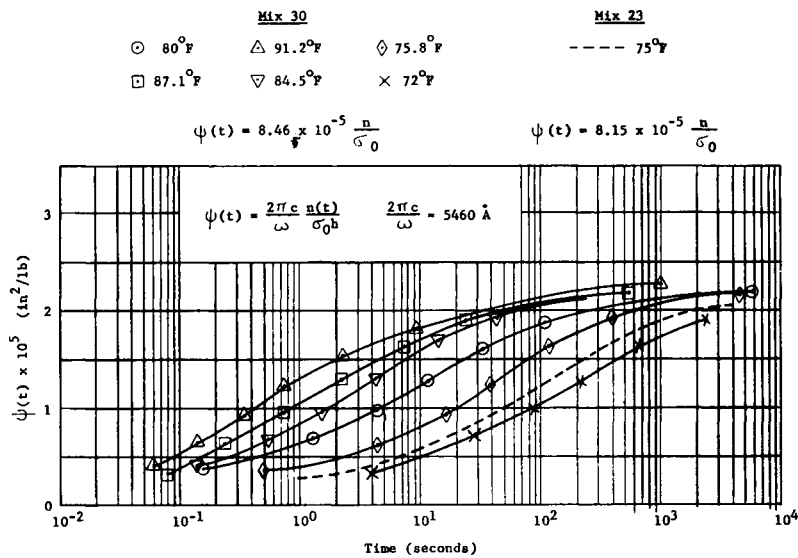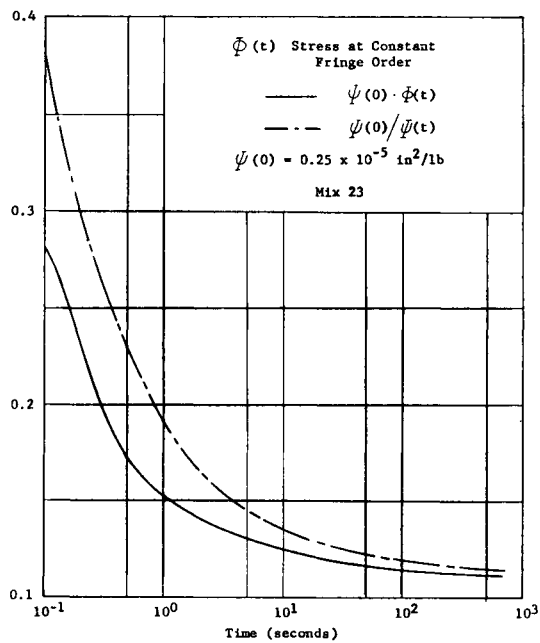
FIG. 10. Inverse optical creep function.
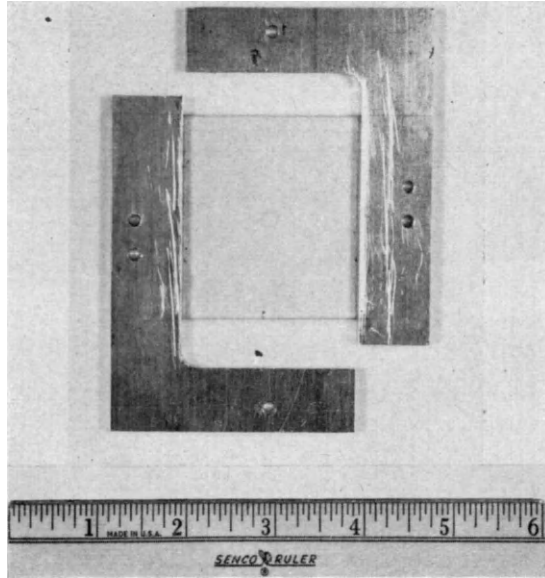
FIG. 11. Shear specimen.
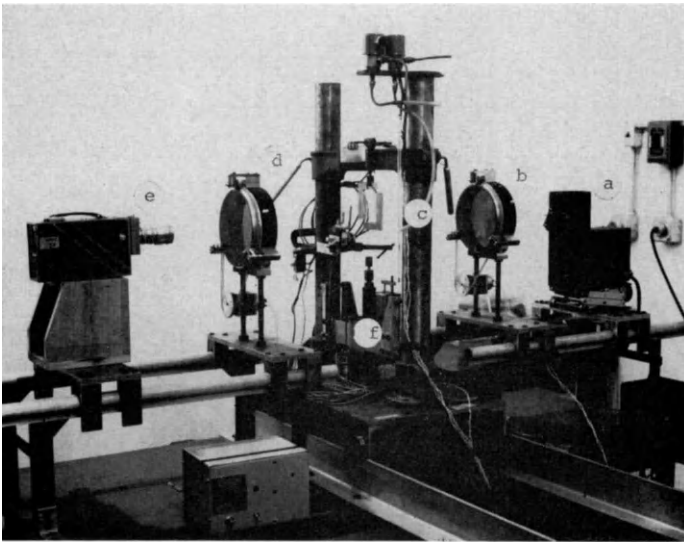
FIG. 12. Photoviscoelastic bench. *a*, Light source, 5460°A. *b*, Polarizer. *c*, Model. *d*, Analyzer. *e*, Camera. *f*, Loading frame.

3.3. *Shear Test*

The shear test specimen is shown in Fig. 11. The model was loaded by constant loads P_1, and the fringe order recorded with an ordinary 16 mm movie camera (Fig. 12). The fringe order at any point on the x_2-axis should be given by (31). The measured fringe order is compared with the value of $\Psi(t)$ measured in the

tensile test in Fig. 13. The agreement is within experimental error except at large times. The stress at the center, computed by (31), is 8.1 psi compared to the value of 8.0 psi for similar loading of an elastic material.
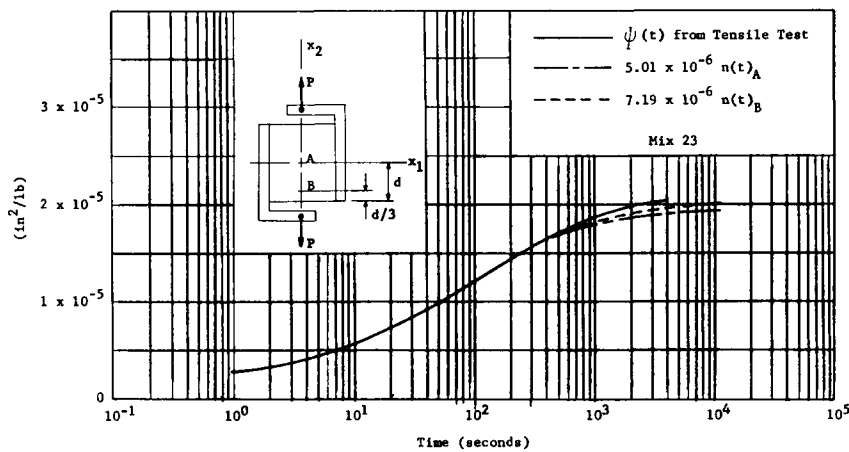
FIG. 13. Fringe order in shear test.
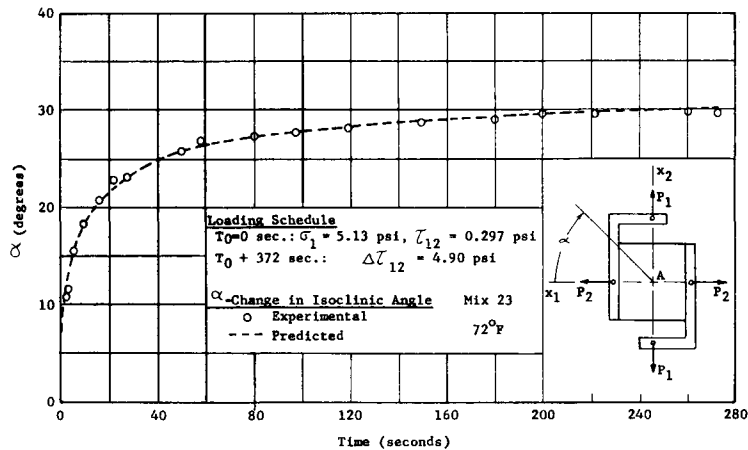
FIG. 14. Isoclinic angle in tension-shear test.

3.4. Tension-Shear Test

The shear model was first loaded by a tensile force P_2. Later a shear load P_1 was added. The principal axis of the dielectric tensor should be given by (33). The isoclinic angle can then be predicted using the value of $\Psi(t)$ from the tensile test. The isoclinic angle was observed to within $\pm\frac{1}{2}$ degree by manually rotating the polaroids to maintain minimum light intensity at the center. The predicted and observed values are compared in Fig. 14. The agreement is within experimental error.

3.5. Plane Stress

The disk specimen is shown in Fig. 15. By means of a frame and diaphragm, a pressure could be applied to the outer edge.

The stress field at room temperature due to a suddenly applied pressure should be constant and given by (29). Thus, the measured fringe order should be proportional to the function $\Psi(t)$ found in the tensile test.
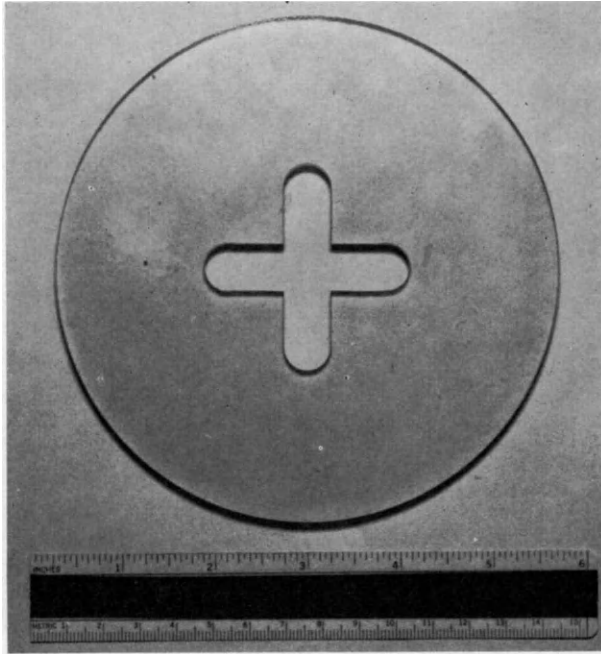
FIG. 15. Disk specimen.

The fringe pattern was recorded by an ordinary movie camera. A typical frame is shown in Fig. 16. The observed fringe order at several points is compared with the results from the tensile test in Fig. 17. The stress at the star root was then calculated by (29).

The specimen was next heated at the inner boundary by radiation from a hot wire (Fig. 18). The model was not loaded until the temperature distribution was steady. The thermal stress at that time did not result in measurable fringes. A pressure was then suddenly applied to the outer edge. The fringe pattern was photographed with a movie camera. The observed fringe order at the root of the star at the inner boundary is shown in Fig. 19. The stress was calculated by numerical integration of (16) using the previously measured inverse creep function, Fig. 10. The result is shown in Fig. 20.

As predicted above, the stress did approach the uniform temperature results at long time and was lower at earlier times. The stress at times less than 0.1 sec
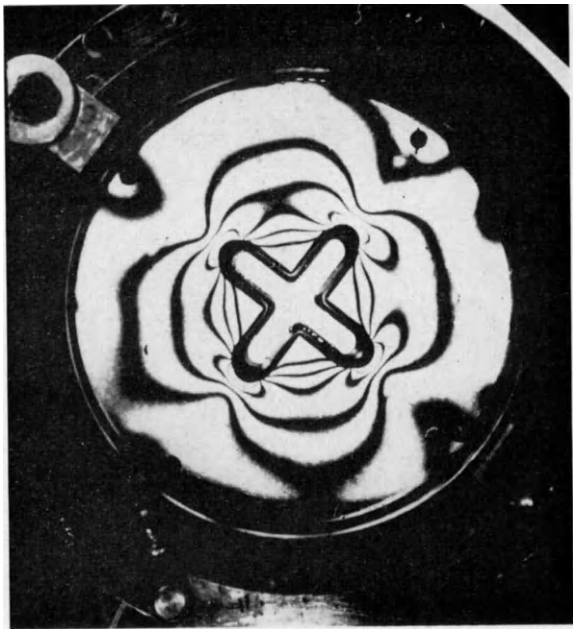
FIG. 16. Isothermal star grain model, light field.
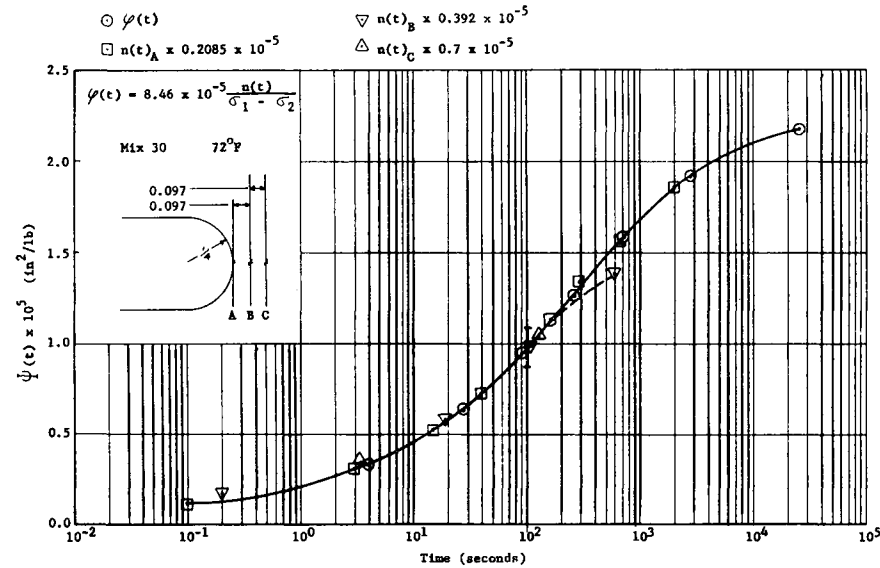
FIG. 17. Fringe order at uniform temperature.

FIG. 18. Pressure loading jig. *a*, Heater. *b*, Diaphragm. *c*, Polaroid-guard.
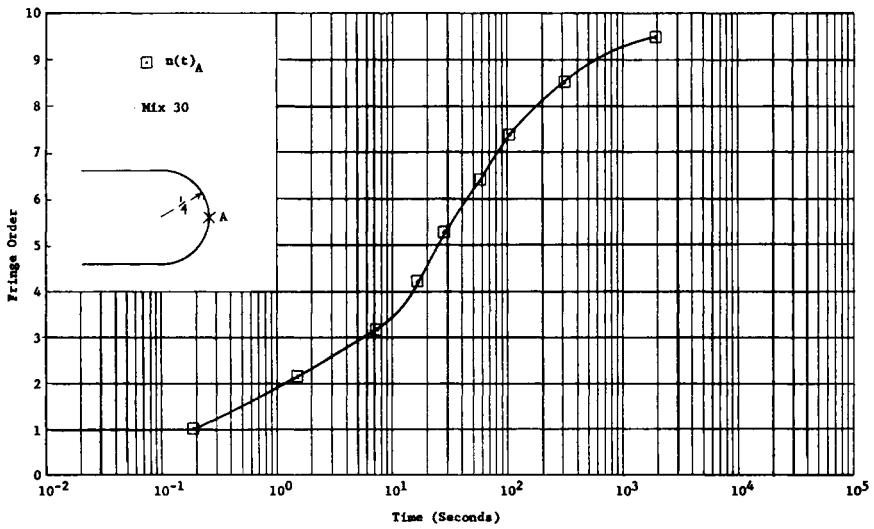
FIG. 19. Fringe order, heated model.
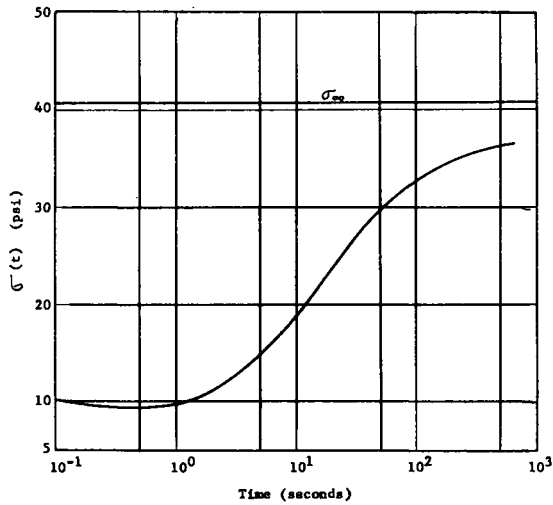
FIG. 20. Stress at root, heated model.

could not be reliably determined. Moreover, the loading was of course not a step change but required about 0.1 sec.

These experiments are quasi-static. Some results on dynamic loading are given in ref. [6]. Other papers may be found in the technical literature.

4. CONCLUSIONS

The tests are in agreement with predictions based upon the assumptions that the dielectric and stress tensors are functionals of the strain history with fading memory. The tests were restricted to small deformations so that the memory functionals reduce to those of linear viscoelasticity.

In particular, the stress in a viscoelastic material was the same as in an elastic material for the case of isothermal proportional loading as predicted by linear viscoelasticity.

The principal axes of stress, strain, and isoclinic angle do not coincide even approximately. This agrees with linear viscoelasticity.

The limiting stress for a steady nonuniform temperature is the same as for a uniform temperature. This agrees with linear viscoelasticity.

The hotter portions of a viscoelastic material experience some momentary stress relief due to the viscoelastic behavior. This fact may be of use in design of rocket motors.

REFERENCES

[1] MINDLIN, R. D., *J. Appl. Phys.*, **20**, 206 (1949), and *Applied Mech. Rev.*, **4** ,164 (1951).
[2] READ, W. T., *J. Appl. Phys.*, **21**, 671 (1950).
[3] STEIN, R. S., ONOGI, S. and KEEDY, D. A., *J. Polymer Sci.*, **57**, 801 (1962).
[4] DILL, E. H., *On the Theory of Photoviscoelasticity*. Univ. of Washington, Dept. of Aero-
    nautics and Astronautics, Report 63–1 (1963).
[5] DILL, E. H. and FOWLKES, C., *Photoviscoelastic Experiments I, The Trend in Engineering*, **16**,
    5 (1964). Published by the Office of Engineering Research at the University of Washington.
[6] DANIEL, J. M., "Two-dimensional dynamic stress analysis in a nonelastic material", IIT
    Research Institute Report RTD–TDR–63–3059 (1963).

DEFORMATION AND FAILURE ANALYSIS
OF REINFORCED GRAINS

A. M. Freudenthal

Columbia University, New York

Abstract—After considering the limitations imposed by the characteristic response of filled elastomers on the performance of case-bonded solid propellant grains, particularly the effect of loss of filler–binder interaction with increasing strain, the significant features of metal-wire or mesh-reinforced grains are discussed. The difference between the design criteria for such grains and for other types of reinforced structures is emphasized and the inapplicability of classical methods of viscoelastic analysis is discussed.

Methods of analysis of elastic orthotropic, inhomogeneous, case-bonded grains are summarized and their limitations shown with respect to optimal utilization of the reinforcement. Such utilization requires the use of reinforcement of variable ductility throughout the wall-thickness of the grain and the consideration of its elastic–plastic response in grain analysis.

1. INTRODUCTION

Current structural design of solid propellant motors is based on the concept of a mechanically weak grain constructed of an elastomeric or polymeric binder, loaded with a high percentage of granular fuel and metallic oxidizer, and cast into a metallic case which provides the essential structural resistance against the forces due to pressurization and the inertia forces arising in operation. The low strength of the grain is utilized only for the transmission of the pressurization and of the inertia forces from the grain surface or from the mass of the grain where they arise, to the metal case by which they are carried.

At a sufficiently large distance from the case the strains associated with the force transmission are relatively large as a result of the high deformability of the binder. On the other hand, effective force transmission from grain to case presupposes continuity of the displacements along the interface between grain and case. The enforcement of this introduces severe strains as well as strain gradients into the grain in the vicinity of the interface, not only because of the large differences between the elastic moduli and the coefficients of thermal expansion of grain and metal case but also because of the considerable shrinkage strains accompanying the curing process of the grain. Thus, both near the burning surface and near the interface large strains arise that might cause failure of the grain by cracking, if its strength at this strain-level is inadequate to ensure force-transmission to the case as well as continuity of the displacements at the interface without crack-development. While such cracking does not significantly affect the mechanical strength of the motor, it seriously interferes with its operation by increasing, sometimes catastrophically, the burning surface.

463

Failure analysis of the motor has therefore the dual aspect of deformation and strength analysis of the case, and deformation and strength analysis of the grain. Only the former is really concerned with "structural integrity"; the latter is concerned with "operational integrity" which, however, presupposes the structural integrity of the grain. The differentiation may seem irrelevant until one recognizes the difference in the concept of "failure" in both cases: while failure criteria of the metal case are reasonably well founded on knowledge of metal behavior and structural mechanics, failure criteria of the grain are somewhat vague. This is due to the fact that only at relatively small strains can the filler–binder compound be considered as a reasonably continuous medium; it loses this continuity by the loss of binder–filler interaction at strains that are considerably below those at which cracks actually start to propagate throughout the medium. It is rather unfortunate for the application of continuum mechanical theory to grain-analysis, particularly close to failure, that the level of maximum operational strains due to pressurization as well as due to thermal cycles are within this intermediate quasi-discontinuous range of behavior. In this range the large numbers of vacuoles surrounding most of the filler particles (Fig. 1) make the transition from the "uncracked" to the cracked condition [in which locally coalescing vacuoles form what may be termed "cracks" (Fig. 2)] rather gradual. Thus, the question of the minimum size of a crack the occurrence of which can produce an instability of the burning process has not yet been clearly answered.

The difficulty of producing a grain of reliable structural integrity to ensure its operational integrity is therefore due to a combination of circumstances:

(a) the interaction of two materials (binder and filler) of highly incompatible deformational characteristics;

(b) the effect of the imperfection of this interaction and of its strong dependence on filler content and geometry (size and shape) and on the overall deformational response of the material;

(c) the pronounced non-linearity of this response which precludes the useful application of classical (elastic or linear viscoelastic) analysis in actual grain design; and

(d) the lack of a clear criterion of "failure" in the grain.

The behavior of the material shows three distinct phases depending on the combination of stress or strain, time, temperature and concentration and size of filler particles. Thus in tensile creep at moderate or high stresses the short-time deformation is characteristic of the response of the "continuous" medium, the long-time deformation of that of the dewetted (unfilled) matrix, while an intermediate stage reflects the process of dewetting itself. Thus moduli of elasticity determined at different stages are quite different, and their dependence on filler content depends on the state of the material.

Within the range of small and moderate strains and small to moderate volume concentrations of a fine-grained chemically inert filler an increase of the filler volume produces a pronounced "strengthening" effect of an elastomeric binder, such as polyurethane rubber, increasing both the elastic modulus and the
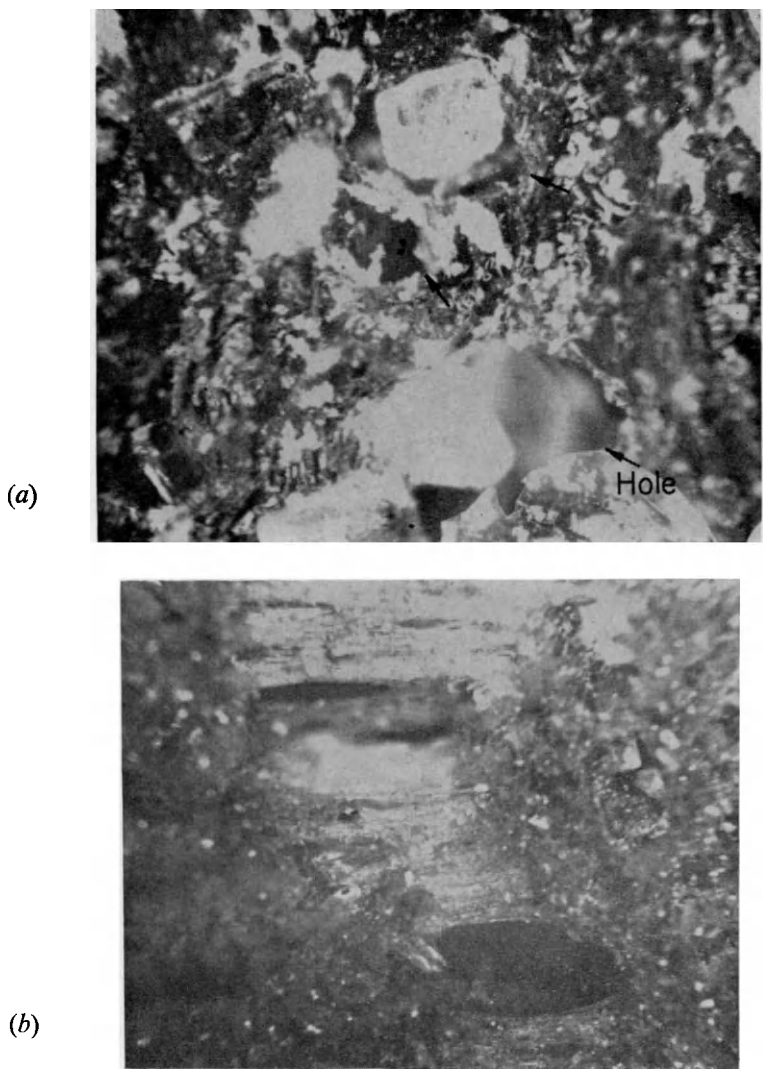
FIG. 1. Initiation of fracture in highly filled polyurethane rubber by formation of vacuoles around (a) filler grains, and (b) isolated holes.

fracture strength of the compound. However, beyond a certain combination of grain-size, volume concentration and strain as well as for large filler particles this effect is reversed (Fig. 3). It is also known that creep under constant tensile stress of the compound material depends so strongly on filler-size geometry and content (Fig. 4) as to support the assumption that a substantial component of the rate sensitivity of highly filled elastomers at moderate strains reflects a time-dependent process of loss of interaction between filler particles and binder, rather than a true viscoelasticity, linear or non-linear.

30

(a)

(b)
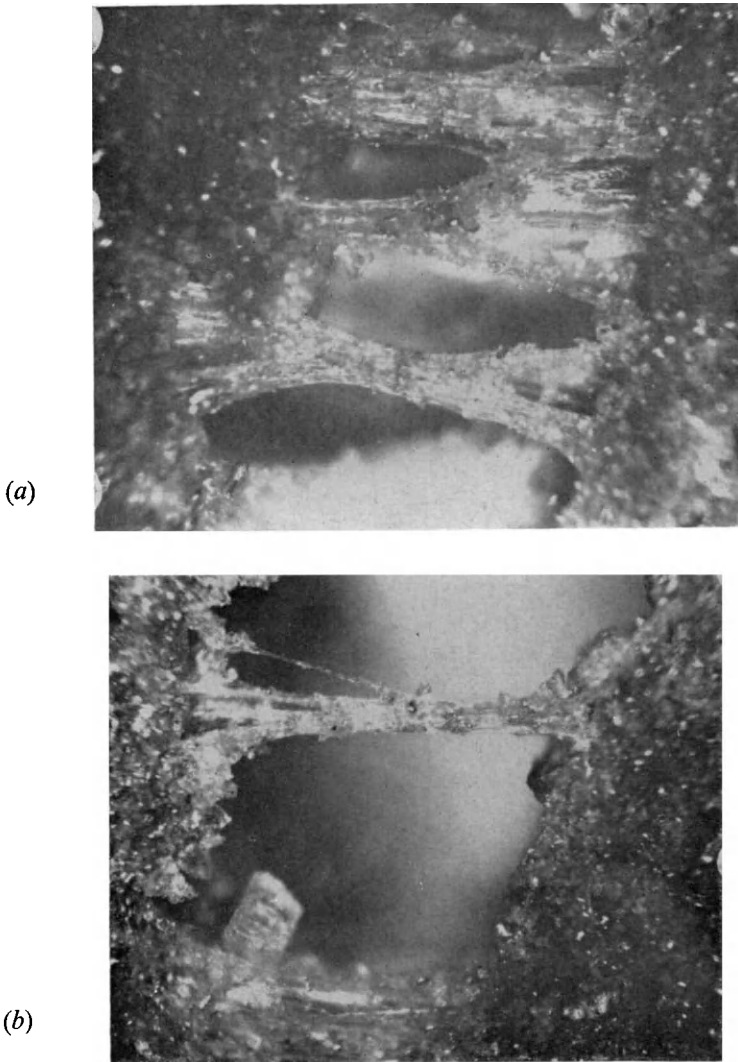
FIG. 2. Development of crack in highly filled polyurethane rubber by (a) opening, and
(b) coalescence, of holes.

The location in time- or strain scale of the dewetting process is also quite
variable, depending on stress but also on filler-concentration and particle-size.
This dependence further complicates the treatment of a filled solid grain under
various critical conditions by analytic theory, a prerequisite of rational design.

In spite of these basically unfavorable structural characteristics of the material
of the solid grain which must necessarily lead to an undesirably high probability
of malfunctioning of the motor in service, the current state of the solid pro-
pellant motor technology seems surprisingly high. To the unbiased observer

this fact points to the conclusion that a remarkable state of balance has been reached between the structural requirements implicit in current motor design and the structural possibilities of the case-bonded solid propellant motor. The fact that most currently operational solid motors have certain common basic
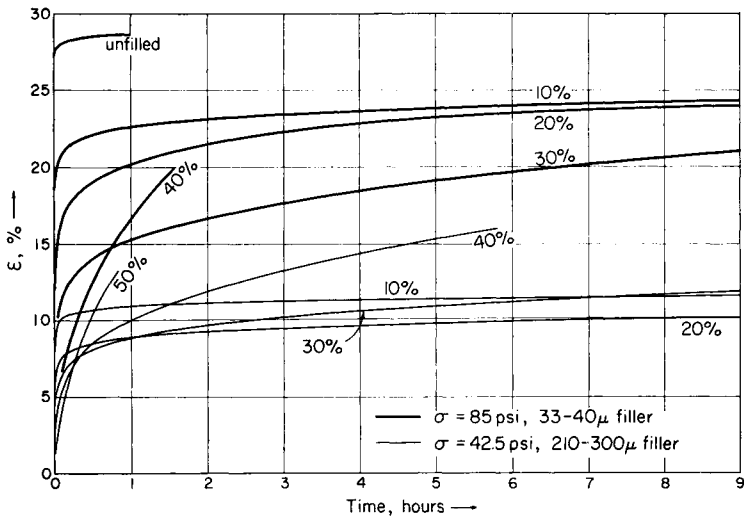
FIG. 3. Creep curves in tension of filled polyurethane for various percentages of filler grain size and stress (effect of filler content on time function clearly observable). (*Courtesy F. R. Schwarzl.*)
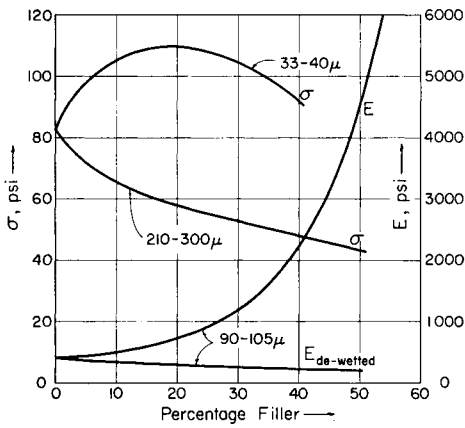
FIG. 4. Effect of filler content and grain size on creep fracture stress σ after 1 hr and on rubber-elastic modulus E in tension creep. (*Courtesy F. R. Schwarzl.*)

features such as relatively low pressure, a characteristic form of the time-pressure profile, low acceleration, and low ratio of length to diameter resulting in low bending moments, suggests that such a balance does in fact exist, the technology having adjusted to the limitations of material performance.

In some way the situation is reminiscent of a similar one that existed about half a century ago in a different field of technology, that of concrete structures.

The material itself had been known to the Romans, if not before, and its technology was perfected within the limitations of material performance; it seemed a satisfactory material for use in structures with predominant compressive stresses, such as vaults and arches, and relatively large span arch bridges were built of pure concrete not more than 40 years ago. Since it was appreciated that the material could not take substantial tensile stresess, structural forms were chosen in which such stresses were avoided. Since the high tensile shrinkage stresses arising during hardening of the cast concrete were undesirable, procedures were developed to avoid them by casting not continuously but in shorter segments.

In 1861 a gardener by the name of Monier in Paris using concrete flower pots decided to reinforce them circumferentially in order to reduce expensive breakage, and took out a number of patents on his process. Between that time and the early twenties so many patent applications were made for different types, systems and configurations of reinforcement that patent offices and courts refused to grant and uphold further patents claiming that no inventiveness but only manual skill was involved in finding different reinforcement configurations. It is interesting to note that reinforced concrete was thus not born because unreinforced concrete technology had reached its technical limits. Years after Monier's and subsequent patents expired, unreinforced concrete structures were still built because not all established builders cared to change the technology to which they had been accustomed. Changes of requirements were met by adjustments in structural forms and not by a radical change-over to a new material. The development of steel-reinforced concrete with its special technology and its potential for completely new structural forms created rather than followed the demands for the use of such forms in new structures. It was the recognition of the potential of the material which provided the incentive for the use of new structural ideas and forms, showing possibilities that could not have been considered before.

It may be interesting to consider the implications of this history of development of steel-reinforced concrete in the light of recent trends to develop a new technology of reinforced solid propellant grains.

2. THE CHARACTERISTICS OF THE REINFORCED GRAIN

From a structural mechanics point of view the idea of replacing the powdered metal oxidizer in a cast monolithic grain with the same quantity of metal in wire form arranged in such a way as to produce a load carrying reinforced composite is quite obvious. The strengthening of a material weak in tension by a reinforcement of high tensile strength is a technological process that has been and is being utilized in various fields, from the manufacture of wooden barrels to that of whisker-reinforced metal or ceramic matrices. The nature, form and arrangement of the reinforcement differs for different materials and different structural forms without in any way affecting the principle that tension is carried by the reinforcement while the matrix must either provide the com-

pressive strength itself, as in reinforced concrete, ceramic or metal matrices, or only provide the continuity and rigidity required for the build-up of an integral composite, such as a glass-filament reinforced structure, in which the reinforcement which is prevented from buckling by the surrounding matrix also contributes to the compressive strength. In the latter case the volume fraction of the reinforcing elements may be as high as 70 per cent, in the former as low as 1 per cent or less. In either case there is a certain disparity between the elastic moduli of reinforcing elements and matrix; however, this ratio is usually of an order of magnitude not exceeding 100. The reinforcement of either type of structure to be structurally effective must be continuous or sufficiently anchored in the matrix to permit it to develop its full tensile strength. This introduces the necessity of providing adequate bond between reinforcement and matrix, which is for instance one of the key problems in reinforced concrete.

Proposed configuration of internally reinforced solid propellant grains include cast propellants with short length of metal wire or screen distributed within the matrix, continuous reinforcing wires wound according to winding patterns that ensure maximum structural efficiency, similar to those used in the manufacture of glass-filament wound structures, and continuous reinforcing metal screens with different percentages of wire in circumferential and longitudinal direction to provide the necessary strength against hoop stresses and longitudinal stresses resulting from acceleration forces and longitudinal bending moments. The principle of the reinforcing wire screen has been extensively used in reinforced concrete plates and shells. In the case of glass-filament reinforcement the high volume percentage of reinforcing material leads automatically to the replacement of the wide-mesh screen by more or less densely woven glass fiber fabrics.

There are two characteristic features of the internally reinforced solid propellant which distinguish it from any other type of reinforced structure:

(a) The reinforcing wires serve the dual purpose of propulsion (combustion) and structural strength; and

(b) the ratio between the elastic moduli of reinforcement and matrix is unusually large, being of the order of magnitude of 10^3 to 10^4.

Because of (a) the percentage, form and distribution of the reinforcement is determined by considerations of combustion, not of strength; strength requirements are necessarily subordinate to those of ballistics. Because of (b) the deformation and failure characteristics of the compound structure are completely dominated by those of the reinforcement.

Since the ballistically desirable total volume percentage of metal reinforcement is of the order of magnitude of 5 to 15 per cent, and thus intermediate between the percentages used in reinforced concrete or ceramic structures and those used in glass-filament wound structures, it is obvious that its closely spaced more or less uniform continuous distribution throughout the volume requires the use of very fine wire, either in the form of wound filaments or in the form of wire-mesh. There are certain structurally desirable non-uniform distributions of such quasi-continuous reinforcement (see Section 4), but their

consideration in actual design is again subject to their compatibility with ballistic requirements.

The large discrepancy between the elastic moduli of reinforcement and matrix introduces the problem of whether a continuous compound can actually be formed by such materials, particularly in view of the low shear and tensile strength of the matrix between the reinforcing layers and the low adhesive bond between reinforcement and matrix, or whether the matrix provides no more than a "spacing" material for the reinforcement. While this question is not of critical importance with respect to the resistance to internal pressure because of the circular symmetry associated with this condition of the structure, the
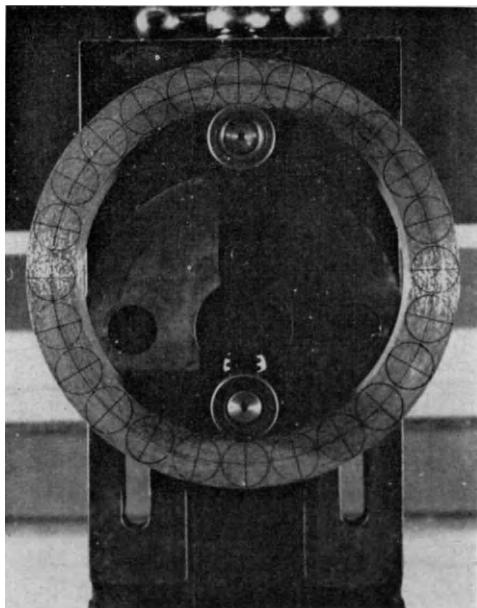
FIG. 5. Ring of metal-fiber wound solid propellant model cylinder in unstrained state before test.

evaluation of the resistance of the reinforced structure to overall and particularly to local bending moments as well as of its resistance to twisting will largely depend on a reliable answer to this particular question.

Preliminary observations of the bending of rings cut from wire-reinforced as well as from screen-reinforced cylinders suggest that the inherent weakness in shear and tension between the reinforcing layers must be expected to produce phenomena that do not arise in the bending of rings of continuous anisotropic materials of adequate shear strength. Figures 5 and 6 clearly show the development of regions of delamination in the vicinity of points of maximum shear under increasing bending moments. At these points the shear strength of the matrix is exceeded with the result that the bending resistance of the cross-section based on its full depth is reduced to that of a section made up of individual lamellae

since the destruction of the continuity of the full section by shearing along the plane of maximum shear produces the critical magnitude of the shear stress in both half-sections. The resulting break-up of these sections by shear is again followed by transfer of the critical shear to new planes along which shearing now proceeds, and so on, until the section is divided by shear planes into several lamellae, a procedure that reduces the elastic bending resistance of the section to $1/n$-th of its initial value, if n denotes the number of lamellae into which this section has been split by shear between reinforcing layers. The sheared sections thus act as some kind of "hinge" in bending ("shear hinge") at which large curvatures can develop under small or no moments (Fig. 7). In reinforced
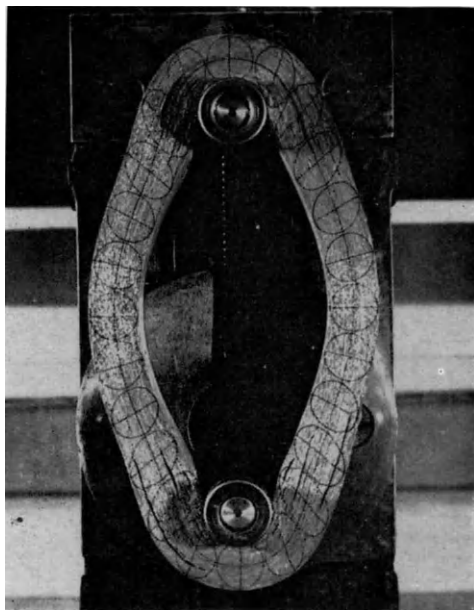
FIG. 6. Ring shown in Fig. 5 strained by two opposing tensile forces. (Delamination at locations of inflexion of bending curvature clearly observable.)

grains designed to carry large over-all as well as highly non-uniform local moments this phenomenon may be highly undesirable; its elimination requires suitable modifications of the reinforcement.

If a real composite structure can be produced by the interaction of the reinforcement with the propellant matrix, the reinforcement will make the composite medium highly anisotropic; it may also make it non-homogeneous. Moreover, the domination of the deformational response of the reinforcement, which may be elastic-plastic, elastic-strain-hardening or elastic-brittle depending on the nature of the metal wire, will considerably reduce the significance of the deformational character of the solid propellant matrix. Obviously the limit of deformation as well as the limit of failure is determined by the metal; hence, failure with respect to fracture as well as maximum deformation of the com-

pound must be based on the resistance of the metal alone. Consequently the rather complex viscoelastic response of the solid propellant matrix, which at present, is being extensively studied in view of the requirements of deformation and failure analysis of non-reinforced monolithic or segmental case-bonded grains is of very little, if any, significance in the structural analysis of a grain with well designed continuous, continuously distributed metal wire reinforcement, since the rate-insensitivity of the metal wire reduces the time-effects arising through wire-matrix interaction to secondary significance. This intuitive conclusion is confirmed by a comparison of the results of an analysis of an orthotropic, inhomogeneous linear viscoelastic cylinder subject to internal pressure with the results of the analysis of the associated orthotropic, inhomogeneous elastic cylinder the moduli of which are the initial values (at time $t = 0$) of the viscoelastic relaxation functions [1].
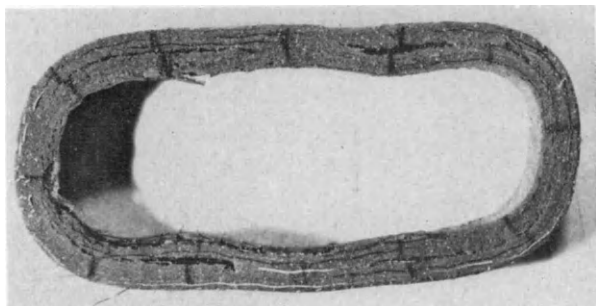
FIG. 7. Effect of "shear-hinges" in wire-mesh reinforced solid propellant ring compressed opposing vertical forces.

This fact considerably simplifies the analysis of reinforced grains. While the structural analysis of anisotropic, inhomogeneous viscoelastic media even for selected relatively simple relaxation functions involves extremely elaborate numerical solutions of integral equations of considerable complexity, methods of analysis of anisotropic elastic media, particularly for the condition of orthotropy that usually arises in reinforced structures, have been developed already by Saint Venant [2] and Voigt [3] and applied to specific problems, such as beams, plates, shells and thick-walled cylinders and spheres by Huber [4], Olszak [5], Lechnitski [6], and others [7]. More recently some problems of the orthotropic non-homogeneous· elastic and elastic-plastic medium, among these the problem of the thick-walled cylinder, have been studied and solved under various simplifying assumptions at the Polish Institute for the Study of Continuous Media, principally by Olszak and co-workers [8]. The fact that the viscoelastic response of the matrix is of minor significance also eliminates the problems of temperature sensitivity and of curing and storage. The analytical complications arising from the necessity of considering a temperature shift of the relaxation functions, which are quite severe in the case of an orthotropic viscoelastic medium, are eliminated for all practical purposes.

3. ANALYSIS OF ELASTIC HOMOGENEOUS ORTHOTROPIC GRAIN

The cylindrical symmetry characteristic of solid-propellant motors and the winding procedures used in their manufacture produce conditions of cylindrical orthotropy with nine independent constants which reduce to six in case of cylindrical symmetric loading. When the reinforcement is uniformly distributed throughout the grain the medium is homogeneous orthotropic; when the distribution is a function of the radial coordinate the medium is inhomogeneous orthotropic. When the viscoelasticity of the matrix is considered, the constants become functions of time. Thus the stress–strain relations of the anisotropic, non-homogeneous viscoelastic medium can be written in the integral form

$$\sigma_{ij}(x, t) = \int_0^t \psi_{ijkl}(x, t - \theta) \frac{\partial}{\partial \theta} \epsilon_{kl}(x, \theta)\, d\theta \qquad (3.1)$$

provided the medium is stress-free at times $t < 0$, where $\psi_{ijkl}(x, t - \theta)$ denotes the fourth-rank tensor of relaxation moduli of the material. Because of the necessity to provide adequate strength both in circumferential and longitudinal directions in order to sustain not only internal pressure but also forces of acceleration as well as bending and twisting moments, the winding of the cylinder reinforcement is done along at least two directions, the winding pattern of the reinforcing wire being selected as the best compromise between the requirements to follow the direction of maximum tension, to avoid shear strains in the direction of the wire, and to avoid slipping of the wire on the surface while being wound, particularly in the vicinity of the transition to the end dome and nozzle. The circumferential and longitudinal directions are therefore reinforced with effective reinforcing percentages depending on the selected winding directions; the radial direction is unreinforced. In the case of wire-screen reinforcement the percentage of wire in the two directions is suitably selected.

Since the deformational response in the reinforced directions is governed by the reinforcement, the relaxation moduli in these directions can, without significant error, be replaced by the elastic moduli in these directions resulting from the effective components of the reinforcement. It is only in the radial direction that the material response remains viscoelastic, which leaves three out of the six relaxation functions. However, in view of the exceptionally low modulus ratio between matrix and reinforcement the effect of time dependence in the radial direction is considerably modified by the interaction of the deformation in this direction with the deformation in the reinforced directions. Therefore, the disproportionate complexity introduced into the analysis by the retention of the relaxation-function in radial direction does not seem warranted, particularly in view of the small differences in the results obtained in the comparative analysis of a thick-walled cylinder under internal pressure with elastic and with viscoelastic response in radial direction [1]. The assumption that the continuously reinforced solid propellant grain with either wound wire reinforcement or reinforcing screens acts like an orthotropic homogeneous or inhomogeneous

elastic medium thus appears to be justified by the physical situation as well as by the simplicity of the methods of structural analysis resulting from it.

The problem of estimation of the orthotropic elastic moduli from the geometry and elastic response of reinforcement and matrix, which has formed the subject of a number of theoretical investigations [9] is not considered here. It is a rather complex problem and it does not seem that these investigations have so far produced results that are physically more acceptable than those obtainable from the rather simple arguments that have been used in the analysis of reinforced concrete structures with small percentages of reinforcement, coupled with the symmetry requirements arising from the association of the stress-strain relations with an elastic potential. Moreover, the relevance of theoretical investigations based on the assumption of undisturbed full interaction between reinforcement and matrix is quite problematic in view of the exceptionally low strength and high deformability of the latter.

For the case of rotational symmetric loading of a homogeneous orthotropic thick-walled cylinder of sufficiently high ratio of length to diameter to justify the assumption of plane strain $\epsilon_z = $ const. the stress-strain relations can be written in the alternative forms

$$\epsilon_r = a_{11}\,\sigma_r + a_{12}\,\sigma_\theta + a_{13}\,\sigma_z$$
$$\epsilon_\theta = a_{12}\,\sigma_r + a_{22}\,\sigma_\theta + a_{23}\,\sigma_z \qquad (3.2)$$
$$\epsilon_z = a_{13}\,\sigma_r + a_{23}\,\sigma_\theta + a_{33}\,\sigma_z$$

since σ_r, σ_θ and σ_z are the principal stress components, or

$$\sigma_r = c_{11}\,\epsilon_r + c_{12}\,\epsilon_\theta + c_{13}\,\epsilon_z$$
$$\sigma_\theta = c_{12}\,\epsilon_r + c_{22}\,\epsilon_\theta + c_{23}\,\epsilon_z \qquad (3.3)$$
$$\sigma_z = c_{13}\,\epsilon_r + c_{23}\,\epsilon_\theta + c_{33}\,\epsilon_z$$

The matrices $[a_{ij}]$ and $[c_{ij}]$ are inversely related

$$[a_{ij}] = [c_{ij}]^{-1} \qquad (3.4)$$

Since eqn. (3.2) can also be written in terms of the engineering constants

$$\epsilon_r = \frac{1}{E_r}\,\sigma_r - \frac{\nu_{\theta r}}{E_\theta}\,\sigma_\theta - \frac{\nu_{zr}}{E_z}\,\sigma_z$$
$$\epsilon_\theta = -\frac{\nu_{r\theta}}{E_r}\,\sigma_r + \frac{1}{E_\theta}\,\sigma_\theta - \frac{\nu_{z\theta}}{E_z}\,\sigma_z \qquad (3.4a)$$
$$\epsilon_z = -\frac{\nu_{rz}}{E_r}\,\sigma_r - \frac{\nu_{\theta z}}{E_\theta}\,\sigma_\theta + \frac{1}{E_z}\,\sigma_z$$

the coefficients a_{ij} can be expressed in terms of these constants

$$a_{11} = \frac{1}{E_r};\ a_{12} = -\frac{\nu_{\theta r}}{E_\theta} = -\frac{\nu_{r\theta}}{E_r};\ a_{13} = -\frac{\nu_{zr}}{E_z} = -\frac{\nu_{rz}}{E_r}$$
$$a_{22} = \frac{1}{E_\theta};\ a_{23} = -\frac{\nu_{z\theta}}{E_z} = -\frac{\nu_{\theta z}}{E_\theta};\ a_{33} = \frac{1}{E_z} \qquad (3.5)$$

which must thus satisfy the symmetry conditions

$$\nu_{r\theta}E_\theta = \nu_{\theta r}E_r; \quad \nu_{zr}E_r = \nu_{rz}E_z; \quad \nu_{z\theta}E_\theta = \nu_{\theta z}E_z \tag{3.5a}$$

In the case of $\epsilon_z = 0$ the third eqn. (3.2) provides the expression

$$\sigma_z = -\frac{a_{13}\sigma_r + a_{23}\sigma_\theta}{a_{33}} \tag{3.6}$$

which, introduced into the first two eqns. (3.2), produces the relations

$$\epsilon_r = a_{11}\,\sigma_r + a_{12}\,\sigma_\theta$$
$$\epsilon_\theta = a_{12}\,\sigma_r + a_{22}\,\sigma_\theta \tag{3.7}$$

where

$$a_{11} = a_{11} - \frac{a^2_3}{a_{33}} = \frac{1}{E_r}\left(1 - \nu^2_{rz}\frac{E_z}{E_z}\right) = \frac{1}{E_z}(1 - \nu_{rz}\,\nu_{zr})$$

$$a_{12} = a_{12} - \frac{a_{13}\,a_{23}}{a_{33}} = -\frac{1}{E_r}(\nu_{r\theta} + \nu_{rz}\nu_{z\theta}) \tag{3.8}$$

$$a_{22} = a_{22} - \frac{a^2_{23}}{a_{33}} = \frac{1}{E_\theta}\left(1 - \nu^2_{\theta z}\frac{E_z}{E_\theta}\right) = \frac{1}{E_\theta}(1 - \nu_{\theta z}\nu_{z\theta})$$

Solving for the stresses in (3.7), we obtain the first two eqns. (3.3):

$$\sigma_r = c_{11}\epsilon_r + c_{12}\epsilon_\theta = c_{11}\frac{du}{dr} + c_{12}\frac{u}{r}$$

$$\sigma_\theta = c_{12}\epsilon_r + c_{22}\epsilon_\theta = c_{12}\frac{du}{dr} + c_{22}\frac{u}{r} \tag{3.9}$$

where $\epsilon_r = du/dr$, $\epsilon = u/r$, $u = u_r$ being the radial displacement, and the coefficients

$$c_{11} = \frac{a_{22}}{a_{11}a_{22} - a^2_{12}}; \quad c_{22} = \frac{a_{11}}{a_{11}a_{22} - a^2_{12}}; \quad c_{12} = -\frac{a_{12}}{a_{11}a_{22} - a^2_{12}} \tag{3.9a}$$

Substituting eqns. (3.9) into the equilibrium condition

$$\sigma_\theta = \frac{d}{dr}(r\sigma_r) \tag{3.10}$$

we obtain the differential equation for the radial displacement

$$\frac{d^2u}{dr^2} + \frac{1}{r}\frac{du}{dr} - \frac{c_{22}}{c_{11}}\frac{u}{r^2} = 0 \tag{3.11}$$

with the integral

$$u = A_1 r^n + A_2 r^{-n} \tag{3.12}$$

where

$$n = \sqrt{\frac{c_{22}}{c_{11}}} = \sqrt{\frac{a_{11}}{a_{22}}} = \sqrt{\frac{a_{11}a_{33} - a^2_{13}}{a_{22}a_{33} - a^2_{13}}} = \sqrt{\frac{E(1 - \nu_{rz}\cdot\nu_{zr})}{E_r(1 - \nu_{\theta z}\cdot\nu_{z\theta})}} \tag{3.13}$$

is an important parameter of the problem which expresses the effect of aniso-
tropy. For the isotropic material, $n = 1$ and eqn. (3.12) becomes the conven-
tional solution of the isotropic elastic plane strain problem. The stress-com-
ponents are easily obtained by introducing eqn. (3.12) into the eqns. (3.9), or
by the direct method of introducing the stress-function F in the simplified
form

$$\sigma_r = \frac{1}{r} F \text{ and } \sigma_\theta = \frac{dF}{dr} \tag{3.14}$$

by which the equilibrium conditions are satisfied, into eqn. (3.7) and satisfying
the compatibility condition

$$\frac{d}{dr}(r\epsilon_\theta) = \epsilon_r \tag{3.15}$$

The resulting differential equation for F

$$\frac{d^2F}{dr^2} + \frac{1}{r}\frac{dF}{dr} - \frac{a_{11}}{a_{22}}\frac{F}{r^2} = 0 \tag{3.16}$$

is of identical form as eqn. (3.11) and its solution is

$$F = B_1 r^n + B_2 r^{-n} \tag{3.17}$$

where n is defined by eqn. (3.13). Hence

$$\sigma_r = B_1 r^{n+1} + B_2 r^{-(n+1)}$$
$$\sigma_\theta = B_1 n r^{n-1} - B_2 n r^{-(n+1)} \tag{3.18}$$

Compatibility of eqns. (3.12) and (3.18) produces the relations between the
constants

$$B_1 = A_1 . (\sqrt{c_{11}c_{22}} + c_{12}) = A_1 m_1$$
$$B_2 = -A_2 . (\sqrt{c_{11}c_{22}} - c_{12}) = -A_2 m_2 \tag{3.19}$$

The constants B_1 and B_2 are obtained by introducing into eqns. (3.18) the
boundary conditions for a cylindrical grain of internal radius a and external
radius b subject to internal pressure p and contained by a thin-walled elastic
case of modulus E_c, Poisson ratio v, wall-thickness δ and radius $R_c = b + \delta/2 \doteq b$:

$$\text{at } r = a: \sigma_r = -p \text{ and at } r = b: \sigma_r = -u(b) . \kappa \tag{3.20}$$

where according to eqn. (3.12) $u(b) = A_1 b^n + A_2 b^{-n}$ and $\kappa = E_c \delta/b^2(1 - v^2)$
characterizes the elastic restraint exerted by the case. From the first eqn. (3.18)
and eqn. (3.20)

$$B_1 = pa^{-n+1} K^{-1} \text{ and } B_2 = -pa^{n+1}(1 + K^{-1}) \tag{3.21}$$

where

$$K = \left[\left(\frac{b}{a}\right)^{2n}\left(\frac{1 + m_1^{-1}b\kappa}{1 - m_z^{-1}b\kappa}\right) - 1\right] \tag{3.21a}$$

expresses the combined effect of the ratio (b/a) and of the case restraint; for a grain without case ($\kappa = 0$)

$$K_{\mathrm{on}} = \left[\left(\frac{b}{a}\right)^{2n} - 1\right]$$ (3.21b)

From eqns. (3.18) therefore

$$\sigma_r = pK^{-1}\left(\frac{r}{a}\right)^{n-1} - p(1 + K^{-1})\left(\frac{a}{r}\right)^{n+1}$$

and

$$\sigma_\theta = npK^{-1}\left(\frac{r}{a}\right)^{n-1} + np\,(1 + K^{-1})\left(\frac{a}{r}\right)^{n+1}$$ (3.22)

The longitudinal stress σ_z is obtained from eqn. (3.6). Since for large values of n the ratio $\sigma_\theta/\sigma_r \gg 1$ the principal contribution to σ_z is from σ_θ and therefore, in first approximation

$$\sigma_z \equiv -\frac{a_{23}}{a_{33}}\sigma_\theta = v_{z\theta}\sigma_\theta$$ (3.6a)

The maximum tangential stress at the inner surface

$$\sigma_\theta\,(a) = np(1 + 2K^{-1})$$ (3.22a)

increases with increasing anisotropy of the medium characterized by $n = \sqrt{c_{22}/c_{11}}$; for large n it does not significantly depend on either diameter or wall-thickness. The effect of the anisotropy on the maximum tangential stress at the inner surface is obtained as the ratio of $\sigma_\theta\,(a)$ according to eqn. (3.22a) and $\sigma_\theta(a)$ for the homogeneous grain

$$\frac{[\sigma_\theta(a)]_n}{[\sigma_\theta(a)]_{n=1}} = n\,\frac{(1 + 2K^{-1})}{(1 + 2K_{01}^{-1})} \sim n$$ (3.22b)

where

$$K_{01} = [K_{\mathrm{on}}]_{(n=1)} = \left[\left(\frac{b}{a}\right)^{2} - 1\right]$$

The tangential stress at the case

$$\sigma_\theta(b) = np\,\left(\frac{a}{b}\right)^{n+1} \cdot \left[K^{-1}\left(\frac{b}{a}\right)^{2n} + (1 + K^{-1})\right]$$ (3.22c)

decreases with increasing wall-thickness and increasing anisotropy so that the tangential stress gradient across the wall becomes increasingly severe.

The radial stress at the interface between grain and case

$$\sigma_r(b) = -p\,\left(\frac{a}{b}\right)^{n+1}\left\{1 - K^{-1}\left[\left(\frac{b}{a}\right)^{2n} - 1\right]\right\}$$ (3.22d)

also decreases with increasing wall-thickness of the grain and increasing anisotropy. It becomes theoretically zero for $(b/a)^{2n} = K + 1$ and thus for $\kappa = 0$

(no case). However, because of the anisotropy, the effect of the case restraint remains small for large values of n even when the value of $(m_2^{-1} b\kappa)$ tends towards one, which produces the case with the maximum restraining effect with required elastic modulus $E_c^* = (b/\delta) \cdot (1 - \nu^2) \cdot (\sqrt{c_{11}c_{22}} - c_{12})$. Since the ratio (b/δ) is between 10^2 and 10^3 and $\sqrt{c_{11}c_{22}}$ is roughly the geometric mean of the anisotropic moduli c_{11} and c_{22} of the reinforced grain, it appears that the value of the modulus of the case must be about one order of magnitude higher than the circumferential modulus of the grain in order to produce a noticeable restraining effect. Therefore glass-fiber cases of metal-wire reinforced grains will not produce a restraining effect even for grains of small wall-thickness.

In order to estimate the maximum value and the gradient across the wall of the circumferential stress in a reinforced filled elastomeric grain, the conventional simplifying assumption is made $c_{22} = (1 - q)\, c_{11} + qE_R$, where c_{11} is the modulus of the matrix, E_R that of the reinforcement and q the percentage of reinforcement. Hence $n \doteq \sqrt{(1 - q) + qE_R/c_{11}} \doteq \sqrt{qE_R/c_{11}}$, or with $q = 0.10$ and $E_R/c_{11} = 2 \times 10^3$: $n \sim 14$. This value of n produces a tangential stress distributed over a narrow region of the wall with a peak stress $\sigma_\theta(a) \doteq np = 14p$ and an extremely sharp gradient at the inner surface.

It follows from eqn. (3.22a) that for large values of n the peak stress does not significantly depend on either the ratio (a/b) or the restraint provided by the case. Hence the grain reinforcement should be designed uniformly for the peak stress $\sigma_\theta(a)$ since this stress will only slowly change as the burning cylindrical surface $r = a$ moves outward towards $a \to b$. Thus, for instance, for $n = 14$ the change of the ratio (a/b) from an initial ratio $(a/b) = 0.2$ to the ratio $(a/b) = 0.9$ towards the end of the combustion process for any reasonable assumption of κ produces an increase of the initial tangential stress at the inner surface of not more than about 10 per cent.

This is of considerable importance in the evaluation of the results of pressurization tests of grains with respect to their actual performance. The steep circumferential stress-gradient makes effective utilization of the elastic reinforcement throughout the initial wall-thickness impossible, a fact which accounts for the relatively low carrying capacity of grains reinforced by high strength reinforcement in hydrostatic pressure tests since premature failure of the reinforcement near the inner surface initiates progressive failure throughout the wall. However, a reinforced grain designed throughout for the maximum elastic stress at the moving inner surface provides in actual operation a structure of constant strength throughout most of the combustion process. The characteristic ineffective utilization of the reinforcement in a pressurization test of an orthotropic grain is therefore not quite relevant to its performance in a firing test in which the constant strength throughout the burning process permits the utilization of pressure-time profiles that show a long sustained pressure level of high intensity.

Since according to eqn. (3.6a) the principal contribution to the longitudinal stress σ_z arises from the stress σ_θ, the distribution of σ_z across the wall is similar to that of σ_θ. The winding angle of the reinforcement must be selected so as to

provide the necessary percentage of reinforcement in the directions of the principal stresses σ_θ and σ_z, in view of the fact that in addition to the longitudinal stresses σ_z according to eqn. (3.6a) longitudinal stresses due to acceleration forces and to bending moments must be considered in the design. These stresses are, however, much more uniformly distributed. Moreover, the understressed reinforcement beyond the region of momentary maximum stress in the vicinity of the burning surface will usually be adequate to carry the longitudinal acceleration and bending stresses without additional reinforcement.

4. INHOMOGENEOUS ORTHOTROPIC GRAINS

The severe circumferential stress-gradients and stress peaks that are characteristic of homogeneous orthotropic elastic grains under internal pressure constitute a serious disadvantage unless the amount of reinforcement required for ballistic reasons is sufficient to design the entire wall thickness of the grain uniformly for the (practically constant) maximum elastic stress at the eroding inner surface. In view of the severity of the peak stress resulting from the exceptionally high modulus ratio of reinforcement and matrix, this condition limits the pressure that can be carried by a homogeneous orthotropic elastic grain with *elastic-brittle* reinforcement. Disregarding the low tensile strength of the matrix, design of uniform reinforcement of percentage q and tensile strength σ_R for the maximum stress $\sigma_\theta(a) \approx np$ produces the condition for the maximum pressure

$$np \doteq q\sigma_R \text{ or } p \leq \sigma_R \sqrt{\frac{qc_{11}}{E_R}} \tag{4.1}$$

with an estimated ratio $(c_{11}/E_R) \approx 10^{-3}$ and a percentage of reinforcement $q \approx 0.10$ to 0.15

$$p \leq 1.0 \text{ to } 1.25 \, \sigma_R \times 10^{-2} \text{ psi}$$

Hence, with $\sigma_R = 70,000$ to $100,000$ psi, the maximum pressure that can be carried by the reinforced grain without case and almost independently of diameter and wall-thickness is about 700 to 1100 psi.

If this pressure is too low or if the ballistically necessary percentage of reinforcement is lower than the assumed values of $0.1 < q < 0.15$, it becomes necessary to alleviate the severe stress gradients and peak stresses so as to ensure a more rational utilization of the reinforcement. Two possible methods suggest themselves:

(a) The reduction of the stress-gradients in the orthotropic elastic medium by reducing the elastic rigidity of the cylinder wall in the vicinity of the inner surface in relation to that of the outer surface. This may be achieved by increasing the percentage of the reinforcement across the cylinder wall or by using uniformly distributed reinforcement of lower elastic modulus in the vicinity of the inner surface and of higher modulus near the outer surface, or by combining both

methods. The result is that the modulus

$$c_{22} \doteq (1 - q) c_{11} + q E_R \approx q(r) E_R(r) = c_{22}(r)$$

becomes an increasing function of r making the orthotropic elastic grain inhomogeneous.

(b) The reduction of the *effect* of the elastic stress-gradient on the carrying capacity of the reinforced grain by providing reinforcement of high ductility and even by reducing the yield-limit of the reinforcement near the inner surface in relation to that near the outer surface so as to permit extensive plastic redistribution of the elastic stresses.

The purpose of both methods is to achieve a uniform distribution of the circumferential stress $\sigma_\theta = $ const. across the wall-thickness and thus to ensure optimal utilization of the reinforcement.

If the introduction of a suitable function $c_{22}(r)$ is sufficient to achieve uniform distribution of the stress σ_θ in the orthotropic inhomogeneous elastic grain, full utilization in the plastic range is assured and the total plastic carrying capacity

$$p_y = q \left(\frac{b}{a} - 1 \right) \sigma_{yR} \tag{4.2}$$

where σ_{yR} denotes the yield-limit of the reinforcing wire can be attained. This limiting pressure p_y is much higher than that given by eqn. (4.1), at least until close to burn-out when $(a/b) \to 1.0$. Hence the method discussed under (a), if feasible, seems to provide the most desirable solution.

The function $c_{22}(r)$ which satisfies the condition $\sigma_\theta = $ const. can be obtained by combining the integral of eqn. (3.10) for $\sigma_\theta = $ const. This satisfies the first boundary condition (3.20) with eqns. (3.9) in which the constant c_{22} has been replaced by $c_{22}(r)$. Integration of eqn. (3.10) produces

$$\sigma_r = \sigma_\theta + \frac{A}{r} \tag{4.3}$$

From the first eqn. (3.20)

$$A = - (p + \sigma_\theta) a$$

and therefore

$$\sigma_r = - \frac{pa}{r} + \sigma_\theta \left(1 - \frac{a}{r} \right) \tag{4.3a}$$

Hence eqns. (3.9) take the form

$$c_{11} \frac{du}{dr} + c_{12} \frac{u}{r} = - p \frac{a}{r} + \sigma_\theta \left(1 - \frac{a}{r} \right)$$

$$c_{12} \frac{du}{dr} + c_{22}(r) \frac{u}{r} = \sigma_\theta \tag{4.4}$$

From the solution of the first eqn. (4.4)

$$u = Br^{-s} + \frac{\sigma_\theta(r - a)}{c_{11}(1 + s)} - \frac{ap(1 + s) + a\sigma_\theta}{c_{11}s(1 + s)} \tag{4.5}$$

where $s = c_{12}/c_{11}$, the integration constant B can be obtained by satisfying the second eqn. (3.20)

$$Bb^{-s} = \left[pa(1 + s) - \sigma_\theta bs \left(1 - \frac{a}{b} \right) + \sigma_\theta a \right] [s(1 + s) c_{11}]^{-1}$$

$$+ \kappa^{-1} \left[p \left(\frac{a}{b} \right) - \sigma_\theta \left(1 - \frac{a}{b} \right) \right] \quad (4.6)$$

Introducing this solution into the second eqn. (4.4), we obtain the function $[c_{22}(r)/c_{22}(a)]$. Its actual evaluation is rather cumbersome, though elementary, and leads to an increase of the reinforcement with r which is at first slow and then rapid as it approaches the case [7].

For the case-less grain ($\kappa = 0$) the integration constant cannot be evaluated from eqn. (4.6). Since in this case the stresses can be directly obtained from the boundary conditions $\sigma_r(a) = \sigma_r(b) = 0$

$$\sigma_\theta = p \left(\frac{b}{a} - 1 \right)^{-1} \quad \text{and} \quad \sigma_r = \sigma_\theta \left(1 - \frac{b}{r} \right) \quad (4.7)$$

it is possible to evaluate the associated displacement from the first eqn. (3.7)

$$\epsilon_r = \frac{du}{dr} = \sigma_\theta \left[(a_{11} + a_{12}) - a_{11} \frac{b}{r} \right] \quad (4.8)$$

which indicates that u is of the form

$$u = \sigma_\theta [Ar + B \ln r + C] \quad (4.9)$$

where the constants in terms of the coefficients c_{11} and c_{12} can be obtained from the boundary conditions through eqns. (3.9). It can be easily shown that for the case-less grain the increase of the reinforcement that would ensure σ_θ according to eqn. (4.7) is of the form

$$\frac{c_{22}(r)}{c_{22}(a)} = \frac{r}{b} \left[M + N \ln \left(\frac{r}{b} \right) + P \left(\frac{r}{b} \right) \right]^{-1} \quad (4.10)$$

where M, N and P are constants. This indicates a somewhat slower than linear increase of the reinforcement throughout the wall [5].

Configurations with such rapidly increasing percentage of reinforcement as indicated by the above analysis are, however, incompatible with ballistic requirements. A limited alleviation of the stress-peaks might be attained by using a uniform percentage of reinforcement of several metals with elastic moduli increasing towards the outer surface although this alone may not be sufficient to attain optimal utilization of the reinforcement. The method referred to under (b) appears therefore as a more effective solution for such utilization of the reinforcement, particularly during the early stages of burning. Because of the high peak stress at the inner surface, yielding will start at the pressure p_0 that is obtained from eqn. (4.1) with $\sigma_R = \sigma_{YR}$ while the limiting pressure is given by eqn. (4.2).

31

An approximate expression for the relation between the internal pressure p and the radius r_0 of the boundary between the elastic and plastic regions can be obtained by fitting the fully plastic region to the elastic region with the aid of the boundary condition $[\sigma_r(r_0)] = -p^*$, so that the peak stress in the elastic-plastic region according to eqn. (3.22a) just attains the yield-limit:

$$\sigma_\theta(r_0) = np^*(1 + 2K^{-1}) = q\sigma_y \tag{4.11}$$

The radial stress in the plastic region is obtained by intergrating eqn. (3.10) for $\sigma_\theta \doteq q\sigma_{YR}$ with the boundary condition $\sigma_r = -p$ at $r = a$. Hence

$$\sigma_r(r_0) = -\left(\frac{a}{r_0}\right)p + q\sigma_Y\left(1 - \frac{a}{r_0}\right) = -p^* \tag{4.12}$$

and therefore

$$p^* = \frac{1}{n}q\sigma_Y(1 + 2K^{-1})^{-1} = \frac{a}{r_0}p - q\sigma_Y\left(1 - \frac{a}{r_0}\right)$$

so that

$$p = q\sigma_Y\left(\frac{r_0}{a} - 1\right) + \frac{1}{n}q\sigma_Y(1 + K^{-1})^{-1} \tag{4.13}$$

Since for $\kappa = 0$ (no case) the term $(1 + K^{-1})^{-1} \to 0$ as $(b/r_0) \to 1$, the pressure p that can be carried by the "elastic-plastic" grain according to eqn. (4.11) tends towards the limit p_Y given by eqn. (4.2) as $r_0 \to b$.

In order to analyze the carrying capacity of the eroding grain subject to internal pressure, the operational pressure-time function must be compared with the carrying-pressure-time function that is obtained from eqn. (4.13) if the constant a is replaced by the function $a(t)$ specifying the process of erosion with time of the inner surface. In order to ensure burn-out of the grain the carrying pressure must remain safely higher than the operational pressure throughout the combustion process.

Since the first term on the right-hand side of eqn. (4.13) is dominating, the significance of the plastic relief of the peak stresses in determining the carrying capacity of the reinforced grain is obvious. However, full utilization of the reinforcement across the wall implied in eqn. (4.2) depends on sufficiently high deformability of the reinforcing wires. Otherwise the extensive plastic deformation near the inner wall associated with relief of the sharp stress gradients will be prematurely interrupted by fracture which, once started, will propagate rather rapidly due to the severity of the stress-peaks in the elastic region. In fact pressure tests to failure of model cylinders of $6\frac{1}{2}$ in. outer diameter and $\frac{3}{4}$ in. wall-thickness reinforced with 9 to 12 per cent of relatively high-strength aluminum filaments showed that only about 45 to 50 per cent of the fully plastic carrying pressure estimated according to eqn. (4.2) could be attained. It seems likely that reinforcement of lower strength and higher ductility may result in a closer approach to the theoretical limiting pressure.

REFERENCES

[1] SOLIMAN, F. and SHINOZUKA, M., *Anistropic Heterogeneous Viscoelastic Cylinder with Eroding Inner Boundary*, Report No. 29, Contract Nonr 266(78), Columbia University, New York (1965).

[2] DE SAINT VENANT, B., *J. de Math. pures et appl. (Liouville)* **10**, 297 (1865).

[3] VOIGT, W., *Kristallphysik*, Teubner Verlag Leipzig, 617 (1928).

[4] HUBER, M., *Theory of Elasticity*, **2**, Warsaw, 203 (1954).

[5] OLSZAK, W., *Final Report, Second Congress Int. Assoc. Bridge and Struct. Eng.*, W. Ernst Berlin, 690 (1936).

[6] LECHNITSKI, S. G., *Theory of Elasticity of an Anisotropic Elastic Body*, Holden Day, San Francisco, 249 (1963).

[7] BIENIEK, M., SPILLERS, W. R. and FREUDENTHAL, A. M., *J. Am. Rocket Soc.*, **32**, 1269 (1962).

[8] OLSZAK, W. and URBANOWSKI, W., *Proc. IUTAM Symposium on Non-Homogeneity in Elasticity and Plasticity*, Warsaw, 1958, Pergamon Press, London, 259 (1959).

[9] HASHIN, Z. and ROSEN, B. W., *J. Appl. Mech.*, **31**, 223 (1964).

MECHANICS OF REINFORCED SOLID PROPELLANTS*

E. L. ALEXANDER and A. A. CAPUTO

Rocketdyne, Division of North American Aviation, Inc.
Canoga, Park, California

Abstract—By replacing powdered metal fuels with high-strength wire, the mechanical strength and modulus of solid propellants can be greatly increased. Progress in developing this technology is reported with emphasis on geometry of reinforcing patterns and experimental tests of reinforced propellant cylinders.

Techniques for measuring strain inside filament reinforced structures are presented in connection with the discussion of tests on filament reinforced structures. Evidence of high internal strain gradients in internally pressurized cylinders is presented.

1. INTRODUCTION

Solid propellants require some kind of support in a rocket motor which may be as simple as a steel motor case bonded to a cast propellant grain. On the other hand, the discussion which follows will bring out some of the structural advantages that may be gained by supporting solid propellant grains both externally with a motor case and internally with fine reinforcing wires. One of several possible versions of this concept is illustrated by Fig. 1. The combustion of the reinforcing wire has been covered by one of the authors in another paper [1].

WIRE REINFORCED PROPELLANT

NOZZLE

FILAMENT WOUND CASE

FIG. 1. Wire reinforced solid propellant motor.

485

Experience has shown that replacing the powdered metal in conventional solid propellants with an equal quantity of fine wire will greatly increase the strength and modulus of the propellant. This simple substitution results in the major change in propellant mechanical properties which is summarized in Table 1.

TABLE 1. TYPICAL MECHANICAL PROPERTIES OF CAST AND
WIRE REINFORCED PROPELLANTS

Cast propellants	Wire reinforced propellants
Tensile strength (psi)	Tensile strength (psi)
Composite 120–200	5000–10,000
Double base 150–1700	
Modulus 1000–3000	Modulus 1,000,000–5,000,000

Thus, without restricting choice of chemical propellant formulations (assuming use of a metallic ingredient), solid propellants can be changed to load bearing materials which can be treated in many respects as just another reinforced composite material. Usually, wire reinforced grains are thick wall structures with greater rigidity than one might expect on the basis of a low volume fraction of wire and a relatively low modulus matrix. The thickness of a typical reinforced grain is a consequence of a requirement to load the propellant in a motor as compactly as possible and need for specified burning time.

Since the propellant serves both as an energy source and structural member, design with respect to the structural function may have certain unconventional aspects. For example, the concept of weight penalties associated with alternate structural designs has no significance when the structure is also required to supply propulsion energy. It follows that even modest progress in a better understanding of the load-bearing capability of reinforced propellants is useful, and it is significant that such progress is being made. For example, experimental evidence indicates that the mechanical response of wire-reinforced propellants is essentially linear and not very time dependent. A typical stress–strain curve for a wire-reinforced propellant is shown in Fig. 2. The elastic response indicated in Fig. 2 was found to be repeatable for several load cycles. These experiments are discussed later in this paper. An attempt is made to compare cast propellant and reinforced propellant in Fig. 2. However, the two materials are obviously so different in physical characteristics that it is necessary to specify how the two types of propellants are to be used in order to develop significant comparisons.

Cast propellants have extremely nonlinear and time-dependent mechanical properties. In this respect, the conventional cast propellants are more difficult to deal with than wire-reinforced propellants. On the other hand, wire-reinforced propellants are very anisotropic so that the grain designer must provide for distributing structural loads so that they can be carried by the reinforcing wires. This may be easy or difficult to do depending on particular applications. In

general, the use of reinforcing wire provides some structural advantages even in complex loading situations where load distribution in the reinforcing wires has not yet been solved. Each step forward in this direction means that the designer can transfer more structural functions to the propellant and reduce the weight of other inert structures in the propulsion system.

In addition to potential advantages associated with the use of reinforced propellants as a pressure vessel, it has been established that reinforced grains are extremely rugged with respect to adverse service conditions. The ability to resist severe temperature cycling, vibration and impact is apparently an intrinsic property of wire-reinforced solid propellants.
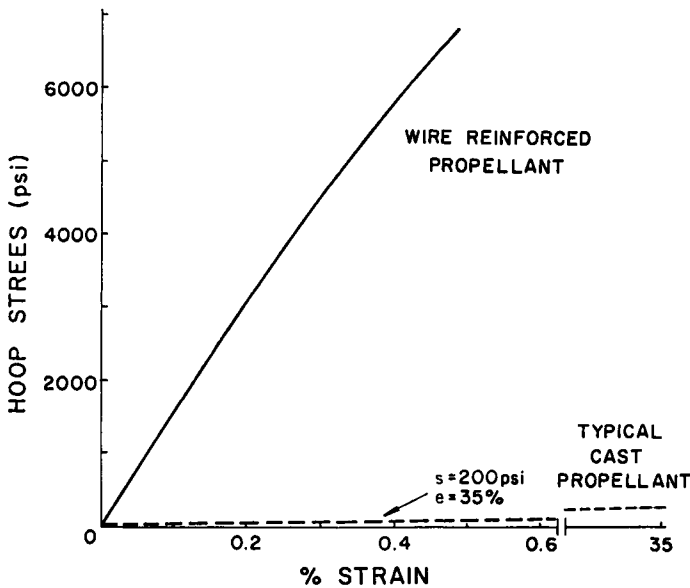
FIG. 2. Typical stress-strain curve for wire reinforced propellant.

Research on the structural properties of reinforced propellants has been in progress long enough to begin to provide useful knowledge of structural characteristics. Results of this research will be discussed along with some interesting techniques for investigating strain fields on the interior of filament reinforced structures. A thorough understanding of internal strain phenomena depends on quantitative measurements and adequate mathematical models. This information is becoming available and may have significance which is not limited to reinforced propellants. The new knowledge should be applicable to filament-wound vessels for high pressure, filament-reinforced structural panels, filament-wound structures for probing ocean depths and related structures designed to withstand an adverse environment.

2. CONFIGURATION OF REINFORCING WIRES

Rocketdyne has evaluated several methods of internally reinforcing solid propellants. Short lengths of metal staple and wire screens have advantages in specific applications. They may be used by themselves [2] or in various combinations with a wire wound-reinforced propellant shell. However, from the structural viewpoint, the logic of using oriented continuous reinforcing wires cannot be denied. By choosing a suitable winding pattern, nearly all of the reinforcing wires can be placed in directions where structural loads can be carried most efficiently. This concept has been applied very successfully to winding wire-reinforced propellant grains. There are differences between the reinforced propellant structure and glass reinforced composites that will be considered in the following discussion.
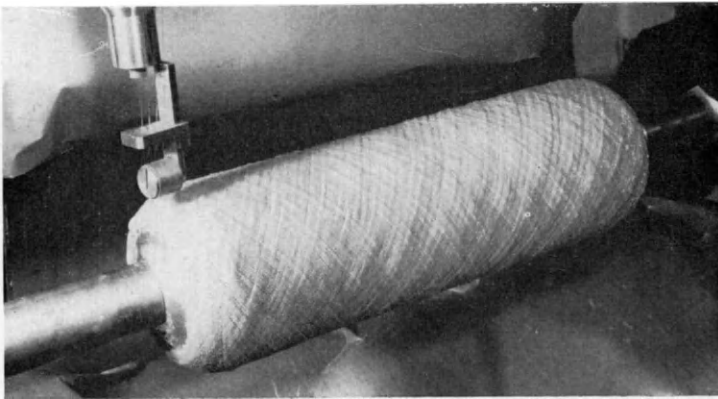
FIG. 3. Winding pattern produced by cam controlled winding machine.

The operation of winding a wire-reinforced propellant grain is shown in Fig. 3 as a basis for discussing winding patterns and structural test results. The winding pattern extends over the end dome which is an ellipse of revolution with the minor axis 0.61 times the major axis. The path traced by the reinforcing wires in the uncured propellant matrix is very close to geodesic both in the cylindrical portion and over the end dome. Propellant matrix is added as required during the winding process until the desired wall thickness is built up. The reinforced grain is cured in an oven using procedures employed with cast propellants.

The problems of fabricating reinforced propellants are actually less difficult than the problem of understanding how the structure will respond to mechanical loads. The structure is obviously anisotropic and is thick enough to require a three-dimensional analysis. We know of no existing mathematical solutions to this problem in its entirety but, at a practical level, useful solutions based on a combination of structural experiments and simple mathematical models are being investigated. The point was made previously that no performance penalties

are involved in using propellant to bear structural loads. It follows that performance advantages should be available to the degree that the propellant can be made to serve a dual role as energy source and structural member. More specifically, it may not be important that the propellant have maximum structural efficiency and, therefore, approximate solutions to design problems may be quite acceptable.

2.1. *Choice of Reinforcing Wire Patterns*

Several years ago the question was posed: What is the optimum pattern of reinforcing wire in a solid propellant pressure vessel? Until now the investigation that grew out of this question has been purely mathematical, but a corresponding series of experimental tests have been planned and will soon be in progress. The mathematical study of winding patterns has produced some results which merit discussion. These include the use of a large digital computer (IBM 7094) to generate winding curves on any surface of revolution. Geometric problems are encountered in generalizing the winding surface to fit the length, diameter, end contours and end openings that may be required in typical rocket motors. In simple terms it is not always possible to find a geodesic path that will cover the whole surface and will assure that the reinforcing elements will not slip while being wound into the propellant grain. The calculations therefore provide families of modified winding curves which deviate to a computed degree from the local geodesic in any particular region. For example, in order to cross a geodesic discontinuity between an end dome and cylindrical section, a winding curve might be specified with a deviation of 0.01 rad/in. compared to the local geodesic. It remains to be established experimentally that this deviation of 1 in. in 100 in. of reinforcing fiber path length would satisfy practical fabrication requirements.

The basic computing programs for generating filament winding curves lead to a series of subprograms which attempt to reduce several aspects of filament winding to a series of logical decisions. It was discovered in the course of this work that good filament-wound structures are nearly always the work of a highly skilled artisan. Although detailed calculations have been developed for some specific filament-wound configurations [3, 4, 5], it usually turns out that a skilled operator winds trial patterns on a machine to match the computed winding curves and that his experience enables him to adjust gear ratios, lever arms, fiber tension and spindle speeds to obtain a "good" pattern. The difference between a good pattern and a bad pattern of filaments which will not cover the mandrel evenly may depend on a slight adjustment of one of the machine settings. Rocketdyne experience indicates that good filament-wound pressure vessels merit respect as an artistic achievement and this situation would probably continue except for the influence of large capacity computers. In essence, a mapping problem must be solved in which points on a winding path are transferred along the filament tangent to a guide on the winding machine. The mathematical transformation then takes characteristics of the winding machine into consideration and ends with a cam contour or a code on tape which controls

the winding pattern. Although the calculations may not be difficult, the volume of mathematical manipulations necessary to define an accurate winding path is beyond the scope of hand calculations.

The objective of work on computer routines to replace decisions by a skilled operator is based on the need for utilizing these skills at a higher level. At present it is feasible to carry only a few alternate designs through preliminary experimental testing. If selection of gear ratios, checking of patterns, etc., can be done on the computer before starting experimental work the relative merits of many more possible configurations can be evaluated. More extensive use of the computer is expected to have less obvious advantages such as increasing the probability that new reinforcing configurations will be found and evaluated. A realistic appraisal of circumstances involved in creation of a new filament-wound product will reveal a large measure of conservatism on the part of the machine operator. There is a strong tendency to use methods that have worked in the past even when new process requirements do not quite fit.
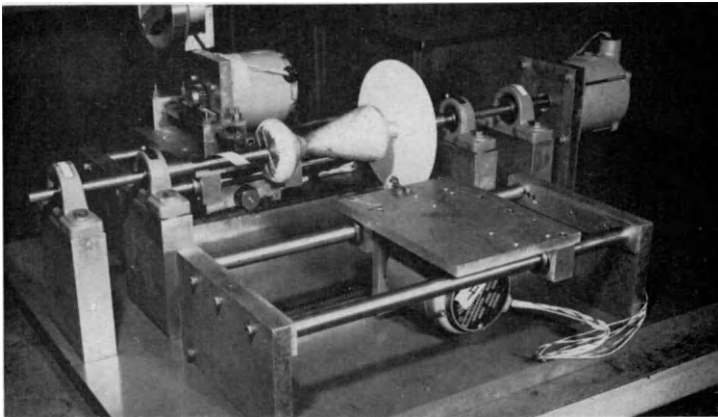
FIG. 4. Punched tape controlled winding machine.

In order to conduct a comprehensive research program on the relative merits of various patterns of reinforcing elements, it was necessary to have winding machines with versatility to match the generality of our computer programs. The Rocketdyne Research Department has designed and built two experimental winding machines using cam control for one machine and punched tape control for the other. In each case there are essentially no restrictions on the winding path except that it should be stable (non-slip) on the wound surface. Both the cams and the punched tape are produced by a computer subprogram which derives input information from the computed winding curve. Figure 4 shows the punched-tape-controlled winding machine and Fig. 5 shows the first course of a winding pattern for a rocket nozzle. In this particular case it was found that the computer program could generate a true geodesic winding path to cover the hourglass-shaped mandrel.

The structural merit of configurations of this type can be measured in part by calculating surface curvature along the path of the reinforcing elements. In practice this is achieved by computing rotation of a unit vector system per unit length of arc as it moves along the winding curve. This orthogonal unit vector system consists of the tangent to the winding curve, the unit normal vector directed away from the surface and the unit binormal vector which may be obtained as the vector cross product of the tangent and the normal. The rotation of the vector system about the binormal per unit length of curve is by definition equivalent to the surface curvature along the winding path. For internal pressure loads tension in a fiber oriented along the winding curve will be
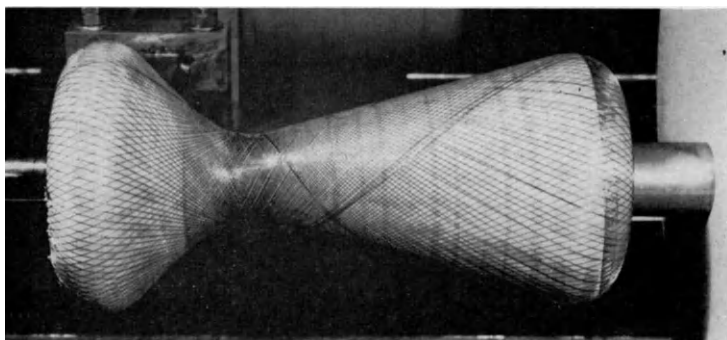
FIG. 5. Geodesic winding pattern for a rocket nozzle.

proportional to the surface curvature. Therefore, computed curvature values serve at least as a relative index of regions in a filament-wound structure which may fail first under pressure loading. It is true that the foregoing analysis presents an oversimplified picture of fiber stress but for complex surfaces of revolution such as the mandrel for rocket nozzles, knowledge of fiber curvature appears to be necessary as point of departure in structural analysis.

Both the surface curvature and the deviations from geodesic are computed as differential vector quantities by the IBM computer program. The deviation from a geodesic path is a vector rotation about the unit normal per unit path length. Both quantities are computed for as many as 1000 points along the winding curves following the lines of procedure found in Refs. [6] and [7].

2.2. Distribution of Reinforcing Filaments

The foregoing discussion has involved only geometry of single winding paths. Another part of the optimization problem is concerned with density and mechanical characteristics of the reinforcing elements. The number of reinforcing elements per unit surface area generally varies from one section of a winding pattern to another. This leads to ridges of piled up fibers at the ends of most filament-wound pressure vessels. In reinforced propellants where the concen-

tration of reinforcing wire is fixed by ballistic considerations, high fiber con-centrations at the ends are even less acceptable than in glass filament-reinforced pressure vessels. Mixed winding patterns are commonly used to "balance" fiber stress in longitudinal and circumferential directions in fiberglass pressure vessels. This relieves the problem of filaments piling up at the ends to a degree but is an unsatisfactory compromise in creating a laminar shear problem between dissimilar winding patterns.

Experimental work is being done by the Rocketdyne Research Department using related families of modified geodesic winding curves to obtain an even or controlled concentration of reinforcing fiber throughout the composite structure and at the same time to minimize the laminar shear problem between layers of different but related winding patterns. This work will also be extended to include varying the mechanical properties of the reinforcing elements layer by layer to meet changing strain requirements which vary with radius in thick wall rein-forced composite structures. Experimental evidence of this problem is discussed later.

3. EXPERIMENTAL EVALUATION
OF WIRE REINFORCED PROPELLANTS

In attempting to obtain information on the physical properties of wire reinforced propellants, small specimens were cut from reinforced grains and subjected to the usual tension and compression tests. In addition to these tests, rings of reinforced propellant were wound to simulate the NOL ring tests and shear tests were made in various directions relative to the reinforcing wires. The principal conclusion resulting from this early evaluation program was that conventional testing methods had been tried and the results were not very useful. Edge and end effects can usually be minimized in testing homogeneous materials, but the effects of cutting reinforcing wires modified the response of reinforced propellant specimens so drastically that test results became essentially meaning-less.

Attention was soon shifted to observing the response of cylinders of reinforced propellant. A logical starting point was the use of internal pressure to load the cylinders. Although the cylinder tests were better suited to the material, problems were still encountered:

1. The volume fraction of reinforcing elements is 10 to 20 per cent compared with about 70 per cent in glass filament-reinforced structures.

2. There is a great disparity between the modulus of the reinforcing elements (10×10^6 psi) and the matrix (about 3000 psi).

It is difficult to measure dimension changes on this mixture of stiff and rubber-like materials. For example, strain gage tabs gave poor readings because they were too rigid to follow strain in the specimens. However, the method of fabri-cating reinforced propellants suggested a way of obtaining strain information. By replacing one of the reinforcing wires with strain gage wire during the wind-

ing process, it appeared feasible to obtain strain information inside the reinforced propellant specimen in addition to more conventional surface strain measurements.

In practice the technique of placing strain gage wires in reinforced grains proved to be a difficult, delicate job. Initially a survival rate of two working gage wires out of 10 wound into the specimen was considered good. Technique in placing gage wires has improved with experience and we now feel that the information obtained has been well worth the effort. Results of some of the more interesting tests will be discussed.

3.1. Internal Strain Measurements during a Motor Firing

At the time techniques were first developed for placing internal strain gage wires, data were also required on the capacity for a long reinforced propellant cylinder to withstand hot combustion gas pressures at rates of loading comparable to ignition in rocket motors. This led to the unusual test set up shown in Fig. 6. A bare cylinder of wire-reinforced propellant was fitted with a nozzle
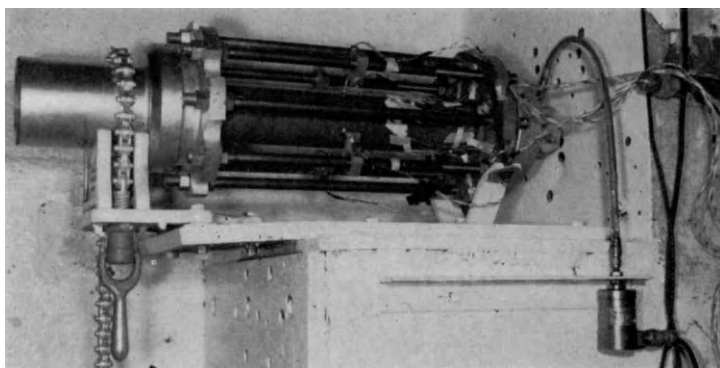
Fig. 6. Bare grain test assembly with strain gages and LVDT's

and head end closure. The test was intended to measure the hoop strength of the reinforced propellant under conditions similar to combustion in a rocket motor. It was intended that the shell of propellant should burst as combustion pressure increased and the wall became thinner.

The figure shows how the nozzle and head end closure were restrained with tie bolts so that a hoop burst would be obtained. The blocks of metal at the center of four tie bolts hold linear differential transformers which gave an oscillograph trace of the increase in outside diameter as combustion pressure increased. The paper tabs near the head end of the bare grain identify strain wire gage leads that were connected to different oscillograph channels. Internal pressure was measured and recorded by means of the pressure transducer shown connected to the head of the motor by the flexible metal tube.

Although this was the first test with internal strain gage wires, we were fortunate in having four gages still in working condition by the time the motor was mounted on the test stand. Moreover, these gage wires were at different locations through the one-inch thick wall of the cylindrical grain. We were therefore able to get an idea of strain gradient across the web of reinforced propellant.

Results of firing the reinforced propellant cylinder as a rocket motor are shown in Fig. 7. The cylinder burst after burning for about 0.07 sec. If this grain had been fired normally in a motor tube or had been designed to burn as a
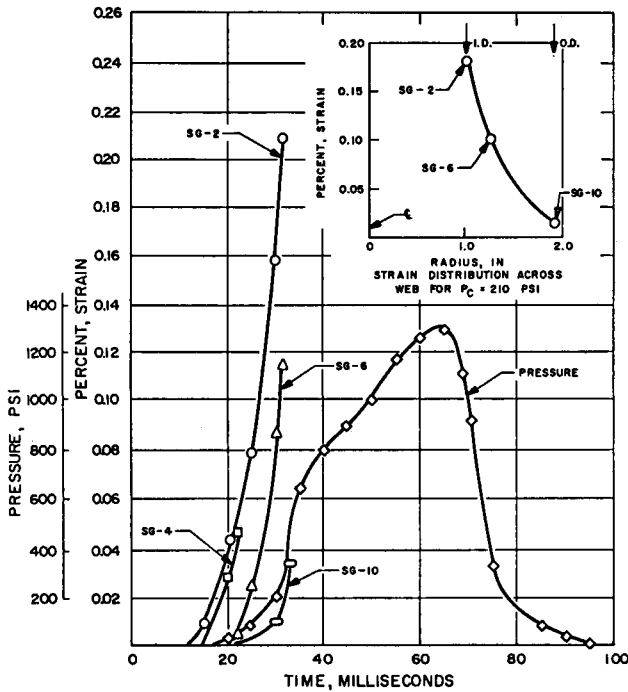
Fig. 7. Hoop strain during ignition of reinforced propellant.

caseless motor, it probably would have burned for about 2 sec. The corrected wall thickness at failure can be computed from ballistic data. However, the pressure trace shows clearly that the remaining thickness of reinforced propellant was capable of supporting combustion pressures up to 1300 psi. Apparently, there was about 10 msec time lag in the pressure readings assuming no time lag for the strain gage wires.

The strain gage corresponding to SG–4 in Fig. 7 was lost very early in the firing and the remaining three gages were lost about 15 msec later. It was unfortunate that the gages became inoperative so early in the test. We had hoped to see the progress of plastic deformation moving across the wall of propellant.

However, replotting strain at three positions versus radial distance in the insert graph in Fig. 7, a high strain gradient is quite evident. This was predicted by theoretical analysis of an orthotropic homogeneous model in Ref. [8].

The magnitude of strains in this and subsequent tests are small indicating the large increase in propellant modulus caused by the reinforcing wire.

3.2. *Internal Strain during a Hydrostatic Test*

The cylinder of reinforced propellant shown in Fig. 8 was burst under hydraulic pressure acting on an internal rubber bladder. Loading was confined to the circumferential mode by use of the test fixture shown. Hydraulic pressure
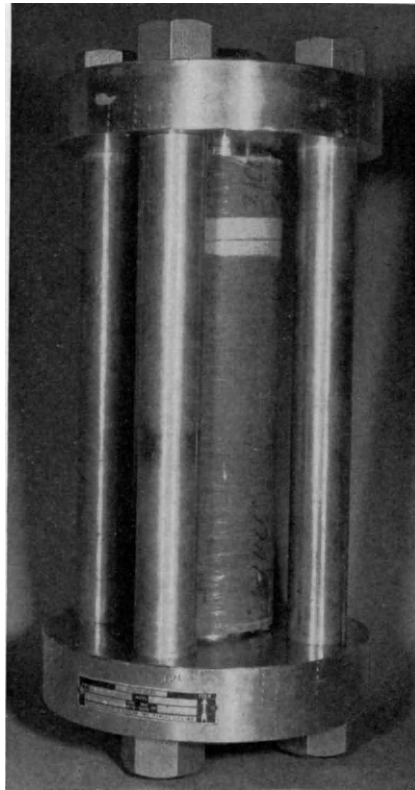
FIG. 8. Assembled Hoop Test apparatus.

was increased slowly (compared to the motor tests just described), and partial unloading was permitted at three successively higher pressures to obtain information on permanent deformation at intermediate loads.

Five strain gage wires were helically wound into this specimen, but only two (internal) gages at $2\frac{1}{2}$ and $2\frac{1}{4}$ in. diameter were operative at the time the test was made.

The quantity of data obtained from the hydrostatic burst test was very gratifying. Strain gage signals were obtained throughout the test until the test specimen burst. Instead of the brief strain signals covering only the ignition phase in the combustion tests, an opportunity existed, as shown in Fig. 9, to follow two strains at different radial positions through three load and unload cycles and, ultimately, to specimen rupture.

The most important aspect of the hydrostatic test data is that they support previous results showing low strain levels in the bare-grain motor firings. This test not only corroborates previous strain data; in addition, it provides new information indicating that the strain gradient follows pressure loading and unloading as predicted by theory in a linear manner until strains are a substantial fraction of limiting values at burst.
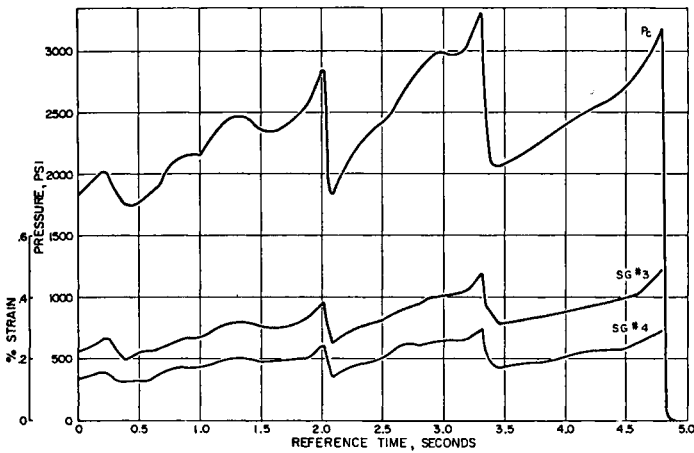
FIG. 9. Oscillograph trace of hydrostatic burst test.

The loading rate can be obtained from Fig. 9, where a maximum slope of 2400 psi/sec is found over a short interval and a more moderate rate of 1070 psi/sec is obtained as the average pressurization rate for the second load cycle. No time lag is discernible between strain gage signals either on pressurization or during the more rapid pressure-relaxation steps. Although the rate of pressurization is 20 to 100 times slower than ignition pressurization in the previous motor tests, the unloading rates are about as steep as the ignition transients; therefore, lack of phase difference or time lag between pressure and strain curves indicates that a viscoelastic model of response to loading may be confined to a lower frequency domain than that encountered in the ignition transient. In other words, the response of the specimen to abrupt loading is, in a practical sense, elastic. If this is substantiated by further experiments of this type, it will greatly simplify the work required to understand behavior of reinforced propellant structures.

The .difference between stress gradient and strain gradient should be emphasized here. As long as the structure is responding elastically, strain and stress gradients are approximately the same except for a multiplying factor. In the plastic response range, however, strain gradients can become quite large without a corresponding linear increase in the stress gradient. This depends upon the degree of nonlinearity of the stress-strain curve for the reinforcing fibers. In practical applications, the inside portion of a reinforced propellant combustion chamber is likely to be in the post-yield condition while the outer portions and the case may be producing an elastic response. The problem is further complicated by combustion of the inner portion of the wall and a variable pressure boundary condition. The mathematical complexity is such that internal strain-gage measurements are expected to be used to a considerable degree in developing a response model that can be used for grain design.
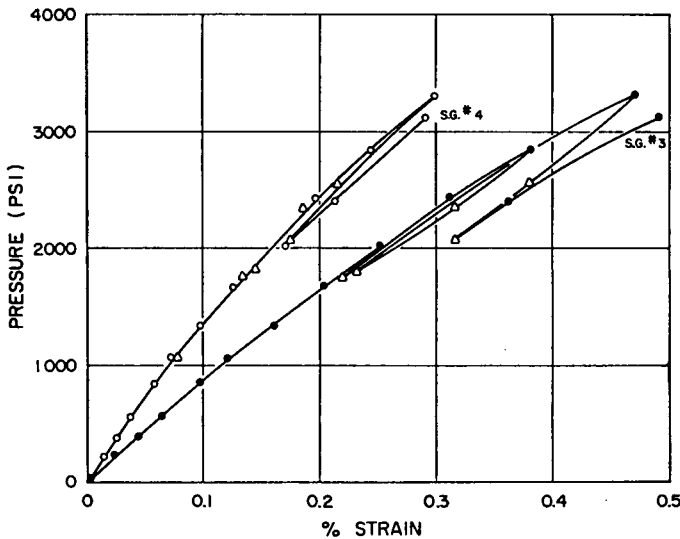
FIG. 10. Strain versus hydrostatic pressure

The curves in Fig. 9 are replotted in Fig. 10 to show more clearly the relation between the two strain-gage signals and internal pressure. SG–3 is located only $\frac{1}{8}$ in. inside SG–4, yet very substantial differences in strain are clearly evident over this small increment of wall thickness. It is noteworthy that through the first two load cycles the loading and unloading curves are nearly identical Displacement of the inner strain-gage curve (SG–3) as the final load cycle is initiated may indicate some damage to the specimen as maximum internal pressure was applied on the second cycle. Some of the reinforcing wires might have been expected to break at the second peak, allowing a slight expansion of the specimen. It is interesting that the slope of the strain–pressure curve is still about the same as loading is resumed for the third and last cycle. This

32

indicates that about the same number of reinforcing wires were resisting expansion as during the previous cycle.

This may also be interpreted to mean that some wires that were not taut and fully loaded in previous cycles assumed the load released by broken filaments, resulting in displacement but no change in slope of the strain-pressure curve.

The preceding discussion involves only comparisons between relative values of strain signals and pressures as opposed to the absolute magnitude of the strains involved. The maximum observed strain was only 0.5 per cent at rupture, which is in agreement with the general level of strain values observed in the motor firings. Although relative values of strain yield considerable information, it is important to establish the accuracy of the absolute values for strain to gain insight into compatibility between propellant grains and a fiberglass motor case or to determine how high- and low-elongation reinforcing wires may be used to obtain more efficient structures.

3.3. *Internal Strain Measured by Radiographic Technique*

The use of X-ray opaque wires to determine displacement under load of reinforcing filaments was suggested by radiographs of some reinforced grains prior to a motor test. The aluminum reinforcing wire cannot be distinguished from the propellant matrix, but these particular grains had strain gage wires wound inside the cylinder and the 5-mil wires were sharply defined on the X-ray film. These observations led to fabricating several reinforced grains with 5-mil tungsten wire wound in parallel with the other wires at intervals as the web thickness increased during the winding process.

Two arrangements were set up to observe the displacement of the tungsten wires by a double exposure with the cylinder unloaded and pressurized. In one case a tangent view was photographed and the other arrangement involved moving the X-ray source closer to accent parallax resulting from displacement of the tungsten filaments. Although the first arrangement is much less complex with respect to geometric interpretation of the photographs, the parallax method yields sharper images. Figure 11 shows a double exposure made by the parallax method. Preliminary measurements have been plotted to show a good correlation between strain at various points and loading, but interpretation of the photographs and reduction of displacements to strain values is very tedious.

This appears to be an ideal application for our Benson–Lerner curve reader which automatically converts position of a point to punch card coordinates. The technique could be refined by adding fiducial points such as drops of solder or kinks to the tungsten wire in order to follow motion of a network of well-defined points. The data conversion could then be accomplished with a computer program which utilizes the dimensional relations of the test set up and projective geometry to arrive at a strain contour map for the structure. The advantage of the radiographic displacement technique is that local strains around discontinuities can be examined while the strain gage wires give average strain over a region. The disadvantage of this method is that it is extremely

tedious and extreme accuracy is necessary in measuring small distances on the photographic plate.
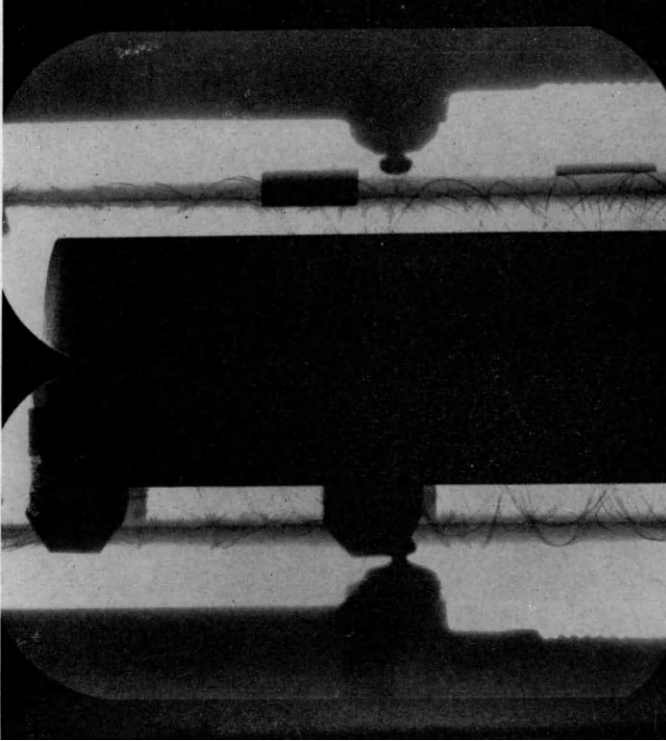
Fig. 11. Wire displacements on double exposure X-rays.

3.4. *Photoelastic Strain Measurements in Filament-Reinforced Structures*

The study of reinforcing fibers in a photoelastic matrix has been in progress for more than a year. This technique shows great promise as a very powerful method for investigating problems of stress transfer between the matrix and reinforcing elements.

Figure 12 illustrates the insight provided by the photoelastic technique into complex stress situations. The specimen shown was intended to provide a simple model of a region in a helical wound structure where reinforcing elements cross over each other. The strain field in Fig. 12 was more complex than expected. Moreover, the observed pattern was not induced by external loads but is solely the result of cure shrinkage of the birefringent plastic matrix. Detailed examination of the 5-mil reinforcing wires under magnification reveals that they have buckled under compressive force and this has produced the periodic strain field extending many wire diameters into the surrounding matrix. This specimen served as the starting point for a mathematical model which proved useful to describe the wavelength of buckled wire in terms of axial force, wire

diameter, wire modulus and modulus of the surrounding matrix. One of the interesting features of the crossed wire pattern is the in-phase enhancement of the strain field at the cross over point. This problem is discussed in detail in Ref. [9].
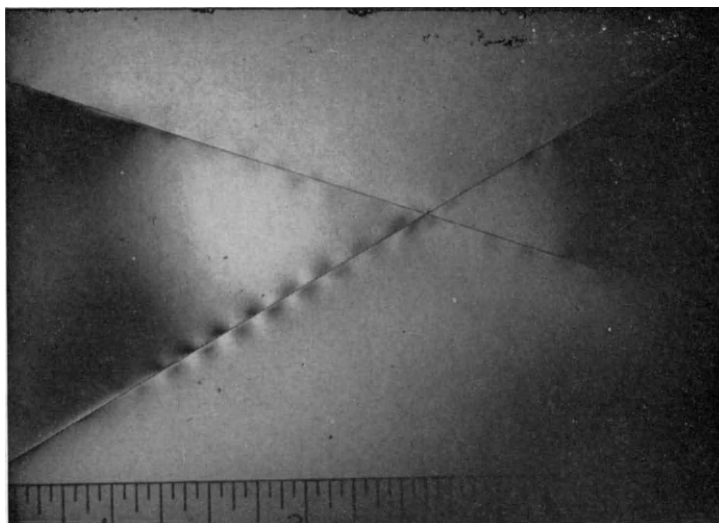
FIG. 12. Strain field around crossed reinforcing wires.

Since modulus of the reinforcing element appeared to have a strong influence on the strain field in the surrounding matrix, a series of 5-mil reinforcing wires were selected to cover a wide modulus range. The specimen in Fig. 13 shows various strain patterns induced in a single birefringent matrix by reinforcing elements ranging from low modulus aluminum wire (10×10^6 psi) at the top of Fig. 13, Constantan $E = 28 \times 10^6$, tungsten $E = 55 \times 10^6$, steel $E = 29 \times 10^6$, to high modulus beryllium wire (46×10^6 psi). The strains were induced only by cure shrinkage of the matrix.

The broad features of the strain patterns in Fig. 13 agree with analysis derived from the mathematical model. The lower modulus wires buckle more easily and exhibit a shorter wavelength in the strain pattern. At the other extreme, the beryllium wire may not have buckled at all. The region at the left end of the wire appears to be an unbonded zone. When the plate is flexed, the stresses do not appear to be transferred to the wire in this region.

4. CONCLUSIONS

An investigation of structural properties of wire-reinforced solid propellants has led to the following concepts and general areas of new knowledge:

1. The mechanical properties of solid propellants can be increased to a level where the propellant can sustain autogenous combustion pressure by simply replacing the powdered metallic ingredient with fine reinforcing wire of the same material.
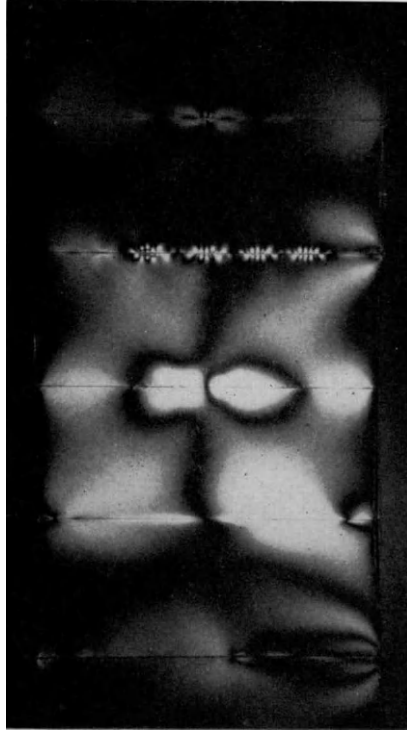
FIG. 13. Strain patterns due to varying modulus of reinforcing elements.

2. The usual methods for evaluating structural characteristics of homogeneous materials are not generally suited to wire-reinforced propellants. Internally pressurized cylinders and dome end cylindrical test specimens have been used to obtain most of the existing information on mechanical properties of reinforced propellants.
3. A new approach to optimize winding patterns of reinforcing elements in filament wound pressure vessels is being investigated. Preliminary results of this research indicate that additional degrees of freedom may be made available to the pressure vessel designer and that it may be possible to set up a quantitative measure of regions in a pressure vessel which present special design problems.
4. Three techniques for measuring internal strains in filament-reinforced structures are expected to be very useful tools for investigating this class of

materials. The three methods using embedded strain wire, radiography and a birefringent matrix supplement each other in the type of information obtained and are not mutually exclusive.

REFERENCES

[1] ALEXANDER, E. L. et al., "Grain designs based on new propellant combustion concepts", 19th Interagency Solid Propulsion Meeting, July (1963).
[2] DEFRIES, M. G. and RICE, A. V., "Internal reinforcement of solid propellant rocket grains", Proceedings ARS Solid Propellant Rocket Conference, Philadelphia, Pa., 2751–2763 (1963).
[3] OUTWATER, J. O., "Filament wound internal pressure vessels", Modern Plastics, (1963).
[4] SCHUERCH, H. U., U.S. Patent 3,121,451, "Isotensoid structure", Feb. 18, 1964.
[5] HARTUNG, R. F., "Membrane analysis of filament wound structures", AIAA Launch and Space Vehicle Shell Structures Conference (1963).
[6] WEATHERBURN, C. E., Differential Geometry, Vol. 1, Cambridge University Press (1961).
[7] WILLS, A. P., Vector and Tensor Analysis, Prentice-Hall, Inc., p. 66 (1949).
[8] BIENIEK, M., SPILLERS, W. R. and FREUDENTHAL, A. M., "Nonhomogeneous thick-walled cylinder under internal pressure", ARS Journal (1962).
[9] GOLDBERG, R. S. and CHU, H. N., "Fiber mechanics of reinforced structures", Bulletin of the 3rd Meeting, Work Group on Mechanical Behavior, Volume I, CPIA (1964).

ON MECHANICAL PROPERTIES OF UNFILLED AND FILLED ELASTOMERS

F. R. SCHWARZL

In collaboration with H. W. BREE, C. J. NEDERVEEN,
L. C. E. STRUIK and C. W. VAN DER WAL

Central Laboratory T.N.O., Delft, Holland

Abstract—The mechanical properties of composite solid propellants depend essentially on the type of binder that is chosen. The viscoelastic behaviour of pure binders is discussed by demonstrating the variation of shear modulus, bulk modulus, Young's modulus, Poisson's ratio and thermal expansion with time, frequency and temperature for unfilled amorphous polymers. The strong frequency and time dependence of the shear properties in the glass–rubber transition region is shown by measurements over many decades in frequency at various temperatures. The validity of the time–temperature shift principle is discussed.

The relationship between filler characteristics and mechanical properties of inert filled composite materials is treated in detail. At small deformations, the mechanical behaviour of composite materials is independent of filler size and is simply related to filler content. This relationship is discussed in the light of various existing theories for the description of composite materials. A theory due to Van der Poel is found to be most satisfactory. At high filler contents with multimodal size distributions, deviations from this theory are found.

The ultimate properties of composite materials are very sensitive to the size of filler. This is demonstrated for two examples: stress–strain diagrams and tensile creep under high stresses. The relationship between strength, dewetting and creep at room temperature is elucidated.

1. INTRODUCTION

In the design of rocket motors, great importance is attached to the mechanical behaviour of solid propellant grains. This is due to the fact that the presence or occurrence of cracks in the propellant during the ignition stage may lead to irregularities in the burning process and to malfunction of the rocket motor. Stress cracking in the propellant may occur either during the storage period, as a result of shrinkage or of thermal stresses, or during the combustion period due to the action of the combustion pressure or that of the acceleration forces.

For the proper understanding of the mechanical behaviour of composite solid propellants, detailed knowledge of the properties of highly filled elastomers is essential. Composite propellants consist of a soft polymeric binder filled with a high amount of hard inorganic oxidizer. As an example, one could think of polyurethane rubber filled with 75 to 80 per cent by volume of ammonium perchlorate.

Some of the mechanical properties of such a system are already fixed by the choice of the binder, e.g. the softening temperature. A wider class of mechanical

properties may be simulated by preparation of an inert model system, consisting of the same type of binder, filled with an analogous amount of a hard, but inert filler. Finally, some special features of live propellants are due to the interaction between oxidizer and binder; these are not likely to be simulated by any model system.

We will attempt to survey the relationship between filler structure and mechanical properties for highly loaded elastomers and proceed in the following order. First, the mechanical properties of unfilled polymers used as binders will be discussed briefly. Secondly, mechanical properties of filled elastomers at small deformations will then be treated. Finally, mechanical properties of filled elastomers at large deformations will be shown to be intimately related to the interaction between binder and filler.

2. THE MECHANICAL PROPERTIES OF UNFILLED RUBBERS

The mechanical properties of unfilled polymers in the region of small deformations may be characterized rather simply. This is due to the validity of the superposition principle of stresses and strains for those materials [1, 2]. Restricting ourselves to amorphous non-oriented polymers, it may be stated that the knowledge of two characteristic functions is sufficient to characterize the mechanical behaviour at small deformations completely. These functions are generalizations of the shear modulus, G, and the bulk modulus, K, well-known from the theory of elasticity. For polymers these functions are not only dependent on the temperature, T, but also on the characteristic time of the experiment. The concept "characteristic time" either relates to the time elapsed since the start of a relaxation or creep experiment, or to the frequency of a vibration experiment.

The behaviour of an elastomer used for the preparation of a composite propellant, is illustrated in Fig. 1. The variation of different characteristic functions with temperature at a fixed time of $1/2\pi$ sec (corrresponding to a frequency of 1 Hz) is shown for an unfilled polyurethane rubber.

Data for the shear modulus have been determined directly by means of the torsional pendulum [3]. Data concerning the bulk modulus were determined by means of a compressional creep technique, which yielded the bulk modulus at a characteristic time of 4 min [4]. From these data, the bulk modulus at 1 Hz was derived by the time–temperature shift procedure to be discussed below. From the experimental data for shear moduli and bulk moduli, the other quantities were calculated by means of the classical formulae:

$$E = \left\{ \frac{1}{3G} + \frac{1}{9K} \right\}^{-1} \tag{1}$$

and

$$1 - 2\mu = \frac{E}{3K} = \frac{3G}{G + 3K} \tag{2}$$
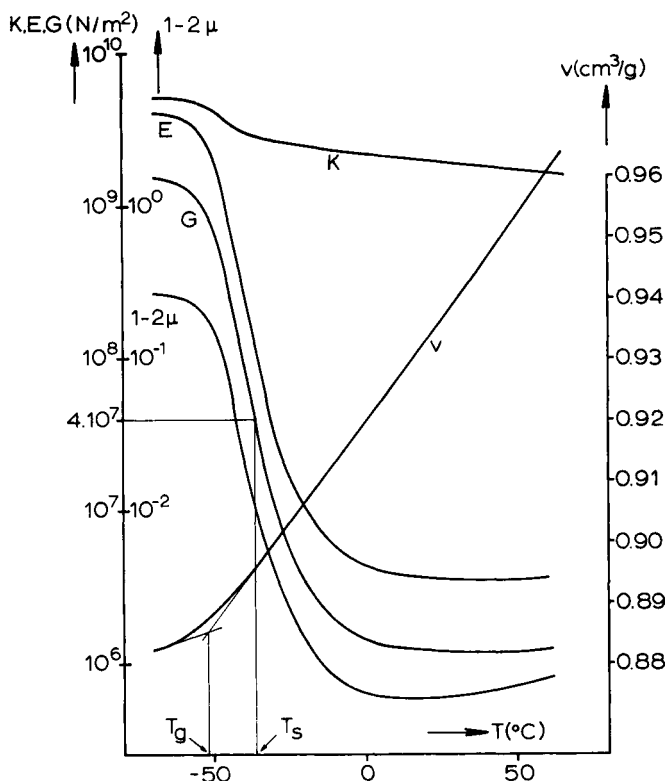
FIG. 1. Characteristic functions vs. temperature for a polyurethane rubber prepared from a linear (polypropylene ether) glycol with toluene diisocyanate and trimethylol propane. Shown are the shear modulus, G, the bulk modulus, K, Young's modulus, E, in N/m^2 and the dimensionless quantity $(1-2\mu)$, where μ is Poisson's ratio. All these functions relate to a characteristic time of $1/2\pi$ sec (a characteristic frequency of 1 Hz). Further, shown is the specific volume, v, in cm^3/g, determined from measurements with a cooling speed of $0.3°C/min$. The definitions of the glass transition temperature, T_g, and the softening temperature in shear, T_s, are illustrated.

A steep transition is seen to occur in the shear modulus, which drops from values of the order of 10^9 N/m^2 to values of the order of 10^6 N/m^2 within a temperature interval of $40°C$.* The midpoint of this transition in a logarithmic modulus scale is situated at about $-38°C$ at 1 Hz. This temperature is called the softening temperature, T_s, of the polymer. At temperatures well below T_s, the material is in the glassy state; at temperatures well above T_s, the material is in the rubbery state; correspondingly, the transition is called the glass–rubber transition of the polymer. The situation of the glass–rubber transition is determined chiefly by the chemical nature of the rubber in question. Clearly, the value of temperature T_s is one of the most important features of a polymeric material for practical purposes.

---

* Throughout this publication, Giorgi units are used. Consequently, stresses and moduli are measured in N(ewton)/m². 10^5 $N/m^2 \approx 1$ $kgf/cm^2 \approx 10^6$ $dyn/cm^2 \approx 14.5$ psi.

The bulk modulus also shows a softening region corresponding with the glass–rubber transition, which is connected with a decrease to about one half of its value in the glassy state. The transition in bulk modulus is also less pronounced than the transition in shear modulus for another reason. Whilst the shear modulus shows an approximately temperature-independent level in the rubbery state, the bulk modulus continues to decrease with temperature there.

The variation of Young's modulus, E, is very similar to that of the shear modulus; from the onset of the transition region, we have with excellent approximation

$$E \approx 3G \tag{3}$$

Poisson's ratio itself is not shown in the figure; instead, the quantity calculated is $(1 - 2\mu)$ which is more important for the calculation of stress distributions in propellant grains [5]. This quantity determines whether a material is to be considered as incompressible or not, depending on whether $(1 - 2\mu)$ is small compared to unity or not.

The specific volume vs. temperature curve shows two regions in which it may be approximated by straight lines. These lines intersect at a temperature, which is defined as the glass transition temperature, T_g. The glass transition temperature is seen to be about 15°C lower than the softening temperature in shear at 1 Hz. Of course, both phenomena reflect the same molecular process, namely the onset of the configurational movement of the long chain molecules of the polymer. The thermal expansion coefficient is about three times larger in the rubbery region of the polymer, than it is in the glassy region.

Both the softening temperature in shear (or bulk modulus) and the glass transition temperature depend on the characteristic time of the experiment. The softening region in shear is shifted to higher temperatures with increase of the frequency of the experiment (with decrease of the characteristic time of the experiment). The glass transition temperature is shifted to higher temperatures with an increase of the speed of cooling.

The strong time-dependence of the mechanical properties in the glass-rubber transition region is illustrated in Fig. 2, where the shear modulus for the same rubber is plotted as a function of characteristic frequency (or time) in a double logarithmic diagram. In the region of steepest slope, shear moduli are seen to decrease one decade in value with two decades change in time or frequency. Similarly, the strong temperature dependence may be noticed. A change of 10°C in temperature corresponds to a parallel shift of the shear modulus–time curve over three decades in logarithmic time scale.

The phenomenon of time–temperature shift of the shear modulus in the glass–rubber transition region has been well established for a large number of polymers [6, 7]. The magnitude of this shift is described by the W.L.F.-equation*:

$$\log a\,(T, T_g) = -\frac{c_1\,(T - T_g)}{c_2 + (T - T_g)} \tag{4}$$
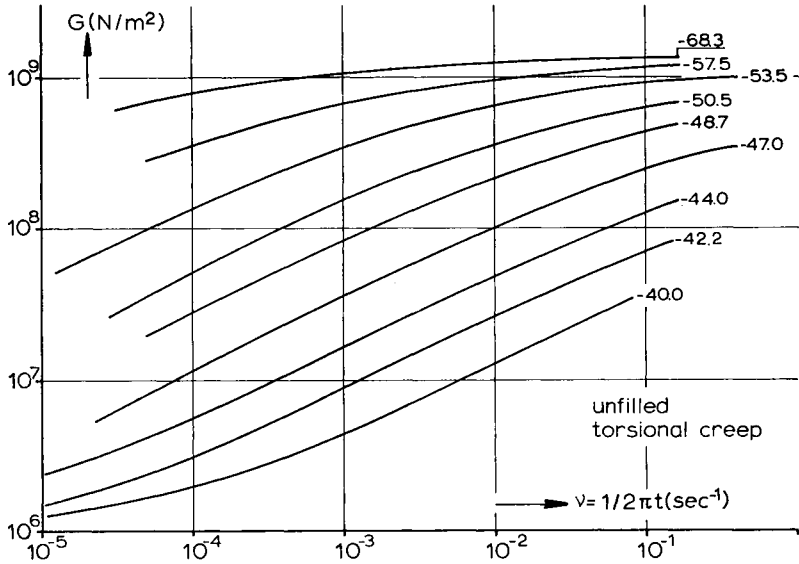
FIG. 2. Dependence of shear modulus on characteristic time at different temperatures in the glass–rubber transition region for an unfilled polyurethane rubber. Shear moduli have been calculated from torsional creep measurements. Temperatures as indicated in °C; the frequency was calculated according to the formula $\nu = 1/2\pi t$, t being the time elapsed in the creep measurement.

where $\log a$ represents the shift in the logarithmic time scale induced by a change in temperature from T_g to T. Furthermore, c_1 and c_2 represent universal constants which are independent of the nature of the polymer, and T_g is taken to be the glass transition temperature of this polymer. These universal values are quoted as [6, 8]:

$$c_1 = 17.44 \qquad c_2 = 51.6°C \tag{5}$$

These statements were formulated for the temperature region

$$T_g < T < (T_g + 100)$$

The data of Fig. 2 can be reduced to a master curve by a time–temperature shift function, which is shown in Fig. 3. This shift function was constructed by use of the results of torsional creep measurements (shown in Fig. 2) and the results of torsional pendulum measurements (not shown here). Function τ of Fig. 3 represents the location of the midpoint of the glass–rubber transition in logarithmic scale (where the shear modulus just passes the value of 4×10^7 N/m²), as a function of temperature; $\log a$ (T, T_s) represents the shift function, counted from the highest temperature investigated, namely $T_s = -24°C$. Also shown is the cubical coefficient of thermal expansion of the same material defined as

$$a = \frac{1}{v}\frac{dv}{dT}, \tag{6}$$

and the location of the glass transition temperature, T_g.
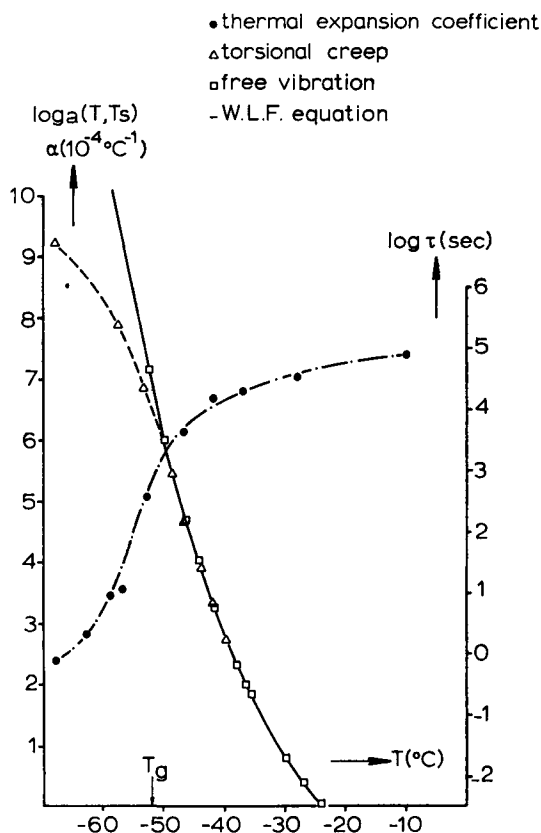
FIG. 3. The position of the glass–rubber transition in the time-temperature plane for an unfilled polyurethane rubber. Shown are the location of the midpoint of the glass–rubber transition in logarithmic scale, τ, the time–temperature shift function, log $a(T,T_s)$, and the W.L.F.-equation with parameter values given in eqn. (7); also shown is the thermal expansion coefficient, a, as function of temperature.

The high temperature part of the shift function is seen to be well described by a W.L.F.-equation with the following parameters:

$$\log a\,(T,\,T_s) = -\,\frac{d_1\,(T - T_s)}{d_2 + (T - T_s)} \tag{7}$$

$$T_s = -\,24°C \qquad d_1 = 6.90 \qquad d_2 = 56.2°C$$

Equation (7) can be transformed [2] into eqn. (4) with the following values for the parameters

$$T_g = -\,52°C \qquad c_1 = 13.8 \qquad c_2 = +\,28°C \tag{8}$$

which do not agree with the universal values, as quoted in (5)*.

---

* It should be mentioned that the claim of the validity of the universal W.L.F-equation (eqns. (4) and (5)) is connected with a temperature independent thermal expansion coefficient. From Fig. 3 it is seen that also in the high temperature part a constant value in a has not yet been reached; this may well be the reason for the discrepancy in c-values.

At temperatures near the glass transition temperature, the W.L.F.-equation fails in describing the shift function. This is in complete agreement with the theoretical derivations of the shift function from the free volume concept. The deviations of the shift function from the W.L.F. form occur in the temperature region where the thermal expansion coefficient decreases strongly with temperature.

The strong time-dependence of the moduli is a feature which is restricted to the glass–rubber transition region. In Fig. 4 we demonstrate the absence of any
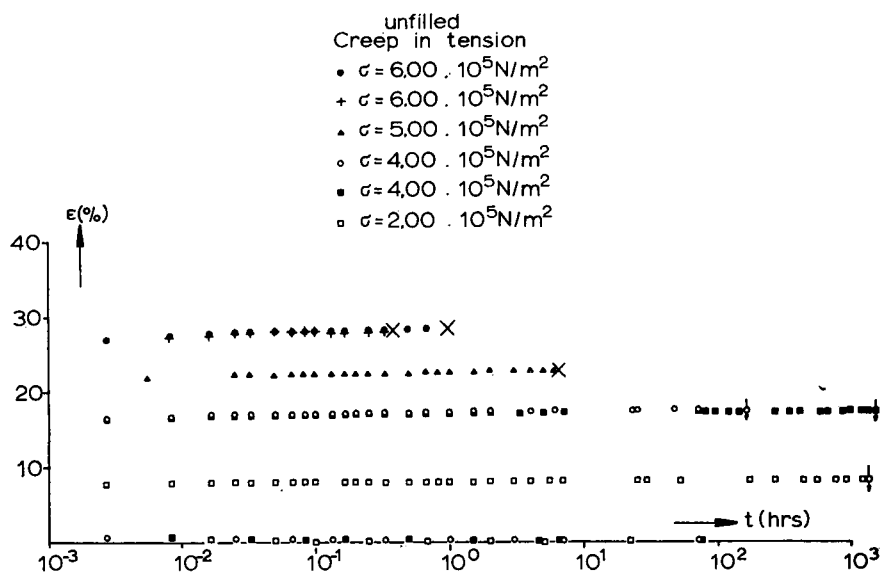
FIG. 4. Tensile creep ϵ as function of time, t, under various constant stresses at 20°C for an unfilled polyurethane rubber. Crosses indicate the occurrence of rupture, arrows indicate unloading and the beginning of a recovery experiment. Points of the recovery experiments are indicated near the abscissa.

appreciable time-dependence of the shear modulus of the same rubber in the rubbery region. This figure shows the results of tensile creep measurements at room temperature under various stresses. The unfilled rubber does not show any appreciable creep, even at stress levels which are high enough to yield rupture within short time. After loading with high stresses, there is still complete and instantaneous recovery of strain.

Before turning to the behaviour of filled materials, a short remark should be made on the mechanical behaviour of unfilled amorphous polymers at large deformations. Not very much is known at present of the ultimate behaviour of polymers in the glass–rubber transition region. However, for polymer behaviour in the rubbery region, important progress has been made recently by Smith [9] and Landel [8].

It was demonstrated that the rupture behaviour of properly crosslinked

amorphous rubbers* at temperatures well above their glass transition tempera-
ture may be described by the "failure envelope". This is the time and tempera-
ture independent locus of all failure points (σ_b, ϵ_b) in tension (σ_b = conventional
tensile stress at rupture, ϵ_b = tensile strain at rupture). An example of a failure
envelope for a butyl rubber, taken from the work by Smith [9], is shown in
Fig. 5.
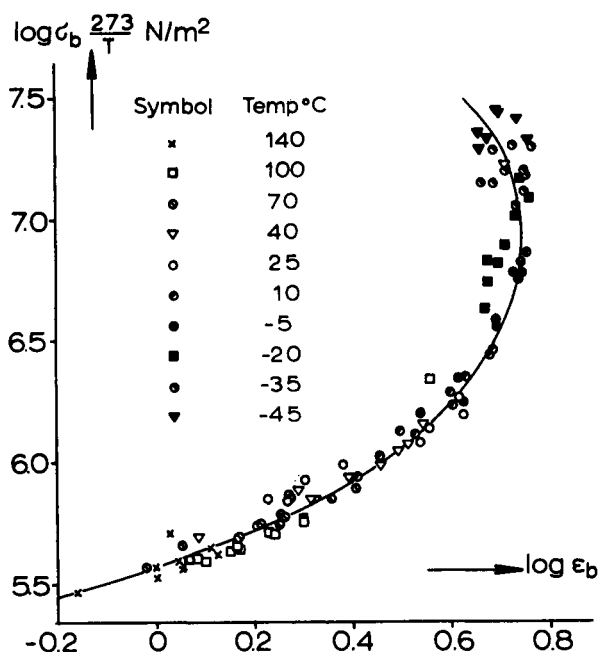
FIG. 5. Failure envelope for a resin cured butyl rubber taken from [9]. Conventional stress
at rupture (σ_b) against strain at rupture (ϵ_b) for tensile tests under different constant
rates of strain and at different temperatures as indicated.

Data obtained at different rates of strain and at different temperatures all
superimpose to lie on one single curve. Furthermore, a change in temperature
is equivalent to a change in strain rate. This equivalence is described by the
same equation which governs the time–temperature shift of the softening region
in small deformations, the W.L.F.-equation (4). A decrease in temperature or
an increase in the rate of strain moves the rupture point counter-clockwise
on the failure envelope. The maximum of breaking strain is reached at a tem-
perature of −20°C, which is about 55°C higher than the glass transition tempera-
ture of this polymer†.

---

* Not only should the rubber be amorphous in the undeformed state, but also no crystal-
should occur in stretching.

† The glass transition temperature of the polymer was not quoted by Smith. From its
chemical structure, the glass transition temperature was estimated to lie around − 75°C.

3. THE MECHANICAL PROPERTIES
OF FILLED ELASTOMERS AT SMALL DEFORMATIONS

3.1. *Dependence of Glass Transition Temperature on Filler Characteristics*

The mechanical behaviour of filled elastomers is still dominated by the viscoelastic properties of the binder, even in cases where the filler content is as high as 70 to 75 per cent by volume. This rather unexpected fact makes it possible to describe the viscoelastic properties of highly filled materials by the same means as the properties of the unfilled binders, and to understand these properties, at least qualitatively, on the basis of polymer physics. It further gives the possibility to simulate the mechanical properties of propellants by inert composite materials.

The most important characteristic of an amorphous high polymer is its glass transition temperature, T_g. For composite materials and composite propellants, the existence of a glass transition temperature was established together with the existence of softening regions in shear moduli and bulk moduli.

The problem, however, whether the glass transition temperature depends on the nature, content and size of the filler material, is not yet completely solved. In Fig. 6, we present divergent results on that question. In the upper part of Fig. 6 are shown results obtained by Landel and Smith [10], due to which the glass transition temperature should increase linearly with filler content (10°C for each 40 per cent by volume). This is not only claimed for propellants, but also for inert model systems, containing glass beads. According to investigations at our own laboratory on polyurethane–sodium chloride composites, as shown in the lower part of Fig. 6, the glass transition temperature should be independent of content and size of filler in the ranges between 1 μm and 500 μm and between 0 and 70 per cent by volume. Note the difference in scale of the temperature axis in the upper and lower parts of Fig. 6. As far as we can see, it is feasible that T_g will depend on filler content in all cases, where the filler interferes chemically with the crosslinking reaction of the binder. This may be the case with some propellants, but it is not expected to be so for glass bead composites.

3.2. *Dependence of Shear Moduli on Filler Characteristics*

Figure 7 illustrates the variation of shear moduli with temperature for polyurethane rubbers filled with increasing amounts of sodium chloride crystals. The size of the filler used for the materials containing less than 50 per cent by volume, was between 125–150 μm, but similar results have been obtained for filler sizes between 30 μm and 500 μm. In this range, the variation of the modulus vs. temperature does not depend on the size of the filler. For the preparation of the materials with higher filler contents (60 and 70 per cent by volume), bimodal mixtures of fractions had to be used.

All samples show a softening temperature, T_s, where the shear modulus drops over more than two orders of magnitude, and where the damping passes through a maximum. At temperatures below T_s, the materials are in the glassy
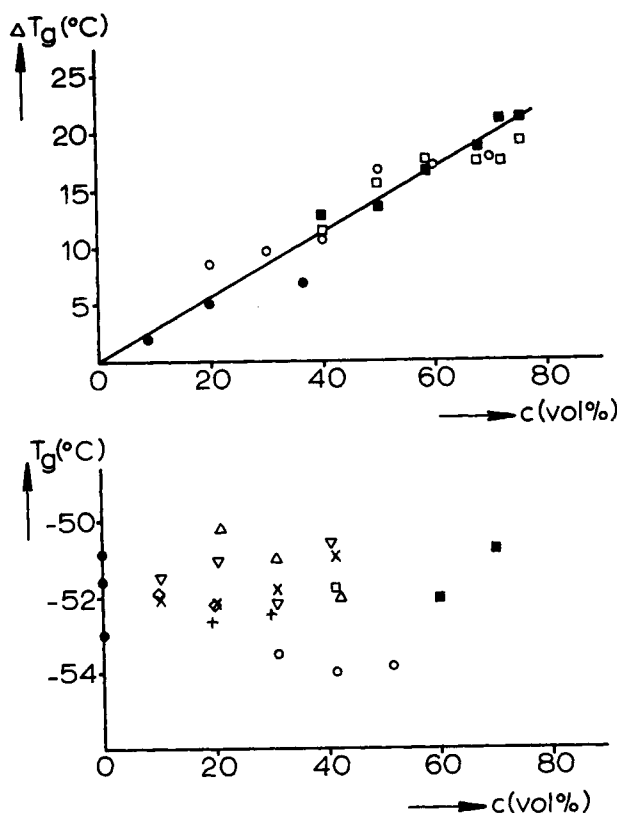
FIG. 6. *Upper part*: increase in glass transition temperatures, ΔT_g, produced by fillers as function of filler content, c, for polyurethane–glass beads ○, polyisobutylene–glass beads ● and two types of propellant □, ■ after Landel and Smith [10].
Lower part: glass transition temperature, T_g, as function of filler content, c, for polyure-thane–sodium chloride composites for different filler sizes: ● unfilled, ○ 300–480 μm, △ 210–300 μm, × 90–105 μm, □ 50–60 μm, ▽ 33–40 μm, + 8–20 μm, ◇ 1–5 μm, ■ bimodally size distribution (210–300 μm; 33–40 μm); Schwarzl *et al.* (unpublished). In both cases, glass transition temperatures were obtained from measurements of the linear thermal expansion coefficient, using a rate of cooling of 0.3°C/min or less.

state and show shear moduli between 10^9 and 10^{10} N/m^2; at temperatures above T_s, the materials are in the rubbery state and show shear moduli between 10^6 and 10^8 N/m^2. The position of the softening temperature only slightly depends on the amount of filler or on the size of filler fractions. The shift of T_s due to an increase of filler content from 0 to 70 per cent does not seem to be larger than 6°C; the shift of T_s due to a change in filler size from 30 to 500 μm does not exceed 6°C.

At first sight, the existence of a remarkable shift of the softening tempera-ture to higher temperatures with increasing filler content might be concluded from Fig. 7. This impression, however, is chiefly due to the vertical shift of the levels of the moduli in the glassy and the rubbery states with increasing filler content. To correct for the latter, the softening temperature should be

defined by the position of the midpoint of the transition of the modulus curve in a logarithmic scale. When defined in this manner, only minor effects are found for the shift of T_s with c. These conclusions agree with conclusions drawn from Figs. 6b and 10.

The value of the shear modulus of the filled elastomer in the glassy state is strongly dependent on the amount of filler, as is the value of the shear modulus
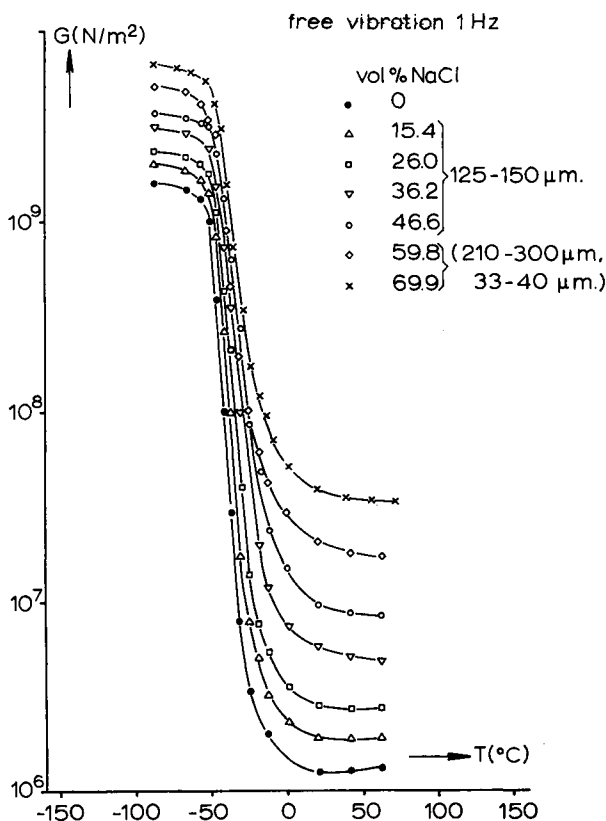
FIG. 7. Shear modulus vs. temperature at 1 Hz for a series of polyurethane rubbers filled with increasing amounts of sodium chloride.

in the rubbery state. In Fig. 8 are plotted the values of the shear moduli at 1 Hz at $-80°C$ (representative for the glassy state) and at $70°C$ (representative for the rubbery state) against the filler content for various sizes of the filler. The modulus is seen to be a function of the filler content only, regardless of the size. The points indicated at 100 per cent filler concentration are the values of the shear moduli for pure sodium chloride crystals. The drawn lines represent the predictions by the Van der Poel theory to be dealt with in Section 3.4.

The relationship between shear modulus in the rubbery region and filler content has been investigated for many other systems. Landel [11] and Landel and Smith [10] investigated polyisobutylene glass bead composites, poly-

33

urethane glass bead composites and different propellants. Their results are presented in Fig. 9b. Data after Payne [12] on natural rubber, filled with glass beads, a non-structure black and ground whiting, are shown in Fig. 9c. Finally, results due to Sabia and Eirich [13] on polyvinyl chloride, filled with calcium carbonate are reproduced in Fig. 9d. All data are compared with the predictions by the Van der Poel theory. Mostly, reasonable agreement is found.
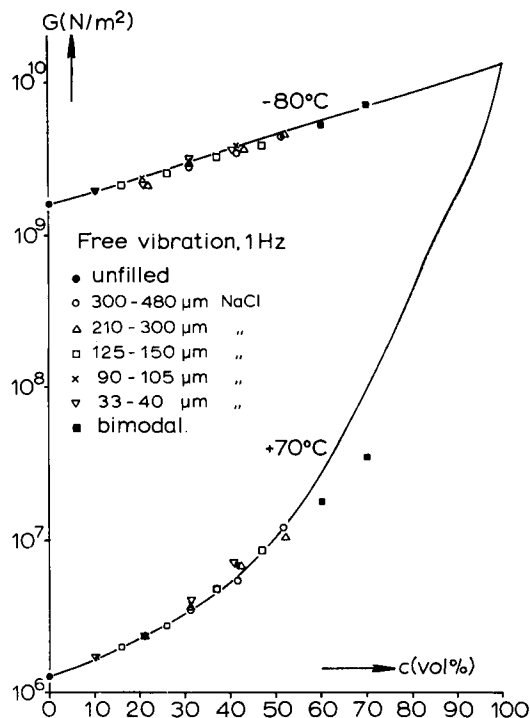
FIG. 8. Shear modulus at 1 Hz at — 80°C (representative for the glassy state) and at + 70°C (representative for the rubbery state) of polyurethane–sodium chloride composites, as a function of filler content for various filler sizes. The full line drawn through experimental points belonging to — 80°C, is the theoretical line according to Van der Poel's theory with parameter values $\mu_1 = 0.25$; $\mu_0 = 0.5$; $G_1/G_0 = 8.4$. The full line drawn through experimental points belonging to + 70°C is the theoretical line according to Van der Poel's theory with parameter values $\mu_1 = 0.25$; $\mu_0 = 0.5$; $G_1/G_0 = 10^4$.

Knowing the influence of filler on the shear modulus-temperature behaviour at constant frequency, we may draw some conclusions on the shear modulus-frequency behaviour at constant temperature. There are indications that the time–temperature shift procedure may also be applied to the glass–rubber transition of filled rubbers, and that the shift function is approximately that of the binder material. Consequently, the position of the glass-rubber transition in a modulus frequency plot is expected to be independent of filler content and size, and the only differences occurring in the master curves due to filler content will be the levels of the glassy and rubbery regions.
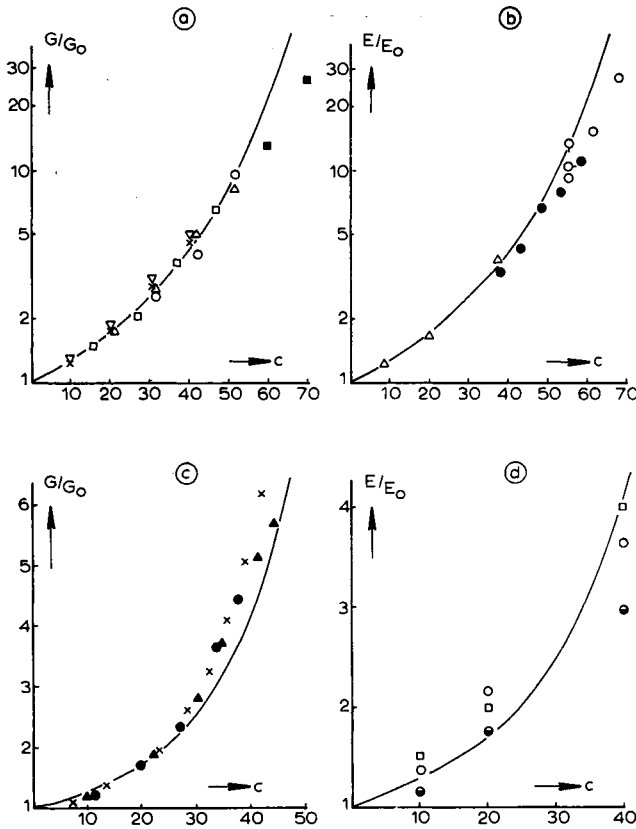
FIG. 9. Dependence of relative modulus on volume fraction of filler for filled polymers in the rubber-like region:

(a) System polyurethane rubber–sodium chloride crystals after [3]. Meaning of symbols as in Fig. 8.

(b) Data after Landel and Smith [10] on:
- △ polyisobutylene–glass beads; size 40 μm
- ○ polyurethane (TMP)–glass beads; size 40 μm
- ○- polyurethane (TDA)–glass beads; size 40 μm
- ○● propellants

(c) Data after Payne [12] on vulcanized natural rubber containing:
- × glass beads; size 100 μm
- ▲ ground whiting
- ● non-structure carbon black P–33

(d) Data after Sabia and Eirich [13] on:
Polyvinyl chloride–calcium carbonate composites; size 0.5–10 μm; different symbols refer to different plasticizers.

3.3. Dependence of Bulk Moduli on Filler Characteristics

Figure 10 illustrates the effect of increasing filler content on the variation of bulk moduli vs temperature for polyurethane–sodium chloride composites. All filled and unfilled samples show a softening region, where the bulk modulus drops to about one half of its value in the glassy state. The position of the

softening region does not depend on the content or size of filler. The values of bulk moduli at three temperatures are shown vs. composition in Fig. 11. The value at $-70°C$ may be taken as representative for the glassy state, and that at $0°C$ as representative for the rubbery state*. Moduli are plotted vs. filler composition for various fractions and are seen to depend on the filler content only. The points indicated at 100 per cent filler concentration are the values of the bulk modulus for pure sodium chloride crystals.
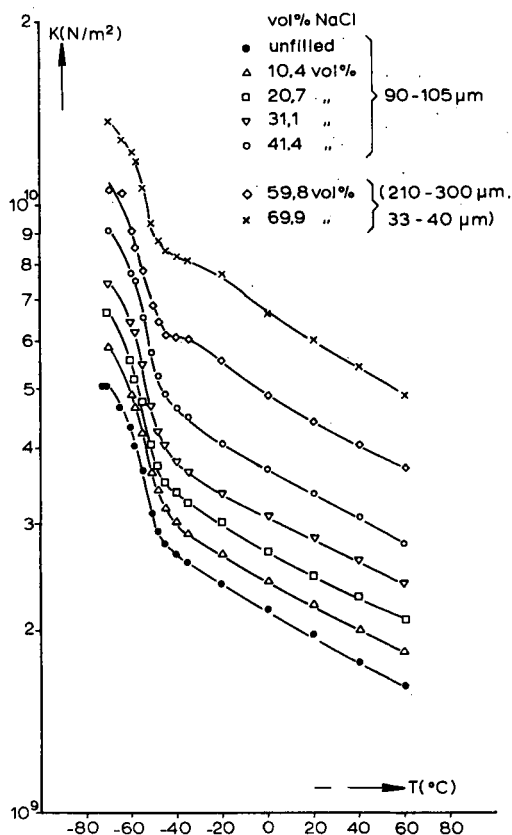
FIG. 10. Bulk modulus, K, vs. temperature for polyurethane rubbers filled with different amounts of sodium chloride. (Measurement 4 min after pressurization under hydrostatic pressure of 1.5×10^7 N/m^2.)

From the measurements of shear moduli and bulk moduli, it is of course possible to calculate Poisson's ratio when use is made of the time–temperature shift principle†. Results of those calculations are presented in Figs. 12 and 13 where $(1 - 2\mu)$ is plotted as function of temperature and composition. Figure 12

---

* Remember the restriction that no rubbery levels exist for the bulk modulus. Therefore, the choice of a representative temperature is quite arbitrary.

† Shear moduli and bulk moduli were measured at different characteristic times.
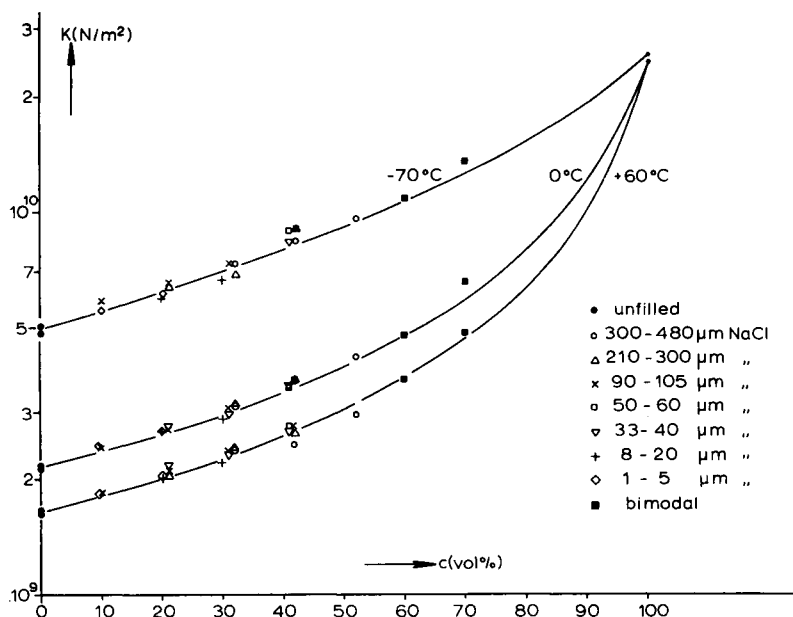
FIG. 11. Bulk moduli at — 70°C, at 0°C and at + 60°C for polyurethane rubbers filled with sodium chloride, as function of filler concentration for different filler sizes. The full line drawn through the experimental points belonging to the temperature of — 70° C, is the theoretical line due to formula (12) with the parameter values $K_1/K_0 = 5.28$; $\mu_0 = 0.36$. The full line drawn through experimental points belonging to 0°C, is the theoretical line due to formula (12) with parameter values $K_1/K_0 = 11.9$; $\mu_0 = 0.50$. The full line drawn through the experimental points belonging to the temperature of 60°C, is the theoretical line due to formula (12) with parameter values $K_1/K_0 = 15.2$; $\mu_0 = 0.50$.

shows the variation of $(1 - 2\mu)$ vs. temperature for rubbers containing respectively 0, 40 and 70 per cent by volume of filler. Figure 13 illustrates the variation of $(1 - 2\mu)$ with filler concentration at —70°C (glassy state of the polymer) and at +60°C (rubbery state of the polymer). The drawn lines represent the predictions of the Van der Poel theory.

3.4. *Theoretical Prediction of the Viscoelastic Properties of Composite Media*

The problem of predicting the bulk mechanical properties of composite media from the knowledge of the corresponding properties of the components and their fractional volumes is today still unsolved. It is only the most simple case, already treated by Einstein [14], of a dilute suspension, which is accessible to a rigorous treatment in closed form. Unfortunately, the range of validity of this case is usually not more than 1 to 2 per cent of filler concentration and, therefore, it is not of interest for our problem.

The difficulty of extending the treatment of the problem to the non-linear concentration range is chiefly due to the statistical nature of the problem [15]. Knowledge of the concentration of the filler particles alone is not sufficient to determine the problem, but detailed information should be available on the
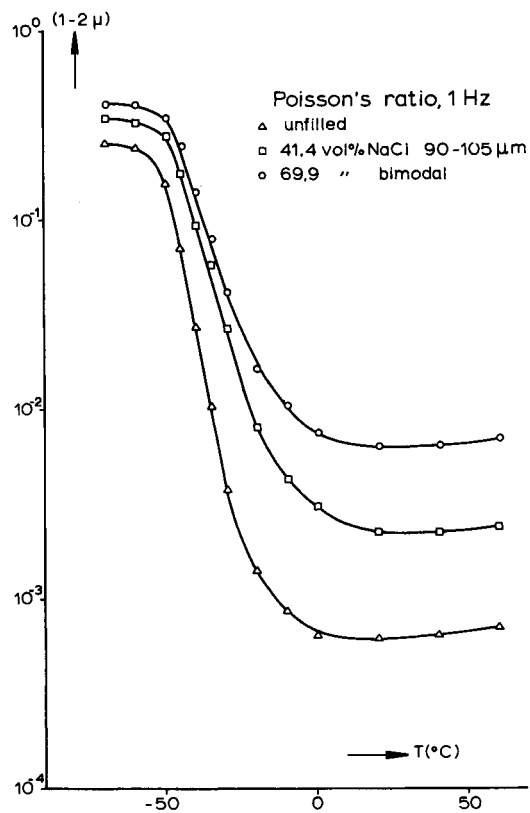
FIG. 12. Variation of Poisson's ratio with temperature for polyurethane rubbers filled with different amounts of sodium chloride; characteristic frequency 1 Hz.

spatial distribution of the dispersed phase. This information is, generally, lacking. Therefore, all that can be done today is either to set up heuristic equations or models to describe experimental results, or to derive upper and lower bounds for the elastic properties of the suspension by means of energy considerations using the restricted knowledge available on the system. The latter has been done by Hashin [15].

The lower and upper bounds for shear modulus and bulk modulus of a two-phase composite medium read as follows [15]:

$$\underline{G} \leq G \leq \tilde{G} \tag{9}$$

$$\underline{K} \leq K \leq \tilde{K} \tag{10}$$

where:

$$\frac{\underline{G}}{G_0} = 1 + \frac{\left(\dfrac{G_1}{G_0} - 1\right) c}{1 + \dfrac{6}{5} \dfrac{\left(\dfrac{G_1}{G_0} - 1\right)\left(\dfrac{K_0}{G_0} + 2\right)}{3 \dfrac{K_0}{G_0} + 4}(1 - c)} \tag{9a}$$
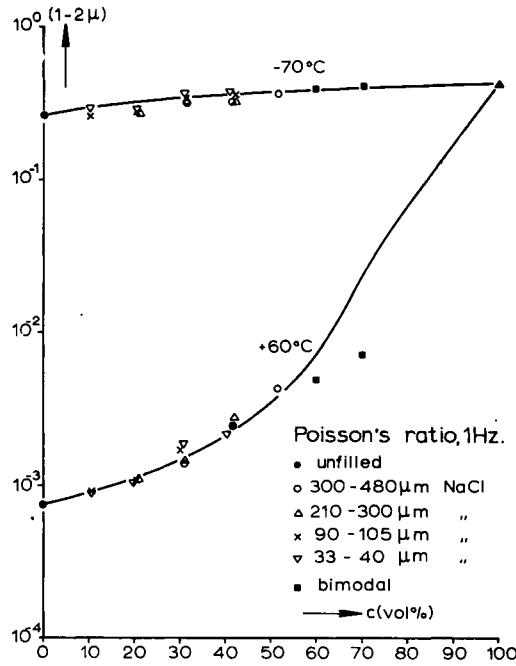
FIG. 13. Variation of Poisson's ratio with filler concentration for polyurethane rubbers filled with sodium chloride, at — 70°C (representative for the glassy state) and at + 60°C (representative for the rubbery state); frequency 1 Hz. The drawn lines represent the predictions of the Van der Poel theory.

$$\frac{\bar{G}}{G_0} = \frac{G_1}{G_0} - \frac{\left(\dfrac{G_1}{G_0} - 1\right)(1 - c)}{1 - \dfrac{6}{5}\left(1 - \dfrac{G_0}{G_1}\right)\dfrac{\dfrac{K_1}{G_1} + 2}{3\dfrac{K_1}{G_1} + 4} c} \tag{9b}$$

$$\frac{K}{K_0} = 1 + \frac{\left(\dfrac{K_1}{K_0} - 1\right) c}{1 + \dfrac{3\left(\dfrac{K_1}{K_0} - 1\right)}{3 + 4\dfrac{G_0}{K_0}}(1 - c)} \tag{10a}$$

$$\frac{\bar{K}}{K_0} = \frac{K_1}{K_0} - \frac{\left(\dfrac{K_1}{K_0} - 1\right)(1 - c)}{1 - \dfrac{3\left(1 - \dfrac{K_0}{K_1}\right)}{3 + 4\dfrac{G_1}{K_1}} c} \tag{10b}$$

In these formulae, index 0 refers to the binder material, index 1 to the filler material, and it is assumed that $G_1 > G_0$ and $K_1 > K_0$; c is the volume fraction of filler.

These bounds are rather close and, therefore, useful in cases where the two components do not differ very much in properties. They are rather useless for the case of a hard filler in a soft binder material, where $G_1/G_0 \sim 10^4$.
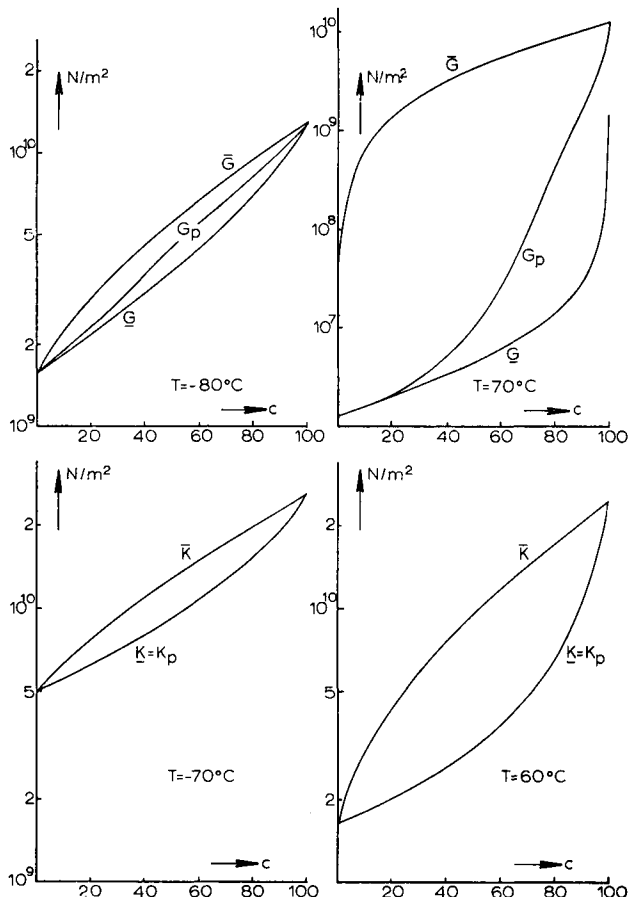
FIG. 14. Upper and lower bounds for shear and bulk moduli for the system polyurethane rubber–sodium chloride after formulae (9) and (10), at two different temperatures (representative for the glassy and rubbery state, respectively); also shown are the predictions by the Van der Poel theory, G_p and K_p.

The bounds for the bulk modulus are the most restrictive that can be obtained in terms of volume fractions and phase elastic moduli only. Whether the bounds for the shear modulus are the most restrictive or not, is not known.

The variation of the bounds with filler volume fraction is illustrated in Fig. 14 for the case of the polyurethane rubber–sodium chloride system. In this figure four cases are treated, viz. the bounds for bulk moduli in the glassy and the rubbery state, and those for shear moduli in the glassy and rubbery state. In all

cases, the course of the modulus due to the Van der Poel theory is shown for comparison. In the case of bulk moduli, the predictions by Van der Poel's theory coincide with the lower bounds. In the case of shear moduli, the predictions by the said theory fall between the bounds somewhat nearer to the lower bound, than to the upper.

The results, presented in Sections 3.2 and 3.3, on the dependence of shear and bulk moduli on filler content, may be well described in terms of a simple macroscopic theory. This theory is far from rigorous, as it is based on the idea of replacing the real composite material by a simple model. Nevertheless, the theory is successful in describing the behaviour of composite materials in shear, in three-dimensional compression and in thermal expansion, at least, for a certain range of filler concentration and particle size. The principles of this theory were first formulated by Bruggeman [16]. These principles were applied by Fröhlich and Sack [17] to the description of dilute dispersions, and by van der Poel [18] to the problem of hard elastic particles dispersed in a soft elastic matrix. Van der Poel also performed the necessary numerical calculations for expressing the shear moduli of the composite in terms of the filler concentration. The thermal expansion behaviour, and the behaviour in three-dimensional compression, were given earlier by Kerner [19]. The model of Bruggeman was applied to the problem of the mechanical properties of an elastic material with holes by Mackenzie [20].

The problem is to predict the shear modulus, G, the bulk modulus, K, and the thermal expansion coefficient, α, of a composite solid which consists of hard particles of shear modulus G_1, bulk modulus K_1, Poisson's ratio μ_1, and thermal expansion coefficient α_1, dispersed in a soft binder of shear modulus G_0, bulk modulus K_0, Poisson's ratio μ_0 and thermal expansion coefficient α_0. The volume concentration of the particles is c. The theory does not account for shape and size explicitly. All calculations are performed within the scope of Hookean thermo-elastic theory for isotropic materials with coefficients of thermal expansion which are independent of temperature.

The composite solid is represented by a sphere in which the inside has been replaced by the microscopic structure of the material: the composite sphere considered consists of three concentric spheres. The inner elastic sphere with material properties G_1, K_1, μ_1, α_1 of radius $c^{1/3}$ is surrounded by and fixed to a spherical shell of outer radius 1 and material properties G_0, K_0, μ_0, α_0; the latter is surrounded by and fixed to a shell of the homogeneous material with, still unknown, material properties G, K, μ, α, and outer radius R. This composite sphere is compared with a homogeneous sphere of material properties G, K, μ, α, and radius R. The thermal expansion and the deformation behaviour under simple shear stress and under hydrostatic pressure is considered for both composite and homogeneous spheres. Stating that the behaviour of both spheres should be identical* results in three conditions which express α, G and K in terms of c and the material properties of matrix and filler.

---

* This is possible only in the approximation $R \gg 1$.

The equations for the thermal expansion coefficient and for the bulk modulus may be written explicitly [19]:

$$\alpha = \alpha_0(1 - c) + \alpha_1 c - (\alpha_0 - \alpha_1) \, c(1 - c) \, \frac{\dfrac{1}{K_0} - \dfrac{1}{K_1}}{\dfrac{1-c}{K_1} + \dfrac{c}{K_0} + \dfrac{3}{4G_0}} \tag{11}$$

$$\frac{K}{K_0} = \frac{1 + 2\,\dfrac{1 - 2\mu_0}{1 + \mu_0}\left[\dfrac{K_0}{K_1}(1 - c) + c\right]}{1 - c + c\,\dfrac{K_0}{K_1} + 2\,\dfrac{K_0}{K_1}\,\dfrac{1 - 2\mu_0}{1 + \mu_0}} \tag{12}$$

The equation for G is not obtained in explicit form. It has been solved numerically by Van der Poel [18] for the special choice $\mu_1 = 0.25$; $\mu_0 = 0.5$. Results are given in Fig. 15, where G/G_0 is plotted as a function of c for different values of ratio G_1/G_0.

Theoretical curves with parameter values G_1/G_0 equal to 10^4 or higher are seen to be indistinguishable for concentrations below 70 per cent. Consequently, the shear modulus of filled rubbers in the rubber-like state (for which $G_1/G_0 > 10^4$ holds) will not depend on the value of the modulus of the filler substance, but only on its volume concentration. In this region, it is therefore possible to approximate the value of the shear modulus by a simple formula which does not depend on the elastic properties of the filler particles. Empirical formulas of this type have been proposed:

Eilers [21] and Van Dijk

$$\frac{G}{G_0} = \left[1 + \frac{1.25\,c}{1 - 1.28\,c}\right]^2 \tag{13}$$

Guth [22] and Smallwood [23]

$$\frac{G}{G_0} = 1 + 2.5\,c + 14.1\,c^2 \tag{14}$$

Both equations have also been plotted in Fig. 15. The Eilers–Van Dijk equation is seen to agree rather well with the Van der Poel theory in the region $G_1/G_0 > 10^3$, $c < 70$ per cent. The minor differences between both expressions will certainly not show up within the accuracy of the experimentally accessible results on filled rubbers. The Guth and Smallwood equation deviated considerably from the Van der Poel theory and from the Eilers–Van Dijk equation even at small concentrations. The Guth–Smallwood equation is clearly not suitable for the description of the modulus–concentration relationship for the filled rubbers under consideration.

Comparisons of the predictions by the Van der Poel theory with experimental results have already been made in Figs. 8, 9 and 11. Within the accuracy of the measurements, reasonable agreement is found between theory and experiment. Bulk moduli are well described by eqn. (12) for filler concentrations between
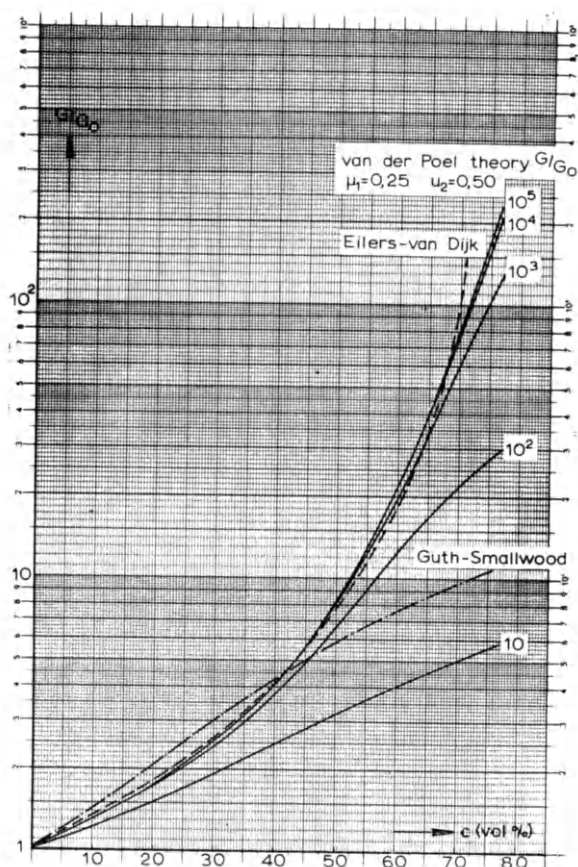
FIG. 15. Theoretical curves of the ratio of shear modulus of composite material to shear modulus of unfilled material as a function of filler concentration according to Van der Poel [18]. Parameter values $\mu_1 = 0.25$; $\mu_0 = 0.50$; G_1/G_0 as indicated. Also shown are the empirical formulae by Eilers and Van Dijk [13] and by Guth and Smallwood [14].

0 and 70 per cent by volume and for filler sizes between 1 μm and 500 μm. Shear moduli in the glassy region of the filled polymer may be predicted by the Van der Poel theory within the same range of size and concentration. For shear moduli in the rubbery region of the filled polymers, however, the range of applicability of the Van der Poel theory is more restricted. Experimental results are well described in the range of moderate concentrations (between 0 and 50 per cent) and for coarse filler sizes (between 30 μm and 500 μm). For higher concentrations, experimental shear moduli are found to be significantly lower than the predictions by the Van der Poel theory (compare Figs. 9a and 9b). In the size range of 10 μm and lower, shear moduli become dependent on the size of filler.

Not many systematic investigations have been performed on the influence of the size of filler on shear moduli of the filled substance. Preliminary indications

of this influence are the following: the softening temperature in shear is slightly increased by a decrease in filler size, and the level of the rubbery region is increased by a decrease in filler size. This is illustrated in Fig. 16, where shear moduli at 1 Hz at three temperatures are plotted as function of filler size for the system polyurethane–sodium chloride.
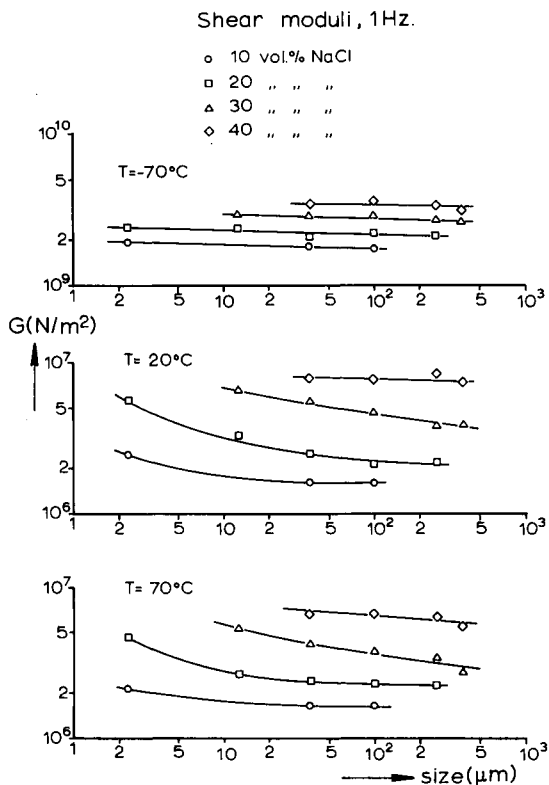
FIG. 16. Influence of the size of filler on the shear moduli at 1 Hz at three different temperatures for the system polyurethane rubber–sodium chloride.

4. THE ULTIMATE PROPERTIES OF FILLED ELASTOMERS

4.1. Dewetting and Stress–strain Behaviour

The influence of increasing content of filler on the stress–strain behaviour of filled elastomers is illustrated in Figs. 17, 18 and 19. In Fig. 17 are shown data due to Bills and others [24] on a polyurethane rubber filled with increasing amounts of glass beads of 60 to 90 μm diameter. In Figs. 18 and 19 are shown data on a different polyurethane rubber filled with increasing amounts of sodium chloride crystals of respectively a fine and a coarse fraction. Note the differences in scale of the stress-axis in these figures. The unfilled polyurethane rubber shown in Fig. 17 has rather good mechanical properties, viz. an ultimate strain

of 300 per cent and a tensile strength of 8×10^5 N/m². When this rubber is filled with increasing amounts of inert filler, its ultimate elongation decreases and its tensile strength increases considerably. The behaviour of the rubber shown in Figs. 18 and 19 is different. This polyurethane rubber has poor mechanical properties in the unfilled state (ultimate strain of only 60 per cent and tensile strength of 13×10^5 N/m²). When this rubber is filled with a fine filler (Fig. 18), the tensile strength increases only slightly. When the rubber is filled with a coarse filler (Fig. 19), its tensile strength decreases considerably. In both cases, the ultimate elongation does not decrease significantly with increasing filler content.
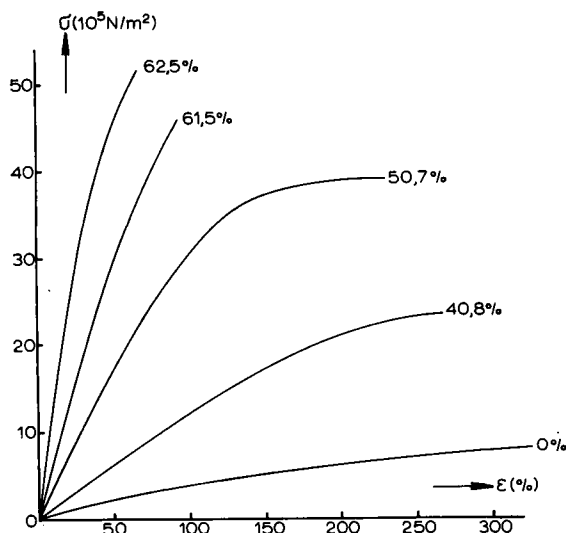
FIG. 17. Uniaxial tensile stress–strain diagrams for a series of polyurethane rubbers filled with different amounts of glass beads (size 60–90 μm) after Bills and others [24]; temperature — 7°C; strain rate 740 per cent per minute.

Next we consider the shape of the stress–strain curves of composite materials containing higher amounts of filler (cf. 50 per cent of glass beads in Fig. 17 or 40 per cent of sodium chloride in Figs. 18 and 19). After a rather straight initial part, these curves show a sharp bend; thereafter, the tensile force remains approximately constant, whereas the overall strain still increases considerably before rupture occurs finally. These stress–strain curves are similar to those for polymers showing the phenomenon of cold drawing. However, the molecular mechanism connected with the yielding is quite different in this case. There is no necking which accompanies the phenomenon in the case of filled rubbers. Instead, there is a change in reflection properties during straining. The specimen is milky, moderately translucent in undeformed state. At yielding, it becomes whiter, but opaque, when observed in incident light, and darker and opaque, when observed in transmitted light. This is in accordance with the development of vacuoles in the binder from the onset of yielding.
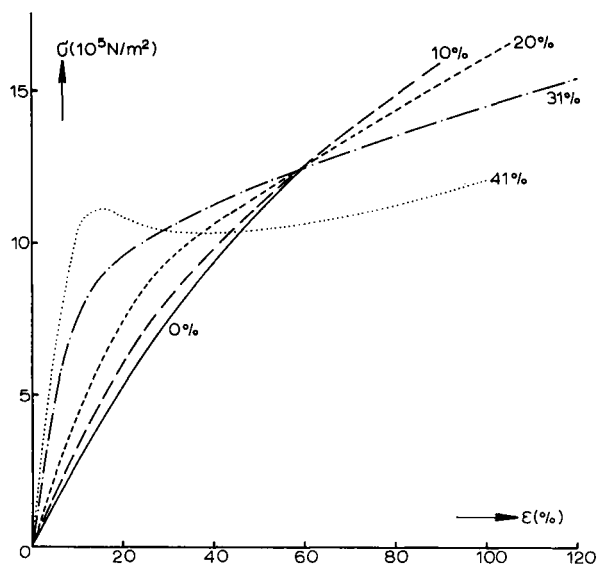
FIG. 18. Uniaxial tensile stress–strain diagrams for a series of polyurethane rubbers filled with increasing amounts of sodium chloride of a small size (50–60 μm); temperature 20°C; strain rate 300 per cent per minute.
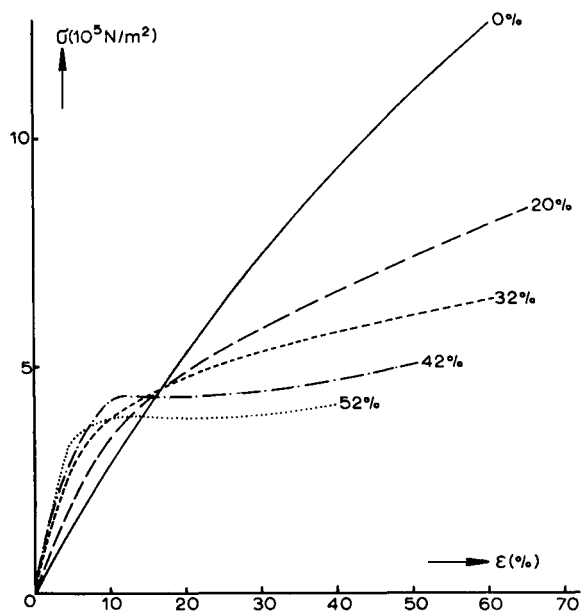
FIG. 19. Uniaxial tensile stress-strain diagrams for a series of polyurethane rubbers filled with increasing amounts of sodium chloride of a coarse size (210–300 μm); temperature 20°C; strain rate 300 per cent per minute.

Depending on the ratio of the strength of the adhesive bond between filler and binder to the cohesive strength of the binder, different phenomena may be observed at the yield point. For good composite propellants [25], and for filled rubbers with high ultimate elongations, the adhesive bond between filler and binder fails first and vacuoles are formed around the filler particles. This phenomenon is called dewetting. After complete dewetting is achieved, a further increase in strain only stretches the binder and enlarges the vacuoles. Finally, a crack propagates from one of the vacuoles and leads to failure [25].

In cases, where the binder material has very poor ultimate strains, the initial failure may occur not at the filler-binder interface, but in the binder itself
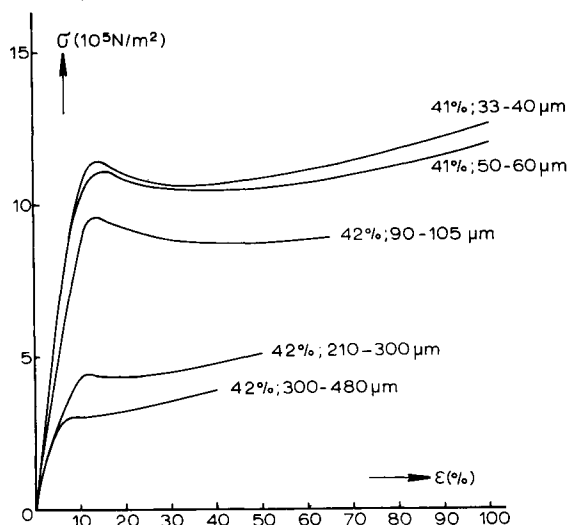
FIG. 20. Uniaxial tensile stress-strain diagrams for polyurethane rubbers filled with 40 per cent of different fractions of sodium chloride; temperature 20°C; strain rate 300 per cent per minute.

due to stress concentration in the vicinity of filler particles. This mechanism will be favoured also by very strong adhesive bonds and by irregular shapes of filler particles. The first type of failure is believed to occur in the samples whose behaviour was shown in Fig. 17, while the latter type of failure is believed to dominate in the samples shown in Fig. 19. It is by no means easy to distinguish in all cases between the two types of failure. Therefore, we will speak of dewetting in general in what follows, also in cases where no evidence is known on the details of the primary failure mechanism.

The stress–strain curve is largely influenced by the size of the filler particles. This is shown in Fig. 20, where the yielding behaviour is compared for polyurethane rubbers containing about 40 per cent of different fractions of sodium chloride. The value of the yield stress is seen to be highly increased by a decrease in the size of the filler particles.

More direct experimental evidence for the dewetting of composites at the yield point may be obtained by a measurement of the volume change during straining. When an unfilled elastomer is stretched, the volume change of the specimen is negligibly small, even at elongations of hundreds of per cent. However, when dewetting and vacuole formation occur in a composite material, the volume will increase considerably with stretching. Thus, a study of the volume change that accompanies the stretching of a filled rubber will yield information on the strain at which dewetting begins, on the strain at which dewetting is complete, and on the deformation properties of the dewetted substance.

The volume changes occurring during stretching of a granular filled elastomer ($c = 73$ per cent), together with the stress–strain diagram, are illustrated in Fig. 21 (Ref. [26]). The steep increase in volume is seen to coincide with the
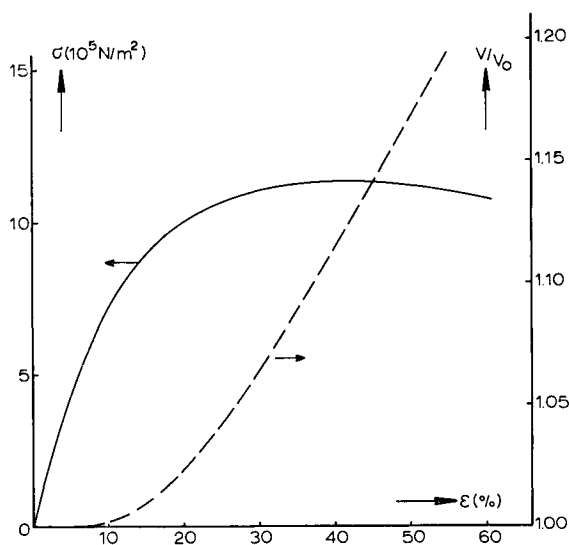
FIG. 21. Stress–strain diagram and volume changes during stretching for a granular filled elastomer ($c = 73$ per cent) after Farris [26]; temperature 25°C; strain rate 666 per cent per minute.

yield region in the stress–strain curve. The occurring volume changes are seen to be as large as 20 per cent (the corresponding volume change of the undewetted substance would not exceed 0.5 per cent).

A thorough investigation of the volume changes due to dewetting of poly-vinyl chloride glass bead composites was performed by Smith [27]. Some of his results on these composites and on a foam of polyurethane rubber are repro-duced in Fig. 22. The abscissae in the two parts of this figure are the logarithm of the longitudinal extension ratio. The ordinates are respectively the logarithm
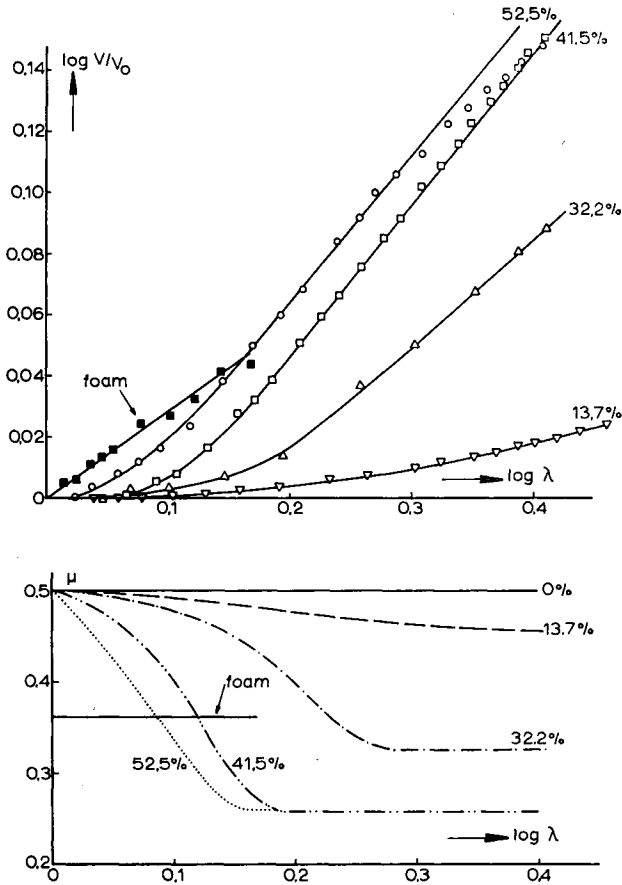
FIG. 22. Volume changes during stretching of polyvinyl chloride–glass bead composites with different filler contents (size 20–60 μm) and of a polyurethane foam (59 vol. per cent of voids) after Smith [27]. Upper part logarithm of relative volume; lower part (derived) Poisson's ratio, μ, defined by eqn. (15); temperature 25° C.

of the volume ratio or Poisson's ratio, which was defined to describe the volume changes in the following way:

Poisson's ratio:

$$\mu = -\frac{d \log \lambda_2}{d \log \lambda} = \tfrac{1}{2} \left[1 - \frac{d \log (V/V_0)}{d \log \lambda} \right] \qquad (15)$$

where:

$\lambda = 1 + \epsilon$	longitudinal extension ratio
λ_2	lateral contraction ratio (< 1)
V/V_0	ratio of stretched to unstretched volume

This definition represents a generalization of the usual definition of Poisson's ratio at small deformations. By this definition, $\mu = \tfrac{1}{2}$ is still connected with a

34

material which does not show any volume change under arbitrarily large deformations, whilst a constant value of Poisson's ratio means that the logarithm of V/V_0 increases linearly with the logarithm of λ:

$$\frac{V}{V_0} = \lambda^{(1-2\mu)} \text{ for } \mu = \text{constant} \tag{16}$$

This behaviour is just shown by a foam which has a constant value of Poisson's ratio over the whole deformation range (Fig. 22). The behaviour of the PVC glass bead composites is different: at small strains there is no volume change (μ being constant and very near to $\frac{1}{2}$); at some critical strain, ϵ_d, volume change and dewetting start leading to a decrease in Poisson's ratio. Finally, at higher strains, Poisson's ratio becomes a strain independent value (considerably lower than $\frac{1}{2}$). From analogy to the behaviour of the foam, it is assumed, that in the latter region dewetting is complete.
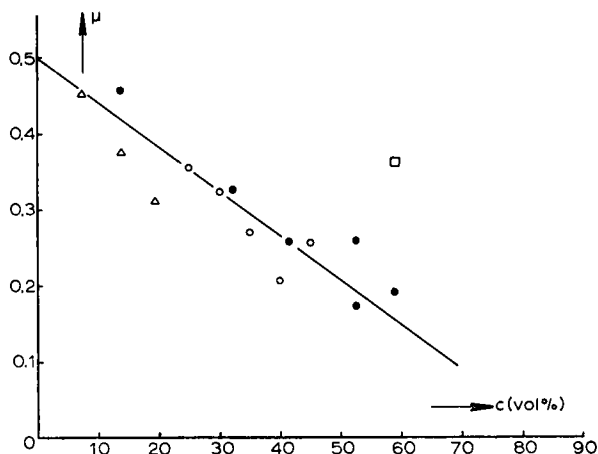
FIG. 23. Poisson's ratio, μ, of stretched composite materials vs. filler content, after Smith [27]:

● polyvinyl chloride–glass bead composites (Smith [27])
□ polyurethane foam 59 per cent voids (Smith [27])
△ vulcanized rubber–zinc oxide (Jones and Yiengst [28])
○ pale creep vulcanizate–whiting (Bryant and Bisset [29])

Thus, Poisson's ratio at large deformations constitutes a characteristic property of the dewetted composite material. Its dependence on filler content is reproduced in Fig. 23. It is remarkable that Poisson's ratio of a foam is larger than Poisson's ratio of a dewetted composite material of corresponding degree of filling, i.e. the volume increase is larger for the dewetted composite. This is to be expected, because the lateral contraction during the elongation of the vacuoles will be largely suppressed by the presence of loose filler particles in the voids.

In Fig. 24 are reproduced strain and stress values at the onset of dewetting as a function of filler content, as well as the moduli of elasticity of the non-dewetted and dewetted material, E_u and E_d. These moduli have been determined as the slopes of the stress–strain diagrams in the initial region and after yielding. As to be expected, E_u increases with filler content, though less than that which would correspond to the Van der Poel theory, and E_d decreases with filler content.
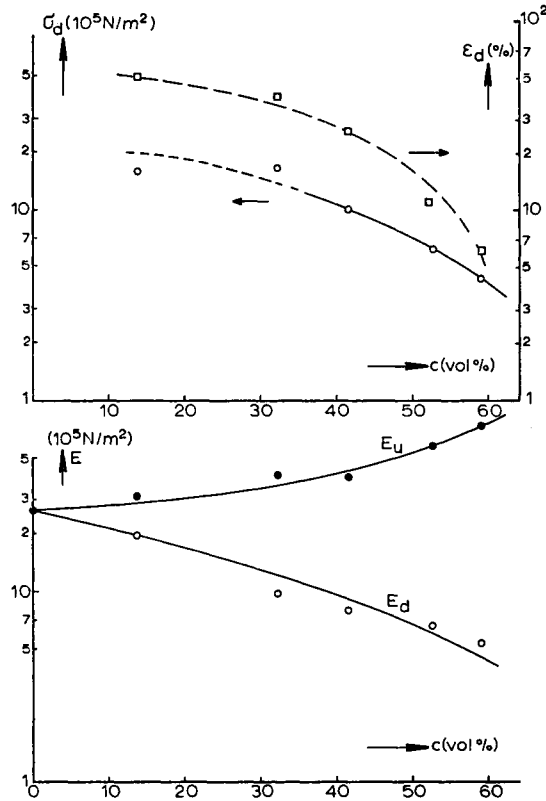
FIG. 24. Yield stress, yield strain, moduli of elasticity of the non-dewetted material, E_u, and of dewetted material, E_d, as function of filler content for polyvinyl chloride–glass bead composites after Smith [27].

4.2. Dewetting and Tensile Creep

A different way to characterize dewetting of a filled rubber is to investigate its creep behaviour under large tensile stresses. Unfilled, well-crosslinked rubbers do not show any appreciable creep in their temperature region of rubber-like elasticity (Fig. 4). If the same rubbers are filled with either inert or active fillers, they show very definite creep behaviour at high stresses. This creep is related to dewetting, as is explained schematically in Fig. 25.

This figure illustrates the variation of tensile strain under three different constant stresses with the logarithm of time for a hypothetical filled material which shows dewetting, but no rupture in the dewetted state. At short times, the material is and exhibits a low strain level independent of time, which is a measure of the modulus of elasticity of the non-dewetted material. After a certain time, dewetting starts and gives additional contribution to tensile deformation. Upon completion of dewetting, a second, much higher, strain level is reached, which is again independent of time and yields the characteristic modulus of the dewetted material. The differences in strain between the
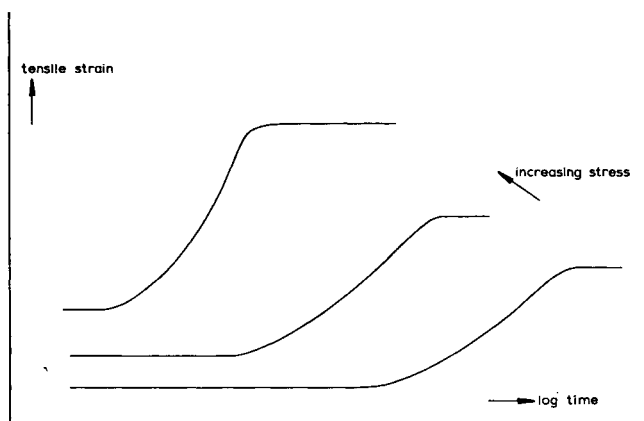
FIG. 25. Tensile creep and dewetting, schematically.

dewetted and non-dewetted state will be clearly the higher, the higher the filler content. Increase in the constant stress level chiefly affects the time of dewetting.

For real composite materials, the picture is complicated by the occurrence of rupture. Only for materials with low filler content is the dewetted state realized generally. In most cases rupture occurs in the upward curved part of the transition region. Thus, under favourable circumstances, these measurements may yield information on the following subjects: elasticity of the non-dewetted sample; elasticity of the dewetted sample; dependence of the dewetting process on stress, time and filler characteristics; and dependence of rupture on stress, time and filler characteristics.

Some examples of tensile creep curves under different stresses are given in Figs. 26, 27 and 28. In these figures, the creep behaviour of polyurethane rubbers filled with increasing amounts of a fraction of coarse sodium chloride is shown. Crosses indicate rupture, while arrows indicate unloading of the sample and the start of a recovery experiment. The creep behaviour clearly becomes more dominant with increasing filler content, and is accelerated with increase of the stress level. Finally, in Fig. 29, the creep behaviour of rubbers with different filler content, all specimens at the same tensile stress level of 3×10^5 N/m^2, is compared.
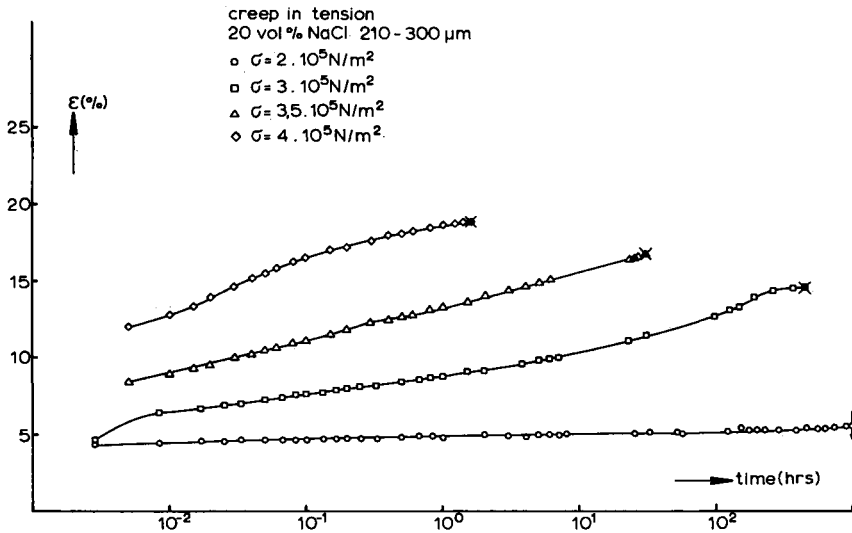
FIG. 26. Tensile creep of polyurethane rubber filled with 20 per cent of NaCl of the size 210–300 μm; stresses as indicated; temperature 20°C.
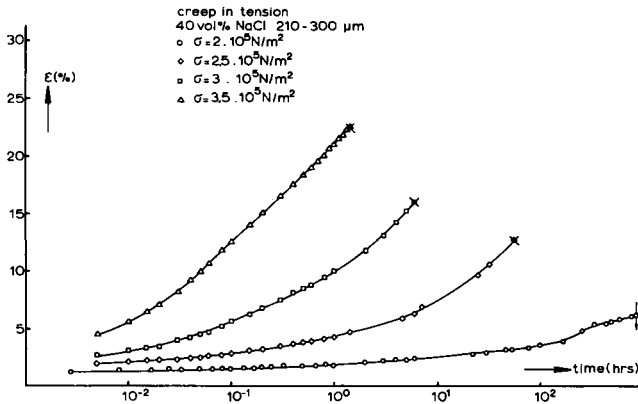
FIG. 27. Tensile creep of polyurethane rubber filled with 40 per cent of NaCl of the size 210–300 μm; stresses as indicated; temperature 20°C.

When a partially or totally dewetted sample is unloaded before the occurrence of rupture, complete recovery of the deformation is observed. About 80 per cent of the deformation recovers instantaneously, and the other 20 per cent retardedly; this retardation extends over several decades in time scale. When a completely recovered sample is reloaded with the original load, the original deformation is reached again after some time. About 80 per cent of this deformation occurs as instantaneous deformation, the other 20 per cent are again retarded. The retarded recovery and the retarded deformation under reload follow about the same dependence on time.
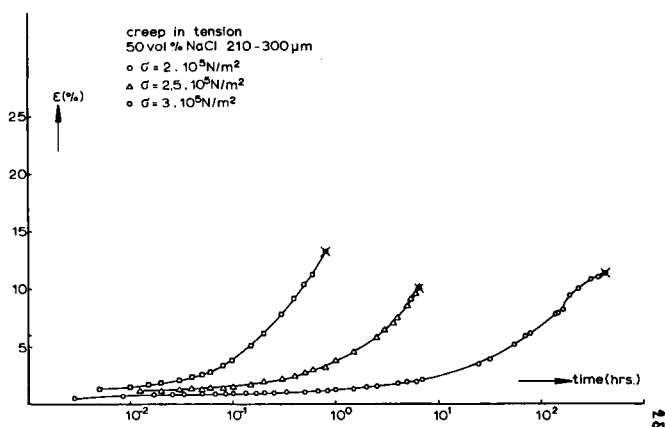
FIG. 28. Tensile creep of polyurethane rubber filled with 50 per cent of NaCl of the size
210–300 μm; stresses as indicated; temperature 20°C.
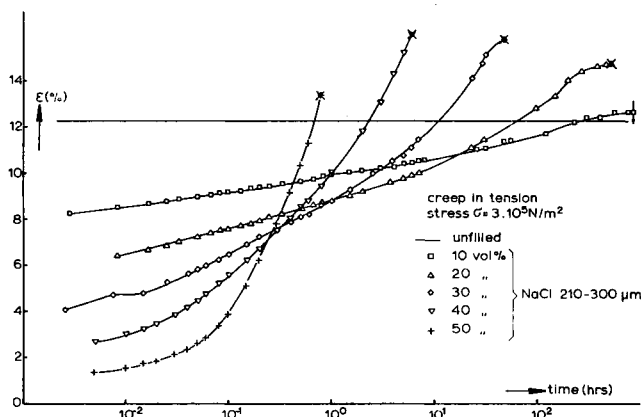
FIG. 29. Tensile creep under the tensile stress of 3×10^5 N/m² for polyurethane rubbers
filled with various amounts of 210–300 μm NaCl; temperature 20°C.

Moduli of elasticity were calculated, before and after dewetting, from the
creep behaviour, using the formulae of the theory of rubber elasticity. These
moduli, E_u and E_d, are shown as functions of filler content in Fig. 30. This
picture should be compared with that of Fig. 24 due to Smith. The moduli of
the non-dewetted material increase considerably with filler content. This increase
conforms to the Van der Poel theory. The moduli of the dewetted samples
decrease with filler content, but less markedly. It is supposed that these samples
do not represent a stage of complete dewetting. A better impression of the
dependence of E_d on c should be obtained by first dewetting the samples
artificially and afterwards measuring them under low strains.

The results of creep measurements also reflect the dependence of dewetting
strength on size of filler particles. This may be seen by comparing results in
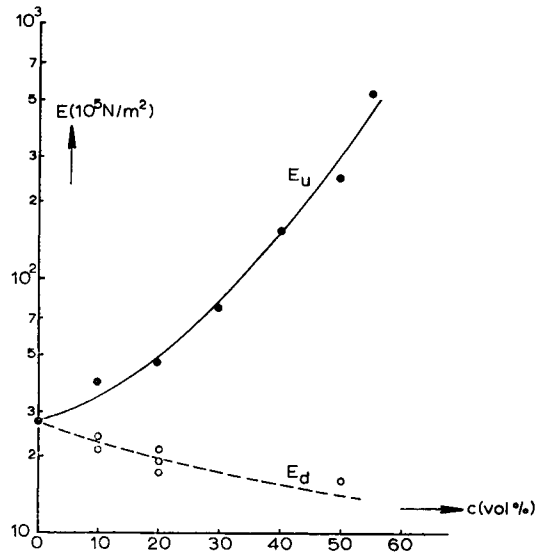
FIG. 30. Moduli of elasticity for non-dewetted samples, E_u, and for dewetted samples, E_d, as function of filler content for urethane rubbers filled with various amounts of 210–300 μm NaCl. E_u and E_d were estimated from the levels of the creep curves before and after dewetting.
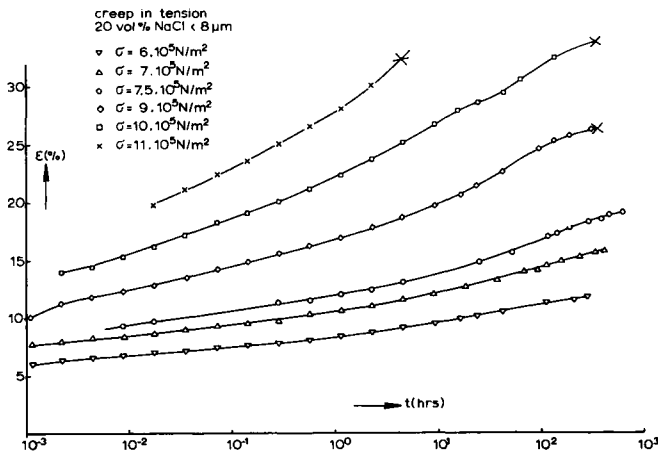
FIG. 31. Tensile creep of polyurethane rubber filled with 20 per cent of NaCl of a size smaller than 8 μm; stresses as indicated; temperature 20°C.

Figs. 31 and 32 with those of Figs. 31 and 29. Figure 26 shows the creep behaviour under different stresses for polyurethane rubbers containing 20 per cent by volume of a sodium chloride fraction with a size smaller than 8 μm. Whilst in Fig. 26 the stress necessary to produce dewetting and rupture was between 2.5 and 4 × 10^5 N/m², it is about twice as high now, namely between 6.0 and 8 × 10^5 N/m². Figure 32 shows some results obtained for polyurethane rubbers
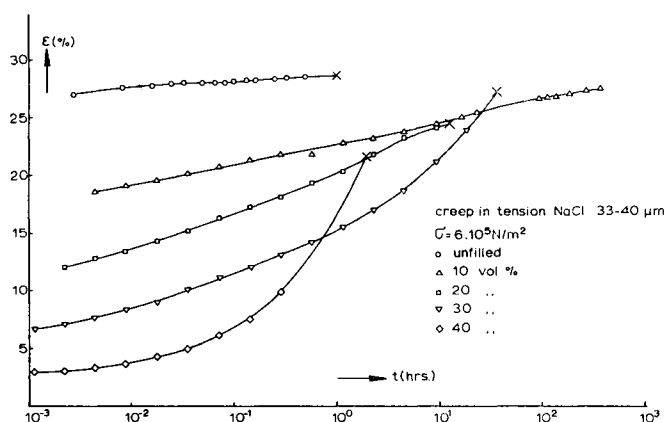
Fig. 32. Tensile creep under the tensile stress of 6×10^5 N/m² for polyurethane rubbers filled with various amounts of 33–40 μm NaCl; temperature 20°C.
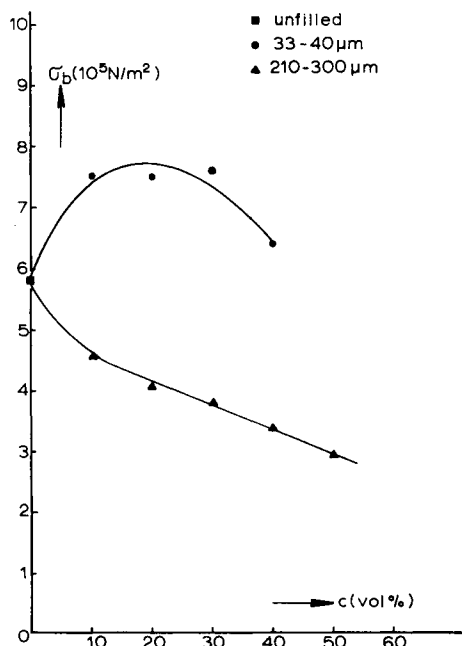
Fig. 33. Rupture stresses after a creep time of 1 hr, as function of filler concentration for polyurethane rubbers, containing various amounts of NaCl of two different sizes.

filled with a sodium chloride fraction of a size between 33–40 μm. These samples are roughly twice as strong as the samples whose behaviour was shown in Fig. 29. Otherwise, both figures are rather similar.

A preliminary survey of the strength of polyurethane–sodium chloride composites obtained by means of tensile creep measurements is presented in Fig. 33. In this figure, rupture stresses corresponding to a rupture time of about 1 hr are

plotted against filler concentration for samples containing sodium chloride crystals. Though the figure is not yet complete, already the trend of the results may be seen clearly. Incorporation of a coarse fraction (210–300 μm) means that the samples are weakened from the very beginning. Incorporation of a small fraction (33–40 μm) results in a material which is first strengthened, and weakened only after an optimum filler concentration is passed. The optimum strength is the higher, the smaller the size of the fraction. A picture which is completely similar to Fig. 33, may be obtained from the stress–strain diagrams of the same materials.

Finally, we would raise the question whether the determination of stress–strain diagrams or the performance of tensile creep may be more suitable to characterize the dewetting behaviour. Clearly, the creep technique is the more involved one, and, therefore, much fewer data have been gathered in this direction. However, when performed properly, it gives information on the long time behaviour, which the stress–strain technique will never yield. Furthermore, the phenomenon to be studied, viz. dewetting, is allowed time to develop more naturally under constant stress (or constant load) conditions. In a stress–strain technique, the critical phenomena of dewetting are enforced and accelerated by the experimental conditions.

REFERENCES

[1] STAVERMAN, A. J. and SCHWARZL, F., "Linear deformation behaviour of high polymers", *Physik der Hochpolymeren*, Vol. IV, Editor H. A. STUART, Springer, Berlin (1956).
[2] SCHWARZL, F. R., "Das mechanische und thermische Verhalten von Polymeren", *Chemie und Technologie der Kunststoffe*, Ed. Houwink, Staverman, Bd. I, 4. Aufl. Akad. Verlagsges. Leipzig (1963).
[3] SCHWARZL, F. R., BREE, H. W. and NEDERVEEN, C. J., "Mechanical properties of highly filled elastomers I. Relationship between filler characteristics, tensile properties and shear moduli", *Proc. 4th Int. Congr. Rheology*, Providence R.I., 1963, vol. 3., 271.
[4] SCHWARZL, F. R., BREE, H. W. and VAN DER WAL, C. W., "Mechanical properties of highly filled elastomers II. Relationship between filler characteristics, thermal expansion and bulk moduli", *J. Appl. Polymer Sci.*, 9 (1965), 2173.
[5] SMITH, T. L., "Elastomeric binder and mechanical property requirements", *Ind. Eng. Chem.*, 52, 776 (1960).

[6] WILLIAMS, M. L., LANDEL, R. F. and FERRY, J. D., "The temperature dependence of relaxation mechanisms in amorphous polymers and other glass-forming liquids", *J. Am. Chem. Soc.*, **77**, 3701 (1955).

[7] TOBOLSKY, A. V., "Stress relaxation studies of the viscoelastic properties of polymers", *Rheology, Theory and Applications II*, Ed. EIRICH, New York, Academic Press Inc. Publishers, N.Y. (1958).

[8] LANDEL, R. F. and FEDORS, R. F., "Rupture of amorphous unfilled rubbers", *Fracture Processes in Polymeric Solids*, Ed. B. Rosen, Interscience Publ. New York (1964).

[9] SMITH, T. L., "Relations between ultimate tensile properties of elastomers and their structure", *Proc. Roy. Soc.*, **A282**, 102 (1964).

[10] LANDEL, R. F. and SMITH, T. L., "Viscoelastic properties of rubber-like composite propellants and filled elastomers", *ARS Journal*, **31**, 599 (1961).

[11] LANDEL, R. F., "The dynamic mechanical properties of a model filled system: Polyisobutylene—glass beads", *Trans. Soc. Rheology*, **2**, 53 (1958).

[12] PAYNE, A. R., "The dynamic properties of carbon black loaded natural rubber vulcanizates", *J. Appl. Polymer Sci.*, **6**, 368 (1962).

[13] SABIA, R. and EIRICH, F. R., "Viscoelastic behaviour of plasticized polyvinyl chloride at large deformations III. The effect of filler", *J. Polymer Sci.*, **A2**, 1909 (1964).

[14] EINSTEIN, A., *Ann. Phys.*, **19**, 289 (1906); **34**, 591 (1911).

[15] HASHIN, Z., "Theory of mechanical behaviour of heterogeneous media", *Applied Mechanics Rev.*, **17**, 1 (1964).

[16] BRUGGEMAN, D. A. G., *Ann. Phys. Lpz.*, **24**, 635 (1935); Ibid. **29**, 160 (1937).

[17] FRÖHLICH, H. and SACK, R., *Proc. Roy. Soc.*, **A185**, 415 (1946).

[18] VAN DER POEL, C., "On the rheology of concentrated dispersions", *Rheologica Acta*, **1**, 198 (1958).

[19] KERNER, E. H., "The elastic and thermoelastic properties of composite media", *Proc. Phys. Soc.*, **B69**, 808 (1956).

[20] MACKENZIE, J. K., "The elastic constants of a solid containing spherical holes", *Proc. Phys. Soc.*, **B63**, 2 (1950).

[21] EILERS, H., Viscosity of emulsions of a highly viscous substance as a function of concentration", *Kolloid-Z.*, **97**, 313 (1941).

[22] GUTH, E., "Theory of filler reinforcement", *J. Appl. Phys.*, **16**, 20 (1945).

[23] SMALLWOOD, H. M., "Limiting law of the reinforcement of rubber", *J. Appl. Phys.*, **15**, 758 (1944).

[24] BILLS, K. W. Jr., SWEENY, K. H. and SALCEDO, F. S., "The tensile properties of highly filled polymers. Effect of filler concentrations", *J. Appl. Polymer Sci.*, **4**, 259 (1960).

[25] BILLS, K. W. Jr. and WIEGAND, J. H., "Relation of mechanical properties to solid rocket motor failure", *A.I.A.A. Journal*, **1**, 2116 (1963).

[26] FARRIS, R. J., "Dilatation of granular filled elastomers under high rates of strain", *J. Appl. Polymer Sci.*, **8**, 25 (1964).

[27] SMITH, T. L., "Volume changes and dewetting in glass bead polyvinyl chloride elastomeric composites under large deformations", *Trans. Soc. Rheology*, **3**, 113 (1959).

[28] JONES, H. C. and YIENGST, H. A., "Dilatometer studies of pigment-rubber systems", *Ind. Eng. Chem.*, **32**, 1354 (1940).

[29] BRYANT, K. C. and BISSET, D. C., *Proceedings of the Third Rubber Technology Conference* (1954), Ed. T. H. Messenger, Heffer, Cambridge, England, p. 655.

THE FAILURE MECHANISM OF
SOLID PROPELLANT GRAINS*

JAMES H. WIEGAND

Aerojet-General Corporation, Sacramento, California

Abstract—The failure behavior of solid propellants has been extensively studied in the laboratory with the objective of providing failure criteria for the design and evaluation of solid rocket motors. Most studies have been focused, therefore, on modes of failure similar to those observed in motors, and only a few studies have been extended into regimes giving a broader picture of the failure process. No single failure criterion is yet clearly established, although the maximum principal strain has been used successfully in empirical correlations where comparison was made with observed motor strains. Several stress criteria are currently being advanced but their applicability has been limited because adequate stress gages for viscoelastic materials are not yet available.

The microscopic examination of events leading to failure have defined the several steps: vacuole formation initiated at points of maximum stress; growth of the cavities; and unbonding of the oxidizer–filler interface unless the filler particles are enclosed in a coating of higher modulis binder. The failure itself appears to be a tearing of the distended binder structure, although this step has not been adequately examined.

The study of failure is complicated by the need to include the whole prior history of the material in any comprehensive theory and by the wide statistical distributions observed for the behavior of real propellants.

1. INTRODUCTION

The solid rocket industry has made significant progress in assessing the stresses and strains that develop in simple motors on storage, thermal cycling, and firing, and in showing that the assessment is consistent with observed motor behavior. Use can now be made of large computers having sufficient capacity to analyze reasonably complex end configurations and predict the effects of stress relaxation. Influences of complex configurations can be measured using "frozen stress" photoelastic techniques to give stress concentrations superimposable on the responses of the simpler tubular grains. Cases are observed, however, in which the change of volume with strain introduces complexities which cannot yet be handled and which produce deviations between predicted and observed strains.

The prediction of motor failure, and hence, development of the design and control requirements to prevent failure, is not yet on a firm basis. Empirical correlations have been developed to relate laboratory failure data to observed motor failures, but little can be said as yet about the adequacy of the safety margins given. Unpredicted failures have occurred as well as unexpected resistance to failure, which indicate that not all factors are yet identified and controlled.

The relation of process variables to motor failures is relatively untouched, and only cursory examinations have been made of the pertinent statistics of extreme values, e.g. how to predict the first failure in a group of production motors.

The failure behavior of solid propellants is complicated by the presence of fillers, thereby necessitating the application of scientific techniques from a number of disciplines. The diversity of needed techniques results from the fact that the failure behavior of solid propellants is associated with the four important areas: (1) the inherent strength and viscoelastic properties of the binder, (2) the binder-filler interactions, (3) the packing characteristics and fracture strength of the filler, and (4) the path dependency of failure phenomena.

Propellant failure is a multiple step process. Except at very low temperatures, these steps are: (1) initiation of vacuoles (voids), (2) increase and growth of vacuoles, and (3) tear of binder films. The mechanism for each step is known in a general way to depend on the binder type and the stress–time–temperature history of the propellant. A thorough understanding of these mechanisms requires more knowledge of path-dependency and cumulative damage than is presently available.

Although most failure studies have been oriented toward the determination of propellant behavior, the observed major role of the propellant-liner bond in motor failures has directed increased attention to that bond. The chemical aspects of adhesion and the difficulties of measuring the quality of bonds in any motor combine to make the bond problem a most serious one.

Attempts are underway to develop general criteria of failure; but, as concluded by Kruse [1] in his comprehensive review of progress on failure criteria,

> Unfortunately, therefore, it is impossible at present to generalize regarding a propellant failure surface; instead the experimentalist must determine, for the particular propellant with which he is concerned, which of the various possible interpretations best fits the data available.

In this paper, I shall not attempt to extend the review of Kruse, but rather to examine some aspects of the mechanism of failure in highly filled solid propellant systems. Following that, the use of empirical data generated for particular systems will be discussed in terms of correlations with observed motor failure behavior.

2. MECHANISMS OF FAILURE

2.1. *General Aspects*

Progress toward propellant failure is determined by mechanisms that control the major steps: (1) initiation of vacuoles, (2) increase and growth of vacuoles, and (3) tear of binder films. At each step, there are several failure mechanisms associated with one or more of the following principal areas: (1) viscoelastic properties of the binder, (2) binder-filler interactions, and (3) filler properties. To further complicate the situation, the behavior of the propellant at any time is influenced by the previous mechanical and thermal history of the material. This influence of previous history is designated here as path dependency. Because

of the obviously great complexity of propellant failure behavior, the chief contributing factors are discussed individually.

2.2. Vacuole Formation and Growth

Preliminary Work

The first step in the failure process in filled elastomers is the formation of vacuoles within the binder or at the binder-filler surface. The formation of these vacuoles and their growth in numbers and size produce the measurable phenomenon of strain dilatation. Ever since this phenomenon was first discovered by
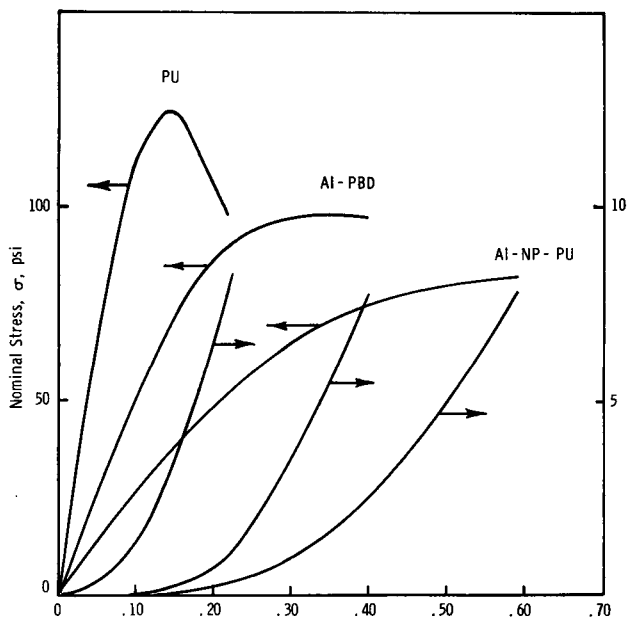
FIG.1 . Typical stress–strain and dilatation–strain behavior of three different propellants at 77° F and strain rate of 0.66 min⁻¹

Schippel [2] in 1919 when he was studying the behavior of filled vulcanizates, efforts have been made to understand it. Many investigators [3–7] have subsequently verified Schippel's findings on solid propellants and other vulcanized and curable rubber systems containing fillers of various kinds. Schippel showed excellent foresight when he said of the vacuoles, "Their cumulative effect in a substance which has the ability to withstand comparatively enormous elastic strains is worthy of serious consideration from a physical standpoint" [2].

Evidence of three kinds indicates the formation of vacuoles in strained propellant. First, laboratory dilatation tests on specimens undergoing tensile tests showed, as in Fig. 1, that the volumes of the specimens increased during the tests. Second, vacuoles have been observed microscopically during the straining

of binder films containing scattered particles of filler. Third, strain dilatation is confirmed by the fact that, when case-bonded motors are cooled, the inner bore hoop strains are considerably smaller than those calculated on the basis of grain geometries and coefficients of thermal expansion.

Sites of Vacuole Formation

Upon application of tensile stress to propellant, vacuoles usually appear first in the binder phase near filler particles. As they grow, these vacuoles usually penetrate to the binder-filler interface and grow into elliptical cavities about the filler particles, as shown typically in Fig. 2. This peeling away of binder from the oxidizer is called dewetting. If the binder near the filler surface has a higher modulus or greater tear strength than the body of the binder, void formation may never penetrate to the filler surface but will produce cavities entirely within the binder phase [7].
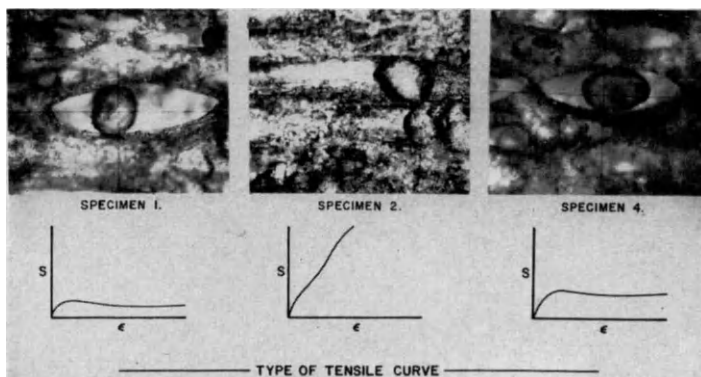
FIG. 2. Micrographs on stretched rubber (approx. 300 per cent elongation) containing 55 vol. per cent filler (7) with corresponding stress–strain curves.

Microscopic examinations of many propellant systems clearly substantiate the presence of vacuoles and furnish much information on the shape and growth of vacuoles during straining. An example of this evidence is presented in Fig. 3, which shows a series of photographs obtained at six different strain levels. These photographs show the formation of new vacuoles while the older ones increase in size as the strains increase.

Once vacuole formation has started, it propagates to the vicinity of neighboring particles to produce a band or region of these failure [8–10]. A band normally lies perpendicular to the direction of straining and varies in thickness, depending on a number of factors including filler content, particle size distributions, the bond strength between the particle and the binder, and the binder strength properties. The manner in which these bands form provides the basis for a propellant classification system [9].

Filler-induced Stresses

To achieve a better understanding of the role of the filler in producing the stresses and strains which create vacuoles in the rubbery binder, microscopic estimates of the strain near large crystals of NH_4ClO_4 were compared with those derived theoretically by Sezawa and Miyazaki [11]. The studies of these
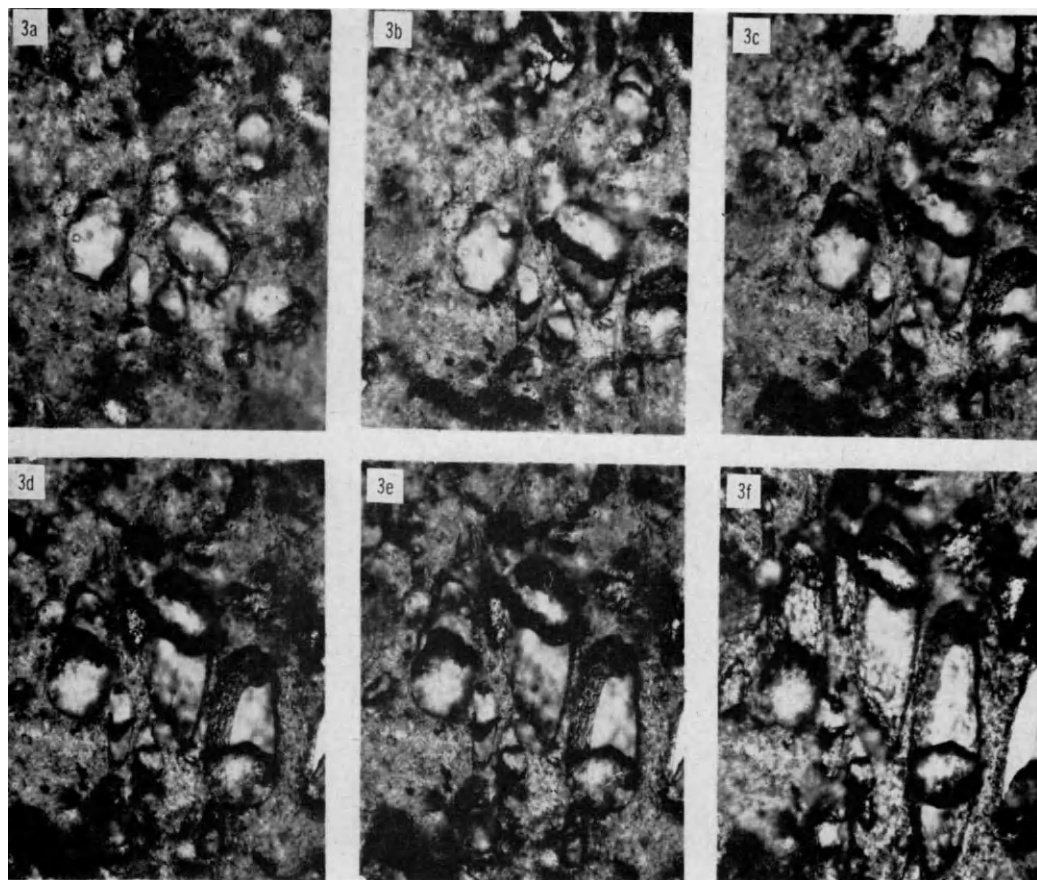
FIG. 3. Void formation seen in serial photomicrographs of a polyurethane propellant elongated from 0 to 80 per cent on Microstrain block.

Japanese investigators were summarized by Rehner [12] in a discussion of the theory of filler reinforcement in natural and synthetic rubbers.

The problem undertaken by Sezawa and Miyazaki is that of determining the stresses (and from these the strains) in the vicinity of a spherical particle of radius, a, which is embedded in an elastic medium of infinite extent. It was assumed that: (1) the elastic material is subjected to a uniform axial tension, T, at an infinite distance from the particle; (2) an infinitesimal deformation occurs; and (3) the fuel is rigidly bonded to the particle. These assumptions permit the

application of the classical theory of elasticity to the problem. The equations were solved by Sezawa and Miyazaki [11] yielding the following stress relation:

$$\frac{\tau_{rr}}{T} = C_1 + C_2 \frac{a^3}{r^3} + C_3 \frac{a^5}{r^5} \tag{1}$$

where τ_{rr} is the radial stress (psi), T is the tension (psi) on the matrix at infinite distance from the particle, a is the radius of the particle, and r the distance to the point at which the stress is calculated, both measured from the center of the particle and expressed in consistent dimensions. The constants, C_1, C_2, and C_3, are complex relations involving the elastic constants of the rubber matrix and of the particle.
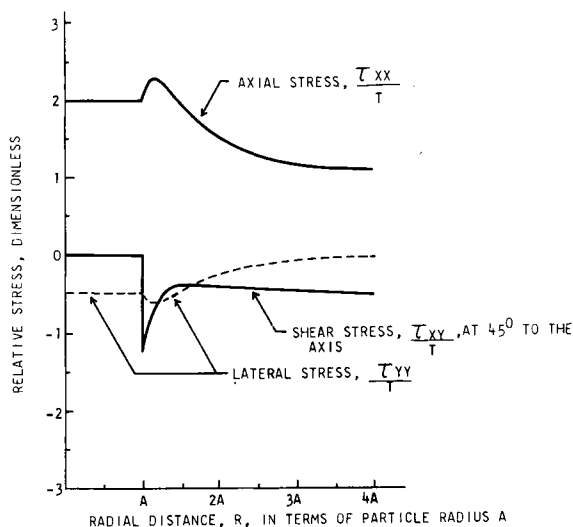
FIG. 4. Relative stress around a spherical particle as a function of the radial distance.

Approximations of the relations have been made for particles of NH_4ClO_4 embedded in polyurethane binder. In these calculations, a bulk modulus value of 2.63×10^6 psi was used for NH_4ClO_4 [13], Poisson's ratio was assumed to be 0.28 and NH_4ClO_4 was treated as though it were isotropic. Use of these assumptions could produce only negligible errors. The bulk modulus of 2.22×10^5 psi and the equilibrium shear modulus of 56 psi for the polyurethane binder were obtained from bulk modulus and stress relaxation measurements.

Inserting these values into eqn. (1) and converting to a Cartesian coordinate system, the relative axial stress, τ_{xx}/T (in the direction of tensile pull) was calculated as a function of the distance, r, from the center of the particles. The results of the calculation are shown in Fig. 4. Note that the stress in the rubber increases to a maximum of 2.28 times the tension, T, at 0.15 radii outside the surface of the particle, then decreases asymptotically to the tension, T, at high values of the radius.

The lateral stress, τ_{yy}/T (perpendicular to the direction of tensile pull) was obtained in a similar manner and is also shown in Fig. 4. The stress is found to be compressive and to reach a minimum of $-0.64\ T$ at $1.2\ a$ and then to approach zero at large distances from the particle.
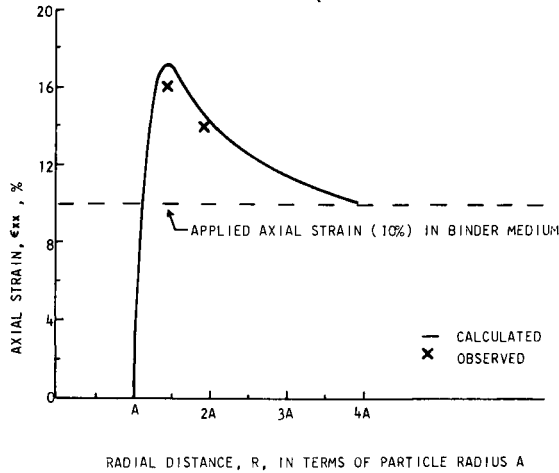
FIG. 5. Axial strain around a spherical particle as a function of radial distance.
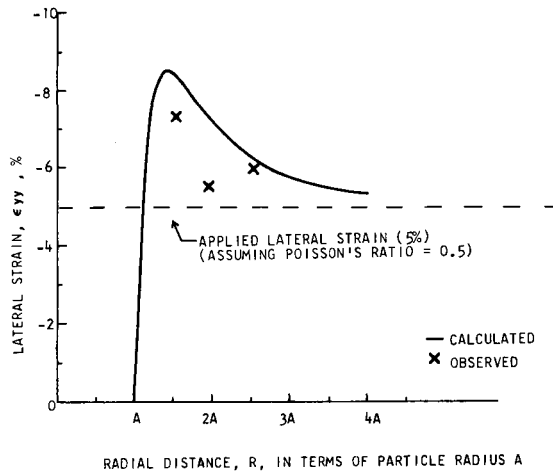
FIG. 6. Lateral strain around a spherical particle as a function of radial distance.

The shear stress, τ_{xy}/T (at a 45° angle to the direction of tensile pull) was calculated by a relation similar to eqn. (1), giving the results shown also in Fig. 4. In this case, the absolute value of the shear stress reaches a maximum at the bond line between the particle and the fuel.

Comparison is made in Figs. 5 and 6, respectively, between the axial and lateral strain values, calculated by the theoretical relations of Sezawa and Miyazaki, and the observed strain values determined during microscopic studies

35

conducted at Aerojet.* The strain values were computed from the stress data presented in Fig. 4, using the classical theory of elasticity. For this computation, the tension, T, for the system under 10 per cent overall macroscopic strain was determined from the ideal theory of rubber elasticity to be 16.7 psi. The observed strains correlate quite well with the calculated strains considering the assumptions made in the calculations and the difficulties encountered in the microscopic measurements of strain.

The calculations described above were extended to yield the entire stress and strain distribution in one plane, shown in Fig. 7. These results provide the stress
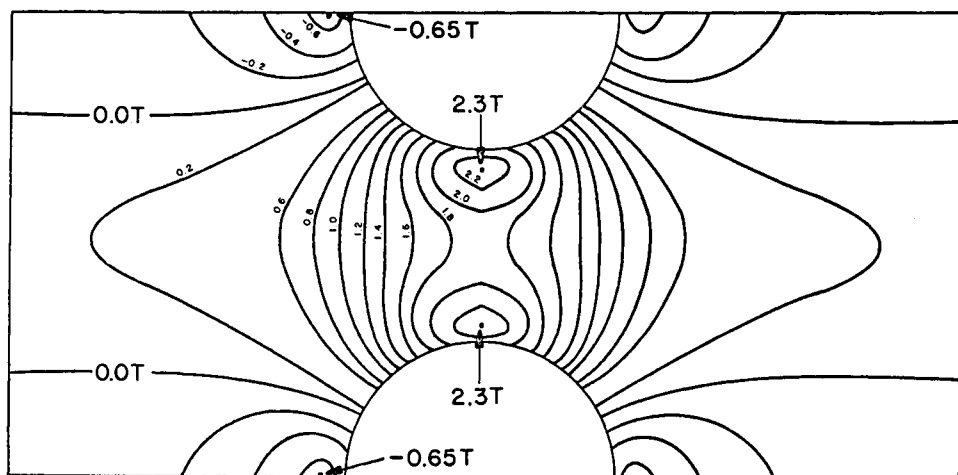
FIG. 7. Binder stresses between adjacent particles with vertical loading. The values are expressed in terms of T, the overall applied tensile stress.

and strain contours, respectively, in the fuel near a spherical particle of ammonium perchlorate of arbitrary radius. A tension of 16.7 psi and a strain of 10 per cent at infinity was assumed in making these calculations. It is important to note that a strain of 17.3 per cent and a stress of 38.4 psi were calculated for a point near the particle. The analysis shows that local stresses and strains can rise significantly above the applied overall stress, with the maxima occurring away from the surface of the particle. The prediction of maximum stress location is borne out by the experiments of Oberth and Bruenner [7], who have related the first appearance of vacuoles to the local stress, as follows.

$$\sigma = \frac{E_B}{2} + 8 \tag{2}$$

where E_B is the modulus of the unfilled binder. They suggest that eqn. (2), derived from tests at atmospheric pressure, can be generalized to other pressures,

* Motion of very fine particles on sheets of the rubber and near embedded large particles of NH_4ClO_4.

P, and stress concentrations, C, other than $C \simeq 2$ for spheres,

$$\sigma = \frac{E_B + P}{C} \tag{3}$$

Rate of Vacuole Formation

Since the vacuoles are the only significant contributors to strain dilatation in filled elastomers, the most appropriate manner in which to study the frequency of these microscopic failures is to analyze dilatation-strain data according to rules developed with the aid of microscopic examinations and statistical analyses.
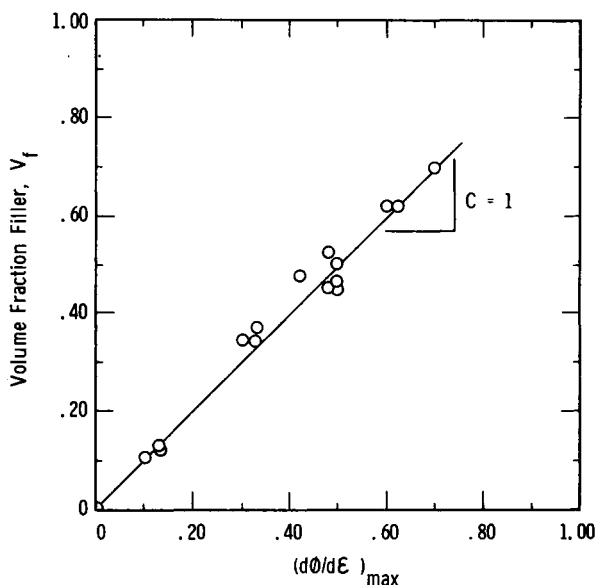
FIG. 8. Effect of fraction of solids on maximum rate of dilatation in constant rate test for systems that tend to dewet completely.

Such a treatment has been developed by Farris [6] in the form of a stochastic model which, from the dilatation-strain behavior, allows calculations of both the cumulative and instantaneous frequencies of vacuole formation in terms of the volume fraction of solids participating. In this model, the first derivative of dilatation with respect to strain is proportional to the volume fraction of filler participating in the dilatation process*, as shown in Fig. 8, for glass and polyethylene bead fillers, including data of Smith [3]. This differential technique eliminates consideration of vacuole growth, leaving only a cumulative frequency. The second derivative of dilatation with respect to strain measures the rate at which new vacuoles are being formed and has the shape of a frequency-distribution or differential probability-density function. Figure 9 illustrates the general shape of the dilatation-strain curve and its first and second strain derivatives.

---

* For a wide range of particle sizes, only the coarser particles appear to enter the process.

Strain, ε , in./in.
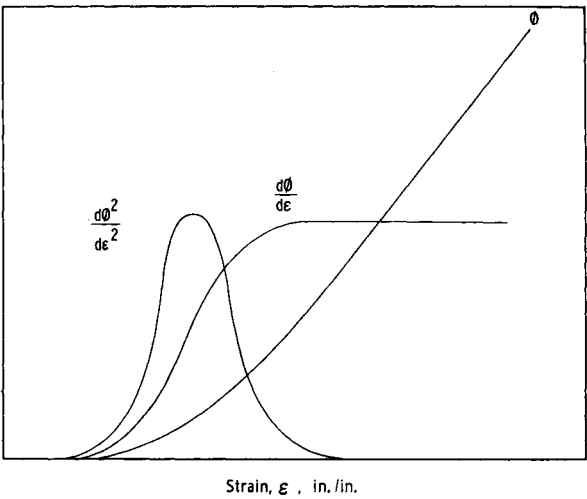
FIG. 9. Typical dilatation, ϕ, with strain, ϵ, showing shape of first and second derivatives.

Strain, ε , in./in.
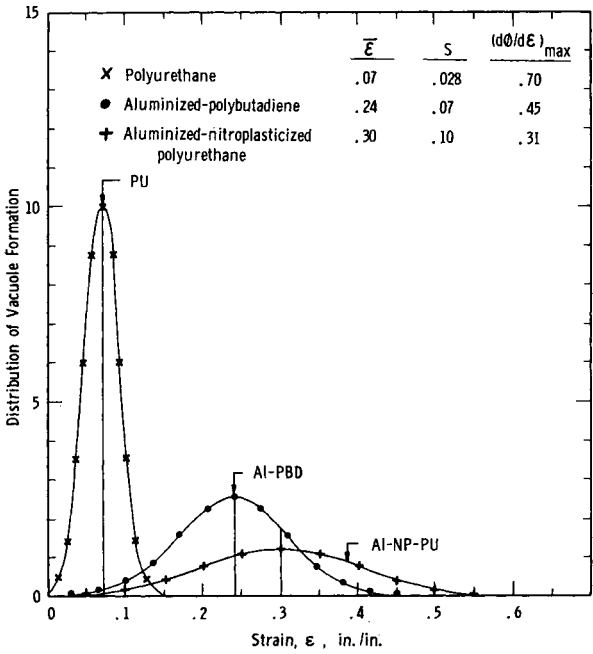
FIG. 10. Typical distributions of vacuole formation as computed for three different Aerojet propellants.

The probability-density functions computed by Farris from observed dilatation curves are almost always normal, or Gaussian, enabling their characterization by normal statistical parameters requiring only a mean, standard deviation, and total probability density. This allows simple comparisons of propellant systems, as the mean strain of the frequency distribution, $\bar\epsilon$, describes the strain
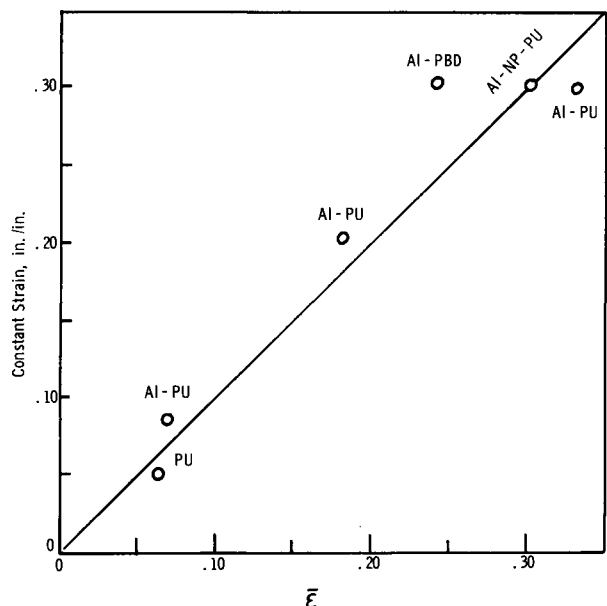
FIG. 11. Comparison of observed constant strain behavior with the mean strain of the dewetting distribution, $\bar{\epsilon}$.

TABLE 1. ULTIMATE STRAIN AND VACUOLE VALUES FOR TYPICAL AEROJET SOLID PROPELLANTS

Propellant	ϵ_b	$\bar{\epsilon}$	S	n_b
Aluminized-nitroplasticized polyurethane	0.58	0.30	0.10	2.8
Aluminized polyurethane	0.80	0.33	0.135	3.5
Aluminized polyurethane	0.42	0.18	0.090	2.9
Aluminized polybutadiene	0.40	0.24	0.070	2.3
Aluminized polyurethane	0.22	0.105	0.044	2.5
Polyurethane	0.15	0.07	0.028	3.0

ϵ_b = strain at break
$\bar{\epsilon}$ = mean of distribution of vacuole formation
S = standard deviation of distribution of vacuole formation
n_b = number of standard deviations above mean where failure occured

value about which the dilatation is centered, the standard deviation, S, measures the range of strain in which the microscopic vacuoles form, and the total probability density, $(d\phi/d\epsilon)_{max}$, describes the total vacuole production. An example of this comparison is given in Fig. 10, which compares the probability-density functions for the three propellants illustrated in Fig. 1.

The fracture properties of propellants under various test conditions can be related to these distributions of microscopic failures in various ways, as illustrated in Fig. 11 and Table 1. Figure 11 shows the correspondence between the maximum strain level at which a propellant can be maintained for one week

without failure and the mean of the probability-density function. Table 1 illustrates that, under similar constant rates of extension to failure, propellants of various strain capabilities fail at essentially the same point in their respective probability-density functions. Where this occurs depends on both rate and temperature, but these data demonstrate again the dominating role that vacuole formation plays in the failure processes of highly filled elastomers.

Classification of Propellants

Propellant dilatation characteristics, as revealed during tensile testing, have been used by Bills and Wiegand [9] as a basis for a propellant classification system. This system, which groups all composite propellants into four classes according to their observed dilatational behavior, is reproduced in Table 2. It is pertinent to the study of failure mechanisms that the dilatational character and, hence, the classification of composite propellants, changes with temperature and strain rate. The dilatation and, hence, the classification, shifts gradually with decreasing temperature or increasing strain rate from the Class 1 to the Class 4 behavior.

TABLE 2. PROPELLANT CLASSIFICATION SYSTEM

Class	Description	Mathematical relation
1	Essentially uniform dilatation is observed as the break point is reached.	For the special case where dilatation may be considered uniform at all points of strain, the finite deformation relations of Blatz [14] offer a good first approximation. A mathematical description by strain energy functions appears to be the most promising approach.
2	Dewetting occurs in two or more bands throughout the gage length of the specimen. Local sites of dewetting occur generally throughout the specimen.	A mathematical approximation by strain energy functions appears to be the most promising approach.
3	Dewetting occurs generally in one narrow band only.	A mathematical approximation by strain energy functions appears to be the most promising approach.
4	No dewetting occurs up to the break point, typical of propellants below their glassy temperature.	The classical theory of elasticity applies quite well to these materials.

Most of the propellants in use today are Class 1 or 2 at 100°F and Class 3 (approaching Class 4) below 0°F. In the high-temperature and low-strain-rate regions (Class 1 or 2 behaviors), the failures tend to be of a ductile nature, whereas at the lower temperatures and higher strain rates (Class 3 or 4), failures show more of the brittle phenomena.

It can be seen from the discussions of vacuoles that their formation and growth constitute the first steps in the propellant failure process. It is clear that the mechanisms, energetics, and statistics of propellant failure on a microscopic scale must be known before grain failures can be clearly understood.

2.3. *Path Dependency of Propellant Behaviors*

Propellant mechanical property research of the last two years has revealed that many of the anomalies that have been troubling us are attributable to the dependency of failure behavior on the stress–strain–time–temperature path that the material traverses. Path dependency is important regardless of whether the imposed stresses and strains are constant or oscillating. Its understanding offers promise of permitting the generation of one general set of criteria that will apply to constant strain (or constant stress), intermittent strain, and oscillating strain regimes applied in any sequence.

Strain–Temperature Paths

The first situation in which path dependency was recognized as a determining factor was in the determination of the strain-bearing capability of a propellant at low temperatures. Propellant in slowly cooled motors survive greater strains than the same propellant (precooled) would withstand in laboratory tensile or constant strain tests. This was clearly illustrated in the results obtained when aluminized polyurethane propellant specimens were strained or cooled along different paths to failure. These paths and the observed failure strains, ϵ_b, are given below:

Path	Description	Results
I	Cool specimen from 40°F to −75°F, then strain to break at strain rate of 0.74 min^{-1}	Average $\epsilon_b = 2.0\%$
II	Simultaneous cooling from 40°F to −75°F at 10°/hr and straining at 1.08%/hr.	Average $\epsilon_b = 7.7\%$ (failure at − 30°F)
III	Specimens were given a 10% strain before following Path II above	Average $\epsilon_b = 21.9\%$ (failure at −75°F)
IV	Strain specimens to various levels at 40°F, then cool to− 75°F	Specimens survived strains up to 25% through 9-day tests at −75°F

From these data it can be seen that cooling before straining (Path I) gives the lowest value for ϵ_b, while straining before cooling (Path IV) gives the largest value. Paths II and III, which are more typical of the experiences of motors, gave intermediate values. Since Path I represents the conditions to which laboratory specimens are subjected in low-temperature tensile tests, it becomes obvious that such tensile test data are of only limited value for appraising the absolute low-temperature capability of propellants in motors, though they may

correlate in a statistical manner the relative quality of different batches of the same formulation.

This strain–time–temperature aspect of path dependency is consistent with what is known about the effects of temperature on the mobility of polymer chain segments. In fact, it should be predictable qualitatively from stress relaxation data measured over the pertinent temperature range.

Constant Strain Failures

Another area of propellant failure study that has proven revealing is the failure of propellant specimens under uniaxial constant strain conditions. The time-dependent effects are attributable in part to viscoelastic characteristics and in part to the accumulation of damage throughout the exposure periods. The strong influence of the sequence of exposure conditions shows that damage under constant strain conditions is definitely path-dependent.

The effects of time, strain level, and path have been studied conveniently on small uniaxial test specimens under both constant and intermittent strain conditions. To assist in interpreting the data, a new method of plotting motor and propellant failure data has been developed, based on the work of Coleman [15].

For propellant samples free from impulsive loading or oscillating loadings with periods equivalent to the relaxation times, the failure distribution can be written in exponential form as

$$- \log \frac{N(t)}{N(0)} = \int_0^t \Psi(\epsilon, t) \, dt \qquad (4)$$

where $N(t)/N(0)$ is the fraction of test specimens remaining unbroken at time, t, and $\Psi(\epsilon, t)$ is a function of strain and time.

This type of analysis has been applied to constant strain data. In one example, data were taken on a nitroplasticized polyurethane propellant at constant temperature and under humidity conditions close to those in equilibrium with the propellant. The strains were applied rapidly (within 20 sec) to each individual specimen; at least 20 specimens were used to generate each line. The results, illustrated in Fig. 12, show that the logarithm of the fraction of surviving specimens is a linear function of the time under strain.

The characteristic behavior, shown in Fig. 12, can be used as a reference for determining changes in the failure rate due to sample history, as well as various treatments designed to alter the properties of the propellant. For example, the curve at the left in Fig. 13 shows the results of a strain followed by a no-strain heat treatment and then by further strain. This test was an attempt to reheal in the survivors any initial tears produced by strain, as suggested by the experiments of Colodny [8]. The results showed rather that the survivors were weakened by the heat treatment.

The above data suggested that the weakening caused by the 135°F heat treatment was a degradation caused by oxygen absorbed during the constant strain period. To investigate this possibility, an experiment was performed to deter-

mine the effects of exposure of the samples to various atmospheres during the constant strain period. The results presented in Fig. 13 showed that the argon atmosphere caused a considerable decrease in the initial constant strain failure rate and a significant increase in the induction time to the first specimen failure. However, the rate of failure after a period of constant strain followed by heat treatment, both under argon, showed the same greatly increased failure rate as in air.
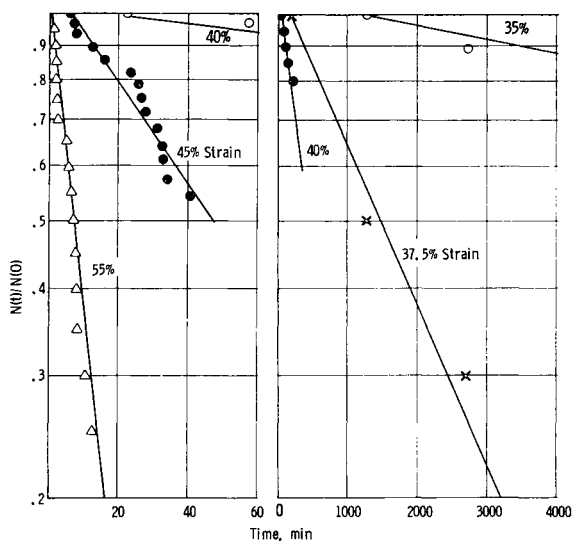
FIG. 12. Effect of increasing strain levels on the failures under constant strain conditions.

Further studies indicated that failure can result from repeated cycles of strain applied over relatively long periods (4 to 14 days) at strain levels less than the lowest level which produces failure under constant strain. The failure rate appears to depend on the number of cycles, as shown in Fig. 14, and on the strain level. It also appears that stress levels exist below which very little damage is done to propellant on repeat cycles and that as this critical stress level is exceeded, the rate of damage incurred by the propellant specimens increases rapidly. This is borne out in Fig. 15 for small motor studies under repeated thermal cycling to provide the strain.

A model, which explains the constant strain test data, assumes that damage is caused by stresses applied for a prolonged period. Short-term stress applications, such as those produced during dynamic testing, produce cavities or flaws which may reheal, but longer term applications allow the migration or rearrangement of broken polymer bonds away from the site of formation so that relatively little chance exists for the failure area to reheal. An additional factor to consider in constant strain tests is the stress relaxation which proceeds in the rubber binder. As binder stresses decay, rates of flaw growth decrease, and if the stress decays below the critical level, the first strain application will not cause failure.

By this concept, a strain level exists below which failure will not occur on the first strain application because the stress causing damage relaxes to a level which will no longer propagate flaws in the time period of the test. Repeated strain applications which are applied before the propellant can recover from the
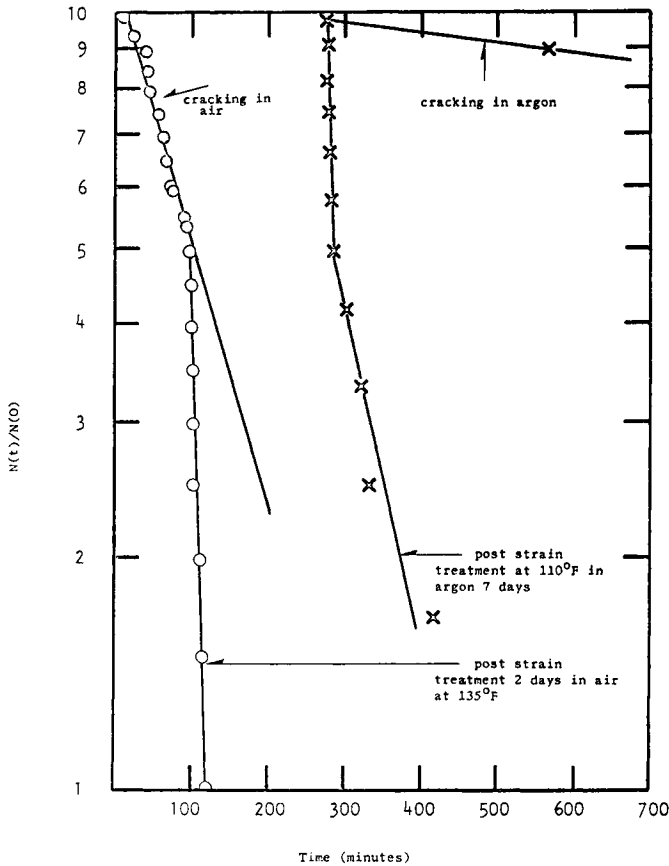
FIG. 13. The effect of combined strain and heat treatment for both air and inert atmospheres on failure of a polyurethane propellant at 40 per cent constant strain.

relaxed strain will also not cause further damage. However, if all restraining forces are removed and the material is allowed, through temporary exposure to higher temperatures, to recover to such an extent that its modulus is increased, restraining will raise the material stresses above the critical no-damage level causing additional flaw growth and further failures.

Cumulative Damage

The cumulative damage concept recognizes that damage effects accumulate in propellant or a propellant-liner bond when either is subjected to repeated loadings. This accumulation of damage continues until, in critical cases, the
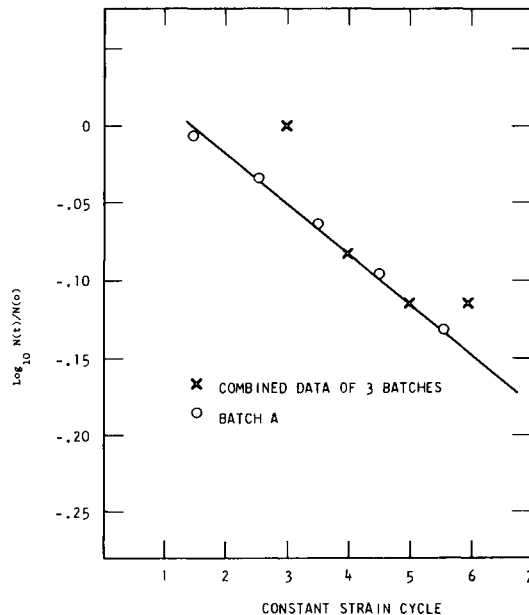
FIG. 14. The effect of repeat constant strain cycles on $\log_{10}$ survival ratio of Instron bars at constant strain of 20 per cent and 77° F. The normal one week test would give no failures at 30 per cent constant strain.
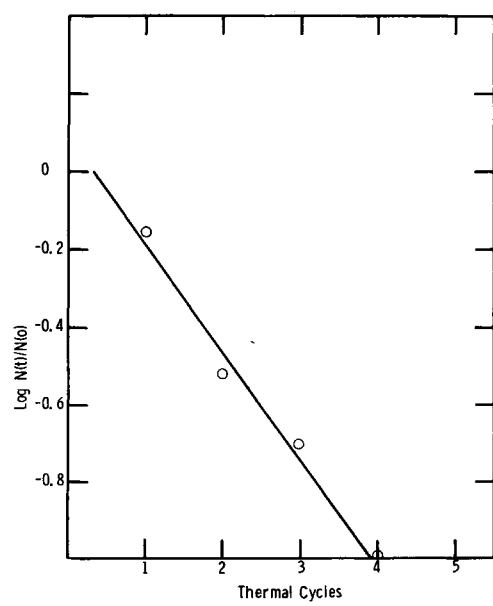
FIG. 15. The effect of repeat thermal cycles on a set of 5-in. diameter strain evaluation cylinders.

total damage equals that required to cause catastrophic failure. Although cumulative damage has not been recognized generally as being path-dependent, recent studies in our laboratories have shown that the extent of damage is somewhat dependent upon the sequence of the exposure conditions.

Considerable progress toward an understanding of the cumulative effects of motor or specimen conditions, including all transient stress conditions, has been accomplished in recent experimental studies on several propellants and propellant-liner systems [16]. In these studies, measurements were made of the failure times of the laboratory specimens under fatigue-cycling and constant-load conditions. Typical data are presented in Fig. 16.
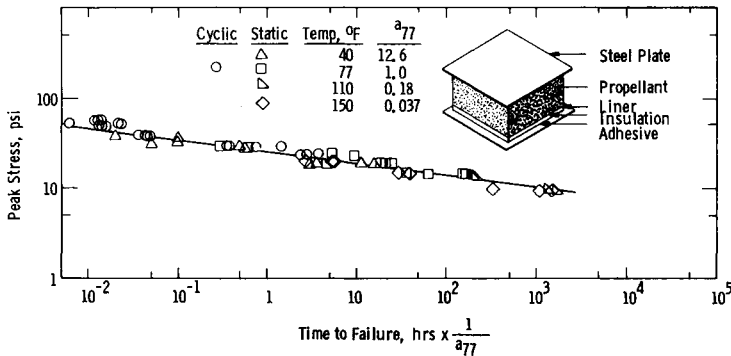
Fig. 16. Failure behavior of propellant-liner bonds subjected to 5 cps cyclic or to static stresses with effect of different temperatures accounted for by the horizontal shift factor a_{77},

In the analysis of the laboratory data, use was made of the exposure ratio, R_i, which is defined as follows:

$$R_i = \frac{\Delta t_i}{t_{fi}} \tag{5}$$

where Δt_i is the increment of time for which a specimen is exposed to the ith loading condition, and t_{fi} is the time required for the specimen to fail under that loading condition. It was hypothesized that the exposure ratio would be related to a damage ratio, D, defined as the ratio of the damage caused by the given exposure to the damage which will cause failure.

In the comparison of various cumulative damage relations between R and D, values of t_{fi} at each of the several load levels studied were taken from the linear regression analyses of all the oscillating-stress and constant-stress tensile data presented in Fig. 16 and used to compute cumulative sums of R_i values. The results are summarized in plots, such as Fig. 17, of ΣR_i versus cumulative failure probability for both the single-stress-level and the multiple-stress-level test data.

Analysis of the laboratory test data using various relations between D and R showed a sufficient agreement with the following

$$\sum_{i=1}^{n} D_i = \sum_{i=1}^{n} R_i \tag{6}$$

that this linear relationship, generally attributed to Miner [17], was selected as the primary cumulative damage relation for the propellant-liner bond and for the propellant of the system studied. The fact that the single straight line in Fig. 17 satisfactorily represents both single-stress-level and multiple-stress-level data sufficiently confirmed the applicability of Miner's relation to these laboratory test data to warrant its application to the prediction of the failure behavior of propellant-liner bonds in full scale solid rocket motors.
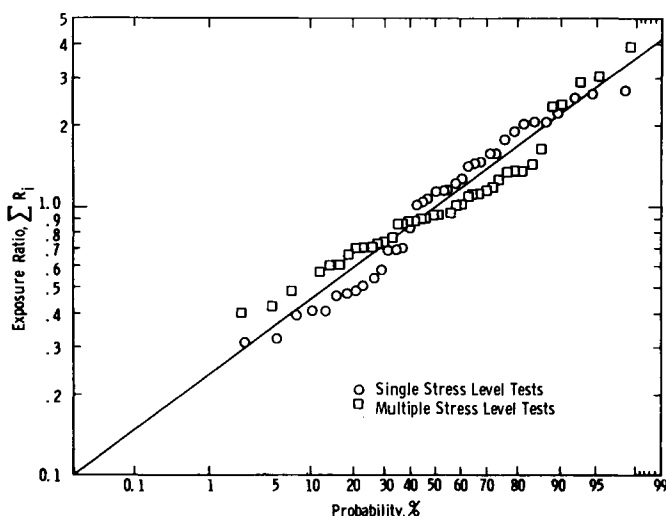
FIG. 17. Probability of failure at given exposure ratios.

Various procedures were compared during the development of the cumulative damage approach. Studies based on strain level were carried out using procedures similar to those subsequently employed by Darwell, Leeming, and Parker [18]. Although controlled strain tests showed some merit, an approach based on stress level appears to be more readily applicable to highly filled composite propellants.

Several conclusions, drawn from these studies, present implications which must be explained by any satisfactory failure theory. These include:

(1) Effects of temperature on log stress-log time-to-failure curves are satisfactorily handled by the Williams–Landel–Ferry technique [39].

(2) In oscillating-stress tests, frequency had little effect on time to failure, thus differing from the behavior of metals wherein the number of cycles determines the damage level.

(3) The energy of activation for constant load failure of one polyurethane composite propellant, as derived from a rate reciprocal temperature plot, was found to be 20 kcal/mole.

(4) Cumulative damage effects were found to be path-dependent in a manner that varies from one propellant to another. For one nitroplasticized polyurethane propellant, a loading sequence involving high initial loads caused

greater damage than did the inverse loading sequence (low initial loads). In a series of tests on another polyurethane propellant, no path-dependency was observed. In a series of tests on a polybutadiene propellant, the damage was greatest when the loads, initially low, were increased during the test.

(5) Recovery of strength has been observed in certain cases in which fatigued specimens were allowed to recover with all external stresses removed.

The results of the above cumulative damage studies indicate that a flaw genesis phenomenon is involved. As the number of vacuoles increases, the dispersion of the failure data will decrease. This prediction, in conjunction with the experimental correlation between constant load failure and cyclic fatigue failure, indicates that failure involves a rate process. Majerus [19] has suggested that this rate phenomenon can be treated by a governing differential equation used in conjunction with the constitutive equation of a multiphased material. It can be studied using statistical mechanics in conjunction with a mathematical material model, with the final multiphase model established from thermodynamic and quasi-static approaches. It appears that the main variables of this constitutive equation are stress, strain, time, volume, temperature, and material environment.

Although past cumulative damage work has demonstrated the role of the stress-time factor in path-dependence, i.e. the effects of frequency and of shifting stress levels, the influence of temperature on cumulative damage effects has not yet been explored.

3. ESTABLISHMENT OF MECHANICAL PROPERTIES CRITERIA

The ultimate objective of a major part of the recent mechanical properties research has been the establishment of mechanical properties criteria for propellants and propellant-liner bonds. The work to establish valid failure criteria for propellant grains can be performed in three major parts: first, the identification of critical motor regions in which the stresses and strains may cause failures in actual motors; second, the laboratory measurement of failure behavior in propellant specimens; and third, the correlation of specimen failure with motor failure.

3.1. *Prediction of Motor Stresses and Strains*

One of the first steps in the establishment of grain failure criteria is the determination of the stress and strain distributions in grains under both storage and firing conditions. These objectives are attained by performing stress analyses on the grain configuration while taking into account the proposed method of mounting the grain in the chamber [20–23]. With the present capacity of computers, such as the IBM 7090, stress analyses usually require the assumption of simple regular shapes, such as grains with cylindrical cores. The results obtained for these simple shapes are modified for grains with complex configurations by the use of photoelastically determined star point stress concentration factors.

The latter can be determined for complex three-dimensional configurations by frozen photoelastic analysis of a scale model [24, 25].

As the studies in this area advanced, it became evident that for pressurization and thermal cycling, the observed strains agreed closely with those calculated for a simple elastic, incompressible material whose modulus had little effect and
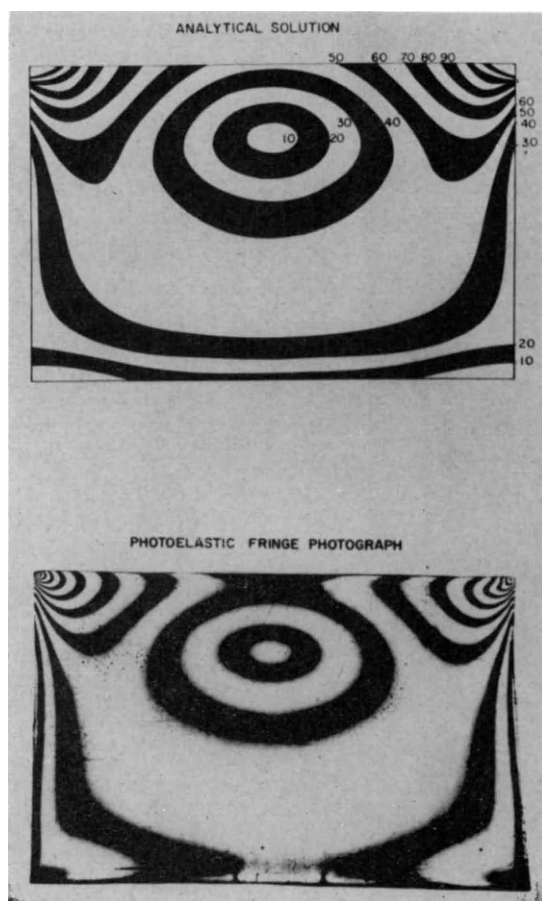
FIG. 18. Comparison of experimental and analytical contours of constant principal stress difference for case-bonded tubular grains.

whose pertinent properties appeared to be only the thermal coefficient of expansion (for temperature cycling) and the bulk modulus (for pressurization). The good correlation between the calculated stress distribution and that observed in a photoelastic scale model for a tubular end-bonded grain can be seen in Fig. 18.

Two methods exist for the modification of a given elastic grain structural analysis to provide for viscoelastic behavior. One method is mathematical and

employs the Laplace transform inversion techniques of R. A. Schapery [26]. This method provides an accurate determination of the time-dependent behavior of the solid propellant grain. The second method is an empirical one employing the experimental observation that time and strain are separate functions in the stress relaxation equations of solid propellant materials [27]. This method proves as satisfactory as the Schapery method if the time-dependent "effective" moduli are substituted for measured moduli. This relationship has a special merit when considering the essentially negligible slump deformations at the inner bore.
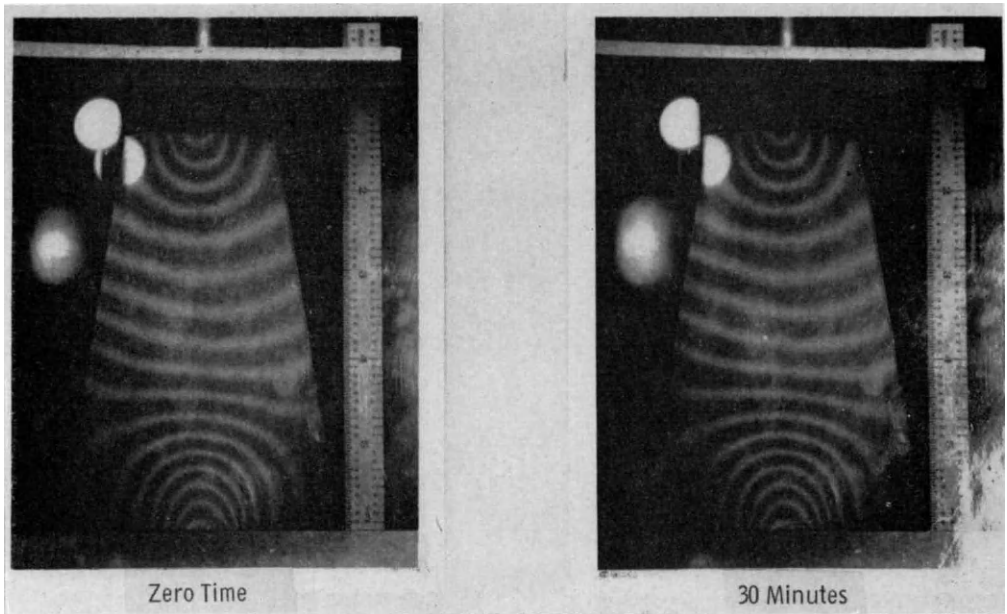
FIG. 19. Separation of strain and time of a complex configuration under stress relaxation conditions shown by Moiré patterns.

The relative rate of stress decay appears to be dependent solely on time and is independent of both the strain level and the complexity of the stress-strain field, except for non-linear effects to be discussed later. This independence was effectively demonstrated on a variety of specimens held under constant strain using the Moiré fringe techniques of optically interfering grid patterns to monitor the strain fields as the stresses relaxed in the specimens. Although the stresses continued to relax markedly, the strain patterns did not change with time, indicating no rearrangement of strains throughout the specimen. An example of this constancy of strain distribution for a truncated disc under constant compression displacement is seen by comparing the patterns at two times, as shown in Fig. 19.

3.2. Empirical Approaches

The difficulties associated with the application of theoretical failure criteria in their current state of development have led to the formulation of design failure criteria based on empirical correlations among laboratory test results, calculated values of stresses and strains, and observed failures in model motors. This empirical approach provides, therefore, a logical foundation for inductive derivation of theories of material failure.

Simulated Use Tests

In one type of laboratory test that has been used to establish failure limits, primary emphasis has been placed on reproducing experimentally the stress-strain environment shown by analysis to characterize the inner bore hoop strains and bond stresses experienced during storage, static firing, or flight, using motor conditions selected to give the most critical condition found in the system under study. For example, since the critical inner bore hoop strains are biaxial, specimens have been designed to test the propellant under biaxial stresses. For storage conditions, constant strain and constant load tests are used at appropriate temperatures. For firing and flight conditions, high strain rates are imposed on specimens subjected to hydrostatic pressure [28]. The ability of specimens to resist interfacial bond failure is measured using propellant-liner bond specimens designed for application of any combination of tension and shear at the interface [29]. The results of these tests, with appropriate safety factors, are compared with calculated requirements to assess probable performance in a motor.

For correlation studies, subscale motor testing has been restricted primarily to thermal cycling, with only limited studies under simulated firing conditions. In the latter tests, cylindrical case-bonded grains are subjected to decreasing temperatures at a specified cooling rate. Inner bore strains are measured at each temperature until the strain at failure is noted. This failure strain is then correlated statistically with various other test parameters.

Each of the above procedures is subject to a number of limitations. First, the assumption of no dilatation leads to estimates of inner bore strain which are higher than the actual strains. The second limitation is the lack of knowledge of local strain distributions as failure is approached and of the steps from initiation to actual failure. Third, these correlations do not account for path-dependency.

Criteria from Empirical Correlations

Correlations of failure in test specimens with the failure of motor grains have been found to involve two temperature regions: (1) above 0°F, and (2) below 0°F [9]. The need for separate correlations above and below 0°F is related to differences in the failure mode. Above 0°F, time under strain is a major factor; below 0°F, strain level is the most important.

Several investigators have proposed the use of design failure criteria derived from the stress-strain curves of laboratory specimens [10, 27, 30]. A typical

curve and the derived parameters are illustrated in Fig. 20. Landel [27] proposed two parameters, ϵ_L and ϵ_C, as indicators of the maximum strain capability of the propellant. The first, ϵ_L, has been taken here as the ratio of the nominal maximum stress, σ_m, to the tensile modulus, E.* The second, ϵ_C, equals two-thirds the strain at the nominal maximum stress in the standard tensile test at 77°F. He also pointed out that ϵ_L is better defined than ϵ_C and suggested that the indicated strain corresponds approximately to the strain level at which separation of the oxidizer and the binder starts. Milloway and Wiegand [10]
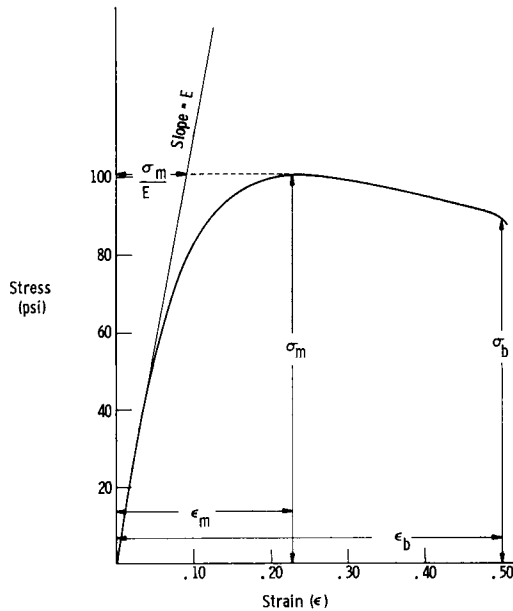
FIG. 20. Typical stress–strain curve for propellant.

suggested that the motor strain should be less than half the ultimate elongation, ϵ_b, of a tensile specimen tested at a strain rate of 0.74 min⁻¹ for no failures to occur, based on tests of forty-one small subscale motors.

That all three of the failure criteria, ϵ_L, ϵ_C, and $\epsilon_b/2$, met with success in predicting failures indicated a degree of correlation among them. Data were gathered [31] from seven different propellant formulations drawn from polyurethane and butadiene types for tests at temperatures from −100°F to 212°F. A plot of ϵ_L versus $\epsilon_b/2$, presented in Fig. 21, shows that many of the points cluster near the correlation line of unit slope. The data suggest that ϵ_L is the more conservative criterion since there are more points below the line than above it. Figure 22 of ϵ_L against ϵ_C shows that these two criteria are in good agreement up to 30 per cent strain with variability increasing with strain.

---

* The value, ϵ_L, was originally defined by Landel in terms of true stress in $\epsilon_L = \lambda_m \sigma_m / E$. This was pointed out by Landel in a recent review article [30] where he noted that this original definition gives better correlations than simply $\epsilon_L = \sigma_m / E$ as used in this paper.

Standard linear regression statistics for the interrelations are given in Table 3, assuming that the correlated variable contains all the variability and the independent variable is accurately known, an assumption clearly not rigorous.
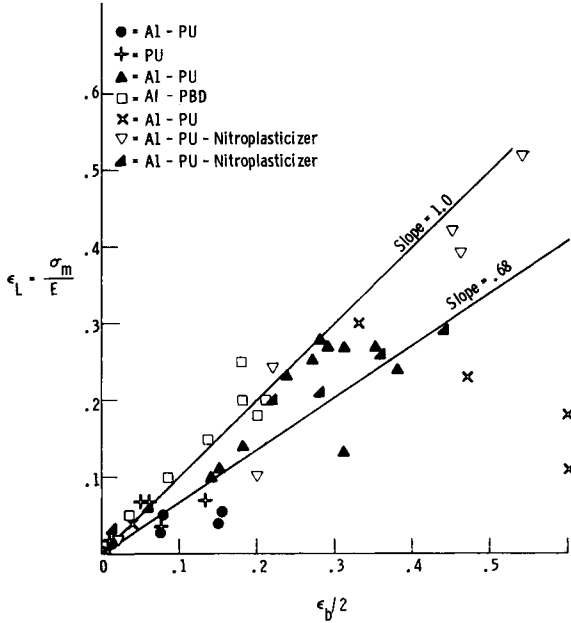
FIG. 21. The relationship between ϵ_L and $\epsilon_B/2$.
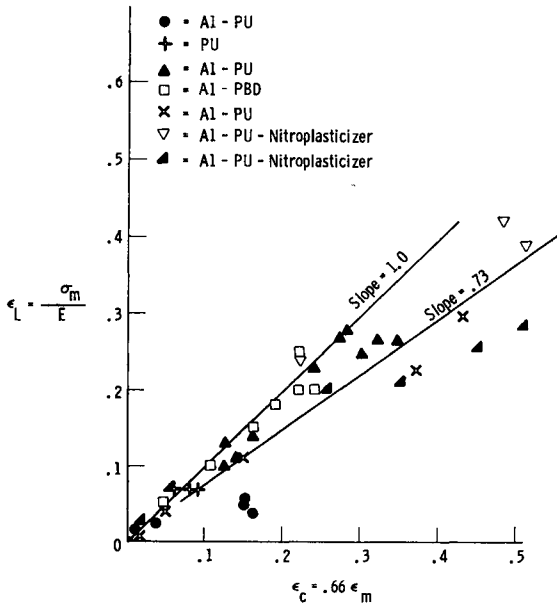
FIG. 22. The relationship between ϵ_L and ϵ_c.

TABLE 3. STATISTICAL DATA RELATING THE VARIOUS
STRESS–STRAIN PARAMETERS

$\epsilon_L = 0.677\,(1/2\;\epsilon_b)$	$r=0.83$	$\sigma_r=4.9$	$n=406$
$\epsilon_L = 0.730\;\epsilon_C$	$r=0.89$	$\sigma_r=3.9$	$n=406$
$\epsilon_b/2=0.918\;\epsilon_C$	$r=0.91$	$\sigma_r=4.5$	$n=406$

r = correlation coefficient
n = number of points
σ_r = standard deviation about the regression line

Since solid propellant exhibits a wide batch-to-batch variability of mechanical behavior, as shown in Fig. 23, any approach to failure prediction must include statistical methods of data analysis. Lack of sufficient full scale motor data has forced the extensive use of subscale motors to generate data. Thus, to provide motor failure data from an equivalent population as required for statistical analysis, subscale motors from a number of propellant batches with differing
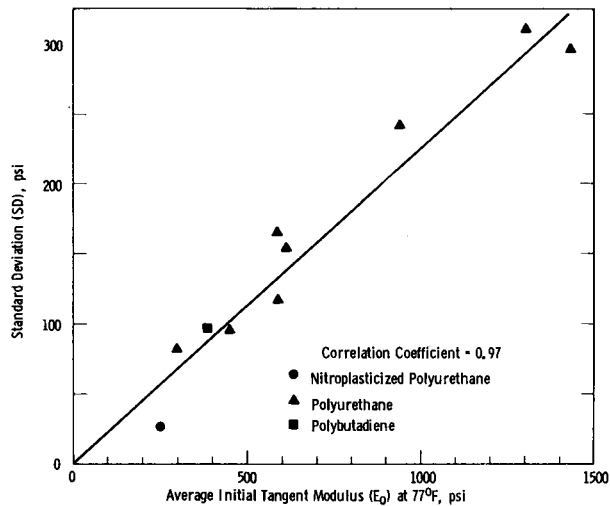
FIG. 23. Relation of modulus to the batch-to-batch standard deviation of production propellants.

properties are deliberately caused to fail by stepwise cooling to successively lower temperatures. Measurements of motor bore strain are made at closely spaced strain intervals prior to cracking to determine failure strain levels. At each inspection temperature, the strain, ϵ_{mm}, is measured at the point in the bore where the strains are maximum. The correlating property value, such as ϵ_L, should be determined in laboratory tensile tests at a strain rate approximating the strain rate developed in the motor during the cooling. An example of how such data can be normalized is illustrated in Fig. 24 for seven motors of a polybutadiene propellant [31]. Two superimposed sets of data are shown in Fig. 24; ϵ_L versus temperature; and the maximum motor strain, ϵ_{mm}, versus

temperature. The point where the ϵ_L and the ϵ_{mm} curves cross is assigned the ratio $\epsilon_{mm}/\epsilon_L = 1.0$ to normalize the data. Crosses are placed along the motor strain line to indicate the points where individual motors failed.

The use of the normalizing procedure of Fig. 24 in assessing the distribution of failure behavior is shown in Fig. 25. The data shown there include five propellant formulations, covering polyurethane, nitroplasticized polyurethane, and polybutadiene systems, with a total of thirteen batches represented. It can be seen that the failures are normally distributed for the bulk of the motors tested, but some few motors behave significantly better than would be predicted
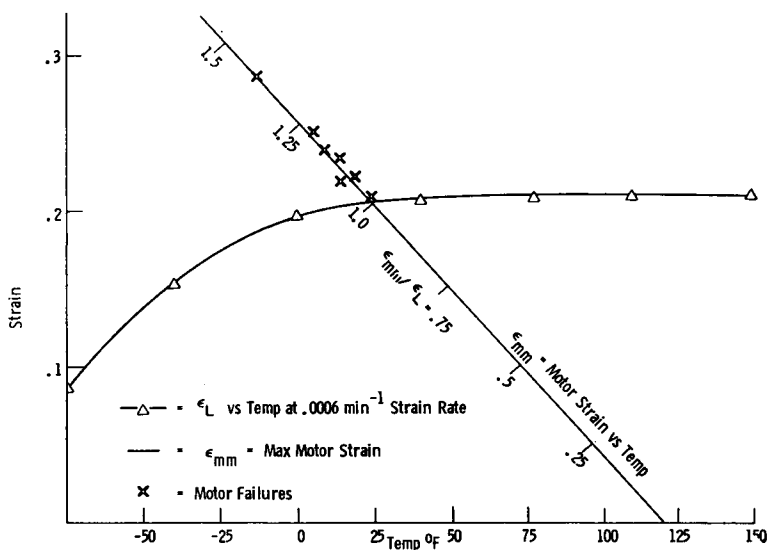
FIG. 24. Comparison of motor strains with very slow rate tensile criteria, showing normalizing procedure.

from the total distribution. These few unusual motors may represent propellant with an unusually small number of those microscopic defects which appear to control the distribution of failures. From a failure view, these successes occur too late to improve the use of the motor, but the causes which make such motors more resistant are of research interest.

Another method of looking at such data, utilizing the interference model [32] for normal or Gaussian distribution curves, is illustrated in Fig. 26. The rules for Gaussian distributions state that the sum or difference of paired values randomly selected from two independent normal distributions is another normal distribution with mean $= \bar{X} = \bar{X}_1 \pm \bar{X}_2$ and standard deviation $\sigma = \sqrt{\sigma_1^2 + \sigma_2^2}$, where the subscripts represent the two different populations. This allows prediction of the distribution of differences between the specimen elongation, ϵ_L, and the motor strains, ϵ_{mm}. When the value of this difference, $\epsilon_L - \epsilon_{mm}$, falls below zero, failure is predicted. The cumulation of these failure incidents, as

shown in Fig. 26, is represented by the area under the difference curve for all negative strain differences.

Studies have been made to determine the relation of propellant failures above 0°F to those occurring below 0°F. One such study of uniaxial data on one carton
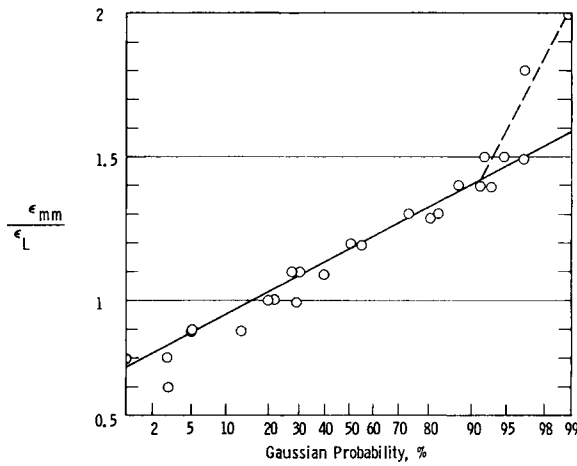
FIG. 25. Cumulative distribution of 95 small motor cycling failures against normalized strain.
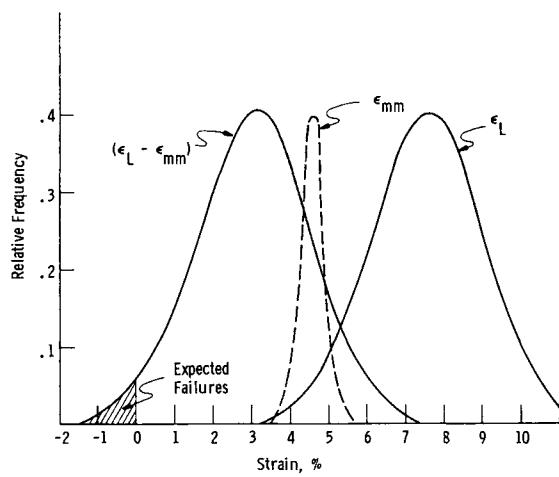
FIG. 26. Interference model for predicting failure distributions from the distributions of motor strain and specimen failures.

from each of forty batches of a polyurethane propellant was made on an Instron testing machine at the constant strain rate of 0.74 min^{-1} and at test temperatures from $-75°F$ to $180°F$. Correlation analysis of elongation at break, ϵ_b, between 77°F and ϵ_b at the other test temperatures show correlation coefficients of 0.932 at 180°F, 0.935 at 0°F, 0.689 at $-40°F$, and 0 at $-75°F$. This lack of correlation appears similar to that described by Landel and Fedors [33] for failure

envelopes developed for a wide range of crosslink densities. Correction factors which brought together the ambient and high temperature data did not decrease the variation of failure values at very low temperatures.

Since tests in the region of 0° to 180°F do not predict the relative order of quality among the batches at very low temperatures, any hypothesis of related failure behavior clearly is limited. This lack of correlation of quality outside of certain limits requires, therefore, a general study of each new system in order to define those limits within which relative quality is described statistically by any one test and outside of which additional tests are required. On the basis of such a study related to the environmental conditions of use, a minimum number of tests and test conditions can be selected to ensure adequate quality in the finally accepted motors.

4. FURTHER COMPLICATIONS

Grain stress analyses are based on assumptions that propellant is elastic or viscoelastic and that usually it is isotropic and incompressible. In some cases, allowance is made for dilatation, described in approximate form by assuming a mean value. Unfortunately, solid propellants display complexities which make these assumptions inaccurate to some extent. In this section, three of these complexities will be discussed briefly: first, the effect on strain distributions of modulus variations within a motor; second, the non-linearity of stress-strain relation in regions of high stress concentrations; and finally, the anisotropy which is always present in propellants to a greater or lesser degree.

4.1. *Structural Effects of Propellant Modulus Variations*

Until recently, it was assumed that propellant modulus had little effect on strains produced in a propellant, since the stiffness of the steel case is so high that the propellant strains, induced by cooling the motor, were determined by the difference in coefficients of thermal expansion of steel and propellant. The firing strains also are determined chiefly by the stiffness of the case, for the reinforcing effect of the propellant generally reduces the strains only slightly. In fiberglass-plastic motor cases, the cycling strains are similar, but the firing strains are much larger due to the greater case expansion. Again, the reduction in strain, caused by reinforcement of the case by the propellant, is not large. There is, however, an interaction between batches of different moduli in the same motor which can cause significant strain increases. The modulus in some instances also becomes critical because it determines the magnitude of the internal stresses produced as a result of the difference in the thermal expansion coefficients of the propellant and the case.

Changes in inner bore hoop strain in a cylindrical grain due to batch-to-batch differences in the modulus of the several propellant batches, cast successively into the motor, have been calculated by Messner [34]. His results are presented in Fig. 27, which shows the assumed modulus versus distance along the bore, and the strains obtained along the bore as influenced by these modulus changes.

The chance of attaining the extreme strain level pattern of Fig. 27 by chance in a four-batch motor is only 1/50,000, however. In the more usual case, a 10 per cent variation in maximum strain is the range to be expected. Since modulus variation also affects the bond stresses, hard propellants at the ends of a grain can increase the hazard of propellant-liner bond failures.
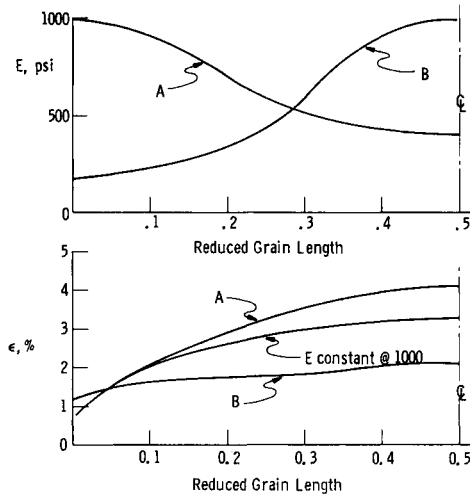
FIG. 27. Different extreme patterns of modulus distribution in a motor, and the maximum strains produced in a motor by these modulus variations, as compared to the strains in a motor with a constant modulus throughout.

4.2. Non-linear Behavior at Stress Concentrations

When strains increase in non-uniform strain regions, such as star points, the possible effects of the non-linear stress-strain behavior should be expected. This was demonstrated by Campbell [35] in experiments with specimens containing central holes and side semi-circular notches. The specimens were 0.5 in. thick, 2 in. wide, and 14 in. long, made of polybutadiene propellant. Moiré fringe patterns were applied and the specimens strained to three levels of strain.

The strain distribution at the minimum section of the central hole specimen, together with a Moiré fringe pattern of 200 lines/in., is shown in Fig. 28. Normalized strains, one minute after load applications, are shown for the three overall strains. The theoretical small deformation elastic strain distribution computed by the method of Howland [36] is also shown.

The measured propellant strain is everywhere greater than the computed elastic strain. Furthermore, the strain concentration increases with increasing displacement. Since the opposite behavior would be predicted for large elastic deformations, the propellant must be classed as a non-linear material. This behavior is also illustrated in Fig. 29 where the strain concentration at the edge of the hole is shown as a function of displacement. Small deformation theory [37] would predict a horizontal line at $\epsilon_x^L/\bar{\epsilon} = 3.14$ and large deformation

behavior would fall below this, varying from 3.14 to approximately 2.90 between the limits of $\bar{\epsilon} = 0$ and 0.07, respectively.

When the overall specimen strain was 5.28 per cent, the ratio, $\epsilon_x^L/\bar{\epsilon}$, increased from 3.30 initially to its maximum value (3.70) within 5 min after load application. These data show non-linearity affecting strain distribution with time not shown by the experiments illustrated in Fig. 19.
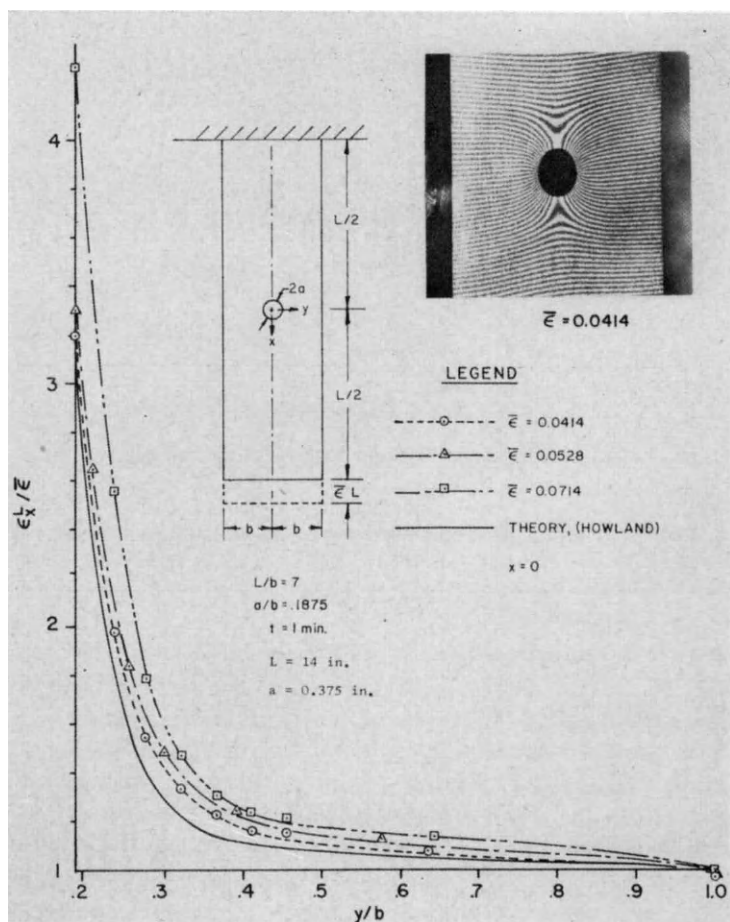
FIG. 28. Strain distribution in the strip specimen with a central circular hole.

4.3. Material Anisotropy

Some propellants have been found to exhibit significant anisotropic modulus effects, i.e. the tensile modulus of the propellant specimen depends on the original orientation of the specimen within the propellant grain, as shown in Table 4. Although this phenomenon is not understood entirely at present, it is felt that anisotropy is related to the volume fraction and particle shape of the

oxidizer. This tentative conclusion is supported also by the burning rate measurements in Table 4 which have shown the same level of anisotropic effects.

Material anisotropy is thus seen to be a further complication which must be recognized in the evaluation of samples and in the drafting of failure criteria.
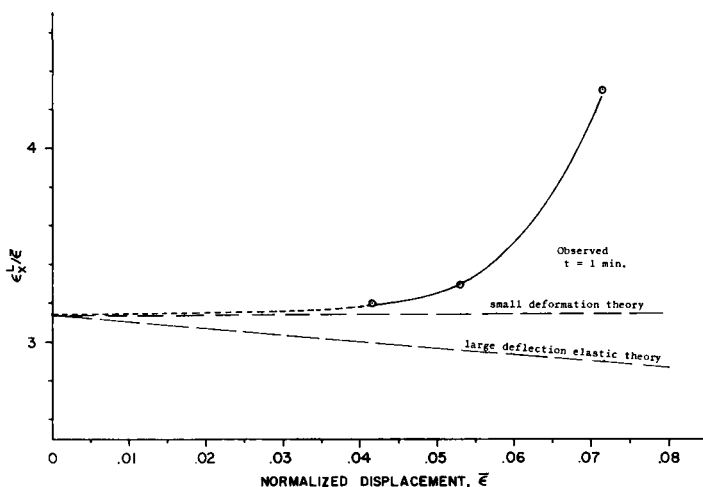
FIG. 29. Displacement-strain behavior at the hole edge.

TABLE 4. ANISOTROPIC BEHAVIORS OF FOUR PROPELLANTS FROM TENSILE AND BURNING RATE TESTS AT 77°F

Propellant	Orientation	σ_{nm}, psi	ϵ_b, %	E, psi	Burning rate, in./sec
Polyurethane No. 1	Vertical	178	83.1	494	0.237
	Horizontal	204	76.1	593	0.269
	Relative difference:	14.6%	8.0%	20.0%	13.5%
	Statistical significance*	Sig.	Sig.	Sig.	Sig.
Polyurethane No. 2	Vertical	114	48.9	629	—
	Horizontal	121	57.2	718	—
	Relative difference:	6.4%	6.7%	14.1%	—
	Statistical significance*	Sig.	N. Sig.	Sig.	—
Polybutadiene No. 1	Vertical	96.6	48.4	451	0.288
	Horizontal	99.3	43.3	567	0.314
	Relative difference:	2.8%	−10.5%	25.7%	9.0%
	Statistical significance*	Sig.	Sig.	Sig.	Sig.
Polybutadiene No. 2	Vertical	114.4	40.0	500	0.392
	Horizontal	118.5	36.1	571	0.448
	Relative difference:	6.5%	−9.7%	14.2%	14.3%
	Statistical significance*	Sig.	Sig.	Sig.	Sig.

* t-test, 95 per cent confidence.

5. DISTRIBUTION OF FAILURES IN FULL SCALE MOTORS

The development of failure criteria through the use of subscale motors has increased rapidly in the solid propellant industry. Confirmation of criteria for full scale motors has been limited because of insufficient and inadequate data.

Most of the available data has come from two sources. When failures of full scale motors have been encountered, statistical analysis is seldom possible because the detailed histories of the motors that failed are too complex. In some cases, however, special tests have been run on selected members of the remaining population to yield data suitable for analysis. The second source results as the
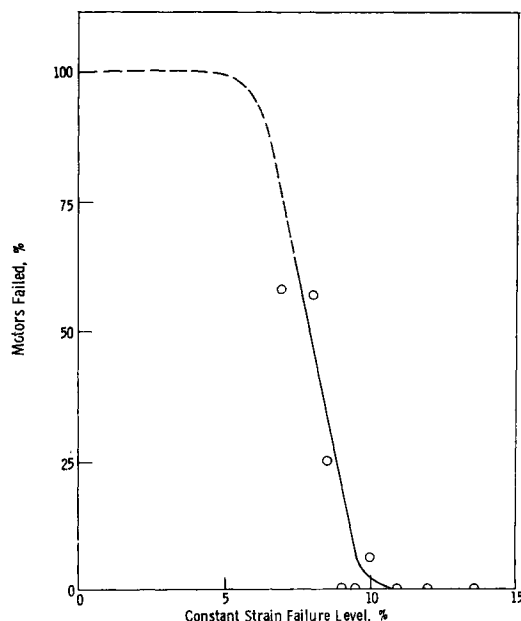
FIG. 30. Relation of fullscale motor failures at about 0° F storage to the constant strain failure levels of laboratory specimens taken from the motors.

large motors used for missile installations reach the end of life, as the reinspections at intervals ultimately show that defects have developed due to age alone. Data on failure or life distributions on such motors are invaluable when correlated with properties measured on the original and on the aged motors.

An example of the amount of information possible from a failure study is shown in Fig. 30. Motors from a suspect population were cooled to 0°F and the incidence of failure recorded. The data were grouped in terms of the constant strain level producing failure in one week for specimens cut from each motor after the cycling test. As one would expect, the failures in motors increase with decrease in strain capability, but the full distribution is not available from these limited data.

In studies of motor aging, recent efforts have been made to study the statistical

distributions of failures at the bond between the propellant and the liner, as a function of motor age. The stresses on this interfacial bond are most severe at the discontinuities, and even with stress relaxation, the force of gravity maintains a continuous stress on this region. Failures of these bonds can be detected by non-destructive techniques [38] on periodic inspections. Predictions of such failures have been attempted using cumulative stress life data, such as those shown in Fig. 16, which describe the statistical distribution of cumulative times to failure. Such cumulative damage behavior can be related to the stresses predicted from stress relaxation data. The predictions are subject to errors which cannot be adequately assessed, since experimental difficulties prevent obtaining adequate long time statistical distribution data on relaxation to characterize a given production. The probable accuracy of stress prediction is suggested by comparing predictions based on laboratory data with the earlier part of the non-destructive test data on some motors aged to end of life. In one case that was studied carefully, good agreement was obtained between calculated and observed life after reducing the mean predicted stress levels by 25 per cent.

The problems of data collection on full scale motors, and the time and care required in long term failure data collection, have delayed full confirmation of the statistical nature of full scale motor failure behavior. The importance of such data in assessing inventories and establishing adequate quality control procedures is bringing increased attention and support to this important area.

6. CONCLUSION

The failure behavior of solid composite propellants cannot as yet be generalized in a single failure criterion, but each formulation requires experimental evaluation over the range of stress–strain conditions expected in the motor. This is probably to be expected from the granular nature of these highly filled systems, modified by the wide variations in mechanical properties of the binder, and the strong role of binder-filler interactions in the failure process. Fortunately, the behavior of a given propellant system is sufficiently reproducible in the several conditions expected in use that a relatively small number of measurements serves to define the relative mechanical behavior of any batch from the total production. This is evidenced by the good agreement reached in empirical correlations of simple mechanical property tests with observed subscale motor behavior. Such correlations must take account of the statistical distribution of mechanical properties of solid propellants as it is reflected in a range of failure behavior of motors on cycling, storage, and firing. Knowledge of the statistical distributions obtainable from laboratory tests and subscale motor tests allows setting conservative design values of maximum motor strain to ensure reliable operation. The limited data available on failures in full-scale motors are consistent with both laboratory measurements and subscale motor experiments.

REFERENCES

[1] KRUSE, R. B., "Laboratory characterization of solid propellant mechanical properties", *AIAA Preprint* 65-147, Jan. 1965.

[2] SCHIPPEL, H. F., "Volume increases of compounded rubber under strain", *Ind. Eng. Chem.*, **12**, 33 (1920).

[3] SMITH, T. L., "Volume changes and dewetting in glass bead–polyvinyl chloride elastomeric composites under large deformations", *Trans. Soc. Rheol.*, **3**, 113 (1959).

[4] SVOB, G. J., COLODNY, P. C., WADDLE, L. A. and LEFFERDINK, T. B., "Volume changes in polyurethane propellants subjected to small strains", JANAF–ARPA–NASA Panel on Physical Properties of Solid Propellant, 20th Meeting Bulletin, SPIA/PP 14U, 295–306 (1961).

[5] FARRIS, R. J., "Dilatation of granular filled elastomers under high rates of strain", *J. Appl. Polymer Sci.*, **8**, 25 (1964).

[6] FARRIS, R. J., "Strain dilatation in solid propellants", *Bulletin of 3rd Annual Meeting of ICRPG Solid Propellant Working Group on Mechanical Behavior*, CPIA Publication No. 61U, Vol. I, p 291–302, October 1964.

[7] OBERTH, A. E. and BRUENNER, R. S., "Tear phenomena around solid inclusions in castable elastomers", *Trans. Soc. Rheol.*, **9**, Part 2, 168–185 (1965).

[8] WIEGAND, J. H., "Study of mechanical properties of solid rocket propellant", Report 0411–10F, Aerojet-General Corporation, May 1962.

[9] BILLS, J. W., Jr. and WIEGAND, J. H., "Relation of mechanical properties to solid rocket motor failure", *AIAA Jour.*, **1**, 2116 (1963).

[10] MILLOWAY, W. T. and WIEGAND, J. H., "Failure criteria for some polyurethane propellants", *J. Appl. Polymer Sci.*, **7**, 1325–39 (1963).

[11] SEZAWA and MIYAZAKI, *J. Soc. Mech. Eng.* (Tokyo), **31**, 625 (1928).

[12] REHNER, J., Jr., *Rubber Chem. and Tech.*, **17**, 865 (1944).

[13] BRIDGEMAN, P. W., *Proc. Am. Acad. Arts and Sciences*, **76**, 9 (1945).

[14] BLATZ, P. J. and KO, W. L., "Application of finite elastic theory to the deformation of rubbery materials", *Trans. Soc. Rheol.*, **6**, 223 (1962).

[15] COLEMAN, B. D., "Time dependence of mechanical breakdown phenomena", *J. Appl. Physics*, **27**, 862–6 (1956).

[16] BILLS, K. W., Jr., SVOB, G. J., PLANCK, R. W. and ERIKSSON, T. L., "A cumulative damage concept for propellant-liner bonds and its application to solid rocket motors", *AIAA Meeting Preprint* 65-191, February (1965).

[17] MINER, M. A., "Cumulative damage in fatigue", *Trans. A.S.M.E.*, **67**, A 159 (1945).

[18] DARWELL, H. M., PARKER, A. and LEEMING, H., "Mechanical behavior of cast-double-base propellants in rocket motors", *AIAA Meeting Preprint* 65-161, February 1965.

[19] MAJERUS, J. N. and TEMAKUNI, M., "Effect of material nonlinearity and failure criteria upon predicted propellant grain reliability", *AIAA Meeting Preprint* 65-158, February 1965.

[20] KRAUSE, I. and SHAFFER, P. W., "Thermal stresses in spherical case-bonded propellant grains", *A.S.M.E. Trans.*, **84B**, 144–148 (1962).

[21] UNGAR, E. E. and SHAFFER, P. W., "Thermally induced bond stresses in case-bonded propellant grains", *ARS Journal*, **30**, 366–8 (1960).

[22] WILLIAMS, M. L., "Some thermal stress design data for rocket grains", *ARS Journal*, **29**, 260–7 (1959).

[23] MESSNER, A. M. and SCHLIESSMANN, D. R., "Transient thermal stresses in solid propellant grains", First AIAA Annual Meeting, Washington, D.C., June 29–July 2, 1964, AIAA Paper No. 64-233.

[24] DANIEL, I. M. and DURELLI, A. J., "Photothermoelastic analysis of bonded propellant grains", *Experimental Mechanics*, **1**, 97–104 (1961).

[25] SAMPSON, R. C., "A three-dimensional photoelastic method for analysis of differential-contraction stresses", experimental mechanics, 3, 1–11 (1963).

[26] SCHAPERY, R. A., "Two simple approximate methods of Laplace transform inversion for viscoelastic stress analysis", GALCIT, 119, Contract No. AF 33(616)–8399, California Institute of Technology, Pasadena, California, November 1961.

[27] LANDEL, R. F., "Tensile testing of composite propellants", Combined Bimonthly Summary No. 66 for the Period 1 June 1958 to 1 August 1958, Jet Propulsion Laboratory, California Institute of Technology, 1958.

[28] HAZELTON, I. G., "Effect of rate and superimposed pressure on tensile properties of composite solid propellants", Presented at the *Fifth International Symposium on High Speed Testing*, Boston, Mass., March 1965.

[29] DIXON, J. D., "Three dimensional photoelastic analysis of a scarf joint for propellant-liner bond strength testing", Aerojet-General Corp., Sacramento, Report PEL–44, Jan. 1964.

[30] LANDEL, R. F., "Rupture of elastomers and propellants", *Solid Rocket Structural Integrity Abstracts*, **2**, 1–22, January 1965.

[31] BRIAR, H. P. and WIEGAND, J. H., "Statistical aspects of propellant behavior", *AIAA Meeting Reprint* 65–148, February 1965, included in survey paper: Majervs, J.N., Brair, H.P., and Wiegand, J. H., "Behaviour and variability of solid propellants and criteria for failure and for rejection", *Jour. Spacecraft and Rockets*, **2**, 833–45 (1965).

[32] REETHOF, G., "Reliability design prediction studies with reference to jet propulsion", *Society of Automotive Engineers, SAE Meeting Preprint* 820 B, January (1964).

[33] LANDEL, R. F. and FEDORS, R. F., "Rupture behavior of elastomers: effects of statistical variability and crosslink density", *Polymer Letters*, **1**, 539–44 (1963).

[34] MESSNER, A. M., "Structural aspects of modulus variations within a solid propellant grain", *Bulletin of the Third Meeting of the Working Group on Mechanical Behavior*, CPIA/61U, Vol. I, pp 119–30, Oct. (1964).

[35] CAMPBELL, D. M. and BROWN, P. E., "Mechanical behavior of solid propellant under the influence of simple strain concentrations by the Moiré method", Aerojet-General Corp. Report PEL–54, Sacramento, November 1964.

[36] HOWLAND, R. C. J., "On the stresses in the neighborhood of a circular hole in a strip under tension", *Phil. Trans. Roy. Soc.* (London), **229A**, 49, (1929–30).

[37] PETERSON, R. E., *Stress concentration design factors*", John Wiley & Sons, N.Y., 1953, p. 25.

[38] LIEBMAN, M. E., "Non-destructive testing of solid rocket motors", *AIAA Meeting Preprint* 65–149, February 1965.

[39] WILLIAMS, M. L., LANDEL, R. F. and FERRY, J. D., "The temperature dependence of relaxation mechanisms in amorphous polymers and other glass-forming liquids", *Jour. Am. Chem. Soc.*, **77**, 3701 (1955).

SOME EFFECTS OF FILLERS ON THE DEFORMATION AND RUPTURE OF AN ELASTOMER*

R. F. LANDEL

Jet Propulsion Laboratory, California Institute of Technology
Pasadena, California

Abstract—Over wide ranges in temperature and time scale the stress–strain behavior of amorphous gum elastomers, up to and including break, is simply and directly related to the molecular architecture. Since rubbery behavior requires a chain-like molecular structure, the architecture of such materials on a molecular scale must be essentially similar. Differences in chain construction, e.g. in the number of chains per unit volume, should therefore give rise to specific differences in the mechanical behavior which are, even at rupture, independent of the chemical nature of the material. This essential similarity in behavior has been confirmed and so it is now possible to establish failure criteria for both uni- and multi-axial conditions which are based only on molecular parameters.

The addition of a filler changes the mechanical behavior in several ways. One of the most thoroughly investigated changes is that in the small-strain modulus as a function of filler content, culminating in the theories of van der Poel, Hashin and Prager. From the first of these theories there may be obtained explicit expression for relative modulus; from the latter two, an upper and lower bound.

At higher strains the rubber tends to rupture internally. At increasing strains the void usually advances to the surface of the particle and the rubber pulls away from the surface in a dewetting phenomenon. At very high loadings, or with particles which interact strongly with each other, it may be necessary to consider the contribution of particle–particle interaction forces to the overall behavior.

In spite of these complications introduced by the filler, many of the characteristics of the fracture behavior of pure rubbers persist in the two-phase system, often to such an extent that the same or very similar correlative procedures may be employed. For example, time–temperature superposition is often obeyed, the rupture properties are a direct function of the number of molecular chains per unit volume of the rubber phase, and the Smith failure envelope criteria for uniaxial rupture is usually applicable. On the other hand, the presence of the filler also provides an upper bound to a strain failure criterion, since lateral contractions are possible only up to the maximum packing density of the particles.

1. INTRODUCTION

The presence of a filler is but one of the wide assortment of parameters which can change the mechanical properties of the polymeric binder in which they are embedded. Thus an adequate understanding of the behavior of a filled system presupposes an adequate understanding of that of the binder. In trying to achieve this understanding, it turns out that the stress-strain properties of an amorphous elastomer have been found to depend only on a rather small number of parameters. The functional form of this dependence can be given either empirically or, more desirably, in terms of molecular parameters. In many cases the latter

goal is reasonably well in hand, as shown by Professor Tobolsky's paper at this Conference on the molecular theory of linear viscoelastic behavior. Ideally we should like to extend this state of knowledge to the case of filled systems, i.e. to be able to describe their behavior in terms of molecular parameters and straight-forward mechanics. This would both assure us that we do indeed have an adequate understanding of the fundamental parameters and at the same time permit us either to predict the response of a given system or to create new systems as the need arises. However, even in the absence of such a complete molecular picture, we should at least use this approach whenever possible in guiding our search for the proper functional forms and in providing a basis for rational correlations. (As an example, we have learned to accept and understand an interaction between time and temperature but the similar interactions between filler content and crosslink density are often only dimly perceived and "cor-rected for" by adjusting the formulation to give some desired modulus without further study.) This will permit us not only to perceive the interrelations between stress, strain and time at fixed values of all other parameters, e.g. crosslink density, but also to gain some insight into further interrelationships as this restriction is relaxed and one of these parameters is varied, e.g. stress vs. cross-link density at fixed strain and time.

Although a wide variety of transient or dynamic mechanical behaviour could be discussed, we shall concentrate here on uniaxial stress–strain behavior because its wide use as a test vehicle has resulted in the largest accrual of experi-mental evidence and, correspondingly, has emphasized the need for understand-ing such behavior. However, we shall refer to multiaxial experiments where pertinent and in later sections we shall turn to dynamic (forced oscillation) behaviour. In all cases we shall first indicate the behavior of the pure polymer and then compare this with that of a filled system.

The determination of the stress–strain response is only part of the problem, however. Specimens cannot be extended indefinitely—they reach a limiting response—hence some failure criterion must be established. Note that this limiting response need not be a condition of complete rupture. Indeed, for cer-tain composite propellant systems, the criterion has for years been that of the stress and strain measured at the maximum load developed in a test conducted at constant cross-head speed.

To be more explicit, Fig. 1 indicates a qualitative formulation of the problem. The stress in a uniaxial experiment σ_u depends on many factors. At small strains, σ_u should be proportional to the strain ϵ, the constant of proportionality assuming the role of the tensile modulus E of classical elasticity theory. As the strain increases, the stress is no longer directly proportional to the strain and an additional function of strain $f(\epsilon)$ must be included to account for the non-linearity. For a filled system, one must next account for the influence of the nature of the filler, its concentration, its size distribution, and the strain at which it dewets. Furthermore, if repetitive experiments are made on the same specimen, the results will markedly depend on the prior strain history.

Even in the limit of small strains, E is not a constant but depends on the time

STRESS–STRAIN RELATIONSHIP:

$$\sigma_u = \sigma(E, \epsilon f(\epsilon), \text{type and amount of filler, degree of dewetting,}$$
$$\text{prior strain, per cent crystallinity, ...})$$
$$E = E(t, T, \nu_e); \text{ i.e. } \nu_e kT \text{ at eqm.}$$
$$\nu_e = \nu_e \text{ (gel fraction of rubber, dangling chain ends)}$$
$$E = E_0 g_1(\phi)$$

for simplicity, take

$$\sigma = E(t, T, \phi) \, \epsilon f(\epsilon, \phi)$$

FAILURE CRITERION:

$$\sigma_b = E\epsilon_b f(\epsilon_b)$$

FIG. 1. The problem stated: to find the functional relationship between the stress and the plethora of variables, consider first the σ, ϵ relationship, then note that the breaking points lie smoothly on the σ, ϵ curve.

scale of the experiment, the temperature and, in the rubbery region, on the crosslink density. Here we shall express the crosslink density in terms of the number of effective chains per cm³ of rubber ν_e. Again, the quantity ν_e is in turn dependent on the gel content of the rubber and the number of dangling chain ends.

In this same small strain region it is known that the modulus of the system E is equal to the product of the modulus of the unfilled rubber E_0 times a corrective factor $g_1(\phi)$. The latter is a function of the volumetric loading ϕ, and it too is a further function of the kind, size and size distribution of the particles.

As a result, it appears that each factor which might be considered is in turn a function of further factors, until we are reminded of the song in which the dog has fleas which have their own fleas which in turn have their own fleas *ad infinitum*. Moreover, the influence of many of these factors may change under multiaxial loading conditions, thus lending still another dimension to the problem.

Because of this complexity, let us consider separately the three regions of small strain, large strain and failure. Prior to failure then, the stress–strain curve might be given in general terms as

$$\sigma = E(t, T, \nu_e, \phi) \, \epsilon f(\epsilon, \phi) \tag{1}$$

To illustrate, consider specimens tested at various temperatures at a given rate; i.e. only T is varied. The stress–strain curves will resemble those of Fig. 2, which depict a crystallizable and non-crystallizable rubber, each filled with 20 parts by weight of ISAF carbon black. As can be seen, the initial slope increases steadily. In addition, the form of the non-linearity, $f(\epsilon)$ is also shown to be strongly temperature-dependent at low temperatures, though this has not been indicated in eqn. (1). Similar plots would have been obtained if the strain rate had been varied widely at a single temperature, because of the close correlation between time and temperature.

The locus of all the rupture points for plots such as shown in Fig. 2 has been called the *failure envelope* by Smith [2]. This locus, giving the relationship between the breaking stress and breaking strain, thus can be considered to

37

represent a failure criterion for the materials. (If the stress–strain curves all had additional characteristic features, such as the maxima found in some propellant stress–strain curves, additional envelopes could also be drawn through these characteristic points.) Of course, any point on the envelope is also a point on the stress–strain curve, and as a result, the envelope at first might appear to be sensitive to all of the parameters already indicated. However, this is not the case.
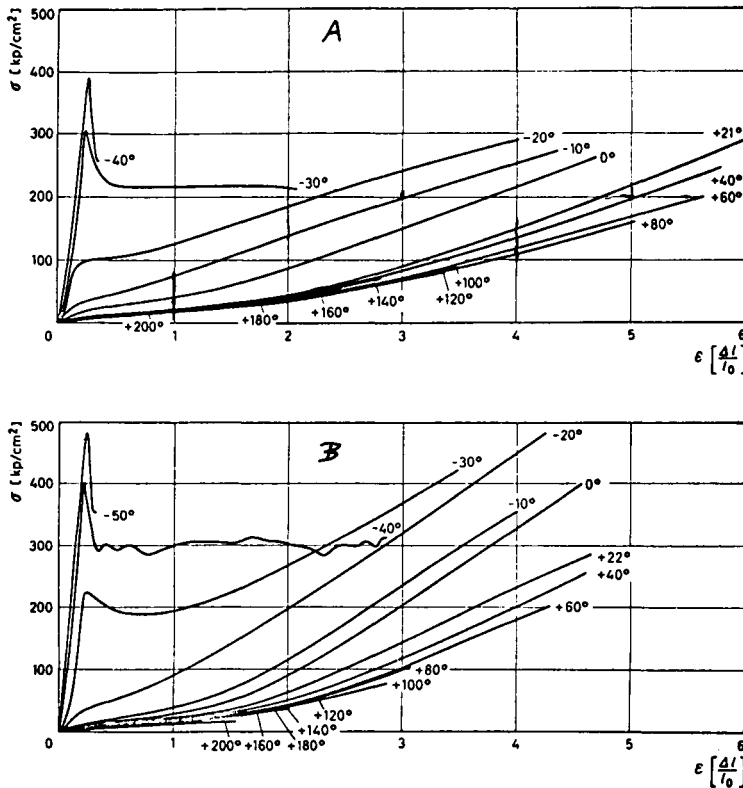
Fig. 2. Stress–strain curves as a function of temperature for, (a) Perbunan N, an amorphous rubber containing 20 per cent carbon black; (b) Urepan E, a crystallizable polyester-based polyurethane rubber, also containing 20 per cent carbon black. (From Ecker [1].)

In particular, it is insensitive to time, temperature and type of test performed, so that in all of these cases the *same* envelope is generated, within experimental error. Thus the envelope seems to be more fundamental than simply one way of showing a relationship between breaking stress and strain. Otherwise a unique curve would not be obtained.

By now we have established our problem as one requiring an investigation of both the stress–strain law and the failure envelope. It is therefore instructive to prepare a three-dimensional graph showing the relationship between stress, strain and time. We shall call the surface thus generated the physical property

surface, in this case the *tensile property surface* [3, 4]. The stress–strain equations determine the shape of this surface, while its boundary is determined by their intersection with an appropriate failure criterion, which we take to be the failure envelope. Such surfaces are illustrated in Figs. 3 and 4, for an elastomer and a propellant, respectively.* Because of the range in values, both figures are plotted on logarithmic coordinates. The stress–strain curves for the elastomers are sigmoidal; those of the propellant pass through a maximum. If the maximum points are *defined* as the failure points, then rupture and failure do not coincide as they do in an elastomer and so there exists both a failure envelope and a
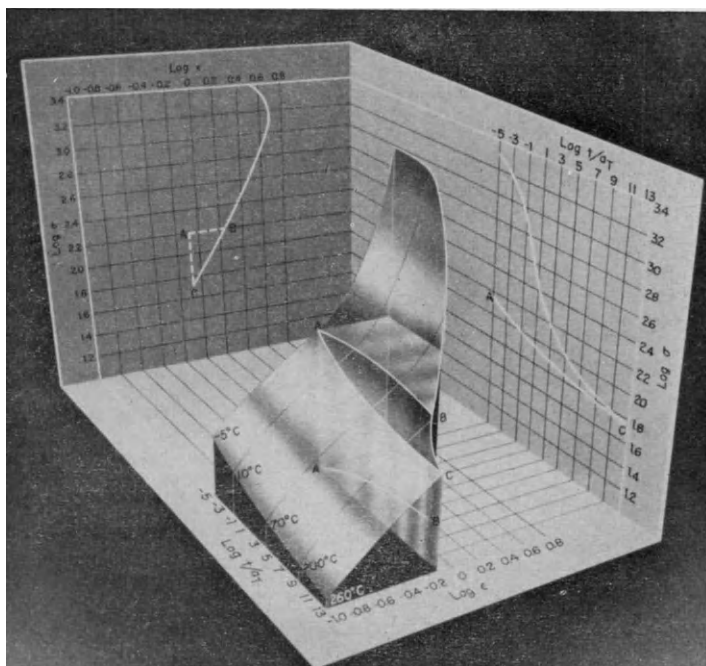
Fig. 3. Tensile property surface for Viton B, a fluorocarbon rubber. Curve *AB* on the surface represents a creep experiment; *AC,* a stress relaxation experiment. (From Landel and Fedors [3].)

rupture envelope for the propellant. In both figures, the projections of the failure points to the σ, t and ϵ, t planes serve to indicate the time dependence of failure, while the projection to the σ, ϵ plane shows that a change in time scale of the experiment changes the location of the response on the envelope but does not change the shape of the envelope.

Considering the elastomer surface, it is clear that the value of the stress at

---

* The materials are assumed to be thermorheologically simple, so that time-temperature superposition is applicable. Thus the time scale here is a reduced time scale t/a_T and a_T is the usual temperature shift factor [5a].

strains so small that the σ, ϵ curve is linear is simply a reflection of the modulus. In this case, the modulus is the same time-dependent modulus which would be obtained in a stress relaxation experiment. Furthermore, to the extent that this time dependence is small, *the shape of the surface should be independent of the path.* Therefore any experiment performed in this region of weak time-dependence is merely a trace of some path across the surface and all paths (experiments) are rather simply interrelated. Thus, if the material were brought to point A it could
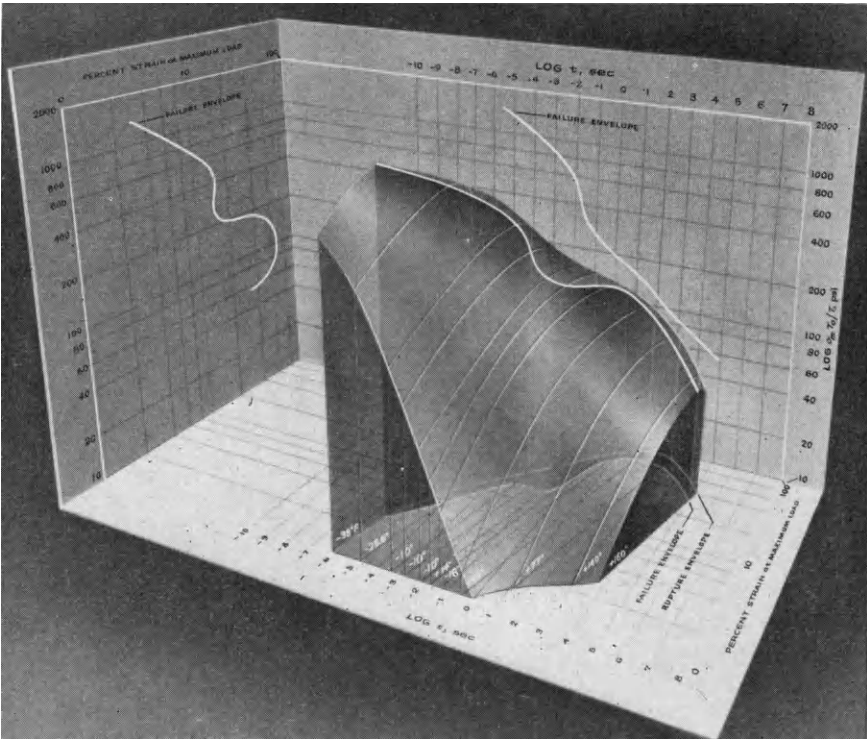
FIG. 4. Tensile property surface for a propellant, showing the relationship of the failure boundary to the surface. Note that failure, as defined here, does not coincide with rupture. (From Landel and Fedors [3]).

either be held at constant stress, as in a creep experiment, or at constant strain, as in a stress relaxation experiment. In former case, path AB would be traced across the surface and the strain as a function of time would be recorded. This ϵ, t relationship is shown as the projection of path AB on the log ϵ, log t plane. In the second case, path AC would be followed and the stress would normally be recorded as a function of time, as shown in the projection of the path on the log σ, log t plane.

The surface is not completely independent of the experiment, because a slight

time dependence does exist, but this dependence is negligibly small. The fact of the near-independence is not generally realized and as a result the possibility of a path-insensitive response has been incorrectly criticized. Typically it requires eight or ten decades of reduced time for the breaking strain to fall from its maximum value $(\epsilon_b)_{max}$ to the final value observed at long reduced times. This final value is not a limiting value of strain, but rather a limiting value of the time scale, beyond which degradation begins to be important. In this same time range
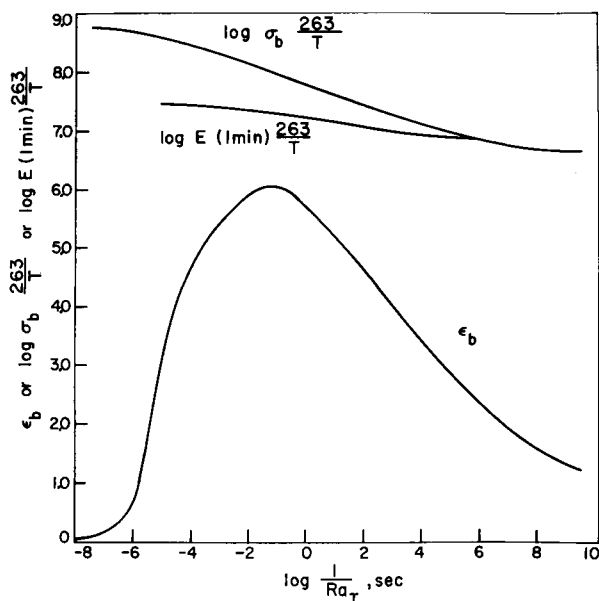
FIG. 5. Comparison [6] of the time-dependence of the breaking stress, the stress-relaxation modulus and the breaking strain for a sytrene–butadiene rubber. All data are reduced to a standard state temperature of $-10°C$.

the breaking stress is decreasing by a factor of more than 10. The modulus, on the other hand, changes by only a factor of 2 or 3, which surely seems to be an acceptably small percentage change. This point has previously been demonstrated [6] by combining Smith's data [7, 8] on SBR to obtain Fig. 5. It may be further illustrated by additional consideration of the data of Fig. 1a. The breaking stress, breaking strain, and modulus at 100 per cent strain E_{100}, as a function of the temperature, have also been reported [1]. The results are shown in Fig. 6. It can be seen that E_{100} is constant up to the point where ϵ_b passes through its maximum.

This time independence over most of the region of interest should also be of importance to those developing finite viscoelastic theories of mechanical properties. In particular, the assumption of weak memory, which has been discussed in earlier papers at the Conference is indeed an excellent approximation and should

be vigorously pursued. At the same time, it is easy to see the region of response in which this assumption should begin to break down.

Turning to the propellant surface, this is not nearly so path-independent as that for elastomers. There is a progressive weakening prior to rupture, associated with the dewetting or unbonding of the rubber from the oxidizer. A hysteresis loop traced out in a loading and unloading cycle is more than just a measure of
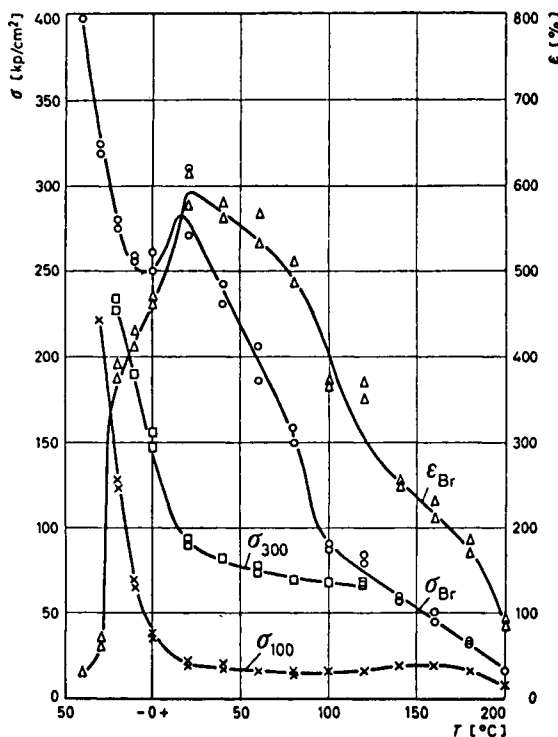
FIG. 6. The breaking stress σ_{br} and breaking strain ϵ_{br} plotted as a function of the test temperature for the butadiene–acrylonitrile rubber of Fig. 2a. Also shown are the stress at 300 per cent strain σ_{300} and that at 100 per cent strain, σ_{100}. The latter may be taken as being equivalent to the small-strain stress relaxation modulus for present purposes. (From Ecker [1].)

viscous losses as it is in unfilled rubbers, because the binder separates from the filler and the structure of the specimen is changed by the loading. Therefore, even for simple loading histories care must be taken that the property surface for a propellant is defined as a "first-stretch" surface, a "second-stretch" surface, etc.

To recapitulate, any consideration of the effect of a filler on the deformation and rupture behaviour of an elastomer must be in essence a comparison of the tensile property surfaces of the unfilled and filled material. Since these surfaces

can be considered as being defined by two separate sets of equations, one for the deformation and one for failure, we shall now examine these aspects in more detail.

2. PHYSICAL PROPERTY SURFACE PRIOR TO RUPTURE

2.1. *Elastomers*

Considering only uniaxial behavior, the surface is described by the stress–strain curve:

$$\sigma = E(t) \, \epsilon f(\epsilon) \tag{2}$$

so long as strain and time are factorable. For many unfilled elastomers this is true over a wide range in time scale or temperature. Specifically, it turns out that the temperature must be about $30°$ or $40°$ above T_g [3, 9], which covers the response from the region of quasi-equilibrium behavior up to the regions of the time or temperature at which the elongation passes through the maximum. Let us now examine this equation term by term.

1. *Time Dependence.*

Taking the modulus term first, the time dependence of E can be ascertained from stress relaxation, creep or dynamic experiments. For stress relaxation experiments, this can be represented by a Prony series:

$$E(t) = E_0 + \sum_{i=1}^{N} e^{-t/\tau_i} \tag{3}$$

where E_0 is an equilibrium value and τ_i is a relaxation time. This series can be given a molecular interpretation, but for present purposes we need only note that the equilibrium value is reached only slowly, if at all.

Therefore, in this quasi-equilibrium zone a simple empirical equation will suffice, viz.

$$E(t) = a - b \log \frac{t}{a_T} \tag{4}$$

2. *Strain Dependence.*

Turning next to the term $\epsilon f(\epsilon)$, the form of the time-independent stress–strain relationship can be stated in several ways, as indicated in Table 1, but ultimately must prove to be compatible with finite deformation theory. For a purely elastic material this means that

$$\sigma_i \lambda_i = \frac{2}{\sqrt{I_3}} \left\{ W_1 \lambda_i^2 + \left[I_2 - \frac{I_3}{\lambda_i^2} \right] W_2 + I_3 W_3 \right\} \tag{5}$$

and the problem is to determine the correct functional form of $W_k \ (\equiv \partial W / \partial I_k)$, where W is the elastically stored energy and $I_{1,\,2,\,3}$ are three strain invariants [10]. For a viscoelastic material the problem is more complicated, although various formulations have been proposed for systems in which the time-dependence is

TABLE 1. ELASTOMER σ, ϵ EQUATIONS

1. Finite deformation theory

$$\sigma_i \lambda_i = (2/\sqrt{I_3})\{W_i \lambda_i^2 + [I_2 - (I_3/\lambda_i^2)] \, W_2 + I_3 W_3\}$$

$$W_1 = \left(\frac{\partial W}{\partial I_1}\right)_{I_2, I_3} \quad \text{etc.}$$

2. Molecular theory (uniaxial)

$$\sigma = (1/6)En^{1/2}[\mathscr{L}^{-1}(\lambda/n^{1/2}) - \lambda^{-3/2}\mathscr{L}^{-1}(1/\lambda^{1/2}n^{1/2})]$$

$$\mathscr{L}(X) = \coth X - 1/X$$

3. Empirical (uniaxial)
   Mooney-Rivlin

$$\sigma = (\lambda - 1/\lambda^2)(C_1 + C_2/\lambda)$$

   Martin-Roth-Stiehler

$$\sigma = E(\epsilon/\lambda^2) \exp A(\lambda - 1/\lambda)$$

---

small (e.g. Refs. [11], [12] and further references cited therein). Since it has been observed that strain and time are separable under uniaxial conditions over the indicated temperature regions, it may ultimately prove more convenient to evaluate isochronal data as though the material were elastic and then find the time-dependence of W_k.

From the molecular viewpoint, the kinetic theory of rubberlike elasticity provides a nonlinear stress–strain law [13]. For strains up to about 100 per cent for elastomers usually encountered, this theory leads to

$$\sigma = \tfrac{1}{3}E(\lambda - \lambda^{-2}). \tag{6}$$

This equation should not be applied to cases involving large deformations.
Under these conditions the more exact expression containing the inverse Langevin function should be applied:

$$\sigma = \frac{1}{6} \, En^{1/2} \left[\mathscr{L}^{-1}\left(\frac{\lambda}{n^{1/2}}\right) - \lambda^{-3/2}\,\mathscr{L}^{-1}\left(\frac{1}{\lambda^{1/2}\,n^{1/2}}\right)\right] \tag{7}$$

where, if the inverse Langevin function is given as:

$$\mathscr{L}^{-1}(X) = \beta \tag{8}$$

then the Langevin function is:

$$\mathscr{L}(\beta) = \coth \beta - \frac{1}{\beta} = X \tag{9}$$

The parameter n is the number of statistical segments in the chain. It has not been measured for many polymers which appear in normal elastomers, though it can be assessed by a combination of light scattering and intrinsic viscosity measurements, among others [14].

Turning to empirical or semi-empirical equations, the best two parameter uniaxial stress–strain law for rubber has been, until recently, the purely empirical

Martin–Roth–Stiehler equation [15], and it is still the simplest to use. Here

$$\sigma = \lambda^{-2} \epsilon E \exp A(\lambda - \lambda^{-1}) \tag{10}$$

This equation is valid over a considerable time-temperature span for many elastomers, so that $E = E(t)$. Wood [16] has pointed out that eqn. (10) is also valid in homogeneous *biaxial* deformation of natural rubber.

It appears that the constant A, which has a value of about 0.40 in regions where the equation is valid, is primarily a measure of the quantity "n" of eqn. (7) [17].

The Mooney–Rivlin stress–strain law [18, 19]

$$\sigma = (\lambda - \lambda^{-2})(C_1 + C_2\lambda^{-1}) \tag{11}$$

$$C_1 + C_2 = E/6 \tag{12}$$

which is also a two-parameter equation, is better known than eqn. (10) and has some theoretical justification. However, (11) has a serious defect for present purposes in that it is not valid up to rupture, while eqn. (10) generally is [20].

Hence, much of the physical property surface can be considered to be completely defined by eqns. (4) and (7) (semi-empirically), or by eqns. (4) and (10) (purely empirically).

3. Crosslink Dependence.

Up to this point we have been considering the response to be expected from a given sample of material. What happens if the material is changed from polymer A to polymer B? Or if we work only with A but change its crosslink concentration? As noted in §1, it can be shown that the modulus which appears in the kinetic theory equations (6) and (7), and thus the stress, should be directly proportional to ν_e* the number of effective chains per cm^3 of gel [3].

In terms of Fig. 3, this proportionality means that the height of the surface can be changed at will by changing the crosslink density. Such modifications to propellants or elastomers are often made in order to achieve a given modulus. In a propellant, for example, the modulus may be adjusted to control the initial deflection of a star point. Or it may be deemed desirable to add a plasticizer, whereupon the modulus will have to be increased in order to counteract the softening effect of the plasticizer. Alternatively, the plasticizer (or any other additive) may contain reactive functional groups which disrupt the cure, and it will be found that the modulus of the propellant with reactive additives differs from that of the normal material. As a result, the formulation must be varied to find a new formulation with equivalent crosslinking. It is important to note that such changes in ν_e can also occur inadvertently too (e.g. by the incorporation of

---

* For a system without sol, and without correcting for chain ends, $\nu_e = \varrho/M_c$, the ratio of the density to the molecular weight between crosslinks. Since M_c depends on the nature of the crosslinking process and the manner in which corrections for chain ends are made [21, 22, 23], while ν_e does not, it is preferable to use ν_e as a measure of crosslink density.

adventitious water in a urethane system) and probably represent one of the major causes of poor batch-to-batch reproducibility. As can be imagined, such changes in crosslink density also affect the ultimate properties very directly, a point which will be discussed subsequently.

Equation (7) also shows that at a given crosslink density the difference in the response of polymer A vs. polymer B is a reflection of the number of statistical segments per chain between crosslink points. Since this quantity is a measure of the degree of chain perfection, decreasing with increasing numbers of dangling chain ends, an explanation is provided for Dr. Klager's observation in his presentation to this Conference that the degree of chain regularity can affect properties. However, if n and ν_e are adjusted to the same value, *the form of the stress–strain equations for A and B should be the same* although they may not have identical σ, ϵ responses because their time-dependencies may not be the same.

2.2. Propellants

1. Time and Crosslink Dependence.

The time dependence of the modulus of propellants parallels that of its elastomeric binder. At room temperature it is usually low for a well-crosslinked composite propellant and eqn. (4) will continue to hold. Time-temperature superposition usually holds over an extended time scale. Lowering the crosslink density lowers the room temperature modulus, just as it does with an elastomer.

2. Strain Dependence.

In contrast to the elastomeric binder, a generally valid stress–strain law for propellants has not been proposed, so that the surface cannot be described mathematically. However, the following may be listed as pertinent attempts.

(a) One of the earliest time-dependent laws was that of Nichols and Nathan [24], derived from a mechanical model consisting of springs, dashpots, and a sliding block friction element. Unfortunately it has never been extensively tested.

(b) Perhaps the most useful stress–strain law has been simply a linear true-stress, Cauchy-strain law:

$$\lambda\sigma = E(t)\epsilon \tag{13}$$

At any rate this expression has proven adequate to permit the calculation of reduced stress–strain plots from constant strain rate data, i.e. plots of

$$\log \frac{\lambda\sigma T_0}{\dot{\epsilon}Ta_T} \text{ vs. } \log \frac{\epsilon}{\dot{\epsilon}a_T}$$

will often superpose stress–strain curves obtained over wide ranges in t and T to a single curve from which the stress relaxation modulus $E(t)$ can be determined [25].

(c) Brock [26] and Bills [27] have both proposed equations based on finite elasticity approaches. The former method has been questioned. The latter is essentially an elegant way of describing the volume change as a function of strain, but the results become so compressed that the direct plot of volume versus strain is easier to work with.

(d) Ferris [28a] has recently derived a very simple and straightforward expression which describes the tensile stress–strain curve through the maximum and out to break. He assumes that a vacuole which forms on dewetting in a tensile experiment is a prolate ellipsoid whose minor axis is the diameter of the particle and whose major axis increases with strain at a rate directly proportional to the particle's radius. The total dilatation is then the sum of the individual ellipsoidal volumes less the volume occupied by its contained particle. The final stress–strain equation is:

$$\sigma = E\epsilon - E_2 \frac{\Delta V}{V_0} \tag{14}$$

where E is the initial modulus, E_2 is a constant, and $\Delta V/V_0$ is the fractional volume change. The latter must be measured independently as a function of strain. The rate of change of volume is proportional to the volume fraction of dewetted solids, ϕ_d

$$\frac{d(\Delta V/V_0)}{d\epsilon} = C\phi_d \tag{15}$$

or

$$\frac{\Delta V}{V_0} = C \int_0^\epsilon \phi_d \, d\epsilon + \phi_d^0 \tag{16}$$

where ϕ_d^0 is the volume fraction of solids already dewetted at the start of the experiment. Thus these equations hold promise of describing the behavior during successive stretches, since provision is automatically made for the extent of dewetting in prior tests. This information is badly needed to assess cumulative damage test results (see below).

It turns out experimentally that the rate of relative volume change with strain $d(\Delta V/V_0)/d\epsilon$ resembles a normal probability curve. This fact and the associated dependence of the dilatation on the fraction of particles already dewetted have previously been noted by Payne [29].

A similar derivation could presumably be worked out for biaxial testing. This would be an important step since it would indicate the failure stress under these conditions and thus give an indication of the geometric failure surface to be expected. A geometric failure surface [10, 30] is one which describes the failure stresses (or failure strains) in terms of the three principle stresses (or strains). Taking these as a Cartesian coordinate system, with both positive (tensile) and negative (compressive) values possible, uniaxial tensile failure would thus be some point on the axes in the first octant; biaxial tensile failure would be a point in each of the planes defined by the axes; and triaxial tensile failures would be a point on the line lying equidistant from all three axes. At stresses less than those indicated by the surface of such a figure, the specimen will not fail and so the surface represents a failure criterion valid for any degree of axiality. Because of the paucity of multiaxial data on filled systems, any *a priori* limitations which can be placed on the shape and magnitude of such a geometric failure surface are of great value.

(e) Fishman and Rinde [31] have also proposed an equation of state which explicitly includes the volume change:

$$\log \frac{V}{V_0} = A \left[\log W' + B \log \frac{t}{b_T} + C \log^2 \frac{t}{b_T} \right]^n \tag{17}$$

where W' is the area under the stress–strain curve and b_T is a temperature shift factor which is not necessarily equal to the WLF factor a_T. This equation was found to hold for constant strain rate, constant load and constant loading rate tests on propellants and so is independent of the path. The values of the constants differ for polyurethanes and carboxyterminated polybutadienes. Since the form of the stress–strain law is left unspecified, eqn. (17) presents a powerful tool for relating stress, strain and volume changes. On the other hand, it cannot be readily related to the tensile property surface.

(f) Rinde and Fishman [32] have also tried two analyses based on finite elasticity theory. They first compared experimental results with the equation of Blatz and Ko [33].

$$\sigma_i \lambda_i = G \left[\lambda_i^2 f - \frac{1-f}{\lambda_i^2} \right] + J_3 W_3 \tag{18}$$

where G is the shear modulus, F is a constant and J_3 is the relative volume change V/V_0. For uniaxial extension, eqn. (18) takes the form:

$$\sigma \left(\lambda - \frac{J_3}{\lambda^2} \right)^{-1} = G \left[f + \frac{1-f}{J_3 \lambda} \right] \tag{19}$$

Defining the left-hand side as the nominal shear modulus G_{nl}, a plot of G_{nl} vs. $(\lambda J_3)^{-1}$ should be linear. The results are shown in Fig. 7 for tests at various strain rates on a polyurethane propellant. The volume changes occurring during the tests were measured in a specially constructed dilatometer. As can be seen, an adequate fit was obtained at high extensions, after extensive dewetting had taken place and the material resembled a foam. Fishman and Rinde also tried an analysis similar to that of Blatz and Ko but based it on the usual strain invariants I_1, I_2, I_3 rather than those employed by Blatz and Ko. In this case the final equation analogous to eqn. (19) should be

$$\frac{\sigma}{\lambda - \sqrt{I_3}/\lambda^2} = C_1 + C_2 \frac{\sqrt{I_3}}{\lambda} \tag{20}$$

and $\sqrt{I_3} = V/V_0$.

The results are shown in Fig. 8, using the same data as employed in Fig. 7. Again the data could be fitted at high extensions, but now the fit extended to lower strains, though still only over the region *beyond* which dewetting had started. Thus both approaches failed to describe the behavior in the important region prior to dewetting.

(g) The stress–strain curve of many propellants through the region of maximum load can be described by the simple expression [34]:

$$\sigma = E\epsilon \exp(-k\epsilon^2) \tag{21}$$
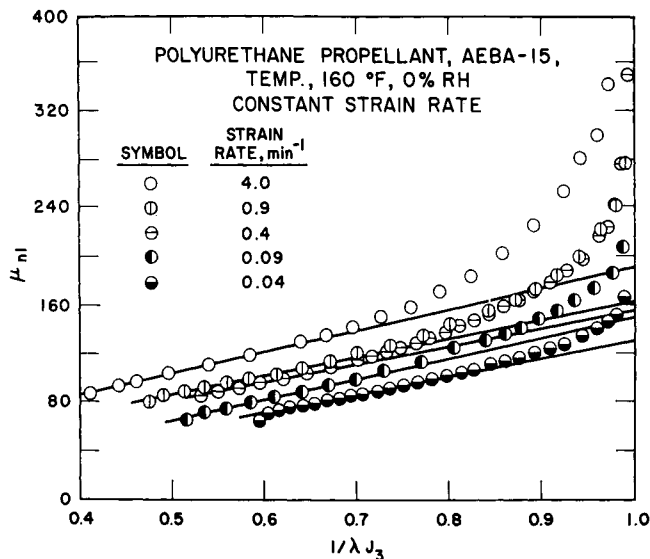
FIG. 7. Uniaxial stress-strain data for a polyurethane propellant plotted according to eqn. (19). Here μ is the same as G of the text. (From Rinde and Fishman [31].)
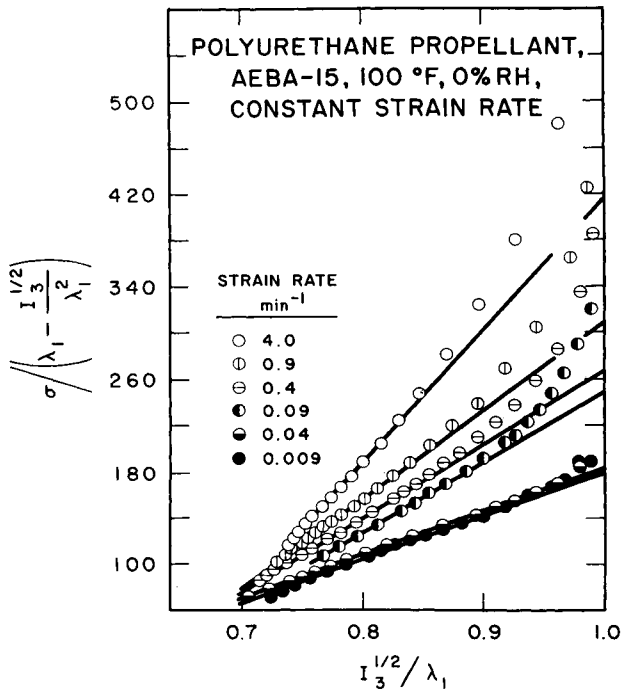
FIG. 8. The data of Fig. 7 replotted according to eqn. (20). (From Rinde and Fishman [31].

Differentiating this and noting that $\epsilon = \epsilon_m$ at the point of zero slope,

$$k^{-1} = 2\epsilon_m^2 \tag{22}$$

This equation can be used to obtain a relationship between $\Delta V/V_0$ and ϵ, which would serve to make Ferris's equation more useful. By equating eqns. (14) and (21),

$$E\epsilon \left[1 - \frac{E_2 \Delta V}{E\epsilon V_0}\right] = E\epsilon \exp\left(-\frac{\epsilon^2}{2\epsilon_m^2}\right) = E\epsilon \left(1 - \frac{\epsilon^2}{2\epsilon_m^2} + \ldots\right) \tag{23}$$

which leads to

$$\frac{\Delta V}{V_0} = \frac{E\epsilon}{E_2}\left[1 - \exp\left(-\frac{\epsilon^2}{2\epsilon_m^2}\right)\right] \tag{24}$$

Hence in the region where $\epsilon < \epsilon_m/2$, the argument of the exponential is small and

$$\frac{\Delta V}{V_0} \approx \left(\frac{E}{2E_2\epsilon_m^2}\right)\epsilon^3 \tag{25}$$

A check of some of Fishman's data points shows this cubic relationship to be true, though Stoker's data [35] are better fitted by a dependence on ϵ^2.

Furthermore, differentiating eqn. (21) to find $d^3(\Delta V/V_0)/d\epsilon^3$, and setting this equal to zero to find the critical strain at which half of the particles have de-wetted, according to Ferris' picture, we find this strain to be 0.63 ϵ_m. This particular value will be recalled later.

Finally, let us use eqn. (21) to investigate the form of the Fishman–Rinde equation. The area under a stress–strain curve is:

$$W' = E\epsilon_m^2 \left[1 - \exp\left(-\frac{\epsilon^2}{2\epsilon_m^2}\right)\right] \tag{26}$$

and combining this with eqn. (24),

$$\frac{\Delta V}{V_0} = \frac{W'\epsilon}{E_2\epsilon_m^2} \tag{27}$$

When ϵ is small,

$$W' = \tfrac{1}{2}E\epsilon^2 \tag{28}$$

and when $\epsilon = \epsilon_m$

$$W' = 0.606\, E\epsilon_m^2 \tag{29}$$

so that in both regions we would therefore predict that:

$$\frac{V}{V_0} \propto (W')^{1.5} \tag{30}$$

Fishman finds that the actual exponent is about 1.8 instead of 1.5.

Thus eqn. (21) is consistent with both the Ferris and the Fishman–Rinde developments and at the same time it permits the volume changes to be expressed in terms of the strain.

Hence, the fundamental problem of describing the first-stretch, stress–strain curve of a propellant seems close to a solution. In addition, Ferris's work

offers some leads for multiple stretching results. Fishman has already shown that eqn. (17) may be applied to a specimen which is pulled at a constant rate for a time and then at a faster rate for the remainder of the time. This means that it should be possible to give a quantitative measure of the changes in the shape of the failure envelope which are expected to be found in cumulative damage tests.

For convenience, the more important of the proposed σ, ϵ equations discussed in this section are listed in Table 2.

TABLE 2. PROPELLANT σ, ϵ EQUATIONS

---

1. True stress, Cauchy strain
$$\lambda\sigma = E(t)\,\epsilon$$

2. Ferris, semi-empirical
$$\sigma = E\epsilon - E_2 \Delta V/V_0$$

3. Fishman and Rinde, empirical
$$\log V/V_0 = A[\log W' + B\log(t/b_T) + C\log^2(t/b_T)]^n$$

4. Empirical
$$\sigma = E\varepsilon \exp(-\epsilon^2/2\epsilon_m^2)$$
which implies:
   (a) $\epsilon_L = (0.606\lambda_L)\epsilon_m$
   (b) for Ferris's 50 per cent dewetting point
   $\epsilon_{50\,\text{per cent}} = 0.63\epsilon_m$

---

3. FAILURE ENVELOPE

3.1. *Time and Temperature Dependence for Elastomers*

As a corollary of the fact that the surface is path-independent for elastomers, the ultimate properties should lie on the same failure envelope for different types of tests. This has been confirmed for SBR, using constant strain rate and constant strain tests [2], and constant strain rate, constant strain and constant load tests [36]. The latter data are shown in Fig. 9; similar agreement has also been found for Viton A, a fluorinated elastomer, in constant load and constant strain rate tests, Fig. 10 [37]. On the other hand, the fact that the ultimate properties lie on the same envelope means that the time to break, t_b, *will* depend on the path. Thus for a creep and a stress relaxation test in which the initial stresses and strains are adjusted so that the same ultimate properties will be observed in the two tests, Smith [2] has shown theoretically that for linearly viscoelastic materials the stress relaxation specimen will break first. For the experimentally easier process of starting from the same *initial* stress and strain values, Landel and Fedors [3] have shown, again theoretically, that the creep specimen will break first and, by implication, the stress at break will be larger. Smith [37] has tested these theories experimentally with inconclusive results. The differences in break times depend on the slope of the stress relaxation modulus, b of eqn. (4). When b is less than about 0.1, a common value in the response region under discussion, then the differences in breaking times are

predicted to be only a decade or less. Since the constant stress and constant load tests suffer from very large statistical distributions in breaking times, this obscures the results. The statistical distributions will be discussed in a later section.

3.2. Propellant Failure Criteria

Before considering the failure envelope for propellants, let us first pause to note that here, in contrast to the case of elastomers, we have not had an equally well-defined criteria of what constitutes failure. While rupture in the elastomer represents an unequivocal response, the rupture points and the rupture failure
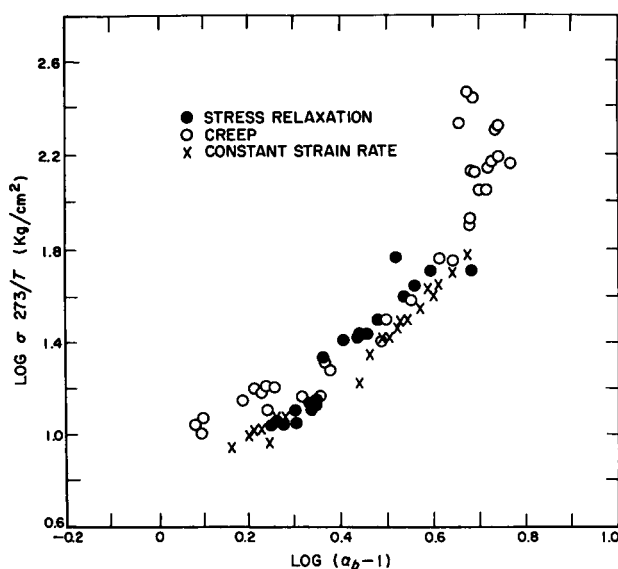
FIG. 9. Comparison of the failure envelopes for SBR rubber as measured in stress relaxation, creep, and constant strain rate experiments. Here a_b is the stretch ratio at break, denoted λ_b in the text. (After Halpin [36]).

envelope of a rubber base composite propellant are of no great practical interest. Instead, the engineering stress (i.e. based on the initial cross-sectional area), and the corresponding strain developed at the maximum load supported by the specimen in a constant strain rate test, σ_m and ϵ_m, have been adopted as a useful, operational definition of failure. It is well recognized that a better definition is needed.

Several years ago a very good failure criterion was proposed as the result of attempting to assess a critical value of volume change associated with dewetting [38]. As an illustration, referring to Fig. 11, if the nominal or engineering stress–strain plot (solid curve) is converted to a true-stress, Cauchy-strain plot*

---

* Assuming Poisson's ratio is 1/2.

(dashed curve), then in the initial regions eqn. (13) will apply. If σ_m is retained as the failure stress and this initial linear region is extrapolated to σ_m, the corresponding value of the strain is defined as the failure strain, ϵ_L. Thus $\epsilon_L/\lambda_L = \sigma_m/E$.

The value and utility of this definition of the failure strain stems from the fact that this is the strain level at which an appreciable amount (*ca.* 2 per cent) of dewetting occurs, yet it can be ascertained without a Ferris–Fishman dilatometer [28b, 31a]. From the curves given in Fig. 8 and 10 of Ref [28a] it appears that this strain level corresponds to about half the dewetting possible for a given propellant subjected to a given strain history.

As a more clear-cut demonstration that ϵ_L corresponds to a critical dewetting, specimens (with milled surfaces) can be immersed in water and quickly tested.
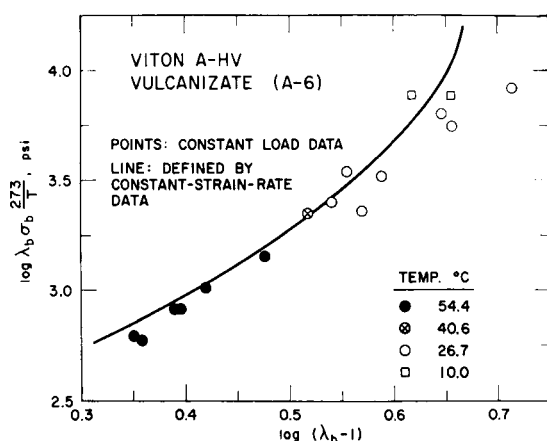
FIG. 10. Comparison of the failure envelopes of Viton A as measured in creep vs. that measured under constant strain rate conditions. The agreement between the data here and in Fig. 9 shows that the results for these two rubbers are insensitive to the experimental path. (From Smith [37].)

So long as the volume change is small, the properties will be unchanged, but when the voids open up enough to admit water, the latter will greatly accelerate the dewetting process and the stress will be less at an equivalent strain value. This effect is also shown in Fig. 11. As can be seen, there is little difference between the dry and submerged curves until just prior to ϵ_L. Beyond this point the stress soon passes through a maximum in the usual fashion, though at a lesser value than σ_m, and then drops to a small constant value while the elongation continues to very large values. This, then is a convenient method for testing for substantial dewetting, though it cannot be used over a very wide time or temperature scale.

Briar and Wiegand [39] have recently employed the quantity σ_m/E to correlate motor failures induced by thermal straining with the propellant properties as measured in uniaxial tension (cf. also Wiegand's paper in this Conference). They called this ratio ϵ_L, after Ref. [38] but the original definition was as given

38

above. Thus their value is actually ϵ_L/λ_m. It is interesting to note that had they used the original definition, they would have improved their correlation, as shown in Fig. 12. Here the number of motors which cracked in one week of thermal cycling is compared with the ratio of the motor bore strain ϵ_{mm} to a critical strain. In the lower abscissa scale, the critical strain is that employed by Wiegand and Briar and it can be seen that when this ratio is unity only about 80 per cent of the specimens will survive. If the original definition is retained, as shown in the upper abscissa scale, the survival probability is raised to 94 per cent, i.e. ϵ_L is a good measure of motor failure.

Returning to the failure envelope discussion *per se*, propellants can thus have a variety of failure envelopes, depending on whether these are referred to ϵ_L, ϵ_m, or ϵ_b conditions. As a rough rule of thumb for many composite systems, $\epsilon_L = \frac{2}{3}$ to $\frac{3}{4}$ ϵ_m at room temperature,* though this generalization breaks down
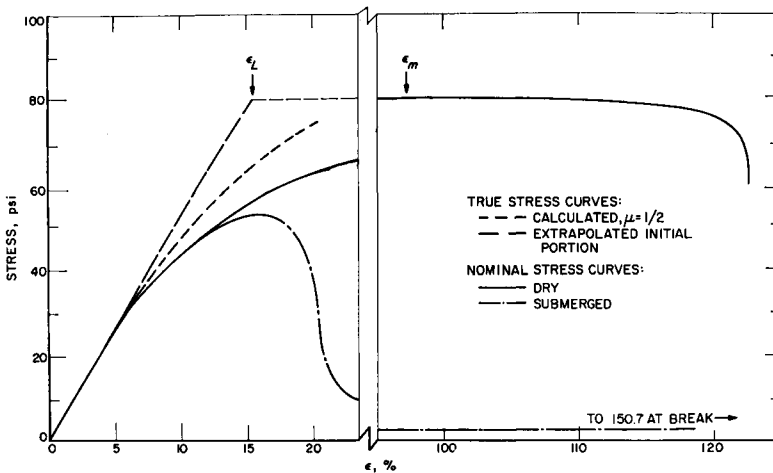
FIG. 11. Stress–strain curves for a polyurethane propellant tested dry and submerged in water. A portion of the former has been converted to a true stress-Cauchy strain curve and the initial linear portion of this extrapolated to σ_m in order to show how ϵ_L is calculated.

for temperatures below or strain rates above those at which ϵ_m or ϵ_b reach their maximum values. Similarly, ϵ_m is often some rather constant fraction of ϵ_b. Thus the three envelopes for a given system, when plotted logarithmically, are similar in shape but are transposed to progressively larger ϵ values. In the low temperature region, below $(\epsilon_m)_{max}$, the three curves draw together into a single curve.

3.3. *Time and Temperature Dependence for Propellants*

Fishman and Rinde [31a] have made studies of the path dependence of the failure envelope of propellants and their data indicate that the *rupture* envelope from creep and constant loading rate tests is very close to that for the ϵ_m envelope

---

* Recall the value of 0.63 ϵ_m derived previously.

in constant strain rate tests. The results are not clear-cut, because of the creep data. Moreover, most of the data fall in the region near $(\epsilon_m)_{max}$, where ϵ_m and ϵ_b envelopes observed in constant strain rate tests would be expected to converge, as just noted. Thus with further data the envelopes would probably diverge. Nevertheless, present indications are that the rupture envelope would be independent of the path, just as it is with an elastomer.
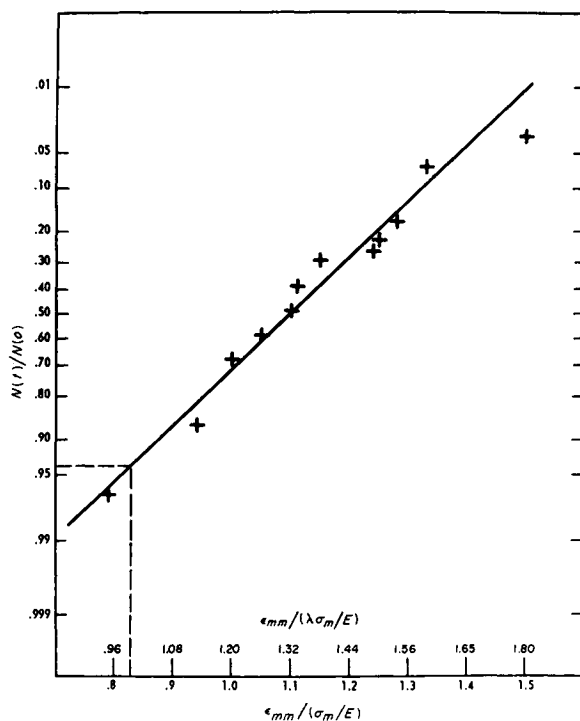
FIG. 12. The fraction of motors successfully passing one week of thermal cycling as a function of the ratio of the motor bore strain to ϵ_L as measured at 77°F. Lower abscissa scale, using an approximate value of ϵ_L; upper abscissa scale, using the originally defined ϵ_L. Only about 6 per cent of the motors failed if the strain was kept at or below the critical value, ϵ_L [after Briar and Wiegand [39]].

For some propellants, such as those described by Wiegand [41], $(\epsilon_m)_{max}$ varies with the temperature as though the crosslink density was temperature-dependent. In such cases the ϵ_m failure envelope must also be changing with temperature.

The failure envelope for cast double-base propellants has a different shape than that for rubber-based ones [42] (Fig. 13). The low and intermediate temperature portions are the same, but after the region of $(\epsilon_m)_{max}$ the value of ϵ_m is essentially constant for the former materials, while for the latter materials the envelopes curve back toward the stress axis just as those for unfilled elastomers do. This lack of curvature toward the stress axis in the double-base systems could

be a reflection of a change in crystallinity with temperature and/or strain. Polyvinylchloride, which is considered to be a crystalline polymer, also shows the same lack of curvature [43].
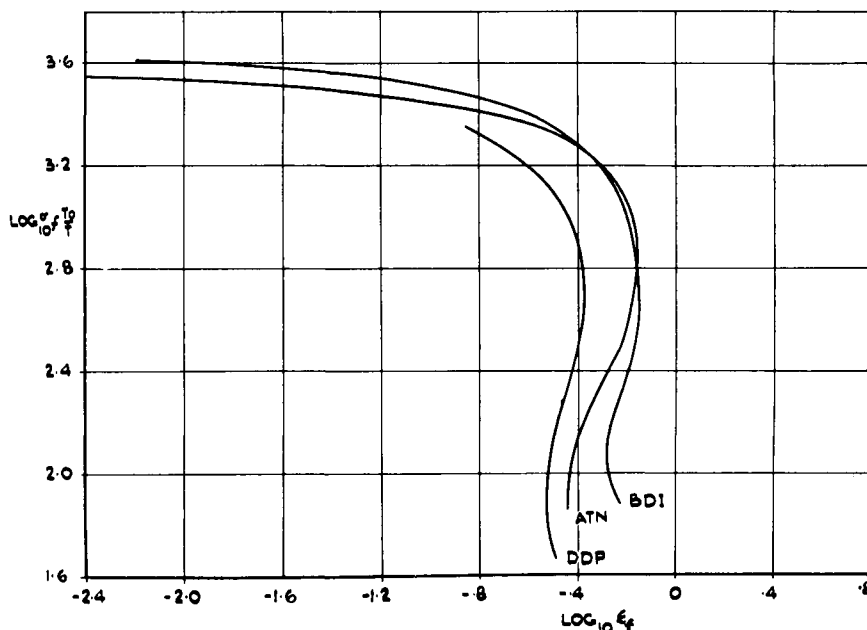
FIG. 13. Failure envelopes for three cast double base propellants. (From Leeming and Parker [42].)

3.4. Crosslink Dependence

At equilibrium, according to the kinetic theory of rubberlike elasticity, σ is directly proportional to ν_e. Since the breaking stress lies on the σ, ϵ curve, σ_b should also be proportional to ν_e. This proportionality is also contained explicitly or implicitly in all the various theories of ultimate strength proposed to date [3]. Therefore, both theory and intuition suggest, and experiment confirms, that a *reduced* failure envelope can be constructed by normalizing the stress to unit crosslink density, i.e. by plotting $\sigma_b T_0/\nu_e T$ versus ϵ_b*. The reduced envelope is thus a measure of the breaking stress per chain as a function of the breaking strain. It has proven to be quite independent of the nature of the polymer backbone systems, when the breaking strains > 100 per cent [2, 43].

Figure 14a indicates how a series of failure envelopes would appear for an elastomer crosslinked to varying degrees; Fig. 14b shows how they will shift and partially superpose when reduced to unit ν_e. Only the high temperature portions

---

* The temperature ratio T_0/T also stems from the kinetic theory of rubber-like elasticity. Here T_0 is an arbitrary standard state temperature and T is the test temperature (both in °K). This ratio must be included, just as when reducing small strain data.

of the envelopes are superposed. The form of reduced envelope up to $(\epsilon_b)_{max}$ is given to a very good approximation by eqn. (10), and more exactly by eqn. (7) [17].

Smith [8] has proposed an alternate form of a reduced failure envelope, obtained by plotting log $\lambda_b \sigma_b T_0 / T$ versus log $\lambda_b E_{equil}$, but this is a restricted case of the above method, valid only over a narrow range in ν_e [44].

REDUCED FAILURE ENVELOPE

a.
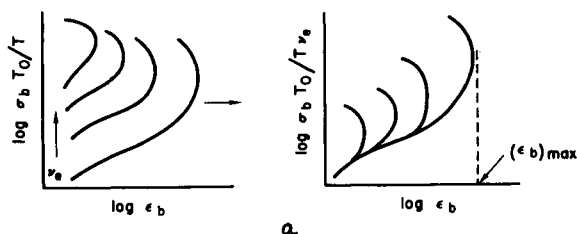
THUS THE RUPTURE BOUNDARIES ARE AS FOLLOWS

b
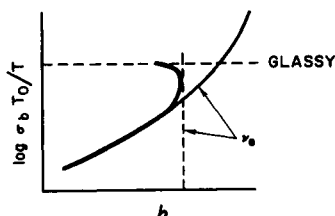
FIG. 14. (a) Schematic representation of unreduced and reduced failure envelope plots; (b) sketch showing that failure is closely bounded by the glassy response on the one hand and the rubbery response through eqn. (7) and ν_e on the other, while between these regions the limit is also set by ν_e, but according to eqn. (31).

Furthermore, $(\epsilon_b)_{max}$, the maximum value of ϵ_b, is expected to vary according to $\nu_e^{-1/2}$, based on the inverse Langevin function form for the stress–strain law, eqn. (7) [3], the Bueche–Halpin theory for the failure envelope [45], and from considerations of the dependence of the breaking strain on the dynamic loss modulus [6]. Experimentally [43]

$$\log (\lambda_b)_{max} = \log [1 + (\epsilon_b)_{max}] = 1.8 - \tfrac{1}{2} \log \nu_e \qquad (31)$$

where ν_e is expressed in micromoles/cm^3.

Since the glassy breaking strength is similar for amorphous polymers (circa 3000 psi), it is clear that the boundaries of the tensile properties of any such system can be predicted rather closely simply from a knowledge of ν_e. Thus, as indicated in Fig. 14b, failure will occur outside the roughly trapezoidal area bounded at the top by the glassy strength and at the right and bottom by ν_e

according to eqns. (31) and (7) respectively. Therefore if a designer can set an acceptable lower limit on his modulus, he will automatically set a lower limit of ν_e. From this he can at once ascertain the upper limit on the ultimate properties.

Since failure envelopes for elastomers which crystallize on straining also fall within these same bounds [8, 37], the same conclusion is also true for these systems. However, the breaking properties actually attained at a given rate and
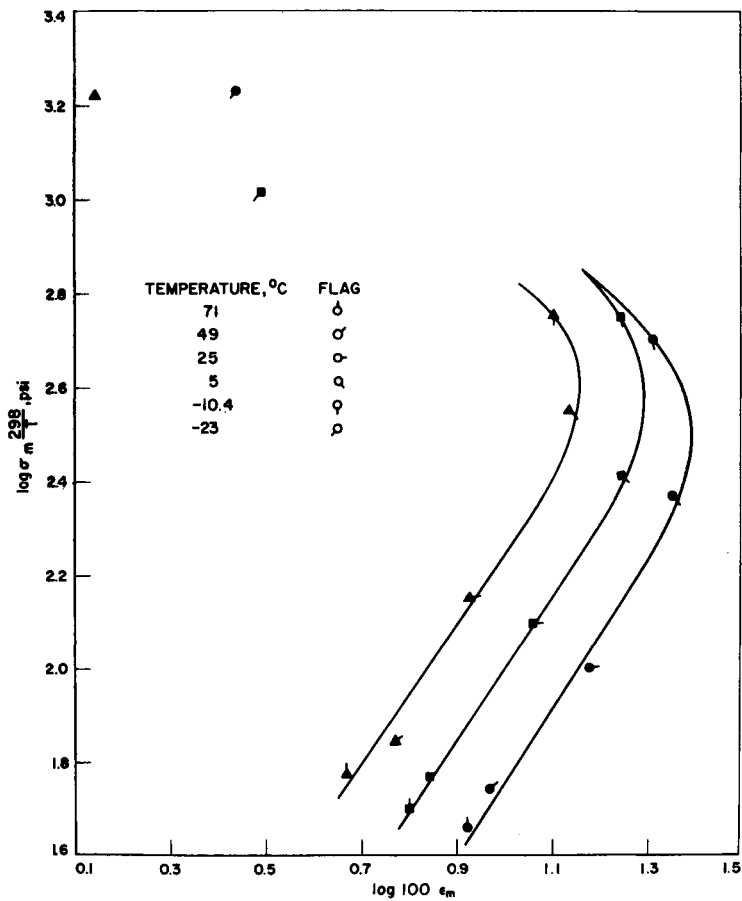
FIG. 15. Failure envelopes at ϵ_m for a polyurethane propellant of three different crosslink densities.

test temperature will lie well within the limits, generally at a higher σ_b for a given ϵ_b, whereas in completely amorphous systems the failure points will lie close to these boundaries.

This same reduction principle will also apply to filled systems, whether the filler is hard, as in a propellant, or soft, as in a foam [17]. However, the reduction factor is still ν_e, or the modulus of the *unfilled* rubber (not the system modulus). To illustrate, Fig. 15 shows some limited data for a polyurethane propellant at

three different crosslink densities. When these are normalized to unit modulus, the curves of Fig. 16 are obtained. Again, the high temperature portions of the ϵ_m envelopes are superposed.

TEMPERATURE, °C	FLAG
71	♂
49	♂
25	♂
5	♀
-10.4	♀
-23	♀
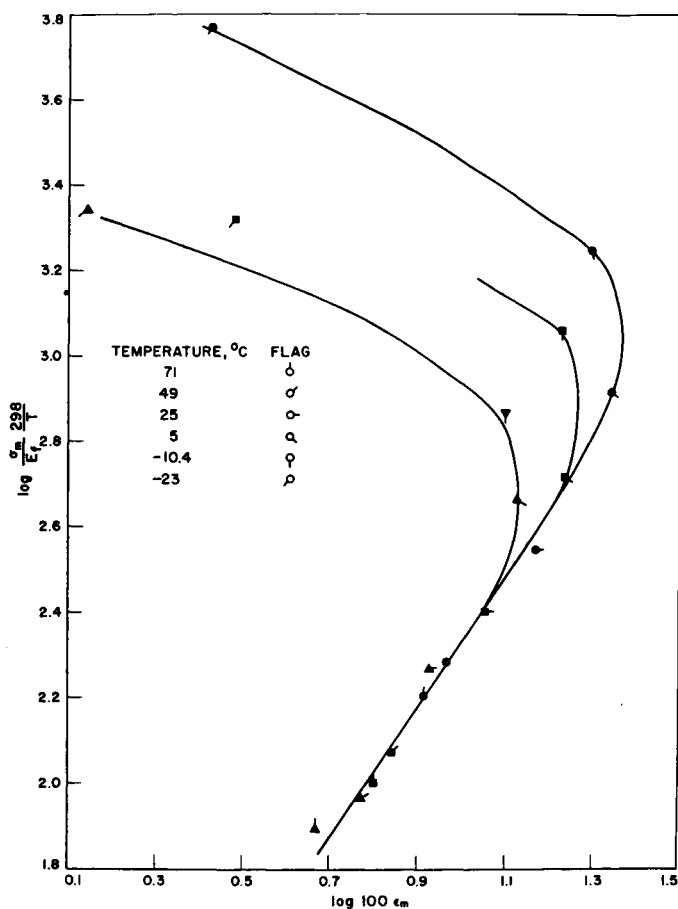
FIG. 16. Data of Fig. 15 reduced to unit modulus, using that of the filled system E_f, rather than that of the binder, as measured at 71°C.

4. THE EFFECT OF FILLER CONTENT

The effect of the amount of filler on the stress–strain curve and thus the tensile property surface can be divided into the effects on the initial modulus, the region of dewetting and the rupture.

4.1. *Initial Modulus*

The effect on the initial modulus should now be well known. A few years ago it was pointed out that the behavior of several systems could be described by the

Eilers–van Dyck equation [25].

$$\frac{E}{E_0} = \left[1 + \frac{k\phi}{1 - \phi/\phi_m}\right]^2 \tag{32}$$

where E_0 is the modulus of the unfilled system, k is a constant which is assumed to have a value of 1.25, ϕ is the volumetric loading, and ϕ_m is the maximum
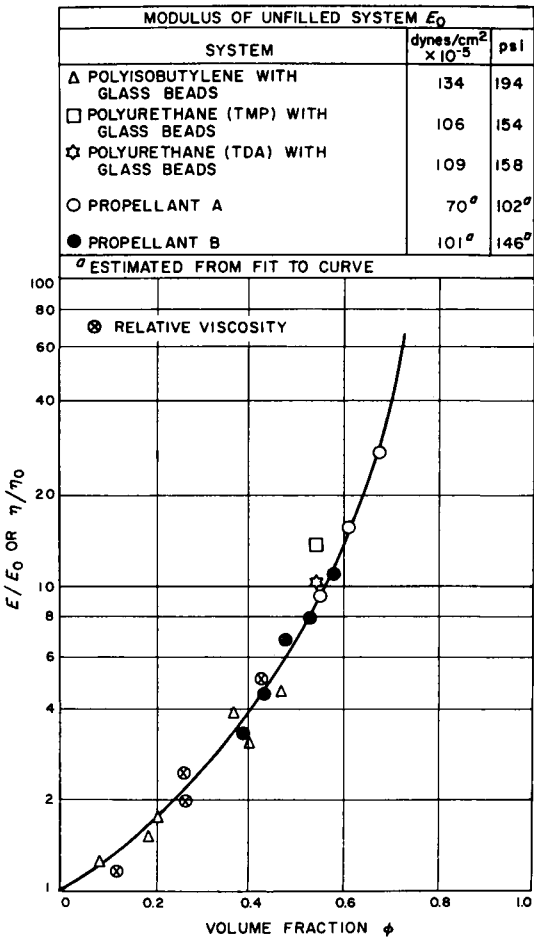
FIG. 17. Relative modulus as a function of the volumetric filler loading for several filled systems. In two cases the binder modulus was unknown. Also shown are relative viscosity data for polypropylene oxide and ammonium perchlorate, as measured with an Ultra-viscoson.

possible loading that can be attained for a given system. Some of the results are shown in Fig. 17. The applicability of eqn. (32) has been confirmed by the more extensive work of Schwarzl [46], who also showed that it was a limiting form of the more general van der Poel equation [47], obtained when the ratio of the filler-to-rubber modulus was high. Equation (32) does not hold in the glassy zone,

while the van der Poel equation does. Schwarzl has also shown that the latter equation holds for the bulk modulus, too. More recent results have been reported at this conference, wherein further references may be found, especially to the theoretical work of Hashin [47] and of Prager and Weissmann [48], as well as a comparison of the van der Poel equation with that of Prager and Weissmann.

Martin [49] recently presented the results of a series of measurements on a polybutadiene-acrylic acid system filled to five different levels. The filler content
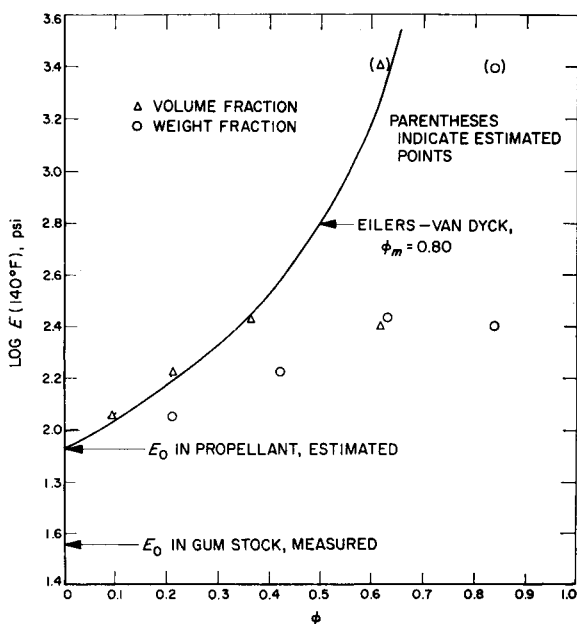
FIG. 18. The modulus data of Martin [49] plotted vs. weight and volume fraction of filler. The latter are also compared with the Eilers-van Dyck curve, eqn. (32), using a reasonable value of ϕ_m.

given in the paper is actually the weight fraction, and some of the data were apparently reduced according to this rather than the more appropriate volumetric loading.

Although interesting correlations were developed on this basis to represent the dependence of the behaviour on filler content, it is preferable to use volume fractions as the dependent variable. If the high temperature (140°F) modulus data are plotted vs. the filler content, as shown in Fig. 18, the points based on weight fraction give an essentially linear relationship, but when these are converted to volume fraction, only the lowest three loadings conform to the Eilers–van Dyck equation as expected. Furthermore, the extrapolated modulus is much higher than the measured value. Both of these apparent discrepancies are not discrepancies at all but instead offer confirmation of the theory. In discussing these results with Martin, it turned out that the binder formulation had to be adjusted at low filler concentrations because the filler affected the cure, and at

high concentrations because the modulus became too high. Both changes are clearly apparent in Fig. 18.

If eqn. (32) is to hold, the specific differences in the properties of a polymer containing different fillers or a given filler at different particle size distributions must be reflected in the parameter ϕ_m. It is not easy to test this thesis because such changes can easily change the crosslink density and thus E_0. However, the same or a similar equation should hold for relative viscosity, too, as indicated in Fig. 16. Using this simpler viscosity technique, it has indeed been found that the relative viscosity* *is* independent of the filler and the liquid medium over wide ranges in filler type, size, size distribution, and surface character [50]. Specifically, it was found that

$$\frac{\eta}{\eta_0} = \left(1 - \frac{\phi}{\phi_m}\right)^{-2.5} \tag{33}$$

Thus the relative viscosity η/η_0 is a simple function of the relative volumetric loading ϕ/ϕ_m which can be attained in the system. Furthermore, ϕ_m emerges as a key parameter in controlling behavior, e.g. for systems in which particles tend to agglomerate, the initial mix viscosity will be high and the cured propellant will be inhomogeneous, containing regions which are more highly filled than the average. Such systems will therefore have a reduced elongation capability. In this connection it is important to return to the work of Fishman and Rinde [31].

Fishman has pointed out that all of the lines of Fig. 8 intersect at a common value of the abscissa. This value is in reality a measure of the transverse contraction of the specimen, since $\sqrt{I_3}/\lambda = \lambda_1 \lambda_2 \lambda_3/\lambda_1 = \lambda_2^2$ for a uniaxial experiment. Thus all specimens rupture just prior to reaching a critical value of the lateral contraction. This critical value is a function of the volumetric loading and corresponds to that contraction at which the particles have achieved a maximum volumetric packing density ϕ_m. Since the latter is insensitive to the medium, if this criterion can be extended to the biaxial case, an absolute upper limit for rupture will have been established.

4.2. *Region of Dewetting*

In the intermediate region, there has been little work done on the form of the stress–strain curve in non-carbon black filled systems, i.e. with non-reinforcing fillers, since 1955, when Bryant and Bisset [51] discussed the plateau which appears in the stress–strain curve at sufficiently high loading density. Schwarzl [46] observed this with his materials too, but has not had time to analyze the results.

Payne [29] has measured the apparent dynamic shear modulus as a function of strain amplitude in systems containing varying filler contents. Typical results are shown in Fig. 19. At low amplitudes, i.e. below 0.001 per cent) strain, the shear modulus G_0 is strain independent and varies with ϕ as indicated by eqn. (32). At intermediate strains the specimen dewets and the modulus decreases.

---

* Apparent viscosity as measured in a parallel plate viscometer.

After complete dewetting, the modulus approaches a constant value, G_∞, which is the same as that for the unfilled rubber. All of these curves can be rectified on a normal probability plot, as shown in Fig. 20. Thus the equation for the strain dependence is

$$\frac{\log G(\epsilon) - \log G_\infty}{\log G_0 - \log G_\infty} = 1 - \frac{2}{\sqrt{\pi}} \int_0^u \exp\left(-\frac{u^2}{2}\right) du \tag{34}$$

where u is a linear function of the strain.
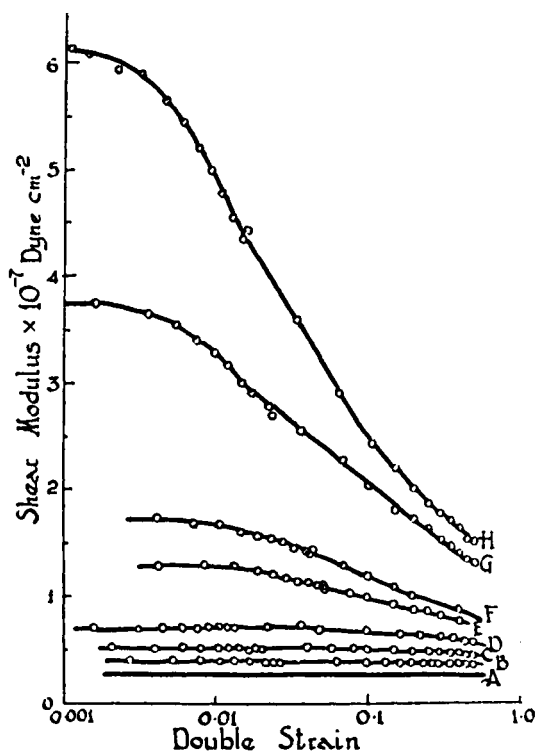
FIG. 19. Dynamic shear modulus as a function of double strain amplitude for natural rubber containing varying amounts of carbon black: A, 0 per cent; B, 5.6 per cent; C, 10.7 per cent; D, 15.2 per cent; E, 19.3 per cent; F, 23.0 per cent; G, 26.4 per cent; H, 29.5 percent. (From Payne [29].)

For small particles such as carbon black ($< 1\mu$), Payne finds strong particle-particle interactions which make a marked contribution to the modulus, beyond that indicated by eqn. (32).

Parkinson [52] has extensively reviewed the reinforcement of rubber by carbon black and silica.

As indicated previously, the work of Fishman [31], using Blatz's treatment for foams [33], and Ferris [28] using a statistical dewetting description, both offer an avenue for informative studies as a function of filler content, though this has not been done to date.

4.3. *Rupture Failure Envelope*

The effect of filler concentration on the failure envelope has not been exten-
sively studied either. Martin's [49] data is presented in Fig. 21 as unreduced
plots of the rupture envelopes. It can be seen that the net effect of the filler on the
envelope resembles that of increasing the modulus of an unfilled system—the
curves shift toward smaller strains. Though not shown here, the time-dependence
of $\lambda\sigma_b$ and ϵ_b in his material were essentially unchanged, aside from the decrease
in $(\epsilon_b)_{max}$. Thus plots of log ϵ_b versus log t_b are very similar in shape.
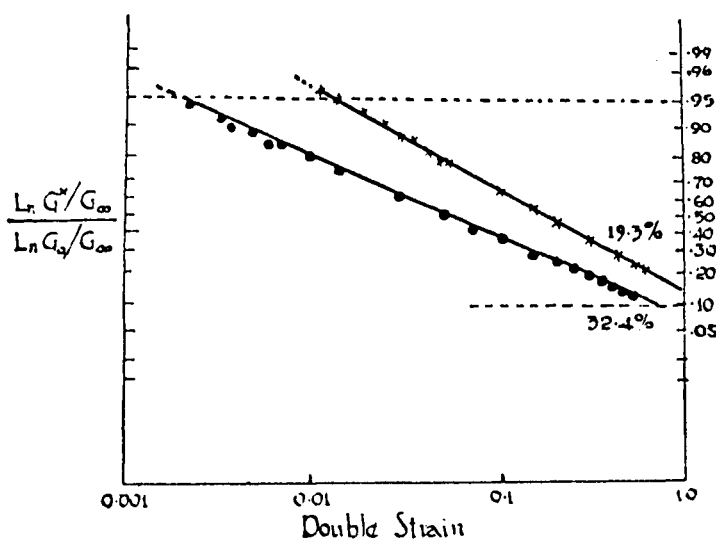
FIG. 20. Data of curve E of Fig. 20 and a similar curve at 32.4 per cent carbon black
rectified according to eqn. (34) of the text. (From Payne [29].)

As shown here, these data include both crosslink density and filler content
variations. To eliminate the former, the reduction to unit crosslink density,
previously discussed, may be employed. The result is illustrated in Fig. 19, where
ν_e has been calculated from the modulus, using the directly observed value for
the unfilled rubber and that deduced from Fig. 18, for the propellants. Just as
with the gum elastomers, all of the high temperature data draw together reason-
ably well and fall on the reduced master curve for gum rubbers [3, 43], which is
shown as the dashed line. This same agreement between the reduced rupture
envelope of filled and unfilled rubber has also been found for model systems
of varying amounts of glass beads in silicone and SBR rubber (up to 50 vol. per
cent beads) [53] as well as in other propellants, where only a single, high volu-
metric loading was employed [54].

In the region of response where the envelopes should superpose, interesting
and useful effects are obtained if the system rather than the binder modulus is
used as the reducing factor. Instead of superposing, the data are spread out into
a grid showing both particle size and volumetric loading effects. Thus if Schwarzl's
data [46] on the ultimate properties of his potassium chloride-filled polyurethane
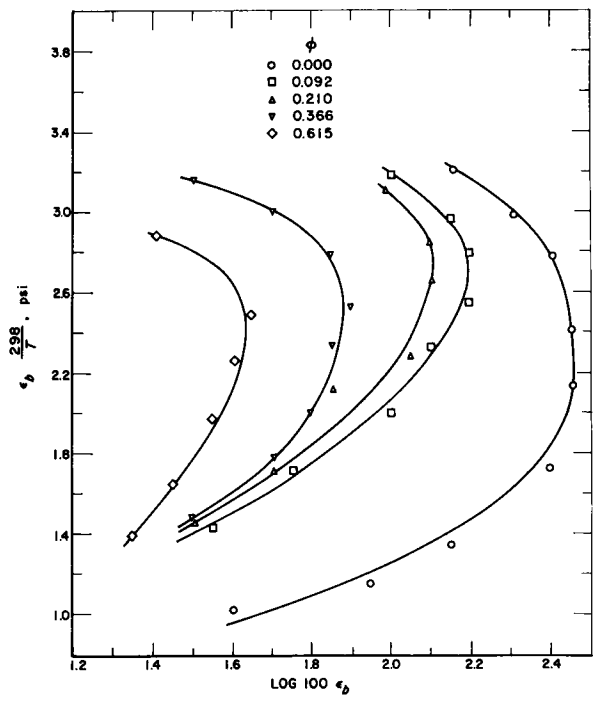
FIG. 21. Martin's [49] failure data plotted as unreduced envelopes.
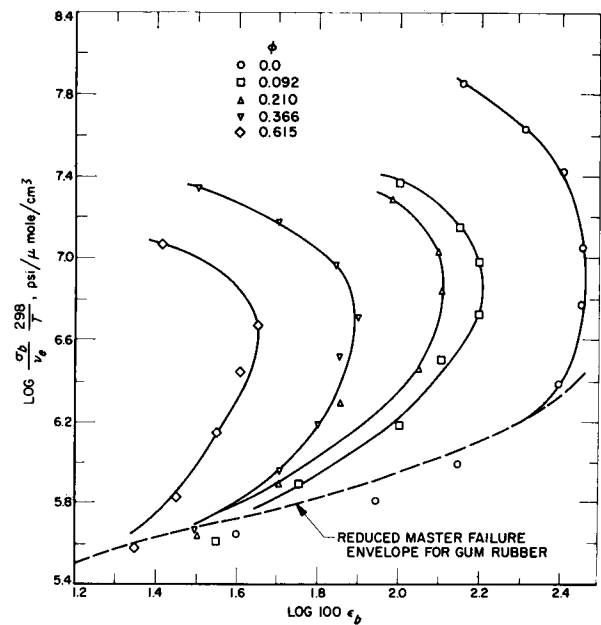
FIG. 22. The data of Fig. 21 reduced to unit chain density. Also shown is the reduced master envelope for unfilled rubber.

rubber are plotted as reduced failure envelopes, Fig. 23 is obtained. If Smith's reduction scheme [9] mentioned above, is attempted, the grid becomes even more clearly defined, Fig. 24. If this should prove to be a general phenomenon, it may offer a useful method of assessing or perhaps predicting both effects.

The shapes of the reduced failure envelopes for foams, rubbers and propellants may differ, of course, since for the filled systems they will always depend on the
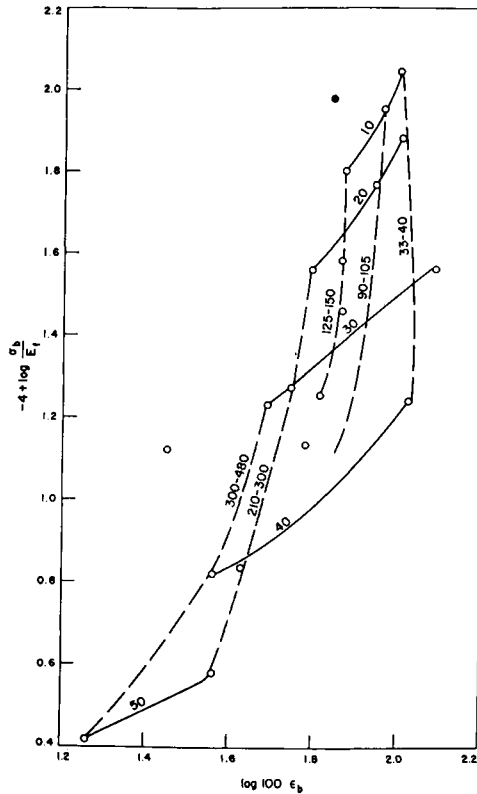
FIG. 23. Grid produced by Schwarzl's ultimate property data for a potassium chloride-filled polyurethane rubber [46], measured at a single rate at room temperature, when plotted as a reduced failure envelope according to the method of Landel and Fedors, but using the system modulus, E_f.

definition of failure, e.g. whether in terms of σ_m and ϵ_m, σ_b and ϵ_b, or σ_m and ϵ_L. Consequently, it is not yet possible to discern a universal expression to describe the envelope, analogous to eqn. (7) for gum rubbers. Nevertheless it should be possible to determine an appropriate envelope at a series of crosslink densities for any given system. Hence, if the stress analyst can ascertain a minimum modulus requirement for a propellant, e.g. from slump or acceleration setback requirements, it will immediately be possible to give the upper limits for σ and ϵ, just as it is for a rubber as shown in Fig. 14b. The stress analysis of the grain will then indicate whether the requirements fall outside this permissible range.
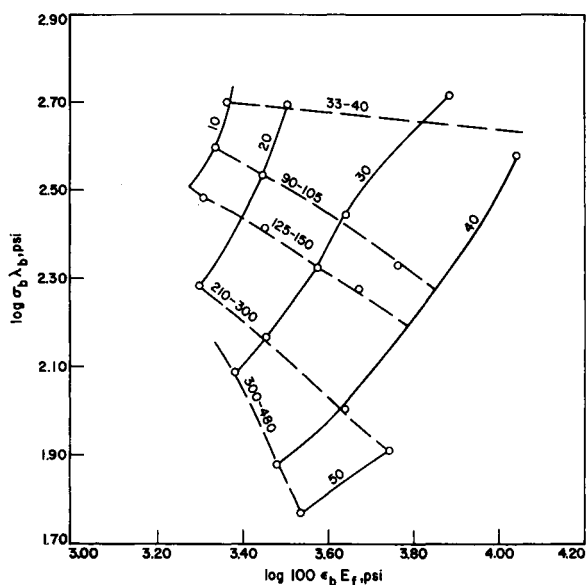
FIG. 24. The data of Fig. 23 plotted as a reduced failure envelope according to the method of Smith. All symbols have the same meaning as in Fig. 23.

5. INTERREGNUM

Because of the lack of experimental data, it is necessary at this point to relax our format of making detailed comparisons between elastomer and propellant behavior. Instead, a series of remarks will follow, summarizing some pertinent observations on multiaxial testing, statistics of rupture, and fatigue.

6. MULTIAXIAL TESTS

Gehman [55] has shown experimentally that time–temperature superposition also holds for an elastomer which is subjected to a triaxial failure test in which a flat-ended probe is forced at different rates and temperatures into a specimen until it is punctured. Presumably this same simplification of experimental studies will also apply to filled systems so long as the binder is thermo-rheologically simple and dominates the response. Preliminary results are very encouraging.

Sharma [56] has made biaxial tests at room temperature on a butadiene–acrylic acid copolymer containing 70 wt. % of aluminum and on an unfilled cellulose acetate butyrate. The tests consisted of tension or tension plus internal pressurization of tubular specimens. The PBAA had a tensile modulus of about 500 psi and was analogous to a composite propellant; the cellulose ester had a modulus of about 250,000 psi and was comparable to a double-base propellant. Pressurization rates were varied from 0.05 to 20 psi/sec for the filled rubber, and from 1 to 60 psi/sec for the hard plastic. The geometric failure criterion for the PBAA seems to be that of octahedral shear stress, while for the cellulose ester it appears to be a maximum principal stress. Thus the criterion for failure appears

to change from one characteristic form to another as specimens pass from the rubbery to the glassy state. On the other hand, the difference in behavior could be the result of the filler.

Jones [57] has performed a variety of biaxial tests on a PBAA propellant and his results indicate a maximum principal stress failure criteria. Harbert [58] is studying triaxial failure in a Rocketdyne propellant and preliminary results indicate again that a maximum principal stress criterion may be applicable.

The corresponding failure strains were not reported in any of these investigations, so the shape of the failure envelope under biaxial conditions cannot be ascertained.
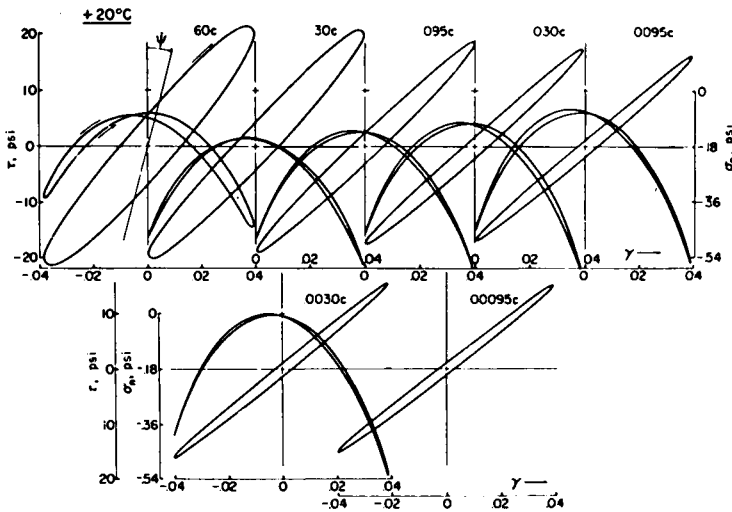
FIG. 25. Shear stress τ vs. shear strain γ ellipses as a function of frequency for a filled polyurethane rubber. Also shown are the corresponding normal stress σ_n vs. γ diagrams, recorded at the same time. (from Albrecht and Freudenthal [59].)

Albrecht and Freudenthal [59] have performed biaxial dynamic shear tests at small strains. This permits the determination of second order elastic constants analogous to the real and imaginary components of the shear modulus. In their apparatus, a Weissenberg rheogoniometer, thin disk-like specimens are subjected to a sinusoidal shearing action and not only the torsional stresses and strains are measured but also the normal stresses which develop perpendicular to the plane of shear. The latter are associated with second order elastic constants, akin to C_2 of eqn. (11), and so it is possible to measure the frequency dependence of both these second order constants and the ordinary constant, i.e. the shear modulus. While the measurements have not progressed far enough to assess the effect of fillers as a function of concentration, this should be a powerful investigative tool because dynamic measurements inherently give more information than transient measurements.

Typical results as a function of frequency are illustrated in Fig. 25 for a filled polyurethane rubber. The upper ellipse, or hysteresis loop, represents the usual

shear stress–shear strain plot, in which the major axis is related to the real part of the usual shear modulus, and the minor axis to the imaginary or loss component. The inverted parabola-like curves represent the normal force developed as a function of the strain. For a purely elastic material, these would be simple parabolas, passing through the origin. For viscoelastic materials at small strains, based on simplifying assumptions, it turns out that there should be two additional loss components, one which displaces the parabola from the origin and slightly modifies its shape, and a second which adds or subtracts according to whether the shear rate is increasing or decreasing. The latter thus has the effect of converting each arm of the parabola into a loop, as shown. The skewness of the parabola-like figures arise from still another term, the angle ψ of Fig. 25. Similar behavior was also found for an unfilled natural rubber. Thus in these highly sensitive dynamic experiments, nonlinear behavior is observed at all values of the shear strain, indicating that second order terms must be included in any consideration of mechanical behavior if precise results are desired. Equivalent second-order effects are also found in precise theories and experimental studies of metals—nonlinearity at small strains is not unique to filled rubbers. Rather it has often been overlooked because of the degree of sophistication required in the experimental techniques.

7. STATISTICS OF RUPTURE

The nature of the statistical distribution of rupture in propellant specimens from a single batch has apparently not been studied. Most attention has been given to batch-to-batch variability, which is mainly a reflection of the variability of the crosslink density. Binders have scarcely fared better, although interest is reviving [43].

In either case, extreme-value statistics must be used. Both Weibull [60] and Gumbel [61] have excellent texts on the subject, the former being eminently readable.

In both natural [62] and styrene–butadiene elastomers [43, 62], it has been found that the distribution of both breaking stress and breaking strain can be described by a double exponential distribution, viz.

$$\Phi = 1 - \exp[-\exp A(x - x^*)] \tag{35}$$

where Φ is the cumulative distribution of failures, A is a measure of the breadth of the distribution and x and x^* are the value and the most probable value of σ (or ϵ), respectively. It is extremely difficult to choose a form for the distribution, since even Kase's data [62] on 200 specimens could also have been fitted by a Weibull distribution [63] instead of the double exponential distribution given above.

Both A and x^* depend on test rate, temperature and crosslink density. The most probable values define the failure envelope, of course, but in addition, at temperatures above the region at which $(\epsilon_b)_{max}$ is found, *all* values lie on the failure envelope (as measured in the usual fashion by testing single specimens at

39

varied test rates and temperatures). Therefore the failure envelope can be obtained by statistical variability experiments [43]. At temperatures below that at which $(\epsilon_b)_{max}$ is observed, the stress-strain curves are not tangent to the failure envelope but cross it at a rather large angle (log–log plots). Thus there will always be a large scatter of data in this region.

The distribution of σ_b broadens up to $(\epsilon_b)_{max}$ while that of ϵ_b gets narrower. The time-dependence has not been explicitly reported, but it is clear that the distribution is broad enough to make it difficult to assess the breaking time in a constant load or constant strain test. The general relationship between the distributions are straightforward, viz., if that of σ_b is $\Phi(\sigma_b)$ and if σ_b is some function of the breaking time $h(t_b)$, then the distribution of t_b is $\Phi[h(t_b)]$. This means that if the time-dependence of σ_b is small, as is generally the case at room temperature and above, then $\Phi(t_b)$ will be very much broader than $\Phi(\sigma_b)$. This shows that the large scatter in breaking times found with constant load (or constant strain) tests is to be expected. Furthermore, comparison of the predicted with the observed difference in breaking times for creep, constant strain rate and stress relaxation tests will probably have to be done via statistical experiments before reliable conclusions can be drawn. Prevorsek [64] has recently discussed the inter-relationships between the distributions in some detail.

One of the important, overlooked aspects of extreme value statistics is that a means is provided for estimating the probability of finding a specimen with a given low (or high) value of σ_b or ϵ_b in a given number of specimens. This is analogous to estimating the height of the greatest flood to be expected in the next 5, 10 or 50 years. Such information is required by a dam designer whose dam would be dangerously weak if designed for a "5-year flood" or outrageously massive and expensive if designed for the highest flood of a thousand years. Similar considerations could be profitably invoked in estimating the reliability of very large grains which require multiple castings.

Wiegand [41] has been pointing out for several years the need to bring statistical methods to bear on analyses of failure data of propellants and motors.

8. CUMULATIVE DAMAGE AND FATIGUE

Little is known of the effects of filler content (non-carbon black) on the cumulative damage and fatigue properties of a rubber. One general comment should be made about fatigue studies, however. The heat generated during cyclic deformation experiments is well known to workers in the rubber field but has only recently been recognized in the propellant field [65, 66]. The energy dissipated $\mathscr{E}$ per quarter cycle at a given strain amplitude ϵ_0 is given as a function of the loss modulus E'' by Ferry [5] as

$$\mathscr{E} = \pi E'' \epsilon_0^2 \tag{36}$$

The power dissipation is thus $2\omega\epsilon_0^2 E''$. The frequency dependence of E'' is essentially the same for all amorphous elastomers at the same reference temperature state $(T - T_g)$, depending only on an internal viscosity parameter (called

the average segmental mobility, ζ_0, in Ferry's book). Thus it should be possible to calculate heat buildup in a rubber, *a priori*, from molecular parameters.

The heat buildup can be quite rapid, even at small strains. For the polybutadiene–acrylonitrile propellant studied by Jones [57], the initial temperature buildup in $4 \times 1 \times 1$ in. specimens at 1.25 per cent peak strain and 45 cps was $7°F/min$; and the final temperature was $200°F$. This is comparable to the 120–$180°F$ final temperature reported by Hoffman [67] for Goodrich flexometer tests on black-filled nitrile rubber, where the test specimen is small, 1×0.7 in. in diameter and the test is run at about 5 cps.

Gehman [68] carried out fatigue studies on carbon-black filled elastomers, under biaxial loading conditions, holding the strain amplitude constant. The break times were best described by a double exponential distribution, i.e. the same type of distribution as would be expected for breaking times in uniaxial constant strain rate tests, according to the earlier comments.

9. CONCLUSION AND COMMENTS

Much of the behavior of unfilled amorphous elastomers is qualitatively well understood at the molecular level [5, 13]. Molecular theories of rupture such as those of Bueche and Halpin [45] and of Knauss [69] are emerging, though they have not been discussed here. Both are hampered by the non-linear response of real polymers. The same approaches used to interrelate fracture and its dependence on time, temperature and degree of crosslinking as well as its statistical nature can be profitably employed for propellants. There is a pressing need for more dilatometric work, so that volumetric effects can be incorporated into theory and description. Multiaxial experiments are now proceeding rapidly in several laboratories [70] and so geometric failure surfaces should soon be described with some exactitude. It is expected that they will lie between that which can be generated from the inverse Langevin description of the amorphous elastomer and that which will be determined by the maximum filler packing density in the propellant.

Finally, tear or crack propagation has not been discussed here. We regard it as uniaxial tensile failure under another guise. Kainradl [71] has recently presented an excellent review of the subject.

REFERENCES

[1] ECKER, R., *Kautschuk u. Gummi*, **16**, 73 (1963).
[2] SMITH, T. L., *Journal of Polymer Science*, Part A, **1**, 3597 (1963); *Rubber Chemistry and Technology*, **37**, 777 (1964).
[3] LANDEL, R. F. and FEDORS, R. V., *Fracture Processes in Polymeric Solids*, Chapter III, B. ROSEN, ed., Interscience/Wiley, New York (1964).
[4] LANDEL, R. F., TM 33–52, Jet Propulsion Laboratory, California Institute of Technology, Pasadena, California, September 25, 1961. Bulletin of the 20th Meeting of the JANAF–ARPA–NASA Panel on Physical Properties of Solid Propellants, Vol. 1, November 1961.
[5] FERRY, J. D., *Viscoelastic Properties of Polymers*, Wiley and Sons, New York (1961), (a) Chapter 11; (b) p. 433.

39§

[6] LANDEL, R. F., "The relation of the small-strain loss compliance to the ultimate elongation capability of an amorphous elastomer", presented at the Society of Rheology Meeting, Pittsburgh, Pa., November 1964.

[7] SMITH, T. L., *J. Polymer Science*, **32**, 89 (1958).

[8] SMITH, T. L., *Journal of Applied Physics*, **35**, 27 (1964); *Rubber Chemistry and Technology*, **37**, 792 (1964).

[9] SMITH, T. L., *Transactions of the Society of Rheology*, **6**, 61 (1962).

[10] BLATZ, P. J., "Application of finite elasticity theory to the behavior of rubberlike materials", *Rubber Chemistry and Technology*, **36**, 1459 (1963).

[11] BERNSTEIN, B., KEARSLEY, E. A. and ZAPAS, L. J., *Transactions of the Society of Rheology*, **7**, 391 (1963).

[12] LIANIS, G., "Constitutive equations of viscoelastic solids under finite deformation", Purdue University Report No. A and ES 63–11, December 1963.

[13] TRELOAR, L. R. G., *The Physics of Rubber Elasticity*, Oxford University Press, London (1958).

[14] See FOX, T. G., *Polymer*, **3**, 111 (1962) and reference cited therein. For background, see Ref. [21] (this paper), Chapters 10 and 14.

[15] MARTIN, G. M., ROTH, F. L. and STIEHLER, R. D., *Transactions of Institute of Rubber Industry*, **32**, 189 (1956).

[16] WOOD, L. A., *J. Res. NBS*, **60**, 193 (1958).

[17] MOSER, B. G., FEDORS, R. F. and LANDEL, R. F., unpublished results.

[18] MOONEY, M., *J. Applied Physics*, **11**, 582 (1940).

[19] RIVLIN, R. S., "Large elastic deformation", in *Rheology*, **1**, F. R. EIRICH, Ed., Academic Press, Inc., New York, N.Y. (1956). (see references cited).

[20] LANDEL, R. F. and STEPRY, P. J., *J. Applied Physics*, **31**, 1885 (1960).

[21] FLORY, P. J., *Principles of Polymer Chemistry*, Cornell University Press, Ithaca, New York, p. 460 (1953).

[22] MULLINS, L. and THOMAS, A. G., *J. Polymer Sci.*, **43**, 13 (1960).

[23] SCANLON, J., *ibid.*, 501 (1960).

[24] NICHOLS, P. L. and NATHAN, R., Progress Report 20-208, Jet Propulsion Laboratory, California Institute of Technology, Pasadena, California, January 1954.

[25] LANDEL, R. F. and SMITH, T. L., *ARS Journal*, 31 599 (1960).

[26] BROCK, F. H., *Journal of Applied Polymer Science*, **7**, 1613 (1963).

[27] BILLS, Jr., K. W., HART, W. D. and HOLLAND, W. E., Bulletin of the 20th Meeting of the JANAF–ARPA–NASA Panel on Physical Properties of Solid Propellants, CPIA, October 1961, p. 61.

[28] FERRIS, R. J., (a) *Journal of Applied Polymer Science*, **8**, 25 (1964). (b) Bulletin of the 3rd Meeting of the ICRPG Working Group on Mechanical Behavior, CPIA, November 1964, p. 291.

[29] PAYNE, A. R., *Journal of Applied Polymer Science*, **6**, 368 (1962).

[30] NADAI, A., *Theory of Flow and Fracture of Solids*, McGraw-Hill, New York, (1950).

[31] FISHMAN, N. and RINDE, J. A., (a) "Solid propellant mechanical properties investigation", Final Report, Contract No. AF 04(611)–9559, Stanford Research Institute, December 1964; (b) Bulletin of the 3rd ICRPG Working Group on Mechanical Behavior, CPIA, November 1964, p. 267.

[32] RINDE, J. A. and FISHMAN, N., *ibid.*, p. 177.

[33] BLATZ, P. J. and KO, W. L., *Transactions of the Society of Rheology*, **6**, 223 (1962).

[34] LANDEL, R. F., previously unpublished.

[35] STOKER, J. H., Bulletin of the 3rd Meeting of the ICRPG Working Group on Mechanical Behavior, CPIA, October, 1964, p. 421.

[36] HALPIN, J. C., *Journal of Applied Physics*, **35**, 3133 (1964).

[37] SMITH, T. L., "Characterization of ultimate tensile properties of elastomers", Air Force Materials Laboratories Report No. ML–TDR–64–264, August 1964.

[38] LANDEL, R. F., "Tensile testing of composite propellants", CBS 66, Jet Propulsion Laboratory, California Institute of Technology, Pasadena, California, August 1958.

[39] BRIAR, H. P. and WIEGAND, J. H., Bulletin of the 3rd Meeting of the ICRPG Working Group on Mechanical Behavior, Vol. 1, CPIA, November 1964, p. 455.

[40] SMITH, T. L. and SMITH, J. R., "Viscoelastic properties of solid propellants and propellant binders", Stanford Research Institute Technical Report No. NOw–61–1057–d, October 1962.

[41] WIEGAND, J. H. and MILLOWAY, W. T., Bulletin of the 20th Meeting of the JANAF-ARPA-NASA Panel on Physical Properties of Solid Propellants, SPIA, October 1961, p. 323.

[42] LEEMING, H. and PARKER, A., Bulletin of the 3rd Meeting of the ICRPG Working Group on Mechanical Behavior, CPIA, October 1964, p. 469.

[43] LANDEL, R. F. and FEDORS, R. F., "The tensile failure envelope of amorphous elastomers: effects of statistical variability and crosslink density", *Proceedings of the 4th International Congress on Rheology*, Brown University, Providence, Rhode Island, 1963, Interscience, New York, Part 2, p. 543 (1965).

[44] LANDEL, R. F. and FEDORS, R. F., Quarterley Summary Report 38-14, Jet Propulsion Laboratory, California Institute of Technology, Pasadena, California. This report is classified but the pertinent section is not and can be provided upon request.

[45] BUECHE, F. and HALPIN, J. C., *Journal of Applied Physics*, **35**, 36 (1964).

[46] SCHWARZL, F. W., "Mechanical properties of highly filled elastomers, I (1962), II (1963), III (1964)". ONR Technical Reports 1, 2, 3, Contract N-62558-2822, -3243, 3581, and 3884; SCHWARZL, F. W., BREE, H. W. and NEDERVEEN, C. J.: "Mechanical Properties of Highly Filled Polymers' *Proceedings of the 4th International Congress on Rheolgy*, Interscience, Part 3, p. 241 (1965).

[47] VAN DER POEL, C., *Rheologica Acta*, **1**, 202 (1958).

[48] WEISSMAN, H. L. and PRAGER, S., "Viscosity of concentrated suspensions by spherical particles", paper presented at the *4th International Congress on Rheology*, Brown University, Providence, R.I., August 1963. Abstract given in *Procedings*, Part 2, p. 709.

[49] MARTIN, D. L., Jr., Bulletin of the 3rd ICRPG Meeting of the Working Group on Mechanical Properties, CPIA, November 1964, p. 303.

[50] LANDEL, R. F., MOSER, B. G. and BAUMAN, A. J., "Rheology of concentrated suspensions: effect of a surfactant", *Proceedings of the 4th International Congress on Rheology*, Brown University, Providence, Rhode Island, August, 1963. Interscience, New York, Part 2, p. 663, (1965).

[51] BRYANT, K. C. and BISSET, D. C., *Proceedings of 3rd Rubber Technology Conference*, London, Butterworths London, p. 655 (1954).

[52] PARKINSON, D., *Reinforcement of Rubbers*. The Institution of the Rubber Industry, London (1957).

[53] FEDORS, R. F., MOSER, B. G. and LANDEL, R. F., work in progress.

[54] KELLY, F. J., private communications.

[55] LIVINGSTON, D. I., YEH, G. S., ROHALL, P. and GEHMAN, S. D., *Journal of Applied Polymer Science*, **5**, 442 (1961); LIVINGSTON, D. I. and YEH, G. S., *Rubber Chemistry and Technology*, **34**, 937 (1961); LIVINGSTON, D. I. and HILDENBRAND, L. E., *Rubber Chemistry and Technology*, **37**, 14 (1964).

[56] SHARMA, M. G. and LIM, K. C., "Experimental investigations on fracture of polymers", presented at the Regional Technical Conference of the Society of Plastics Engineers, Newark, N.J., November, 1964.

[57] JONES, J. W., Bulletin of the 3rd ICRPG Meeting of the Working Group on Mechanical Behavior, CPIA, October 1964, p. 371.

[58] HARBERT, B. C., *ibid.*, p. 357.

[59] ALBRECHT, B. and FREUDENTHAL, A. M., Report Nonr 266 (78), No. 27, Columbia University, New York, 1965.

[60] WEIBULL, W., *Fatigue Testing and the Analysis of Results*. Pergamon Press, New York (1961).

[61] GUMBEL, E. J., *Statistics of Extremes*. Columbia University Press, New York (1958).

[62] KASE, S., *Journal of Polymer Science*, **11**, 425 (1953).

[63] SCHWARZL, F. and STAVERMAN, A. J., Chapter III, Vol. IV. "Bruchspannung und Festigkeit von Hochpolymeren", in *Die Physik der Hochpolymeren*, H. A. STUART, Ed. Springer, Berlin (1956).

[64] PREVORSEK, D. and LYONS, W. J., *Textile Research Journal*, **33**, 963 (1963).

[65] TORMEY, J. F. and BRITTON, S. C., *AIAA Journal*, August 1963.

[66] BURTON, J. D., JONES, W. B. and FRAZEE, J. D., Bulletin of the 3rd Meeting of the ICRPG Working Group on Mechanical Behavior, November 1964, p. 191.

[67] HOFFMAN, W., "Nitrile rubber". A Rubber Review for 1963, *Rubber Chemistry and Technology*, **37**, 178 (1964).

[68] GEHMAN, S. D., ROHALL, P. and LIVINGSTON, D. I., *Rubber Chemistry and Technology*, **34,** 506 (1964).

[69] KNAUSS, W. G., Bulletin of the 3rd Meeting of the ICRPG Working Group on Mechanical Behavior, CPIA, November 1964, p. 437.

[70] JONES, T. M. and KRUSE, R. B., "Failure behavior of composite hydrocarbon fuel binder propellants", to be presented at 6th AIAA Solid Propellant Rocket Conference, New York City, Feburary 1965. According to the abstract it is suggested that the surface consists of a deviatoric stress cylinder capped by a dilatational failure surface in the positive stress octant.

[71] KAINDRADL, P. and HANDLER, F., *Kautschuk und Gummi*, **12,** WT 239, 284, 336 (1959); *Rubber Chemistry and Technology*, **33,** 1438 (1960).

[72] HASHIN, Z. and SHTRIKEMAN, S., "A variational approach to the theory of the elastic behaviour of multiphase materials", *J. mech. Phys. Solids*, **11,** 127, (1963) and prior references cited therein.

AUTHOR INDEX

615

SUBJECT INDEX

621